UNIVERSITY OF BELGRADE
FACULTY OF PHYSICS

Stefan Đorđević

Page curve in models of 2D dilaton gravity

Doctoral Dissertation

Belgrade, 2026.

UNIVERZITET U BEOGRADU
FIZIČKI FAKULTET

Stefan Đorđević

Pejdžova kriva u modelima 2D dilatonske gravitacije

Doktorska disertacija

Beograd, 2026.

Mentor

prof. dr Voja Radovanović
redovni profesor
Univerzitet u Beogradu – Fizički fakultet

Komisija za odbranu doktorske disertacije

prof. dr Maja Burić
redovni profesor
Univerzitet u Beogradu – Fizički fakultet

dr Branislav Cvetković
naučni savetnik
Univerzitet u Beogradu – Institut za fiziku

prof. dr Marija Dimitrijević Ćirić
redovni profesor
Univerzitet u Beogradu – Fizički fakultet

Datum odbrane doktorske disertacije

____

Abstract

This dissertation investigates quantum gravity effects and black hole unitarity within the framework of semiclassical two-dimensional dilaton gravity with the aim at resolving the information loss paradox. A central objective is to reproduce the Page curve for the experimentally relevant dimensionally reduced Schwarzschild black hole, in both evaporating and eternal configurations. To this end, we first develop a coherent method for constructing eternal and evaporating black hole geometries based on a symmetric ansatz for two-dimensional spacetimes that admits a Killing vector. With this ansatz in place, we obtain the classical static vacuum solutions to the equations of motion. Next, we describe a classical collapse scenario by smoothly matching two such vacuum regions across an infalling matter shockwave. We then incorporate quantum corrections and solve the quantum-corrected equations of motion in perturbations around the classical vacuum black hole and the classical collapse scenario by specifying the Hartle–Hawking state and the Unruh state, respectively, as the underlying quantum states. The Hartle–Hawking state leads to an eternal black hole solution, whereas the Unruh state describes an evaporating black hole. Finally, by invoking the island rule, we successfully derive the Page curve in both of these setups.

The second part of this work investigates how spacetime torsion enters black hole thermodynamics, with the specific aim of preparing the ground for studying its influence on the island formula by identifying viable two-dimensional spacetimes with nonzero torsion. To construct such two-dimensional torsional models, we carry out a dimensional reduction of a five-dimensional Chern–Simons theory. Examining minimal couplings to various matter fields, we uncover distinct cosmological solutions and a charged Riemannian black hole. In particular, coupling gravity to Dirac spinors gives rise to a fermionic soliton-star that undergoes a characteristic phase transition: a fully regular fermionic star configuration collapses into a localized, non-extremal singular horizon once a critical parameter is surpassed. Finally, we incorporate Polyakov–Liouville quantum corrections and thereby obtain an eternal black hole configuration with two singular horizons, analogous to the rotating 3D BTZ black hole. We then employ the standard island prescription, using the Wald entropy as the area term, to investigate how torsion influences the fine-grained entropy. Our analysis shows that turning on torsion enforces stringent constraints on the allowed position of the black hole boundary hypersurface. In summary, this work develops a robust computational framework for studying evaporating black holes and supplies two-dimensional spacetime solutions with torsion that can be employed in future analyses of how spacetime torsion alters fine-grained entropy.

Key words: *2D dilaton gravity, black hole thermodynamics, information loss paradox, black hole evaporation, Page curve, island formula, dimensional reduction, Chern-Simons gravity, spacetime torsion*

Research field: **physics**

Research subfield: **high energy physics**

Apstrakt

Ova disertacija istražuje efekte kvantne gravitacije i unitarnost crnih rupa u okviru semiklasične dvodimenzionalne dilatonske gravitacije sa ciljem razrešenja paradoksa gubitka informacija. Glavni cilj disertacije je reprodukcija Pejdžove krive za eksperimentalno relevantnu dimenziono redukovanu Švarcšildovu crnu rupu, kako u isparavajućoj tako i u večnoj konfiguraciji. Najpre razvijamo metod za konstruisanje geometrije večnih i isparavajućih crnih rupa zasnovan na simetričnom ansatzu za dvodimenzionalno prostor-vreme sa Kilingovim vektorom. Koristeći ovaj ansatz, dobijamo klasična statička vakuumska rešenja jednačina kretanja. Zatim opisujemo scenario klasičnog kolapsa glatkim spajanjem dve odgovarajuće vakuumske oblasti preko kolapsirajućeg talasa materije. Potom dodajemo u naš model kvantne korekcije i rešavamo kvantno-korigovane jednačine kretanja korisreći perturbativni razvoj oko klasične vakuumske crne rupe, kao i klasičnog scenarija kolapsa, birajući Hartli-Hokingovo kvatno stanje i Unruhovo kvantno stanje, redom. Na kraju, uspešno izvodimo Pejdžovu krivu u obe konfiguracije.

Drugi deo ove disertacije bavi se uticajem nenulte torzije u prostor-vremenu na termodinamiku crne rupe, sa ciljem izučavanja efekata u formuli sa ostrvom pomoću nalaženja odgovarajućih dvodimenzionalnih prostor-vremena sa nenultom torzijom. Da bismo konstruisali takve dvodimenzionalne modele sa torzijom, primenjujemo dimenzionu redukciju petodimenzionalne Čern–Sajmonsove teorije. Ispitujući minimalna kuplovanja sa različitim poljima materije, otkrivamo razna kosmološka rešenja kao i naelektrisnanu crnu rupu u Rimanovskom sektoru teorije. Posebno, sprezanje gravitacije sa Dirakovim spinorima dovodi do fermionske solitonske zvezde koja doživljava karakterističan fazni prelaz: potpuno regularna konfiguracija fermionske zvezde se kondenzuje u lokalizovani, neekstremalni singularni horizont nakon što se desi fazni prelaz. Konačno, uključujemo Poljakov-Liuvilove kvantne korekcije i time dobijamo konfiguraciju večne crne rupe sa dva singularna horizonta, analognu rotirajućoj 3D BTZ crnoj rupi. Zatim primenjujemo standardnu preskripciju ostrva, koristeći Voldovu entropiju kao površinski član, kako bismo ispitali uticaj torzije na fino-granuliranu entropiju. Naša analiza pokazuje da uključivanje torzije nameće stroga ograničenja na dozvoljeni položaj granične hiperpovrši crne rupe. Ukratko, ovaj rad razvija računarski okvir za proučavanje isparavajućih crnih rupa i pruža rešenja za dvodimenzionalna prostor-vreme sa torzijom.

Ključne reči: *2D dilatonska gravitacija, termodinamika crnih rupa, pardoks gubitka informacija, isparavanje crnih rupa, Pejdžova kriva, pravilo ostrva, dimenziona redukcija, Čern-Sajmons gravitacija*

Naučna oblast: **fizika**

Uža naučna oblast: **fizika visokih energija**

Acknowledgements

First, I would like to express my sincere gratitude to my supervisor, Dr Voja Radovanović, who has been my primary collaborator on the papers that constitute the core of this thesis. As I am also deeply interested in topological phases of matter, I am very grateful to my collaborator, Dr Vladimir Juričić, with whom I have recently posted an e-print on arXiv on the subject of non-Hermitian topology in condensed matter physics. I am equally grateful to my third collaborator and dear friend, Dr Dušan Đorđević, with whom I am working on Chern-Simons aspects of the research presented here. Furthermore, I wish to express my gratitude to all my colleagues from the Belgrade Group for Gravitation, Particles, and Fields, with whom I have collaborated and discussed a wide range of topics.

I would also like to acknowledge the constant and invaluable support of my family and friends. I am especially indebted to my wife, Ana Đorđević, for the tremendous help she has provided whenever I needed it, both in everyday matters and in my scientific work, including numerous insightful discussions about physics. She is also responsible for creating all the figures in this dissertation. I further wish to thank Hana Schiff Toman for her many useful suggestions on writing in English, which is not my native language, though it is hers.

I am grateful to my elementary school and high school physics teachers, Selma Popović and Nataša Čaluković, without whose influence I would not have developed such a strong passion for physics. Similarly, I am deeply grateful to my parents, Jelica and Dragan Đorđević, who have consistently supported the scientific path I chose and encouraged me to embark on it from the very beginning. Finally, I would like to thank everyone who has shared part of this journey with me.

I am also thankful to the Petnica Science Center and the Mathematical Grammar School for providing me with an excellent teaching experience over the past five years. It has been an honor to teach talented young people, some of whom, I am certain, will become outstanding physicists one day. At Petnica, I have met many friends who share my enthusiasm for physics. Some are now my collaborators on projects at various levels, and I hope that others will become collaborators in the future.

To my lovely wife Ana,
and my dearest parents Jelica and Dragan

Table of Contents

List of Figures

Chapter 1

Introduction

In this dissertation, we study certain thermodynamic aspects of black holes. Black holes arise as some of the earliest known solutions to Einstein's field equations. In 1915, Einstein presented his *General Theory of Relativity* [2], and in that same year Karl Schwarzschild found the first spherically symmetric solution of Einstein's equations [3]. This solution is characterized by the presence of a singularity, that is, a point where the curvature of spacetime ceases to be well defined. In addition, this singularity is concealed behind a surface called the *event horizon*. More precisely, the event horizon is a boundary that separates spacetime into two distinct regions. Inside the region enclosed by the horizon, the future evolution of all particles, including light, is the same: they inevitably end at the singularity. Put differently, once a particle crosses the event horizon, the gravitational field becomes so intense that escaping would demand a speed exceeding that of light, which is physically impossible. As a result, the particle remains confined. Because of these characteristics, this solution is known as a *black hole*.

1.1 Historical overview of the black hole thermodynamics

As research progressed, further black hole solutions were identified, the most general of which is the *Kerr–Newman solution* [4, 5]. This solution provides the most general vacuum configuration of Einstein's equations coupled to electrodynamics, describing a singularity concealed behind an event horizon. Black holes can, in fact, be fully characterized by only a few parameters, i.e., conserved quantities: the mass M, the angular momentum (spin) J, the electric charge Q, and the magnetic charge P. Using Killing vectors, which encode spacetime symmetries, one can determine these conserved quantities. They are connected via the *Smarr relation* [6], which can be derived purely from the spacetime geometry [7]:

$$M = \frac{\kappa A}{4\pi G} + 2\Omega_{\mathrm{H}} J + \Phi_{\mathrm{H}} Q + \Psi_{\mathrm{H}} P, \tag{1.1}$$

where κ denotes the *surface gravity*, A is the area of the event horizon, G is Newton's gravitational constant, Ω_{H} is the angular velocity of the horizon, Φ_{H} is the electric scalar potential at the horizon, and Ψ_{H} is the magnetic scalar potential at the horizon. This formula closely resembles Euler's equation in thermodynamics [8], which prompted many researchers to regard black holes as thermodynamic systems. Taking into account that $M = M(A, J, Q^2, P^2)$ is a homogeneous function of degree $1/2$, together with the Hawking area theorem [9], $\Delta A \geqslant 0$, which is always satisfied, the first law of black hole thermodynamics was established in the mid-20th century in the form [10]:

$$dM = \frac{\kappa}{8\pi G} dA + \Omega_{\mathrm{H}} dJ + \Phi_{\mathrm{H}} dQ + \Psi_{\mathrm{H}} dP. \tag{1.2}$$

From Eq. (1.2), up to an overall numerical factor, Bekenstein inferred which quantities should be interpreted as the temperature and entropy of a black hole:

$$T = \alpha \frac{\kappa}{8\pi} \quad \wedge \quad S = \frac{A}{\alpha G}. \tag{1.3}$$

Information loss paradox

From a classical standpoint, a black hole that "swallows" everything that comes near it should not exhibit any temperature. Thus, the quantity obtained earlier could not be regarded as a genuine temperature; it was instead understood merely as a mathematical construct highlighting a formal analogy with thermodynamics. This interpretation remained dominant until 1974, when Hawking performed the quantization of fields on the fixed Schwarzschild black hole background. He showed that this semiclassical framework—combining quantum field theory with general relativity—implies that a stationary observer at infinity measures black hole radiation with a thermal spectrum and a well-defined temperature. This result determines the previously undetermined parameter to be $\alpha = 4$ [11, 12, 13]. It was the first clear indication that black holes behave as genuine thermal systems.

Two years before Hawking's discovery, Bekenstein had hypothesized that black holes must carry entropy [14], and the following year he argued that the proportionality constant should be very close to $\alpha = 4$ [15]. Consequently, the expression for black hole entropy is known as the *Bekenstein–Hawking formula* and is written as

$$S_{BH} = \frac{k_B A}{4 l_p^2}, \tag{1.4}$$

where $l_p = \sqrt{\frac{G\hbar}{c^3}}$ denotes the Planck length. Up to this point we have employed natural units with $c = k_B = \hbar = 1$, whereas here the constants have been reinstated to emphasize the physical dimensions.

Thus, the notion that black holes possess entropy was confirmed; however, this led to a new set of problems. The subsequent task was to compute the entropy of the radiation emitted by the black hole, known as *Hawking radiation*. Because this entropy is associated with the subsystem corresponding to the radiation, it is actually the *fine-grained entropy*. In contrast, the Bekenstein–Hawking entropy is a *coarse-grained entropy*, defined as a thermodynamic quantity. Hawking's analysis demonstrated that the fine-grained entropy grows monotonically over time throughout the evaporation process, up until the black hole has completely evaporated. This behavior is incompatible with unitary time evolution in quantum mechanics. Specifically, if the black hole is formed by the collapse of a pure state, as is generally assumed, then after evaporation one is left with a mixed state of radiation. Such an evolution is non-unitary. This inconsistency is referred to as the *Hawking information paradox*. Hawking himself did not consider it a paradox, but instead interpreted it as evidence that black holes act as systems into which information can fall and be permanently lost [16].

In contrast, numerous researchers challenged this conclusion and sought to pinpoint a mistake in Hawking's calculation of the radiation entropy. As a result, in 1992 Page introduced a particular time dependence for the entropy of Hawking radiation so that the overall evolution would remain unitary [17, 18]. This time dependence is now referred to as the *Page curve*.

Throughout the 1990s, a large number of papers on black hole entropy appeared, aiming to address the information paradox, that is, to understand why information seems to be lost. Many authors followed Hawking's argument and assumed that quantum fields propagating on a black hole background do not evolve unitarily. To study this issue, two-dimensional dilaton gravity models were developed as simplified frameworks. The most prominent among these are the CGHS model [19] (named after Callan, Giddings, Harvey, and Strominger) and the JT model [20, 21] (named after Jackiw and Teitelboim). These are not realistic models but rather "toy models," designed to capture only the qualitative features of black hole evaporation; a precise, quantitative treatment still requires numerical computations.

To model black hole evaporation, quantum corrections to the classical theories must be taken into account. When the matter sector consists of massless scalar fields, this leads to the inclusion of the *Polyakov–Liouville term* [22] in the action. However, adding this term alone does not yield analytic solutions, so additional correction terms were introduced to preserve analyticity. For the CGHS model, there are two widely used such extensions: the RST model [23, 24] (named after Russo, Susskind, and Thorlacius) and the BPP model [25] (named after Bose, Parker, and Peleg). In the 1990s, analyses of both of these models pointed to the same outcome: black hole evaporation leads to information loss [26, 25]. These constructions were originally motivated by, and derived from, *string theory*.

Fine-grained entropy in gravitational systems

In parallel with efforts to resolve the information paradox, Gerard 't Hooft introduced the *holographic principle* in 1993 [27]. By revisiting Hawking's original results from the 1970s, he argued that the number of degrees of freedom associated with a black hole scales with the area of its horizon. This notion was then developed further by Susskind in his 1995 work [28], where he treated the entire spacetime as the boundary of a higher-dimensional bulk, effectively portraying the universe as a hologram. The most influential development inspired by the holographic principle came shortly thereafter in Juan Maldacena's 1997 paper, which introduced the AdS/CFT correspondence [29] (Anti-de Sitter/conformal field theory). This work rapidly became the most cited publication in the history of theoretical high-energy physics.

Drawing on ideas from string theory, and AdS/CFT correspondence in particular, Ryu and Takayanagi proposed in 2006 a relation between fine-grained (entanglement) entropy and the conformal field theory defined on the boundary of Anti-de Sitter spacetime. This relation is now known as the *Ryu–Takayanagi formula* [30]. A covariant generalization of this formula was presented in 2007 [31]. The central idea is grounded in the Bekenstein–Hawking expression for black hole entropy:

$$S_I = \min_I \left\{ \operatorname*{\mathbf{ext}}_I \left[\frac{A[I]}{4G} \right] \right\}, \tag{1.5}$$

where I denotes a subregion of the boundary of a space-like hypersurface, and $A[I]$ is the area of the corresponding surface I.

Even so, most researchers in this area aimed primarily at reproducing the Page curve, because the principle of unitarity in quantum mechanics is broadly accepted. The Ryu–Takayanagi formula on its own failed to yield the Page curve in any concrete model, but it served as the initial step toward formulating a general expression for the fine-grained entropy of gravitational systems. Substantial advances followed. By carrying out a more sophisticated analysis of the *gravitational path integral*, originally introduced by Gibbons and Hawking [32], Maldacena and Lewkowycz in 2013 derived a formula for the *generalized fine-grained entropy in gravitational systems* [33, 34]:

$$S_{FG} = \min_{I} \left\{ \underset{I}{\mathbf{ext}} \left[\frac{A[I]}{4G} + S_{semi-cl} \left(\Sigma_I \cup \Sigma_{rad} \right) \right] \right\}. \tag{1.6}$$

In this work, they introduced the concept of **islands** Σ_I and their boundary I, which appears in the formula via the Ryu–Takayanagi area term. In addition, they included the semiclassical fine-grained entropy of the combined region made up of the island Σ_I and the Hawking-radiation region Σ_{rad}.

The key insight is that, contrary to the earlier assumption that only a single saddle—the Hawking saddle—contributes, the gravitational path integral actually has two saddle points. Using the replica-wormholes construction, a second saddle point, the replica-wormhole saddle, was identified. The Hawking saddle yields a contribution to the fine-grained entropy that grows indefinitely, whereas the replica-wormhole saddle gives a contribution that decreases monotonically. Taking the minimum of these two competing contributions, the formula (1.6) reproduces the Page curve correctly. Since the replica-wormhole construction arises simply as an implementation of the replica trick in theories with dynamical gravity, it is expected that the island rule should apply to essentially any type of black hole.

In the years that followed, many works appeared that refined this formula into its now-standard form [35, 36, 37]. The main issue was whether it genuinely reproduces the Page curve in explicit models. This was ultimately demonstrated first in JT gravity in 2019 [35, 38, 39], and subsequently in the RST/BPP model in 2021 [40, 41] and the DREH model between 2022 and 2025 [42, 43]. Building on this foundational derivation of the Page curve, it has since been obtained in a broad class of two-dimensional dilaton gravity theories [44, 45, 46, 47, 48, 49, 50, 51, 52, 53, 54, 55, 56, 57, 58, 59], as well as in several higher-dimensional constructions [60, 61, 62, 63, 64]. Additional noteworthy investigations of entanglement entropy in gravitational settings include [65, 66, 67, 68, 69]. At face value, these results may suggest that the information paradox has been resolved. Nonetheless, important issues remain open, such as the detailed quantum state of Hawking radiation, the reconstruction of the relevant causal diamond [70, 71, 72], and related questions.

1.1.1 Chern-Simons theory of gravity

Another major line of research that emerged over the last century is Chern–Simons theory. What started as a purely mathematical construction for analyzing topological invariants of manifolds—especially the Pontryagin characteristic classes—has become a central pillar of contemporary theoretical physics. It is applied not only in gravitational and topological quantum field theory contexts, but also in condensed matter physics to characterize topological phases of matter, such as those appearing in the fractional quantum Hall effect. The theory was first introduced by mathematicians Shiing-Shen Chern and James Simons in their seminal 1974 paper [73]. In this work, they identified a boundary term that cannot be defined globally by a gauge-invariant tensor, yet whose integral over a closed odd-dimensional manifold yields a topological invariant.

The first appearance of Chern-Simons theory in physics occurred when researchers recognized that this mathematical construct exhibits distinctive physical features, largely because its action does not depend on the metric and is therefore topologically invariant. In 1982, Stanley Deser, Roman Jackiw, and Stephen Templeton brought the Chern-Simons term into the realm of physics [74]. They demonstrated that incorporating this term into the Einstein–Hilbert or Maxwell actions in $(2+1)$ dimensions generates a mass for the graviton or photon without violating gauge invariance—a mechanism now known as Topologically Massive Gravity or Topologically Massive Electromagnetism. In 1989, Edward Witten transformed the subject by proving that Chern-Simons theory defines a Topological Quantum Field Theory (TQFT) [75]. He famously employed it to formulate a quantum field theoretic description of the Jones polynomial, a knot invariant in mathematics. This achievement forged a deep link between physics and topology and played a key role in Witten's award of the Fields Medal.

The first concrete application to general relativity appeared in 1988. In $(2+1)$ dimensions, general relativity becomes strikingly simple: it lacks local propagating degrees of freedom and thus realizes a TQFT. Achúcarro and Townsend [76], followed by Witten [77], showed that ordinary three-dimensional general relativity is mathematically equivalent to a pure Chern-Simons gauge theory. This was the first explicit realization of gravity as a pure gauge theory. Building on this, in 1992 Bañados, Teitelboim, and Zanelli found that 3D gravity with a negative cosmological constant admits black hole solutions [78]. Since the bulk theory is purely topological (Chern-Simons), the degrees of freedom accounting for the black hole entropy are entirely localized on the boundary. This represented a major conceptual advance and anticipated the holographic principle.

In the early 1990s, Ali Chamseddine and collaborators formulated Chern-Simons gravity and supergravity in arbitrary odd dimensions [79], exploiting the fact that the CS form exists only in odd-dimensional spacetimes. In contrast to standard Einstein gravity, higher-dimensional Chern-Simons theories for gravity include higher powers of the curvature, yet they uniquely evade the occurrence of pathological "ghosts" (negative-energy modes) that usually plague higher-derivative models. In 1996, Strominger and Vafa demonstrated that string theory can account for the microscopic origin of Bekenstein–Hawking entropy by employing the five-dimensional Chern-Simons term in minimal 5D supergravity and, in this way, successfully counted the microstates of five-dimensional black holes [80].

A key feature of the five-dimensional Chern-Simons theory of gravity is that, although the action has no explicit dependence on torsion, torsion does not vanish on shell, unlike in standard four-dimensional General Relativity. Consequently, one must adopt the Riemann–Cartan geometric framework to correctly analyze solutions with nonzero torsion [81]. More generally, in any spacetime dimension there exists a class of Lagrangians—known as *Lovelock Lagrangians* [82]—that contain higher-order curvature terms while preserving properties analogous to those of ordinary General Relativity. A thorough and foundational exposition of the geometric formulation of Chern-Simons gravity in all odd dimensions is provided by Zanelli in his 2012 work [83], which details the gauge-theoretic construction, the structure of local degrees of freedom, and the way in which one passes from standard General Relativity to these Lovelock-type gravitational theories.

In studying the thermodynamics of any gravitational theory, boundary terms play a crucial rule. The asymptotic symmetries of AdS_3 spacetime were first analyzed by Brown and Henneaux in their 1986 work [84]. A systematic treatment of boundary terms in Chern–Simons theories in odd dimensions was later developed by Mišković and Olea in [85]. Their paper introduces an elegant framework for handling boundary conditions, counterterms, and the regularized evaluation of Noether charges, which is further extended in [86].

The thermodynamics of three-dimensional Chern–Simons gravity with torsion has been explored in [87, 88]. In [87], the authors present a thorough study of three-dimensional black holes in Einstein–Maxwell theory endowed with both gravitational and electromagnetic

Chern–Simons terms. They construct intrinsically rotating, geodesically complete solutions and confirm that their mass, angular momentum, and entropy obey the first law of black hole thermodynamics. In contrast, [88] derives generalized asymptotic configurations for 3D Maxwell Chern–Simons gravity and proposes a new extension that introduces torsion through a deformed Maxwell algebra. They show that, whereas the torsionless sector leads to flat cosmological spacetimes, the torsional sector gives rise to BTZ-like geometries in which the entropy depends not only on the horizon area but also on additional spin-2 fields integrated over the horizon. Finally, in five dimensions, one finds a well-defined BTZ-type black hole with torsion, whose thermodynamics, when coupled to an $SU(2)$ soliton, is analyzed in the recent work [89].

1.2 Motivation

The Einstein–Hilbert action and its black hole predictions form the foundation of contemporary gravitational theory. Over the decades, numerous experiments have been carried out with the aim of testing Einstein's theory of gravity [2], and all have confirmed its validity. The first key success was the explanation of the anomalous precession of Mercury's orbit around the Sun, where the general relativistic correction matches observations with remarkable precision. This was followed by the confirmation of gravitational lensing, in which a single source (typically a galaxy) appears in two distinct directions in the sky as seen from Earth. This effect arises because light is deflected when it passes near a massive body such as a black hole, exactly as predicted by general relativity. The most recent observational breakthroughs provide especially compelling evidence for Einstein's theory: the first ever image of a black hole [90] and the observation of gravitational waves [91].

Another central feature of general relativity is the set of cosmological solutions it admits, many of which describe our universe quite accurately. In this domain, there is an even larger body of experimental data, most notably the observations of the cosmic microwave background (CMB) radiation. Yet general relativity by itself does not account for the small temperature fluctuations observed in the CMB. These are generally viewed as phenomena that require a complete theory of quantum gravity. Consequently, researchers turn to semiclassical methods—where quantum fields are defined on a curved spacetime background—to explain these features, and such approaches have achieved partial success.

The same technique is employed to account for the thermal character of black holes. Consequently, they must emit radiation and lose energy—an effect that cannot be understood without invoking quantum field theory in curved spacetime. Although this phenomenon has not yet been confirmed experimentally, because the predicted temperature of a black hole is on the same order of magnitude as the CMB temperature, it is regarded as an unavoidable aspect of black hole physics. Therefore, it deserves deeper study.

This leads to crucial questions, such as: Do black holes—and by extension, general relativity—respect the principles of quantum mechanics? In particular: Is black hole radiation governed by a unitary time evolution? Furthermore, this issue should be investigated in more intricate settings as well, including cosmological solutions of Einstein's equations.

The island formula (1.6), obtained from the gravitational path integral, offers a framework that reproduces the Page curve and thereby suggests that the underlying evolution is unitary. Nonetheless, this does not yet guarantee that the Hawking radiation itself evolves unitarily, since the Page curve only captures the correct time dependence of the fine-grained entropy. Several questions remain unresolved. For instance: Is it possible, in principle, to reconstruct the full information about the initially infalling matter solely from measurements performed on the Hawking radiation?

At present, the explicit form of the island formula is well understood only in two spatial dimensions. Consequently, the Page curve has been computed primarily in a limited set of "toy models" based on two-dimensional dilaton gravity, and often in the unphysical context of an eternal black hole, which describes a black hole in thermal equilibrium with its surroundings. In this work, we succeed in reproducing the Page curve within a physically relevant DREH model, derived from experimentally tested Einstein's general relativity. Moreover, we achieve this for both the eternal black hole case and the fully evaporating black hole scenario.

The importance of torsion

The second line of research in this dissertation focuses on the dimensionally reduced five-dimensional Chern–Simons theory. Although this is not a physical theory, the first giveaway being that it is defined in five spacetime dimensions it nevertheless admits black hole solutions with non-vanishing torsion. In contrast, general relativity is intrinsically torsion-free, as it is formulated on a Riemannian manifold. However, such manifolds do not exhaust all geometries that can arise from the fundamental postulates of general relativity. In particular, the equivalence principle can be viewed as implying that gravity results from the localization of the Poincaré symmetry. When the Poincaré group is localized in this way, the most general resulting manifold is a Riemann–Cartan manifold, which allows for non-zero torsion.

The presence of torsion has not yet been confirmed experimentally, but we still cannot definitively claim that spacetime is torsion-free. In many theoretical frameworks, torsion is intimately connected to the nontrivial interaction between Dirac fermions and gravity, for example in configurations such as fermionic soliton star solutions. The canonical case is the Einstein–Cartan theory, which extends general relativity to a Riemann–Cartan spacetime. In fact, when fermions are absent in this theory, the resulting equations of motion reduce to Einstein's field equations, which enforce vanishing torsion.

The central question to be addressed is: How does non-vanishing torsion affect the fine-grained entropy of gravitational systems such as black holes? Since this problem is too broad, a more precise first step is to ask: How should the island formula (1.6) be modified to incorporate the effects of torsion? At the time of writing this dissertation, this remains unresolved. Even the correct torsion-inclusive generalization of the Ryu–Takayanagi formula is not yet known. In this context, five-dimensional Chern–Simons theory provides an excellent testing ground for exploring torsion, as it admits a BTZ-like black hole solution with torsion. From the viewpoint of the island formula, however, it is natural to dimensionally reduce the full five-dimensional Chern–Simons theory to two dimensions and consequently recast it as a two-dimensional dilaton gravity theory that includes both torsion fields inherited from higher dimensions and torsion intrinsic to two dimensions.

The initial task in pursuing these questions is to obtain solutions with torsion in two-dimensional dilaton gravity. This is the specific goal of this dissertation within this broader research program. Having achieved this paves the way for the next step: trying to modify the Ryu–Takayanagi formula so that torsion is properly taken into account. Ultimately, once the correct torsion-inclusive formula is established, it should be applied to compute the Page curve in the dimensionally reduced, experimentally tested Einstein–Cartan theory of gravity.

1.3 Key results

This dissertation pursues two separate directions within the framework of two-dimensional dilaton gravity. The first focuses on analyzing the fine-grained entropy of gravitational systems, while the second explores a dimensionally-reduced model of five-dimensional Chern-Simons theory, with the ultimate aim of understanding how non-zero torsion influences the fine-grained entropy in such systems. We begin by outlining the central method used to compute the various solutions developed in this thesis.

The first key result is the construction of the symmetric ansatz in Sec. 3.1, designed to describe 2D spacetimes that admit at least one Killing vector. This ansatz provides a straightforward route to obtain the equations of motion for any static configuration in 2D dilaton gravity, including classical vacuum solutions, asymptotically flat Minkowski-like vacua, and eternal black hole scenarios. Every such solution is characterized by $(\mathrm{F}^+, \mathrm{F}^-, C, f)$, where $\mathrm{F}^\pm$ encode the coordinate transformations from an arbitrary coordinate system to the Eddington-Finkelstein coordinates associated with the chosen Killing vector, and C denotes a set of integration constants (or charges) that specify the particular solution. The quantity f represents a collection of arbitrary functions that typically emerge from residual gauge freedoms in the higher-dimensional parent theory from which the 2D dilaton gravity model is obtained.

The same ansatz can be employed to formulate the classical collapse scenario, as discussed in Sec. 3.4, where infalling matter propagates along a null hypersurface. In this framework, the spacetime on each side of the null hypersurface must be given by one of the static vacuum solutions. By requiring a continuous matching of these vacuum regions across the infalling matter hypersurface, one relates the parameters of the two solutions. Specifically, the presence of falling matter induces a discontinuity in F^- and in charges C, while the other coordinate transformation remains unchanged. In most situations, these junction conditions fully fix the remaining gage freedom and thereby determine any arbitrary functions that may appear in the general vacuum solutions.

Another important aspect of this matching procedure is that it allows one to obtain a formal expression for the mass of the spacetime in terms of its parameters, providing an alternative route to determine the thermodynamic properties of the theory.

However, in many cases, these equations of motion cannot be solved exactly. In such situations, one employs a perturbative expansion in the natural parameter $\hbar$ and determines the equations of motion only up to the first order in $\hbar$. This allows the ansatz to be applied to obtain the evaporating black hole solution as well. Because the EMT associated with quantum corrections is of order $\hbar$, one first uses the zeroth-order static solutions to evaluate the EMT and only then integrates the equations of motion. The solutions in the regions of spacetime separated by the infalling-matter hypersurface are then characterized by $(\mathrm{F}^+, \mathrm{F}^-, C, t_+(\sigma^+), t_-(\sigma^-))$, where the additional functions $t_\pm(\sigma^\pm)$ encode the specific quantum state of the fields. After enforcing the continuous matching of the two solutions across the dividing hypersurface, the coordinate transformation F^- and constants C receive additional quantum corrections, leading to a quantum-corrected collapse scenario. This procedure is described in full detail in Sec. 3.4.1.

We employ this method to obtain both the eternal and evaporating black hole solutions in the DREH model, as presented in Secs. 5.2.3 and 5.3, respectively. An analogous procedure is applied in the Riemannian sector of the DR5DCS model, where the corresponding solutions are constructed in Secs. 6.2.3 and 6.3, respectively. One might anticipate difficulties near the endpoint of evaporation, since the standard non-perturbative solutions in the BPP and RST models exhibit non-analytic behavior in this region of spacetime. Our method, however, captures precisely this non-analyticity and correctly reproduces the energy balance, the thunderpop, and the end-state geometry in each model.

The central findings of this research program are summarized in Chap. 10, where we successfully obtain the Page curve for the DREH model in both the eternal and evaporating black hole scenarios. The perturbative analysis reproduces the expected behavior of the Page curve, determines the Page time, and thereby establishes the unitary time evolution of the fine-grained entropy in the DREH model.

The central result of the second line of research is derived in Sec. 2.3, where the complete 5DCS theory is dimensionally reduced to two dimensions over the 3-sphere, yielding the following action:

$$\begin{aligned} S_{\mathrm{DRCS}_5} =& \frac{k\pi^2}{(\lambda l)^3}\int \mathrm{d}^2x\sqrt{-g}e^{-3\phi}\Bigg\{\left(1+\frac{3}{\mathrm{x}^2}\left(1-\Phi^2-\theta^2\right)\right)\left[\mathrm{R}+2\varepsilon^{\alpha\beta}\partial_\alpha \mathrm{K}_\beta+\frac{2}{l^2}\right] \\ &+\frac{4}{l^2}+\frac{6}{l\mathrm{x}^3}\theta^2\nabla_\alpha\phi^\alpha+\frac{6}{l\mathrm{x}}\left(1+\frac{1}{\mathrm{x}^2}\left(1-\Phi^2-\theta^2\right)\right)\left[\nabla_\alpha\phi^\alpha-\varepsilon^{\alpha\beta}\phi_\alpha \mathrm{K}_\beta\right] \\ &-\frac{6}{\mathrm{x}^2}\left[\nabla_\alpha\phi^\beta\nabla_\beta\phi^\alpha-\nabla_\alpha\phi^\alpha\nabla_\beta\phi^\beta-\varepsilon^{\alpha\beta}\mathrm{K}_\alpha\nabla_\beta\Phi^2\right]\Bigg\}+S_{\mathrm{mat}}, \end{aligned} \tag{1.7}$$

In this manner, a two-dimensional dilaton gravity theory with torsion is obtained. Its properties are examined in detail in Chap. 7. There, it is shown that the general vacuum geometry is inherited from the original 5DCS theory and corresponds to a BTZ black hole with a non-vanishing five-dimensional torsion field, which manifests in the 2D theory as a scalar field θ. This field θ effectively serves as a Lagrange multiplier, imposing a constraint that substantially restricts the phase space of admissible solutions. In Sec. 7.2.1, we adopt the symmetric ansatz and exploit this constraint to explicitly determine all additional fields originating from the dimensional reduction and the two-dimensional torsion as well, in the presence of two-dimensional matter. We demonstrate that, as long as $\theta \neq 0$, the 2D torsion is necessarily non-vanishing as well.

In Sec. 7.3 we solve the ensuing equations of motion in the presence of matter that is minimally coupled to gravity. We consider several types of matter fields. The most compelling solutions are found when a Dirac spinor field is minimally-coupled to both gravity and torsion. In that setting, we demonstrate that the system supports a fermionic soliton star configuration with a clearly defined phase transition mechanism. The transition is governed by two parameters, μ and P. For $\left|\frac{\mu}{P}\right| > \frac{\pi}{4}$, the solution corresponds to a completely regular spacetime, free of horizons and singularities. Once this critical threshold is crossed, however, the fermions condense at a particular spacetime location where the fermion density $\bar{\psi}\psi$ diverges. This divergence in density produces a curvature singularity and a horizon precisely at that location. The associated horizon has non-vanishing surface gravity, so the resulting configuration is non-extremal. We anticipate that including quantum corrections will remove, or "smooth out," this singularity.

Beyond the fermionic star configuration, we uncover a wide variety of additional solutions. In most situations, coupling to scalar fields, with or without electromagnetism, leads to cosmological solutions. These are typically singular and often describe spacetimes oscillating between a big bang and a big crunch events. In some cases, additional singularities arise in between them, occurring at spacetime locations where the scale factor remains finite. Singularities of this kind are referred to as sudden singularities and have been thoroughly studied in the literature [92, 93]. In addition, we demonstrate that once the Polyakov–Liouville quantum corrections are taken into account, the geometry develops a structure analogous to that of the

Reissner–Nordström or rotating BTZ black hole solutions, featuring two singular horizons that shield a singularity lying beyond them.

The main results of the second research program are discussed in Chap. 11, where we analyze the fine-grained entropy in the DR5DCS framework. There, we explicitly obtain the Page curve for an eternal black hole in the Riemannian sector of the theory. Furthermore, we derive several noteworthy results concerning how torsion influences the Page curve by computing the fine-grained entropy of a quantum-corrected eternal black hole solution featuring two singular horizons. This computation is carried out using the standard island rule, with the Wald entropy serving the role of the area term. Our analysis indicates that torsion imposes stringent constraints on the placement of the cut-off hypersurface that defines the boundary of the black hole region. Nevertheless, these findings should be interpreted cautiously, since they are somewhat conjectural: it is currently unclear whether the usual island rule remains valid in theories with non-zero torsion.

1.4 Organization

The dissertation is divided into two main parts. The first part, comprising Chaps. 2-7, focuses on two-dimensional dilaton gravity. Various models are presented, their equations of motion are solved, and quantum corrections are incorporated, leading to both eternal and evaporating black hole solutions. The second part, consisting of Chaps. 8-11, is devoted to the study of fine-grained entropy in the framework of 2D dilaton gravity, where the Page curve is recovered for several different models. The final chapter provides concluding remarks.

In Chap. 2 we present the framework of dimensional reduction. This framework is central to the thesis, since all theories under consideration are obtained from higher-dimensional ones by dimensional reduction. We begin by formulating a dimensional reduction on a general Riemannian manifold with a well-defined topology. Using this setup, we then derive the action for a theory reduced over an n-sphere manifold, and subsequently apply it explicitly to reduce the five-dimensional Chern-Simons (5DCS) theory and the four-dimensional Einstein-Hilbert action to two-dimensional dilaton gravity over $\mathbb{S}^3$ and $\mathbb{S}^2$, respectively. In the final section, we carry out the dimensional reduction of the full 5DCS theory to a two-dimensional dilaton gravity with torsion over $\mathbb{S}^3$ by employing the most general spherically symmetric ansatz for both the vielbein and the spin-connection.

Chap. 3 is devoted to the general structure of two-dimensional dilaton gravity. We first introduce the most general symmetric ansatz for a two-dimensional spacetime that admits at least one Killing vector. The ansatz for scalar, spinor, vector, and tensor fields is constructed, as well as for the metric and the dilaton. We then derive the most general covariant conservation laws in 2D dilaton gravity when non-minimal couplings to curvature and torsion are included. Next, we incorporate quantum corrections through the Polyakov–Liouville action and study the transformation properties of the resulting quantum energy-momentum tensor (EMT). The concluding section of this chapter develops the framework for both classical and quantum-corrected gravitational collapse, with particular emphasis on a perturbative expansion in $\hbar$ in the quantum-corrected case.

In Chap. 4 we present an in-depth review of the CGHS model of 2D dilaton gravity, treated as a fundamental toy model for investigating the entropy of Hawking radiation in an asymptotically flat spacetime. We begin by deriving the equations of motion and their general solutions. We then impose a static ansatz setup, solve the resulting static equations of motion, and formulate the classical gravitational collapse scenario. After that, we incorporate Polyakov–Liouville quantum corrections, examine various choices of counterterms that render the quantum-corrected equations exactly solvable, and determine the most general static vacuum solution of these quantum-corrected equations. In the following section, we provide a detailed analysis of the BPP model, which we adopt as our preferred route. We first construct the exact quantum-corrected collapse scenario and then apply the perturbative method developed in Chap. 3 to demonstrate that it leads to consistent results. The chapter concludes with a discussion of the thermodynamic properties of the CGHS model.

Chap. 5 focuses on the dimensionally reduced four-dimensional Einstein–Hilbert action and is organized into three sections. As before, we start by deriving the classical equations of motion and demonstrate that Birkhoff's theorem is inhered through dimensional reduction, in the sense that the most general solution of the vacuum equations of motion is the Schwarzschild black hole spacetime. The second section explains how to incorporate Polyakov–Liouville quantum corrections in this setting, derives the most general quantum-corrected static solutions, and discusses both the asymptotically flat static vacuum configuration and the eternal black hole scenario. The final section systematically introduces evaporating black hole solutions. In this part, we explicitly compute the end point of evaporation, determine the final state of black hole radiation, and show that the end-state geometry is the quantum-corrected Minkowski vacuum solution.

In Chap. 6 we study the Riemannian sector of the dimensionally reduced five-dimensional Chern-Simons theory (DR5DCS). The organization closely parallels that of the preceding chapter. In the first section, we derive the classical equations of motion together with their most general vacuum solutions, and then construct the classical collapse scenario and the associated Penrose diagram. The following section introduces quantum corrections into this framework. There we obtain the general static solutions to the quantum-corrected equations of motion and formulate the eternal black hole scenario. The final section is dedicated to the evaporating black hole solution. We explicitly determine the end-point of evaporation, the corresponding final state, and the geometry characterizing this end state.

Chap. 7 is devoted to the full dimensionally reduced 5DCS theory with non-vanishing torsion. Because the equations of motion are, in general, extremely challenging to solve, we immediately adopt the symmetric ansatz of Sec. 3.1. Within this framework, we derive the most general symmetric vacuum solution and formulate the classical gravitational collapse. The second section addresses the general solution of the gravitational equations of motion. We manage to express all additional fields arising from dimensional reduction, as well as the two-dimensional contorsion, solely in terms of the metric, the dilaton, and their derivatives, and from this we obtain the resulting equations for the dilaton and the metric in terms of the matter EMT and the contorsion current. We then analyze three distinct cases. First, we consider matter with a completely vanishing contorsion current; in this regime the matter EMT is entirely determined by the metric. Next, we investigate how non-vanishing components of the contorsion current modify the equations of motion. The penultimate section examines the coupling of gravity to various matter field theories. We start with a real scalar field, pure electrodynamics, and spinor field theory, then proceed to scalar electrodynamics, and conclude with ideal fluid hydrodynamics. Finally, in the last section we incorporate Polyakov-Liouville quantum corrections.

We now turn to the second part of the dissertation. Chap. 8 is devoted to various notions of entropy in gravitational systems. It is divided into four sections. In the first section, we highlight the distinction between coarse-grained and fine-grained entropy, and clarify what is meant by the fine-grained entropy of quantum fields in a gravitational background. We stress that the crucial ingredient in defining entanglement entropy is the spacetime region in which the degrees of freedom inaccessible to a static observer reside.

The second section focuses on the Von Neumann entropy in gravity. We begin by computing the Von Neumann entropy for a Rindler observer and derive the Unruh effect. In subsequent subsections, we examine how changing the inaccessible region affects the fine-grained entropy and extend the resulting formulas to curved spacetimes, both with and without reflective boundaries. The next subsection analyzes how the entropy depends on the choice of quantum state of the matter fields. This section concludes with a definition of the Hawking information paradox.

The final section reviews the recent Maldacena–Lewkowycz prescription for evaluating fine-grained entropy in gravitational systems, following [1]. We begin by presenting the central dogma, which states that a black hole can be treated as an ordinary quantum system up to a certain cutoff hypersurface, and then proceed to discuss the reconstruction of the Page curve, the replica wormhole method, and the problem of entanglement wedge reconstruction.

In Chap. 9 we revisit the derivation of the Page curve in the BPP model. We begin by computing the Page curve for an eternal black hole and subsequently analyze the evaporating black hole case. For both setups, we first examine the no-island configuration, in which one recovers the standard Hawking result, and then demonstrate explicitly how incorporating the island correctly yields the Page curve. At the end of this chapter, we address the reliability of the Page curve calculation and offer a comment on the Page time.

Chap. 10 is devoted to the central result of this dissertation, namely the Page curve in the DREH model. It is organized into three sections. In the first section, we derive the Page curve for an eternal black hole, analyze the island and no-island configurations, and comment on their connection to Wald entropy. The second section focuses on the Page curve in a classical collapse setup, where we show that the resulting Page curve exhibits the same asymptotic behavior as in the eternal black hole case, as expected in the absence of quantum back-reaction on the classical geometry. The final section recovers the Page curve for an evaporating black hole, with particular emphasis on distinguishing between the island and no-island configurations.

In the final Chap. 11 of the second part of the dissertation, we study the Page curve in the context of the DR5DCS theory. We begin by introducing a coupling of the black hole spacetime to a thermal bath region, which is required whenever the spacetime is asymptotically AdS-like. The following section evaluates the coarse-grained entropy in this model by using the Wald entropy formula. We then reproduce the Page curve for an eternal black hole in this framework, examining both island and no-island configurations, as usual. In the final section, we explore how to compute the Page curve when the spacetime exhibits non-vanishing torsion, again employing the Wald entropy formula as the area term in the island rule.

The main text is supplemented by four appendices. App. A introduces the Riemann-Cartan geometry and the spinor conventions employed throughout this dissertation. App. B provides further technical details on the polynomials that appear in the evaporating black hole solution of the DREH model discussed in Sec. 5.3. In App. C we present a brief review of the standard four-dimensional Schwarzschild solution. The final App. D is devoted to quantum field theory in curved spacetime, with particular focus on the scalar field. We begin by discussing canonical quantization in curved spacetime, Bogoliubov transformations, and the Unruh effect. The fourth section highlights the role of event and Killing horizons within the black hole spacetimes, while the fifth section derives the Kruskal coordinates and the surface gravity by imposing regularity of the metric at the horizon. In the last section, we examine the Hawking effect and Hawking radiation.

Chapter 2

Dimensional reduction

Higher-dimensional gravitational theories are generally difficult to solve. To address this, one often attempts to simplify the problem by reducing the number of dimensions. There exist many consistent methods to carry out such a dimensional reduction. The original historical proposal, due to Kaluza and Klein [94, 95], suggested introducing a fifth coordinate in order to unify Einstein's general relativity with Maxwell's electromagnetism. To account for the fact that we do not observe this fifth coordinate, they assumed it is compactified on a tiny circle with a radius so small that it cannot be detected. Although this framework did not yield the correct value for the electron mass-to-charge ratio, it nonetheless remains a foundational idea in modern string theory, where the compactification is done over small complex Calabi–Yau manifolds, thereby reducing higher-dimensional string theories to an effective four-dimensional theory.

In this chapter, we present an alternative approach to dimensional reduction. The idea is to impose a symmetric ansatz such that the resulting metric has the required topology, and then integrate out the redundant coordinates. In this way, any solution of the original theory that possesses the specified topology and symmetries automatically becomes a solution of the dimensionally reduced theory. Since it is considerably easier to study the thermodynamic properties in the lower-dimensional framework, this method is particularly valuable, as it ensures that the desired solutions are indeed captured by the reduced theory.

The chapter is divided into three sections. In Sec. 2.1, we present a general method for performing this type of dimensional reduction on a Riemannian manifold. In the following Sec. 2.2, we carry out the dimensional reduction over the n-sphere and, as illustrative examples, consider the Einstein–Hilbert action and the Riemannian sector of five-dimensional Chern–Simons theory. In the final Sec. 2.3, we perform a dimensional reduction of the complete five-dimensional Chern–Simons theory of gravity, which exhibits a black hole solution with torsion, which is of great importance for the study of fine-grained entanglement entropy in gravitational systems with torsion.

2.1 Dimensional reduction of Riemannian manifold

Here we introduce an alternative symmetry-based approach to dimensional reduction of a Riemannian manifold. We begin with an N-dimensional manifold that can be decomposed in $K+1$ disjunctive sub-manifolds $\mathcal{M}_N = \mathcal{M}_n \times \mathcal{M}_{d_1} \times \mathcal{M}_{d_2} \times \cdots \times \mathcal{M}_{d_K}$, each characterized by its own dimension d_a, topology and symmetry properties. The component $\mathcal{M}_n$ represents the final

n-dimensional manifold that remains after the reduction process. The metric on each submanifold is written as $\mathrm{d}s_a^2 = \gamma^{(a)}_{i_a j_a}\mathrm{d}x^{i_a}\mathrm{d}x^{j_a}$. Accordingly, for the metric on the original manifold we adopt the following ansatz:

$$\mathrm{d}s^2 \equiv G_{AB}\mathrm{d}X^A\mathrm{d}X^B = g_{\mu\nu}\mathrm{d}x^\mu\mathrm{d}x^\nu + \sum_{a=1}^{K}\frac{1}{\lambda_a^2}e^{-2\phi_a}\gamma^{(a)}_{i_a j_a}\mathrm{d}x^{i_a}\mathrm{d}x^{j_a}, \tag{2.1}$$

where we have introduced K dilaton fields ϕ_a and dimensional constants λ_a associated with the corresponding submanifolds. We emphasize that the symmetry requirement is that the dilaton fields depend solely on the coordinates of the final manifold, namely $\phi_a = \phi_a(x^\mu)$. We denote the coordinates collectively as $X^A \in \{x^\mu, x^{i_1}, x^{i_2}, ..., x^{i_K}\}$, where Latin indices label the submanifolds and Greek indices are reserved for the final manifold.

The action of the higher-dimensional Riemannian gravity theory may depend only on the curvature invariants, namely:

$$S = \int_{\mathcal{M}_N}\mathrm{d}^N X\sqrt{-G}\mathcal{L}\left(\mathcal{R}, \mathcal{R}_{AB}\mathcal{R}^{AB}, \mathcal{R}_{ABCD}\mathcal{R}^{ABCD}\right). \tag{2.2}$$

Hence, we evaluate these invariants using the ansatz (2.1). In addition to $\Gamma^\rho_{\mu\nu}$ for the resulting manifold and $\Gamma^{k_a}_{i_a j_a}$ for each submanifold over which the dimensional reduction is carried out, the remaining non-vanishing Christoffel symbols are:

$$\begin{aligned}\Gamma^\mu_{i_a j a} &= \frac{1}{\lambda_a^2}e^{-2\phi_a}\gamma^{(a)}_{i_a j_a}\nabla^\mu\phi_a, && \forall a \in \{1, 2, ..., K\},\\ \Gamma^{j_a}_{i_a\mu} &= -\delta^{j_a}_{i_a}\nabla_\mu\phi_a, && \forall a \in \{1, 2, ..., K\}.\end{aligned} \tag{2.3}$$

The next step is to compute the Riemannian curvature tensor of the initial manifold using Christoffel symbols (2.3) and ansatz (2.1). For non-zero components of the Riemannian tensor, we get:

$$\begin{aligned}\mathcal{R}^\mu{}_{i_a\nu j_a} &= \frac{1}{\lambda_a^2}e^{-2\phi_a}\gamma^{(a)}_{i_a j_a}\Big(\nabla^\mu\nabla_\nu\phi_a - \nabla^\mu\phi_a\nabla_\nu\phi_a\Big),\\ \mathcal{R}^{i_a}{}_{\mu j_a\nu} &= \delta^{i_a}_{\ j_a}\Big(\nabla_\mu\nabla_\nu\phi_a - \nabla_\mu\phi_a\nabla_\nu\phi_a\Big),\\ \mathcal{R}^{i_a}{}_{j_a k_a l_a} &= R^{(a)i_a}{}_{j_a k_a l_a} + \frac{1}{\lambda_a^2}e^{-2\phi_a}\left(\nabla\phi_a\right)^2\Big(\delta^{i_a}_{\ l_a}\gamma^{(a)}_{j_a k_a} - \delta^{i_a}_{\ k_a}\gamma^{(a)}_{j_a l_a}\Big),\\ \mathcal{R}^{i_a}{}_{i_b j_a j_b} &= -\delta^{i_a}_{\ j_a}\frac{1}{\lambda_b^2}e^{-2\phi_b}\gamma^{(b)}_{i_b j_b}\nabla_\mu\phi_a\nabla^\mu\phi_b,\\ \mathcal{R}^\mu{}_{\nu\rho\sigma} &= R^\mu{}_{\nu\rho\sigma},\end{aligned} \tag{2.4}$$

where $R^\mu{}_{\nu\rho\sigma}$ and $R^{i_a}{}_{j_a k_a l_a}$ are the Riemannian curvature tensors of the final manifold and the a-th submanifold, respectively. The Ricci tensor is defined by $\mathcal{R}_{AB} = \mathcal{R}^D{}_{ADB}$, and is given by:

$$\begin{aligned}\mathcal{R}_{\mu\nu} &= R_{\mu\nu} + \sum_{a=1}^{K} d_a\Big(\nabla_\mu\nabla_\nu\phi_a - \nabla_\mu\phi_a\nabla_\nu\phi_a\Big),\\ \mathcal{R}_{i_a j_a} &= R^{(a)}_{i_a j_a} + \frac{1}{\lambda_a^2}e^{-2\phi_a}\gamma^{(a)}_{i_a j_a}\Big(\Box\phi_a - \nabla_\mu\phi_a\nabla^\mu\phi\Big),\end{aligned} \tag{2.5}$$

where $R_{\mu\nu}$ and $R_{i_a j_a}$ are the Ricci tensors of the final manifold and the a-th submanifold, respectively. In addition, we introduce $\phi \equiv \sum_{a=1}^{K} d_a\phi_a$. The first curvature invariant, the scalar curvature, is directly computed from Eq. (2.5):

$$\mathcal{R} = R + (\nabla\phi)^2 - 2e^{\phi}\Box e^{-\phi} + \sum_{a=1}^{K}\left(\lambda_a^2 R^{(a)} e^{2\phi_a} - d_a\left(\nabla\phi_a\right)^2\right), \tag{2.6}$$

where R and $R^{(a)}$ denote the scalar curvatures associated with their respective manifolds. Finally, we evaluate the quadratic curvature terms. The Ricci squared is as follows:

$$\begin{aligned}\mathcal{R}^{AB}\mathcal{R}_{AB} = R_{\mu\nu}R^{\mu\nu} + &+ \sum_{a=1}^{K}\lambda_a^4 e^{4\phi_a} R^{(a)}_{i_a j_a} R^{i_a j_a}_{(a)} + \sum_{a,b=1}^{K} d_a d_b e^{\phi_a+\phi_b}\nabla_\mu\nabla_\nu e^{-\phi_a}\nabla^\mu\nabla^\nu e^{-\phi_b} \\ &+ 2R^{\mu\nu}\sum_{a=1}^{K} d_a\left(\nabla_\mu\nabla_\nu\phi_a - \nabla_\mu\phi_a\nabla_\nu\phi_a\right) + 2\sum_{a=1}^{K}\lambda_a^2 e^{2\phi_a}R^{(a)}\left(\Box\phi_a - \nabla_\mu\phi_a\nabla^\mu\phi\right) \\ &+ \sum_{a=1}^{K} d_a\left(\Box\phi_a - \nabla_\mu\phi_a\nabla^\mu\phi\right)^2,\end{aligned} \tag{2.7}$$

while the Kreshman scalar is given by:

$$\begin{aligned}\mathcal{R}_{ABCD}\mathcal{R}^{ABCD} = R_{\mu\nu\rho\sigma}R^{\mu\nu\rho\sigma} &+ 4\sum_{a=1}^{K} d_a e^{2\phi_a}\nabla_\mu\nabla_\nu e^{-\phi_a}\nabla^\mu\nabla^\nu e^{-\phi_a} + 4\sum_{1\leqslant a<b\leqslant K} d_a d_b\left(\nabla_\mu\phi_a\nabla^\mu\phi_b\right)^2 \\ &+ \sum_{a=1}^{K}\left[\lambda_a^4 e^{4\phi_a} R^{(a)}_{i_a j_a k_a l_a} R^{i_a j_a k_a l_a}_{(a)} - 4\lambda_a^2 e^{2\phi_a}R^{(a)}(\nabla\phi_a)^2 + 2d_a(d_a-1)(\nabla\phi_a)^4\right].\end{aligned} \tag{2.8}$$

We can see that the resulting action is at most fourth order in derivatives of the dilaton fields.

All of these invariants depend on the corresponding invariants of the submanifold on which the reduction is carried out. These are the only terms that explicitly depend on the submanifold coordinates. Substituting Eqs. (2.6-2.8) into the gravitational action (2.2) and then integrating over the submanifold coordinates yields an action defined on the final manifold. If one or more of the submanifolds is non-compact, divergences can arise when attempting to integrate out the submanifold coordinates. In such cases, an appropriate regularization procedure must be employed to tame those divergences. In most cases the invariants appear in specific combination known as Gauss-Bonnet term [96], firstly introduced in Lovelock gravity [97], and later refined as main ingredient in Gauss-Bonnet gravity:

$$GB = \mathcal{R}^2 - 4\mathcal{R}^{\mu\nu}\mathcal{R}_{\mu\nu} + \mathcal{R}^{\mu\nu\rho\sigma}\mathcal{R}_{\mu\nu\rho\sigma}. \tag{2.9}$$

This term becomes relevant only in theories with more than five dimensions. In two- and three-dimensional theories it is exactly equal to zero; while in four dimensions it appears as a topological term, proportional to the Euler characteristic of the manifold. It arises in topological gravity theories, most notably in five-dimensional Chern–Simons theory.

Finally, we need to substitute the ansatz (2.1) in order to rewrite $\sqrt{-G}$ from Eq. (2.2) in terms of the dilaton fields. Because the metric ansatz is block diagonal, its determinant factorizes into a product of $\sqrt{-g}$ contributions, one from each submanifold:

$$\sqrt{-G} \equiv \sqrt{-g}\prod_{a=1}^{K}\sqrt{|\gamma_a|}\left(\frac{1}{\lambda_a}e^{-\phi_a}\right)^{d_a} = \sqrt{-g}e^{-\phi}\prod_{a=1}^{K}\frac{\sqrt{|\gamma_a|}}{\lambda_a^{d_a}}. \tag{2.10}$$

Consequently, the integration decomposes into K separate integrals over submanifolds, each of which can be computed individually. The corresponding action is then defined on the final submanifold. Note that, from the standpoint of this final action, Lagrangian terms of the form $e^{\phi}\nabla_\mu \xi^\mu$ are total derivatives and can therefore be disregarded when deriving the equations of motion.

2.2 Dimensional reduction over n-sphere

In this section we preform the dimensional reduction of manifold $\mathcal{M} \times \mathbb{S}^n$ over the submanifold $\mathbb{S}^n$. Since the n-sphere is a maximally symmetric space, the curvature invariants are given by:

$$R^{(n)} = n(n-1) \quad \wedge \quad R^{(n)}_{ij} R^{ij}_{(n)} = n(n-1)^2 \quad \wedge \quad R^{(n)}_{ijkl} R^{ijkl}_{(n)} = 2n(n-1). \tag{2.11}$$

Placing this into the scalar curvature yields the following:

$$\mathcal{R} = R + n(n-1)\left[(\nabla\phi)^2 + \lambda^2 e^{2\phi}\right] - 2e^{n\phi}\Box e^{-n\phi}. \tag{2.12}$$

The last term in this expression is a surface term. Consequently, it may be omitted from the action, since it does not contribute to the equations of motion. The remaining invariants can likewise be obtained by straightforward substitution. Instead of presenting the full expressions from this procedure, we only provide the resulting form of the Gauss–Bonnet (2.9) term:

$$\begin{aligned} GB =& n(n-1)(n-2)(n-3)\left(\lambda^4 e^{4\phi} + 2\lambda^2 e^{2\phi}(\nabla\phi)^2 - (\nabla\phi)^4\right) \\ &+ 2n(n-1)\left(\lambda^2 e^{2\phi} R + (n-2)(\nabla\phi)^2\left(\Box\phi - (\nabla\phi)^2\right) - 2e^{n\phi}\nabla_\mu \xi^\mu\right), \end{aligned} \tag{2.13}$$

where the last term in the second row $\propto e^{n\phi}\nabla_\mu\xi^\mu$ represents a total derivative in the action and as such can be disregarded.

2.2.1 Dimensional reduction of 4D Einstein-Hilbert action over $\mathbb{S}^2$

In this section, we consider the dimensional reduction of the Einstein–Hilbert action, commonly referred to as the DREH model. The four-dimensional action is given by:

$$S = \frac{1}{16\pi G_N}\int d^4x \sqrt{-G}\mathcal{R}, \tag{2.14}$$

where G_N is the Newton gravitational constant in four dimensions. Since the reduction is preformed over the $\mathbb{S}^2$, the specific four-dimensional metric is given by:

$$G_{AB} = \left(\begin{array}{c|c} g_{\mu\nu} & 0 \\ \hline 0 & \gamma_{ij} \end{array}\right) \quad \wedge \quad \gamma_{ij} = \frac{1}{\lambda^2}\begin{pmatrix} e^{-2\phi} & 0 \\ 0 & e^{-2\phi}\sin^2\theta \end{pmatrix}. \tag{2.15}$$

where the indices correspond to $i, j \in \{2, 3\}$, while $\mu, \nu \in \{0, 1\}$. Here λ is simply a dimensional parameter. We also assume that $g_{\mu\nu} = g_{\mu\nu}(x^0, x^1)$. In this case, the scalar curvature (2.12) and the Jacobian (2.10) read:

$$\mathcal{R} = R + 2(\nabla\phi)^2 + 2\lambda^2 e^{2\phi} - 2e^{2\phi}\Box e^{-2\phi}. \tag{2.16}$$

$$\mathrm{d}^4X\sqrt{-G} = d^2x \mathrm{d}\theta \mathrm{d}\varphi \frac{1}{\lambda^2}\sqrt{-g}e^{-2\phi}\sin\theta. \tag{2.17}$$

After integrating out the angles and neglecting the surface term, we arrive at the following dimensionally reduced action:

$$S_{red} = \frac{1}{4G_N\lambda^2}\int \mathrm{d}^2x\sqrt{-g}e^{-2\phi}\left[R + 2(\nabla\phi)^2 + 2\lambda^2 e^{2\phi}\right]. \tag{2.18}$$

Let us discuss the dimensionality of the constant appearing in front of the action. Its dimension matches that of the gravitational constant in two dimensions. This correspondence enables us to define the two-dimensional gravitational constant as $G = \lambda^2 G_N$. To construct the complete theory, we must also incorporate matter. We introduce matter in the form of a two-dimensional massless scalar field f. The DREH action then takes the following final form:

$$S_{\mathrm{DREH}} = \frac{1}{4G}\int d^2x\sqrt{-g}e^{-2\phi}\left[R + 2(\nabla\phi)^2 + 2\lambda^2 e^{2\phi}\right] - \frac{1}{2}\int d^2x\sqrt{-g}\,(\nabla f)^2. \tag{2.19}$$

Note that, as a consequence of the dimensional reduction, the reduced action exhibits a cosmological constant term as well. In some cases, matter may instead be introduced as a quantity obtained through dimensional reduction by starting from the four-dimensional scalar field action and then performing the reduction. In this formulation, the matter Lagrangian is multiplied by a factor $e^{-2\phi}$ [98].

2.2.2 Dimensional reduction of 5D Chern-Simons theory over $\mathbb{S}^3$

In this subsection, we preform the dimensional reduction of the five-dimensional Chern–Simons (5DCS) action over $\mathbb{S}^3$, obtaining a two-dimensional dilaton gravity theory. Although 5DCS gravity generally allows for non-zero torsion, here we restrict our analysis to the torsion-free Riemannian sector. The action can be written as [99]:

$$S^{(5)}_{\mathrm{CS}} = \frac{k}{2l^3}\int \mathrm{d}^5x\sqrt{-g}\Big[\mathcal{R} + \frac{6}{l^2} + \frac{l^2}{4}\big(\mathcal{R}^2 - 4\mathcal{R}^{AB}\mathcal{R}_{AB} + \mathcal{R}^{ABCD}\mathcal{R}_{CDAB}\big)\Big]. \tag{2.20}$$

In the same way as in the case of Einstein-Hilbert action, we assume that the metric has a block diagonal form:

$$\mathrm{d}s^2 = g_{\mu\nu}\mathrm{d}x^\mu\mathrm{d}x^\nu + \frac{1}{\lambda^2}e^{-2\phi}\mathrm{d}\Omega_3^2, \tag{2.21}$$

where $\phi = \phi(x^0, x^1)$ is a newly introduced dilaton field, $g_{\mu\nu} = g_{\mu\nu}(x^0, x^1)$ is a two-dimensional metric, and $\mathrm{d}\Omega_3^2 = \mathrm{d}\psi^2 + \sin^2\psi(\mathrm{d}\theta^2 + \sin^2\theta\mathrm{d}\varphi^2) \equiv \gamma_{ij}\mathrm{d}x^i\mathrm{d}x^j$ is a $\mathbb{S}^3$ metric. We use Greek indices $\mu, \nu = 0, 1$ for the remaining two-dimensional manifold, and Latin indices $i, j = 2, 3, 4$ for the $\mathbb{S}^3$. For the $\mathbb{S}^3$ reduction, the scalar curvature. For the $\mathbb{S}^3$ reduction, the scalar curvature (2.12), the Gauss-Bonnet term (2.13) and the Jacobian (2.10) read:

$$\mathcal{R} = R + 6\left((\nabla\phi)^2 + \lambda^2 e^{2\phi}\right) - 2e^{3\phi}\Box e^{-3\phi}, \tag{2.22}$$

$$GB = 12\left(\lambda^2 Re^{2\phi} + (\nabla\phi)^2\left(\Box\phi - (\nabla\phi)^2\right) - 2e^{3\phi}\nabla_\mu\xi^\mu\right), \tag{2.23}$$

$$\mathrm{d}^5X\sqrt{-G} = \mathrm{d}^2x\mathrm{d}\psi\mathrm{d}\vartheta\mathrm{d}\varphi\frac{1}{\lambda^3}e^{-3\phi}\sin^2\psi\sin\vartheta. \tag{2.24}$$

Placing Eqs. (2.22-2.24) into the action (2.20) we get the following final expression for the action of the dimensionally reduced theory:

$$\begin{aligned} S_{\mathrm{DR5DCS-R}} = \frac{k\pi^2}{(\lambda l)^3}\int \mathrm{d}x^2\sqrt{-g}e^{-3\phi}\Big[&R\left(1 + 3(\lambda l)^2 e^{2\phi}\right) \\ &+ 6\left((\nabla\phi)^2 + \lambda^2 e^{2\phi}\right) + \frac{6}{l^2} + 3l^2(\nabla\phi)^2\left(\Box\phi - (\nabla\phi)^2\right)\Big] + S_{\mathrm{mat}}, \end{aligned} \tag{2.25}$$

where S_{mat} is a mater action in two dimensions.

2.3 Dimensional reduction of the full 5DCS theory over $\mathbb{S}^3$

Let us first introduce the five-dimensional theory of Chern-Simons gravity, following the introduction in [99]. As a first step, we introduce the $SO(4,2)$ gauge connection:

$$\mathcal{A} = \frac{1}{2}\Omega^{AB}J_{AB} + \frac{1}{l}E^A P_A, \tag{2.26}$$

where J_{AB} and P_A are generators of the $\mathfrak{so}(4,2)$ Lie algebra, satisfying:

$$\begin{aligned}
&[J_{AB}, J_{CD}] = \eta_{AD}J_{BC} + \eta_{BC}J_{AD} - (C \leftrightarrow D),\\
&[J_{AB}, P_C] = \eta_{BC}P_A - \eta_{AC}P_B,\\
&[P_A, P_B] = J_{AB}.
\end{aligned} \tag{2.27}$$

The parameter l denotes the AdS radius. Using this gauge connection, we can then build the Chern–Simons Lagrangian, which in five dimensions takes the form:

$$-\frac{ik}{3}\int \mathrm{Tr}\Big(\mathcal{F}\wedge\mathcal{F}\wedge\mathcal{A} - \frac{1}{2}\mathcal{F}\wedge\mathcal{A}\wedge\mathcal{A}\wedge\mathcal{A} + \frac{1}{5}\mathcal{A}\wedge\mathcal{A}\wedge\mathcal{A}\wedge\mathcal{A}\wedge\mathcal{A}\Big), \tag{2.28}$$

where the trace is taken in a particular representation of the gauge group. After evaluating this trace, the resulting action can be written in the following form:

$$S^{(5)}_{\mathrm{CS}} = \frac{k}{8}\int \varepsilon_{ABCDE}\Big(\frac{1}{l}\mathcal{R}^{AB}\wedge\mathcal{R}^{CD}\wedge E^E + \frac{2}{3l^3}\mathcal{R}^{AB}\wedge E^C\wedge E^D\wedge E^E + \frac{1}{5l^5}E^A\wedge E^B\wedge E^C\wedge E^D\wedge E^E\Big). \tag{2.29}$$

By varying the action (2.29) we arrive at the following set of equations of motion:

$$\begin{aligned}
&\varepsilon_{ABCDE}\big(\mathcal{R}^{AB} + E^A\wedge E^B\big)\big(\mathcal{R}^{CD} + E^C\wedge E^D\big) = 0,\\
&\varepsilon_{ABCDE}\mathcal{T}^A\big(\mathcal{R}^{BC} + E^B\wedge E^C\big) = 0,
\end{aligned} \tag{2.30}$$

These equations do not require the torsion $\mathcal{T}^A = \mathrm{d}E^A + \Omega^A{}_B\wedge E^B$ to vanish. On the other hand, they are satisfied when the torsion is set to zero. Consequently, it is consistent to focus on the torsionless sector of the theory defined by the action (2.20). This is the most common approach in studies of this class of Lovelock gravity, where Riemannian geometry is assumed from the outset, as we did in the previous section.

What is interesting about the 5DCS gravity is that it admits the dimensionally continued BTZ black hole solution [78, 100].

$$\mathrm{d}s^2 = -\left(r^2-\mu\right)\mathrm{d}t^2 + \frac{1}{(r^2-\mu)}\mathrm{d}r^2 + r^2\mathrm{d}\Omega_3^2, \tag{2.31}$$

where $\mathrm{d}\Omega_3^2$ denotes the metric on the 3-sphere. It is straightforward to see that the choice $\mu=-1$ yields AdS space-time. The field Eqs. (2.30) admit solutions not only with spherical symmetry, but also with more general geometries in which $\mathrm{d}\Omega_3^2$ is replaced by an arbitrary $\mathrm{d}\Sigma_3^2$, where Σ_3 is any fixed manifold describing the horizon geometry [101]. A notable characteristic of this BH solution is that it allows for nontrivial axial torsion. Adopting conventions where the indices $\{i,j,k\}\in\{2,3,4\}$ label directions along Σ_3, the nonvanishing torsion components are given by:

$$\mathcal{T}^i = -\frac{\delta}{r}\varepsilon^{ijk}e^j e^k, \tag{2.32}$$

with δ an arbitrary constant, while all remaining torsion components vanish.

The existence of this black hole with torsion makes this theory an interesting testing ground for the effects of torsion on the fine-grained entropy of gravitational systems. Since most of the Page curve reconstructions are carried out within the framework of two-dimensional dilaton gravity, for simplicity, we preform the dimensional reduction of the full 5DCS to two dimensions.

The first step in this procedure is to find ansatz for the spin-connection and the vielbein which exhibits a spherical symmetry of a 3-sphere. We decompose indices as $(A) = (a, i)$, where lower Latin indices from the beginning of the alphabet indicate two-dimensional Lorentz indices, while indices $i, j, k \dots \in \{2, 3, 4\}$. The five-dimensional vielbein is given by:

$$E^a = e^a_0 \mathrm{d}t + e^a_1 \mathrm{d}r \equiv e^a \quad \wedge \quad E^i = \frac{e^{-\phi}}{\lambda} e^i, \tag{2.33}$$

where $e^2 = \mathrm{d}\psi$, $e^3 = \sin\psi\,\mathrm{d}\vartheta$, and $e^4 = \sin\psi\,\sin\vartheta\,\mathrm{d}\varphi$; while $\phi = \phi(x^0, x^1)$ is the dilaton field. The most general static, spherically symmetric Riemann–Cartan space-time in five dimensions [102] admits the following ansatz for the spin connection:

$$\begin{aligned}
&\Omega^{01} = A(x^0, x^1)\mathrm{d}x^1 + B(x^0, x^1)\mathrm{d}x^0 \equiv \omega^{01}, \quad \Omega^{0i} = \phi^0 e^i, \\
&\Omega^{1i} = \phi^1(x^0, x^1)e^i, \quad \Omega^{23} = -\cos\psi\mathrm{d}\vartheta + \theta(x^0, x^1)e^4, \\
&\Omega^{24} = -\cos\psi\sin\vartheta\mathrm{d}\varphi - \theta(x^0, x^1)e^3, \quad \Omega^{34} = -\cos\vartheta\mathrm{d}\varphi + \theta(x^0, x^1)e^2,
\end{aligned} \tag{2.34}$$

where A, B, ϕ^0, ϕ^1 and θ are arbitrary functions defined on the final manifold. Then the components of Riemann-Cartan curvature tensor $\mathcal{R}^{AB} = \mathrm{d}\Omega^{AB} + \Omega^A{}_C \wedge \Omega^{CB}$ can be directly computed. To illustrate how one computes components of the form $\mathcal{R}^{ai}$ we explicitly evaluate component $\mathcal{R}^{02}$:

$$\begin{aligned}
\mathcal{R}^{02} &= \mathrm{d}\Omega^{02} + \Omega^0{}_1 \wedge \Omega^{12} + \Omega^0{}_3 \wedge \Omega^{32} + \Omega^0{}_4 \wedge \Omega^{42} \\
&= \mathrm{d}\phi^0 \wedge \mathrm{d}\psi + \omega^0{}_1\phi^1 \wedge \mathrm{d}\psi - \phi^0\theta\left(e^3 \wedge e^4 - e^4 \wedge e^3\right).
\end{aligned} \tag{2.35}$$

Furthermore, we demonstrate the procedure for calculating the components R^{ij} by explicitly working out $\mathcal{R}^{23}$:

$$\begin{aligned}
\mathcal{R}^{23} &= \mathrm{d}\Omega^{23} + \Omega^2{}_4\Omega^{43} + \Omega^2{}_0\Omega^{03} + \Omega^2{}_1\Omega^{13} \\
&= \sin\psi\,\mathrm{d}\psi \wedge \mathrm{d}\vartheta + \mathrm{d}\theta - \theta^2\sin\psi\,\mathrm{d}\psi \wedge \mathrm{d}\vartheta - (\phi_0\phi^0 + \phi_1\phi^1)\sin\psi\,\mathrm{d}\psi \wedge \mathrm{d}\vartheta.
\end{aligned}$$

Generalizing this procedure to other components of the Riemannian curvature tensor, we conclude that:

$$\mathcal{R}^{ai} = (\mathrm{d}\phi^a)e^i - \theta\phi^a\varepsilon^{ijk}e^je^k, \tag{2.36}$$

$$\mathcal{R}^{ij} = (1 - \phi^a\phi_a - \theta^2)e^ie^j + \mathrm{d}\theta\,\varepsilon^{ijk}e^k. \tag{2.37}$$

One must show that ϕ^a indeed forms a two-dimensional Lorentz vector multiplet. Under $SO(4,2)$ gauge transformations, A transforms according to $\mathcal{A} \mapsto \mathcal{A}_\epsilon = \mathcal{A} - \mathrm{d}\epsilon$, with $\epsilon = \frac{1}{2}\epsilon^{AB}J_{AB} + \epsilon^A P_A$. Two-dimensional Lorentz transformations are produced by choosing $\epsilon = \varepsilon J_{01}$. A straightforward calculation yields:

$$\delta\mathcal{A} = -\mathrm{d}\varepsilon J_{01} - \varepsilon\left(\Omega^{0i}J_{i1} + \Omega^{i1}J_{i0} - \frac{1}{l}E^0P_1 + \frac{1}{l}E^1P_0\right), \tag{2.38}$$

from which we conclude:

$$\begin{aligned}\mathcal{A}_\varepsilon = &\left(\omega^{01} - \mathrm{d}\varepsilon\right) J_{01} + \left(\Omega^{0i} + \varepsilon\Omega^{i1}\right) J_{0i} + \left(\Omega^{1i} + \varepsilon\Omega^{0i}\right) J_{1i} \\ &+ \frac{1}{2}\Omega^{ij} J_{ij} + \frac{1}{l}\left(e^0 - \varepsilon e^1\right) P_0 + \frac{1}{l}\left(e^1 + \varepsilon e^0\right) P_1.\end{aligned} \tag{2.39}$$

Substituting Eq. (2.34), we obtain the following transformation law for ϕ^a:

$$\phi^0 e^i \to \phi^0 e^i - \varepsilon\phi^1 e^i \quad \wedge \quad \phi^1 e^i \to \phi^1 e^1 + \varepsilon\phi^0 e^i, \quad \Longrightarrow \quad \phi^a \mapsto \phi^a + \varepsilon\varepsilon^a{}_b\phi^b. \tag{2.40}$$

Since this quantity indeed transforms as Lorentz vector, we can utilize a vielbein $e_a{}^\mu$ to define a two-dimensional vector ϕ^μ as $\phi^\mu = e_a{}^\mu\phi^a$. Additionally, Eq. (2.39) shows that ϕ is a scalar field.

The next step is to evaluate the whole action (2.29) using the ansatz for the spin-connection (2.34) and for the vielbein (2.33). The resulting reduced action is then given by:

$$\begin{aligned}S_{red} = &-\frac{k\pi^2}{(\lambda l)^3}\int_{\mathcal{N}} \varepsilon_{ab}\, e^{-3\phi}\Big[\big(1 + 3(\lambda l)^2 e^{2\phi}(1 - \phi_c\phi^c)\big)\tilde{R}^{ab} + \frac{3}{l^2}\big(1 + (\lambda l)^2 e^{2\phi}(1 - \phi_c\phi^c)\big)e^a \wedge e^b \\ &+ 6\lambda e^{\phi}\big(1 + (\lambda l)^2 e^{2\phi}(1 - \phi_c\phi^c)\big)e^a \wedge \mathrm{d}\phi^b + 6(\lambda l)^2 e^{2\phi}\mathrm{d}\phi^a \wedge \mathrm{d}\phi^b\Big] \\ &- 3(\lambda l)^2\theta^2 e^{-\phi}\left[\tilde{R}^{ab} + \frac{e^a \wedge e^b}{l^2} - 2\lambda e^{\phi}\phi^a T^b\right].\end{aligned}$$

Note that after performing integration by parts in the last term, it becomes clear that θ^2 plays the role of a Lagrange multiplier. When the two-dimensional torsion vanishes, the precise structure of the term containing θ^2 coincides with that of JT gravity [20, 21]. Consequently, assigning a non-zero value to this field greatly simplifies the resulting equations. The action (2.25) reduces to the Riemannian action (2.25) upon setting $\theta = 0$ and imposing $\phi_\mu = \frac{e^{-\phi}}{\lambda}\nabla_\mu\phi$, with $\phi_\mu = e_\mu{}^a\phi_a$. These relations are implied by the torsion-free condition $T^a = 0$.

Now we rewrite the Riemann-Cartan action (2.41) into a more suitable Riemannian form. Using the notation defined in App. A, different terms appearing in Eq. (2.41) can be expressed in terms of the metric $g_{\mu\nu}$ and the contorsion 1-form K_μ as follows:

$$\varepsilon_{ab}R^{ab} = -\tilde{R} = -\left(\mathrm{R} + 2\varepsilon^{\alpha\beta}\partial_\alpha\mathrm{K}_\beta\right), \tag{2.41}$$
$$\varepsilon_{ab}e^a \wedge e^b = -1, \tag{2.42}$$
$$\varepsilon_{ab}\phi^a T^b = -\phi^\mu T^\nu{}_{\mu\nu} = -\varepsilon^{\mu\nu}\phi_\mu\mathrm{K}_\nu, \tag{2.43}$$
$$\varepsilon_{ab}e^a \wedge \mathrm{d}\phi^b = -\tilde{\nabla}_\mu\phi^\mu = -\left(\nabla_\mu\phi^\mu - \varepsilon^{\mu\nu}\phi_\mu\mathrm{K}_\nu\right), \tag{2.44}$$
$$\varepsilon_{ab}\mathrm{d}\phi^a \wedge \mathrm{d}\phi^b = -\left(\tilde{\nabla}_\mu\phi^\mu\tilde{\nabla}_\nu\phi^\nu - \tilde{\nabla}_\mu\phi^\nu\tilde{\nabla}_\nu\phi^\mu\right), \tag{2.45}$$

where R and $\tilde{R}$ are the Riemannian and Riemann-Cartan scalar curvatures, respectively. In addition, Eqs. (2.42-2.45) should be multiplied by $\mathrm{d}^2x\sqrt{-g}$. To further simplify equations, we define a reduced dilaton filed x by:

$$\mathrm{x} = \frac{1}{\lambda l}e^{-\phi}. \tag{2.46}$$

Putting all terms (2.42-2.45) into action (2.41) and using the reduced field (2.46), the action becomes:

$$
\begin{aligned}
S_{\mathrm{DRCS}_5} =& \frac{k\pi^2}{(\lambda l)^3} \int \mathrm{d}^2x \sqrt{-g} e^{-3\phi} \Bigg\{ \left(1 + \frac{3}{\mathrm{x}^2}\left(1 - \Phi^2 - \theta^2\right)\right) \left[\mathrm{R} + 2\varepsilon^{\alpha\beta}\partial_\alpha \mathrm{K}_\beta + \frac{2}{l^2}\right] \\
& + \frac{4}{l^2} + \frac{6}{l\mathrm{x}^3}\theta^2 \nabla_\alpha \phi^\alpha + \frac{6}{l\mathrm{x}}\left(1 + \frac{1}{\mathrm{x}^2}\left(1 - \Phi^2 - \theta^2\right)\right) \left[\nabla_\alpha \phi^\alpha - \varepsilon^{\alpha\beta}\phi_\alpha \mathrm{K}_\beta\right] \\
& - \frac{6}{\mathrm{x}^2}\left[\nabla_\alpha \phi^\beta \nabla_\beta \phi^\alpha - \nabla_\alpha \phi^\alpha \nabla_\beta \phi^\beta - \varepsilon^{\alpha\beta}\mathrm{K}_\alpha \nabla_\beta \Phi^2\right]\Bigg\} + S_{\mathrm{mat}},
\end{aligned}
\tag{2.47}
$$

where $\Phi^2 \equiv \phi^\alpha \phi_\alpha$, and S_{mat} denotes the action of the matter fields. The remaining part of the action is attributed to gravity. This action is a functional of the metric $g_{\mu\nu}$, the contorsion K_μ, the vector field ϕ^μ arising from the five-dimensional spin connection, the scalar field θ linked to the five-dimensional torsion, and the dilaton field ϕ, which plays the role of the radial coordinate in five dimensions.

Chapter 3

Dilaton gravity in two dimensions

In the previous chapter, we developed a systematic procedure for performing dimensional reduction of a gravitational theory between arbitrary spacetime dimensions. This process necessarily led to the appearance of new dilaton fields as an integral part of the reduction. Dimensional reduction offers several advantages. First, it yields an effective theory in fewer dimensions, which is significantly more tractable. Second, and more importantly, the reduced theory preserves the solutions of the original higher-dimensional theory that reflect the topology of the manifold used in the reduction. For instance, if one is interested in spherically symmetric vacuum solutions of a higher-dimensional theory, then performing a reduction over a sphere ensures that these configurations remain valid solutions in the lower-dimensional theory. Third, some fine-grained thermodynamic quantities, such as entanglement entropy, are known in closed analytic form only in a smaller number of dimensions. Therefore, applying dimensional reduction is a much need prerequisite for examining these thermodynamic properties.

The dimensionality of the final manifold has not yet been specified. In this chapter, we focus on the general features of two-dimensional dilaton gravity. A two-dimensional spacetime offers an excellent setting for studying entanglement entropy, because in two dimensions there exist well-defined formulas for computing it. As these theories arise from a dimensional reduction of a higher-dimensional theory, their thermodynamic characteristics retain traces of the original higher-dimensional system, thereby providing a window into the thermodynamics of higher dimensional black hole solutions.

In order to study Hawking radiation and its thermodynamic characteristics, one must take into account the back-reaction of quantum fields on the spacetime geometry. This requires computing an effective action, at least up to one-loop order. In the case of a two-dimensional massless scalar field, this effective action is known as the Polyakov–Liouville (PL) action [22]. An additional remarkable feature of the 2D setting is that the PL action is exact at the one-loop level.

As established in the previous chapter, performing a dimensional reduction of a Riemannian spacetime leads to the emergence of several dilaton fields ϕ_a, whose number and structure are determined by the topology of the manifold on which the reduction is carried out. Imposing that the original action contains terms at most quadratic in the curvature, the resulting reduced action has the following form:

$$S[\phi_a, g_{\mu\nu}] \propto \int \mathrm{d}^2x\sqrt{-g}e^{-\sum_a d_a\phi_a}\left(\mathcal{F}_0[\phi_a] + \mathcal{F}_1[\phi_a]R + \mathcal{F}_2[\phi_a]R^2\right), \tag{3.1}$$

where the functionals $\mathcal{F}_i[\phi_a]$ depend on the dilaton fields and involve at most four derivatives. This structure follows directly from Eqs. (2.6-2.8). Moreover, we have exploited the specific features of the two-dimensional spacetime (A.15) to express both the Riemann curvature tensor and the Ricci tensor solely in terms of the Ricci scalar. Note that for higher-dimensional gravity theories involving the Gauss-Bonnet term (2.9), there is no second-order curvature term in the reduced action as Gauss-Bonnet in 2D vanishes.

For a dimensional reduction of a full Riemann–Cartan theory with non-vanishing torsion, the resulting action involves many additional fields. Besides the dilaton associated with the higher-dimensional vielbeins, there appear both scalar and vector fields arising from the higher-dimensional spin connection. The two-dimensional geometry is then characterized by the metric $g_{\mu\nu}$ and the contorsion K_μ (see App. A).

This chapter consists of four main parts. In Sec. 3.1, we present an ansatz for the metric, 1-form, vector field, spinor field, and more generally for any tensor field in spacetimes that admit at least one non-null Killing vector. To construct this ansatz, we choose one of the dilatons ϕ_a as a radial coordinate, thereby expressing all remaining fields as functions of that single dilaton. The following Sec. 3.2 addresses how the covariant conservation laws of the energy–momentum tensor are modified in the presence of non-vanishing torsion. Our derivation closely follows [81], but we additionally incorporate non-minimally coupled fields, which leads to an even more intricate structure of the conservation laws. These laws are crucial in deriving several thermodynamical properties of gravitational theories. The penultimate Sec. 3.3 presents the Polyakov–Liouville action, which serves as the framework for incorporating the quantum corrections. The transformations of the energy-momentum tensor, as well as different vacuum states are discussed in detail. Finally, in the concluding Sec. 3.4, we examine how to construct a gravitational collapse scenario within the framework of two-dimensional dilaton gravity. As a by-product of this analysis, we obtain an alternative method for deriving the mass of the spacetime.

3.1 Symmetric ansatz setup for two-dimensional spacetime

We consider an ansatz for symmetric solutions in a two-dimensional spacetime. That implies the presence of at least one Killing vector. We focus on configurations with a single Killing vector, which may be either time-like or space-like. Because these two situations are analogous with respect to the ansatz for the field content of the theory,, we will present the procedure specifically for the case of a time-like Killing vector.

In two dimensions, any stationary spacetime is necessarily static. This indicates that the existence of a time-like Killing vector is the only requirement for the geometry to be static. The ansatz for the metric is taken to have the form:

$$\mathrm{d}s^2 = -e^{2\rho}\mathrm{d}x^+\mathrm{d}x^-, \tag{3.2}$$

so that the conformal gauge is satisfied. This is always possible in two dimensions. Using this ansatz, the Christoffel symbols and scalar curvature are as follows:

$$\Gamma^{\pm}_{\pm\pm} = 2\partial_\pm\rho \quad \wedge \quad R = 8e^{-2\rho}\partial_+\partial_-\rho. \tag{3.3}$$

In this gauge, for an arbitrary function f, the scalar quantities are given by:

$$\Box f = -4e^{-2\rho}\partial_+\partial_- f \quad \wedge \quad (\nabla f)^2 = -4e^{-2\rho}\partial_+ f\partial_- f. \tag{3.4}$$

Let us assume that there exists a time-like Killing vector:

$$\xi = \partial_t = \mathrm{F}^-(x^-)\partial_- - \mathrm{F}^+(x^+)\partial_+. \tag{3.5}$$

The functions $\mathrm{F}^{\pm}$ are the coordinate transformations from arbitrary coordinates $x^{\pm}$ to the Eddington–Finkelstein–type coordinates $\sigma^{\pm} = t \pm \sigma$, defined by the following relation:

$$\frac{\mathrm{d}\sigma^{\pm}}{\mathrm{d}x^{\pm}} = -\frac{1}{\mathrm{F}^{\pm}}. \tag{3.6}$$

Stating that the spacetime is in the Eddington-Finkelstein gauge amounts to fixing $\mathrm{F}^{+} = -1$ and $\mathrm{F}^{-} = 1$. In this way, we preserve the arbitrary choice of the coordinates within the conformal gauge. Note that we use the same label ξ to denote both the Killing vector and the associated Killing one-form.

The reduced field x can always be introduced by selecting one of the dilatons such that:

$$L\,\mathrm{x} = \frac{1}{\lambda_r} e^{-\phi_r} \equiv r, \tag{3.7}$$

where L is the characteristic length scale of the model (for the AdS spacetime, it is the AdS radius l as in Eq. (2.46), while for the Schwarzschild black hole, it equals the Schwarzschild radius a). The quantity r therefore acts as the radial coordinate in the higher-dimensional theory. In two dimensions, we can similarly take $l\mathrm{x}$ to serve as the radial coordinate. This choice is also convenient for comparing the two-dimensional theory with the higher-dimensional one from which it is derived.

For any scalar field f, including the remaining dilaton fields, the presence of a time-like Killing vector implies $\xi^{\mu}\nabla_{\mu} f = 0$, which means that f depends only on the spatial coordinate, $f = f(\mathrm{x})$. The norm of ξ defines the metric function $\Lambda(\mathrm{x})$:

$$\xi^2 = \xi^{\mu}\xi_{\mu} = \mathrm{F}^{+}\mathrm{F}^{-} e^{2\rho} \equiv \Lambda(\mathrm{x}), \tag{3.8}$$

which represents the g_{tt} component of the metric in the (t, r) coordinates. It depends only on the dilaton field (coordinate r) since there is a time-like Killing vector.

In two-dimensional spacetime, a basis in the space of 1-forms can be chosen to be $\{\xi, \star\xi\}$, since these two are orthogonal in a sense $\xi^{\mu}(\star\xi)_{\mu} = 0$. There are also restrictions on the vector fields (1-forms) related to the existence of ξ. Any 1-form A can be expressed as:

$$A = A^{\parallel}(x^{+}, x^{-})\xi - A^{\perp}(x^{+}, x^{-}) \star \xi, \tag{3.9}$$

where $A^{\parallel}$ and $A^{\perp}$ are parallel and perpendicular components of 1-form A with regard to Killing 1-form ξ. Then, the restrictions are given by:

$$\mathcal{L}_{\xi} A = 0 \quad \Longleftrightarrow \quad \xi^{\alpha}\nabla_{\alpha} A_{\beta} + A^{\alpha}\nabla_{\beta}\xi_{\alpha} = 0, \tag{3.10}$$

where $\mathcal{L}_{\xi}$ is a Lie derivative along the ξ vector field. Inserting ansatz (3.9) reduces Eq. (3.10) to:

$$\left(\xi^{\alpha}\nabla_{\alpha} A^{\parallel}\right)\xi_{\beta} + \left(\xi^{\alpha}\nabla_{\alpha} A^{\perp}\right)\varepsilon_{\beta\delta}\xi^{\delta} = 0. \tag{3.11}$$

The terms in Eq. (3.11) are mutually orthogonal, which implies that each one of them is equal to zero. This in turn means that $A^{\parallel} = A^{\parallel}(\mathrm{x})$ and $A^{\perp} = A^{\perp}(\mathrm{x})$. We conclude that any 1-form can be expressed as:

$$A_{\mu} = A^{\parallel}(\mathrm{x})\xi_{\mu} + A^{\perp}(\mathrm{x})\varepsilon_{\mu\nu}\xi^{\nu}. \tag{3.12}$$

The 1-form $\nabla_{\mu}\mathrm{x}$ can also be written in form Eq. (3.12), but the condition $\xi^{\mu}\nabla_{\mu}\mathrm{x} = 0$ implies that there is no parallel component:

$$\nabla_{\mu}\mathrm{x} = \frac{1}{L}\mathcal{D}(\mathrm{x})\varepsilon_{\mu\nu}\xi^{\nu}. \tag{3.13}$$

By applying the same reasoning, namely that $\mathcal{L}_\xi T = 0$ for a rank-2 tensor T, we are led to the following ansatz for T:

$$T_{\mu\nu} = T^{\parallel\parallel}(\mathrm{x})\xi_\mu\xi_\nu + T^{\perp\perp}(\mathrm{x})\varepsilon_{\mu\rho}\varepsilon_{\nu\sigma}\xi^\rho\xi^\sigma + \left(T^{\parallel\perp}(\mathrm{x})\xi_\mu\varepsilon_{\nu\rho} + T^{\perp\parallel}(\mathrm{x})\xi_\nu\varepsilon_{\mu\rho}\right)\xi^\rho. \tag{3.14}$$

This procedure can be easily generalized to tensors of any rank. A symmetric ansatz for a spinor field can likewise be formulated. We begin by writing the Kosmann-Lie derivative for a spinor field [103, 104]:

$$\mathcal{L}_\xi\psi = \xi^\mu\nabla_\mu\psi + \frac{1}{4}\nabla_a\xi_b\gamma^a\gamma^b\psi. \tag{3.15}$$

For further information on the spinor notation employed in this work, refer to App. A. Imposing that the spinor field satisfies the symmetry condition leads to the following equation:

$$\mathcal{L}_\xi\psi \equiv \begin{pmatrix} -\mathrm{F}^+\partial_+ + \mathrm{F}^-\partial_- + \frac{1}{4}\left(\partial_+\mathrm{F}^+ + \partial_-\mathrm{F}^-\right) \\ -\mathrm{F}^+\partial_+ + \mathrm{F}^-\partial_- - \frac{1}{4}\left(\partial_+\mathrm{F}^+ + \partial_-\mathrm{F}^-\right) \end{pmatrix}\psi = 0. \tag{3.16}$$

Then, the ansatz for the spinor field is given by:

$$\psi = \begin{pmatrix} \left|\frac{\mathrm{F}^+}{\mathrm{F}^-}\right|^{\frac{1}{4}}\varphi(\mathrm{x})e^{i\alpha(\mathrm{x})} \\ \left|\frac{\mathrm{F}^-}{\mathrm{F}^+}\right|^{\frac{1}{4}}\chi(\mathrm{x})e^{i\beta(\mathrm{x})} \end{pmatrix}, \tag{3.17}$$

where φ, χ, α, and β denote unknown functions that depend solely on the dilaton field x.

Now, we can express the tortoise coordinate $\sigma(\mathrm{x}) = \frac{1}{2}(\sigma^+ - \sigma^-) = -\frac{1}{2}\left(\int\frac{\mathrm{d}x^+}{\mathrm{F}^+} + \int\frac{\mathrm{d}x^-}{\mathrm{F}^-}\right)$ and subsequently the metric in the $(t, l\mathrm{x})$ coordinates:

$$\frac{\sigma}{L} = -\int\frac{\mathrm{dx}}{\Lambda\mathcal{D}} = -\frac{1}{2L}\left(\int\frac{\mathrm{d}x^+}{\mathrm{F}^+} + \int\frac{\mathrm{d}x^-}{\mathrm{F}^-}\right), \tag{3.18}$$

$$\mathrm{d}s^2 = \Lambda\mathrm{d}t^2 - \frac{l^2\mathrm{dx}^2}{\Lambda\mathcal{D}^2}. \tag{3.19}$$

Eq. (3.18) gives the coordinate dependence of the dilaton field $\mathrm{x} = \mathrm{x}(x^+, x^-)$, while Eq. (3.19) implies that another coordinate transformation can be performed to change the metric to a standard form associated with the black hole solutions:

$$\frac{\mathrm{dx}}{\mathrm{d\bar{x}}} = \mathcal{D} \quad \Longrightarrow \quad \mathrm{d}s^2 = \Lambda(\bar{\mathrm{x}})\mathrm{d}t^2 - \frac{l^2\mathrm{d\bar{x}}^2}{\Lambda(\bar{\mathrm{x}})}. \tag{3.20}$$

In some cases, another coordinate transformation may be performed:

$$\frac{\mathrm{dz}}{\mathrm{d\bar{x}}} = -\frac{1}{\sqrt{-\Lambda}} \quad \Longrightarrow \quad \mathrm{d}s^2 = \Lambda(\mathrm{z})\mathrm{d}t^2 + l^2\mathrm{dz}^2, \tag{3.21}$$

when $\Lambda < 0$. In a case when $\Lambda > 0$ a substitution $\mathrm{z} = i\tilde{\mathrm{z}}$ is consistent. New coordinate $\tilde{\mathrm{z}}$ is time-like, implying that the Killing vector ξ is space-like. In this case, we have a cosmological solution.

To summarize, by demanding the existence of a time-like Killing vector field ξ the two-component vector field A^μ is replaced with two scalar functions $A^\parallel(\mathrm{x})$ and $A^\perp(\mathrm{x})$, one orthogonal and the other perpendicular to the Killing field; the two-component spinor field ψ is equivalent to four scalar functions $\varphi(\mathrm{x})$, $\chi(\mathrm{x})$, $\alpha(\mathrm{x})$ and $\beta(\mathrm{x})$; metric is replaced with a function $\Lambda(\mathrm{x})$, while the dilaton field x is regarded as a coordinate and a derivatives of a dilaton field introduce another scalar function $\mathcal{D}(\mathrm{x})$.

Note that the arguments presented here are not applicable when the Killing vector is light-like, because ξ and $\star\xi$ cease to span the entirety of the 1-form space. Since we had to include an auxiliary function $\mathcal{D}$ to play the role of the derivative of the dilaton, an additional integration constant may appear when solving the equations of motion. This constant has no physical significance and therefore must be fixed by imposing suitable conditions. Up to this point, we have not specified the asymptotic behavior of the solution. Requiring the spacetime to be asymptotically flat yields extra conditions on the norm of the time-like Killing vector at infinity and on the behavior of the tortoise coordinate (3.18) at large distances. Interpreting the dilaton x as a radial coordinate, these two constraints read:

$$\lim_{\mathrm{x}\to\infty} \Lambda = -1 \qquad \wedge \qquad \lim_{\mathrm{x}\to\infty} \sigma = +\infty. \tag{3.22}$$

If, instead, the spacetime approaches AdS at infinity, a different set of asymptotic conditions must be enforced:

$$\Lambda \sim -\mathrm{x}^2(\mathrm{x}),\ \mathrm{x}\to\infty \qquad \wedge \qquad \lim_{\mathrm{x}\to\infty} \sigma = +\infty. \tag{3.23}$$

In summary, one must always prescribe the asymptotic form of the norm of the Killing vector, consistent with the spacetime symmetries, and at the same time require that the tortoise coordinate (3.18) diverges to $+\infty$ as the radial coordinate is taken to infinity.

At the end of this subsection, we give a collection of useful expressions involving different vector fields is given here:

$$\nabla_\mu \xi_\nu = \frac{\mathcal{D}}{2L}\frac{\mathrm{d}\Lambda}{\mathrm{dx}}\varepsilon_{\mu\nu}, \tag{3.24}$$

$$\nabla_\mu A^\mu = -\frac{\mathcal{D}}{L}\frac{\mathrm{d}}{\mathrm{dx}}\left(\Lambda A^\perp\right), \tag{3.25}$$

$$\varepsilon^{\mu\nu}\nabla_\mu A_\nu = -\frac{\mathcal{D}}{L}\frac{\mathrm{d}}{\mathrm{dx}}\left(\Lambda A^\parallel\right), \tag{3.26}$$

$$\varepsilon^{\mu\nu}A_\mu B_\nu = \Lambda\left(A^\parallel B^\perp - A^\perp B^\parallel\right), \tag{3.27}$$

$$A^\mu B_\mu = \Lambda\left(A^\parallel B^\parallel - A^\perp B^\perp\right), \tag{3.28}$$

where ξ is the Killing vector field, $\Lambda = \xi^2$, while A and B are two arbitrary vector fields. For the scalars, we have the following set of formulas:

$$R = \frac{\mathcal{D}}{L^2}\frac{\mathrm{d}}{\mathrm{dx}}\left(\mathcal{D}\frac{\mathrm{d}\Lambda}{\mathrm{dx}}\right), \tag{3.29}$$

$$\tilde{R} = \frac{\mathcal{D}}{L^2}\frac{\mathrm{d}}{\mathrm{dx}}\left(\mathcal{D}\frac{\mathrm{d}\Lambda}{\mathrm{dx}} - 2L\Lambda \mathrm{K}^\parallel\right), \tag{3.30}$$

$$\Box \mathrm{x} = -\frac{\mathcal{D}}{L^2}\frac{\mathrm{d}}{\mathrm{dx}}\left(\Lambda\mathcal{D}\right), \tag{3.31}$$

$$\left(\nabla \mathrm{x}\right)^2 = -\frac{\Lambda\mathcal{D}^2}{L^2}, \tag{3.32}$$

where $\mathrm{K}^\parallel$ is a component of contorsion parallel to the Killing field ξ, $\tilde{R}$ is the Riemann-Cartan scalar curvature, while R is the Riemannian scalar curvature. Finally, for the rank-2 tensor field $T_{\mu\nu}$ we have:

$$g^{\mu\nu}T_{\mu\nu} \equiv T = \Lambda\left(T^{\parallel\parallel} - T^{\perp\perp}\right), \tag{3.33}$$

$$\mathrm{F}^{\pm 2}T_{\pm\pm} = \frac{\Lambda^2}{4}\left[T^{\parallel\parallel} + T^{\perp\perp} \mp \left(T^{\parallel\perp} + T^{\perp\parallel}\right)\right]. \tag{3.34}$$

Note that, in the case of a symmetric tensor, we obtain $T^{\parallel\perp} = T^{\perp\parallel}$.

3.2 Covariant conservation laws

In this section, we investigate the modifications to the covariant conservation law for the energy-momentum tensor due to the presence of a non-zero torsion within the two-dimensional theory. In this prescription, the main sources are the energy-momentum tensor $T_{\mu\nu}$ and the contorsion current T^{K}_{μ}, the latter of which is obtained by taking the variational derivative of the matter action with respect to the contorsion. In Sec. 2.3 we show that the fundamental fields of the theory transform as expected with respect to the local Lorentz transformations (2.40) in the case of the dimensional reduction of 5D Chern-Simons theory. Naturally, it is expected that this holds true for any well-defined dimensional reduced theory. We analyze the symmetry properties according to the Poincaré gauge theory (for more details, see [81]). The idea is to localize the Poincaré group. The compensating fields, which are introduced within this process of localization, are interpreted as spin-connection $\omega^{ab}{}_{\mu}$ and vielbeins $e_a{}^{\mu}$, and subsequently the resulting geometry is interpreted as Riemann-Cartan geometry discussed in App. A.

The infinitesimal local Poincaré transformations in two dimensions are parametrized by a translation vector $\varepsilon^{\mu}(x)$ and a rotation angle $\theta(x)$, namely:

$$x^{\mu} \mapsto x'^{\mu} = x^{\mu} + \zeta^{\mu}(x) \equiv x^{\mu} + \varepsilon^{\mu}(x) + \theta(x)\varepsilon^{\mu\nu}x_{\nu}, \tag{3.35}$$

where we have used $\theta_{\mu\nu} = \theta\varepsilon_{\mu\nu}$ in two dimensions. The matter fields then transform according to the following law:

$$\phi(x) \mapsto \phi'(x) = e^{\frac{1}{2}\theta_{\mu\nu}(x)M^{\mu\nu}+\varepsilon_{\mu}(x)P^{\mu}}\phi(x), \tag{3.36}$$

where $M_{\mu\nu} = x_{\mu}\partial_{\nu} - x_{\nu}\partial_{\mu} - \Sigma\varepsilon_{\mu\nu}$ and $P_{\mu} = -\partial_{\mu}$ are generators of rotations and translations that belong to the respective representation of the Poincaré group associated with the field ϕ, and $\Sigma_{\mu\nu} = -\Sigma\varepsilon_{\mu\nu}$ is the matrix part of the Lorentz generator. Infinitesimally, the form-variation of the matter fields can be expressed as:

$$\delta_0\phi(x) = \mathcal{P}\phi(x) \equiv (\theta\Sigma - \zeta^{\mu}\partial_{\mu})\,\phi(x). \tag{3.37}$$

When there is a global Poincaré symmetry present, the derivative of a field transforms according to:

$$\delta_0(\partial_{\mu}\phi) = \mathcal{P}\partial_{\mu}\phi - \partial_{\mu}\zeta^{\nu}\partial_{\nu}\phi. \tag{3.38}$$

The localization procedure consists of two steps. First, one introduces a connection (gauge field) so that the transformation law of the newly defined covariant derivative of the field (A.3) has the same form as Eq. (3.38), i.e.

$$\delta_0\left(\tilde{\nabla}_{\mu}\phi\right) \equiv \mathcal{P}\tilde{\nabla}_{\mu}\phi - \partial_{\mu}\zeta^{\nu}\tilde{\nabla}_{\nu}\phi. \tag{3.39}$$

Then, one demands that, in the local reference frame, the covariant derivative transforms the same way as in the flat case:

$$\delta_0(\tilde{\nabla}_a\phi) \equiv \mathcal{P}\tilde{\nabla}_a\phi + \theta\varepsilon_a{}^b\tilde{\nabla}_b\phi, \tag{3.40}$$

where $\tilde{\nabla}_a\phi \equiv e_a{}^{\mu}\tilde{\nabla}_{\mu}\phi$. Eq. (3.40) introduces another set of compensating fields, i.e. vielbeins $e_a{}^{\mu}$. For more details on spinor notations see App. A. Using Eqs. (3.39) and (3.40) one derives the form variations of the compensating fields ω_{μ} and $e_a{}^{\mu}$, given by:

$$\delta_0\omega_{\mu} = -\zeta^{\alpha}\partial_{\alpha}\omega_{\mu} - \omega_{\alpha}\partial_{\mu}\zeta^{\alpha} - \partial_{\mu}\theta, \tag{3.41}$$

$$\delta_0 e_a{}^{\mu} = \theta\varepsilon_a{}^b e_b{}^{\mu} + e_a{}^{\alpha}\partial_{\alpha}\zeta^{\mu} - \zeta^{\alpha}\partial_{\alpha}e_a{}^{\mu}. \tag{3.42}$$

Next, we define the gauge-invariant quantities, that is, the field-strength tensors for the $\omega^{ab}{}_{\mu}$ connection and the vielbein $e_a{}^{\mu}$, $\tilde{R}^{ab}{}_{\mu\nu}$, and $T^a{}_{\mu\nu}$, respectively, given by Eqs. (A.13) and (A.14). From a geometric standpoint, they represent the curvature and torsion of the underlying Riemann-Cartan manifold. The metric $g_{\mu\nu}$, defined by Eq. (A.1), transforms in the following way (using the transformation law for vielbein (3.42)):

$$\delta_0 g^{\mu\nu} = \left(g^{\nu\alpha}\delta^{\mu}{}_{\beta} + g^{\mu\alpha}\delta^{\nu}{}_{\beta}\right)\partial_\alpha\zeta^\beta - \zeta^\alpha\partial_\alpha g^{\mu\nu}. \tag{3.43}$$

Using Eqs. (3.41-3.42) the separate parts of the spin-connection have the following form variations:

$$\delta_0\Delta_\mu = -\zeta^\alpha\partial_\alpha\Delta_\mu - \Delta_\alpha\partial_\mu\zeta^\alpha - \partial_\mu\theta, \tag{3.44}$$
$$\delta_0\mathrm{K}_\mu = -\zeta^\alpha\partial_\alpha\mathrm{K}_\mu - \mathrm{K}_\alpha\partial_\mu\zeta^\alpha. \tag{3.45}$$

From these equations, it is evident that contorsion K_μ behaves as a 1-form, in contrast to Δ_μ. Finally, we find the transformation laws for the curvature and the torsion. They are given by:

$$\delta_0\tilde{R} = -\zeta^\alpha\partial_\alpha\tilde{R}, \tag{3.46}$$
$$\delta_0 T^\mu = \mathrm{K}^\alpha\partial_\alpha\zeta^\mu - \zeta^\alpha\partial_\alpha\mathrm{K}^\mu. \tag{3.47}$$

It is easy to check that the torsion transforms as a vector under the local Poincaré transformations, that is:

$$\delta T^a = \theta\varepsilon^a{}_b T^b. \tag{3.48}$$

The condition for the invariance of the action results in the following equation for the Lagrangian of the theory:

$$\Delta\tilde{\mathcal{L}} \equiv \delta_0\tilde{\mathcal{L}} + \partial_\alpha\left(\tilde{\mathcal{L}}\zeta^\alpha\right) = 0, \tag{3.49}$$

where $\tilde{\mathcal{L}} \equiv \sqrt{-g}\mathcal{L}$ [81]. For instance, by its very construction, the action (2.47) is invariant under Poincaré transformations. Moreover, it is straightforward to verify that the condition (3.49) holds, making use of the transformation laws (3.42-3.47) and (2.40). This is expected to occur for all properly defined dimensionally reduced theories.

Now, we investigate the conditions which are imposed on the action of the matter fields due to the local Poincaré invariance. To make the matter action manifestly invariant, we demand that its Lagrangian depends only on the quantities that transform covariantly under the Poincaré group, i.e.

$$\mathcal{L}_{\mathrm{M}} = \mathcal{L}_{\mathrm{M}}\left(g^{\mu\nu}, \omega_\mu, \phi, \tilde{\nabla}_\mu\phi, \tilde{R}, T^\mu\right). \tag{3.50}$$

Notice that a non-minimal coupling is allowed since the matter action can directly depend on curvature and torsion. This violates the equivalence principle. Nonetheless, we will continue to examine these scenarios as well. Next, we define the following dynamical currents:

$$\tau_{\mu\nu} \equiv -\frac{2}{\sqrt{-g}}\frac{\partial\tilde{\mathcal{L}}_{\mathrm{M}}}{\partial g^{\mu\nu}}, \quad \sigma^\mu \equiv \frac{\partial\mathcal{L}_{\mathrm{M}}}{\partial\omega_\mu}, \quad \varrho \equiv \frac{\partial\mathcal{L}_{\mathrm{M}}}{\partial\tilde{R}}, \quad \tau_\mu \equiv \frac{\partial\mathcal{L}_{\mathrm{M}}}{\partial T^\mu}. \tag{3.51}$$

Using the form-variations (3.41), (3.43), (3.46-3.47), on-shell condition (3.49) for the matter Lagrangian can be expressed in the following form:

$$\Delta\tilde{\mathcal{L}}_{\mathrm{M}} \equiv \sqrt{-g}\zeta^\beta\mathrm{I}_\beta + \theta\mathrm{I} + \partial_\alpha\left(\sqrt{-g}\Lambda^\alpha\right) = 0, \tag{3.52}$$

where the quantities I, I_β and Λ^α are given by:

$$\Lambda^\alpha = \theta\left[\frac{\partial\mathcal{L}_\mathrm{M}}{\partial(\tilde{\nabla}_\alpha\phi)}\Sigma\phi - \sigma^\alpha\right] - \zeta^\beta\left[\frac{\partial\mathcal{L}_\mathrm{M}}{\partial(\tilde{\nabla}_\alpha\phi)}\partial_\beta\phi - \mathcal{L}_\mathrm{M}\delta^\alpha{}_\beta + \tau^\alpha{}_\beta + \sigma^\alpha\omega_\beta - \tau_\beta\mathrm{K}^\alpha\right], \tag{3.53}$$

$$\mathrm{I} = \partial_\mu\left(\sqrt{-g}\sigma^\mu\right), \tag{3.54}$$

$$\mathrm{I}_\beta = \frac{1}{\sqrt{-g}}\partial_\alpha\left[\sqrt{-g}\left(\tau^\alpha{}_\beta + \sigma^\alpha\omega_\beta - \tau_\beta\mathrm{K}^\alpha\right)\right] + \frac{1}{2}\tau_{\mu\nu}\partial_\beta g^{\mu\nu} - \sigma^\alpha\partial_\beta\omega_\alpha - \tau_\alpha\partial_\beta\mathrm{K}^\alpha - \varrho\partial_\beta\tilde{R}. \tag{3.55}$$

Because the parameters θ and ε^α (or ζ^α) can take any values, nullifying the term $\Delta\tilde{\mathcal{L}}_\mathrm{M}$ requires that I, I_β, and Λ^α be equal to zero. With Λ^α being dependent on these parameters as well, each term within the brackets in Eq. (3.53) must thus vanish, leading to the following two conditions:

$$\sigma^\alpha = \frac{\partial\mathcal{L}_\mathrm{M}}{\partial(\tilde{\nabla}_\alpha\phi)}\Sigma\phi \equiv S^\alpha \tag{3.56}$$

$$-\tau^\alpha{}_\beta + \tau_\beta\mathrm{K}^\alpha = \frac{\partial\mathcal{L}_\mathrm{M}}{\partial(\tilde{\nabla}_\alpha\phi)}\tilde{\nabla}_\beta\phi - \delta^\alpha{}_\beta\mathcal{L}_\mathrm{M} \equiv T^{(\mathrm{M})\alpha}{}_\beta. \tag{3.57}$$

The first Eq. (3.56) demonstrates that the dynamical spin-current σ^α matches the spin tensor of the matter fields S^α. In contrast, the subsequent Eq. (3.57) illustrates the relationship between the covariant energy-momentum tensor of the matter fields $T^{(\mathrm{M})\alpha}{}_\beta$ and the dynamical currents specified in Eq. (3.51). Note that this quantity is not equal to the energy-momentum tensor derived by varying the matter action with respect to the metric.

By setting $\mathrm{I} = 0$ (3.54) and employing the Riemannian covariant derivative ∇_μ associated with the Levi-Civita connection, we derive the ensuing conservation law for the dynamical spin-current:

$$\nabla_\mu\sigma^\mu = 0. \tag{3.58}$$

Finally, imposing the condition $\mathrm{I}_\beta = 0$ leads to the covariant conservation law associated with the dynamical current $\tau^{\alpha\beta}$, specifically:

$$\nabla_\alpha\tau^{\alpha\beta} = -\frac{1}{2}\tilde{R}\varepsilon^{\beta\alpha}\sigma_\alpha + \nabla_\alpha\left(\mathrm{K}^\alpha\tau^\beta\right) + \tau_\alpha\nabla^\beta\mathrm{K}^\alpha + \varrho\nabla^\beta\tilde{R}, \tag{3.59}$$

where we have once more employed the Riemannian covariant derivative.

Currently, the covariant conservation laws have been identified, but they are related to the dynamical currents specified by Eq. (3.51), and not directly to the energy-momentum tensor $T^{\mu\nu}$, which is obtained by varying the matter action in relation to the metric, nor to the contorsion current T^μ_K, which results from variation with respect to the contorsion. Since the metric and contorsion are the only independent variables present in the theory, given that torsion, curvature, and the spin connection are intrinsically determined by their derivatives, it inevitably follows that there exist conservation laws that are reliant solely on $T^{\mu\nu}$ and T^μ_K. To obtain these, we first express the contorsion current and energy-momentum tensor in terms of dynamical currents. Varying the matter action with respect to contorsion results in:

$$-T^\mu_\mathrm{K} = \sigma^\mu + \tau^\mu + 2\varepsilon^{\mu\nu}\partial_\nu\varrho, \tag{3.60}$$

while, the variation with respect to the metric yileds:

$$T^{\mu\nu} = \tau^{\mu\nu} + \frac{1}{2}\left(\varepsilon^{\mu\alpha}g^{\nu\beta} + \varepsilon^{\nu\alpha}g^{\mu\beta}\right)\nabla_\alpha\sigma_\beta + 2\left[\nabla^\mu\nabla^\nu\varrho - g^{\mu\nu}\left(\Box\varrho + \frac{1}{2}\varrho\tilde{R}\right)\right] - \left(\tau^\mu\mathrm{K}^\nu + \tau^\nu\mathrm{K}^\mu\right). \tag{3.61}$$

The next step is to find the covariant derivatives $\nabla_\mu T^\mu_{\mathrm{K}}$ and $\nabla_\mu T^{\mu\nu}$. With the help of covariant conservation laws for σ^μ (3.58) and $\tau^{\mu\nu}$ (3.59) we arrive at the following expressions:

$$\nabla_\mu T^\mu_{\mathrm{K}} = -\nabla_\mu \tau^\mu, \tag{3.62}$$

$$\nabla_\mu T^{\mu\nu} = -\frac{1}{2}\mathrm{R}[\mathrm{K}]\varepsilon^{\nu\rho}\left(\sigma_\rho + \tau_\rho + 2\varepsilon_{\rho\sigma}\nabla^\sigma \varrho\right) - \mathrm{K}^\nu \nabla_\rho \tau^\rho, \tag{3.63}$$

where $\mathrm{R}[\mathrm{K}] = 2\varepsilon^{\mu\nu}\partial_\mu \mathrm{K}_\nu$. In the case of minimal coupling, that is, $\tau^\mu = 0$ and $\varrho = 0$, the covariant conservation laws reduce to the expressions obtained in [81]. As anticipated, dynamical currents, as mentioned in (3.51), can be completely removed from conservation laws and replaced with the contorsion current and energy-momentum tensor. This is achieved by inserting Eqs. (3.60) and (3.62) into Eq. (3.63). The resulting expression for the covariant conservation law of the energy-momentum tensor is presented below:

$$\nabla_\mu T^{\mu\nu} = \frac{1}{2}\mathrm{R}[\mathrm{K}]\varepsilon^{\nu\rho}T^{\mathrm{K}}_\rho + \mathrm{K}^\nu \nabla_\rho T^\rho_{\mathrm{K}}. \tag{3.64}$$

Applying the ansatz defined in the Sec. 3.1, Eq. (3.64) can be rewritten in the following form:

$$\Lambda \frac{\mathrm{d}T^{\shortparallel\perp}}{\mathrm{d}\bar{\mathrm{x}}} + 2T^{\shortparallel\perp}\frac{\mathrm{d}\Lambda}{\mathrm{d}\bar{\mathrm{x}}} = \mathrm{K}^{\shortparallel}\frac{\mathrm{d}}{\mathrm{d}\bar{\mathrm{x}}}\left(\Lambda T^\perp_{\mathrm{K}}\right) + T^\perp_{\mathrm{K}}\frac{\mathrm{d}}{\mathrm{d}\bar{\mathrm{x}}}\left(\Lambda \mathrm{K}^{\shortparallel}\right), \tag{3.65}$$

$$\Lambda \frac{\mathrm{d}T^{\perp\perp}}{\mathrm{d}\bar{\mathrm{x}}} + \frac{1}{2}\left(3T^{\perp\perp} + T^{\shortparallel\shortparallel}\right)\frac{\mathrm{d}\Lambda}{\mathrm{d}\bar{\mathrm{x}}} = \mathrm{K}^{\perp}\frac{\mathrm{d}}{\mathrm{d}\bar{\mathrm{x}}}\left(\Lambda T^\perp_{\mathrm{K}}\right) + T^{\shortparallel}_{\mathrm{K}}\frac{\mathrm{d}}{\mathrm{d}\bar{\mathrm{x}}}\left(\Lambda \mathrm{K}^{\shortparallel}\right), \tag{3.66}$$

where we have employed the $\bar{\mathrm{x}}$ coordinate (3.20). The first Eq. (3.65) can be integrated, yielding the following:

$$T^{\shortparallel\perp} = \mathrm{K}^{\shortparallel}T^\perp_{\mathrm{K}} + \frac{A}{\Lambda^2}, \tag{3.67}$$

where A is an arbitrary constant. Placing $T^{\shortparallel}_{\mathrm{K}} = T^\perp_{\mathrm{K}} = A = 0$ into Eqs. (3.67) gives $T^{\shortparallel\perp} = 0$, while Eq. (3.66) reduces to the standard conversation law of the energy-momentum tensor, i.e.:

$$\nabla_\mu T^{\mu\nu} \equiv -\frac{\mathcal{D}}{2L}\left[\Lambda \frac{\mathrm{d}T^{\perp\perp}}{\mathrm{d}\bar{\mathrm{x}}} + \frac{1}{2}\left(3T^{\perp\perp} + T^{\shortparallel\shortparallel}\right)\frac{\mathrm{d}\Lambda}{\mathrm{d}\bar{\mathrm{x}}}\right]\varepsilon^{\nu\rho}\xi_\rho = 0. \tag{3.68}$$

As a final consistency check of our approach, we verify that, upon setting the non-minimally coupled terms τ^μ and ϱ to zero, we reproduce the result of [81]. The spin-current conservation law (3.58) is already identical in form to that given in [81]. Next, from Eq. (3.60) we obtain $T^\mu_{\mathrm{K}} = -\sigma^\mu$. Using the spin-current conservation law (3.58), this implies $\nabla_\mu T^\mu_{\mathrm{K}} = 0$. Inserting this into Eq. (3.64) yields:

$$\nabla_\mu T^{\mu\nu} = -\frac{1}{2}\mathrm{R}[\mathrm{K}]\varepsilon^{\nu\rho}\sigma_\rho, \tag{3.69}$$

$$\nabla_\mu \sigma^\mu = 0, \tag{3.70}$$

which coincide with the conservation laws for the two-dimensional gravitational theory derived in [81].

3.3 Quantum corrections

In the preceding sections, we have constructed the framework of classical 2D dilaton gravity. To study Hawking radiation, however, it is necessary to account for the back-reaction of quantum fields on the classical geometry. This is achieved by adding the Polyakov–Liouville action [22], which represents the 1-loop effective action of a two-dimensional massless scalar field, namely:

$$e^{\frac{i}{\hbar}S_{\mathrm{PL}}} = \int \mathcal{D}\chi e^{\frac{i}{\hbar}\int \mathrm{d}^2x\sqrt{-g}\left(-\frac{1}{2}(\nabla\chi)^2\right)}, \tag{3.71}$$

After computing this Gaussian functional integral, we arrive at:

$$S_{\mathrm{PL}} = -\frac{\hbar}{96\pi}\int d^2x \int d^2y \sqrt{-g(x)}\sqrt{-g(y)}R(x)G(x-y)R(y). \tag{3.72}$$

Here, $G(x-y)$ denotes the Green's function of the massless Klein–Gordon equation in a curved (1+1)-dimensional spacetime, defined by $\Box G(x-y) = \frac{1}{\sqrt{-g}}\delta^{(2)}(x-y)$. A striking feature of this action is that it is 1-loop exact. In the form given above, the action is manifestly nonlocal. However, one can render it local by introducing an auxiliary scalar field ψ, in terms of which the action becomes:

$$S_{PL} = -\frac{\hbar}{96\pi}\int d^2x\sqrt{-g}\left[2R\psi + (\nabla\psi)^2\right], \tag{3.73}$$

which is on-shell equivalent to Eq. (3.72). The field equation of the auxiliary field is as follows:

$$\Box\psi = R. \tag{3.74}$$

By varying the action with respect to the metric we obtain the following energy-momentum tensor of the quantum fields:

$$\langle \Delta T^f_{\mu\nu}\rangle = \frac{\hbar}{48\pi}\left[-2\nabla_\mu\nabla_\nu\psi + \nabla_\mu\psi\nabla_\nu\psi + g_{\mu\nu}\left(2\Box\psi - \frac{1}{2}(\nabla\psi)^2\right)\right]. \tag{3.75}$$

It corresponds to the expectation value of the quantum energy-momentum tensor operator. The limitation of this approach is that it requires the introduction of an additional field. However, Eq. (3.74) can be readily solved once we substitute Eq. (3.3) into it:

$$\psi = -2\rho + f_+(x^+) + f_-(x^-), \tag{3.76}$$

where $f_\pm$ represent a set of arbitrary functions. Using this result, the energy-momentum tensor is given by:

$$\langle \Delta T^f_{\pm\pm}\rangle = \frac{\hbar}{12\pi}\left[\partial^2_\pm\rho - (\partial_\pm\rho)^2 - t_\pm(x^\pm)\right], \quad \langle \Delta T^f_{+-}\rangle = -\frac{\hbar}{12\pi}\partial_+\partial_-\rho, \tag{3.77}$$

where the functions $t_\pm$ are given in terms of $f_\pm$ by the following relations:

$$t_\pm(x^\pm) = \frac{1}{2}\partial^2_\pm f_\pm - \frac{1}{4}\left(\partial_\pm f_\pm\right)^2. \tag{3.78}$$

The quantity $\varepsilon = \frac{\hbar}{12\pi}$ serves as a natural expansion parameter in perturbation theory and will be employed in later chapters whenever we deal with a theory that cannot be solved exactly. Finally, we rewrite the EMT of the PL action (3.75) once more, now employing the symmetric ansatz introduced in Sec. 3.1:

$$\begin{aligned}\langle \Delta T^{(f)}_{\mu\nu}\rangle = -\frac{\hbar}{12\pi}\frac{1}{(2L\Lambda)^2}\Bigg\{ &\left[4L^2\big(t_+(\sigma^+) + t_-(\sigma^-)\big) + \frac{1}{2}\Big(\mathcal{D}\frac{\mathrm{d}\Lambda}{\mathrm{dx}}\Big)^2 - 2\Lambda\mathcal{D}\frac{\mathrm{d}}{\mathrm{dx}}\Big(\mathcal{D}\frac{\mathrm{d}\Lambda}{\mathrm{dx}}\Big)\right]\xi_\mu\xi_\nu \\ &+ \left[4L^2\big(t_+(\sigma^+) + t_-(\sigma^-)\big) + \frac{1}{2}\Big(\mathcal{D}\frac{\mathrm{d}\Lambda}{\mathrm{dx}}\Big)^2\right]\varepsilon_{\mu\rho}\varepsilon_{\nu\sigma}\xi^\rho\xi^\sigma \\ &- 4L^2\big(t_+(\sigma^+) - t_-(\sigma^-)\big)\big(\varepsilon_{\mu\rho}\xi_\nu + \varepsilon_{\nu\rho}\xi_\mu\big)\xi^\rho\Bigg\},\end{aligned} \tag{3.79}$$

where we have used the form of the EMT in the arbitrary coordinates $x^{\pm}$, namely expression (3.77), together with the observation that, after inserting the metric ansatz (3.2), the functions $t_{\pm}(x^{\pm})$ transform to the Eddington–Finkelstein coordinates, due to the appearance of the coordinate transformation functions $\mathrm{F}^{\pm}$:

$$\begin{aligned}(\partial_{\pm}\rho)^2 - \partial_{\pm}^2\rho + t_{\pm}(x^{\pm}) &= \frac{1}{4}\left(\partial_{\pm}\ln \mathrm{F}^{\pm}\right)^2 + \frac{1}{2}\partial_{\pm}^2 \ln \mathrm{F}^{\pm} + t_{\pm}(x^{\pm}) + \left(\frac{\lambda}{2\mathrm{F}^{\pm}}\right)^2 \mathcal{F}[\mathrm{x}] \\ &= t_{\pm}(x^{\pm}) - \frac{1}{2}D_{x^{\pm}}\left[\sigma^{\pm}\right] + \left(\frac{\lambda}{2\mathrm{F}^{\pm}}\right)^2 \mathcal{F}[\mathrm{x}] = \frac{1}{\mathrm{F}^{\pm 2}}t_{\pm}(\sigma^{\pm}) + \left(\frac{\lambda}{2\mathrm{F}^{\pm}}\right)^2 \mathcal{F}[\mathrm{x}],\end{aligned} \tag{3.80}$$

where $\mathcal{F}[\mathrm{x}]$ denotes a function which depends only on metric function Λ (3.8) and its derivatives. Note that for Eq. (3.79) to be only a function of the dilaton x, functions $t_{\pm}(\sigma^{\pm})$ must be constants.

3.3.1 Transformation properties of the energy–momentum tensor

To proceed with our analysis of these equations, we must first clarify the meaning of the seemingly arbitrary functions $t_{\pm}$ (3.78). To this end, we examine how the energy–momentum tensor behaves under coordinate transformations. To preserve the conformal gauge, we limit our consideration to conformal coordinate transformations, specifically those of the form $y^{\pm} = y^{\pm}(x^{\pm})$. It is enough to focus on the quantum part of the energy–momentum tensor, because the classical contribution is already known to obey the standard tensor transformation law. Under the conformal transformations, the metric function ρ changes in the following way:

$$\rho(y) = \rho(x) + \frac{1}{2}\ln\frac{dy^+}{dx^+} + \frac{1}{2}\ln\frac{dy^-}{dx^-}. \tag{3.81}$$

Since the energy–momentum tensor is required to transform as a tensor, and its classical component already obeys the standard tensor transformation law, the quantum fluctuation of the energy–momentum tensor (3.77) must likewise satisfy this same tensor transformation law, namely:

$$\langle \Delta T^f_{\pm\pm}(y)\rangle = \left(\frac{dx^{\pm}}{dy^{\pm}}\right)^2 \langle \Delta T^f_{\pm\pm}(x)\rangle. \tag{3.82}$$

By enforcing condition (3.82), we arrive at the following expression for the transformation law of the $t_{\pm}$ functions:

$$t_{\pm}(y^{\pm}) = \left(\frac{dx^{\pm}}{dy^{\pm}}\right)^2\left[t_{\pm}(x^{\pm}) - \frac{1}{2}D_{x^{\pm}}\left[y^{\pm}\right]\right], \quad D_{x^{\pm}}\left[y^{\pm}\right] = \frac{y^{+'''}}{y^{+'}} - \frac{3}{2}\left(\frac{y^{+''}}{y^{+'}}\right)^2. \tag{3.83}$$

The quantity $D_{x^{\pm}}\left[y^{\pm}\right]$ is called the Schwarzian derivative. It represents a functional acting on a function of a single variable. In Eq. (3.83) the quantity $y^{+'}$ denotes the first derivative of the function $y^+ = y^+(x^+)$. In order to better understand the nature of the quantity $t_{\pm}$, we perform canonical quantization of the scalar field in curved spacetime (see App. D.1). The equation for the scalar field, and its solution, are given by:

$$\Box f = 0 \quad \Longrightarrow \quad \partial_+\partial_- f = 0 \quad \Longrightarrow \quad f(x^+, x^-) = f_+(x^+) + f_-(x^-). \tag{3.84}$$

We define positive-frequency modes as:

$$\partial_0 f^{\omega} = -i\omega f^{\omega} \implies \frac{df^{\omega}_{\pm}(x^{\pm})}{dx^{\pm}} = -i\omega f^{\omega}(x^{\pm}) \implies f^{\omega}_{\pm}(x^{\pm}) = A^{\pm}_{\omega}e^{-i\omega x^{\pm}}. \tag{3.85}$$

The standard scalar product is given by:

$$\left(f_\pm^{\omega_1}, f_\pm^{\omega_2}\right) = -i\int_{x^0=0} dx\sqrt{\gamma}n^\mu\Big[f_\pm^{\omega_1}(x^\pm)\nabla_\mu f_\pm^{\omega_2 *}(x^\pm) - f_\pm^{\omega_2 *}(x^\pm)\nabla_\mu f_\pm^{\omega_1}(x^\pm)\Big], \tag{3.86}$$

where: $n^\mu = (e^{-\rho}, 0, 0, 0)^T$ i $\sqrt{\gamma} = e^\rho$. By imposing the orthogonality condition of the modes: $(f_\pm^{\omega_1}, f_\pm^{\omega_2}) = \delta(\omega_1 - \omega_2)$, we arrive at the following quantized scalar field:

$$f_\pm(x^\pm) = \int_0^\infty \frac{d\omega}{\sqrt{4\pi\omega}}\Big[a_\pm(\omega)e^{-i\omega x^\pm} + a_\pm^\dagger e^{i\omega x^\pm}\Big], \tag{3.87}$$

where $a_\pm(\omega)$ and $a_\pm^\dagger(\omega)$ represent the creation and annihilation operators of the modes $f_\pm^\omega$.

We now compute the two–point Green's function. Because the definition of the vacuum state is coordinate–dependent, we label it as $|0, x\rangle$ to underline that it is specified with respect to the $x^\pm$ coordinates. Since the explicit dependence on $\hbar$ is relevant for what follows, we reinstate the factor of $\sqrt{\hbar}$ multiplying the field. The two-point correlation function then takes the form:

$$\begin{aligned} G(x, x') = \langle 0, x|\, f_\pm(x^\pm) f_\pm(x'^\pm)\,|0, x\rangle &= \hbar \iint_0^\infty \frac{d\omega d\omega'}{4\pi\sqrt{\omega\omega'}} e^{i\omega' x' - i\omega x^\pm}\,\langle 0, x|\, a_\pm(\omega)a_\pm^\dagger(\omega')\,|0, x\rangle \\ = \hbar\int_0^\infty \frac{d\omega}{4\pi\omega}e^{i\omega(x'^\pm - x^\pm)} &= -\frac{\hbar}{4\pi}\ln\left|x'^\pm - x^\pm\right| + const. \end{aligned} \tag{3.88}$$

Next, we evaluate the expectation value of the energy–momentum tensor by applying $\partial_\pm\partial'_\pm$ to the Green's function and then taking the limit $x' \to x$, which yields:

$$\langle 0, x|\, \hat{T}^f_{\pm\pm}(x)\,|0, x\rangle = \lim_{x'^\pm\to x^\pm}\frac{\partial}{\partial x^\pm}\frac{\partial}{\partial x'^\pm}G(x, x') = -\frac{\hbar}{4\pi}\lim_{x'^\pm\to x^\pm}\frac{1}{\left(x'^\pm - x^\pm\right)^2}. \tag{3.89}$$

The energy–momentum tensor operator can be decomposed as $\hat{T}_{\mu\nu} =: \hat{T}_{\mu\nu} : + \langle 0, x|\, \hat{T}_{\mu\nu}\,|0, x\rangle$, leading to:

$$\hat{T}^f_{\pm\pm}(x) =: \hat{T}^f_{\pm\pm}(x) : -\frac{\hbar}{4\pi}\lim_{x'^\pm\to x^\pm}\frac{1}{\left(x'^\pm - x^\pm\right)^2}, \tag{3.90}$$

where $: \hat{T}^f_{\mu\nu} :$ denotes the normally ordered part of the energy–momentum tensor expressed in the $x^\pm$ coordinates. This represents the energy–momentum tensor as measured by an observer in the $x^\pm$ frame. The key question is what an observer in the $y^\pm$ frame measures if, for example, the energy–momentum tensor is normally ordered with respect to the $x^\pm$ coordinates (so that an observer in the $x^\pm$ frame detects no excitations of the matter fields). More generally, we may ask how the normally ordered part of the energy–momentum tensor changes under the transformation $x^\pm \mapsto y^\pm$, assuming that the complete energy–momentum tensor satisfies the usual tensor transformation law. We find:

$$\begin{aligned} : \hat{T}^f_{\pm\pm}(y^\pm) : &= \hat{T}^f_{\pm\pm}(y^\pm) + \frac{\hbar}{4\pi}\lim_{y'^\pm\to y^\pm}\frac{1}{\left(y'^\pm - y^\pm\right)^2} \\ &= \lim_{y'^\pm\to y^\pm}\frac{dx^\pm}{dy^\pm}\frac{dx'^\pm}{dy'^\pm}\hat{T}^f_{\pm\pm}(x^\pm) + \frac{\hbar}{4\pi}\lim_{y'^\pm\to y^\pm}\frac{1}{\left(y'^\pm - y^\pm\right)^2} \\ &= \left(\frac{dx^\pm}{dy^\pm}\right)^2 : \hat{T}^f_{\pm\pm}(x) : -\frac{\hbar}{4\pi}\underbrace{\lim_{x'^\pm\to x^\pm}\left[\frac{1}{\left(x'^\pm - x^\pm\right)^2}\frac{dx^\pm}{dy^\pm}\frac{dx'^\pm}{dy'^\pm} - \frac{1}{\left(y'^\pm - y^\pm\right)^2}\right]}_{L}. \end{aligned} \tag{3.91}$$

It remains to evaluate the limit L. We assume that the transformation $y^{\pm} = y^{\pm}(x^{\pm})$ is differentiable, so that whenever $x'^{\pm} \to x^{\pm}$ it follows that $y'^{\pm} \to y^{\pm}$. For convenience, in the calculation of the limit L, we will denote $x^{\pm}$ simply by x and $y^{\pm}$ simply by y. We set $x' - x = \varepsilon \to 0$ and perform an expansion in powers of ε. A representative behavior of such functions is illustrated in Fig. 3.1:

$$\begin{aligned} y^{'} &= y + \varepsilon\frac{dy}{dx} + \frac{\varepsilon^2}{2}\frac{d^2y}{dx^2} + \frac{\varepsilon^3}{6}\frac{d^3y}{dx^3}, \\ \frac{dy^{'}}{dx^{'}} &= \frac{dy}{dx} + \varepsilon\frac{d^2y}{dx^2} + \frac{\varepsilon^2}{2}\frac{d^3y}{dx^3}. \end{aligned} \tag{3.92}$$

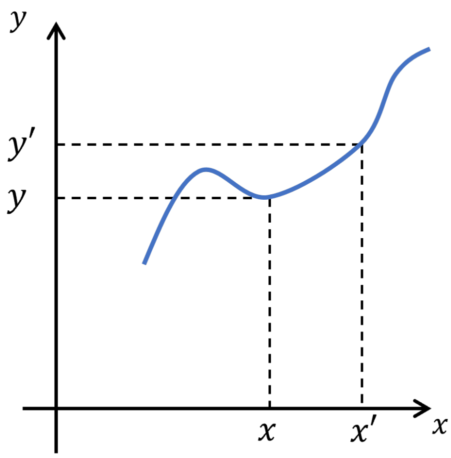

Figure 3.1: Representation of the behavior of the transformation $y(x)$

Furthermore, we use the notation $\frac{dy}{dx} = y'$, $\frac{d^2y}{dx^2} = y''$, and similarly for higher derivatives. We now proceed to evaluate the desired limit of L.:

$$\begin{aligned} L &= \lim_{\varepsilon\to 0}\left[\frac{\frac{dx}{dy}\frac{dx'}{dy'}}{(x'-x)^2} - \frac{1}{(y'-y)^2}\right] = \lim_{\varepsilon\to 0}\frac{(y'-y)^2 - (x'-x)^2\frac{dy}{dx}\frac{dy'}{dx'}}{(x'-x)^2(y'-y)^2\frac{dy}{dx}\frac{dy'}{dx'}} \\ &= \lim_{\varepsilon\to 0}\frac{\left(\varepsilon y' + \frac{\varepsilon^2}{2}y'' + \frac{\varepsilon^3}{6}y'''\right)^2 - \varepsilon^2 y'\left(y' + \varepsilon y'' + \frac{\varepsilon^2}{2}y'''\right) + o(\varepsilon^4)}{\varepsilon^4 (y')^4} \\ &= \lim_{\varepsilon\to 0}\frac{(y')^2 + \varepsilon y'y'' + \frac{\varepsilon^2}{3}y'y''' + \frac{\varepsilon^2}{4}(y'')^2 - (y')^4 - \varepsilon y'y'' - \frac{\varepsilon^2}{2}y'y'' + o(\varepsilon^2)}{\varepsilon^2(y')^4} \\ &= \lim_{\varepsilon\to 0}\frac{\frac{1}{4}(y'')^2 - \frac{1}{6}y'y''' + o(1)}{(y')^4} = -\frac{1}{6(y')^2}\left[\frac{y'''}{y'} - \frac{3}{2}\left(\frac{y''}{y'}\right)^2\right] = -\frac{1}{6(y')^2}D_x\left[y\right]. \end{aligned} \tag{3.93}$$

Finally, the transformation law can be written as $:\hat{T}^f_{\pm\pm}(x^{\pm}):$

$$:\hat{T}^f_{\pm\pm}(y^{\pm}) := \left(\frac{dx^{\pm}}{dy^{\pm}}\right)^2\left[:\hat{T}^f_{\pm\pm}(x^{\pm}): + \frac{\hbar}{24\pi}D_{x^{\pm}}\left[y^{\pm}\right]\right]. \tag{3.94}$$

This formula corresponds to a standard transformation law for the energy-momentum tensor in conformal field theory [105]. The coefficient in front of the Schwarzian derivative, when multiplied by $\frac{\hbar}{24\pi}$, defines the central charge, which takes the value $c = 1$ for a free massless boson.

From this we conclude that an energy–momentum tensor that is normally ordered with respect to one coordinate system will, in general, not remain normally ordered after a change of coordinates. This is consistent with the fact that one observer can perceive the vacuum, while another detects a particle spectrum (see App. D.1). It is also crucial to note that the Schwarzian derivative enters the transformation, so the transformation law coincides with the one in Eq. (3.83) for the quantity $t_{\pm}(x^{\pm})$. Consequently, we obtain

$$\langle\psi|:\hat{T}^f_{\pm\pm}:(x^{\pm})\,|\psi\rangle = -\frac{\hbar}{12\pi}t_{\pm}(x^{\pm}), \tag{3.95}$$

where $|\psi\rangle$ denotes the quantum state of the field. Eq. (3.95) gives the expectation value of the normally ordered energy–momentum tensor, and thus indicates whether an observer associated with a particular reference frame measures a particle spectrum or not. On this basis, we characterize the quantum state in which the system is found. The central issue is whether a particle spectrum is present at asymptotic infinity, i.e. at $\mathcal{J}^{\pm}$. Three distinct choices of vacuum state are commonly considered [26, 106]:

- **Boulware state** $|B\rangle$: This is a state that exhibits no energy flux through either of the asymptotic null infinities, $\mathcal{J}^+$ or $\mathcal{J}^-$. In other words, it describes a non-radiating black hole. For this requirement to hold, the energy–momentum tensor must be normally ordered with respect to the Eddington–Finkelstein, asymptotically flat coordinates $\sigma^{\pm}$, specifically:

$$\langle B| : \hat{T}^f_{\pm\pm}(\sigma^{\pm}) : |B\rangle = -\varepsilon t_{\pm}(\sigma^{\pm}) = 0 \quad \Longrightarrow \quad |B\rangle = |0, \sigma\rangle \, . \tag{3.96}$$

- **Hartle–Hawking state** $|HH\rangle$: This is a state in which the energy flux through $\mathcal{J}^+$ and $\mathcal{J}^-$ is equal. In other words, the black hole is in thermal equilibrium with its surroundings [107], evaporating at the same rate at which it absorbs. For this requirement to hold, the energy–momentum tensor must be normally ordered with respect to the Kruskal coordinates $x^{\pm}$, i.e. the coordinates in which the metric remains regular at the horizon, namely:

$$\langle HH| : \hat{T}^f_{\pm\pm}(x^{\pm}) : |HH\rangle = -\varepsilon t_{\pm}(x^{\pm}) = 0 \quad \Longrightarrow \quad |HH\rangle = |0, x\rangle \, . \tag{3.97}$$

- **Unruh state** $|U\rangle$: This state corresponds to a black hole that has no energy flux at $\mathcal{J}^-$ in the distant past, but does exhibit energy flux at $\mathcal{J}^+$ in the far future. In other words, we are dealing with a scenario where, at some point in time, matter collapses and a black hole forms. Prior to the collapse, there is no energy flux, and the energy–momentum tensor is normally ordered with respect to the asymptotically flat coordinates $\sigma^{\pm}$. Once the collapse occurs, the appropriate asymptotically flat coordinates switch to $\hat{\sigma}^{\pm}$. Because the quantum state is defined in terms of the original $\sigma^{\pm}$ coordinates, the energy–momentum tensor is no longer normally ordered in the new asymptotically flat coordinates $\hat{\sigma}^{\pm}$. This mismatch produces an energy flux at $\mathcal{J}^+$, implying that the black hole evaporates.

$$\langle U| : \hat{T}^f_{\pm\pm}(\sigma^{\pm}) : |U\rangle = -\varepsilon t_{\pm}(\sigma^{\pm}) = 0 \quad \Longrightarrow \quad |U\rangle = |0, \sigma\rangle \, . \tag{3.98}$$

In recent years, a new class of quantum states, known as hybrid quantum states, has been explored. This idea was first put forward in [108, 109] within the framework of the RST model [23, 24], where it was shown that the entanglement entropy of quantum fields can exhibit a Page-curve-like behavior even without invoking an island [110]. The core concept is to introduce non-physical, ghost-like fields arranged in a hybrid state. A hybrid state is a mixture of two quantum states (for example, a Hartle–Hawking state for the physical fields together with a Boulware state for the auxiliary non-physical fields, i.e. $|\psi\rangle \equiv |HH\rangle \otimes |B\rangle$). Because of the inclusion of these non-physical fields, the effective central charge of the conformal field theory can become negative. When this occurs, the space-time singularity is removed, which appears to be the primary mechanism driving the Page-curve-like evolution of the entanglement entropy in this setting. In contrast, the resolution of space-time singularities has long been expected to be a hallmark of a fully consistent theory of quantum gravity. Although the island formula (1.6) reproduces a Page curve, it does not, by itself, resolve singularities. This shortcoming can be viewed as a consequence of working within the semiclassical approximation.

3.4 Gravitational collapse scenario

In this section, we explain how to construct a gravitational collapse scenario within the framework of two-dimensional dilaton gravity. For studying the Page curve, one needs an evaporating black hole solution, i.e. a dynamical semi-classical configuration that does not admit a global timelike Killing vector field.

We begin by setting up the classical collapse scenario. The infalling matter is represented as a null shockwave of mass M propagating along the $x^+ = x_0^+$ hypersurface. Once this shockwave reaches the boundary of spacetime, namely the x = 0 hypersurface, a singularity forms together with an event horizon. The energy-momentum tensor for the simplest ingoing shockwave is described using a Dirac δ-function as follows:

$$T_{++} = s\delta\left(x^+ - x_0^+\right), \quad T_{--} = T_{+-} = 0, \tag{3.99}$$

where s is a constant connected to the mass of the shockwave. The mass carried by the energy-momentum tensor is given by [106]:

$$M = \int_\Sigma \mathrm{d}\sigma \sqrt{\gamma} n^\mu \xi^\nu T_{\mu\nu}, \tag{3.100}$$

where Σ is a space-like hypersurface, n is an orthogonal vector to the surface Σ normalized as $n_\mu n^\mu = -1$, ξ is the time-like Killing vector, γ is the induced metric on Σ and $T_{\mu\nu}$ is the energy-momentum tensor. Since ξ is orthogonal to Σ, we can choose n to be proportional to ξ, i.e. $n^\mu = \frac{\xi^\mu}{\sqrt{-\xi\cdot\xi}}$. The induced metric on the hypersurface Σ is then: $\mathrm{d}s^2 = -\Lambda \mathrm{d}\sigma^2$. Substituting all of this into Eq. (3.100) gives:

$$M = \int_\Sigma \mathrm{d}\sigma\sqrt{-\Lambda}\xi^\mu \frac{\xi^\nu}{\sqrt{-\Lambda}} T_{\mu\nu} = \int_\Sigma \mathrm{d}\sigma \mathrm{F}^{+2} T_{++} = -\int \frac{\mathrm{d}x^+}{\mathrm{F}^+} s\mathrm{F}^{+2}\delta\left(x^+ - x_0^+\right) = -s\mathrm{F}^+(x_0^+). \tag{3.101}$$

The collapse scenario is illustrated in Fig. 3.2. The blue line, representing the matter shockwave, divides the diagram into two parts. Because matter is confined to the shockwave itself, regions I and II are described by vacuum solutions of the form $(\mathrm{F}^+, \mathrm{F}^-, C)$, where $\mathrm{F}^\pm(x^\pm)$ denote conformal transformations from arbitrary coordinates $x^\pm$ to Eddington–Finkelstein coordinates $\sigma^\pm$, and C is a set of constants specifying the solution in Eddington–Finkelstein coordinates (such as the black hole mass or charge). In this way, one encodes the most general static vacuum solution within the formalism developed in Sec. 3.1. When crossing the shockwave hypersurface, two of these three parameters can jump, namely C and F^-. To determine these discontinuities, we impose appropriate gluing conditions on the metric and dilaton field.

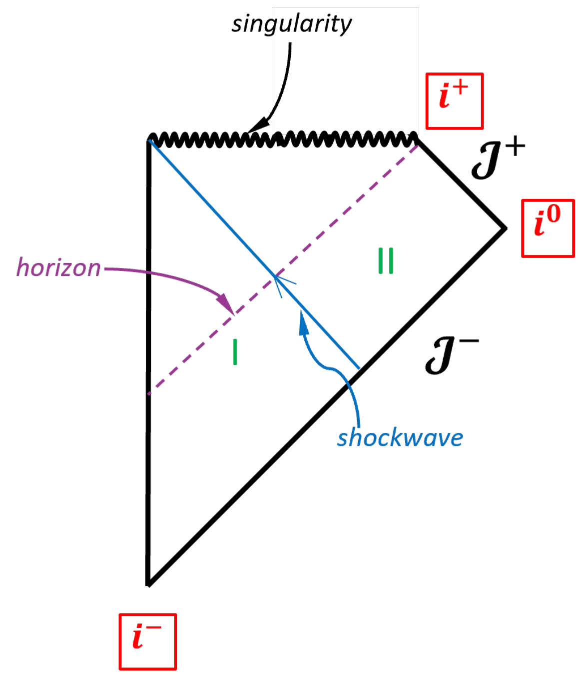

Figure 3.2: Penrose diagram of the gravitational collapse

Both the metric and the dilaton must remain continuous functions of x^+ and x^- across the hypersurface $x^+ = x_0^+$, which implies:

$$e^{2\rho_{\mathrm{I}}}\Big|_{x^+=x_0^+-\epsilon} = e^{2\rho_{\mathrm{II}}}\Big|_{x^+=x_0^++\epsilon}\,, \qquad e^{-\phi_{\mathrm{I}}}\Big|_{x^+=x_0^+-\epsilon} = e^{-\phi_{\mathrm{II}}}\Big|_{x^+=x_0^++\epsilon}\,, \tag{3.102}$$

when $\epsilon \to 0$, where the indices I and II refer, respectively, to region I and region II of space-time (see Fig. 3.2). In addition to these two continuity conditions, all derivatives of the metric and the dilaton with respect to the coordinate x^- must also be continuous. Finally, we have to examine the $++$ component of the metric equation, since its source term, T_{++}, is proportional to a Dirac δ-function. This function can always be expressed in the following form:

$$\partial_+\mathcal{F} + \mathcal{G}_<\eta(x_0^+ - x^+) + \mathcal{G}_>\eta(x^+ - x_0^+) = \frac{M}{\mathrm{F}^+}\delta\left(x^+ - x_0^+\right), \tag{3.103}$$

where it is repeatedly used that the metric and the dilaton field and their derivatives with respect to x^- must be continuous along the hypersurface $x^+ = x_0^+$. Integrating this equation from $x_0^+ - \epsilon$ to $x_0^+ + \epsilon$ and then taking the limit $\epsilon \to 0$ yields:

$$\mathcal{F}\Big|_<^> = \frac{M}{\mathrm{F}^+(x_0^+)}. \tag{3.104}$$

What we have essentially done here is to split the $++$ equation into a term proportional to the Dirac δ-function, $\partial_+\mathcal{F}$, and a term, $\mathcal{G}_{>/<}$, which is discontinuous at $x^+ = x_0^+$. The latter contribution is integrable at $x^+ = x_0^+$ and therefore its integral vanishes in the limit $\epsilon \to 0$. This constitutes the final condition imposed on the fields. Solving Eqs. (3.102) and (3.104) then determines the parameters of region II of the spacetime in terms of those of region I, or equivalently:

$$\mathrm{F}_{\mathrm{II}}^-(x^-) = \mathrm{F}_{\mathrm{II}}^-\left(\mathrm{F}_{\mathrm{I}}^-(x^-), \phi(x^-, x_0^+), \mathrm{F}_{\mathrm{I}}^+(x_0^+), C_{\mathrm{I}}, M\right), \quad \mathrm{F}_{\mathrm{II}}^+ = \mathrm{F}_{\mathrm{I}}^+, \quad C_{\mathrm{II}} = C_{\mathrm{II}}\left(\mathrm{F}_{\mathrm{I}}^+(x_0^+)), C_{\mathrm{I}}, M\right). \tag{3.105}$$

The net result of this kind of construction is that the static vacuum solutions remain present in both spacetime regions I and II. What does change is the Killing vector, because the component ξ^- becomes discontinuous, rendering the spacetime as a whole non-stationary. As a consequence, the asymptotically flat Eddington–Finkelstein coordinates are modified, going from $\sigma^\pm$ to $\hat{\sigma}^\pm$, since they are defined by:

$$\frac{\mathrm{d}\sigma^\pm}{\mathrm{d}x^\pm} = \mp\frac{1}{\mathrm{F}_{\mathrm{I}}^\pm}, \qquad \frac{\mathrm{d}\hat{\sigma}^\pm}{\mathrm{d}x^\pm} = \mp\frac{1}{\mathrm{F}_{\mathrm{II}}^\pm}, \tag{3.106}$$

specifically the σ^- coordinate. For later convenience, we introduce a new set of coordinates adapted to the shockwave hypersurface:

$$\hat{\mathrm{x}} \equiv \frac{\sigma_0^+ - \sigma^-}{2L}, \quad \wedge \quad \delta \equiv e^{-\frac{\sigma^+ - \sigma_0^+}{2L}}, \tag{3.107}$$

where the first coordinate plays the role of a redefined σ^-, and the second encodes a shift in the σ^+ coordinate. Note that $\delta \in (0,1)$, and it monotonically decreases from 1 to 0 (the latter corresponding to infinity) throughout region II of the spacetime, where the black hole is located. When region I is the flat Minkowski space, we have $\hat{\mathrm{x}} = \mathrm{x}$ at the shockwave hypersurface.

According to the cosmic censorship conjecture [106], any singularity must remain concealed behind some kind of horizon, typically the event horizon. In dynamical spacetimes, however, another type of horizon can arise, known as the apparent horizon, which can lie outside and thus obscure the event horizon. The apparent horizon is defined as the surface behind which all trapped surfaces are located (i.e., all null geodesics converge, preventing light from escaping that region). In dilaton gravity the apparent horizon is determined by the condition $\partial_+ e^{-n\phi} = 0$, because this expression is proportional to the area of the n-sphere in the higher-dimensional theory from which the model is obtained via spherical reduction (see Chap. 2). For considerations involving entropy, the apparent horizon is in fact more relevant than the event horizon itself [26].

3.4.1 Quantum-corrected collapse scenario

Here we assume that quantum corrections are incorporated via the PL action defined in Eq. (3.72). The starting point is the same as in the previous section: the infalling matter is modeled as an ingoing null shockwave located on the $x^+ = x_0^+$ hypersurface, which splits the spacetime into two regions. Region I denotes the portion of spacetime prior to the passage of the shockwave, i.e. $x^+ < x_0^+$, and coincides with the corresponding region in the classical setup. The essential new element is that we must now specify the quantum state of the fields, because in the quantum-corrected framework the geometry is characterized by the ordered quintuple $(\mathrm{F}^+, \mathrm{F}^-, t_+, t_-, C)$. Choosing $t_\pm = 0$ then selects the quantum state in which the EMT is normal ordered, as in Eq. (3.95).

In region I we introduce the Eddington–Finkelstein coordinates $\sigma^\pm$ and impose that the EMT is normal ordered with respect to these coordinates, i.e. $t_\pm(\sigma^\pm) = 0$. This condition guarantees the absence of Hawking radiation at the $\mathcal{J}^-$ hypersurface, prior to the introduction of the infalling matter. Without the shockwave, this would indicate that the matter fields are prepared in the Boulware state (3.96).

Once the infalling matter is introduced, the asymptotically flat coordinates change from $\sigma^\pm$ to a new set $\hat{\sigma}^\pm$. This is already apparent in the purely classical collapse setup (3.106), and therefore should remain valid when quantum effects are included. Moreover, upon incorporating quantum corrections, these coordinate transformations are expected to receive additional contributions. Since the EMT is no longer normal ordered in the new asymptotically flat coordinates, Hawking radiation is present on the $\mathcal{J}^+$ hypersurface. Consequently, the underlying quantum state is in fact the Unruh state (3.98).

Classically, the model features two stationary geometries with distinct time-like Killing vectors, which are smoothly matched across the $\sigma^+ = \sigma_0^+$ hypersurface. Thus, each region can be regarded as stationary on its own, even though the full spacetime is dynamical. Once quantum corrections are turned on, this picture changes. The geometry in region I may still be treated as stationary with respect to its corresponding Killing vector, but this is no longer true for region II. The key point is that, upon crossing the matching hypersurface, not only the coordinate transformations $\mathrm{F}^\pm$ change, but the functions $t_\pm$ also undergo a change.

In many practical situations, the full vacuum solution $(\mathrm{F}^+, \mathrm{F}^-, t_+, t_-, C)$ cannot be obtained in closed analytic form. When this is the case, one possible approach is to carry out a formal perturbative expansion in the natural small parameter $\varepsilon = \frac{\hbar G}{12\pi}$ (often written without G), which multiplies the EMT components (3.77). At zeroth order in ε one recovers the classical collapse solution. The next step is to expend the fields to first order in ε, namely:

$$\rho \mapsto \rho(\mathrm{x}) + \varepsilon\alpha, \quad \wedge \quad e^{-\phi} \mapsto e^{-\phi(\mathrm{x})} + \varepsilon\theta. \tag{3.108}$$

Since the quantum correction to the EMT already appears at first order in the expansion parameter ε, we insert the fields at zeroth order and evaluate it. The resulting expression is:

$$\begin{aligned}\langle \Delta T^{(f)}_{\pm\pm}\rangle &= -\frac{\varepsilon}{(2L\mathrm{F}^{+})^{2}}\left[4L^{2}t_{\pm}(\sigma^{\pm})+\frac{1}{4}\left(\mathcal{D}_0\frac{\mathrm{d}\Lambda_0}{\mathrm{dx}}\right)^{2}-\frac{\Lambda_0\mathcal{D}_0}{2}\frac{\mathrm{d}}{\mathrm{dx}}\left(\mathcal{D}_0\frac{\mathrm{d}\Lambda_0}{\mathrm{dx}}\right)\right],\\ \langle \Delta T^{(f)}\rangle &= \frac{\varepsilon}{2L^{2}}\mathcal{D}_0\frac{\mathrm{d}}{\mathrm{dx}}\left(\mathcal{D}_0\frac{\mathrm{d}\Lambda_0}{\mathrm{dx}}\right),\end{aligned}\tag{3.109}$$

where Λ_0 and $\mathcal{D}_0$ are given by Eqs. (3.8) and (3.13), respectively. The explicit dependence on the $x^{\pm}$ coordinates arises from the term $-\frac{\varepsilon}{\mathrm{F}^{\pm}}t_{\pm}(\sigma^{\pm})$. The "$\pm\pm$" equations of motion can always be rewritten as a first-order differential equations for the quantity $e^{-2\rho}\mathcal{D}_0^{-1}\partial_{\pm}\theta-\frac{1}{L}\alpha\mathrm{F}^{\mp}$, that is:

$$\partial_{\pm}\left(\frac{e^{-2\rho}}{\mathcal{D}_0}\partial_{\pm}\theta-\frac{\alpha\mathrm{F}^{\mp}}{L}\right)=\frac{\mathcal{F}\mathrm{F}^{\mp}t_{\pm}(\sigma^{\pm})}{\mathrm{F}^{\pm}}+\frac{\mathrm{F}^{\mp}}{2L}\frac{\mathcal{F}[\mathrm{x}]}{\mathcal{D}_0\Lambda_0^{2}}\left[\frac{1}{4}\left(\mathcal{D}_0\frac{\mathrm{d}\Lambda_0}{\mathrm{dx}}\right)^{2}-\frac{\Lambda_0\mathcal{D}_0}{2}\frac{\mathrm{d}}{\mathrm{dx}}\left(\mathcal{D}_0\frac{\mathrm{d}\Lambda_0}{\mathrm{dx}}\right)\right]\partial_{\pm}\mathrm{x}.\tag{3.110}$$

The first term on the right-hand side is fixed by the choice of a vacuum state and therefore remains in integral form as a source. The second term depends only on x and is multiplied by a function that is independent of the coordinate associated with the derivative on the left-hand side. Finally, the function $\mathcal{F}[\mathrm{x}]$ depends on the model. Consequently, integration can be carried out. The result is:

$$\partial_{\pm}\theta=\frac{1}{2L}\left[\mathrm{F}^{\mp}(\mathcal{D}_1+2\alpha)+\mathrm{G}^{\mp}\right]\mathcal{D}_0e^{2\rho}+\mathrm{F}^{\mp}\mathcal{D}_0e^{2\rho}\int\frac{\mathrm{d}x^{+}}{\mathrm{F}^{\pm}}t_{\pm}(\sigma^{\pm})\mathcal{F}[\mathrm{x}],\tag{3.111}$$

where a new set of arbitrary functions $\mathrm{G}^{\pm}=\mathrm{G}^{\pm}(x^{\pm})$ is introduced. They represent the quantum corrections to the coordinate transformations $\mathrm{F}^{\pm}$. The new function $\mathcal{D}_1$ is defined via:

$$\frac{\mathrm{d}\mathcal{D}_1}{\mathrm{dx}}=\frac{\mathcal{F}[\mathrm{x}]}{\mathcal{D}_0\Lambda_0^{2}}\left[\frac{1}{4}\left(\mathcal{D}_0\frac{\mathrm{d}\Lambda_0}{\mathrm{dx}}\right)^{2}-\frac{\Lambda_0\mathcal{D}_0}{2}\frac{\mathrm{d}}{\mathrm{dx}}\left(\mathcal{D}_0\frac{\mathrm{d}\Lambda_0}{\mathrm{dx}}\right)\right].\tag{3.112}$$

Employing a combination of the dilaton equation and the trace equation makes it possible to remove the unknown function α and therefore make Eq. (3.111) integrable once more. This integration gives a solution for θ in terms of the derivatives of θ, thus making it a first order differential equation for θ. Solving this equation gives a closed form of the θ function in terms of x and the integrals of the sources. These two integrations result in another set of integration constants C_1, which represent quantum corrections to the constants of the classical solution. Combining the zeroth and first order corrections together:

$$\rho(\mathrm{x})+\varepsilon\alpha\mapsto\rho,\;\; e^{-\phi(\mathrm{x})}+\varepsilon\theta\mapsto e^{-\phi},\;\; \mathrm{F}^{\pm}+\varepsilon\mathrm{G}^{\pm}\mapsto\mathrm{F}^{\pm},\;\; C+\varepsilon C_1\mapsto C,\tag{3.113}$$

we get the quantum-corrected solution that depends on x and the sources $t_{\pm(}\sigma^{\pm})$.

With this, the general vacuum solution to the quantum-corrected equations of motion has been determined to first order in ε. We now turn to the collapse setup. As in the classical analysis, the spacetime is split into two regions, each described by a vacuum solution. In the first part, we select a solution with vanishing energy flux at both future and past null infinity. Consequently, the quantum state is $|0,\sigma\rangle$, which implies $t_{\pm}(\sigma^{\pm})=0$. Upon entering the second part of the spacetime, the asymptotically flat coordinates are replaced by $\hat{\sigma}^{\pm}$, but the quantum state itself remains unchanged. In contrast, the solution in part II depends on $t_{\pm}(\hat{\sigma}^{\pm})$. Since this dependence is of order ε, it suffices to evaluate it at zeroth order, so that it is governed solely by the classical coordinate transformations $\mathrm{F}^{\pm}$, namely:

$$t_{\pm}(\hat{\sigma}^{\pm}) = \mathrm{F}^{\pm 2}\left[\frac{1}{4}\left(\partial_{\pm}\ln \mathrm{F}^{\pm}\right)^2 + \frac{1}{2}\partial_{\pm}^2 \ln \mathrm{F}^{\pm}\right]. \tag{3.114}$$

Because only the σ^- coordinate is transformed non-trivially, we have $t_-(\hat{\sigma}^-) \neq 0$ as the only non-vanishing component. In this way, the functions $t_{\pm}$ that specify the quantum state are determined in part II of the spacetime. The continuity conditions (3.102) and (3.104) must then be imposed, yielding the quantum-corrected coordinate transformations into part II, as well as the quantum-corrected discontinuity in the constants C, which encode the mass and other charges of the theory. The geometry in part II of the spacetime is thus completely specified.

The quantum-corrected collapse scenario is depicted in Fig. 3.3. It closely resembles the classical collapse shown in Fig. 3.2. The key distinction is the emergence of region III within the second part of the spacetime. This feature arises from the non-stationary geometry, which gives rise to an evaporating black hole located in region II of the spacetime. In this region, the geometry is such that the apparent horizon, defined by $\partial_+ e^{-n\phi} = 0$, and the singularity determined by solving $1/R = 0$ meet at a finite point in spacetime, denoted as the end-point of the evaporation $(\sigma_{\mathrm{E}}^+, \sigma_{\mathrm{E}}^-)$. Nevertheless, in many 2D dilaton gravity models [23, 24, 25], the black hole has not radiated away all of its mass by this stage. In accordance with the cosmic censorship conjecture [106], a naked singularity cannot be allowed to form; thus, the remaining mass is discharged as an outgoing shockwave along the hypersurface $\sigma^- = \sigma_{\mathrm{E}}^-$. This shockwave is commonly referred to in the literature as "the thunderpop."

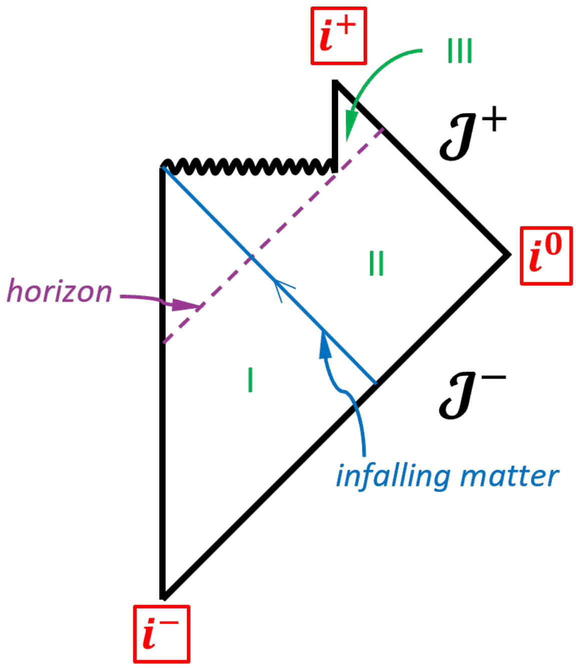

Figure 3.3: Penrose diagram of the quantum-corrected gravitational collapse featuring an evaporating black hole

Next, we need to identify the end-state geometry. The first step is to rewrite the solution using the radial coordinate x and the σ^- coordinate, since the hypersurface that separates the evaporating black hole in region II from the end-state geometry of region III is specified by the condition $\sigma^- = \sigma_{\mathrm{E}}^-$. We then recast the metric and the dilaton field in region II by introducing a running constant $\hat{C} = \hat{C}(\sigma^-)$, expanded as $\hat{C} = C + \varepsilon\, C_1(\sigma^-)$. This quantity closely follows the apparent horizon. Because the singularity is typically of ε-order,, the parameter $\hat{C}$ becomes small when the apparent horizon meets the singularity, i.e. near the end point of evaporation. Consequently, in the vicinity of the hypersurface $\sigma^- = \sigma_{\mathrm{E}}^-$ we can take the limit $\hat{C} \to 0$ within the first-order terms in the solution. In this limit, the solution reduces to one of the static configurations without energy flux at asymptotic infinity. Therefore, the metric and the dilaton field are already smoothly matched across the hypersurface $\sigma^- = \sigma_{\mathrm{E}}^-$.

Since no further coordinate transformation takes place in this step, the EMT in region III is already normal ordered with respect to the $\hat{\sigma}^{\pm}$ coordinates. We also identify the final vacuum state as $|0, \hat{\sigma}\rangle$. Consequently, the evolution both starts and ends in a pure state, implying that no information is lost during this process. Nevertheless, the final state does not depend on the detailed structure of the initial infalling matter shockwave. To determine whether information is genuinely lost, one must evaluate the entanglement entropy and verify whether it exceeds the coarse-grained limit set by the thermodynamic entropy.

Finally, as already noted, the black hole does not radiate away all of its mass by the time the evaporation reaches its end-point. One should determine how much mass remains by evaluating the emitted energy:

$$E_{rad} = -\varepsilon \int_{-\infty}^{\sigma_{\mathrm{E}}^{-}} \frac{\mathrm{d}\sigma^{-}}{\mathrm{F}^{-}} t_{-}(\hat{\sigma}^{-}) = M + M_{\mathrm{S}_1} - M_{\mathrm{S}_2} - M_0, \tag{3.115}$$

where M is the mass carried by the infalling matter shockwave, M_{S_1} denotes the mass of the initial spacetime of region I, M_{S_2} the mass of the final spacetime of region III, and $M_0 = \mathcal{O}(\varepsilon)$ is the small residual mass of the black hole at the end-point of the evaporation. This remaining mass is expected to be released as an outgoing energy shockwave. Eq. (3.115) is referred to as the energy balance equation.

To verify the internal consistency of this treatment, one has to evaluate the EMT at the $\sigma^{-} = \sigma_{\mathrm{E}}^{-}$ hypersurface and demonstrate explicitly that it contains a term proportional to the Dirac-δ function, with mass equal to M_0. This confirms the presence of an outgoing shockwave originating from the evaporation end-point. One way to show this is to use the "$--$" component of the metric equation and integrate it across the $\sigma^{-} = \sigma_{\mathrm{E}}^{-}$ hypersurface. This procedure is analogous to the one previously used when the spacetime was matched across the infalling shockwave hypersurface in Eq. (3.104).

Chapter 4

Review of the CGHS model

The classical CGHS model [19] is an example of a $2D$ dilaton gravity theory emerging from string theory. We are not be concerned here with the detailed derivation of its action. It can be obtained by dimensionally reducing an extremal magnetically charged black hole. Because the Einstein–Hilbert term in two dimensions is purely topological, gravitational dynamics originates from the interplay between the dilaton, acting as a scalar field, and the spacetime curvature. Furthermore, the model includes matter in the form of N massless scalar fields. The role of these N fields becomes crucial once quantum fluctuations are taken into account. The action of the CGHS model is given by:

$$S_{\text{CGHS}} = \frac{1}{2\pi G}\int \mathrm{d}^2x\sqrt{-g}e^{-2\phi}\left[R + 4\left(\nabla\phi\right)^2 + 4\lambda^2\right] - \frac{1}{2}\sum_{i=1}^{N}\int \mathrm{d}^2x\sqrt{-g}\left(\nabla f_i\right)^2, \tag{4.1}$$

where ϕ denotes the dilaton field, R the Ricci scalar curvature, λ a constant with dimensions of inverse length, and f_i is the one of the N scalar matter fields in the model. The constant G appearing in the first term is the two-dimensional Newton constant. Although it is often set to one or omitted in the literature, we keep it explicit to maintain dimensional consistency. We refer to the first term as S_g (the gravitational action) and the second as S_m (the matter action).

The chapter is organized into five sections. In the first Sec. 4.1, we derive the equations of motion of the model. We then obtain their general solution and impose the static ansatz of Sec. 3.1. Among the resulting configurations, besides the usual linear dilaton vacuum and the static black hole, we study a particular cosmological solution with charged scalar matter fields. The section concludes with the introduction of a dynamical collapse scenario.

In Sec. 4.2, we incorporate quantum fluctuations through the Polyakov–Liouville action (3.72), together with an additional correction term in the action designed to render the resulting equations exactly solvable. We examine how this new term modifies the equations of motion and determine the general static solutions using a symmetric ansatz.

The next Sec. 4.3 is devoted to the BPP model [25], specified by a particular choice of the correction terms. Within the BPP framework, we analyze the linear dilaton vacuum solution, a Minkowski vacuum solution characterized by a vanishing EMT at asymptotic infinity, as well as eternal and evaporating black hole solutions.

The penultimate Sec. 4.4 focuses on the perturbative treatment of the BPP model introduced in Sec. 3.4.1, specifically the quantum-corrected gravitational collapse scenario. Whereas the final Sec. 4.5 discusses the thermodynamical quantities within the classical CGHS model.

4.1 Equations of Motion

By varying the action with respect to the metric $g^{\mu\nu}$ and the dilaton field ϕ, we obtain the corresponding equations of motion:

$$\begin{aligned}
\delta S_g &= \frac{1}{2\pi G}\int \mathrm{d}^2x\sqrt{-g}e^{-2\phi}\Big\{\left(\delta\ln\left(\sqrt{-g}\right)-2\delta\phi\right)\left[R+4\left(\nabla\phi\right)^2+4\lambda^2\right]+\delta R+4\delta\left(\nabla\phi\right)^2\Big\}\\
&= \frac{1}{2\pi G}\int \mathrm{d}^2x\sqrt{-g}e^{-2\phi}\Big\{\left(-\frac{1}{2}g_{\mu\nu}\delta g^{\mu\nu}-2\delta\phi\right)\left[R+4\left(\nabla\phi\right)^2+4\lambda^2\right]\\
&\qquad +R_{\mu\nu}\delta g^{\mu\nu}+g^{\mu\nu}\delta R_{\mu\nu}+4\nabla_\mu\phi\nabla_\nu\phi\delta g^{\mu\nu}+8g^{\mu\nu}\nabla_\nu\phi\nabla_\mu\left(\delta\phi\right)\Big\}\\
&= \frac{1}{2\pi G}\int \mathrm{d}^2x\sqrt{-g}e^{-2\phi}\Big\{\left[-2\left(\left(\nabla\phi\right)^2+\lambda^2\right)g_{\mu\nu}+4\nabla_\mu\phi\nabla_\nu\phi+\cancelto{0}{G_{\mu\nu}}\right]\delta g^{\mu\nu}\\
&\qquad +\underbrace{g^{\mu\nu}\delta R_{\mu\nu}}_{A}-2\left[R+4\left(\nabla\phi\right)^2+4\lambda^2\right]\delta\phi+\underbrace{8g^{\mu\nu}\nabla_\nu\phi\nabla_\mu(\delta\phi)}_{B}\Big\}. \qquad (4.2)
\end{aligned}$$

In the second line, we employed the standard relation for the variation of the metric determinant, $\delta\sqrt{-g}=-\frac{1}{2}\sqrt{-g}g_{\mu\nu}\delta g^{\mu\nu}$, along with $\delta(\nabla\phi)^2=\nabla_\mu\phi\nabla_\nu\phi\delta g^{\mu\nu}+2g^{\mu\nu}\nabla_\nu\phi\nabla_\mu(\delta\phi)$ [106]. Due to the enhanced symmetry of a $2D$ spacetime, the Ricci tensor is proportional to the metric, which makes the Einstein tensor $G_{\mu\nu}=R_{\mu\nu}-\frac{1}{2}Rg_{\mu\nu}$, appearing in the third line, vanish identically. Thus, we are left with simplifying the terms A and B in Eq. (4.2). The term B can be directly simplified via partial integration. Neglecting boundary terms (as they do not influence the equations of motion), we obtain:

$$B=\frac{1}{2\pi G}\int \mathrm{d}^2x\sqrt{-g}e^{-2\phi}\left[-8\Box\phi+16(\nabla\phi)^2\right]\delta\phi. \qquad (4.3)$$

The simplification of term A in Eq. (4.2) is more complex. We begin by evaluating the variation $\delta R_{\mu\nu}$. To this end, let us examine the situation in a locally flat reference frame (where $\Gamma^\rho_{\mu\nu}=0$ but $\partial_\sigma\Gamma^\rho_{\mu\nu}\neq 0$):

$$\delta R_{\mu\nu}=\delta R^\rho{}_{\mu\rho\nu}=\delta\left(\partial_\rho\Gamma^\rho_{\mu\nu}-\partial_\nu\Gamma^\rho_{\rho\mu}-\Gamma^\rho_{\rho\alpha}\Gamma^\alpha_{\mu\nu}-\Gamma^\rho_{\nu\alpha}\Gamma^\alpha_{\mu\rho}\right)=\partial_\rho\left(\delta\Gamma^\rho_{\mu\nu}\right)-\partial_\nu\left(\delta\Gamma^\rho_{\rho\mu}\right). \qquad (4.4)$$

It is well established that Christoffel symbols themselves do not transform as tensor components. However, it is also known that the difference between two Christoffel symbols does behave as a tensor component [106]. Since we are dealing with such a quantity, specifically $\delta\Gamma^\rho_{\mu\nu}$, we are allowed to use the principle of minimal substitution. Consequently, we obtain

$$\delta R_{\mu\nu}=\nabla_\rho\left(\delta\Gamma^\rho_{\mu\nu}\right)-\nabla_\nu\left(\delta\Gamma^\rho_{\rho\mu}\right). \qquad (4.5)$$

Inserting this relation into the expression for A and carrying out a partial integration (discarding boundary terms) leads to:

$$A=\frac{1}{\pi G}\int \mathrm{d}^2x\sqrt{-g}e^{-2\phi}g^{\mu\nu}\left[\nabla_\rho\phi\,\delta\Gamma^\rho_{\mu\nu}-\nabla_\nu\phi\,\delta\Gamma^\rho_{\mu\rho}\right]. \qquad (4.6)$$

Because this quantity is a tensor, it is more convenient to evaluate it in a locally flat reference frame (LFRF). The transformation to such a locally flat reference frame is given by:

$$g_{\mu\nu}\longleftrightarrow\eta_{\mu\nu}\quad\wedge\quad\nabla_\mu\longleftrightarrow\partial_\mu\quad\wedge\quad d^2x\sqrt{-g}\longleftrightarrow d^2x\quad\wedge\quad\partial_\rho g_{\mu\nu}=0\quad\wedge\quad\partial_\sigma\partial_\rho g_{\mu\nu}\neq 0. \qquad (4.7)$$

Therefore, under this transition, the variations of the Christoffel symbols persist, even though the Christoffel symbols themselves vanish. The term A in the locally flat reference frame then takes the following form:

$$\begin{aligned} A\Big|_{\mathrm{LFRF}} &= \frac{1}{\pi G}\int \mathrm{d}^2x e^{-2\phi}\eta^{\mu\nu}\left[\partial_\rho\phi\,\delta\Gamma^\rho_{\mu\nu} - \partial_\nu\phi\,\delta\Gamma^\rho_{\mu\rho}\right] \\ &= \frac{1}{\pi G}\int \mathrm{d}^2x e^{-2\phi}\partial_\rho\phi\left(\eta^{\lambda\nu}\eta^{\rho\mu} - \eta^{\mu\nu}\eta^{\lambda\rho}\right)\partial_\lambda(\delta g_{\mu\nu}) \\ &= \frac{1}{\pi G}\int \mathrm{d}^2x\left(\eta^{\mu\nu}\eta^{\lambda\rho} - \eta^{\lambda\nu}\eta^{\rho\mu}\right)\partial_\lambda\left(e^{-2\phi}\partial_\rho\phi\right)\delta g_{\mu\nu}. \end{aligned} \tag{4.8}$$

In the first line we applied the transition to the LFRF. In the second line we substituted the expressions for the variation of the metric in the LFRF: $\delta\Gamma^\rho_{\mu\nu} = \frac{1}{2}\eta^{\lambda\rho}\left[\partial_\mu(\delta g_{\nu\lambda}) + \partial_\nu(\delta g_{\mu\lambda}) - \partial_\lambda(\delta g_{\mu\nu})\right]$ and simplified the expression. In the third line we applied partial integration. Following the principle of minimal substitution and returning to a general reference frame, as well as using the relation: $\delta g_{\rho\sigma} = -g_{\rho\mu}g_{\sigma\nu}\delta g^{\mu\nu}$ the term A becomes:

$$A = \frac{1}{2\pi G}\int \mathrm{d}^2x\sqrt{-g}\left[-\nabla_\mu\nabla_\nu e^{-2\phi} + g_{\mu\nu}\Box e^{-2\phi}\right]\delta g^{\mu\nu}. \tag{4.9}$$

By substituting back into the expression (4.2) for the variation of the gravitational action S_g, we obtain:

$$\begin{aligned} \delta S_g = \frac{1}{2\pi G}\int \mathrm{d}^2x\sqrt{-g}e^{-2\phi}\Big\{ &\left[2\nabla_\mu\nabla_\nu\phi + \left(2(\nabla\phi)^2 - 2\Box\phi - 2\lambda^2\right)g_{\mu\nu}\right]\delta g^{\mu\nu} \\ &+ \left[-2R + 8(\nabla\phi)^2 - 8\lambda^2 - 8\Box\phi\right]\delta\phi\Big\}. \end{aligned} \tag{4.10}$$

To derive the complete set of equations of motion, one must also vary the matter action S_m with respect to both the metric $g^{\mu\nu}$ and the matter fields f_i. This procedure mirrors the one applied to the gravitational action S_g. As a consequence, we arrive at the following result:

$$\delta S_m = -\sum_{i=1}^{N}\int \mathrm{d}^2x\sqrt{-g}\left\{\frac{1}{2}\left[\nabla_\mu f_i\nabla_\nu f_i - \frac{1}{2}g_{\mu\nu}(\nabla f_i)^2\right]\delta g^{\mu\nu} - (\Box f_i)\,\delta f_i\right\}. \tag{4.11}$$

We observe that the energy–momentum tensor (EMT), given by $T^f_{\mu\nu} \equiv \frac{-2}{\sqrt{-g}}\frac{\delta S_m}{\delta g^{\mu\nu}} = \sum_{i=1}^N T^{(i)}_{\mu\nu}$, coincides with the EMT of massless scalar fields. In this expression, $T^{(i)}_{\mu\nu}$ denotes the EMT corresponding to the i-th particle species, obtained from the action $S^{(i)}_m$ of the associated i-th matter field. Therefore, enforcing Hamilton's principle, $\delta S_{CGHS} = \delta S_g + \delta S_m = 0$, yields the following equations of motion:

$$\begin{aligned} \frac{\delta S}{\delta g^{\mu\nu}} = 0: &\quad \nabla_\mu\nabla_\nu\phi\, e^{-2\phi} + g_{\mu\nu}\left((\nabla\phi)^2 - \Box\phi - \lambda^2\right)e^{-2\phi} = \frac{\pi G}{2}T^f_{\mu\nu}, \\ \frac{\delta S}{\delta\phi} = 0: &\quad \Box\phi = (\nabla\phi)^2 - \lambda^2 - \frac{1}{4}R, \\ \frac{\delta S}{\delta f_i} = 0: &\quad \Box f_i = 0;\ \ \forall i \in \{1, 2, ..., N\} \\ T^{(i)}_{\mu\nu} \equiv \frac{-2}{\sqrt{-g}}\frac{\delta S^{(i)}_m}{\delta, g^{\mu\nu}}: &\quad T^{(i)}_{\mu\nu} = \nabla_\mu f_i\nabla_\nu f_i - \frac{1}{2}g_{\mu\nu}(\nabla f_i)^2\ \ \forall i \in \{1, 2, ..., N\}. \end{aligned} \tag{4.12}$$

Up to this point, we have treated the first term in the CGHS action as the gravitational action, but it can be interpreted in another way. More precisely, it encodes the coupling between the dilaton and the spacetime curvature and can therefore be viewed as the matter action associated with the dilaton. The truly gravitational contribution is instead given by the Einstein–Hilbert action. Since it appears in the field equations as $0 = G_{\mu\nu} \propto T_{\mu\nu}$, we infer that, in two dimensions, the equations of motion reduce to $T_{\mu\nu} = 0$. With this in mind, we can introduce the dilaton energy–momentum tensor:

$$T^{\phi}_{\mu\nu} = \frac{-2}{\sqrt{-g}} \frac{\delta S_g}{\delta g^{\mu\nu}} = -\frac{2}{\pi G} \left[\nabla_\mu \nabla_\nu \phi + \left((\nabla\phi)^2 - \Box\phi - \lambda^2 \right) g_{\mu\nu} \right] e^{-2\phi}. \tag{4.13}$$

We thus find that the equations of motion take the expected form, $T^{\phi}_{\mu\nu} + T^{f}_{\mu\nu} = 0$. This observation will play a crucial role when we later discuss the interpretation of the limit $N \gg 1$ for the matter fields.

4.1.1 General solution of the equations of motion

In this subsection, we proceed to solve the equations of motion (4.12). We adopt light-cone coordinates $x^{\pm} = t \pm x$ and work in the conformal gauge introduced in Chap. 3. Substituting the conformal-gauge metric (3.2) together with the scalar invariants (3.4) into (4.12), we obtain the corresponding equations for ρ and ϕ. Using the identity $\partial_+\partial_- e^{-2\phi} = (-2\partial_+\partial_-\phi + 4\partial_+\phi\,\partial_-\phi)\, e^{-2\phi}$, the equations of motion can be rewritten in the following form:

$$\begin{aligned}
+- : &\quad \partial_+\partial_- e^{-2\phi} + \lambda^2 e^{2(\rho-\phi)} = \pi G T^f_{+-}, && (4.14)\\
\pm\pm : &\quad -\partial_\pm^2 e^{-2\phi} + 4\partial_\pm\phi\partial_\pm(\phi-\rho) e^{-2\phi} = \pi G T^f_{\pm\pm}, && (4.15)\\
\phi : &\quad \partial_+\partial_- e^{-2\phi} - 2\partial_+\partial_-(\phi-\rho) e^{-2\phi} + \lambda^2 e^{2(\rho-\phi)} = 0, && (4.16)
\end{aligned}$$

where the first two equations follow from the metric equation, while the third is derived from the dilaton field equation. Since $T^{(i)}_{+-} = 0$ for massless scalar matter fields and $T^{(i)}_{\pm\pm} = (\nabla_\pm f_i)^2$, Eqs. (4.14) and (4.16) can be combined to yield:

$$\partial_+\partial_-(\phi - \rho) = 0, \tag{4.17}$$

whose general solution takes the form:

$$2(\rho - \phi) = \omega_-(x^-) + \omega_+(x^+) \tag{4.18}$$

where ω_+ and ω_- denote arbitrary functions of a single variable. We can now insert this expression back into Eq. (4.14). Doing so gives:

$$e^{-2\phi} = -\lambda^2 \int \mathrm{d}x^- e^{\omega_-} \int \mathrm{d}x^+ e^{\omega_+} + F_+(x^+) + F_-(x^-), \tag{4.19}$$

where $F_\pm(x^\pm)$ constitute another set of arbitrary single-variable functions. We now transition to the $y^\pm$ coordinates, which offer a more suitable description while maintaining the conformal gauge, defined by $\frac{dy^\pm}{dx^\pm} = e^{\omega_\pm}$, leading to the following form of the metric:

$$ds^2 = \frac{dy^+ dy^-}{-\lambda^2 y^+ y^- + F_+(y^+) + F_-(y^-)}. \tag{4.20}$$

Using Eq. (4.19), we can readily determine $e^{-2\phi}$ as follows:

$$e^{-2\phi} = -\lambda^2 y^+ y^- + F_+(y^+) + F_-(y^-). \tag{4.21}$$

In this way, we have demonstrated that one can choose coordinates such that $\rho = \phi$. This particular choice is referred to as the Kruskal gauge condition, as it is directly connected to the Kruskal coordinates appearing in the Schwarzschild solution (see App. C.3). From this point onward, we work in the Kruskal gauge. Moreover, instead of denoting the coordinates by $y^\pm$, we use $x^\pm$ to represent the Kruskal coordinates. The remaining task is to solve Eq. (4.15), which simplifies to:

$$\frac{d^2 F_\pm}{dx^{\pm 2}} = -\pi G T^f_{\pm\pm}(x^\pm), \tag{4.22}$$

which leads to the following form of the functions $F_\pm$ expressed in terms of the given EMT:

$$F_\pm(x^\pm) = -\pi G \int \mathrm{d}x^\pm \int \mathrm{d}x^\pm T^f_{\pm\pm}(x^\pm) + a_\pm x^\pm + \frac{b}{2}. \tag{4.23}$$

where $a_\pm$ and b are arbitrary constants. From Eq. (4.22), it follows that $T^f_{\pm\pm}$ can depend only on $x^\pm$. By inspecting the matter field equations from Eq. (4.12), we confirm that this requirement is indeed fulfilled:

$$\Box f_i = 0 \Longrightarrow \partial_+\partial_- f_i = 0 \implies f_i = f_{i+}(x^+) + f_{i-}(x^-) \implies T^{(i)}_{\pm\pm}(x^\pm) = \left(\frac{df_{i\pm}}{dx^\pm}\right)^2. \tag{4.24}$$

Therefore, the general solution of the equations of motion in the Kruskal gauge is given by:

$$e^{-2\phi} = -\lambda^2 x^+ x^- - \pi G \int \mathrm{d}x^+ \int \mathrm{d}x^+ T_{++} - \pi G \int \mathrm{d}x^- \int \mathrm{d}x^- T_{--} + a_+ x^+ + a_- x^- + b. \tag{4.25}$$

In this setup, the geometry is characterized by three constants, $a_\pm$ and b, together with the EMT of the matter fields, $T^f_{\pm\pm}(x^\pm)$. In the absence of matter, the constants $a_\pm$ can be eliminated by an appropriate change of coordinates, $x^\pm \mapsto x^\pm - \frac{a_\mp}{\lambda^2}$. Depending on this choice, we obtain various distinct solutions, i.e. different geometries. It should be remembered that all of this has been formulated in the Kruskal gauge. If required, we can easily switch to other coordinate systems.

4.1.2 Applying the static ansatz setup

In the preceding subsection, we described the standard procedure for solving the CGHS equations of motion in the Kruskal gauge. We now instead employ the symmetric ansatz introduced in Sec. 3.1, which is obtained by imposing the presence of a time-like Killing vector. In this setup, the natural length scale is determined by λ, implying $L = 1/\lambda$, and the reduced field defined in Eq. (3.7) becomes $\mathrm{x} = e^{-\phi}$. By rewriting the metric equation using Eq. (3.8) for the metric function Λ, together with Eq. (3.13), we obtain:

$$\frac{\mathcal{D}}{4\Lambda}\left[\frac{\mathrm{d}}{\mathrm{dx}}\left(\mathrm{x}^2\mathcal{D}\frac{\mathrm{d}\Lambda}{\mathrm{dx}}\right)\xi_\mu\xi_\nu - \left(\frac{\mathrm{d}}{\mathrm{dx}}\left(\mathrm{x}^2\mathcal{D}\frac{\mathrm{d}\Lambda}{\mathrm{dx}}\right) + 4\mathrm{x}^2\Lambda\frac{\mathrm{d}}{\mathrm{dx}}\left(\frac{\mathcal{D}}{\mathrm{x}}\right)\right)\varepsilon_{\mu\rho}\varepsilon_{\nu\sigma}\xi^\rho\xi^\sigma\right] = \frac{\pi G}{2\lambda^2}T^f_{\mu\nu}, \tag{4.26}$$

where we have employed the auxiliary relations (3.32) and (3.33) for the scalar invariants $\Box\mathrm{x}$ and $(\nabla\mathrm{x})^2$, respectively, as well as Eqs. (3.24) and (3.29) for the covariant derivative of the Killing vector and the scalar curvature. This equation implies that the only non-zero components of the EMT are the one aligned with the Killing vector, $T^{\|\|}$, and the one orthogonal to it, $T^{\perp\perp}$, while all mixed components vanish. Similarly, for the dilaton equation one gets:

$$\mathcal{D}\frac{\mathrm{d}}{\mathrm{dx}}\left(\Lambda\mathcal{D}\right)+\mathrm{x}+\frac{\mathrm{x}}{4}\mathcal{D}\frac{\mathrm{d}}{\mathrm{dx}}\left(\mathcal{D}\frac{\mathrm{d}\Lambda}{\mathrm{dx}}\right)=0. \tag{4.27}$$

Since the matter field are massless scalar fields, we can use the fact that their EMT is traceless in two dimensions. Thus, taking the trace of the metric Eq. (4.26) gives:

$$\frac{\mathrm{d}}{\mathrm{dx}}\left(\mathrm{x}^2\mathcal{D}\frac{\mathrm{d}\Lambda}{\mathrm{dx}}\right)+2\mathrm{x}^2\Lambda\frac{\mathrm{d}}{\mathrm{dx}}\left(\frac{\mathcal{D}}{\mathbf{x}}\right)=0. \tag{4.28}$$

This equation is integrable, resulting into:

$$\frac{1}{2}\mathcal{D}\frac{\mathrm{d}\Lambda}{\mathrm{dx}}+\frac{\Lambda\mathcal{D}}{\mathrm{x}}=C, \tag{4.29}$$

where C is an integration constant. This equation can be regarded as a solution for $\mathcal{D}$. Substituting this solution into the dilaton Eq. (4.27) we once again get an integrable equation, the solution being as follows:

$$\Lambda\mathrm{x}^2+C\mathrm{x}\Lambda\mathcal{D}=\mu, \tag{4.30}$$

where μ is another integration constant. Combining Eqs. (4.29) and (4.30) results into a differential equation for Λ whose solution is:

$$\Lambda\mathrm{x}^2-\mu\ln\left|\Lambda\mathrm{x}^2\right|=b-C^2\mathrm{x}^2, \tag{4.31}$$

where yet another integration constant b is introduced. Next, we compute the tortoise coordinate (3.18). Direct calculation, yields

$$\lambda\sigma=-\frac{1}{2C}\ln\left|\Lambda\mathrm{x}^2\right|. \tag{4.32}$$

Finally, one has to enforce the constraints (3.22) for the asymptotical flat solution at infinity. Taking the limit $\mathrm{x}\to\infty$ of Eq. (4.31), gives $\Lambda\to-C^2$, implying that $C=\pm1$. Then, from Eq. (4.32) we deduce that $C=-1$, by demanding that $\sigma\to+\infty$ in this limit. Hence, the solution in the asymptotically flat coordinates depends on two constants b and μ and is given by:

$$\Lambda=\begin{cases}-\dfrac{1}{1+(b+2\mu\lambda\sigma)e^{-2\lambda\sigma}}, & \Lambda<0,\\ -\dfrac{1}{1-(b+2\mu\lambda\sigma)e^{-2\lambda\sigma}}, & \Lambda>0,\end{cases}\qquad \mathrm{x}=\begin{cases}\sqrt{b+2\mu\lambda\sigma+e^{2\lambda\sigma}}, & \Lambda<0,\\ \sqrt{b+2\mu\lambda\sigma-e^{2\lambda\sigma}}, & \Lambda>0.\end{cases} \tag{4.33}$$

Next, we compute the components of the EMT by substituting this solution into Eq. (4.26). This gives:

$$\Lambda^2T^{\|\|}=\Lambda^2T^{\perp\perp}=\frac{2\mu\lambda^2}{\pi G}. \tag{4.34}$$

In contrast, evaluation of the components of the EMT using the scalar field f and the equation of motion for the i-th field yields the following.

$$T^{\|\|}=T^{\perp\perp}=\frac{\lambda^2}{2}\sum_{i=1}^{N}\left(\mathcal{D}\frac{\mathrm{d}f_i}{\mathrm{dx}}\right)^2,\quad \frac{\mathrm{d}}{\mathrm{dx}}\left(\Lambda\mathcal{D}\frac{\mathrm{d}f_i}{\mathrm{dx}}\right)=0. \tag{4.35}$$

Hence, the physical interpretation of the constant $\mu>0$ is that it is some type of a charge carried by the matter fields. Since the Eq. (4.31) is transcendental when $\mu\neq0$, we cannot write down the explicit expression for Λ in terms of x.

4.1.3 Static vacuum solutions

In this subsection, we examine the static vacuum solution, defined by the condition $T^f_{\mu\nu} = 0$, which holds when $\mu = 0$, as can be seen from Eq. (4.34). From Eq. (4.31) it follows that $\mathcal{D} = \mathrm{x}$, and Eq. (4.32) provides an expression for Λ solely as a function of x, namely:

$$\Lambda = \frac{b}{\mathrm{x}^2} - 1, \quad \mathcal{D} = \mathrm{x}, \quad 2\lambda\sigma = \ln\left|b - \mathrm{x}^2\right|, \tag{4.36}$$

where the last expression determines the tortoise coordinate (4.32). There are three possible scenarios depending on the sign of the constant b. To see if this solution possesses any singularity, we compute the scalar curvature. Using Eq. (3.29) we obtain:

$$R = \frac{4\lambda^2 b}{\mathrm{x}^2}. \tag{4.37}$$

It is now evident that as long as $b \neq 0$ there is a singularity at $\mathrm{x_S} = 0$. When $b = 0$, we have $\Lambda = -1$ throughout the entire spacetime and $R = 0$, so the geometry is simply flat Minkowski spacetime. For $b \neq 0$, in order to determine whether the solution describes a black hole or a naked singularity, we must check for the presence of an event horizon. The event horizon is defined as the hypersurface on which the time-like Killing vector becomes null, i.e., where $\Lambda = 0$. If $b < 0$, then $\Lambda < 0$ everywhere, indicating that no event horizon exists. Conversely, for $b > 0$, imposing $\Lambda = 0$ gives $\mathrm{x_H} = \sqrt{b}$. It is therefore clear that in this case the solution corresponds to a static black hole. Hence, the solutions can be classified according to the sign of the constant b as follows:

- $b = 0$: Flat Minkowski spacetime,
- $b < 0$: Naked singularity,
- $b > 0$: Static black hole.

The cosmic censorship conjecture rules out the formation of naked singularities, which in turn requires that the constant b be nonnegative. Now we examine each of the two allowed cases in detail.

Linear dilaton vacumm

Within the CGHS model, the vacuum configuration is referred to as the linear dilaton vacuum. This terminology stems from the fact that, for $b = 0$, the dilaton field ϕ depends linearly on the spatial coordinate σ. Explicitly, the solution is

$$\mathrm{d}^2 s = -\mathrm{d}t^2 + \mathrm{d}\sigma^2, \quad \phi = -\lambda\sigma, \tag{4.38}$$

and it arises as the limit $b \to 0$ of the general static vacuum solution (4.36). This solution exhibits the full two-dimensional Poincaré symmetry, meaning that, in addition to the Killing vector ∂_t, there are two more Killing vectors: ∂_σ corresponding to spatial translations, and $L = \sigma\partial_t + t\partial_\sigma$ corresponding to Lorentz boosts.

Static black hole

This scenario corresponds to a choice $b > 0$ in the general static solution (4.36). As mentioned before, the event horizon is $\mathrm{x_H} = \sqrt{b}$, while the singularity is $\mathrm{x_S} = 0$. The two extra Killing vectors vanish, leaving only the Killing vector of time translations. Transitioning to the Eddington-Finkelstein coordinates, similarly to the general solution of the CGSH model with matter (4.33), we get:

$$\Lambda = \begin{cases} -\dfrac{1}{1+be^{-2\lambda\sigma}}, & \Lambda < 0, \\ -\dfrac{1}{1-be^{-2\lambda\sigma}}, & \Lambda > 0, \end{cases} \qquad \mathrm{x} = \begin{cases} \sqrt{b+e^{2\lambda\sigma}}, & \Lambda < 0, \\ \sqrt{b-e^{2\lambda\sigma}}, & \Lambda > 0. \end{cases} \tag{4.39}$$

In this coordinate system, the horizon is shifted to infinity, that is, $\sigma_H = -\infty$. Consequently, the two cases in Eq. (4.39) represent two coordinate charts that are joined along the event horizon hypersurface located at infinity. The singularity is still determined by $\mathrm{x}_S = 0$, which gives $b = e^{2\lambda\sigma}$ in Eddington-Finkelstein coordinates.

To construct the maximally extended black hole solution, as in the Schwarzschild case, we need to switch to Kruskal coordinates (see App. D.5). Our first task is to determine the surface gravity at the horizon:

$$\kappa = \frac{\lambda}{2}\left|\mathcal{D}\frac{\mathrm{d}\Lambda}{\mathrm{dx}}\right|_{\mathrm{H}} = \lambda, \tag{4.40}$$

accordingly, the Kruskal coordinates follow from exponentiating the Eddington–Finkelstein coordinates using the surface gravity, that is:

$$|\lambda x^+| = e^{\lambda\sigma^+} \quad \wedge \quad |\lambda x^-| = e^{-\lambda\sigma^-}, \tag{4.41}$$

where the signs of $x^\pm$ determine four patches connected by the event horizon. In all four patches, the metric and the dilaton exhibit the same form:

$$ds^2 = -\frac{\mathrm{d}x^+\mathrm{d}x^-}{-\lambda^2x^+x^- + b}, \qquad e^{-2\phi} = -\lambda^2x^+x^- + b. \tag{4.42}$$

As anticipated, in Kruskal coordinates we have $\phi = \rho$. This solution coincides with the general solution (4.33) once the condition of a vanishing EMT is enforced (along with $a_\pm = 0$).

The transformation (4.41) divides the spacetime into four distinct regions, classified according to the signs of the Kruskal coordinates $x^\pm$. As an illustration, region III is characterized by $x^+ < 0$ and $x^- < 0$. Collectively, these four regions serve as coordinate charts that together constitute an atlas for the spacetime manifold. In practical applications, one typically focuses on region I and, in some cases, region II. Region I describes the exterior of the black hole and directly corresponds to the $\Lambda < 0$ case in Eq. (4.36), whereas region II describes the black hole interior, where the Killing vector is space-like, i.e. $\Lambda > 0$.

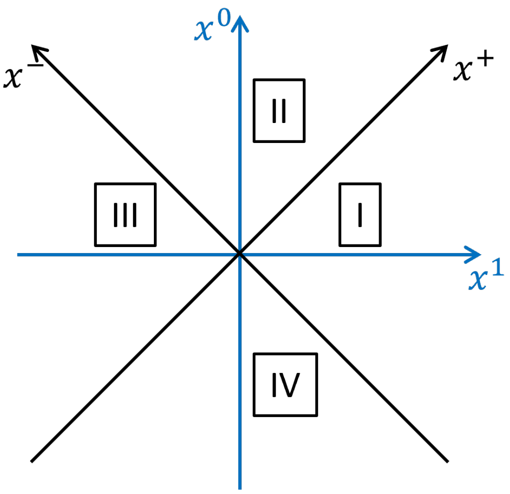

Figure 4.1: Different patches of the spacetime

We now examine the coordinate curves $t =$ const. and $\sigma =$ const. in Kruskal coordinates:

$$t = c: \frac{x^+}{x^-} = e^{2\lambda t} \implies x^+ = c\,x^-,$$
$$\sigma = c: \lambda^2 x^+ x^- = \pm e^{2\lambda\sigma} \implies x^+ x^- = c.$$

In Fig. 4.2, the $t =$ const. curves are plotted in red, whereas the $\sigma =$ const. curves appear in blue. The Killing horizons (i.e., the event horizons) lie at $\sigma \to -\infty$ and are drawn in green. Singularities occur in regions I and IV of Fig. 4.1, specified by the relation $\lambda^2 x^+ x^- = b$, i.e. $2\lambda\sigma = \ln b$, and are indicated in the figure by a black wavy line.

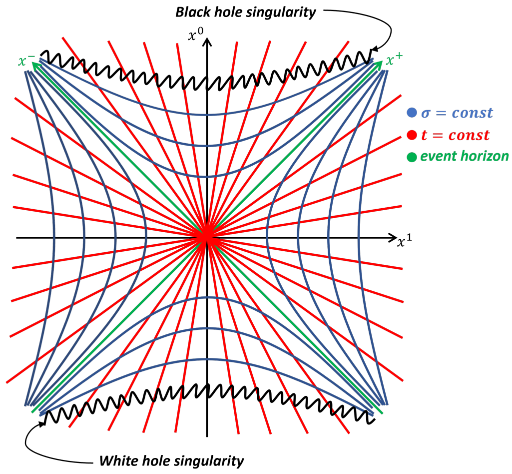

Figure 4.2: Kruskal diagram in CGHS model

We observe that the resulting diagram is completely analogous to the Kruskal diagram of the Schwarzschild solution (see App. C.3). Consequently, the corresponding conformal diagrams also match (see App. C.4). Even the singularity is described by the same functional relation $x^+ = x^+(x^-)$. We now proceed to identify the standard black-hole (t, r) coordinates, in which the metric assumes the following form:

$$ds^2 = -l(r)dt^2 + \frac{dr^2}{l(r)} \implies \frac{dr}{d\sigma} = \frac{1}{1 \pm be^{-2\lambda\sigma}} \implies e^{2\lambda r} = C\left(e^{2\lambda\sigma} \pm b\right). \tag{4.43}$$

We note that the $\pm$ signs in these expressions determine whether the solution is defined in quadrants I and II or in quadrants III and IV, respectively. Enforcing the condition $r = r_H$ at the horizon leads to $C = \pm\frac{e^{2\lambda r_H}}{b}$. Thus, for $l(r)$ we find:

$$l(r) = 1 - e^{-2\lambda(r-r_H)}, \quad 2\lambda\sigma = \ln\left[\pm b\left(e^{2\lambda(r-r_H)} - 1\right)\right]. \tag{4.44}$$

The singularity is located at:

$$r_S = r_H + \frac{1}{2\lambda}\ln b. \tag{4.45}$$

As in the Schwarzschild case, regions I and II are both represented by the same metric in the (t, r) coordinate system. Spacetime terminates at the value of the radial coordinate r associated with the singularity. The domain $r > r_H$ represents region I in Fig. 4.1, while $r < r_H$ denotes region II. Moreover, the dilaton reduces to a linear function of r, namely:

$$\phi = -\frac{1}{2}\ln b - \lambda(r - r_H). \tag{4.46}$$

We still have to clarify the physical interpretation of the constant b, namely how it relates to the black hole mass. Although one could determine this using the ADM formalism, we will not adopt that approach here. Instead, we will deduce the form of this relation from the dynamical setup introduced in the following subsection.

4.1.4 Cosmological solution with charged matter

In this subsection, we examine the general static solution (4.90) in the case where the matter charged with $\mu \neq 0$. The event horizon is defined by the condition $\Lambda = 0$. From Eq. (4.31) we infer that, as long as $\mu \neq 0$, there is no finite value of x that satisfies this condition. Let us first consider the case $\Lambda < 0$. Attempting to determine the apparent horizon from $\partial_+ \mathrm{x}^2 = 0$ leads to the equation $\mu + e^{2\lambda\sigma} = 0$. Since $\mu > 0$, this equation admits no solutions. The curvature scalar is given by

$$R = 4\lambda^2 \left[\left(\frac{e^{2\lambda\sigma} + \mu}{b + 2\mu\lambda\sigma + e^{2\lambda\sigma}} \right)^2 - 1 \right]. \tag{4.47}$$

It is evident that the curvature diverges along the hypersurface $\mathrm{x} = 0$. This equation always admits a solution for a negative value of the coordinate σ. Consequently, this configuration describes a naked singularity and is therefore excluded by the cosmic censorship conjecture.

For $\Lambda > 0$ we are effectively looking for the cosmological solution. The first order of business is to determine under which conditions $\Lambda > 0$ holds. This is the case when:

$$e^{2\lambda\sigma} \leqslant b + 2\mu\lambda\sigma. \tag{4.48}$$

For a fixed value of μ, with $\mu > 0$, there is a critical value of b above which the inequality admits a solution. In Fig. 4.3 we plot the functions $f(x) = e^x$ and $g_b(x) = b + \mu x$, where $x = 2\lambda\sigma$. For sufficiently small b, a solution does not always exist. As b increases, one reaches a critical point at which $g_b(x)$ becomes tangent to $f(x)$. Differentiating Eq. (4.48), we obtain $2\lambda\sigma_{cr} = \ln \mu$. Substituting this back into Eq. (4.48) yields the condition on b:

$$b \geqslant \mu \left(1 - \ln \mu\right). \tag{4.49}$$

For $\mu > e$, this inequality is automatically fulfilled for any positive b.

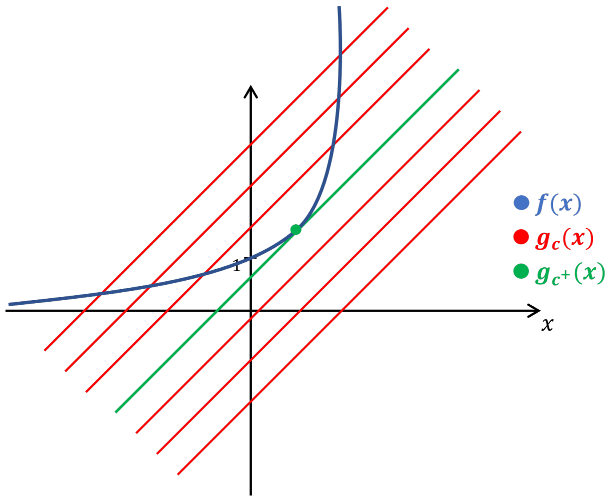

Figure 4.3: Graphical solution to inequality (4.48)

Now assume that condition (4.49) holds. As illustrated in Fig. 4.3, inequality (4.48) admits two critical values, denoted by σ_1 and σ_2. Because $\Lambda > 0$, the Killing vector ξ is space-like, which means that σ plays the role of a time coordinate. We therefore relabel it as $\sigma \mapsto \tau$. The metric then takes the form

$$\mathrm{d}s^2 = \frac{-\mathrm{d}\tau^2 + \mathrm{d}r^2}{(b + 2\mu\lambda\tau)e^{-2\lambda\tau} - 1}, \tag{4.50}$$

which can be cast into the standard cosmological form $\mathrm{d}s^2 = -\mathrm{d}t^2 + a(t)^2 \mathrm{d}r^2$, where the new time coordinate t and the derivative of the scale factor $a = \sqrt{\Lambda}$, namely $\dot{a}(t)$, are given by

$$t = \int \frac{\mathrm{d}\tau}{\sqrt{(b + 2\mu\lambda\tau)e^{-2\lambda\tau} - 1}}, \qquad \dot{a}(t) = \lambda \frac{b - \mu + 2\mu\lambda\tau}{\left((b + 2\mu\lambda\tau)e^{-2\lambda\tau} - 1\right)^{3/2}} e^{-2\lambda\tau}. \tag{4.51}$$

From this expression we observe that $\dot{a}(t) < 0$ for $\tau_1 < \tau < \frac{b-\mu}{2\lambda\mu}$, and $\dot{a}(t) > 0$ for $\frac{b-\mu}{2\lambda\mu} < \tau < \tau_2$. Hence, the universe undergoes a contraction phase with $\dot{a}(t) > 0$ until the moment $\tau = \frac{b-\mu}{2\lambda\mu}$, after which it begins to expand to infinity. The curvature becomes singular at both endpoints, so this solution corresponds to a universe that originates as an infinite universe at $\tau = \tau_1$ and terminates in a big rip at $\tau = \tau_2$, once again diverging to infinity.

4.1.5 Dynamical solution and gravitational collapse

In this section, we consider the dynamical solution of the equations of motion (4.14-4.16), closely following the method described in Sec. 3.4. The overall setup is illustrated in Fig. 3.2. The matter content is represented by an infalling shockwave localized on the hypersurface $x^+ = x_0^+$. We begin by re-deriving Eq. (3.104) within this framework. Because both ϕ and ρ must remain continuous throughout spacetime, as required by Eq. (3.102), the derivatives $\partial_+\phi$ and $\partial_+\rho$ do not contain contributions proportional to the Dirac δ-function. Integrating the equations across the shockwave then yields:

$$\partial_+ e^{-2\phi}\Big|_{>}^{<} = \frac{\pi G M}{\mathrm{F}^+(x_0^+)}. \tag{4.52}$$

Using the ansatz for the derivative of the dilaton (3.13), together with the general static vacuum solution (4.36), we find:

$$2\mathrm{x}\frac{\lambda}{2}\mathrm{F}^-\mathcal{D}e^{2\rho}\Big|_{<}^{>} = \frac{\pi G M}{\mathrm{F}^+(x_0^+)} \quad\Longrightarrow\quad \Lambda\mathrm{x}^2\Big|_{<}^{>} = \frac{\pi G M}{\lambda} \quad\Longleftarrow\quad b_> - b_< = \frac{\pi G M}{\lambda}. \tag{4.53}$$

Imposing continuity of the metric then determines the jump in the function F^-:

$$\frac{\Lambda_{\mathrm{I}}}{\mathrm{F}^-_{\mathrm{I}}} = \frac{\Lambda_{\mathrm{II}}}{\mathrm{F}^-_{\mathrm{II}}} \quad\Longrightarrow\quad \mathrm{F}^-_{\mathrm{II}} = \mathrm{F}^-_{\mathrm{I}}\frac{b_> - \hat{\mathrm{x}}^2}{b_< - \hat{\mathrm{x}}^2} \quad\Longrightarrow\quad \mathrm{F}^-_{\mathrm{II}} = \mathrm{F}^-_{\mathrm{I}}\left(1 + \frac{\frac{\pi G M}{\lambda}}{b_< - \hat{\mathrm{x}}^2}\right), \tag{4.54}$$

where we have introduced the coordinate $\hat{\mathrm{x}}$ defined in Eq. (3.107). Hence, the general discontinuity of the solution when crossing the shockwave hypersurface is described by the following relation:

$$\left(\mathrm{F}^+, \mathrm{F}^-, b\right) \mapsto \left(\mathrm{F}^+, \mathrm{F}^-\left(1 + \frac{\frac{\pi G M}{\lambda}}{b - \hat{\mathrm{x}}^2}\right), b + \frac{\pi G M}{\lambda}\right). \tag{4.55}$$

This equation shows how the solution evolves when an additional mass M is added to the total mass of the black hole. The gravitational collapse corresponds to a scenario in which the initial spacetime is the linear dilaton vacuum, specified by $(-1, 1, 0)$, expressed in Eddington–Finkelstein coordinates. The subsequent transition to a black hole solution in region II of the spacetime is then:

$$(-1, 1, 0) \mapsto \left(-1, 1 - \frac{\pi G M}{\lambda}\frac{1}{\hat{\mathrm{x}}^2}, \frac{\pi G M}{\lambda}\right). \tag{4.56}$$

At this stage, the physical relation between the constant b and the black hole mass becomes clear: $b = \frac{\pi G M}{\lambda}$. The final step in the computation is to write down the explicit form of the dilaton field in the $(\delta, \hat{\mathrm{x}})$ coordinate system. In region II of spacetime, the solution takes the form:

$$\Lambda = \frac{\pi G M}{\lambda}\frac{1}{\mathrm{x}^2} - 1, \qquad \mathcal{D} = \mathrm{x}, \qquad \ln\left|b - \mathrm{x}^2\right| = -2\ln\delta + \ln\left|b - \hat{\mathrm{x}}^2\right|. \tag{4.57}$$

From this relation, it is immediately evident that at the shockwave hypersurface $\delta = 1$, we recover the expected identity $\mathrm{x} = \hat{\mathrm{x}}$.

We now rewrite the solution in terms of the Kruskal coordinates (4.41). A straightforward calculation gives:

$$e^{-2\phi} = e^{-2\rho} = -\lambda^2 x^+\left(x^- + \frac{\pi G M}{\lambda^3 x_0^+}\right) + \frac{\pi G M}{\lambda}. \tag{4.58}$$

Conversely, substituting $T_{++} = \frac{M}{\lambda x_0^+}\delta(x^+ - x_0^+)$, together with $\mathrm{F}^+(x_0^+) = -\lambda x_0^+$, into the general CGHS solution (4.81) and then carrying out the integration reproduces the same result, provided that continuity of both the metric and the dilaton field is enforced. For later convenience, we also define the notation $\Delta = \frac{\pi G M}{\lambda^3 x_0^+}$.

Using the coordinate transformations in region II of the spacetime (4.56), we directly calculate the new Eddington-Finkelstein coordinates in region II of the spacetime:

$$\lambda x^+ = e^{\lambda \hat{\sigma}^+} \quad \wedge \quad \lambda(x^- + \Delta) = -e^{-\lambda \hat{\sigma}^-}. \tag{4.59}$$

Inserting these expressions into the solution (4.58), we can immediately confirm that the solution depends solely on the coordinate $\hat{\sigma}$. Therefore, the solution is genuinely static within region II of the spacetime. It should be kept in mind, however, that although the solutions in each of the two spacetime regions are static, the spacetime as a whole does not possess a time-translation symmetry.

To obtain the Penrose diagram, we switch to compactified coordinates. The transformation that produces the required form is:

$$\lambda x^+ = \frac{\pi M G}{\lambda^2 \Delta} \tan y^+ \qquad \wedge \qquad \lambda\left(x^- + \Delta\right) = \lambda \Delta \tan y^-. \tag{4.60}$$

Under this transformation, the point x_0^+ is mapped to $y_0^+ = \frac{\pi}{4}$. In these new coordinates, the metric takes the form:

$$\mathrm{d}s^2 = \begin{cases} \dfrac{\mathrm{d}y^+ \mathrm{d}y^-}{\lambda^2 \cos^2 y^+ \cos^2 y^- \tan y^+ \left(\tan y^- - 1\right)}, & y^+ < \dfrac{\pi}{4} \\[2ex] \dfrac{\mathrm{d}y^+ \mathrm{d}y^-}{\lambda^2 \cos^2 y^+ \cos^2 y^- \left(\tan y^+ \tan y^- - 1\right)}, & y^+ > \dfrac{\pi}{4} \end{cases} \tag{4.61}$$

In Fig. 4.4, the conformal diagram of the dynamical black hole is displayed. The singularity is specified by $\tan y^+ \tan y^- = 1$, i.e. $y^+ + y^- = \frac{\pi}{2}$, and is depicted as the black wavy line. The infalling matter is shown as the red arrowed curve. The hypersurfaces $i^\pm$ denote future and past timelike infinity (in red), while i^0 represents spatial infinity (in blue). The hypersurfaces $\mathcal{J}^\pm$ correspond to future and past null infinity (in green). The spacetime boundary is drawn as a solid black line. In region II, the event horizon is present, indicated by the solid blue line and given by $x_\mathrm{H}^- = -\Delta$. This expression follows from extremizing the two-dimensional area of a sphere, namely by imposing $\partial_+ e^{-2\phi} = 0$ (see Sec. 3.4). We find that the apparent horizon and the event horizon are identical.

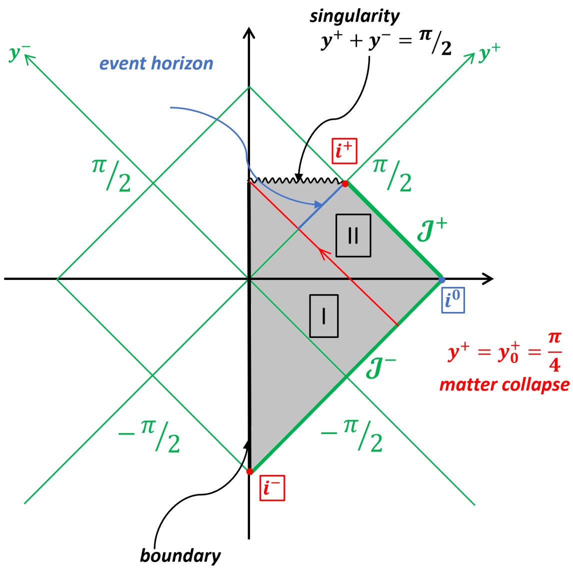

Figure 4.4: Penrose diagram of the dynamical scenario

This configuration does not describe an evaporating black hole. Indeed, the apparent horizon and the singularity meet at future time infinity i^+. Moreover, in region II of the spacetime, the fields are independent of the new time coordinate. To obtain a genuinely evaporating black hole solution, quantum corrections must be taken into account. For more details, see Sec. 3.4.

4.2 Adding quantum fluctuations

In this section, we incorporate quantum corrections into the classical CGHS model. Gravity is kept classical, while the scalar matter fields are quantized via the Polyakov–Liouville action (3.72). Further details on the quantization procedure for the scalar fields are provided in Sec. 3.3. Thus, we work within the semiclassical framework of quantum field theory on a fixed classical background geometry [26, 25]:

The central objective of these toy models is to obtain exactly solvable equations of motion that still capture the essential qualitative features of the system. The full CGHS action supplemented only with the PL term is not exactly solvable. For this reason, we introduce an additional correction term in the action, denoted by S_{cor}, which depends exclusively on the dilaton and the geometry. The complete action then takes the form:

$$S_{\text{QC}} = S_g[g,\phi] + S_m[g,f_i] + NS_{\text{PL}}[g,\psi] + S_{\text{cor}}[g,\phi]. \tag{4.62}$$

The first two contributions reproduce the classical CGHS model (4.1). Since S_{PL} is independent of the detailed structure of the matter fields, it is simply multiplied by N when there are N distinct matter fields. In two-dimensional models, the equations of motion reduce to the condition $T_{\mu\nu} = 0$, so we obtain:

$$T^{\phi}_{\mu\nu} + \Delta T^{\phi}_{\mu\nu} + T^{f,cl}_{\mu\nu} + N < \Delta T^{f}_{\mu\nu} >= 0, \tag{4.63}$$

where the various energy–momentum tensors are defined as follows:

$$T^{\phi}_{\mu\nu} = \frac{-2}{\sqrt{-g}}\frac{\delta S_g}{\delta g^{\mu\nu}},\quad \Delta T^{\phi}_{\mu\nu} = \frac{-2}{\sqrt{-g}}\frac{\delta S_{cor}}{\delta g^{\mu\nu}},\quad T^{f,cl}_{\mu\nu} = \frac{-2}{\sqrt{-g}}\frac{\delta S_m}{\delta g^{\mu\nu}},\quad \langle \Delta T^{f}_{\mu\nu}\rangle = \frac{-2}{\sqrt{-g}}\frac{\delta S_{PL}}{\delta g^{\mu\nu}}. \tag{4.64}$$

The correction term S_{corr} can be interpreted as a classical modification of the original CGHS model; consequently, the EMT derived from this part of the action is labeled $\Delta T^{\phi}_{\mu\nu}$. We do not interpret this contribution as a quantum effect. In contrast, the only genuine quantum contributions stem from the Polyakov–Liouville term, so the corresponding EMT is written as $\langle \Delta T^{f}_{\mu\nu}\rangle$. Hence, the total EMT of the matter fields is:

$$T^{f}_{\mu\nu} = T^{f,cl}_{\mu\nu} + \langle \Delta T^{f}_{\mu\nu}\rangle\,. \tag{4.65}$$

Since the correction term must cancel the part of the PL action that renders the equations of motion not exactly solvable, it must scale as $N\hbar$. This creates an apparent tension: the correction term is intended to be classical, yet it is proportional to $\hbar$. To resolve this, let us consider a very large number of matter fields. In that case, the combination $N\hbar$ can be treated as a constant of the same order as $\frac{1}{2\pi G}$. Thus, we need not view it as a small quantum correction, but instead as a finite constant. Since the overall factor in front of the correction term can be chosen as an arbitrary constant that is not intrinsically of order $\hbar$, we are free to set it equal to the constant $N\hbar$.

Due to this correction term, the dilaton field equation of motion is modified as well and takes the following form:

$$\frac{\delta S_g}{\delta\phi} + \frac{\delta S_{corr}}{\delta\phi} = 0. \tag{4.66}$$

4.2.1 The correction term in the action

Here we examine which forms of the correction term in the action can make the equations of motion exactly solvable. While the main body of this work focuses on the BPP model, we introduce here a more general expression for the correction term. It is given by [26, 25]:

$$S_{cor} = \frac{N\hbar}{2\pi} \int \mathrm{d}^2x\sqrt{-g}\left[-C_1\phi R + \frac{C_2}{12}\left(\nabla\phi\right)^2\right], \tag{4.67}$$

where C_1 and C_2 are free parameters whose specific values determine the particular model. In the next section, we demonstrate how to choose these constants so that the resulting model possesses exactly solvable equations of motion. For the moment, we simply note which choices correspond to the most relevant models, namely the RST [23, 24] and BPP [25] models.

- **BPP model**: $C_1 = \frac{1}{12} \quad \wedge \quad C_2 = 1$
- **RST model**: $C_1 = \frac{1}{24} \quad \wedge \quad C_2 = 0$

By explicitly solving the equations of motion in detail, we can see why the constants are fixed in exactly this way. In this section, we keep the constants arbitrary. We now vary the action with respect to the metric and the dilaton field. The same type of term appears repeatedly in this calculation as in Eq. (4.2). After performing a large number of simplifications, we arrive at

$$\begin{aligned}\delta S_{cor} = \frac{N\hbar}{2\pi}\int \mathrm{d}^2x\sqrt{-g}\Bigg\{&\left[C_1\Big(\nabla_\mu\nabla_\nu\phi - g_{\mu\nu}\Box\phi\Big) + \frac{C_2}{12}\left(\nabla_\mu\phi\nabla_\nu\phi - \frac{1}{2}g_{\mu\nu}\left(\nabla\phi\right)^2\right)\right]\delta g^{\mu\nu}\\ &+\left[-C_1R - \frac{C_2}{6}\Box\phi\right]\delta\phi\Bigg\}.\end{aligned} \tag{4.68}$$

After a direct identification with Eq. (4.64), we can read off the correction to the energy–momentum tensor and the variation of the correction term with respect to the field ϕ, which are given by:

$$\begin{aligned}\Delta T^{\phi}_{\mu\nu} &= -\frac{N\hbar}{\pi}\left[C_1\Big(\nabla_\mu\nabla_\nu\phi - g_{\mu\nu}\Box\phi\Big) + \frac{C_2}{12}\left(\nabla_\mu\phi\nabla_\nu\phi - \frac{1}{2}g_{\mu\nu}\left(\nabla\phi\right)^2\right)\right],\\ \frac{\delta S_{cor}}{\delta\phi} &= \frac{N\hbar}{2\pi}\left[-C_1R - \frac{C_2}{6}\Box\phi\right].\end{aligned} \tag{4.69}$$

4.2.2 Equations of motion and their general solutions

Now we can write down the full set of equations of motion. On the left–hand side we collect the geometric contributions, i.e. all terms arising from the dilaton energy–momentum tensor, while on the right–hand side we put all matter contributions. Using Eqs. (3.75) and (4.69), we arrive at the following system:

$$\begin{aligned}&\nabla_\mu\nabla_\nu\phi\, e^{-2\phi} + g_{\mu\nu}\left((\nabla\phi)^2 - \Box\phi - \lambda^2\right)e^{-2\phi}\\ &+\frac{N\hbar G}{2}\left[C_1\Big(\nabla_\mu\nabla_\nu\phi - g_{\mu\nu}\Box\phi\Big) + \frac{C_2}{12}\left(\nabla_\mu\phi\nabla_\nu\phi - \frac{1}{2}g_{\mu\nu}\left(\nabla\phi\right)^2\right)\right] = \frac{\pi G}{2}T^f_{\mu\nu},\\ &\left(-2R + 8\left(\nabla\phi\right)^2 - 8\lambda^2 - 8\Box\phi\right)e^{-2\phi} = N\hbar G\left(C_1R + \frac{C_2}{6}\Box\phi\right),\end{aligned} \tag{4.70}$$

where the only source term entering the equations of motion is the quantum–corrected energy–momentum tensor,

$$T^f_{\mu\nu} = T^{f,cl}_{\mu\nu} + \frac{N\hbar}{48\pi}\Big[- 2\nabla_\mu\nabla_\nu\psi + \nabla_\mu\psi\nabla_\nu\psi + g_{\mu\nu}\left(2\Box\psi - \frac{1}{2}(\nabla\psi)^2\right)\Big]. \tag{4.71}$$

The second term in Eq. (4.70) precisely coincides with the EMT derived from the PL action in Eq. (3.75). Consequently, these equations merely represent a compact rewriting of the relations we have already obtained in the preceding sections. Our next task is to solve this coupled system. Expressing the equations of motion (4.70) in light–cone coordinates $x^\pm$ and choosing the conformal gauge metric (3.2), we find:

$$+- : \partial_+\partial_- e^{-2\phi} + \lambda^2 e^{2(\rho-\phi)} - N\hbar G C_1 \partial_+\partial_-\phi = \pi G T^f_{+-}, \tag{4.72}$$

$$\begin{aligned}\pm\pm : &-\partial^2_\pm e^{-2\phi} + 4\partial_\pm\phi\partial_\pm(\phi-\rho)e^{-2\phi} + \\ &N\hbar G\left[C_1\left(\partial^2_\pm\phi - 2\partial_\pm\rho\partial_\pm\phi\right) + \frac{C_2}{12}(\partial_\pm\phi)^2\right] = \pi G T^f_{\pm\pm},\end{aligned} \tag{4.73}$$

$$\phi : \partial_+\partial_- e^{-2\phi} - 2\partial_+\partial_-(\phi-\rho)e^{-2\phi} + \lambda^2 e^{2(\rho-\phi)} = N\hbar G\left[-C_1\partial_+\partial_-\rho + \frac{C_2}{12}\partial_+\partial_-\phi\right] \tag{4.74}$$

$$T : T^f_{+-} = -\frac{N\hbar}{12\pi}\partial_+\partial_-\rho \quad \wedge \quad T^f_{\pm\pm} = T^{f,cl}_{\pm\pm} + \frac{N\hbar}{12\pi}\left[\partial^2_\pm\rho - (\partial_\pm\rho)^2 - t_\pm(x^\pm)\right], \tag{4.75}$$

where, in the last line, we have written the components of the quantum–corrected EMT explicitly in terms of the PL EMT components introduced in Eq. (3.77).

Next, we choose the constants such that the resulting system of equations admits an exact solution. In the classical CGHS model, the key requirement for obtaining a closed-form analytic solution was the Kruskal gauge condition, which followed from Eqs. (4.14) and (4.16). We now investigate what happens when we combine Eqs. (4.72) and (4.74). This yields

$$N\hbar\left(C_1 - \frac{C_2}{12}\right)\partial_+\partial_-\phi + N\hbar\left(C_1 - \frac{1}{12}\right)\partial_+\partial_-\rho - \frac{2}{G}\partial_+\partial_-(\phi-\rho)e^{-2\phi} = 0. \tag{4.76}$$

In order to obtain the equation $\partial_+\partial_-(\phi-\rho) = 0$, which is required to impose the Kruskal gauge, the constants must satisfy

$$C_1 - \frac{C_2}{12} = -\left(C_1 - \frac{1}{12}\right) \quad \Longrightarrow \quad C_1 = \frac{C_2+1}{24}. \tag{4.77}$$

With this choice, the equation simplifies to

$$\left[N\hbar\left(C_1 - \frac{C_2}{12}\right) - \frac{2}{G}e^{-2\phi}\right]\partial_+\partial_-(\phi-\rho) = 0. \tag{4.78}$$

Consequently, we can also impose the Kruskal gauge condition $\rho = \phi$ in the quantum-corrected case. In both the RST and BPP models, the relation (4.77) between the constants C_1 and C_2 is indeed fulfilled. After enforcing the Kruskal gauge condition, the equations of motion (4.72-4.74) take the form:

$$+- : \quad \partial_+\partial_-\left[e^{-2\phi} + N\hbar G\left(\frac{1}{12} - C_1\right)\phi\right] = -\lambda^2, \tag{4.79}$$

$$\pm\pm : \quad \partial^2_\pm\left[e^{-2\phi} + N\hbar G\left(\frac{1}{12} - C_1\right)\phi\right] = \frac{N\hbar G}{12}t_\pm(x^\pm) - \pi G T^{f,cl}_{\pm\pm}(x^\pm). \tag{4.80}$$

It is clear that this system of equations can be solved exactly by directly integrating the sources, which are now determined by $T^{f,cl}_{\pm\pm}$ together with the function $t_\pm$ defined in Eq. (3.78). The particular choice of the functions $t_\pm$ is tied to the specification of the quantum vacuum state (see Sec. 3.3). The general solution to the quantum-corrected equations of motion is given by:

$$\begin{aligned} e^{-2\phi} + N\hbar G\left(\frac{1}{12} - C_1\right)\phi = -\lambda^2 x^+ x^- - \pi G \int \mathrm{d}x^+ \int \mathrm{d}x^+ \left(T^{f,cl}_{++} - \varepsilon t_+\right) \\ - \pi G \int \mathrm{d}x^- \int \mathrm{d}x^- \left(T^{f,cl}_{--} - \varepsilon t_-\right) + a_+ x^+ + a_- x^- + b. \end{aligned} \tag{4.81}$$

We also introduce the constant $\varepsilon = \frac{N\hbar}{12\pi}$, which multiplies the quantum correction to the matter energy–momentum tensor. Eq. (4.81) is transcendental in ϕ, except in the special case $C_1 = \frac{1}{12}$, which corresponds to the BPP model. The quantities $a_\pm$ and b are integration constants, just as in the classical CGHS solution (4.25). Hence, in the BPP case the equations coincide exactly with the classical ones, and for this reason that model will be of particular interest in the following analysis..

4.2.3 General static solution

In this subsection, we solve the system of Eqs. (4.70) by employing the symmetric ansatz introduced in Sec. 3.1. Once this ansatz is implemented, the equations of motion reduce to:

$$\begin{aligned} &\left[\frac{\mathrm{d}}{\mathrm{dx}}\left(\mathrm{x}^2\mathcal{D}\frac{\mathrm{d}\Lambda}{\mathrm{dx}}\right) + \frac{N\hbar G C_1}{2}\left(\frac{\mathrm{d}}{\mathrm{dx}}\left(\mathcal{D}\frac{\mathrm{d}\Lambda}{\mathrm{dx}}\right) - 4\Lambda\frac{\mathrm{d}}{\mathrm{dx}}\left(\frac{\mathcal{D}}{\mathrm{x}}\right) - \frac{2}{\mathrm{x}}\mathcal{D}\frac{\mathrm{d}\Lambda}{\mathrm{dx}}\right) + \frac{N\hbar G}{12}\frac{C_2}{\mathrm{x}}\frac{\mathrm{d}\left(\Lambda\mathcal{D}\right)}{\mathrm{dx}}\right]\xi_\mu\xi_\nu \\ &- \left[\frac{\mathrm{d}}{\mathrm{dx}}\left(\mathrm{x}^2\mathcal{D}\frac{\mathrm{d}\Lambda}{\mathrm{dx}}\right) + 4\mathrm{x}^2\Lambda\frac{\mathrm{d}}{\mathrm{dx}}\left(\frac{\mathcal{D}}{\mathrm{x}}\right) + \frac{N\hbar G C_1 \mathrm{x}^2}{2}\frac{\mathrm{d}}{\mathrm{dx}}\left(\frac{\mathcal{D}}{\mathrm{x}^2}\frac{\mathrm{d}\Lambda}{\mathrm{dx}}\right) + \frac{N\hbar G C_2}{12}\frac{\mathrm{d}}{\mathrm{dx}}\left(\frac{\Lambda\mathcal{D}}{\mathrm{x}^2}\right)\right]\varepsilon_{\mu\rho}\varepsilon_{\nu\sigma}\xi^\rho\xi^\sigma \\ &= \frac{\pi G}{2\lambda^2}T^f_{\mu\nu} = \frac{\pi G}{2\lambda^2}\left(T^{f,cl}_{\mu\nu} + \langle\Delta T^{(f)}_{\mu\nu}\rangle\right), \end{aligned} \tag{4.82}$$

$$\mathcal{D}\mathrm{x}\frac{\mathrm{d}(\Lambda\mathcal{D})}{\mathrm{dx}} + \frac{\mathrm{x}^2}{4}\mathcal{D}\frac{\mathrm{d}}{\mathrm{dx}}\left(\mathcal{D}\frac{\mathrm{d}\Lambda}{\mathrm{dx}}\right) + \mathrm{x}^2 + \frac{N\hbar G}{8}\mathcal{D}\left[C_1\frac{\mathrm{d}}{\mathrm{dx}}\left(\mathcal{D}\frac{\mathrm{d}\Lambda}{\mathrm{dx}}\right) + \frac{C_2}{6}\frac{\mathrm{d}}{\mathrm{dx}}\left(\frac{\Lambda\mathcal{D}}{\mathrm{x}}\right)\right] = 0, \tag{4.83}$$

where the symmetric-ansatz form of the EMT $\langle\Delta T^{(f)}_{\mu\nu}\rangle$ is provided in Eq. (3.79). Because the left-hand side of Eq. (4.82) contains no mixed parallel–normal component, the constants associated with the functions $t_\pm$ must coincide. We denote their common value by $t_+(\sigma^+) = t_-(\sigma^-) = \frac{\lambda^2}{4}\Xi$. Subtracting the parallel and orthogonal components of Eq. (4.82), we arrive at:

$$\frac{N\hbar G}{2}\left[\frac{1}{2}\left(C_1 - \frac{1}{12}\right)\frac{\mathrm{d}}{\mathrm{dx}}\left(\mathcal{D}\frac{\mathrm{d}\Lambda}{\mathrm{dx}}\right) + \left(\frac{C_2}{12} - C_1\right)\frac{\mathrm{d}}{\mathrm{dx}}\left(\frac{\Lambda\mathcal{D}}{\mathrm{x}}\right)\right] + \mathrm{x}^2\frac{\mathrm{d}}{\mathrm{dx}}\left(\frac{1}{2}\mathcal{D}\frac{\mathrm{d}\Lambda}{\mathrm{dx}} + \frac{\Lambda\mathcal{D}}{\mathrm{x}}\right) = 0. \tag{4.84}$$

This equation is akin to taking the trace of the original system (4.82), together with the property that the EMT of a massless scalar field is traceless. It coincides with Eq. (4.76). For this equation to be explicitly integrable, the constants C_1 and C_2 must obey condition (4.77). Imposing that condition and integrating yields

$$\frac{1}{2}\mathcal{D}\frac{\mathrm{d}\Lambda}{\mathrm{dx}} + \frac{\Lambda\mathcal{D}}{\mathrm{x}} = C, \tag{4.85}$$

which is equivalent to Eq. (4.29) and encodes the Kruskal gauge condition for a static geometry. Proceeding in complete analogy with the purely classical static solution, we now integrate the dilaton Eq. (4.83). The result is

$$\Lambda \mathrm{x}^2 + C\left[\mathrm{x} + \frac{N\hbar G}{2}\left(C_1 - \frac{1}{12}\right)\frac{1}{\mathrm{x}}\right]\Lambda\mathcal{D} = Q, \tag{4.86}$$

where Q denotes an integration constant. Combining Eqs. (4.85) and (4.86) leads to the following expression for the metric function Λ:

$$\Lambda \mathrm{x}^2 - Q\ln\left|\Lambda \mathrm{x}^2\right| = b - C^2\left(\mathrm{x}^2 + N\hbar G\left(C_1 - \frac{1}{12}\right)\ln \mathrm{x}\right), \tag{4.87}$$

with b introduced as the final integration constant. The tortoise coordinate σ keeps the same form as in Eq. (4.32). The last step is to insert all these results back into the original Eq. (4.82) and extract the constraints on the classical part of the EMT. We obtain

$$\Lambda^2 T^{\Vert\Vert}_{f,cl} = \Lambda^2 T^{\perp\perp}_{f,cl} = \frac{2\lambda^2}{\pi G}\left(Q + \frac{N\hbar G}{48}\left(\Xi + C^2\right)\right). \tag{4.88}$$

This matches our expectations, as the equation of motion for the matter sector coincides with that of the classical static configuration, thereby introducing an additional charge μ. Consequently, we express Q in terms of the remaining parameters:

$$Q = \mu - \frac{N\hbar G}{48}\left(\Xi + C^2\right). \tag{4.89}$$

As in the purely classical setup, the constant C must be chosen such that the metric satisfies $\Lambda \to -1$ when $\mathrm{x} \to \infty$ and $\sigma \to +\infty$. From Eq. (4.87) it follows that $\Lambda \to -C^2$ in this limit, hence the second condition fixes $C = -1$. Finally, we rewrite the solution (4.87) for the metric function in Kruskal coordinates by using $|\Lambda \mathrm{x}^2| = e^{2\lambda\sigma} = -\lambda^2 x^+ x^-$ and reverting to $\mathrm{x} = e^{-\phi}$:

$$e^{-2\phi} + N\hbar G\left(\frac{1}{12} - C_1\right)\phi = -\lambda^2 x^+ x^- - \left(\frac{N\hbar G}{48}(\Xi + 1) - \mu\right)\ln\left|\lambda^2 x^+ x^-\right| + b. \tag{4.90}$$

Note that for $\mu \neq 0$, the geometry remains very similar to the classical case analyzed in Sec. 4.1.4. The resulting spacetime is a cosmological solution that describes an infinite universe shrinking from an infinite scale factor and subsequently re-expanding back to an infinite scale factor. We now turn to specific vacuum configurations: the linear dilaton vacuum, the static solution, and the static black hole, all specified with $\mu = 0$.

Linear dilaton vacuum

Here we determine which values the constants must take so that the linear dilaton vacuum solves the original field equations. The general solution of this model is given by Eq. (4.90). Imposing the condition $e^{-2\phi} = -\lambda^2 x^+ x^-$ leads to:

$$N\hbar G\left(\frac{1}{12} - C_1\right)\phi = \left(\frac{N\hbar G}{24}(\Xi + 1) - 2\mu\right)\phi + b. \tag{4.91}$$

From this relation it follows that the state must be massless, i.e. $b = 0$. Setting $\mu = 0$, the constraint becomes:

$$\frac{1}{24} - C_1 = \Xi. \tag{4.92}$$

For the static configuration with no energy flux at infinity—namely, the Boulware state—the energy-momentum tensor is normal ordered in Eddington–Finkelstein coordinates, which enforces $t_\pm(\sigma^\pm) = \Xi = 0$. Consequently, the linear dilaton vacuum represents a genuine vacuum state, devoid of any particle content, only in the RST model, where one has $C_1 = 1/24$. While in the BPP model, we instead obtain $\Xi = -1$, which corresponds to the Hartle–Hawking state. This connection is demonstrated in the following sections.

Static vacuum solution

A static vacuum solution is defined as one that carries no energy flux through either past or future null infinity. This requirement leads to the choice:

$$\Xi = 0. \tag{4.93}$$

Imposing this together with $\mu = 0$ simplifies the general solution (4.90) to:

$$e^{-2\phi} + N\hbar G\left(\frac{1}{12} - C_1\right)\phi = -\lambda^2 x^+ x^- - \frac{N\hbar G}{48}\ln\left|\lambda^2 x^+ x^-\right| + b. \tag{4.94}$$

In general, this relation is transcendental in ϕ. It becomes algebraically solvable for ϕ only in the BPP model, characterized by $C_1 = 1/12$. This is the main advantage of the BPP model. However, the drawback is that no choice of b can recover the linear dilaton vacuum from this solution. Consequently, the linear dilaton vacuum necessarily carries a nonvanishing energy flux at future null infinity.

Static vacuum black hole solution

Note that for any non-vanishing Q, no event horizon appears at a finite value of x. Since the presence of an event horizon is a prerequisite for a solution to qualify as a black hole [106], we must therefore set $Q = 0$. Moreover, because we are interested in a vacuum configuration, we also impose $\mu = 0$. Under these conditions, we obtain a constraint on the parameter Ξ, namely:

$$\Xi = -1. \tag{4.95}$$

Inserting this relation into the general solution (4.90) yields:

$$e^{-2\phi} + N\hbar G\left(\frac{1}{12} - C_1\right)\phi = -\lambda^2 x^+ x^- + b. \tag{4.96}$$

Here again, we see the benefit of working with the BPP model rather than the RST model. For $C_1 = 1/12$, this solution coincides with the classical expression (4.42).

4.3 BPP model

In this section, we study the various solutions within the BPP model, following the derivation of [25]. Unlike in the previous section, we begin with the most general solution in Kruskal coordinates, and then obtain different geometries by specifying in advance the vacuum state of the quantum fields. We then explicitly compute which of these geometries give rise to a non-vanishing energy flux at infinity. Moreover, we clarify why $\Xi = -1$ (4.95) holds for the static black hole.

As already stated, the BPP model arises when the constants in the correction term of the action (4.67) are fixed to $C_1 = \frac{1}{12}$ and $C_2 = 1$ [25]. With this choice, the general solution to the BPP equations of motion takes the form

$$\begin{aligned} e^{-2\phi} = -\lambda^2 x^+ x^- - \pi G \int \mathrm{d}x^+ \int \mathrm{d}x^+ \left(T^{f,cl}_{++} - \varepsilon t_+\right) \\ - \pi G \int \mathrm{d}x^- \int \mathrm{d}x^- \left(T^{f,cl}_{--} - \varepsilon t_-\right) + a_+ x^+ + a_- x^- + b, \end{aligned} \tag{4.97}$$

which is obtained by substituting $C_1 = 1/12$ into the general solution of the quantum-corrected CGHS model (4.81).

Eq. (4.97) gives the solution for the dilaton (and thus for the metric as well, since $\rho = \phi$ in Kruskal gauge), with $T^{f,cl}_{\pm\pm}$, $t_\pm$, $a_\pm$, and b serving as sources. Relative to the classical CGHS solution (4.25), the only new ingredients are the functions $t_\pm$, which encode the choice of quantum state of the matter fields. Recall that $\varepsilon = \frac{N\hbar}{12\pi}$ is the parameter signaling the presence of quantum corrections in the model; in the limit $\varepsilon \to 0$, the solutions revert to their classical forms.

We now briefly comment on the dimensions of the constants appearing in these expressions. In D spatial dimensions, Newton's law takes the form $F = G\frac{m_1 m_2}{r^{D-1}}$. For $D = 1$, this implies $[G] = \frac{\mathrm{m}}{\mathrm{kg\,s^2}}$. It follows that the combination $\frac{\hbar G}{c^3}$ is dimensionless. Hence, in the product εG the factor $1/c^3$ is effectively absent.

4.3.1 Linear dilaton vacuum

The linear dilaton vacuum corresponds to a solution with flat spacetime, as is already known from the classical CGHS model. For this case, the appropriate choice of sources in Eq. (4.97) is:

$$T^{f,cl}_{\pm\pm} = 0 \quad \wedge \quad a_\pm = 0 \quad \wedge \quad b = 0 \quad \wedge \quad t_\pm(x^\pm) = 0. \tag{4.98}$$

The last condition specifies that the quantum state is the Hartle–Hawking vacuum (3.97) (because the energy–momentum tensor is normal ordered in Kruskal coordinates). The metric takes the form:

$$\mathrm{d}s^2 = -\frac{\mathrm{d}x^+ \mathrm{d}x^-}{-\lambda^2 x^+ x^-} \quad \wedge \quad \phi = -\frac{1}{2}\ln\left|\lambda^2 x^+ x^-\right|. \tag{4.99}$$

To verify that we truly have the Hartle–Hawking state, we compute the energy–momentum tensor in the $x^\pm$ coordinates:

$$\langle \Delta T^f_{\pm\pm}(x^\pm)\rangle = \varepsilon\left[\partial^2_\pm \rho - (\partial_\pm \rho)^2 - \cancelto{0}{t_\pm(x^\pm)}\right] = \frac{\varepsilon\lambda^2}{4}\frac{1}{(\lambda x^\pm)^2}. \tag{4.100}$$

Next, we must determine whether there is any energy flux at infinity. To this end, we transform to the asymptotically flat coordinates $\sigma^\pm$ and consider the limit $\sigma \to \infty$:

$$\langle \Delta T^f_{\pm\pm}(\sigma^\pm)\rangle = \left(\frac{\mathrm{d}x^\pm}{\mathrm{d}\sigma^\pm}\right)^2 \langle \Delta T^f_{\pm\pm}(x^\pm)\rangle = \frac{\varepsilon\lambda^2}{4} \Longrightarrow \langle 0, x|\, \Delta\hat{T}^f_{\pm\pm}(\sigma^\pm)\,|0, x\rangle\Big|_{\mathcal{J}^\pm} = \frac{\varepsilon\lambda^2}{4}. \tag{4.101}$$

We observe that an energy flux is present both at $\mathcal{J}^+$ and $\mathcal{J}^-$, and thus we identify the configuration as a system in thermal equilibrium. Evaluating the temperature of the radiation, we obtain:

$$T = \frac{\kappa}{2\pi\hbar} = \frac{\lambda}{4\pi\hbar}\left|\mathcal{D}\frac{\mathrm{d}\Lambda}{\mathrm{dx}}\right| = \frac{\lambda}{2\pi\hbar}. \tag{4.102}$$

For more details see App. D.5. This shows that, even though the geometry is that of Minkowski flat spacetime, there is still a nonvanishing energy flux. This is the same outcome as in the preceding section. Therefore, this solution cannot be identified with the true Minkowski vacuum. The geometry behaves as the geometry in the vicinity of a black hole, although no singularity exists, leading us to classify it as nonphysical.

4.3.2 Eternal black hole solution

Here we present the quantum–corrected static black hole solution, corresponding to the Hartle–Hawking vacuum (3.97) for the matter fields. We require the energy–momentum tensor to be normal ordered in the $x^\pm$ coordinates. Consequently, the setup is specified by the following choice of sources in Eq. (4.97):

$$T^{f,cl}_{\pm\pm} = 0 \quad \wedge \quad a_\pm = 0 \quad \wedge \quad b = \frac{\pi GM}{\lambda} \quad \wedge \quad t_\pm(x^\pm) = 0. \tag{4.103}$$

Just as for the linear dilaton vacuum, the metric here also coincides exactly with the classical one (see Eq. (4.42)):

$$\mathrm{d}s^2 = -\frac{\mathrm{d}x^+\mathrm{d}x^-}{-\lambda^2 x^+x^- + \frac{\pi GM}{\lambda}} \quad \wedge \quad \phi = -\frac{1}{2}\ln\left|-\lambda^2 x^+x^- + \frac{\pi GM}{\lambda}\right|. \tag{4.104}$$

Note that this solution is equivalent to Eq. (4.96). We now investigate whether this configuration gives rise to an energy flux at infinity, as is necessary for describing a black hole in thermal equilibrium:

$$\langle \Delta T^f_{\pm\pm}(x^\pm)\rangle = \varepsilon\left[\partial^2_\pm\rho - (\partial_\pm\rho)^2 - \cancelto{0}{t_\pm}(x^\pm)\right] = \frac{\varepsilon\lambda^2}{4}\left[\frac{\lambda x^\mp}{-\lambda^2 x^+x^- + \frac{\pi GM}{\lambda}}\right]^2. \tag{4.105}$$

Expressing the energy–momentum tensor in the $\sigma^\pm$ coordinates and then taking the limit $\sigma \to \infty$ yields:

$$\langle \Delta T^f_{\pm\pm}(\sigma^\pm)\rangle = \frac{\varepsilon\lambda^2}{4}\frac{1}{\left(1 + \frac{\pi GM}{\lambda}e^{-2\lambda\sigma}\right)^2} \implies \langle 0, x|\, \Delta\hat{T}^f_{\pm\pm}(\sigma^\pm)\, |0, x\rangle\Big|_{\mathcal{J}^\pm} = \frac{\varepsilon\lambda^2}{4}. \tag{4.106}$$

Thus, the energy flux at $\mathcal{J}^\pm$ matches that of the linear dilaton vacuum (4.101). The crucial distinction is that in the present case there is an actual black hole of mass M. In this way we have obtained the eternal black hole configuration, which will serve as the basis for our analysis of the fine-grained entropy of Hawking radiation in Chap. 9.

At the conclusion of this subsection, we determine the value of the Ξ parameter that corresponds to the static black hole configuration. By transforming $t_\pm(x^\pm)$ to Eddington–Finkelstein coordinates using the transformation law (3.83), we obtain:

$$t_\pm(\sigma^\pm) = \left(\frac{\mathrm{d}x^\pm}{\mathrm{d}\sigma^\pm}\right)^2\left[\cancelto{0}{t_\pm}(x^\pm) - \frac{1}{2}D_{x^\pm}[\sigma^\pm]\right] \implies t_\pm(\sigma^\pm) = -\frac{\lambda^2}{4}. \tag{4.107}$$

On the other hand, Ξ is defined by $t_\pm(\sigma^\pm) = \frac{\lambda^2}{4}\Xi$, which immediately implies $\Xi = -1$. This coincides with the value previously obtained by requiring the presence of an event horizon in the general static vacuum solution (4.95).

4.3.3 Minkowski vacuum

Since our aim is to study gravitational collapse, we require a vacuum configuration that does not emit radiation at infinity, unlike the situation for the linear dilaton vacuum (4.101). Such a configuration is realized by the Boulware vacuum (3.96), defined by the condition $t_\pm(\sigma^\pm) = 0$. Consequently, the setup is characterized by the following values for the sources in Eq. (4.97):

$$T^{f,cl}_{\pm\pm} = 0 \quad \wedge \quad a_\pm = 0 \quad \wedge \quad b = 0 \quad \wedge \quad t_\pm(\sigma^\pm) = 0. \tag{4.108}$$

Let us now examine in more detail the requirement $t_\pm(\sigma^\pm) = 0$. This condition implies that the energy–momentum tensor is normal ordered with respect to the $\sigma^\pm$ coordinates. Equivalently, there is no energy flux through $\mathcal{J}^\pm$. We can verify this explicitly:

$$\langle \Delta T^f_{\pm\pm}(\sigma^\pm)\rangle\Big|_{\mathcal{J}^\pm} = \varepsilon\left[\partial^2_\pm\rho - (\partial_\pm\rho)^2 - t_\pm(\sigma^\pm)\right]\Big|_{\mathcal{J}^\pm} = -\varepsilon t_\pm(\sigma^\pm)\Big|_{\mathcal{J}^\pm}. \tag{4.109}$$

The contributions involving derivatives of the metric must vanish, because ρ must remain finite as $\sigma \to \infty$. A necessary and sufficient condition for this behavior is $t_\pm(\sigma^\pm) = 0$.

To determine the metric, we must now compute $t_\pm(x^\pm)$. This can be achieved by applying the transformation law (3.83) for this quantity, derived in Sec. 3.3. This yields:

$$t_\pm(x^\pm) = \left(\frac{d\sigma^\pm}{dx^\pm}\right)\left[\cancelto{0}{t_\pm}(\sigma^\pm) - \frac{1}{2}D_{\sigma^\pm}\left[x^\pm\right]\right] = \frac{1}{(\lambda x^\pm)^2}\left(-\frac{1}{2}\right)\left(-\frac{1}{2}\lambda^2\right) = \frac{1}{4(x^\pm)^2}. \tag{4.110}$$

All the required source parameters in Eq. (4.97) have now been evaluated. Performing the corresponding integrations yields

$$e^{-2\phi} = e^{-2\rho} = -\lambda^2 x^+ x^- - \frac{\varepsilon\pi G}{4}\ln\left(-\lambda^2 x^+ x^-\right) + C. \tag{4.111}$$

Here C is an arbitrary constant, playing the role of the constant b. We adopt the notation C in order to align with the conventions of [25]. We now determine the metric and dilaton in asymptotically flat coordinates (in quadrant I of Fig. 4.1):

$$ds^2 = \frac{-dt^2 + d\sigma^2}{1 - \left(\frac{\varepsilon\pi G}{2}\lambda\sigma - C\right)e^{-2\lambda\sigma}} \;\wedge\; \phi(\sigma) = -\lambda\sigma - \frac{1}{2}\ln\left[1 - \left(\frac{\varepsilon\pi G}{2}\lambda\sigma - C\right)e^{-2\lambda\sigma}\right]. \tag{4.112}$$

It is immediately evident that this configuration is static. Moreover, in the limit $\sigma \to \infty$, we recover the linear dilaton vacuum, precisely as desired. A straightforward computation of the energy–momentum tensor in the $x^\pm$ coordinates, followed by a transformation to the $\sigma^\pm$ coordinates, leads to:

$$\langle \Delta \hat{T}^f_{\pm\pm}(\sigma^\pm)\rangle = \frac{\varepsilon\lambda^2}{4}\left[\left(\frac{1 - \frac{\varepsilon\pi G}{4}e^{-2\lambda\sigma}}{1 - \left(\frac{\varepsilon\pi G}{2}\lambda\sigma - C\right)e^{-2\lambda\sigma}}\right)^2 - \frac{\frac{\varepsilon\pi G}{2}e^{-2\lambda\sigma}}{1 - \left(\frac{\varepsilon\pi G}{2}\lambda\sigma - C\right)e^{-2\lambda\sigma}} - 1\right]$$
$$\Longrightarrow \langle 0,\sigma|\, \Delta\hat{T}^f_{\pm\pm}(\sigma^\pm)\, |0,\sigma\rangle\Big|_{\mathcal{J}^\pm} = 0. \tag{4.113}$$

All these solutions approach the linear dilaton vacuum at $\mathcal{J}^\pm$ because $e^{2\phi}$ vanishes exponentially fast in this region. We now address the interpretation of the constant C [25]. For the spacetime mass (for example, in the ADM formalism) one finds $\frac{\pi GM}{\lambda} = C - C_0$, where C_0 is a reference value corresponding to the massless solution. However, the ADM mass of both the linear dilaton vacuum and the static black hole diverges. This divergence arises from the presence of radiation at $\mathcal{J}^{\pm}$. Since the static solutions have a smaller ADM mass, we are led to expect that the true ground state is given by one of these static configurations.

This also clarifies why the linear dilaton vacuum actually corresponds to the Hartle–Hawking state. It is smoothly connected to the choice $b = 0$ in the general eternal black hole solution (4.104), and not to any particular value of the constant C in the family of static vacuum solutions (4.111). Consequently, it must display the same Hawking radiation as the eternal black hole. We therefore conclude that the genuine vacuum state associated with flat Minkowski spacetime, once quantum corrections are switched off, is represented by one of the static vacuum solutions (4.111).

We now examine the behavior of solution (4.111) in greater detail. From a mathematical standpoint, it closely resembles the cosmological solution discussed in Sec. 4.1.4. Setting $\mu = -\frac{\varepsilon\pi G}{4}$ renders the two solutions identical. Nonetheless, flipping the sign of μ has significant physical implications. For the cosmological solution, μ is positive, which implies $\Lambda > 0$. By contrast, solution (4.111) is a vacuum solution with $\Lambda < 0$. Consequently, unlike the cosmological case, it should not contain any singularity, as it does not describe a black hole. As in the cosmological case, we begin our analysis with the scalar curvature. A straightforward computation gives:

$$R = 4\lambda^2 \frac{\frac{\varepsilon\pi G}{2} + \frac{(\varepsilon\pi G)^2}{16\lambda^2 x^+ x^-} - \frac{\varepsilon\pi G}{4}\ln\left(-\lambda^2 x^+ x^-\right) + C}{-\lambda^2 x^+ x^- - \frac{\varepsilon\pi G}{4}\ln\left(-\lambda^2 x^+ x^-\right) + C}. \tag{4.114}$$

Two different kinds of singularities appear in this setting. First, the curvature clearly blows up at $x^{\pm} = 0$. These singularities can be handled in a straightforward way by removing the hypersurfaces $x^+ = 0$ and $x^- = 0$ from the manifold. More interesting, however, is the situation in which the denominator vanishes:

$$-\lambda^2 x^+ x^- - \frac{\varepsilon\pi G}{4}\ln\left(-\lambda^2 x^+ x^-\right) + C = 0 \quad\Longrightarrow\quad e^{2\lambda\sigma} - \frac{\varepsilon\pi G}{2}\lambda\sigma + C = 0. \tag{4.115}$$

We carry out an analysis analogous to that in Sec. 4.1.4. A graphical representation of the solution to Eq. (4.115) is depicted in Fig. 4.5. We introduce the functions $f(x) = e^x$ and $g_C(x) = \frac{\varepsilon\pi G}{4}x - C$, and determine their point of intersection. An intersection occurs only when $C < C^*$. The critical value C^* is obtained by identifying the straight line $g_{C^*}(x)$ that is tangent to the curve $f(x)$. The tangency point is located at $x_0 = \ln\frac{\varepsilon\pi G}{4}$. Consequently, for the constant C^* we obtain:

$$C^* = -\frac{\varepsilon\pi G}{4}\left[1 - \ln\frac{\varepsilon\pi G}{4}\right]. \tag{4.116}$$

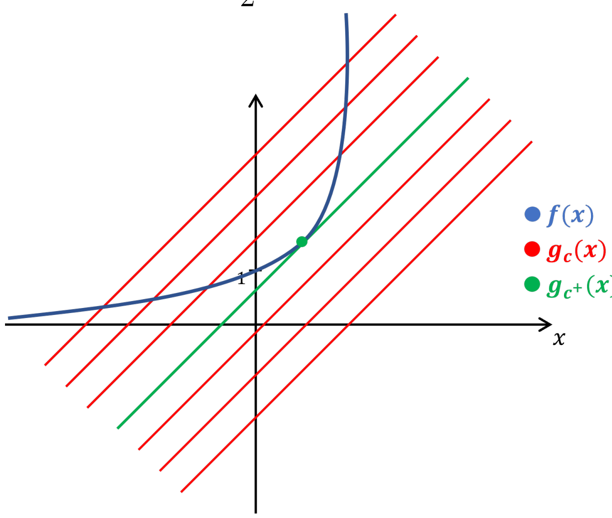

Figure 4.5: The intersection of the functions f and g_C

We conclude that for $C < C^*$ there exist spacelike hypersurfaces given by $\sigma = \sigma_s$, which solve this equation. In this regime, the curves intersect twice, producing two distinct hypersurfaces.

This defines the **strong coupling region**, where strong quantum correlations are expected and the semiclassical approximation breaks down. Consequently, we choose to discard this region.

For $C > C^*$, divergences appear at the hypersurfaces $x^\pm = 0$. In this case, the previously studied equation has no solutions, but we can still identify a strong coupling region. It is located in the neighborhood of the point $2\lambda\sigma_{\min} = \ln \frac{\varepsilon\pi G}{4}$, where the curves are closest to each other.

The terminology "strong coupling region" arises because $e^{2\phi}$ becomes very large there; this factor acts as the coupling strength between the curvature and the dilaton in the action. In our static vacuum configuration, we must avoid both singularities and strong coupling regions. We eliminate them by imposing reflective boundary conditions at the boundary of spacetime. This boundary coincides with one of the hypersurfaces $\sigma = \sigma_b$, so we enforce reflective boundary conditions at $\sigma = \sigma_b$ via:

$$\langle \Delta T^f_{++} \rangle \Big|_{\sigma=\sigma_b} = \langle \Delta T^f_{--} \rangle \Big|_{\sigma=\sigma_b} . \tag{4.117}$$

Hence, a well-defined Minkowski vacuum exists only in the region $\sigma > \sigma_s$ when $C < C^*$, or in the region $\sigma > \sigma_{\min}$ when $C > C^*$, with reflective boundary conditions imposed at $\sigma_b = \sigma_s + \delta$ or $\sigma_b = \sigma_{\min} + \delta$, respectively, where $\delta > 0$.

4.3.4 Evaporating black hole solution

In this subsection, we construct the dynamical scenario for an evaporating black hole. In contrast to Sec. 4.1.5, the spacetime here is divided not into two, but into three distinct regions. Specifically, evaporation ends at a finite point in the spacetime, and beyond this point the geometry returns to a static vacuum solution. This third region is absent in the purely classical case, where no radiation is present. The solution is fixed by the following choice of source parameters in Eq. (4.97):

$$T^{f,cl}_{++} = \frac{M}{\lambda x_0^+} \delta\left(x^+ - x_0^+\right) \quad \wedge \quad T^{f,cl}_{--} = 0 \quad \wedge \quad a_\pm = 0 \quad \wedge \quad t_\pm(\sigma^\pm) = 0. \tag{4.118}$$

For an evaporating black hole, there is no energy flux in the distant past, i.e. at $\mathscr{I}^-$ $(x^+ < x_0^+)$, whereas in the far future $(x^+ > x_0^+)$ there is an energy flux at $\mathscr{I}^+$. Consequently, the appropriate quantum state is $|\psi\rangle = |0, \sigma\rangle$, namely the Unruh state (3.98). This implies that the metric before the collapse corresponds to one of the Minkowski vacuum states (4.111) with some constant C (region I). After collapse, the metric is determined, as in the classical scenario, by imposing the continuity of both the metric and the dilaton field along the hypersurface $x^+ = x_0^+$. We then obtain:

$$ds^2 = \begin{cases} -\dfrac{dx^+dx^-}{-\lambda^2 x^+ x^- - \frac{\varepsilon\pi G}{4}\ln\left(-\lambda^2 x^+ x^-\right) + C}, & x^+ < x_0^+ \\ -\dfrac{dx^+dx^-}{-\lambda^2 x^+\left(x^- + \Delta\right) - \frac{\varepsilon\pi G}{4}\ln\left(-\lambda^2 x^+ x^-\right) + \frac{\pi G M}{\lambda} + C}, & x^+ > x_0^+ \end{cases} \tag{4.119}$$

We now focus on region I of the spacetime, i.e. the portion after the shockwave. If the spacetime boundary is fixed by $\sigma = \sigma_b$, then the coordinate x_0^+ coordinate is determined by $-\lambda^2 x_0^+ x_0^- = e^{2\lambda\sigma_b}$. Two distinct possibilities arise. In the first, when the infalling mass satisfies $M < M_{cr}$, it is too small to create a singularity, and the matter shockwave is simply reflected due to the reflective boundary conditions (4.117). Our primary interest, however, lies in the second situation, where the mass exceeds the critical value and a singularity forms, thereby generating region II of the spacetime. By evaluating the curvature, we obtain that the curve along which it diverges, i.e. the singularity, is given by:

$$-\lambda^2 x_{\mathrm{S}}^+ \left(x_{\mathrm{S}}^- + \Delta\right) - \frac{\varepsilon\pi G}{4} \ln\left(-\lambda^2 x_{\mathrm{S}}^+ x_{\mathrm{S}}^-\right) + \frac{\pi G M}{\lambda} + C = 0. \tag{4.120}$$

According to the cosmic censorship hypothesis, an event horizon must exist to conceal this singularity. In addition, there may be an apparent horizon that encloses the event horizon and, therefore, also hides the singularity. The apparent horizon is obtained by solving the equation $\partial_+ e^{-2\phi} = 0$, which yields

$$-\lambda^2 x_{\mathrm{AH}}^+ \left(x_{\mathrm{AH}}^- + \Delta\right) = \frac{\varepsilon\pi G}{4}. \tag{4.121}$$

Once the singularity has formed, the black hole starts to evaporate. To demonstrate this explicitly, one needs to compute the components of the energy–momentum tensor in the asymptotically flat coordinates, which in this case are the $\hat{\sigma}^\pm$ coordinates defined in Eq. (4.59). The relevant component is $\langle \Delta T_{--}^f(\hat{\sigma}^-)\rangle$ evaluated along the $\mathcal{J}^+$ hypersurface. Since the metric approaches a constant on $\mathcal{J}^+$, the EMT there is given by $\langle \Delta T_{--}^f(\hat{\sigma}^-)\rangle|_{\mathcal{J}^+} = -\varepsilon\, t_-(\hat{\sigma}^-)$. Moreover, from Eq. (4.110) we know how the condition $t_-(\sigma^-) = 0$ is modified when we transform to Kruskal gauge coordinates, namely $t_-(x^-) = \frac{1}{4(x^-)^2}$. Thus, using Eq. (3.83), we obtain:

$$t_-(\hat{\sigma}^-) = \left(\frac{dx^-}{d\hat{\sigma}^-}\right)^2 \left[t_-(x^-) - \frac{1}{2} D_{x^-}\left[\hat{\sigma}^-\right]\right] = \lambda^2 \left(x^- + \Delta\right)^2 \left[\frac{1}{4\left(x^-\right)^2} - \frac{1}{4\left(x^- + \Delta\right)^2}\right]. \tag{4.122}$$

Expressing this relation in $\hat{\sigma}^-$ coordinate, the EMT along the $\mathcal{J}^+$ hypersurface reads:

$$\langle 0, \sigma | \, \Delta \hat{T}_{--}^f(\hat{\sigma}^-) \, | 0, \sigma\rangle \Big|_{\mathcal{J}^+} = \frac{\varepsilon\lambda^2}{4} \left[1 - \frac{1}{\left(1 + \lambda\Delta e^{\lambda\hat{\sigma}^-}\right)^2}\right]. \tag{4.123}$$

The dynamical nature of this setup manifests itself in the explicit dependence of the EMT on the $\hat{\sigma}^-$ coordinate, in contrast with the static configurations discussed in the previous subsections. As the black hole continues to evaporate, the apparent horizon gradually contracts until it eventually meets the singularity. To locate this event in the spacetime, we have to solve the pair of Eqs. (4.120) and (4.121). Solving for the intersection coordinates x_{E}^+ and x_{E}^-, we find:

$$x_{\mathrm{E}}^+ = \frac{1}{\lambda^2 \Delta} \left[e^{1 + \frac{4(\pi G M + \lambda C)}{\varepsilon\pi G\lambda}} - \frac{\varepsilon\pi G}{4}\right] \quad \wedge \quad x_{\mathrm{E}}^- = -\frac{\Delta}{1 - \frac{\varepsilon\pi G}{4} e^{-1 - \frac{4(\pi G M + \lambda C)}{\varepsilon\pi G\lambda}}}. \tag{4.124}$$

Thus, the intersection takes place within a finite time interval. At that moment, the singularity becomes naked. According to the cosmic censorship theorem [106], this is not allowed to occur. This issue is resolved, however, if the entire black hole has evaporated by the time the intersection is reached. For this reason, it is also referred to as the evaporation end-point. We now verify whether the black hole has completely evaporated by calculating the energy emitted via Hawking radiation up to this point. Since the metric at $\mathcal{J}^+$ is flat, namely $\mathrm{d}s^2 = -\mathrm{d}\hat{\sigma}^+ \mathrm{d}\hat{\sigma}^-$, the radiated energy is given by:

$$\begin{aligned} E_{rad} &= \int_{-\infty}^{\hat{\sigma}_{\mathrm{E}}^-} d\hat{\sigma}^- \langle \Delta T_{--}^f(\hat{\sigma}^-)\rangle \Big|_{\mathcal{J}^+} = \frac{\varepsilon\lambda^2}{4} \int_{-\infty}^{\hat{\sigma}_{\mathrm{E}}^-} d\hat{\sigma}^- \left[1 - \frac{1}{(1 + \lambda\Delta e^{\lambda\hat{\sigma}^-})^2}\right] \\ &= \frac{\varepsilon\lambda}{4} \int_1^{\xi_{\mathrm{E}}} d\xi \frac{\xi + 1}{\xi^2} = \frac{\varepsilon\lambda}{4} \left[\ln \xi_{\mathrm{E}} + 1 - \frac{1}{\xi_{\mathrm{E}}}\right], \end{aligned} \tag{4.125}$$

where in the second line, we make a change of variables, defining $\xi = 1+\lambda\Delta e^{\lambda\hat{\sigma}^-}$, which implies $\xi_{\rm E} = \frac{4}{\varepsilon\pi G}e^{1+\frac{4(\pi GM+\lambda C)}{\varepsilon\pi G\lambda}}$ and $1+\frac{1}{\xi_{\rm E}} = -\frac{\Delta}{x^-_{\rm E}}$. With these relations, we can then write the radiated energy in an explicit form:

$$\begin{aligned} E_{rad} &= \frac{\varepsilon\lambda}{4}\left[-\ln\frac{\varepsilon\pi G}{4}+1+\frac{4M}{\varepsilon\lambda}+\frac{4C}{\varepsilon\pi G}-\frac{\Delta}{x^-_{\rm E}}\right] \\ &= M+\frac{\lambda}{\pi G}\left[C+\frac{\varepsilon\pi G}{4}\left(1-\ln\frac{\varepsilon\pi G}{4}\right)\right]-\frac{\varepsilon\lambda\Delta}{4x^-_{\rm E}} = M+\frac{\lambda}{\pi G}\left(C-C^*\right)-\frac{\varepsilon\lambda\Delta}{4x^-_{\rm E}}, \end{aligned} \tag{4.126}$$

where the quantity C^*, defined in Eq. (4.116), appears in the second line. This shows that the black hole does not fully evaporate by the time the evaporation process reaches its endpoint. We now compute the residual mass. A straightforward calculation gives:

$$\delta M = \left(M+\frac{\lambda}{\pi G}(C-C_0)\right)-E_{rad} = \frac{\lambda}{\pi G}(C^*-C_0)+\frac{\varepsilon\lambda\Delta}{4x^-_{\rm E}}. \tag{4.127}$$

We observe that, up to the end-point of the evaporation, the black hole emits nearly all of its energy. Yet, the cosmic censorship conjecture requires that the entire initial mass is radiated away at the end-point. We now try to smoothly match the solution along the line $x^- = x^-_{\rm E}$, so that in region III of the spacetime ($x^- > x^-_{\rm E}$) we obtain a Minkowski vacuum solution (4.111) characterized by a new constant C' and asymptotically flat coordinates $\hat{\sigma}^\pm$, namely:

$$\mathrm{d}s^2 = -\frac{\mathrm{d}\hat{\sigma}^+\mathrm{d}\hat{\sigma}^-}{1-\left(\frac{\varepsilon\pi G}{2}\lambda\hat{\sigma}-C'\right)e^{-2\lambda\hat{\sigma}}} = -\frac{\mathrm{d}x^+\mathrm{d}x^-}{-\lambda^2x^+\left(x^-+\Delta\right)-\frac{\varepsilon\pi G}{4}\ln\left(-\lambda^2x^+\left(x^-+\Delta\right)\right)+C'}. \tag{4.128}$$

To ensure a continuous matching of both the metric and the dilaton field across the hypersurface $x^- = x^-_{\rm E}$, the following condition must be satisfied:

$$e^{-2\rho}\Big|_{x^-=x_p^{-(+)}} = e^{-2\rho}\Big|_{x^-=x_p^{-(-)}} \quad\Longrightarrow\quad C^{'} = C^*. \tag{4.129}$$

One might then conclude that the difference in the mass of spacetime prior to the beginning of the evaporation and after the evaporation ends $\frac{\lambda}{\pi G}\left(C^*-C_0\right)$ is equal to the mass (4.127), but this is incorrect because Eq. (4.127) contains an additional contribution. We must therefore determine the physical origin of this extra term. In regions II and III, the field $e^{-2\phi}$ is given by:

$$\begin{aligned} e^{-2\phi} = -\lambda^2x^+\left(x^-+\Delta\right) &+ \left[-\frac{\varepsilon\pi G}{4}\ln\left(-\lambda^2x^+x^-\right)+\frac{\pi GM}{\lambda}+C\right]\eta(x^-_{\rm E}-x^-) \\ &+ \left[-\frac{\varepsilon\pi G}{4}\ln\left(-\lambda^2x^+(x^-+\Delta)\right)+C^*\right]\eta(x^--x^-_{\rm E}), \end{aligned} \tag{4.130}$$

where η is the Heaviside function. After a careful calculation of the second derivative of $e^{-2\phi}$, we obtain:

$$\begin{aligned} \partial_+^2 e^{-2\phi} &= \frac{\varepsilon\pi G}{4(x^+)^2}, \\ \partial_-^2 e^{-2\phi} &= \frac{\varepsilon\pi G}{4}\left[\frac{1}{(x^-)^2}\eta(x^-_{\rm E}-x^-)+\frac{1}{(x^-+\Delta)^2}\eta(x^--x^-_{\rm E})\right]+\frac{\varepsilon\pi G\Delta}{4x^-_{\rm E}\left(x^-_{\rm E}+\Delta\right)}\delta(x^--x^-_{\rm E}), \\ \partial_+\partial_- e^{-2\phi} &= -\lambda^2. \end{aligned} \tag{4.131}$$

These three equations correspond to the original system (4.79-4.80), with the third equation exactly coinciding with Eq. (4.79). Because the expression for the asymptotically flat coordinate x^+ is identical in all three spacetime regions, we deduce that $t_+(x^+) = \frac{1}{4(x^+)^2}$ holds everywhere. This is precisely what the first equation states. To interpret the second equation, we must determine $t_-(x^-)$ in the third region. Region III is defined to be the Minkowski vacuum in the $\hat{\sigma}^{\pm}$ coordinates, so the quantum state there is $|\psi\rangle = |0, \hat{\sigma}\rangle$. This implies $t_-(\hat{\sigma}^-) = 0$, which in turn leads to $t_-(x^-) = \frac{1}{4(x^-+\Delta)^2}$. Therefore, we can now identify the meaning of each term appearing in the second equation:

$$t_-(x^-) = \frac{\eta(x_{\mathrm{E}}^- - x^-)}{4(x^-)^2} + \frac{\eta(x^- - x_{\mathrm{E}}^-)}{4\left(x^- + \Delta\right)^2}, \quad T_{--}^{f,cl}(x^-) = -\frac{\varepsilon\Delta}{4x_{\mathrm{E}}^-\left(x_{\mathrm{E}}^- + \Delta\right)}\delta(x^- - x_{\mathrm{E}}^-). \tag{4.132}$$

Due to the presence of a term proportional to the Dirac δ-function, an additional matter shockwave arises, which exits the black hole and travels to future null infinity at the precise instant when the singularity meets the apparent horizon. To compute the mass transported by this outgoing shockwave, we employ Eq. (3.100), taking n^μ to be proportional to the time-like Killing vector in region III, $\xi = \lambda x^+\partial_+ - \lambda\left(x^- + \Delta\right)\partial_-$. The calculation simplifies to:

$$M' = \int_\Sigma \sqrt{\gamma}d\hat{\sigma}\; n^\mu \xi^\nu T_{\mu\nu} = -\frac{\varepsilon\Delta}{4x_{\mathrm{E}}^-\left(x_{\mathrm{E}}^- + \Delta\right)}\mathrm{F}^-(x_{\mathrm{E}}^-) = \frac{\varepsilon\lambda\Delta}{4x_{\mathrm{E}}^-}, \tag{4.133}$$

where we have used $\mathrm{F}^-(x_{\mathrm{E}}^-) = -\lambda(x_{\mathrm{E}}^- + \Delta)$.

Therefore, we find that the mass carried away by this shockwave precisely matches the second term in the expression for δM (4.127). Let us briefly recapitulate the physical picture. At the instant when the singularity reaches the apparent horizon, a small amount of negative energy (since $x_{\mathrm{E}}^- < 0$) is emitted as an outgoing shockwave (the so-called *thunderpop* [23, 24, 25, 26]), which transports the surplus energy to infinity. After this emission, what remains is a static universe with no energy flux at $\mathcal{J}^+$, described by the Minkowski vacuum metric.

What is noteworthy is that the constant C' determining the Minkowski vacuum state in region III of the spacetime is independent of the initial choice of C and in fact coincides with the critical value C^*. As before, we must discard the strong-coupling region, implying that the spacetime boundary in region III is located at $2\lambda\hat{\sigma}_{\mathrm{B}} = \ln\frac{\varepsilon\pi G}{4}$, which, upon rewriting in $x^\pm$ coordinates, becomes:

$$-\lambda^2 x_{\mathrm{B}}^+\left(x_{\mathrm{B}}^- + \Delta\right) = \frac{\varepsilon\pi G}{4}. \tag{4.134}$$

Hence, the boundary in region III is simply the extension of the apparent horizon from region II. It is also evident that the event horizon (in region II) is given by:

$$x_{\mathrm{H}}^- = x_{\mathrm{E}}^-. \tag{4.135}$$

If we expand the metric near the strong-coupling region, i.e., close to the boundary $\hat{\sigma} = \hat{\sigma}_{\mathrm{B}} + \delta$, where $\delta > 0$ is a small parameter, we find:

$$\mathrm{d}s^2 = \frac{-\mathrm{d}t^2 + \mathrm{d}\delta^2}{2\lambda^2\delta^2 + o(\delta^3)}. \tag{4.136}$$

Thus, in the vicinity of $\delta = 0$, the spacetime exhibits the geometry of a semi-infinite throat. The proper distance diverges logarithmically as one approaches the boundary, mirroring the behavior found in higher-dimensional black holes. Furthermore, the curvature remains finite everywhere, so the spacetime is geodesically complete.

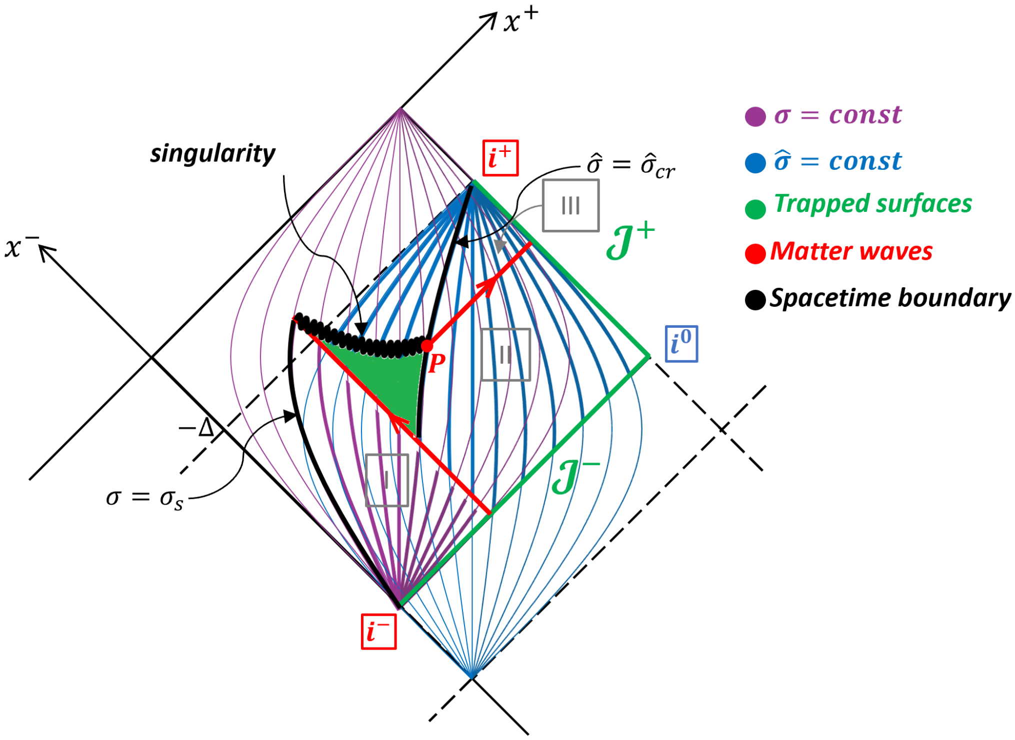

Figure 4.6: Penrose diagram of the evaporating black hole solution in the BPP model

There is still one "degree of freedom" remaining that we have not fixed: the constant C_0, which selects which particular static Minkowski vacuum corresponds to the massless solution. It is natural to demand that the ADM mass of the final spacetime vanish. Under this assumption, the natural assignment is $C_0 = C^*$. However, for this choice, the spacetime in region I acquires a nonzero mass unless $C = C^*$. This consideration motivates us to fix the initial constant C as well. Although such a choice is not strictly required within this model, it provides the most physically meaningful specification of the constants.

The full dynamical picture of the evaporating black hole is presented in Fig. 4.6. The axes represent the compactified Kruskal coordinates. One can clearly track the evolution of the spacetime boundary (black line). Initially, it coincides with the boundary of the strongly coupled region of the Minkowski vacuum solution in region I, which is described by Eq. (4.115). In this stage, it is a constant-σ hypersurface, $\sigma = \sigma_s$, subject to the reflective boundary conditions (4.117). Entering region II, the boundary turns into a singularity (4.120), indicated by the wavy line in Fig. 4.6. In region III, it again becomes a constant-$\hat{\sigma}$ hypersurface, $\hat{\sigma} = \hat{\sigma}_{\mathrm{B}}$ (4.134), representing the continuation of the apparent horizon of region II, defined in Eq. (4.121). The trapped surfaces, located between the apparent horizon and the singularity, are shown in green. The initial ingoing shockwave is colored red. The end-point of evaporation (4.124) is explicitly marked, with the outgoing shockwave emerging from it also drawn in red, while in the opposite direction the event horizon (4.135) of the black hole in region II extends.

In region III, the energy–momentum tensor is normal ordered with respect to the $\hat{\sigma}$ coordinates, which implies that the final quantum state is $|\psi\rangle = |0, \hat{\sigma}\rangle$, i.e., a pure state. Since there is no Hawking radiation in this region, the evolution appears to be unitary. Nevertheless, the only parameter describing the initial matter is its mass, and this is also the only piece of information that can be inferred from the final spacetime. Consequently, the model seems to exhibit information loss. However, because there are strong correlations in the vicinity of the boundary, we might expect substantial quantum gravitational effects there, which could provide a mechanism for recovering the apparently lost information. Whether information is actually lost depends on the behavior of the entanglement entropy, more specifically, on whether or not it follows the Page curve. This is discussed in detail in Chap. 9.

Evaporation time

At the end of this section, we determine the total evaporation time. We begin with the relation

$$e^{2\lambda t_{\mathrm{E}}} = -\frac{x_p^+}{x_{\mathrm{E}}^- + \Delta}. \tag{4.137}$$

The evaporation time is evaluated by fixing the integration constant C according to the above choice, i.e. by setting $C = C^*$. With this choice, the intersection point takes the form

$$x_{\mathrm{E}}^+ = \frac{\varepsilon\pi G}{4\lambda^2\Delta}\left[e^{\frac{4M}{\varepsilon\lambda}-1}\right] \quad \wedge \quad x_{\mathrm{E}}^- = -\frac{\Delta}{1 - e^{-\frac{4M}{\varepsilon\lambda}}}. \tag{4.138}$$

Substituting these expressions into Eq. (4.137) for the evaporation time yields

$$e^{2\lambda t_{\mathrm{E}}} = \frac{\varepsilon\pi G}{4(\lambda\Delta)^2}\left(e^{\frac{4M}{\varepsilon\lambda}} - 1\right)^2 \implies 2\lambda t_{\mathrm{E}} = 2\ln\left(e^{\frac{4M}{\varepsilon\lambda}} - 1\right) - \ln\frac{4\pi GM^2}{\varepsilon\lambda^2} + 2\ln\left(\lambda x_0^+\right). \tag{4.139}$$

If we now assume that the black hole mass is very large, namely $\frac{4M}{\varepsilon\lambda} \gg 1$, the evaporation time simplifies to

$$\lambda t_p = \frac{4M}{\varepsilon\lambda} - \frac{1}{2}\ln\frac{4\pi GM^2}{\varepsilon\lambda^2} + \ln\left(\lambda x_0^+\right). \tag{4.140}$$

In the large-mass regime, the second term in this expression can also be neglected, since the logarithmic contribution grows much more slowly than the linear one. Let us next consider the behavior of the event horizon (4.135) in this limit: $x^- = x_{\mathrm{E}}^- \approx -\Delta$. Thus, in this regime, the horizon is located slightly below the hypersurface $x^- = -\Delta$. Restoring the physical constants, the evaporation time becomes

$$\Delta t_{\mathrm{E}} = \frac{48\pi M}{N\hbar\lambda^2}, \tag{4.141}$$

where we have discarded the last term in Eq. (4.140) as well, since it is constant and therefore negligible compared to the leading term, which scales linearly with the mass.

4.4 Perturbative treatment of the gravitational collapse

In this section, we demonstrate how the perturbative method introduced in Sec. 3.4.1 can be employed to derive the quantum-corrected collapse scenario discussed in the previous section. We work in Eddington–Finkelstein coordinates. Because the linear dilaton vacuum in the BPP model carries a non-vanishing energy flux at infinity, both spacetime regions I and II (see Fig. 3.3) must be quantum-corrected. When solving the equations, it is not necessary to treat these two regions separately, since the Minkowski vacuum should emerge as the $b \to 0$ limit of the solution in the region $x^+ > x_0^+$, where the black hole exists. We therefore first determine the general solution of the BPP equations of motion.

We begin by expanding the equations of motion (4.72-4.74) for the BPP model to first order in ε, using an expansion analogous to Eq. (3.108), namely $\rho \mapsto \rho + \varepsilon\alpha$ and $\phi \mapsto \phi + \varepsilon\theta$. The equations of motion then become:

$$\begin{aligned} &\lambda\alpha e^{2\rho} = \frac{1}{\lambda}\partial_+\partial_-\theta + e^{2\rho}\left(\mathrm{F}^+\partial_+\theta + \mathrm{F}^-\partial_-\theta\right), \\ &\partial_\pm\left(e^{-2\rho}\left(\partial_\pm\theta + \lambda\alpha\mathrm{F}^\pm e^{2\rho}\right)\right) = -\frac{1}{2}e^{\phi-\rho}\partial_\pm^2 e^{\phi-\rho}, \\ &\partial_+\partial_-\theta = \partial_+\partial_-\alpha. \end{aligned} \tag{4.142}$$

Since the right-hand side of Eq. (4.73) is already of ε order, a simple substitution of $\phi - \rho$ in zeroth order from Eq. (4.36) yields:

$$\partial_\pm\left(e^{-2\rho}\left(\partial_\pm\theta + \lambda\alpha\mathrm{F}^\mp e^{2\rho}\right)\right) = \frac{e^{2(\phi-\rho)}}{\mathrm{F}^{\pm 2}}\left[t_\pm(\hat\sigma^\pm) + \frac{\lambda^2}{4}\right], \tag{4.143}$$

where Eq. (4.73) has been recast into the form in Eq. (3.109). To determine the normal ordered components of the energy-momentum tensor $t_\pm(\hat\sigma^\pm)$ in region II of the spacetime, we make use of Eq. (3.114). These components read:

$$t_+(\hat\sigma^+) = 0 \ \wedge \ t_-(\hat\sigma^-) = \frac{\lambda^2}{4}\left(\mathrm{F}^{-2} - 1\right). \tag{4.144}$$

Expressing F^- in terms of ϕ and δ (3.107) with the help of Eq. (4.57) and substituting in Eq. (4.143), after integration, yields:

$$\begin{aligned} &\partial_+\theta = -\frac{\lambda}{2}\mathrm{F}^- e^{2\rho}\left[2\alpha + \frac{\mathrm{G}^-}{\mathrm{F}^-} + \frac{1}{4}\frac{1}{b - e^{-2\phi}}\right], \\ &\partial_-\theta = -\frac{\lambda}{2}\mathrm{F}^+ e^{2\rho}\left[2\alpha + \frac{\mathrm{G}^+}{\mathrm{F}^+} + \frac{1}{4}\frac{\delta^2}{\delta^2\left(b - e^{-2\phi}\right) - b}\right], \end{aligned} \tag{4.145}$$

where another set of arbitrary fictions $\mathrm{G}^\pm(\sigma^\pm)$ is introduced. These two expressions correspond to Eq. (3.111). The function $\mathcal{D}_1$ is determined by direct comparison. Following further the method introduced in Sec. 3.4.1 we express α from the first equation in Eq. (4.142) and substitute it in Eq. (4.145). The subsequent integration gives:

$$\begin{aligned} &\lambda b\theta e^{2\phi} = \frac{\lambda}{2}\frac{\mathrm{G}^-}{\mathrm{F}^-} - \mathrm{F}^-\partial_-\theta + \frac{\lambda}{8}e^{2\phi}\left(\ln\left|b - e^{-2\phi}\right| + \mathrm{H}^-\right), \\ &\lambda b\theta e^{2\phi} = \frac{\lambda}{2}\frac{\mathrm{G}^+}{\mathrm{F}^+} - \mathrm{F}^+\partial_+\theta + \frac{\lambda}{8}e^{2\phi}\left(\ln\left|b - \delta^2\left(b - e^{-2\phi}\right)\right| + \mathrm{H}^+\right), \end{aligned}$$

with an additional pair of functions $\mathrm{H}^\pm(x^\pm)$. Requiring these two equations to coincide determines the form of the functions $\mathrm{H}^\pm$ in terms of another constant D, resulting in the following expression:

$$\lambda b\theta e^{2\phi} = \frac{\lambda}{2}\left(be^{2\phi} - 1\right)\left[2\alpha + \frac{\mathrm{G}^+}{\mathrm{F}^+} + \frac{\mathrm{G}^-}{\mathrm{F}^-}\right] + \frac{\lambda}{8}e^{2\phi}\left[-2\ln\delta - D + 1 + \ln\left|b - \delta^2\left(b - e^{-2\phi}\right)\right|\right]. \tag{4.146}$$

To obtain the function θ, we follow the same procedure once again. Solving Eq. (4.145) for α and substituting the result into Eq. (4.146) yields a pair of first-order differential equations for θ (one involving $\partial_+\theta$ and the other involving $\partial_-\theta$). Integrating these two equations introduces a new family of arbitrary functions, which are then fixed by requiring that the two resulting expressions for θ agree. The final form of θ is given by:

$$\theta = \frac{\lambda}{2}\left(be^{2\phi}-1\right)\left(\int \mathrm{d}x^{+}\frac{\mathrm{G}^{+}}{\mathrm{F}^{+2}} + \int \mathrm{d}x^{-}\frac{\mathrm{G}^{-}}{\mathrm{F}^{-2}}\right) + \frac{1}{8}e^{2\phi}\left(1 - D - 2\ln\delta + \ln\left|b - \delta^{2}\left(b - e^{-2\phi}\right)\right|\right) \tag{4.147}$$

We now switch back to the quantum-corrected fields $\phi + \varepsilon\theta \mapsto \phi$ and $\rho + \varepsilon\alpha \mapsto \rho$, as described in Eq. (3.113) by substituting the solutions for α (4.146) and θ (4.147). In this way, we obtain the quantum-corrected counterparts of the expressions in Eq. (4.57):

$$\begin{aligned}
&\mathrm{F}^{+}\mathrm{F}^{-}e^{2\rho} = be^{2\phi} - 1 + \frac{\varepsilon\pi G}{4}e^{2\phi}\left[2\ln\delta + D - 1 - \ln\left|b - \delta^{2}\left(b - e^{-2\phi}\right)\right|\right],\\
&\ln\left|b - e^{-2\phi}\right| + \frac{\varepsilon\pi G}{4}e^{2\phi}\frac{2\ln\delta + D - 1 - \ln\left|b - \delta^{2}\left(b - e^{-2\phi}\right)\right|}{be^{2\phi}-1} = -\lambda\left(\int\frac{\mathrm{d}x^{+}}{\mathrm{F}^{+}} + \int\frac{\mathrm{d}x^{-}}{\mathrm{F}^{-}}\right) \equiv 2\lambda\hat{\sigma},
\end{aligned} \tag{4.148}$$

where $\mathrm{F}^{\pm} + \varepsilon\mathrm{G}^{\pm} \mapsto \mathrm{F}^{\pm}$. Taking the limit $b \to 0$ gives the following quantum-corrected Minkowski vacuum solution:

$$\begin{aligned}
\mathrm{F}^{+}\mathrm{F}^{-}e^{2\rho} &= -1 + \frac{\varepsilon\pi G}{2}\left(\phi + \phi_0\right)e^{2\phi},\\
\phi + \frac{\varepsilon\pi G}{4}\left(\phi + \phi_0\right)e^{2\phi} &= \frac{\lambda}{2}\left(\int\frac{\mathrm{d}x^{+}}{\mathrm{F}^{+}} + \int\frac{\mathrm{d}x^{-}}{\mathrm{F}^{-}}\right),
\end{aligned} \tag{4.149}$$

where ϕ_0 denotes the integration constant. Choosing Eddington–Finkelstein coordinates as the starting coordinate system is equivalent to fixing $\mathrm{F}^{+} = -1$ and $\mathrm{F}^{-} = 1$. If one then performs an additional coordinate transformation to Kruskal coordinates (4.41), it is straightforward to check that, to first order in perturbation theory, the solution (4.149) coincides with the exact Minkowski vacuum solution (4.111). Under this identification, the constant C appearing in Eq. (4.111) is related to ϕ_0 via $C = \frac{\varepsilon\pi G}{2}\phi_0$.

In Sec. 3.4.1, the next step is to smoothly match the solution (4.148) to the initial Minkowski vacuum configuration (4.149). This is done by imposing continuity of $e^{2\rho}$ and ϕ, while allowing their derivatives $\partial_{+}\rho$ and $\partial_{+}\phi$ to exhibit discontinuities across the hypersurface $x^{+} = x_0^{+}$. Under these conditions, the evaporating black hole solution is fixed by specific choices of the constants b, D, and coordinate transformations F^{+} and F^{-} that enter the general solution (4.148):

$$b = \frac{\pi GM}{\lambda},\ D = 1 + 2\phi_0,\ \mathrm{F}^{+} = -1,\ \mathrm{F}^{-} = 1 - be^{-2\hat{\mathrm{x}}}. \tag{4.150}$$

As we can see, the coordinate transformations do not gain any quantum corrections in this procedure, and the coordinates are the same as in the classical case:

$$2\lambda\hat{\sigma} = -2\ln\delta + \ln\left|b - e^{2\hat{\mathrm{x}}}\right|. \tag{4.151}$$

A direct check shows that solution (4.150) coincides with the exact solution (4.119) expanded to first order in ε.

The end-state of the evaporation

To find the apparent horizon, we solve the equation $\partial_{+}e^{-2\phi} = 0$. Employing the solution (4.148), the apparent horizon hypersurface to first order in ε is given by

$$e^{2\hat{\mathrm{x}}} = b + \frac{\varepsilon\pi G}{4}\delta^{2}. \tag{4.152}$$

The scalar curvature, defined as $R = 8e^{-2\rho}\partial_+\partial_-\rho$, is found to be

$$R = \frac{4\lambda^2\tilde{b}\delta^2}{\tilde{b}\delta^2 - b + e^{2\hat{\mathrm{x}}}}, \tag{4.153}$$

where the quantum-corrected constant b is introduced as $\tilde{b} = b - \frac{\varepsilon\pi G}{2}(\hat{\mathrm{x}} - \ln\delta - \phi_0)$. The singularity line is described by

$$e^{2\hat{\mathrm{x}}} = b - \tilde{b}\delta^2, \tag{4.154}$$

since this corresponds to the hypersurface along which the curvature diverges. To obtain the end-point of the evaporation, one must determine where the apparent horizon and singularity hypersurfaces intersect. This intersection can be computed from Eqs. (4.152) and (4.154) to first order in ε, yielding the following result:

$$\delta_{\mathrm{E}}^2 = be^{-\frac{4b}{\varepsilon\pi G}-1-2\phi_0} \quad \wedge \quad e^{2\hat{\mathrm{x}}_{\mathrm{E}}} = b\left[1 + \frac{\varepsilon\pi G}{4}e^{-\frac{4b}{\varepsilon\pi G}-1-2\phi_0}\right]. \tag{4.155}$$

By rewriting the solution in Kruskal coordinates and employing $\delta_{\mathrm{E}}^2 = \frac{x_0^+}{x_{\mathrm{E}}^+}$ together with $e^{2\hat{\mathrm{x}}_{\mathrm{E}}} = -\lambda^2 x_0^+ x_{\mathrm{E}}^-$, we obtain that these expressions reproduce the precise end-point (4.124) to first order in ε.

Next, we show how to extract the end-state geometry. As a first step, we rewrite the solution in terms of the radial coordinate ϕ and the coordinate $\hat{\mathrm{x}}$, since the hypersurface that separates the evaporating black hole from the end-state geometry is defined using this coordinate, specifically by the condition $\hat{\mathrm{x}} = \hat{\mathrm{x}}_{\mathrm{E}}$. For this purpose, we introduce the running b constant:

$$\hat{b} = b + \frac{\varepsilon\pi G}{2}\phi_0 + \frac{\varepsilon\pi G}{4}\ln\left|be^{-2\hat{\mathrm{x}}} - 1\right|. \tag{4.156}$$

Since the deviation from the constant b is of order ε, we can replace every occurrence of b in the first-order perturbation theory with $\hat{b}$. Consequently, Eqs. (4.148) are modified as follows:

$$\begin{aligned} \mathrm{F}^+\mathrm{F}^- e^{2\rho} &= \hat{b}e^{2\phi} - 1 - \frac{\varepsilon\pi G}{4}e^{2\phi}\ln\left|\hat{b} - e^{-2\phi}\right|, \\ \ln\left|\hat{b} - e^{-2\phi}\right| - \frac{\varepsilon\pi G}{4}\frac{\ln\left|\hat{b} - e^{-2\phi}\right|}{\hat{b} - e^{-2\phi}} &= 2\lambda\hat{\sigma}. \end{aligned} \tag{4.157}$$

These two relations are valid for every value of the coordinate $\hat{\mathrm{x}}$. As we move toward the event horizon at $\hat{\mathrm{x}} = \hat{\mathrm{x}}_{\mathrm{E}}$, the quantity $\hat{b}$ decreases smoothly and takes the value:

$$\hat{b}_{\mathrm{E}} = \frac{\varepsilon\pi G}{4}\left(\ln\frac{\varepsilon\pi G}{4} - 1\right), \tag{4.158}$$

at $\hat{\mathrm{x}} = \hat{\mathrm{x}}_{\mathrm{E}}$. Because $\hat{b}_{\mathrm{E}}$ is of order ε at this point, we may set $\hat{b} \to 0$ in the first-order perturbative expansion. After taking this limit, Eqs. (4.157) reduce to the Minkowski vacuum solution (4.149) with constant $\phi_0' = \frac{2}{\varepsilon\pi G}\hat{b}_{\mathrm{E}}$. Comparing with the exact solution (4.128), we find that, upon transforming to Kruskal coordinates, the two solutions coincide to first order.

To determine whether a further outgoing shockwave emerges from the evaporation end-point, we integrate the "$--$" equation in (4.73) from $\sigma_{\mathrm{E}}^- - \epsilon$ to $\sigma_{\mathrm{E}}^- + \epsilon$, and then take the limit $\epsilon \to 0$, which yields:

$$\lim_{\epsilon\to 0} e^{-2\rho}\left[\partial_-\phi + \frac{\varepsilon\pi G}{2}e^{2\phi}\partial_-(\phi - \rho)\right]\Bigg|_{\sigma_{\mathrm{E}}^- - \epsilon}^{\sigma_{\mathrm{E}}^- + \epsilon} = \frac{\lambda b_0}{2\mathrm{F}^-}e^{2(\phi-\rho)}, \tag{4.159}$$

where $b_0 = \frac{\pi G \Delta M}{\lambda}$ and ΔM denotes the mass of the shockwave. By substituting the derivatives directly, we obtain:

$$-\frac{b_0}{\mathrm{F}^-} e^{2(\phi-\rho)} = \frac{\varepsilon\pi G}{4} e^{2\phi} + \frac{\varepsilon\pi G}{2}\frac{1}{b - e^{-2\phi}} + \frac{\varepsilon\pi G}{4}\frac{\delta^2}{b - \delta^2\left(b - e^{-2\phi}\right)}. \tag{4.160}$$

A careful calculation of this expression yields the following:

$$b_0 = -\frac{\varepsilon\pi G}{4} b e^{-2\hat{\mathrm{x}}_{\mathrm{E}}} - \frac{\varepsilon\pi G}{4} b e^{-2\phi}. \tag{4.161}$$

Since $e^{-2\hat{\mathrm{x}}_{\mathrm{E}}} \propto 1/b$, the first term remains finite in the limit $b \to 0$, whereas the second term vanishes. Consequently, the mass of the thunderpop is:

$$\Delta M = -\frac{\varepsilon\lambda}{4} b e^{-2\mathrm{x}_{\mathrm{E}}} = \frac{\varepsilon\lambda\Delta}{4x_{\mathrm{E}}^-}, \tag{4.162}$$

which matches the exact expression.

Finally, we turn to verifying the energy balance (3.115) in the BPP model. We begin by evaluating the total energy emitted by the black hole throughout its entire evaporation process:

$$E_{rad} = \varepsilon\int_{-\infty}^{\sigma_{\mathrm{E}}^-} \frac{\mathrm{d}\sigma^-}{\mathrm{F}^-} t_-(\hat{\sigma}^-) = \frac{\varepsilon\lambda}{4}\left[b e^{-2\hat{\mathrm{x}}_{\mathrm{E}}} - \ln\left|b e^{-2\hat{\mathrm{x}}_{\mathrm{E}}} - 1\right|\right] = M + \frac{\varepsilon\lambda}{4}\left[2\phi_0 - \ln\frac{\varepsilon\pi G}{4} + 1 - \frac{\Delta}{x_{\mathrm{E}}^-}\right], \tag{4.163}$$

where, in the last step, we have made use of the expression (4.144) for $t_-(\hat{\sigma}^-)$. Observe that this result matches exactly the exact formula (4.126). This agreement arises because the coordinate transformation F^-, which enters the computation of the radiated energy, does not acquire quantum corrections in the BPP model. The energy balance can be reformulated in terms of the b-parameters as:

$$b_{rad} = b + \frac{\varepsilon\pi G}{2}\phi_0 - \frac{\varepsilon\pi G}{2}\phi_0' - b_0, \tag{4.164}$$

In this relation, $\frac{\varepsilon\pi G}{2}\phi_0$ represents the mass of the spacetime before the collapse, while $\frac{\varepsilon\pi G}{2}\phi_0'$ corresponds to the mass of the final configuration. The parameter $b = \frac{\pi G M}{\lambda}$ is the b-parameter associated with the incoming shockwave, b_0 denotes the b-parameter of the outgoing shockwave, and $b_{rad} = \frac{\pi G E_{rad}}{\lambda}$ is the b-parameter describing the Hawking radiation.

4.5 Thermodynamical quantities

In this section, we derive the temperature and entropy of the static black hole in the CGHS model. At first glance, discussing black hole entropy might seem meaningless unless one adopts the framework of quantum field theory in curved spacetime. Nonetheless, the temperature can actually be obtained purely from the geometric data (see App. D.6). In general, the temperature is given by $T = \frac{\kappa}{2\pi\hbar}$, where κ is the surface gravity calculated in Eq. (4.40). For our case, this yields:

$$T = \frac{\lambda}{2\pi} \quad \Longrightarrow \quad T = \frac{\lambda\hbar c}{2\pi k_B}. \tag{4.165}$$

We observe that the temperature is independent of the mass. Applying the thermodynamic relation $\mathrm{d}M = T\,\mathrm{d}S$, we obtain the entropy as $S = \frac{M}{T}$. The integration constant is chosen such that $S = 0$ at $M = 0$. It is customary to express the entropy in terms of the value of the dilaton at the horizon, namely:

$$e^{-2\phi_H} = b = \frac{\pi G M}{\lambda c^2} \quad \Longrightarrow \quad M = \frac{\lambda c^2}{\pi G} e^{-2\phi_H} \quad \Longrightarrow \quad S = k_B \frac{2c^3}{G\hbar} e^{-2\phi_H}, \tag{4.166}$$

where we have employed the expression for the temperature (4.165) together with the static black hole solution (4.42). Finally, by setting $k_B = \hbar = c = G = 1$, we arrive at the following expressions for the temperature and entropy of a static black hole in the CGHS model:

$$T = \frac{\lambda}{2\pi} \quad \wedge \quad S = 2e^{-2\phi_H}. \tag{4.167}$$

Note that these expressions remain valid even after quantum corrections are included, since the surface gravity stays unchanged.

Chapter 5

Dimensionally-reduced Einstein gravity

In this chapter, we set the stage for studying the information loss paradox by computing the Page curve for the theory of dimensionally reduced Einstein–Hilbert gravity (the DREH model). Our primary goal here is to construct the eternal and evaporating black hole scenarios within this theory. In the preceding chapter, we pursued the same objective using the CGHS model of dilaton gravity. That model has the key benefit that its equations of motion remain exactly solvable even after incorporating quantum corrections. This feature is absent in the DREH model. Nonetheless, since Einstein gravity is a thoroughly experimentally tested theory, analyzing entanglement entropy in the DREH model is highly significant. Once quantum corrections are introduced, we employ the perturbative approach described in Sec. 4.3.4. The reduced action (2.19) was obtained in Chap. 2. For convenience, we rewrite it here:

$$S_{\mathrm{DREH}} = \frac{1}{4G}\int d^2x\sqrt{-g}e^{-2\phi}\left[R + 2(\nabla\phi)^2 + 2\lambda^2 e^{2\phi}\right] - \frac{1}{2}\int d^2x\sqrt{-g}\,(\nabla f)^2\,. \tag{5.1}$$

The first term in Eq. (5.1) represents the gravitational action, denoted by S_g, whereas the second term introduces the matter contribution as a single scalar field, labeled S_m. Unlike in the CGHS model, we do not require additional scalar fields, since no correction term can be incorporated into the action that would make the equations of motion exactly solvable.

The chapter is divided into three main sections. In the first Sec. 5.1, we solve the classical equations of motion derived from (5.1). We begin by analyzing the vacuum solution, then determine the solution with charged matter, and finally formulate the classical gravitational collapse. In this part we largely follow [111].

In the next Sec. 5.2, quantum corrections are included through the Polyakov–Liouville action Eq. (3.72). The general static vacuum solution is obtained by employing the static ansatz introduced in Sec. 3.1. We then examine two specific cases: the vacuum solution associated with the Boulware state of the quantum fields and the eternal black hole solution. Here, our presentation is based on the arguments given in both [42] and [111].

The concluding Sec. 5.3 addresses the evaporating black hole scenario. We obtain the solution that satisfies the Unruh vacuum condition, and then demonstrate that the apparent horizon and the singularity meet at a finite point in the spacetime. We also show that the end-state geometry is again described by the static Boulware vacuum solution, and that there is no need to invoke a thunderpop. The entire analysis is carried out to first order in a perturbative expansion in $\hbar$. In this section we mainly follow [111].

5.1 Equations of motion and their solutions

We now proceed to determine the equations of motion obtained by varying the action 5.1.First, we address the gravitational part of the action:

$$\begin{aligned}
\delta S_g &= \frac{1}{4G}\int d^2x\left\{\delta\left(\sqrt{-g}e^{-2\phi}R\right)+2\delta\sqrt{-g}\left[(\nabla\phi)^2+\lambda^2e^{2\phi}\right]e^{-2\phi}+2\sqrt{-g}\delta\left(e^{-2\phi}(\nabla\phi)^2\right)\right\}\\
&= \frac{1}{4G}\int d^2x\sqrt{-g}e^{-2\phi}\Big\{-e^{2\phi}\left[\nabla_\mu\nabla_\nu e^{-2\phi}+g_{\mu\nu}\Box e^{-2\phi}\right]\delta g^{\mu\nu}-2R\delta\phi\\
&\quad -g_{\mu\nu}\left[(\nabla\phi)^2+\lambda^2e^{2\phi}\right]e^{-2\phi}\delta g^{\mu\nu}+2\nabla_\mu\phi\nabla_\nu\phi\delta g^{\mu\nu}+4\left[(\nabla\phi)^2-\Box\phi\right]\delta\phi\Big\}\\
&= \frac{1}{4G}\int d^2x\sqrt{-g}e^{-2\phi}\Big\{\left[2\nabla_\mu\nabla_\nu\phi-2\nabla_\mu\phi\nabla_\nu\phi+g_{\mu\nu}\left(3(\nabla\phi)^2-2\Box\phi-\lambda^2e^{2\phi}\right)\right]\delta g^{\mu\nu}\\
&\qquad +\left[4(\nabla\phi)^2-4\Box\phi-2R\right]\delta\phi\Big\}.
\end{aligned}\tag{5.2}$$

Throughout this computation, the same terms as in the CGHS model appear. In the second line, we employ Eq. (4.9) for the variation of the scalar curvature, together with $\delta\ln\left(\sqrt{-g}\right)=-\frac{1}{2}g_{\mu\nu}\delta g^{\mu\nu}$. Moreover, we make use of the enhanced symmetry of the 2D spacetime, which leads to a vanishing Einstein tensor, $G_{\mu\nu}=0$. The matter contribution is exactly the same as in the CGHS model (4.11), so we simply reproduce it here:

$$\delta S_m=-\int d^2x\sqrt{-g}\left\{\frac{1}{2}\left[\nabla_\mu f\nabla_\nu f-\frac{1}{2}g_{\mu\nu}(\nabla f)^2\right]\delta g^{\mu\nu}-(\Box f)\,\delta f\right\},\tag{5.3}$$

where we have omitted the sum, since the DREH model involves only a single scalar field. Using the same notation for the energy–momentum tensor as in the CGHS model, we arrive at the following equations of motion:

$$\begin{aligned}
\frac{\delta S}{\delta g^{\mu\nu}}=0: &\quad 2\nabla_\mu\nabla_\nu\phi e^{-2\phi}-2\nabla_\mu\phi\nabla_\nu\phi e^{-2\phi}+g_{\mu\nu}\left(3(\nabla\phi)^2-2\Box\phi-\lambda^2e^{2\phi}\right)e^{-2\phi}=2GT^f_{\mu\nu},\\
\frac{\delta S}{\delta\phi}=0: &\quad (\nabla\phi)^2-\Box\phi=\frac{R}{2},\\
\frac{\delta S}{\delta f}=0: &\quad \Box f=0,\\
T_{\mu\nu}=\frac{-2}{\sqrt{-g}}\frac{\delta S_m}{\delta g^{\mu\nu}}: &\quad T_{\mu\nu}=\nabla_\mu f\nabla_\nu f-\frac{1}{2}g_{\mu\nu}(\nabla f)^2
\end{aligned}\tag{5.4}$$

The metric equation in Eq. (5.4) can be simplified. Contracting it with the metric tensor $g^{\mu\nu}$ yields $\Box e^{-2\phi}=2\lambda^2+2GT$, where $T=g^{\mu\nu}T_{\mu\nu}$. Defining a new field $\varphi=e^{-\phi}$ and using the dilaton equation, we arrive, after some algebraic manipulations, at:

$$\nabla_\mu\nabla_\nu\varphi-\frac{1}{2}R_{\mu\nu}\varphi=-G\left(T_{\mu\nu}-\frac{1}{2}g_{\mu\nu}T\right)\varphi^{-1},\tag{5.5}$$

$$\Box\varphi^2=2\lambda^2+2GT.\tag{5.6}$$

Note that we have not introduced the reduced field x (2.46) in the same manner as in the CGHS model. Instead, we use φ. The reduced field is defined later, and its definition involves the Schwarzschild radius.

5.1.1 Vacuum solution of classical equations of motion

We now determine the general solution of the classical vacuum equations of motion in the conformal gauge $\mathrm{d}s^2 = -e^{2\rho}\mathrm{d}x^+\mathrm{d}x^-$, introduced in Eq. (3.2). In this gauge, the non-zero components of the connection, Ricci tensor, and scalar curvature are listed in Eq. (3.3), and the scalar field invariants are specified in Eq. (3.4). With these choices, the equations of motion (5.5) and (5.6) take the form:

$$\partial_\pm\left(e^{-2\rho}\partial_\pm\varphi\right) = -GT_{\pm\pm}\varphi^{-1}e^{-2\rho}, \tag{5.7}$$
$$\partial_+\partial_-\varphi + \varphi\partial_+\partial_-\rho = 0, \tag{5.8}$$
$$\partial_+\partial_-\varphi^2 + \frac{\lambda^2}{2}e^{2\rho} = 0. \tag{5.9}$$

In this step, we have made explicit use of the symmetry of the scalar field EMT, the fact that its trace is zero, and that the only non-vanishing components are $T_{\pm\pm}$, which are set to zero when considering the vacuum solution. Integrating Eq. (5.7), we obtain:

$$\partial_\pm\varphi = \frac{\lambda}{2}\mathrm{F}^\mp(x^\mp)e^{2\rho}, \tag{5.10}$$

where $\mathrm{F}^\pm(x^\pm)$ denote a set of arbitrary functions. Shortly, it will become evident that they are identified with the Killing vector (3.5) associated with time translations. The functions $\partial_\pm\varphi$ obey the consistency condition $\partial_+\partial_-\varphi = \partial_-\partial_+\varphi$. Making use of this property leads to:

$$\nabla_+\mathrm{F}^+ = \nabla_-\mathrm{F}^-, \tag{5.11}$$
$$\partial_+\partial_-\varphi = \frac{\lambda}{2}\nabla_+\mathrm{F}^+e^{2\rho}. \tag{5.12}$$

Combining this expression with Eqs. (5.9) and (5.10), we can write φ in terms of $\mathrm{F}^\pm$ and ρ as

$$\varphi = -\frac{\lambda}{2}\frac{1+\mathrm{F}^+\mathrm{F}^-e^{2\rho}}{\nabla_+\mathrm{F}^+}. \tag{5.13}$$

We now determine $\partial_+\partial_-\rho$ by inserting Eqs. (5.13) and (5.12) into Eq. (5.8):

$$\partial_+\partial_-\rho = \frac{\left(\nabla_+\mathrm{F}^+\right)^2e^{2\rho}}{1+\mathrm{F}^+\mathrm{F}^-e^{2\rho}}. \tag{5.14}$$

One readily verifies that $\partial_-\left(1+\mathrm{F}^+\mathrm{F}^-e^{2\rho}\right) = \mathrm{F}^+\nabla_+\mathrm{F}^+e^{2\rho}$ and that $\partial_+\partial_-\rho = \frac{\partial_-\left(\nabla_+\mathrm{F}^+\right)}{2\mathrm{F}^+}$. Using these relations together with Eq. (5.14), we obtain

$$\nabla_+\mathrm{F}^+ = \mathrm{G}^+(x^+)\left(1+\mathrm{F}^+\mathrm{F}^-e^{2\rho}\right)^2, \tag{5.15}$$

where $\mathrm{G}^+(x^+)$ is an arbitrary function. Differentiation with respect to x^+ reproduces the same relation, implying that we also find:

$$\nabla_+\mathrm{F}^+ = \mathrm{G}^-(x^-)\left(1+\mathrm{F}^+\mathrm{F}^-e^{2\rho}\right)^2, \tag{5.16}$$

where $\mathrm{G}^-(x^-)$ is likewise an arbitrary function. Because these two expressions coincide, the functions $G^\pm$ must in fact be equal to the same constant: $\mathrm{G}^+(x^+) = \mathrm{G}^-(x^-) = -\frac{1}{2a}$, where the significance of a will be clarified shortly. Therefore, using Eq. (5.13), we arrive at the following result:

$$\nabla_+\mathrm{F}^+ = -\frac{1}{2a}\left(1+\mathrm{F}^+\mathrm{F}^-e^{2\rho}\right)^2 = -\frac{\lambda}{2}\frac{\lambda a}{\varphi^2}. \tag{5.17}$$

We can check that $\nabla_+ \mathrm{F}^+$ likewise obeys $\nabla_+ \mathrm{F}^+ = \mathrm{F}^\pm \partial_\pm \ln \left(\mathrm{F}^+ \mathrm{F}^- e^{2\rho}\right)$. Combined with Eqs. (5.17) and (5.13), this allows the derivatives of φ to be written as:

$$\partial_\pm \varphi = -\frac{\lambda}{2\mathrm{F}^\pm} \frac{\varphi - \lambda a}{\varphi}. \tag{5.18}$$

By integrating this equation, we obtain the final result, which is expressed by the following two equations:

$$\varphi + \lambda a \ln\left(\frac{\varphi}{\lambda a} - 1\right) = -\frac{\lambda}{2}\left(\int \frac{\mathrm{d}x^+}{\mathrm{F}^+} + \int \frac{\mathrm{d}x^-}{\mathrm{F}^-}\right) \equiv \lambda\sigma, \tag{5.19}$$

$$\mathrm{F}^+ \mathrm{F}^- e^{2\rho} = \frac{\lambda a}{\varphi} - 1. \tag{5.20}$$

The general solution of the classical vacuum Eqs. (5.19-5.20) is characterized by one integration constant and two arbitrary functions. We denote it by the ordered triplet $(\mathrm{F}^+, \mathrm{F}^-, a)$. It is clear that this solution is expressed in the form Eqs. (3.18-3.19). The first line gives the dilaton field and defines the tortoise coordinate, whereas the second line provides the metric functions Λ. The functions $\mathrm{F}^\pm$ represent the coordinate transformations from an arbitrary coordinate system to the Eddington–Finkelstein coordinates. Therefore, we conclude that the most general vacuum solution of the DREH equations of motion corresponds to the static Schwarzschild black hole. A natural choice for the dilaton field is $\varphi = e^{-\phi} = \lambda r$, thereby introducing the radial coordinate. Expressing the metric in terms of this radial coordinate yields

$$\mathrm{d}s^2 = -\left(1 - \frac{a}{r}\right)\mathrm{d}t^2 + \frac{\mathrm{d}r^2}{1 - \frac{a}{r}}. \tag{5.21}$$

Thus, the Schwarzschild metric is recovered within the DREH model. By direct comparison with the standard Schwarzschild solution, we identify the constant a as the Schwarzschild radius. The appearance of the Schwarzschild black hole as the most general solution of the vacuum equations of motion in the DREH model is precisely how Birkhoff's theorem [106] manifests itself in this two-dimensional framework. This observation also makes it clear that the model arises from dimensional reduction over $\mathbb{S}^2$. For more details on the standard Schwarzschild solution see App. C.

5.1.2 General static solution with charged matter

The key conclusion of the previous subsection is that the most general vacuum solution coincides with a static black hole configuration corresponding to the 4D Schwarzschild geometry. We now turn to determining the most general static solution when the matter fields are permitted to carry a certain type of charge, similarly to the CGHS model in Sec. 4.1.4. In doing so, we make explicit use of the fact that the classical scalar field EMT is traceless. After imposing the static ansatz of Sec. 3.1, the equations of motion (5.5-5.6) take the following form:

$$\begin{aligned}
&\frac{2G\Lambda}{\lambda^2\varphi} T_{\mu\nu} = \left[\mathcal{D}^2 \frac{\mathrm{d}\Lambda}{\mathrm{d}\varphi} + \frac{\mathcal{D}\varphi}{2}\frac{\mathrm{d}}{\mathrm{d}\varphi}\left(\mathcal{D}\frac{\mathrm{d}\Lambda}{\mathrm{d}\varphi}\right)\right]\xi_\mu \xi_\nu - \left[\frac{\mathrm{d}\left(\Lambda \mathcal{D}^2\right)}{\mathrm{d}\varphi} + \frac{\mathcal{D}\varphi}{2}\frac{\mathrm{d}}{\mathrm{d}\varphi}\left(\mathcal{D}\frac{\mathrm{d}\Lambda}{\mathrm{d}\varphi}\right)\right]\varepsilon_{\mu\rho}\varepsilon_{\nu\sigma}\xi^\rho \xi^\sigma, \\
&\mathcal{D}\frac{\mathrm{d}}{\mathrm{d}\varphi}\left(\Lambda \mathcal{D}\varphi\right) = -1.
\end{aligned} \tag{5.22}$$

The trace of the metric equation gives:

$$\mathcal{D}^2\frac{\mathrm{d}\Lambda}{\mathrm{d}\varphi}+\frac{\mathrm{d}\left(\Lambda\mathcal{D}^2\right)}{\mathrm{d}\varphi}+\mathcal{D}\varphi\frac{\mathrm{d}}{\mathrm{d}\varphi}\left(\mathcal{D}\frac{\mathrm{d}\Lambda}{\mathrm{d}\varphi}\right)=0. \tag{5.23}$$

Substituting the second equation from Eq. (5.22) into Eq. (5.23) yields an integrable equation. Solving it introduces a positive charge $\mu>0$, associated with the scalar field in the same way as in Eq. (4.34) of the CGHS model, namely:

$$\varphi\Lambda^2\mathcal{D}\frac{\mathrm{d}\mathcal{D}}{\mathrm{d}\varphi}=-\mu, \qquad \mathcal{D}^2=\left(\frac{\mu}{\Lambda}-1\right)\left(\frac{\mathrm{d}\left(\Lambda\varphi\right)}{\mathrm{d}\varphi}\right)^{-1}, \qquad \Lambda^2T^{\Vert\Vert}=\Lambda^2T^{\perp\perp}=\frac{\lambda^2\mu}{2G}. \tag{5.24}$$

Inserting this form of $\mathcal{D}_1$ leads to a second-order differential equation for Λ. Integrating once, we obtain:

$$\left(1-\frac{\mu}{\Lambda}\right)\frac{\mathrm{d}\left(\Lambda\varphi\right)}{\mathrm{d}\varphi}=-A-2\mu\ln\left|\Lambda\varphi\right|, \tag{5.25}$$

where A is an additional integration constant. Putting Eq. (5.25) back into the expression for $\mathcal{D}_1$ in Eq. (5.24) we see that $A+2\mu\ln|\Lambda\varphi|>0$. Treating Eq. (5.25) as a differential equation for φ as a function of $\Lambda\varphi$, we find the solution:

$$\varphi=\frac{\Lambda\varphi}{\mu}+\sqrt{A+2\mu\ln|\Lambda\varphi|}\left[B-\frac{\sqrt{2\pi}\,\mathrm{sgn}(\Lambda)}{2\mu^{3/2}}e^{-\frac{A}{2\mu}}\mathrm{erfi}\left(\sqrt{\ln|\Lambda\varphi|+\frac{A}{2\mu}}\right)\right], \tag{5.26}$$

where B is the final integration constant, and $\mathrm{erfi}(x)$ denotes the imaginary error function, defined by

$$\mathrm{erfi}(x)=\frac{2}{\sqrt{\pi}}\int_0^x e^{t^2}\mathrm{d}t. \tag{5.27}$$

The tortoise coordinate (3.18) can likewise be expressed in terms of $\Lambda\varphi$ and takes the form:

$$\lambda\sigma=\frac{1}{\sqrt{2\mu}}\left[\varphi\sqrt{\ln|\Lambda\varphi|+\frac{A}{2\mu}}+\frac{\sqrt{\pi}\,\mathrm{sgn}(\Lambda)}{2\mu}e^{-\frac{A}{2\mu}}\mathrm{erfi}\left(\sqrt{\ln|\Lambda\varphi|+\frac{A}{2\mu}}\right)\right]. \tag{5.28}$$

The asymptotic behavior of this solution is given by $\varphi=\frac{\Lambda\varphi}{2\mu\ln|\Lambda\varphi|}$. Hence, the geometry is not asymptotically flat, and the solution is therefore completely disconnected from the standard Schwarzschild black hole solution.

5.1.3 Classical gravitational collapse

To describe classical gravitational collapse, we adopt the approach presented in Sec. 3.4. The energy-momentum tensor is specified as an incoming shockwave with components $T_{++}=-\frac{M}{\mathrm{F}^+(x_0^+)}\delta(x^+-x_0^+)$ and $T_{--}=0$, where M denotes the mass carried by the shockwave. The associated Penrose diagram is depicted in Fig. 3.2. The spacetime consists of two regions (I and II in Fig. 3.2), which must be joined smoothly. In particular, the metric and the dilaton field are required to match continuously across the hypersurface $x^+=x_0^+$, as imposed by condition (3.102):

$$e^{2\rho_{\mathrm{I}}}\Big|_{x^+=x_0^+-\epsilon}=e^{2\rho_{\mathrm{II}}}\Big|_{x^+=x_0^++\epsilon}, \tag{5.29}$$

$$\varphi_I\Big|_{x^+=x_0^+-\epsilon}=\varphi_{II}\Big|_{x^+=x_0^++\epsilon}, \tag{5.30}$$

when $\epsilon \to 0$, and the indices I and II label parts I and II of the spacetime, respectively, in the same manner as in Sec. 3.4. In region I, the vacuum solution is specified by $(\mathrm{F}_{\mathrm{I}}^{+}, \mathrm{F}_{\mathrm{I}}^{-}, a_{\mathrm{I}})$, whereas in region II it is characterized by $(\mathrm{F}_{\mathrm{II}}^{+}, \mathrm{F}_{\mathrm{II}}^{-}, a_{\mathrm{II}})$. The final condition (3.104) follows from integrating Eq. (5.7). This yields:

$$e^{-2\rho_{\mathrm{II}}}\partial_{+}\varphi_{II}\bigg|_{x^+=x_0^+ +\epsilon} - e^{-2\rho_{\mathrm{I}}}\partial_{+}\varphi_{I}\bigg|_{x^+=x_0^+ -\epsilon} = \frac{GM}{\mathrm{F}^+}e^{-2\rho}\varphi^{-1}\bigg|_{x^+=x_0^+}. \tag{5.31}$$

Eq. (5.31), together with Eqs. (5.10) and (5.29), leads to a discontinuity in the derivatives of the dilaton field and consequently to a discontinuity in the F^- coordinate transformation, which is given by:

$$\mathrm{F}_{\mathrm{II}}^{-} = \mathrm{F}_{\mathrm{I}}^{-} + \frac{2MG}{\lambda \mathrm{F}^+}e^{-2\rho}\varphi^{-1}\bigg|_{x^+=x_0^+}. \tag{5.32}$$

From Eq. (5.29) and solution (5.20), together with Eq. (5.30), we also find that the constant a undergoes a change at $x^+ = x_0^+$.

$$a_{\mathrm{II}} = a_{\mathrm{I}} + \frac{2GM}{\lambda^2}. \tag{5.33}$$

Hence, we conclude that the solution in region II of the spacetime takes the following form:

$$\left(\mathrm{F}_{\mathrm{I}}^{+}, \mathrm{F}_{\mathrm{I}}^{-}\left(1 + \frac{2MG/\lambda}{\lambda a_{\mathrm{I}} - \varphi(x_0^+, x^-)}\right), a_{\mathrm{I}} + \frac{2MG}{\lambda^2}\right). \tag{5.34}$$

Eq. (5.34) specifies the structure of the solution in region II, given that region I already contains a black hole solution and that this black hole consumes matter of mass M. Without loss of generality, we may adopt the Eddington–Finkelstein gauge in region I, which corresponds to choosing $\mathrm{F}_{\mathrm{I}}^{+} = -1$ and $\mathrm{F}_{\mathrm{I}}^{-} = 1$. To investigate gravitational collapse, we further set the metric in region I to be that of Minkowski spacetime by taking $a_{\mathrm{I}} = 0$. The associated dilaton field is then $\varphi_{\mathrm{I}} = \frac{\lambda}{2}(\sigma^+ - \sigma^-)$. With these choices, Eq. (5.34) shows that the geometry in region II indeed contains a black hole of mass M:

$$\left(-1, 1 - \frac{4MG/\lambda^2}{\sigma_0^+ - \sigma^-}, \frac{2MG}{\lambda^2}\right). \tag{5.35}$$

Let us now introduce the notation that will be used from this point onward. To begin with, we take the solution in region I of the spacetime to be the Minkowski vacuum, specified by $(-1, 1, 0)$. We then define $\hat{\varphi}(\sigma^-) = \frac{\lambda}{2}\left(\sigma_0^+ - \sigma^-\right)$. With this function, the coordinate transformations in region II can be written as:

$$\mathrm{F}^+ = -1, \quad \mathrm{F}^- = \frac{\hat{\varphi} - \lambda a}{\hat{\varphi}}. \tag{5.36}$$

Here we omit the index II on the functions $\mathrm{F}_{\mathrm{II}}^{\pm}$ as well as on the constant a_{II}, and simply write $a = \frac{2MG}{\lambda^2}$. In region II of the spacetime, relation (5.19) remains valid, so we define new Eddington–Finkelstein coordinates $\hat{\sigma}^{\pm}$ via Eq. (3.106). Expressed in terms of $\sigma^{\pm}$, these are:

$$\hat{\sigma}^+ = \sigma^+, \tag{5.37}$$

$$\hat{\sigma}^- = \sigma_0^+ - \frac{2}{\lambda}\left[\hat{\varphi} + \lambda a \ln\left(\frac{\hat{\varphi}}{\lambda a} - 1\right)\right]. \tag{5.38}$$

Next, we define the reduced dilaton field (2.46) using the Schwarzschild radius a as:

$$\mathrm{x} = \frac{\varphi}{\lambda a}. \tag{5.39}$$

Moreover, the solutions (5.19) and (5.20) in region II of the spacetime can be recast in terms of the coordinates δ and $\hat{\mathrm{x}}$, defined in Eq. (3.107) and the reduced field x:

$$\begin{aligned} &\mathrm{x}+\ln(\mathrm{x}-1)=-\ln\delta+\hat{\mathrm{x}}+\ln(\hat{\mathrm{x}}-1),\\ &\mathrm{F}^{+}\mathrm{F}^{-}e^{2\rho}=\frac{1}{\mathrm{x}}-1. \end{aligned} \tag{5.40}$$

Now we analyze solution (5.40). From the metric equation we infer the presence of a black hole, with a singularity located at $\mathrm{x}=0$ and an event horizon at $\mathrm{x}=1$. Recall that $\varphi=\lambda\hat{r}$, where $\hat{r}$ is the radial coordinate in region II of the spacetime. Inspecting solution (5.40) once more, we find that the condition $\varphi=\lambda a$ translates into $\hat{\varphi}=\lambda a$. Consequently, the hypersurfaces corresponding to the horizon and the singularity are given by:

$$\sigma^{-}_{\mathrm{H}}=\sigma^{+}_{0}-2a, \tag{5.41}$$

$$\ln\delta_{S}=\hat{\mathrm{x}}_{\mathrm{S}}+\ln|\hat{\mathrm{x}}_{\mathrm{S}}-1|, \tag{5.42}$$

respectively. In the limit $t\to\infty$, we obtain $\sigma^{+}\to\infty$, which is equivalent to $\delta\to 0$. Applying Eq. (5.42), we conclude that the horizon and the singularity meet at future time infinity i^{+}. This is precisely what one expects, as quantum corrections are absent in this scenario. Both of these lines are depicted in the conformal diagram (see Fig. 3.2). In both spacetime regions there exists a timelike Killing vector, but its form changes upon crossing the separating hypersurface. Therefore, the full spacetime is not stationary. This configuration corresponds to the classical CGHS gravitational collapse analyzed in Sec. 4.1.5.

5.2 Adding quantum corrections

In close analogy with the treatment of the CGHS model in Secs. 4.2 and 4.3, we now consider the quantum-corrected DREH model by supplementing the classical DREH action (5.1) with the Polyakov–Liouville term (3.72). Further details on the PL action are provided in Sec. 3.3. Unlike in the CGHS case, here no additional correction terms can be introduced that render the quantum-corrected equations of motion exactly solvable. Consequently, the dilaton equation of motion in Eq. (5.4) remains unchanged. The metric equation, on the other hand, is modified solely through the contribution of the energy–momentum tensor of the quantum fluctuations (3.75), and takes the form:

$$\begin{aligned} \Big[2\nabla_\mu\nabla_\nu\phi-2\nabla_\mu\phi\nabla_\nu\phi+g_{\mu\nu}\Big(3(\nabla\phi)^2-2\Box\phi-\lambda^2e^{2\phi}\Big)\Big]e^{-2\phi}=2G_{\mathrm{N}}\Bigg\{\nabla_\mu f\nabla_\nu f-\frac{1}{2}g_{\mu\nu}(\nabla f)^2\\ +\frac{\hbar}{48\pi}\Bigg[-2\nabla_\mu\nabla_\nu\psi+\nabla_\mu\psi\nabla_\nu\psi+g_{\mu\nu}\left(2\Box\psi-\frac{1}{2}(\nabla\psi)^2\right)\Bigg]\Bigg\}, \end{aligned} \tag{5.43}$$

where the EMT of the PL-type quantum fluctuations is explicitly presented in the second line. In this section, we focus exclusively on quantum-corrected vacuum solutions. Therefore, the classical contribution to the EMT is set to zero. In the conformal gauge (3.2), the equations of motion become:

$$\partial_{\pm}\left(e^{-2\rho}\partial_{\pm}\varphi\right)=\frac{\hbar G}{12\pi}\left[(\partial_{\pm}\rho)^2-\partial^2_{\pm}\rho+t_{\pm}(x^{\pm})\right]\varphi^{-1}e^{-2\rho}, \tag{5.44}$$

$$\partial_+\partial_-\varphi+\varphi\partial_+\partial_-\rho=0, \tag{5.45}$$

$$\partial_+\partial_-\varphi^2+\frac{\lambda^2}{2}e^{2\rho}+\frac{\hbar G}{6\pi}\partial_+\partial_-\rho=0, \tag{5.46}$$

where the explicit forms of the quantum-corrected EMT components in Eq. (3.77) have been employed. From this, we clearly observe that the dilaton Eq. (5.45) coincides with Eq. (5.8), and therefore remains unchanged. In contrast, the trace Eq. (5.9), associated with its quantum-corrected counterpart (5.46), is modified. This modification arises due to the gravitational trace anomaly. Specifically, the trace of the quantum-corrected EMT takes the form $\langle \delta T^{(f)} \rangle = \frac{\hbar}{3} e^{-2\rho}\partial_+\partial_-\rho$, whereas in the classical case the scalar field EMT is traceless.

These quantum-corrected equations are not exactly solvable. Instead, we treat them perturbatively to first order in the expansion parameter $\varepsilon = \frac{\hbar G}{12\pi}$, following the procedure outlined in Sec. 3.4.1. We apply this method in complete analogy with the BPP model discussed in Sec. 4.3.4. Concretely, we perform the perturbative expansion by shifting the dilaton as $\varphi \mapsto \varphi + \varepsilon\theta$ and the metric as $\rho \mapsto \rho + \varepsilon\alpha$, as specified in Eq. (3.108). The quantum correction to Eqs. (5.44-5.46), expressed in terms of θ and α, is then given by:

$$\partial_\pm \left[e^{-2\rho}\partial_\pm\theta - 2\alpha e^{-2\rho}\partial_\pm\varphi \right] = \left[(\partial_\pm\rho)^2 - \partial_\pm^2\rho + t_\pm(x^\pm) \right] \varphi^{-1} e^{-2\rho}, \tag{5.47}$$

$$\partial_+\partial_-\theta + \varphi\partial_+\partial_-\alpha + \theta\partial_+\partial_-\rho = 0, \tag{5.48}$$

$$\partial_+\partial_- \left(\theta\varphi + \rho \right) + \frac{\lambda^2}{2}\alpha e^{2\rho} = 0. \tag{5.49}$$

The first step in solving these equations is to integrate the first one, Eq. (5.47). By expressing ρ from Eq. (5.20) and substituting it into $(\partial_\pm\rho)^2 - \partial_\pm^2\rho + t_+(x^\pm)$, this equation can be recast into the form (3.110). After further using the relation (5.18), we obtain:

$$\partial_\pm \left(e^{-2\rho}\partial_\pm\theta - \lambda\alpha \mathrm{F}^\mp \right) = \frac{1}{\mathrm{F}^{\pm 2}} t_\pm(\sigma^\pm) e^{-2\rho}\varphi^{-1} + \frac{\lambda}{2}\mathrm{F}^\mp \lambda a \frac{\varphi - \frac{3}{4}\lambda a}{\varphi^3(\varphi - \lambda a)^2}\partial_\pm\varphi, \tag{5.50}$$

Since $\mathcal{D}_0 = 1$, it follows that $\mathcal{F}[\varphi] = -1/(\varphi - \lambda a)$. We then introduce the function $\mathcal{D}_1(\varphi)$ via its derivative:

$$\frac{\mathrm{d}\mathcal{D}_1}{\mathrm{d}\varphi} = \lambda a \frac{\varphi - \frac{3}{4}\lambda a}{\varphi^3(\varphi - \lambda a)^2}. \tag{5.51}$$

This relation is precisely equivalent to Eq. (3.112). Upon integrating Eq. (5.50), we arrive at the expressions for the derivatives of θ:

$$\partial_+\theta = \frac{\lambda}{2}\left[\mathrm{F}^-(\mathcal{D}_1 + 2\alpha) + \mathrm{G}^- \right] e^{2\rho} - \mathrm{F}^- e^{2\rho} \int \frac{\mathrm{d}x^+}{\mathrm{F}^+} \frac{t_+(\sigma^+)}{\varphi - \lambda a}, \tag{5.52}$$

$$\partial_-\theta = \frac{\lambda}{2}\left[\mathrm{F}^+(\mathcal{D}_1 + 2\alpha) + \mathrm{G}^+ \right] e^{2\rho} - \mathrm{F}^+ e^{2\rho} \int \frac{\mathrm{d}x^-}{\mathrm{F}^-} \frac{t_-(\sigma^-)}{\varphi - \lambda a}, \tag{5.53}$$

where $G^\pm(x^\pm)$ are arbitrary functions encoding the quantum corrections to the coordinate transformations. At this stage, the derivatives $\partial_\pm\theta$ are still not known in closed form, because the integrals in Eqs. (5.52) and (5.53) cannot yet be performed explicitly. The obstacle is the functional dependence $\varphi = \varphi(x^+, x^-)$, which is only implicitly determined by the transcendental Eq. (5.19). For the moment, we therefore keep the solution in this integral representation. In order to integrate Eq. (5.52) once more, we must remove the undetermined function α. This can be achieved by using Eq. (5.49), together with Eqs. (5.10) and (5.20), from which we obtain:

$$\theta + \frac{2\mathrm{F}^-}{\lambda}\left(\varphi\partial_-\theta + \theta\partial_-\varphi + \partial_-\rho \right) = \int \mathcal{D}_1 \mathrm{d}\varphi + \frac{\mathrm{G}^-}{\mathrm{F}^-}\varphi - \int \frac{\mathrm{d}x^+}{\mathrm{F}^+}\left(\frac{\lambda a}{\varphi} - 1 \right) \int \frac{\mathrm{d}x^+}{\mathrm{F}^+} \frac{t_+(\sigma^+)}{\varphi - \lambda a} + \mathrm{H}^-, \tag{5.54}$$

where we have introduced an additional arbitrary function $\mathrm{H}^-(x^-)$. By eliminating the derivatives $\partial_-\varphi$ and $\partial_-\theta$ using Eqs. (5.18) and (5.53), respectively, and then applying the same procedure once more to Eq. (5.53), we obtain:

$$\theta = \frac{\varphi(\varphi-\lambda a)}{\lambda a}\left(\mathcal{D}_1 + 2\alpha + \frac{\mathrm{G}^+}{\mathrm{F}^+}\right) + \frac{\varphi^2}{\lambda a}\frac{\mathrm{G}^-}{\mathrm{F}^-} + \frac{1}{2\varphi} \tag{5.55}$$
$$+ \frac{\varphi}{\lambda a}\left[\int \mathcal{D}_1 \mathrm{d}\varphi - \frac{2}{\lambda}(\varphi-\lambda a)\int \frac{\mathrm{d}x^-}{\mathrm{F}^-}\frac{t_-(\sigma^-)}{\varphi-\lambda a} - \int \frac{\mathrm{d}x^+}{\mathrm{F}^+}\left(\frac{\lambda a}{\varphi}-1\right)\int \frac{\mathrm{d}x^+}{\mathrm{F}^+}\frac{t_+(\sigma^+)}{\varphi-\lambda a} - \mathrm{H}^-\right],$$
$$\theta = \frac{\varphi(\varphi-\lambda a)}{\lambda a}\left(\mathcal{D}_1 + 2\alpha + \frac{\mathrm{G}^-}{\mathrm{F}^-}\right) + \frac{\varphi^2}{\lambda a}\frac{\mathrm{G}^+}{\mathrm{F}^+} + \frac{1}{2\varphi} \tag{5.56}$$
$$+ \frac{\varphi}{\lambda a}\left[\int \mathcal{D}_1 \mathrm{d}\varphi - \frac{2}{\lambda}(\varphi-\lambda a)\int \frac{\mathrm{d}x^+}{\mathrm{F}^+}\frac{t_+(\sigma^+)}{\varphi-\lambda a} - \int \frac{\mathrm{d}x^-}{\mathrm{F}^-}\left(\frac{\lambda a}{\varphi}-1\right)\int \frac{\mathrm{d}x^-}{\mathrm{F}^-}\frac{t_-(\sigma^-)}{\varphi-\lambda a} - \mathrm{H}^+\right].$$

By equating Eqs. (5.55) and (5.56) we obtain the following consistency condition:

$$\mathrm{H}^- + \lambda a\frac{\mathrm{G}^-}{\mathrm{F}^-} - \frac{2}{\lambda}\int \frac{\mathrm{d}x^-}{\mathrm{F}^-}t_-(\sigma^-) = \mathrm{H}^+ + \lambda a\frac{\mathrm{G}^+}{\mathrm{F}^+} - \frac{2}{\lambda}\int \frac{\mathrm{d}x^+}{\mathrm{F}^+}t_+.(\sigma^+) = C, \tag{5.57}$$

where C denotes an arbitrary constant. Adding Eqs. (5.55) and (5.56), and making use of Eq. (5.57), we express θ in terms of φ and α as:

$$\theta = \frac{\varphi(\varphi-\lambda a)}{\lambda a}\left[\mathcal{D}_1 + 2\alpha + \frac{\mathrm{G}^+}{\mathrm{F}^+} + \frac{\mathrm{G}^-}{\mathrm{F}^-}\right] + \frac{1}{2\varphi} + \frac{\varphi}{\lambda a}\int \mathcal{D}_1 \mathrm{d}\varphi \tag{5.58}$$
$$-\frac{\varphi}{\lambda a}\left[\int \frac{\mathrm{d}x^+}{\mathrm{F}^+}\left(\frac{\lambda a}{\varphi}-1\right)\int \frac{\mathrm{d}x^+}{\mathrm{F}^+}\frac{t_+(\sigma^+)}{\varphi-\lambda a} + \int \frac{\mathrm{d}x^-}{\mathrm{F}^-}\left(\frac{\lambda a}{\varphi}-1\right)\int \frac{\mathrm{d}x^-}{\mathrm{F}^-}\frac{t_-(\sigma^-)}{\varphi-\lambda a}\right].$$

At this stage, a single integration has been performed. As in Sec. 3.4.1, another integration is required. This is clear from the fact that Eq. (5.58) is not yet the final form of the field θ, since it still involves the unknown function α, which must be eliminated. A straightforward way to accomplish this is to use either Eq. (5.52) or Eq. (5.53), thereby obtaining another first-order differential equation for θ. Note that the constant C defined in Eq. (5.57) does not appear explicitly in Eq. (5.58); instead, it is absorbed as the integration constant of $\int \mathcal{D}_1 \mathrm{d}\varphi$. We later demonstrate that C represents a quantum correction to the constant a. Proceeding with either Eq. (5.53) or Eq. (5.52) leads to the same outcome: one derives two alternative expressions for θ, each containing its own arbitrary functions, which are then removed by setting these expressions equal to each other. The resulting final expression for θ is:

$$\theta = \frac{\varphi-\lambda a}{\varphi}\left[\frac{\lambda}{2}\left(\int \mathrm{d}x^+\frac{\mathrm{G}^+}{\mathrm{F}^{+2}} + \int \mathrm{d}x^-\frac{\mathrm{G}^-}{\mathrm{F}^{-2}}\right) - \int d\varphi\left(\frac{\lambda a}{2\varphi(\varphi-\lambda a)^2} + \frac{\varphi}{(\varphi-\lambda a)^2}\int \mathcal{D}_1 \mathrm{d}\varphi\right)\right.$$
$$\left. + \int \frac{\mathrm{d}x^+}{\mathrm{F}^+}\frac{1}{\varphi-\lambda a}\int \frac{\mathrm{d}x^+}{\mathrm{F}^+}t_+(\sigma^+) + \int \frac{\mathrm{d}x^-}{\mathrm{F}^-}\frac{1}{\varphi-\lambda a}\int \frac{\mathrm{d}x^-}{\mathrm{F}^-}t_-(\sigma^-)\right], \tag{5.59}$$

in terms of x^+, x^-, $t_+(\sigma^+(x^+))$, $t_-(\sigma^-(x^-))$ and $\varphi(x^+,x^-)$. The next step would be to determine α. One possible approach is to use Eq. (5.52), from which it is straightforward to derive an expression for α in terms of x^+ and x^-. However, as discussed in Sec. 3.4.1, this is not required, because we already possess all the information needed to write down the quantum-corrected forms of Eqs. (5.19-5.20).

Let us first simplify the expressions by using the reduced field $\mathrm{x} = \frac{\varphi}{\lambda a}$ and the coordinate $\hat{\mathrm{x}} = \frac{\hat{\varphi}}{\lambda a}$. In terms of x, the function $\mathcal{D}_1(\mathrm{x})$ and its integral can be written as:

$$\mathcal{D}_1 = \frac{1}{4(\lambda a)^2}\left[\ln\left|1-\frac{1}{\mathrm{x}}\right| - \frac{1}{\mathrm{x}-1} + \frac{3}{2}\frac{1}{\mathrm{x}^2} + \frac{2}{\mathrm{x}}\right], \tag{5.60}$$

$$\int \mathcal{D}_1 \mathrm{d}\varphi = \frac{1}{4\lambda a}\left[(\mathrm{x}-2)\ln\left|1-\frac{1}{\mathrm{x}}\right| - \frac{3}{2}\frac{1}{\mathrm{x}}\right] + C, \tag{5.61}$$

where C is the constant introduced in Eq. (5.57). For later convenience, we now define the function:

$$\theta_0(\varphi) = -\int \mathrm{d}\varphi \left(\frac{\lambda a}{2\varphi(\varphi-\lambda a)^2} + \frac{\varphi}{(\varphi-\lambda a)^2}\int \mathcal{D}_1 \mathrm{d}\varphi\right), \tag{5.62}$$

which, upon using Eq. (5.61), takes the form:

$$\theta_0(\mathrm{x}) = \frac{-1}{4\lambda a}\frac{1}{\mathrm{x}-1}\left[\frac{1}{2} + (\mathrm{x}^2-3\mathrm{x}+3)\ln|\mathrm{x}-1| - (\mathrm{x}^2-2\mathrm{x}+2)\ln \mathrm{x}\right] + C\left(\frac{1}{\mathrm{x}-1} - \ln|\mathrm{x}-1|\right). \tag{5.63}$$

We furthermore introduce the integrals:

$$\mathrm{I}_\pm = \int \frac{\mathrm{d}x^\pm}{\mathrm{F}^\pm}\frac{1}{\varphi-\lambda a}\int \frac{\mathrm{d}x^\pm}{\mathrm{F}^\pm} t_\pm(\sigma^\pm). \tag{5.64}$$

Using this notation, Eq. (5.59) can be recast in a considerably more compact form:

$$\theta = \frac{\mathrm{x}-1}{\mathrm{x}}\left[\frac{\lambda}{2}\left(\int \mathrm{d}x^+ \frac{\mathrm{G}^+}{\mathrm{F}^{+2}} + \int \mathrm{d}x^- \frac{\mathrm{G}^-}{\mathrm{F}^{-2}}\right) + \theta_0 + \mathrm{I}\right], \tag{5.65}$$

where $\mathrm{I} = \mathrm{I}_+ + \mathrm{I}_-$. We now proceed to demonstrate that the functions $\mathrm{G}^\pm$ represent the quantum corrections to the coordinate transformations, by examining how Eq. (5.19) is modified when these quantum corrections are included. From Eq. (5.65) we extract the term involving $\mathrm{G}^\pm$, multiply it by ε, and add it to the right-hand side of Eq. (5.19):

$$\varphi + \lambda a \ln\left(\frac{\varphi}{\lambda a} - 1\right) + \varepsilon\frac{\varphi\theta}{\varphi-\lambda a} - \varepsilon\theta_0 - \varepsilon \mathrm{I} = -\frac{\lambda}{2}\left[\int \frac{\mathrm{d}x^+}{\mathrm{F}^+}\left(1-\varepsilon\frac{\mathrm{G}^+}{\mathrm{F}^+}\right) + \int \frac{\mathrm{d}x^-}{\mathrm{F}^-}\left(1-\varepsilon\frac{\mathrm{G}^-}{\mathrm{F}^-}\right)\right]. \tag{5.66}$$

The final step is to revert to the quantum-corrected fields (3.113). If we expand Eq. (5.19) to first order in ε, we obtain precisely the term linear in θ that appears in Eq. (5.66). On the right-hand side of Eq. (5.66), we have the first-order expansion in ε of $(\mathrm{F}^\pm + \varepsilon \mathrm{G}^\pm)^{-1}$, implying that the transformation $\mathrm{F}^\pm + \varepsilon\mathrm{G}^\pm \mapsto \mathrm{F}^\pm$ should be interpreted as the quantum-corrected coordinate transformation. Furthermore, observe that the constant C in Eq. (5.63) represents the quantum correction in $\lambda a + \varepsilon C \mapsto \lambda a$. This can be verified straightforwardly by expanding $(\lambda a + \varepsilon C)\ln(\varphi/(\lambda a + \varepsilon C) - 1)$ to first order in ε. We are similarly interested in how quantum corrections modify Eq. (5.20). To this end, we now employ the newly defined quantum-corrected coordinate transformations:

$$\mathrm{F}^+\mathrm{F}^- e^{2\rho} \mapsto \mathrm{F}^+\mathrm{F}^- e^{2\rho}\left[1 + \varepsilon\left(2\alpha + \frac{\mathrm{G}^+}{\mathrm{F}^+} + \frac{\mathrm{G}^-}{\mathrm{F}^-}\right)\right]. \tag{5.67}$$

The quantity in brackets of Eq. (5.67) also appears in Eq. (5.58), which allows us to isolate it from that expression. Before doing so, we introduce another set of integrals:

$$\mathrm{I}'_\pm = -\int \frac{\mathrm{d}x^\pm}{\mathrm{F}^\pm}\left(\frac{\lambda a}{\varphi} - 1\right)\int \frac{\mathrm{d}x^\pm}{\mathrm{F}^\pm}\frac{t_\pm(\sigma^\pm)}{\varphi-\lambda a}. \tag{5.68}$$

We then define $\mathrm{I}' = \mathrm{I}'_+ + \mathrm{I}'_-$, insert this into Eq. (5.67), and make use of Eq. (5.20) to obtain:

$$\mathrm{F}^+\mathrm{F}^- e^{2\rho} \mapsto \frac{\lambda a}{\varphi} - 1 - \varepsilon\frac{\lambda a\theta}{\varphi^2} + \varepsilon\left[\frac{\varphi-\lambda a}{\varphi}\mathcal{D}_1 + \frac{\lambda a}{2\varphi^3} + \frac{1}{\varphi}\int \mathcal{D}_1\mathrm{d}\varphi + \frac{1}{\varphi}\mathrm{I}'\right]. \tag{5.69}$$

The first three terms are precisely the expansion of $\lambda a(\varphi+\varepsilon\theta)^{-1}-1$. Because C is the integration constant of $\int \mathcal{D}_1 \mathrm{d}\varphi$, the only term in which it appears is $\varepsilon C/\varphi$, which, once again, demonstrates that C corresponds to the quantum correction to the constant λa. Expressing Eqs. (5.66) and (5.69) in terms of the quantum-corrected reduced field x and the quantum-corrected constant λa, we finally obtain:

$$\mathrm{x}+\ln|\mathrm{x}-1|+\frac{\varepsilon}{4(\lambda a)^2}\frac{1}{\mathrm{x}-1}\left[\frac{1}{2}+(\mathrm{x}^2-3\mathrm{x}+3)\ln|\mathrm{x}-1|-(\mathrm{x}^2-2\mathrm{x}+2)\ln\mathrm{x}\right]-\frac{\varepsilon}{\lambda a}\mathrm{I}$$
$$=-\frac{1}{2a}\left(\int\frac{\mathrm{d}x^+}{\mathrm{F}^+}+\int\frac{\mathrm{d}x^-}{\mathrm{F}^-}\right)\equiv\frac{\sigma}{a}, \tag{5.70}$$

$$\mathrm{F}^+\mathrm{F}^-e^{2\rho}=\frac{1}{\mathrm{x}}-1+\frac{\varepsilon}{4(\lambda a)^2}\left[\frac{2\mathrm{x}-3}{\mathrm{x}}\ln\left|1-\frac{1}{\mathrm{x}}\right|+\frac{1}{\mathrm{x}}-\frac{2}{\mathrm{x}^2}+\frac{1}{2}\frac{1}{\mathrm{x}^3}\right]+\frac{\varepsilon}{\lambda a}\frac{\mathrm{I}'}{\mathrm{x}}. \tag{5.71}$$

Eqs. (5.70) and (5.71) provide the general solution to the vacuum Eqs. (5.47–5.49). They therefore represent the quantum-corrected analogues of Eqs. (5.19) and (5.20) obtained from the classical equations of motion. Consequently, the solution to the quantum-corrected equations of motion is specified by an ordered quintuple $(\mathrm{F}^+,\mathrm{F}^-,a,t_+,t_-)$. Note that $\mathrm{F}^\pm$ and a are now quantum-corrected quantities. An explicit solution can be constructed once the integrals I and I' have been evaluated. These integrals are not independent, but are linked through Eqs. (5.52) and (5.53), so that it suffices to compute only one of them. Since the condition $t_\pm(x^\pm)=0$ specifies the vacuum we adopt (see Sec. 3.3), the integrals I and I' are closely related to the particular choice of vacuum state.

5.2.1 Applying the static ansatz

The general static solution in the classical DREH model is obtained in Sec. 5.1.2. Once quantum corrections are incorporated, the main distinction is the presence of the gravitational trace anomaly. Consequently, the trace of the EMT on the right-hand side of Eq. (5.5) can no longer be neglected. For the quantum-corrected EMT (3.79) it reads:

$$\frac{2G\Lambda}{\lambda^2\varphi}\left(T_{\mu\nu}-\frac{1}{2}g_{\mu\nu}T\right)=\frac{\varepsilon}{\Lambda\mathrm{x}}\left[\frac{\mu}{\varepsilon}-\Xi-\frac{1}{4}\mathcal{D}^2\left(\frac{\mathrm{d}\Lambda}{\mathrm{d}\varphi}\right)^2+\frac{1}{2}\Lambda\mathcal{D}\frac{\mathrm{d}}{\mathrm{d}\varphi}\left(\mathcal{D}\frac{\mathrm{d}\Lambda}{\mathrm{d}\varphi}\right)\right](\xi_\mu\xi_\nu+\varepsilon_{\mu\rho}\varepsilon_{\nu\sigma}\xi^\rho\xi^\sigma), \tag{5.72}$$

where μ and ξ denote the scalar-field charge and the parameter specifying the quantum vacuum state, respectively, defined through:

$$\Lambda^2T^{\shortparallel\shortparallel}=\Lambda^2T^{\perp\perp}=\frac{\lambda^2\mu}{2G},\qquad t_+(\sigma^+)=t_-(\sigma^-)=\frac{\lambda^2}{4}\Xi. \tag{5.73}$$

Because the action itself does not receive correction terms, the left-hand side of (5.5) remains identical to the classical expression (5.22). Thus, the resulting system of equations takes the form:

$$\mathcal{D}^2\frac{\mathrm{d}\Lambda}{\mathrm{d}\varphi}+\frac{\mathrm{d}\left(\Lambda\mathcal{D}^2\right)}{\mathrm{d}\varphi}+\mathcal{D}\varphi\frac{\mathrm{d}}{\mathrm{d}\varphi}\left(\mathcal{D}\frac{\mathrm{d}\Lambda}{\mathrm{d}\varphi}\right)=0, \tag{5.74}$$

$$\mathcal{D}\frac{\mathrm{d}}{\mathrm{d}\varphi}(\Lambda\mathcal{D}\varphi)+1+\frac{\varepsilon}{2}\mathcal{D}\frac{\mathrm{d}}{\mathrm{d}\varphi}\left(\mathcal{D}\frac{\mathrm{d}\Lambda}{\mathrm{d}\varphi}\right)=0, \tag{5.75}$$

$$\mathcal{D}^2\frac{\mathrm{d}\Lambda}{\mathrm{d}\varphi}+\frac{\mathcal{D}\varphi}{2}\frac{\mathrm{d}}{\mathrm{d}\varphi}\left(\mathcal{D}\frac{\mathrm{d}\Lambda}{\mathrm{d}\varphi}\right)=\frac{\varepsilon}{\Lambda\mathrm{x}}\left[\frac{\mu}{\varepsilon}-\Xi-\frac{1}{4}\mathcal{D}^2\left(\frac{\mathrm{d}\Lambda}{\mathrm{d}\varphi}\right)^2+\frac{1}{2}\Lambda\mathcal{D}\frac{\mathrm{d}}{\mathrm{d}\varphi}\left(\mathcal{D}\frac{\mathrm{d}\Lambda}{\mathrm{d}\varphi}\right)\right]. \tag{5.76}$$

Since we are not interested in the classical charged matter in this subsection, we set $\mu = 0$. By combining the three equations in a particular way, we obtain an expression for $\mathcal{D}$ in terms of Λ and its derivative:

$$\mathcal{D}^2 \left[\varphi \frac{\mathrm{d}\Lambda}{\mathrm{d}\varphi} + \Lambda + \frac{\varepsilon}{4\Lambda} \left(\frac{\mathrm{d}\Lambda}{\mathrm{d}\varphi} \right)^2 \right] = -1 - \frac{\varepsilon \Xi}{\Lambda}. \tag{5.77}$$

Substituting this into Eq. (5.74) yields an expression for $\frac{\mathrm{d}\mathcal{D}^2}{\mathrm{d}\varphi}$ in terms of Λ and its derivatives. Consequently, Eq. (5.75) reduces to a second-order nonlinear differential equation that determines the metric function Λ:

$$\left(\varphi^2 - \varepsilon\right) \frac{\mathrm{d}^2\Lambda}{\mathrm{d}\varphi^2} + 2\varphi \frac{\mathrm{d}\Lambda}{\mathrm{d}\varphi} + \frac{3\varepsilon}{2\Lambda} \left(\frac{\mathrm{d}\Lambda}{\mathrm{d}\varphi} \right)^2 + \frac{\varepsilon\varphi}{4\Lambda^2} \left(\frac{\mathrm{d}\Lambda}{\mathrm{d}\varphi} \right)^3 = \varepsilon \Xi \left[2 + \varphi \frac{\mathrm{d}\ln\Lambda}{\mathrm{d}\varphi} - \left(\varphi^2 - \varepsilon\right) \frac{\mathrm{d}^2 \ln \Lambda}{\mathrm{d}\varphi^2} \right]. \tag{5.78}$$

In general, Eq. (5.78) is extremely difficult to solve. In the special case $\Xi = 0$, it can be recast as a first-order differential equation for $u = \frac{\mathrm{d}\ln\Lambda}{\mathrm{d}\varphi}$:

$$\left(\varphi^2 - \varepsilon\right) \frac{\mathrm{d}u}{\mathrm{d}\varphi} + 2\varphi u + \left(\varphi^2 + \frac{\varepsilon}{2}\right) u^2 + \frac{\varepsilon}{4} \varphi u^3 = 0 \tag{5.79}$$

This is an Abel differential equation, which is well known to be highly nontrivial to solve; closed-form solutions exist only for a limited set of specific relations among the coefficients multiplying the powers of u. In our situation, these conditions are not met, and an exact analytic solution is not available. Therefore, as anticipated, we resort to a perturbative approach. In the limit $\varepsilon \to 0$, Eq. (5.78) simplifies to:

$$\varphi \frac{\mathrm{d}^2\Lambda}{\mathrm{d}\varphi^2} + 2\frac{\mathrm{d}\Lambda}{\mathrm{d}\varphi} = 0 \qquad \Longrightarrow \qquad \Lambda = A + \frac{B}{\varphi}, \tag{5.80}$$

where A and B are integration constants. Imposing the asymptotic condition (3.22), i.e. $\Lambda \to -1$ as $\varphi \to \infty$ yields the Schwarzschild solution (5.21) with $B = \lambda a$, as expected. Expanding $\Lambda = \Lambda_0 + \varepsilon \Lambda_1$, where Λ_0 denotes the Schwarzschild solution, we obtain the following general solution:

$$\Lambda = \frac{1}{\mathrm{x}} - 1 + \frac{\varepsilon}{4(\lambda a)^2} \left[\frac{2\mathrm{x} - 3}{\mathrm{x}} \ln \left| 1 - \frac{1}{\mathrm{x}} \right| + \frac{2}{\mathrm{x}} - \frac{2}{\mathrm{x}^2} + \frac{1}{2}\frac{1}{\mathrm{x}^3} \right] + \varepsilon \Xi \left(\frac{2\mathrm{x} - 3}{\mathrm{x}} \ln |\mathrm{x} - 1| + \frac{1}{2\mathrm{x}} \right), \tag{5.81}$$

where we have employed the reduced field (5.39) and have also dropped the two integration constants in Λ_1. In the most general case, the solution can be written as $\Lambda_1 \mapsto \Lambda_1 + D_1 + \frac{D_2}{\mathrm{x}}$. The constant D_2, however, is absorbed into a as its quantum correction, whereas D_1 represents the quantum-corrected contribution to the constant A in Eq. (5.80) and thus merely rescales the entire Killing vector. Consequently, it can be removed by a redefinition of the time coordinate and will be disregarded here. Inserting Eq. (5.81) into the expression (5.77) for $\mathcal{D}$, we find:

$$\mathcal{D} = 1 + \frac{\varepsilon}{4(\lambda a)^2} \left[\ln \left| 1 - \frac{1}{\mathrm{x}} \right| - \frac{1}{\mathrm{x} - 1} + \frac{3}{2}\frac{1}{\mathrm{x}^2} + \frac{2}{\mathrm{x}} \right] + \varepsilon \Xi \left[\frac{1}{2} + \ln|\mathrm{x} - 1| - \frac{1}{\mathrm{x} - 1} \right]. \tag{5.82}$$

Finally, we derive the tortoise coordinate (3.18). A straightforward integration gives:

$$\begin{aligned} \frac{\sigma}{a} = \mathrm{x} + \ln|\mathrm{x} - 1| + \frac{\varepsilon}{4(\lambda a)^2} \frac{1}{\mathrm{x} - 1} &\left[\left(\mathrm{x}^2 - 2\mathrm{x} + 2\right) \ln \left| 1 - \frac{1}{\mathrm{x}} \right| + \mathrm{x} - \frac{3}{2} \right] \\ + \frac{\varepsilon \Xi}{\mathrm{x} - 1} &\left[\left(\mathrm{x}^2 - \mathrm{x} + 1\right) \ln|\mathrm{x} - 1| - \frac{1}{2} - \frac{1}{2}(3\mathrm{x} - 5)(\mathrm{x} - 1) \right]. \end{aligned} \tag{5.83}$$

5.2.2 Solution without energy flux at the asymptotic infinity

Here, we focus on the solution for which there is no energy flux in either of the two asymptotic regions of the spacetime. The associated vacuum state is the Boulware vacuum $|0,\sigma\rangle$ (3.96). It is characterized by normal ordering of the EMT with respect to the Eddington–Finkelstein coordinates, that is, by the condition $t_\pm(\sigma^\pm) = 0$. For the general static solution discussed in the previous section, this requirement implies $\Xi = 0$. Consequently, the solution takes the form:

$$\begin{aligned}
\Lambda &= \frac{1}{\mathrm{x}} - 1 + \frac{\varepsilon}{4(\lambda a)^2}\left[\frac{2\mathrm{x}-3}{\mathrm{x}}\ln\left|1-\frac{1}{\mathrm{x}}\right| + \frac{2}{\mathrm{x}} - \frac{2}{\mathrm{x}^2} + \frac{1}{2}\frac{1}{\mathrm{x}^3}\right], \\
\mathcal{D} &= 1 + \frac{\varepsilon}{4(\lambda a)^2}\left[\ln\left|1-\frac{1}{\mathrm{x}}\right| - \frac{1}{\mathrm{x}-1} + \frac{3}{2}\frac{1}{\mathrm{x}^2} + \frac{2}{\mathrm{x}}\right], \\
\frac{\sigma}{a} &= \mathrm{x} + \ln|\mathrm{x}-1| + \frac{\varepsilon}{4(\lambda a)^2}\frac{1}{\mathrm{x}-1}\left[\left(\mathrm{x}^2 - 2\mathrm{x} + 2\right)\ln\left|1-\frac{1}{\mathrm{x}}\right| + \mathrm{x} - \frac{3}{2}\right].
\end{aligned} \tag{5.84}$$

In contrast to the BPP model (see Sec. 4.3.3), solution (5.84) admits a well-defined $a \to 0$ limit, which yields Minkowski spacetime, i.e. $\Lambda = -1$, $\mathcal{D} = 1$, and $\sigma = \mathrm{x}a$. This indicates that the Minkowski solution is a regular configuration with no energy flux at null infinities. The solution was first obtained in [111].

One can also derive this solution from the general solution of the quantum-corrected model (5.70-5.71). In that framework, imposing $t_\pm(\sigma^\pm) = 0$ is equivalent to requiring that the integrals $\mathrm{I}_\pm$ (5.64) and $\mathrm{I}'_\pm$ (5.68) vanish. At first glance, the resulting solution appears to diverge in the limit $a \to 0$. However, we must recall that the constant λa is modified as $\lambda a \mapsto \lambda a + \varepsilon C(\lambda a)$. The apparent divergence can be removed by a suitable choice of the constant $C(\lambda a)$, namely $C(\lambda a) = \frac{1}{4\lambda a}$. With this specific choice, the metric function and the tortoise coordinate are exactly transformed into Eq. (5.84). Finally, for the function $\mathcal{D}$ in Eq. (5.84) we have $\mathcal{D} = 1 + \varepsilon\mathcal{D}_1$, where $\mathcal{D}_1$ is defined in Eq. (5.60). Hence, the two derivations are mutually consistent.

Since these configurations correspond to solutions with no energy flux at infinity, they are expected to be horizonless and therefore not to resemble black hole solutions. It has been shown in [112, 113] that the classical horizon disappears once quantum corrections are incorporated. The horizon is defined as the hypersurface on which the Killing vector (3.5) becomes null, i.e. where $\Lambda = 0$. In a perturbative framework, if a horizon is present, its position should be written as $\mathrm{x_H} = \mathrm{x_H^{(0)}} + \varepsilon\mathrm{x_H^{(1)}}$. From Eq. (5.84), we immediately deduce that $\mathrm{x_H^{(0)}} = 1$, which represents the classical horizon. The first-order correction is then found by taking the limit $\mathrm{x} \to 1$ of the first-order terms in Eq. (5.84). This limit diverges, showing that the perturbative expansion breaks down in the region of spacetime near the classical horizon. Equivalently, one may interpret this divergence as evidence that the quantum corrections actually eliminate the classical horizon. We thus reach the same conclusion as in [112, 113].

Another significant property of solution (5.84) is that it exhibits a curvature singularity whenever the mass parameter is non-vanishing. This can be checked explicitly by evaluating the scalar curvature, which to first order in the perturbative expansion is given by:

$$R = 2\lambda^2\frac{\lambda a}{(\varphi^2 - \varepsilon)^{3/2}}. \tag{5.85}$$

As expected, this expression vanishes in the massless limit, $a = 0$. This leads to the same conclusion as in the RST and BPP dilaton gravity models [23, 24, 25]. There is, however, a subtle difference between our model and the BPP construction. Furthermore, we find that if the central charge of the conformal matter fields obeys $\varepsilon < 0$, the singularity disappears from this Boulware state at first order in perturbation theory. This phenomenon has been analyzed thoroughly in the context of the RST model [108, 109]. A negative central charge may result from the presence of unphysical, ghost-like fields. Moreover, numerical investigations within the DREH model [114] likewise suggest the appearance of this type of behavior.

5.2.3 Eternal black hole scenario

An eternal black hole solution describes a black hole that is in thermal equilibrium with its environment. Consequently, the quantum fields are in the Hartle–Hawking state (3.97), which is defined by imposing that the normal-ordered EMT vanishes in Kruskal coordinates, $t_\pm(x^\pm) = 0$. By construction, this configuration is static and therefore must belong to the family of solutions (5.81-5.83) for a particular value of the constant Ξ. The defining property of a static black hole is the presence of an event horizon [106]. This horizon is the hypersurface on which the Killing vector becomes null, i.e., where $\Lambda = 0$. However, solving this condition perturbatively in the form $\mathrm{x_H} = 1 + \varepsilon \mathrm{x_H^{(1)}}$ is not feasible as long as the term $\ln|\mathrm{x} - 1|$ is present in expression (5.81). Fortunately, there exists a particular choice of Ξ that removes this term. It is given by:

$$\Xi = -\frac{1}{4(\lambda a)^2}. \tag{5.86}$$

The solution can now be written as:

$$\begin{aligned}
\Lambda &= \frac{1}{\mathrm{x}} - 1 + \frac{\varepsilon}{4(\lambda a)^2}\left[-\frac{2\mathrm{x}-3}{\mathrm{x}}\ln\mathrm{x} + \frac{3}{2}\frac{1}{\mathrm{x}} - \frac{2}{\mathrm{x}^2} + \frac{1}{2}\frac{1}{\mathrm{x}^3}\right],\\
\mathcal{D} &= 1 + \frac{\varepsilon}{4(\lambda a)^2}\left[-\ln\mathrm{x} + \frac{3}{2}\frac{1}{\mathrm{x}^2} + \frac{2}{\mathrm{x}} - \frac{1}{2}\right],\\
\frac{\sigma}{a} &= \mathrm{x} + \ln|\mathrm{x}-1| + \frac{\varepsilon}{4(\lambda a)^2}\left[-\ln|\mathrm{x}-1| + \left(1 - \mathrm{x} - \frac{1}{\mathrm{x}-1}\right)\ln\mathrm{x} + \frac{3}{2}(\mathrm{x}-1)\right].
\end{aligned} \tag{5.87}$$

We observe that the integration constants in the Ξ term are fixed such that $\mathrm{x_H} = 1$, because for this value of the dilaton the associated Killing vector becomes null. To locate the singularity, we evaluate the curvature (3.29), which takes the form:

$$R = \frac{2}{a^2\mathrm{x}^3}\left[1 + \frac{\varepsilon}{4(\lambda a)^2}\left(\ln\mathrm{x} + \mathrm{x} - \frac{7}{2} - \frac{1}{\mathrm{x}} + \frac{15}{2}\frac{1}{\mathrm{x}}\right)\right]. \tag{5.88}$$

Consequently, the curvature diverges along the hypersurface approaching the classical singularity at $\mathrm{x_S} \approx 0$. The surface gravity (see App. D.5) is given by:

$$\kappa = \frac{1}{2a}\left|\mathcal{D}\frac{\mathrm{d}\Lambda}{\mathrm{dx}}\right|_{\mathrm{H}} = \frac{1}{2a}\left(1 + \frac{\varepsilon}{4(\lambda a)^2}\right). \tag{5.89}$$

We now confirm that the condition (5.86) imposed on the parameter Ξ indeed implements normal ordering of the EMT in Kruskal coordinates. To move to the Kruskal coordinates we use the classical part of the surface gravity. After applying the transformations (see App. D.5), we obtain:

$$\frac{\lambda^2}{4}\Xi = t_\pm(\sigma^\pm) = \left(\frac{\mathrm{d}x^\pm}{\mathrm{d}\sigma^\pm}\right)^2\left[\cancelto{0}{t_\pm}(x^\pm) - \frac{1}{2}D_{x^\pm}[\sigma^\pm]\right] = -\frac{\kappa^2}{4} \implies \Xi = -\frac{\kappa^2}{\lambda^2} = -\frac{1}{4(\lambda a)^2}. \tag{5.90}$$

Therefore, the choice (5.86) for Ξ, originally obtained by requiring the presence of an event horizon, is precisely equivalent to selecting the Hartle–Hawking state. Finally, we should examine the nature of the pole of the tortoise coordinate appearing in Eq. (5.87). Using the expression for the surface gravity (5.89), we obtain

$$\sigma = \frac{1}{2\kappa}\left[\mathrm{x} + \ln|\mathrm{x}-1| + \frac{\varepsilon}{4(\lambda a)^2}\left(\left(1-\mathrm{x}-\frac{1}{\mathrm{x}-1}\right)\ln\mathrm{x} + \frac{5}{2}\mathrm{x} - \frac{3}{2}\right)\right]. \tag{5.91}$$

Expressed in this way, the tortoise coordinate exhibits precisely the same near-horizon behavior as in the classical case, namely $\sigma = \frac{1}{2\kappa}\ln|\mathrm{x}-1|$, because the term of order ε vanishes at the horizon $\mathrm{x_H} = 1$. This is made possible by the specific choice of the integration constant of the Ξ term in Eq. (5.83).

Next, we demonstrate how to obtain the same result starting from the general solution (5.70-5.71). The sources are the functions $t_\pm(\sigma^\pm)$. For the Hartle–Hawking state, they are specified by Eq. (5.90). Hence, we can easily evaluate the integrals I (5.64) and (5.68). Performing the integration, we find:

$$\mathrm{I}' = \Xi\lambda a\left[(2\mathrm{x}-4)\ln|\mathrm{x}-1| + \big(A_+(x^+) + A_-(x^-)\big)\,\mathrm{x} + B_+(x^+) + B_-(x^-)\right], \tag{5.92}$$

where $A_\pm(x^\pm)$ and $B_\pm(x^\pm)$ are arbitrary functions. At this point, one has to proceed with caution. If these arbitrary functions are simply discarded, the correct Ξ term in Eq. (5.81) cannot be recovered. This issue appears as an artifact of the procedure in which the quantum corrections to the coordinate transformations $\mathrm{G}^\pm$ are eliminated in Eq. (5.57) after the first integration. Consequently, choosing $A_\pm$ and $B_\pm$ arbitrarily effectively corresponds to performing an additional coordinate transformation. The appropriate choice of this transformation is fixed by requiring that $\mathrm{F}^\pm$ represent the components of the time-like Killing vector (3.5), i.e. that $\nabla_+\mathrm{F}^+ = \nabla_-\mathrm{F}^-$. Imposing this condition uniquely determines the arbitrary functions and restores the original solution (5.81).

The solution (5.87) was first derived in [42], albeit in a slightly different form. There, the metric ansatz is taken to be:

$$\mathrm{d}s^2 = -\left(1-\frac{a}{r}+\frac{\varepsilon m(r)}{r}\right)e^{2\varepsilon\varphi(r)}\mathrm{d}t^2 + \frac{\mathrm{d}r^2}{1-\frac{a}{r}+\frac{\varepsilon m(r)}{r}}, \tag{5.93}$$

with the functions m and φ specified by:

$$m(r) = \frac{a}{4(\lambda a)^2}\left[-\frac{7}{2}\left(\frac{a}{r}\right)^2 + \frac{a}{r} + \ln\frac{a}{r} - \frac{r}{a}\right] + aC_1, \tag{5.94}$$

$$\varphi(r) = \frac{1}{4(\lambda a)^2}\left[-\frac{3}{2}\left(\frac{a}{r}\right)^2 - 2\frac{a}{r} - \ln\frac{a}{r}\right] + C_2, \tag{5.95}$$

where $r = \mathrm{x}a$. We also use the notation $h = 1-(a-\varepsilon m)/r$. In this framework, the norm of the Killing vector is as follows:

$$\Lambda = -\left(1-\frac{a}{r}+\frac{\varepsilon m(r)}{r}\right)e^{2\varepsilon\varphi(r)}. \tag{5.96}$$

Requiring this expression to coincide with the solution (5.81) fixes the constants C_1 and C_2 to

$$C_1 = \frac{7}{8(\lambda a)^2} \quad \wedge \quad C_2 = \frac{1}{8(\lambda a)^2}. \tag{5.97}$$

As an additional consistency check, we note that this particular choice of constants reduces the surface gravity in [42] to Eq. (5.89). Moreover, comparing the tortoise coordinate in [42] with Eq. (5.91), we find that they coincide up to an integration constant.

5.3 Evaporating black hole scenario

The evaporating black hole scenario describes both the gravitational collapse leading to black hole formation and the subsequent evaporation driven by Hawking radiation. This framework is introduced in Sec. 3.4. Here we follow [111], where this scenario was first developed within the DREH model.

The purely classical gravitational collapse was analyzed in Sec. 5.1.3. Since the classical treatment does not include the back-reaction of quantum fields on the geometry, the black hole does not evaporate in that setting. Unlike in the BPP model discussed in Sec. 4.3, where the Minkowski vacuum carries a non-vanishing energy flux at infinity, in the DREH model the initial spacetime can still be chosen as Minkowski space after quantum corrections are included. This is because the Minkowski metric satisfies the quantum-corrected field Eqs. (5.44)–(5.46) and does not exhibit any energy flux. For the evaporating black hole case, the relevant vacuum state is the Unruh state (3.98), defined by $t_\pm(\sigma^\pm) = 0$. While the initial spacetime has vanishing energy flux at infinity, a non-zero flux appears at future null infinity once the black hole forms, arising from the change in asymptotically flat coordinates (see Sec. 3.4).

Before the black hole forms (region I of the spacetime in Fig. 3.3), we work in the Eddington–Finkelstein gauge, which corresponds to choosing the $\sigma^\pm$ coordinates for the solution (5.70-5.71). In this gauge, the solution takes the form $(-1, 1, a, 0, 0)$. In region II of the spacetime an evaporating black hole is present. There, the Eddington–Finkelstein coordinates are denoted by $\hat{\sigma}^\pm$, and the solution is characterized by $(-1, \mathrm{F}^-, 0, t_-(\hat{\sigma}^-))$. Consequently, we need to determine the functions $t_\pm(\hat{\sigma}^\pm)$ using the transformation law (3.83). Since the coordinate transformation (3.106) is expressed in terms of the functions $\mathrm{F}^\pm$, defined in Eq. (5.36), the problem reduces to computing the Schwarzian derivative. The final expression is written in terms of the coordinate $\hat{\mathrm{x}}$:

$$t_+(\hat{\sigma}^+) = 0, \qquad t_-(\hat{\sigma}^-) = -\frac{\lambda^2}{4(\lambda a)^2}\frac{\hat{\mathrm{x}} - \frac{3}{4}}{\hat{\mathrm{x}}^4}. \tag{5.98}$$

Observe that the spacetime depicted in Fig. 3.2 differs from that in Fig. 3.3 by the presence of a third region (III). This additional region corresponds to the spacetime that remains after the black hole has fully evaporated and is characterized by the end-state geometry. With all necessary ingredients specified, the next task is to determine θ, whose general expression is given in Eq. (5.65). This solution, however, is only fixed up to the integral I in Eq. (5.64). The problem therefore reduces to computing these integrals for the particular choice (5.98). Because $t_+ = 0$, the integral I_+ vanishes, leaving us solely with the integral I_-:

$$\mathrm{I} = \int \frac{\mathrm{d}\sigma^-}{\mathrm{F}^-}\frac{1}{\varphi - \lambda a}\int \frac{\mathrm{d}\sigma^-}{\mathrm{F}^-} t_-(\hat{\sigma}^-). \tag{5.99}$$

The inner integral, expressed in terms of the coordinate $\hat{\mathrm{x}}(\sigma^-)$, takes the form

$$\int \frac{\mathrm{d}\sigma^-}{\mathrm{F}^-} t_-(\hat{\sigma}^-) = \frac{1}{8a}\,\mathrm{F}(\hat{\mathrm{x}}) = \frac{1}{8a}\left[\ln\!\left(1 - \frac{1}{\hat{\mathrm{x}}}\right) + \frac{1}{\hat{\mathrm{x}}} - \frac{3}{2}\frac{1}{\hat{\mathrm{x}}^2}\right], \tag{5.100}$$

where we have introduced the function $\mathrm{F}(\hat{\mathrm{x}})$. With this, the integral I can be rewritten as

$$\mathrm{I} = -\frac{1}{4\lambda a}\int \frac{\hat{\mathrm{x}}\,\mathrm{d}\hat{\mathrm{x}}}{\hat{\mathrm{x}} - 1}\frac{\mathrm{F}(\hat{\mathrm{x}})}{\mathrm{x} - 1}. \tag{5.101}$$

The key difficulty is that we must integrate with respect to $\hat{\mathrm{x}}$, even though the integrand still involves the field x, and the two variables are related by the transcendental Eq. (5.40), which can be cast in the following form:

$$e^{\hat{\mathrm{x}}}(\hat{\mathrm{x}}-1)=\delta\, e^{\mathrm{x}}(\mathrm{x}-1). \tag{5.102}$$

To proceed, we must solve Eq. (5.102) for $\hat{\mathrm{x}}$, i.e. obtain $\hat{\mathrm{x}}=\hat{\mathrm{x}}(\mathrm{x},\delta)$. Since in region II of the spacetime we have $\delta<1$, this equation admits an analytic solution. The full derivation, including a rigorous proof of the uniform convergence of the resulting series, is presented in App. B, see Theorems 1 and 3. Here we simply state the final result:

$$\hat{\mathrm{x}}=\begin{cases}1-\displaystyle\sum_{n=1}^{\infty}\frac{\delta^n}{n!}\,e^{n(\mathrm{x}-1)}(1-\mathrm{x})^n\,\mathrm{P}_{n-1}(1), & \mathrm{x}\leqslant 1,\\[2ex] \mathrm{x}-\displaystyle\sum_{n=1}^{\infty}\frac{(1-\delta)^n}{n!}\left(1-\frac{1}{\mathrm{x}}\right)^n\mathrm{P}_{n-1}\!\left(\frac{1}{\mathrm{x}}\right), & \mathrm{x}>1,\end{cases} \tag{5.103}$$

where $\mathrm{P}_n(x)$ are the polynomials introduced in Theorem 1. In the subsequent calculation we also require the function $\ln\hat{\mathrm{x}}=\ln\hat{\mathrm{x}}(\mathrm{x},\delta)$, which is given by (Theorems 5 and 7)

$$\ln\hat{\mathrm{x}}=\begin{cases}-\displaystyle\sum_{n=1}^{\infty}\frac{\delta^n}{n!}\,e^{n(\mathrm{x}-1)}(1-\mathrm{x})^n\,\mathrm{Q}_{n-1}(1), & \mathrm{x}\leqslant 1,\\[2ex] \ln\mathrm{x}-\displaystyle\sum_{n=1}^{\infty}\frac{(1-\delta)^n}{n!}\left(1-\frac{1}{\mathrm{x}}\right)^n\mathrm{Q}_{n-1}\!\left(\frac{1}{\mathrm{x}}\right), & \mathrm{x}>1,\end{cases} \tag{5.104}$$

where $\mathrm{Q}_n(x)$ are the polynomials defined in Corollary 1. Making use of the series representations (5.103) and (5.104), together with their uniform convergence (see App. B), one readily finds that I can be written as

$$\mathrm{I}(\mathrm{x},\delta)=\frac{1}{8\lambda a}\begin{cases}\mathrm{I}_0^{<}(\mathrm{x})+\mathrm{I}_{-1}^{<}(\mathrm{x})\ln\delta-\displaystyle\sum_{n=1}^{\infty}\frac{\delta^n}{n!}\,\mathrm{I}_n^{<}(\mathrm{x}), & \mathrm{x}<1,\\[2ex] \mathrm{I}_0^{>}(\mathrm{x})+\mathrm{I}_{-1}^{>}(\mathrm{x})\ln\delta-\displaystyle\sum_{n=1}^{\infty}\frac{(1-\delta)^n}{n!}\,\mathrm{I}_n^{>}(\mathrm{x}), & \mathrm{x}>1,\end{cases} \tag{5.105}$$

where the newly introduced functions I_n are given by

$$\begin{aligned}
\mathrm{I}_0^{<}(\mathrm{x})&=\frac{1}{\mathrm{x}-1}-\frac{\mathrm{x}-3}{\mathrm{x}-1}\ln(1-\mathrm{x})-\ln^2(1-\mathrm{x})-2\mathrm{x}+c_0,\\
\mathrm{I}_0^{>}(\mathrm{x})&=\frac{1}{\mathrm{x}-1}-\frac{\mathrm{x}-3}{\mathrm{x}-1}\ln\!\left(1-\frac{1}{\mathrm{x}}\right)-\ln^2(\mathrm{x}-1)-2\mathrm{L}(\mathrm{x})+c_0,\\
\mathrm{I}_{-1}^{>}(\mathrm{x})&=\mathrm{I}_{-1}^{<}(\mathrm{x})=2\left(\frac{1}{\mathrm{x}-1}-\ln|\mathrm{x}-1|+c_{-1}\right),\\
\mathrm{I}_n^{>}(\mathrm{x})&=\int\frac{(2\mathrm{x}-1)\,d\mathrm{x}}{(\mathrm{x}-1)^2}\left(1-\frac{1}{\mathrm{x}}\right)^n\mathrm{P}_{n-1}\!\left(\frac{1}{\mathrm{x}}\right)+\int\frac{(2\mathrm{x}-3)\,d\mathrm{x}}{(\mathrm{x}-1)^2}\left(1-\frac{1}{\mathrm{x}}\right)^n\mathrm{Q}_{n-1}\!\left(\frac{1}{\mathrm{x}}\right)\\
&\quad-\left(1-\frac{1}{\mathrm{x}}\right)^n\frac{\mathrm{P}_{n-1}\big(\frac{1}{\mathrm{x}}\big)+3\mathrm{Q}_{n-1}\big(\frac{1}{\mathrm{x}}\big)}{\mathrm{x}-1}+c_n,\\
\mathrm{I}_n^{<}(\mathrm{x})&=\mathrm{P}_{n-1}(1)\int\frac{(2\mathrm{x}-1)\,d\mathrm{x}}{(\mathrm{x}-1)^2}\,e^{n(\mathrm{x}-1)}(1-\mathrm{x})^n+\mathrm{Q}_{n-1}(1)\int\frac{(2\mathrm{x}-3)\,d\mathrm{x}}{(\mathrm{x}-1)^2}\,e^{n(\mathrm{x}-1)}(1-\mathrm{x})^n\\
&\quad+e^{n(\mathrm{x}-1)}(1-\mathrm{x})^{n-1}\big(\mathrm{P}_{n-1}(1)+3\mathrm{Q}_{n-1}(1)\big)+\tilde{c}_n,
\end{aligned} \tag{5.106}$$

where $\mathrm{L}(\mathrm{x}) = \frac{\pi^2}{6} - \int_0^{\mathrm{x}} \frac{ds}{s-1} \ln s$, so that $\mathrm{L}(1) = 0$. The constants c_n are free parameters. By comparing Eq. (5.106) with Eq. (5.70), we can interpret these constants as being associated with a redefinition of the σ^+ coordinate, because the contribution to I that contains them depends solely on $\delta = \delta(\sigma^+)$. On the other hand, the constants $\tilde{c}_n$ are fixed, since the functions I_n must be continuous across the hypersurface at $\mathrm{x} = 1$, which imposes the matching condition $\mathrm{I}_n^{>}(1) = \mathrm{I}_n^{<}(1)$.

The integral in Eq. (5.101) has been reduced to the simple integrals appearing in Eq. (5.106). Consequently, we can express the function $\theta(\mathrm{x}, \delta)$ from Eq. (5.65) as

$$\theta(\mathrm{x}, \delta) = \frac{\mathrm{x}-1}{\mathrm{x}} \left[\frac{\lambda}{2} \left(\int \mathrm{d}\sigma^+ \frac{\mathrm{G}^+}{\mathrm{F}^{+2}} + \int \mathrm{d}\sigma^- \frac{\mathrm{G}^-}{\mathrm{F}^{-2}} \right) + \frac{1}{8\lambda a} \left(\mathrm{S}_0(\mathrm{x}) + \mathrm{S}_{-1}(\mathrm{x}) \ln \delta - \sum_{n=1}^{\infty} \frac{\tilde{\delta}^n}{n!} \mathrm{S}_n(\mathrm{x}) \right) \right]. \tag{5.107}$$

Here, $\mathrm{S}_0(\mathrm{x}) = \mathrm{I}_0(\mathrm{x}) + (8\lambda a)\theta_0(\mathrm{x})$, $\mathrm{S}_{-1} = \mathrm{I}_{-1}$, and $\mathrm{S}_n = \mathrm{I}_n$. The function $\theta_0(\mathrm{x})$ is defined in Eq. (5.63). Note that Eq. (5.107) simultaneously covers the cases $\mathrm{x} < 1$ and $\mathrm{x} > 1$, with $\tilde{\delta} = \delta$ for $x < 1$ and $\tilde{\delta} = 1 - \delta$ for $x > 1$. The explicit expression for $\mathrm{S}_0(\mathrm{x})$ is given in Eq. (5.109). For $n \geq 1$, the functions $\mathrm{S}_n(\mathrm{x})$ coincide with the corresponding $\mathrm{I}_n(\mathrm{x})$, so we do not rewrite them here. It is straightforward to verify that the set of functions $\mathrm{S}_n(\mathrm{x})$ obeys the recurrence relation

$$n \frac{\mathrm{dS}_n}{\mathrm{dx}} - \frac{1}{\mathrm{x}-1} \frac{\mathrm{d}}{\mathrm{dx}} \left(\frac{(\mathrm{x}-1)^2}{\mathrm{x}} \frac{\mathrm{dS}_n}{\mathrm{dx}} \right) = \begin{cases} \dfrac{\mathrm{dS}_{n+1}}{\mathrm{dx}}, & \mathrm{x} > 1, \\ 0, & \mathrm{x} < 1. \end{cases} \tag{5.108}$$

The function S_0 is explicitly given by:

$$\mathrm{S}_0(\mathrm{x}) = \begin{cases} 2\dfrac{\mathrm{x}^2 - 2\mathrm{x} + 2}{\mathrm{x}-1} \ln \mathrm{x} - (2\mathrm{x}-3) \ln(1-\mathrm{x}) - \ln^2(1-\mathrm{x}) - 2\mathrm{x} & \\ \qquad + 8\lambda a C \left(\dfrac{1}{\mathrm{x}-1} - \ln(1-\mathrm{x}) \right) + c_0, & \mathrm{x} \leqslant 1, \\ (2\mathrm{x}-1) \ln \mathrm{x} - (2\mathrm{x}-3) \ln(\mathrm{x}-1) - \ln^2(\mathrm{x}-1) - 2\mathrm{L}(\mathrm{x}) & \\ \qquad + 8\lambda a C \left(\dfrac{1}{\mathrm{x}-1} - \ln(\mathrm{x}-1) \right) + c_0, & \mathrm{x} \geqslant 1. \end{cases} \tag{5.109}$$

Using Eq. (5.52), we can then compute $\alpha(\mathrm{x}, \delta)$ directly. Substituting the obtained expressions for θ and α into the equations of motion (5.47–5.49) confirms that Eq. (5.107) indeed provides the required solution.

5.3.1 Evaporating black hole solution

In the preceding subsections, we obtained a solution in region II of the spacetime (see Fig. 3.3), where the black hole has already formed. This solution involves several constants: c_0, c_{-1}, c_n, $\tilde{c}_n$, and C. Since the constants c_n and $\tilde{c}_n$ are arbitrary (they encode the choice of the function G^+), we fix them by imposing $\mathrm{S}_n(1) = 0$ and setting $c_0 = 0$. Using Eq. (5.52), one can then straightforwardly compute $\alpha(\mathrm{x}, \delta)$. Next, by repeating the same procedure as before, namely $\rho + \varepsilon\alpha \mapsto \rho$, $\mathrm{x} + \frac{\varepsilon}{\lambda a}\theta \mapsto \mathrm{x}$, and $\mathrm{F}^{\pm} + \varepsilon \mathrm{G}^{\pm} \mapsto \mathrm{F}^{\pm}$ (see Eqs. (5.66) and (5.67)), we arrive at the following set of equations:

$$\begin{aligned} \mathrm{x} + \ln|\mathrm{x}-1| - \frac{\varepsilon}{8(\lambda a)^2}\left[\mathrm{S}_0(\mathrm{x}) + \mathrm{S}_{-1}(\mathrm{x})\ln\delta - \sum \frac{\tilde{\delta}^n}{n!}\mathrm{S}_n(\mathrm{x})\right] \\ = -\frac{\lambda}{2}\frac{1}{\lambda a}\left[\int \frac{\mathrm{d}\sigma^+}{\mathrm{F}^+} + \int \frac{\mathrm{d}\sigma^-}{\mathrm{F}^-}\right] \equiv \frac{\hat{\sigma}^+ - \hat{\sigma}^-}{2a}, \end{aligned} \tag{5.110}$$

$$\mathrm{F}^+\mathrm{F}^- e^{2\rho} = \begin{cases} \left(\frac{1}{\mathrm{x}} - 1\right)\left\{1 + \frac{\varepsilon}{8(\lambda a)^2}\left[\frac{\mathrm{x}-1}{\mathrm{x}}\frac{\mathrm{dS}_0(\mathrm{x})}{\mathrm{dx}} + \frac{\mathrm{x}-1}{\mathrm{x}}\frac{\mathrm{dS}_{-1}(\mathrm{x})}{\mathrm{dx}}\ln\delta - 2c_{-1} \right.\right. & \\ \left.\left. \quad -c_1 - \sum_{n=1}^{\infty}\frac{(1-\delta)^n}{n!}\left(\frac{\mathrm{x}-1}{\mathrm{x}}\frac{\mathrm{dS}_n(\mathrm{x})}{\mathrm{dx}} + \mathrm{S}_{n+1}(\mathrm{x}) - n\mathrm{S}_n(\mathrm{x})\right)\right]\right\}, & \mathrm{x} \geqslant 1, \\ \left(\frac{1}{\mathrm{x}} - 1\right)\left\{1 + \frac{\varepsilon}{8(\lambda a)^2}\left[\frac{\mathrm{x}-1}{\mathrm{x}}\frac{\mathrm{dS}_0(\mathrm{x})}{\mathrm{dx}} - \mathrm{S}_{-1}(\mathrm{x}) - 8(\lambda a)^2\mathcal{D}(\mathrm{x}) \right.\right. & \\ \left.\left. \quad + \frac{\mathrm{x}-1}{\mathrm{x}}\frac{\mathrm{dS}_{-1}(\mathrm{x})}{\mathrm{dx}}\ln\delta - \sum_{n=1}^{\infty}\frac{\delta^n}{n!}\left(\frac{\mathrm{x}-1}{\mathrm{x}}\frac{\mathrm{dS}_n(\mathrm{x})}{\mathrm{dx}} - n\mathrm{S}_n(\mathrm{x})\right)\right]\right\}, & \mathrm{x} \leqslant 1. \end{cases} \tag{5.111}$$

The only remaining free constants are c_{-1} and C. The solution in region II of the spacetime must match continuously with the solution in region I across the hypersurface $\sigma^+ = \sigma_0^+$, i.e., at $\delta = 1$ (see Fig. 3.2). Let us first consider the "$++$" component of Eq. (5.44):

$$\partial_+(e^{-2\rho}\partial_+\varphi) = \frac{\lambda}{2}\frac{\lambda a}{\mathrm{F}^+}\delta(\sigma^+ - \sigma_0^+)\varphi^{-1}e^{-2\rho} + \varepsilon\big((\partial_+\rho)^2 - \partial_+^2\rho\big)\varphi^{-1}e^{-2\rho}. \tag{5.112}$$

Integrating this relation yields

$$e^{-2\rho}\partial_+\varphi_> - e^{-2\rho}\partial_+\varphi_< = -\frac{\lambda}{2}\lambda a\,\varphi^{-1}e^{-2\rho} - \varepsilon(\partial_+\rho_> - \partial_+\rho_<)\varphi^{-1}e^{-2\rho}, \tag{5.113}$$

where the subscript "$>$" denotes the region $\sigma^+ > \sigma_0^+$ and "$<$" the region $\sigma^+ < \sigma_0^+$. The origin of the last term in Eq. (5.113) deserves clarification: it is inherited from the final term in Eq. (5.112). Since $\partial_+\rho = \frac{\lambda}{4}\frac{\lambda a}{\varphi^2}\eta(\sigma^+ - \sigma_0^+) + o(\varepsilon)$, with $\eta(\sigma^+ - \sigma_0^+)$ the Heaviside step function, it follows that $\partial_+^2\rho$ contains a contribution proportional to a Dirac δ-function. Using Eq. (5.52), one can then establish that

$$\partial_+\varphi_> = \frac{\lambda}{2}\mathrm{F}_>^- e^{2\rho}\left(1 + \varepsilon\mathcal{D}(\mathrm{x})\right). \tag{5.114}$$

At $\delta = 1$ we have $\mathrm{x} = \hat{\mathrm{x}}$, $e^{2\rho} = 1$, and $\partial_+\varphi_< = \lambda/2$. A straightforward computation then leads to the following form for the function $\mathrm{F}^-(\hat{\mathrm{x}})$:

$$\mathrm{F}^- = \left(1 - \frac{1}{\hat{\mathrm{x}}}\right)\left[1 - \varepsilon\mathcal{D}(\hat{\mathrm{x}}) - \frac{\varepsilon}{2(\lambda a)^2}\frac{1}{\hat{\mathrm{x}}^2(\hat{\mathrm{x}}-1)}\right]. \tag{5.115}$$

Now we impose the continuity conditions on ρ and θ. This analysis will be carried out independently in the two separate regions of the spacetime, specifically for $\mathrm{x} > 1$ and for $\mathrm{x} < 1$. We begin with the case $\mathrm{x} > 1$. Substituting $\delta = 1$ into Eq. (5.111) and using Eq. (5.115), we obtain:

$$\frac{8\lambda a C - 2}{\hat{\mathrm{x}} - 1} + 2c_{-1} + c_1 = 0. \tag{5.116}$$

From Eq. (5.116) it follows that $C = \frac{1}{4\lambda a}$ and $c_{-1} = -c_1/2$. Since $c_1 = 7$ was already fixed by the condition $\mathrm{S}_1(1) = 0$, where $S_1(\mathrm{x}) = 2\ln \mathrm{x} - \frac{4}{\mathrm{x}} - \frac{3}{\mathrm{x}^2} + c_1$, we obtain $c_{-1} = -\frac{7}{2}$. The remaining continuity requirement is $\theta(\hat{\mathrm{x}}, 1) = 0$. Using Eq. (5.110), this condition becomes:

$$\frac{\lambda}{2}\int \mathrm{d}\sigma^+ \frac{\mathrm{G}^+}{\mathrm{F}^{+2}}\bigg|_{\delta=1} + \frac{\lambda}{2}\int \mathrm{d}\sigma^- \frac{\mathrm{G}^-}{\mathrm{F}^{-2}} = -\frac{\mathrm{S}_0(\hat{\mathrm{x}})}{8\lambda a}. \tag{5.117}$$

To fully specify the solution, we set $\mathrm{G}^+ = 0$, which then yields the following coordinate transformations:

$$\mathrm{F}^- = \left(1 - \frac{1}{\hat{\mathrm{x}}}\right)\left[1 + \frac{\varepsilon}{8(\lambda a)^2}\frac{\hat{\mathrm{x}}-1}{\hat{\mathrm{x}}}\frac{\mathrm{dS}_0(\hat{\mathrm{x}})}{\mathrm{d}\hat{\mathrm{x}}}\right], \tag{5.118}$$

$$\mathrm{F}^+ = -1, \tag{5.119}$$

$$\hat{\sigma}^- = \sigma_0^+ - 2a\left[\hat{\mathrm{x}} + \ln|\hat{\mathrm{x}} - 1| - \frac{\varepsilon}{8(\lambda a)^2}\mathrm{S}_0(\hat{\mathrm{x}})\right], \tag{5.120}$$

$$\hat{\sigma}^+ = \sigma^+. \tag{5.121}$$

Next, we turn to the region $x < 1$ of the spacetime. Setting $\delta = 1$ in Eq. (5.111) yields the following condition:

$$2\ln\hat{\mathrm{x}} - 2\frac{\ln\hat{\mathrm{x}}}{\hat{\mathrm{x}}-1} - \frac{3}{\hat{\mathrm{x}}} - 2 - 2c_{-1} + 2\frac{1-4\lambda a C}{\hat{\mathrm{x}}-1} = \sum_{n=1}^{\infty}\frac{1}{n!}\left[\frac{\hat{\mathrm{x}}-1}{\hat{\mathrm{x}}}\frac{\mathrm{dS}_n(\hat{\mathrm{x}})}{\mathrm{d}\hat{\mathrm{x}}} - n\mathrm{S}_n(\hat{\mathrm{x}})\right]. \tag{5.122}$$

Inserting $\delta = 1$ into Eqs. (5.103) and (5.104) gives:

$$\hat{\mathrm{x}} = 1 - \sum_{n=1}^{\infty}\frac{\mathrm{P}_{n-1}(1)}{n!}e^{n(\hat{\mathrm{x}}-1)}(1-\hat{\mathrm{x}})^n, \tag{5.123}$$

$$\ln\hat{\mathrm{x}} = -\sum_{n=1}^{\infty}\frac{\mathrm{Q}_{n-1}(1)}{n!}e^{n(\hat{\mathrm{x}}-1)}(1-\hat{\mathrm{x}})^n. \tag{5.124}$$

From Eq. (5.106) we obtain the following expression for the derivatives of $\mathrm{S}_n(\mathrm{x})$:

$$\frac{\mathrm{dS}_n^<(\hat{\mathrm{x}})}{\mathrm{d}\hat{\mathrm{x}}} = \hat{\mathrm{x}}(1-\hat{\mathrm{x}})^{n-2}e^{n(\hat{\mathrm{x}}-1)}\Big[(2-n)\mathrm{P}_{n-1}(1) + (2-3n)\mathrm{Q}_{n-1}(1)\Big]. \tag{5.125}$$

Substituting Eq. (5.125) into the first series on the right-hand side of Eq. (5.122) and using Eqs. (5.123) and (5.124), the sum can be evaluated straightforwardly, giving:

$$\frac{\hat{\mathrm{x}}-1}{\hat{\mathrm{x}}}\sum_{n=0}^{\infty}\frac{1}{n!}\frac{\mathrm{dS}_n^<(\hat{\mathrm{x}})}{\mathrm{d}\hat{\mathrm{x}}} = -2 - 2\frac{\ln\hat{\mathrm{x}}}{\hat{\mathrm{x}}-1} + \frac{1}{\hat{\mathrm{x}}} + \frac{3}{\hat{\mathrm{x}}^2}. \tag{5.126}$$

The second series in Eq. (5.122) can be obtained in a similar way: we first differentiate, use the same technique as for the preceding sum, and then integrate, imposing the condition that the sum vanishes at $\hat{\mathrm{x}} = 1$. This procedure leads to:

$$-\sum_{n=1}^{\infty}\frac{\mathrm{S}_n^<(\hat{\mathrm{x}})}{(n-1)!} = 2\ln\hat{\mathrm{x}} - \frac{4}{\hat{\mathrm{x}}} - \frac{3}{\hat{\mathrm{x}}^2} + 7 \equiv \mathrm{S}_1^>(\hat{\mathrm{x}}). \tag{5.127}$$

By inserting Eqs. (5.126) and (5.127) into Eq. (5.122), one indeed recovers condition (5.116). The remaining requirement is the continuity of the function θ. Using Eq. (5.110), this continuity condition can be rewritten as:

$$\mathrm{S}_0^{>}(\hat{\mathrm{x}}) = \mathrm{S}_0^{<}(\hat{\mathrm{x}}) - \sum_{n=1}^{\infty} \frac{\mathrm{S}_n^{<}(\hat{\mathrm{x}})}{n!}. \tag{5.128}$$

Once again, employing Eqs. (5.123) and (5.124), the series in Eq. (5.128) can be evaluated, yielding:

$$\sum_{n=1}^{\infty} \frac{\mathrm{S}_n^{<}(\hat{\mathrm{x}})}{n!} = 2\mathrm{L}(\hat{\mathrm{x}}) - 2\hat{\mathrm{x}} - \frac{\hat{\mathrm{x}} - 3}{\hat{\mathrm{x}} - 1} \ln \hat{\mathrm{x}}. \tag{5.129}$$

Substituting Eq. (5.129) into Eq. (5.128) one readily verifies that the continuity condition is met.

5.3.2 Asymptotically flat solution

Our final task is to verify whether the solution defined by Eqs. (5.110) and (5.111) is asymptotically flat. For this purpose, it is useful to clarify the behaviour of $\mathrm{S}_n^{>}(\mathrm{x})$ as $\mathrm{x} \to \infty$. We demonstrate that, for $n > 1$, the following relation holds:

$$\mathrm{S}_n^{>}(\mathrm{x}) = (n-1)!\mathrm{S}_1^{>}(\mathrm{x}) + \frac{6}{\mathrm{x}^4} \mathrm{Z}_{2(n-2)}\left(\frac{1}{\mathrm{x}}\right) - 6\mathrm{Z}_{2(n-2)}(1), \tag{5.130}$$

where $\mathrm{Z}_{2(n-2)}(x)$ denotes polynomials of degree $2(n-2)$. Expression (5.130) is written so as to incorporate the condition $\mathrm{S}_n(1) = 0$, given that $\mathrm{S}_1(1) = 0$. We will collectively denote the last two terms in Eq. (5.130) by $\mathrm{R}_n(\mathrm{x})$. Using the recurrence relation (5.108), one can derive the following recurrence relation for the functions R_n:

$$\frac{\mathrm{dR}_{n+1}}{\mathrm{dx}} - n\frac{\mathrm{dR}_n}{\mathrm{dx}} = -(n-1)!\frac{24}{\mathrm{x}^5} - \frac{1}{\mathrm{x}-1}\frac{\mathrm{d}}{\mathrm{dx}}\left(\frac{(\mathrm{x}-1)^2}{\mathrm{x}}\frac{\mathrm{dR}_n}{\mathrm{dx}}\right). \tag{5.131}$$

We now substitute $\frac{\mathrm{dR}_n}{\mathrm{dx}} = -\frac{24}{\mathrm{x}^5}\mathrm{M}_n(\mathrm{x})$ into Eq. (5.131), which leads to:

$$\mathrm{M}_{n+1} - n\mathrm{M}_n = (n-1)! + 2\left(\frac{2}{\mathrm{x}} - \frac{3}{\mathrm{x}^2}\right)\mathrm{M}_n - \frac{\mathrm{x}-1}{\mathrm{x}}\frac{\mathrm{dM}_n}{\mathrm{dx}}. \tag{5.132}$$

Since $\mathrm{M}_2(\mathrm{x}) = 1$, Eq. (5.132) shows that the functions $\mathrm{M}_n(\mathrm{x})$ can be expressed as polynomials in $1/\mathrm{x}$, and that their degree increases by two each time n is incremented by one. Consequently, the degree of the n-th polynomial is $2(n-2)$. After integrating the functions $\mathrm{M}_n/\mathrm{x}^5$, we obtain the representation (5.130) for the functions $\mathrm{S}_n^{>}(\mathrm{x})$. For later convenience, we introduce the shorthand $6\mathrm{Z}_{2(n-2)}(1) = z_n$. To determine whether the spacetime is asymptotically flat, we examine the large–x behavior of the metric, i.e., the limit $\mathrm{x} \to \infty$. We do this term by term using Eq. (5.111). The δ-independent term is given by:

$$\left(\frac{\mathrm{x}-1}{\mathrm{x}}\right)^2 \frac{\mathrm{dS}_0^{>}}{\mathrm{dx}} = -2\frac{\mathrm{x}-1}{\mathrm{x}} \ln\left(1 - \frac{1}{\mathrm{x}}\right) - \frac{2}{\mathrm{x}} + \frac{1}{\mathrm{x}^2} - \frac{1}{\mathrm{x}^3}, \tag{5.133}$$

from which it follows that this contribution goes to zero as $\mathrm{x} \to \infty$. The term proportional to $\ln\delta/\mathrm{x}$ also vanishes in the limit $\mathrm{x} \to \infty$. Furthermore, since $\frac{\mathrm{dS}_n^{>}}{\mathrm{dx}} \sim (n-1)!\frac{2}{\mathrm{x}}$ for $\mathrm{x} \to \infty$, this contribution likewise tends to zero. The only remaining term in the sum is

$$\mathrm{S}_{n+1}^{>} - n\mathrm{S}_n^{>} = -(z_{n+1} - nz_n) + \mathcal{O}\left(\frac{1}{\mathrm{x}^4}\right). \tag{5.134}$$

Thus, we are finally left with the following expression:

$$\lim_{\mathrm{x}\to\infty} \mathrm{F}^+\mathrm{F}^- e^{2\rho} = -1 - \frac{\varepsilon}{8(\lambda a)^2}\sum_{n=1}^{\infty}\frac{(1-\delta)^n}{n!}(z_{n+1}-nz_n). \tag{5.135}$$

From Eq. (5.135) we infer that, in the $\hat{\sigma}^{\pm}$ coordinates introduced in Eqs. (5.120) and (5.121), the metric is not asymptotically flat. Since its asymptotic form depends solely on σ^+, we attempt to perform a coordinate transformation that renders the metric flat at infinity:

$$\mathrm{d}s^2 = e^{2\rho}\mathrm{d}\sigma^+\mathrm{d}\sigma^- = -\mathrm{F}^+\mathrm{F}^- e^{2\rho}\mathrm{d}\hat{\sigma}^+\mathrm{d}\hat{\sigma}^- = -\mathrm{F}^+\mathrm{F}'^+\mathrm{F}^- e^{2\rho}\mathrm{d}\hat{\sigma}'^+\mathrm{d}\hat{\sigma}^-. \tag{5.136}$$

Requiring that the metric be asymptotically flat in the coordinates $\hat{\sigma}^-$ and $\hat{\sigma}'^+$ is equivalent to choosing

$$\mathrm{F}'^+ = 1 - \frac{\varepsilon}{8(\lambda a)^2}\sum_{n=1}^{\infty}\frac{(1-\delta)^n}{n!}(z_{n+1}-nz_n). \tag{5.137}$$

To determine the new coordinate $\hat{\sigma}'^+$, one must evaluate the integral $\int \frac{\mathrm{d}\hat{\sigma}^+}{\mathrm{F}'^+}$. The resulting expression is

$$\hat{\sigma}'^+ = -2a\ln\delta + \frac{a\varepsilon}{4(\lambda a)^2}\sum_{n=1}^{\infty}\frac{(1-\delta)^n}{n!}z_n + 2aD, \tag{5.138}$$

where D denotes an arbitrary integration constant. We now investigate the behavior of Eq. (5.110) for the dilaton field at infinity. Solving Eq. (5.138) for $\ln\delta$ and substituting the result into Eq. (5.110) leads to:

$$\mathrm{x}+\ln(\mathrm{x}-1)-\frac{\varepsilon}{8(\lambda a)^2}\left[\mathrm{S}_0^{>}(\mathrm{x})+\mathrm{S}_{-1}(\mathrm{x})\ln\delta-\sum_{n=1}^{\infty}\frac{(1-\delta)^n}{n!}\left(\mathrm{S}_n^{>}(\mathrm{x})+z_n\right)\right] = \frac{\hat{\sigma}'^+-\hat{\sigma}^-}{2a}-D. \tag{5.139}$$

First, we extract the δ-dependent contributions from Eq. (5.139). For large x we have

$$\mathrm{S}_n(\mathrm{x}) \sim (n-1)!\big(2\ln\mathrm{x}+7\big) - z_n, \tag{5.140}$$

which allows us to rewrite the sum appearing in Eq. (5.139) as:

$$-\sum_{n=1}^{\infty}\frac{(1-\delta)^n}{n!}\left(\mathrm{S}_n^{>}(\mathrm{x})+z_n\right) \sim \ln\delta\big(2\ln\mathrm{x}+7\big). \tag{5.141}$$

In the limit $\mathrm{x}\to\infty$, the contribution in Eq. (5.141) cancels exactly with the term $\mathrm{S}_{-1}(\mathrm{x})\ln\delta$. The $\mathrm{S}_0^{>}(\mathrm{x})$ contribution in Eq. (5.139) behaves as:

$$\lim_{\mathrm{x}\to\infty}\mathrm{S}_0^{>}(\mathrm{x}) = 2+\frac{\pi^2}{3}, \tag{5.142}$$

as $\mathrm{x}\to\infty$. The key ingredient in deriving Eq. (5.142) is the asymptotic form of $\mathrm{L}(\mathrm{x})$:

$$\mathrm{L}(\mathrm{x}) \sim -\frac{1}{2}\ln^2(\mathrm{x}-1)-\frac{\pi^2}{6}. \tag{5.143}$$

Thus, in the limit $\mathrm{x}\to\infty$, Eq. (5.139) simplifies to:

$$\mathrm{x}+\ln(\mathrm{x}-1)-\frac{\varepsilon}{4(\lambda a)^2}\left(\frac{\pi^2}{6}+1\right) = \frac{\hat{\sigma}'^+-\hat{\sigma}^-}{2a}-D. \tag{5.144}$$

Imposing that the asymptotic behavior of the dilaton field remains unchanged under quantum corrections fixes the constant to be $D = \frac{\varepsilon}{4(\lambda a)^2}\left(\frac{\pi^2}{6}+1\right)$. For simplicity, we can redefine the coordinate transformation for σ^+ by taking $\mathrm{F}^+\mathrm{F}'^+ \mapsto \mathrm{F}^+$ and $\hat{\sigma}'^+ \mapsto \hat{\sigma}^+$. In this new notation, the coordinate transformations become:

$$\mathrm{F}^- = \left(1-\frac{1}{\hat{\mathrm{x}}}\right)\left[1+\frac{\varepsilon}{8(\lambda a)^2}\frac{\hat{\mathrm{x}}-1}{\hat{\mathrm{x}}}\frac{\mathrm{dS}_0(\hat{\mathrm{x}})}{\mathrm{d}\hat{\mathrm{x}}}\right], \tag{5.145}$$

$$\mathrm{F}^+ = -1+\frac{\varepsilon}{8(\lambda a)^2}\sum_{n=1}^{\infty}\frac{(1-\delta)^n}{n!}(z_{n+1}-nz_n), \tag{5.146}$$

and the corresponding asymptotically flat coordinates read:

$$\hat{\sigma}^- = \sigma_0^+ - 2a\left[\hat{\mathrm{x}}+\ln|\hat{\mathrm{x}}-1|-\frac{\varepsilon}{8(\lambda a)^2}\mathrm{S}_0(\hat{\mathrm{x}})\right], \tag{5.147}$$

$$\hat{\sigma}^+ = \sigma^+ + \frac{2a\varepsilon}{8(\lambda a)^2}\left[\frac{\pi^2}{3}+2+\sum_{n=1}^{\infty}\frac{(1-\delta)^n}{n!}z_n\right]. \tag{5.148}$$

We then introduce a new coordinate $\hat{\delta}$ in terms of $\hat{\sigma}^+$:

$$\hat{\delta} = \exp\left\{\left(-\frac{\hat{\sigma}^+-\sigma_0^+}{2a}\right)\right\}. \tag{5.149}$$

With these definitions, the final forms of the metric and the dilaton field in region II of the spacetime (see Fig. 3.2) are as follows,

$$\begin{aligned}\mathrm{F}^+\mathrm{F}^-e^{2\rho} = &\left[1-\frac{\varepsilon}{8(\lambda a)^2}\sum_{n=1}^{\infty}\frac{(1-\delta)^n}{n!}(z_{n+1}-nz_n)\right]\left(\frac{1}{\mathrm{x}}-1\right)\left\{1+\frac{\varepsilon}{8(\lambda a)^2}\left[\frac{\mathrm{x}-1}{\mathrm{x}}\frac{\mathrm{dS}_0^>(\mathrm{x})}{\mathrm{dx}}\right.\right.\\ &\left.\left.-\frac{2\ln\delta}{\mathrm{x}-1}-\sum_{n=1}^{\infty}\frac{(1-\delta)^n}{n!}\left(\frac{\mathrm{x}-1}{\mathrm{x}}\frac{\mathrm{dS}_n^>(\mathrm{x})}{\mathrm{dx}}+\mathrm{S}_{n+1}^>(\mathrm{x})-n\mathrm{S}_n^>(\mathrm{x})\right)\right]\right\}\end{aligned} \tag{5.150}$$

$$\begin{aligned}\mathrm{F}^+\mathrm{F}^-e^{2\rho} = &\left[1-\frac{\varepsilon}{8(\lambda a)^2}\sum_{n=1}^{\infty}\frac{(1-\delta)^n}{n!}(z_{n+1}-nz_n)\right]\left(\frac{1}{\mathrm{x}}-1\right)\left\{1+\frac{\varepsilon}{8(\lambda a)^2}\left[\frac{\mathrm{x}-1}{\mathrm{x}}\frac{\mathrm{dS}_0^<(\mathrm{x})}{\mathrm{dx}}\right.\right.\\ &\left.\left.+\mathrm{S}_1^>(\mathrm{x})-\frac{2\ln\delta}{\mathrm{x}-1}-\sum_{n=1}^{\infty}\frac{\delta^n}{n!}\left(\frac{\mathrm{x}-1}{\mathrm{x}}\frac{\mathrm{dS}_n^<(\mathrm{x})}{\mathrm{dx}}-n\mathrm{S}_n^<(\mathrm{x})\right)\right]\right\}\end{aligned} \tag{5.151}$$

$$\begin{aligned}&\mathrm{x}+\ln(\mathrm{x}-1)-\frac{\varepsilon}{8(\lambda a)^2}\left[\mathrm{S}_0^>(\mathrm{x})-\frac{\pi^2}{3}-2+\ln\delta\mathrm{S}_{-1}(\mathrm{x})-\sum_{n=1}^{\infty}\frac{(1-\delta)^n}{n!}(\mathrm{S}_n^>(\mathrm{x})+z_n)\right]\\ &\qquad=-\ln\hat{\delta}+\hat{\mathrm{x}}+\ln(\hat{\mathrm{x}}-1)-\frac{\varepsilon}{8(\lambda a)^2}\mathrm{S}_0^>(\hat{\mathrm{x}})\equiv\frac{\hat{\sigma}^+-\hat{\sigma}^-}{2a}\equiv\frac{\hat{\sigma}}{a},\end{aligned} \tag{5.152}$$

$$\begin{aligned}&\mathrm{x}+\ln(1-\mathrm{x})-\frac{\varepsilon}{8(\lambda a)^2}\left[\mathrm{S}_0^<(\mathrm{x})-\frac{\pi^2}{3}-2+\ln\delta\mathrm{S}_{-1}(\mathrm{x})-\sum_{n=1}^{\infty}\frac{\delta^n}{n!}\mathrm{S}_n^<(\mathrm{x})-\sum_{n=1}^{\infty}\frac{(1-\delta)^n}{n!}z_n\right]\\ &\qquad=-\ln\hat{\delta}+\hat{\mathrm{x}}+\ln(1-\hat{\mathrm{x}})-\frac{\varepsilon}{8(\lambda a)^2}\mathrm{S}_0^>(\hat{\mathrm{x}})\equiv\frac{\hat{\sigma}^+-\hat{\sigma}^-}{2a}\equiv\frac{\hat{\sigma}}{a}.\end{aligned} \tag{5.153}$$

Eq. (5.150) provides the form of the metric for $\mathrm{x}\geqslant 1$, while Eq. (5.151) gives the corresponding expression for $\mathrm{x}\leqslant 1$. The relations (5.152) and (5.153) are the quantum-corrected transcendental equations for the dilaton field $\mathrm{x} = \frac{1}{\lambda a} e^{-\phi}$ in the regimes $\mathrm{x} \geqslant 1$ and $\mathrm{x} \leqslant 1$, respectively, expressed in terms of the coordinates σ^+ (via their dependence on δ) and σ^- (through the dependence on $\hat{\mathrm{x}}$). The functions $\mathrm{S}_0^{>/<}$ and $\mathrm{S}_n^{>/<}(\mathrm{x})$ appearing in Eqs. (5.150)–(5.153) are defined in Eqs. (5.109) and (5.106), respectively. Observe that for $\delta = 1$ both Eqs. (5.150) and (5.151) reduce to Eq. (5.145) for the coordinate transformation F^-. Consequently, $e^{2\rho} = 1$ when $\delta = 1$, which enforces continuity of the metric. Moreover, Eqs. (5.152) and (5.153) show that $\mathrm{x} = \hat{\mathrm{x}}$ when $\delta = 1$, ensuring continuity of the dilaton field. In Eqs. (5.152) and (5.153) we also identify new asymptotically flat coordinates $\hat{\sigma}^\pm$, defined in Eqs. (5.147) and (5.148). Note that in the following subsections we alternate between the original $\hat{\sigma}^\pm$ coordinates and the ones introduced in this subsection.

5.3.3 Evaporation adapted form of the solution

The terms involving $\ln\delta$ appear in the evaporating black hole solution (5.150-5.153). Since $\ln\delta \sim \sigma^+$, these contributions grow without bound at late evaporation times. One might therefore conclude that this behavior leads to a divergent metric at $\mathcal{J}^+$. However, they cancel precisely against the δ terms coming from the sums, so that the metric remains asymptotically flat. Still, their presence in this explicit form is somewhat unexpected. From a physical point of view, the apparent horizon should shrink as the black hole continues to evaporate. Hence, it is natural to expect that the $\ln\delta$ terms are effectively incorporated into the constant λa as part of its quantum corrections. In this subsection, we rewrite the solution (5.150-5.153) guided by this line of reasoning.

As a consequence, the solution is well defined on hypersurfaces specified by $\mathrm{x} = 1 + \mathcal{O}(\tilde{\varepsilon})$ or equivalently $\hat{\mathrm{x}} = 1 + \mathcal{O}(\tilde{\varepsilon})$. We also introduce the notation $\tilde{\varepsilon} = \frac{\varepsilon}{(\lambda a)^2}$. This is relevant because many hypersurfaces of physical interest (apparent horizon, horizon, island, QES, etc.) are described by relations of this form. From the structure of the equations of motion (5.44-5.46) and the method by which they are solved (5.47-5.59), one is naturally led to expect that the formulas for $\partial_\pm \mathrm{x}$ (5.52-5.53) remain well defined when $\mathrm{x} = 1 + \mathcal{O}(\tilde{\varepsilon})$, since they follow from straightforward integration of the original equations of motion. This expectation is indeed confirmed:

$$\partial_+ \mathrm{x} = \frac{1}{2a}\left\{1 - \frac{1+\frac{\tilde{\varepsilon}}{4}\ln\delta}{\sqrt{\mathrm{x}^2-\tilde{\varepsilon}}}\left[1 - \frac{\tilde{\varepsilon}}{8}\left(2(\mathrm{x}-2)\ln\mathrm{x} - 8 + 5\mathrm{x} + \frac{3}{\mathrm{x}}\right.\right.\right.$$
$$\left.\left.\left. - (\mathrm{x}-1)\sum_{n=1}^{\infty}\frac{\delta^n}{n!}\left(\frac{\mathrm{x}-1}{\mathrm{x}}\frac{d\mathrm{S}_n^<}{d\mathrm{x}} - n\mathrm{S}_n^<\right)\right)\right]\right\}, \tag{5.154}$$

$$\partial_- \mathrm{x} = -\frac{1}{2a\mathrm{F}^-}\left\{1 - \frac{1+\frac{\tilde{\varepsilon}}{4}\ln\delta}{\sqrt{\mathrm{x}^2-\tilde{\varepsilon}}}\left[1 - \frac{\tilde{\varepsilon}}{8}\left(2(\mathrm{x}-2)\ln\mathrm{x} - 2(\mathrm{x}-1)\ln(1-\mathrm{x}) + 1 - 2\mathrm{x} + \frac{3}{\mathrm{x}}\right.\right.\right.$$
$$\left.\left.\left. - \frac{(\mathrm{x}-1)^2}{\mathrm{x}}\sum_{n=1}^{\infty}\frac{\delta^n}{n!}\frac{d\mathrm{S}_n^<}{d\mathrm{x}}\right)\right]\right\}. \tag{5.155}$$

This indicates that the problem emerges in the course of performing the final integration in Eqs. (5.58-5.59). We now introduce a new coordinate:

$$\mathrm{y} = \frac{\mathrm{x}}{1+\frac{\tilde{\varepsilon}}{4}\ln\delta} \equiv \frac{\mathrm{x}}{\tilde{a}}, \tag{5.156}$$

such that $a\tilde{a}$ can be interpreted as a quantum-corrected version of the constant a. With this substitution, Eqs. (5.154-5.155) take the form:

$$\partial_+ \mathrm{x} = \frac{1}{2a}\left\{1 - \frac{1}{\sqrt{\mathrm{y}^2-\tilde{\varepsilon}}}\left[1 - \frac{\tilde{\varepsilon}}{8}\left(2(\mathrm{y}-2)\ln \mathrm{y} - 8 + 5\mathrm{y} + \frac{3}{\mathrm{y}} \right.\right.\right.$$
$$\left.\left.\left. -(\mathrm{y}-1)\sum_{n=1}^{\infty}\frac{\delta^n}{n!}\left(\frac{\mathrm{y}-1}{\mathrm{y}}\frac{\mathrm{dS}_n^<}{\mathrm{dy}} - n\mathrm{S}_n^<\right)\right)\right]\right\}, \tag{5.157}$$

$$\partial_- \mathrm{x} = -\frac{1}{2a\mathrm{F}^-}\left\{1 - \frac{1}{\sqrt{\mathrm{y}^2-\tilde{\varepsilon}}}\left[1 - \frac{\tilde{\varepsilon}}{8}\left(2(\mathrm{y}-2)\ln \mathrm{y} - 2(\mathrm{y}-1)\ln(1-\mathrm{y}) + 1 - 2\mathrm{y} + \frac{3}{\mathrm{y}} \right.\right.\right.$$
$$\left.\left.\left. -\frac{(\mathrm{y}-1)^2}{\mathrm{y}}\sum_{n=1}^{\infty}\frac{\delta^n}{n!}\frac{\mathrm{dS}_n^<}{\mathrm{dy}}\right)\right]\right\}. \tag{5.158}$$

We therefore expect the evaporation dynamics to be determined by the zeroth-order term in $\tilde{\varepsilon}$ in Eqs. (5.157) and (5.158), because the first-order contribution vanishes at $\mathrm{y} = 1$. Hence, we temporarily ignore the $\mathcal{O}(\tilde{\varepsilon})$ term in the square brackets of Eq. (5.157), which yields:

$$\partial_+ \mathrm{x}^{(0)} = \frac{1}{2a}\left(1 - \frac{1}{\sqrt{\mathrm{y}^2-\tilde{\varepsilon}}}\right). \tag{5.159}$$

Next, we introduce a function $\mathcal{J}(\mathrm{x})$ defined implicitly through

$$\tilde{a}\mathcal{J}(\mathrm{y}) = \frac{\sigma^+}{2a}. \tag{5.160}$$

Differentiating Eq. (5.160) with respect to σ^+ and substituting Eq. (5.159) leads to the following differential equation for $\mathcal{J}$:

$$\frac{\mathrm{d}\mathcal{J}}{\mathrm{dy}} - \frac{\tilde{\varepsilon}}{4}\frac{\sqrt{\mathrm{y}^2-\tilde{\varepsilon}}}{(1+\frac{\tilde{\varepsilon}}{4}\mathrm{y})\sqrt{\mathrm{y}^2-\tilde{\varepsilon}}-1}\mathcal{J} = \frac{\sqrt{\mathrm{y}^2-\tilde{\varepsilon}}}{(1+\frac{\tilde{\varepsilon}}{4}\mathrm{y})\sqrt{\mathrm{y}^2-\tilde{\varepsilon}}-1}. \tag{5.161}$$

A solution of Eq. (5.161) can then be written as:

$$\mathcal{J}(\mathrm{y}) = -\frac{4}{\tilde{\varepsilon}} + S\exp\left\{\left(\frac{\tilde{\varepsilon}}{4}\tilde{f}(\mathrm{y})\right)\right\}, \tag{5.162}$$

where S is an integration constant to be fixed, and $\tilde{f}(\mathrm{y})$ is defined by:

$$\tilde{f}(\mathrm{y}) = \int \frac{\sqrt{\mathrm{y}^2-\tilde{\varepsilon}}}{(1+\frac{\tilde{\varepsilon}}{4}\mathrm{y})\sqrt{\mathrm{y}^2-\tilde{\varepsilon}}-1}\mathrm{dy}. \tag{5.163}$$

Upon performing the substitution $\mathrm{z} = \sqrt{\frac{\mathrm{y}-\sqrt{\tilde{\varepsilon}}}{\mathrm{y}+\sqrt{\tilde{\varepsilon}}}}$, the integral (5.163) takes the form

$$\tilde{f} = 8\tilde{\varepsilon}\int \frac{\mathrm{z}^2\mathrm{dz}}{(\mathrm{z}^2-1)R(z)}, \tag{5.164}$$

where

$$R(\mathrm{z}) = \mathrm{z}^4 + 2\sqrt{\tilde{\varepsilon}}\left(1 - \frac{\tilde{\varepsilon}^{3/2}}{4}\right)\mathrm{z}^3 - 2\mathrm{z}^2 - 2\sqrt{\tilde{\varepsilon}}\left(1 + \frac{\tilde{\varepsilon}^{3/2}}{4}\right)\mathrm{z} + 1. \tag{5.165}$$

This quartic polynomial can be factorized as

$$R(\mathrm{z}) = (\mathrm{z}^2 + \alpha_1 \mathrm{z} + \beta_1)(\mathrm{z}^2 + \alpha_2 \mathrm{z} + \beta_2). \tag{5.166}$$

The coefficients $\alpha_{1,2}$ and $\beta_{1,2}$ are constrained by

$$\begin{aligned} \alpha_1 + \alpha_2 &= 2\sqrt{\tilde{\varepsilon}}\left(1 - \frac{\tilde{\varepsilon}^{\frac{3}{2}}}{4}\right), \quad \beta_1 + \beta_2 = -2 - \alpha_1\alpha_2, \\ \alpha_1\beta_2 + \alpha_2\beta_1 &= -2\sqrt{\tilde{\varepsilon}}\left(1 + \frac{\tilde{\varepsilon}^{\frac{3}{2}}}{4}\right), \quad \beta_1\beta_2 = 1. \end{aligned} \tag{5.167}$$

Although the system (5.167) can be solved exactly, we instead determine its solution perturbatively up to $\mathcal{O}(\tilde{\varepsilon}^4)$. This yields

$$\begin{aligned} \alpha_1 &= 2\sqrt{\tilde{\varepsilon}}\left(1 - \frac{\tilde{\varepsilon}^{\frac{3}{2}}}{4}\right)\left[1 - \frac{\tilde{\varepsilon}^2}{16}\left(1 + \frac{\tilde{\varepsilon}^{\frac{3}{2}}}{2}\right)\right], \quad \alpha_2 = \frac{\tilde{\varepsilon}^{\frac{5}{2}}}{8}\left(1 + \frac{\tilde{\varepsilon}^{\frac{3}{2}}}{4}\right), \\ \beta_1 &= -1 + \frac{\tilde{\varepsilon}^{\frac{3}{2}}}{2}\left(1 - \frac{\tilde{\varepsilon}^{\frac{3}{2}}}{4} + \frac{\tilde{\varepsilon}^2}{8}\right), \quad \beta_2 = -1 - \frac{\tilde{\varepsilon}^{\frac{3}{2}}}{2}\left(1 + \frac{\tilde{\varepsilon}^{\frac{3}{2}}}{4} + \frac{\tilde{\varepsilon}^2}{8}\right). \end{aligned} \tag{5.168}$$

The corresponding expressions for the roots of the polynomial $R(\mathrm{z})$ are:

$$\mathrm{z}_2^+ = 1 + \frac{\tilde{\varepsilon}^{\frac{3}{2}}}{4} - \frac{\tilde{\varepsilon}^{\frac{5}{2}}}{16} + \frac{\tilde{\varepsilon}^3}{32} + \frac{\tilde{\varepsilon}^{\frac{7}{2}}}{32} - \frac{\tilde{\varepsilon}^4}{64} \tag{5.169}$$

$$\mathrm{z}_2^- = -1 - \frac{\tilde{\varepsilon}^{\frac{3}{2}}}{4} - \frac{\tilde{\varepsilon}^{\frac{5}{2}}}{16} - \frac{\tilde{\varepsilon}^3}{32} - \frac{\tilde{\varepsilon}^{\frac{7}{2}}}{32} - \frac{\tilde{\varepsilon}^4}{64} \tag{5.170}$$

$$\mathrm{z}_1^+ = 1 - \tilde{\varepsilon}^{\frac{1}{2}} + \frac{\tilde{\varepsilon}}{2} - \frac{\tilde{\varepsilon}^{\frac{3}{2}}}{4} + \frac{\tilde{\varepsilon}^2}{8} - \frac{\tilde{\varepsilon}^{\frac{5}{2}}}{16} + \frac{\tilde{\varepsilon}^3}{32} - \frac{\tilde{\varepsilon}^4}{128}, \tag{5.171}$$

$$\mathrm{z}_1^- = -1 - \tilde{\varepsilon}^{\frac{1}{2}} - \frac{\tilde{\varepsilon}}{2} + \frac{\tilde{\varepsilon}^{\frac{3}{2}}}{4} + \frac{3\tilde{\varepsilon}^2}{8} + \frac{3\tilde{\varepsilon}^{\frac{5}{2}}}{16} - \frac{\tilde{\varepsilon}^3}{32} + \frac{5\tilde{\varepsilon}^4}{128}. \tag{5.172}$$

Now the integral (5.164) can be evaluated in a straightforward manner, yielding

$$\begin{aligned} \tilde{f}(\mathrm{z}) =& \frac{4}{\tilde{\varepsilon}} \ln\left|\frac{\mathrm{z}^2 + \alpha_2 \mathrm{z} + \beta_2}{1 - \mathrm{z}^2}\right| + \left(1 - \frac{5}{4}\tilde{\varepsilon}\right)\ln|\mathrm{z} - \mathrm{z}_1^+| - \left(1 - \frac{1}{4}\tilde{\varepsilon}\right)\ln|\mathrm{z} - \mathrm{z}_1^-| \\ &- \left(1 - \frac{3}{4}\tilde{\varepsilon}\right)\ln|\mathrm{z} - \mathrm{z}_2^+| + \left(1 + \frac{3}{4}\tilde{\varepsilon}\right)\ln|\mathrm{z} - \mathrm{z}_2^-| + \frac{\tilde{\varepsilon}}{4}\ln\frac{\tilde{\varepsilon}}{16}. \end{aligned} \tag{5.173}$$

A convenient and consistent choice for the constant S in Eq. (5.162) is $S = \frac{4}{\tilde{\varepsilon}} + \frac{9}{2}$, which ensures that the divergent contributions in Eqs. (5.152) and (5.153) are entirely absorbed into the function $\mathcal{J}(\mathrm{y})$. By expanding $\mathcal{J}$, we obtain

$$\mathcal{J}(\mathrm{y}) = \mathrm{y} + \ln|\mathrm{y} - 1| - \frac{\tilde{\varepsilon}}{8}\left[-4\ln \mathrm{y} - (2\mathrm{y} - 1)\ln|\mathrm{y} - 1| - \ln^2|\mathrm{y} - 1| + \frac{2}{\mathrm{y} - 1} - 5\mathrm{y}\right] + \frac{9}{2}. \tag{5.174}$$

From Eq. (5.174) it follows that the function $\mathcal{J}$ incorporates all divergent terms, including the $\ln\delta$ contribution (after substituting $\mathrm{y} = \frac{\mathrm{x}}{\tilde{a}}$) appearing in Eqs. (5.152) and (5.153). These equations can therefore be recast in the form:

$$\left(1+\frac{\varepsilon}{4(\lambda a)^2}\ln\delta\right)\mathcal{J}(\mathrm{y})-\frac{\varepsilon}{8(\lambda a)^2}\left[(2\mathrm{y}+3)\ln\mathrm{y}+5\mathrm{y}-2\mathrm{L}(\mathrm{y})-\sum_{n=1}^{\infty}\frac{(1-\delta)^n}{n!}\mathrm{S}_n^{>}(\mathrm{y})\right] \tag{5.175}$$
$$=-\ln\delta+\mathcal{J}(\hat{\mathrm{x}})-\frac{\varepsilon}{8(\lambda a)^2}\left[(2\hat{\mathrm{x}}+3)\ln\hat{\mathrm{x}}+5\hat{\mathrm{x}}-2\mathrm{L}(\hat{\mathrm{x}})\right], \quad \text{when } \mathrm{y}>1$$

$$\left(1+\frac{\varepsilon}{4(\lambda a)^2}\ln\delta\right)\mathcal{J}(\mathrm{y})-\frac{\varepsilon}{8(\lambda a)^2}\left[\frac{2\mathrm{y}^2}{\mathrm{y}-1}\ln\mathrm{y}+3\mathrm{y}-\sum_{n=1}^{\infty}\frac{\delta^n}{n!}\mathrm{S}_{\mathrm{n}}^{<}(\mathrm{y})\right] \tag{5.176}$$
$$=-\ln\delta+\mathcal{J}(\hat{\mathrm{x}})-\frac{\varepsilon}{8(\lambda a)^2}\left[(2\hat{\mathrm{x}}+3)\ln\hat{\mathrm{x}}+5\hat{\mathrm{x}}-2\mathrm{L}(\hat{\mathrm{x}})\right], \quad \text{when } \mathrm{y}<1.$$

Note that both equations are well defined in the vicinity of $\mathrm{y}=1+\mathcal{O}(\tilde{\varepsilon})$, which was the primary objective of this subsection. Next, we determine the general solution under the assumption $\mathrm{y}=1+\frac{\varepsilon}{(\lambda a)^2}\eta$ and $\tilde{a}\gg 0$. This condition yields $\hat{\mathrm{x}}=1+\frac{\varepsilon}{(\lambda a)^2}\mu$. Consequently, both Eqs. (5.175) and (5.176) reduce to:

$$\tilde{a}\mathcal{J}\left(1+\tilde{\varepsilon}\eta\right)=-\ln\delta+\mathcal{J}\left(1+\tilde{\varepsilon}\mu\right). \tag{5.177}$$

Formula (5.177) can be further recast as:

$$\tilde{a}\exp\left\{\left(\frac{\tilde{\varepsilon}}{4}\tilde{f}(1+\tilde{\varepsilon}\eta)\right)\right\}=\exp\left\{\left(\frac{\tilde{\varepsilon}}{4}\tilde{f}(1+\tilde{\varepsilon}\mu)\right)\right\}. \tag{5.178}$$

A detailed analysis of the function $\tilde{f}(\mathrm{z})$ then yields:

$$\tilde{a}^{\frac{4}{\tilde{\varepsilon}}}=\left|\frac{4\mu-1}{4\eta-1}\right|. \tag{5.179}$$

Because the solution is derived only to first order in perturbation theory, we obtain $\tilde{a}^{4/\tilde{\varepsilon}}=\delta$. We expect that this relation will remain valid at higher orders in perturbation theory as well. Under this assumption, Eq. (5.179) reduces to:

$$\delta=\left|\frac{4\mu-1}{4\eta-1}\right|. \tag{5.180}$$

Substituting back, yields the following expression:

$$\hat{\mathrm{x}}=1+\frac{\varepsilon}{4(\lambda a)^2}\left(1+(4\eta-1)\delta\right). \tag{5.181}$$

Together with Eqs. (5.157) and (5.158), derivative we give a closed form for the metric derivatives: $\partial_{\pm}\rho$:

$$\partial_+\rho=\frac{1}{4a\tilde{a}}\frac{\mathrm{y}}{(\mathrm{y}^2-\tilde{\varepsilon})^{\frac{3}{2}}}\left\{1+\frac{\tilde{\varepsilon}}{4}\left[(3+2\mathrm{y})\left(1-\frac{1}{\mathrm{y}^2}\right)+2\ln\mathrm{y}\right.\right. \tag{5.182}$$
$$\left.\left.+\frac{1}{2}\sum_{n=1}^{\infty}\frac{\delta^n}{n!}\left(n(1-n\mathrm{y}^2)\mathrm{S}_n^{<}-\frac{\mathrm{y}-1}{\mathrm{y}}(\mathrm{y}^2+\mathrm{y}-1)\frac{\mathrm{dS}_n^{<}}{\mathrm{dy}}\right)\right]\right\},$$

$$\partial_-\rho=-\frac{1}{4a\mathrm{F}^-}\left\{\frac{\hat{\mathrm{x}}^2-1}{\hat{\mathrm{x}}^2}\left(1-\frac{\tilde{\varepsilon}}{4}\mathrm{F}(\hat{\mathrm{x}})\right)-\frac{1}{\tilde{a}}\left(1-\frac{1}{\mathrm{y}^2}\right)\right. \tag{5.183}$$
$$\left.+\frac{\tilde{\varepsilon}}{4\tilde{a}\mathrm{y}^2}\left[(\mathrm{y}^2-1)\left(\ln(1-\mathrm{y})+(2\mathrm{y}-3)\frac{\mathrm{y}^2+2}{2\mathrm{y}^2}\right)+2\ln\mathrm{y}+\frac{(\mathrm{y}^2+1)(\mathrm{y}-1)^2}{2}\sum_{n=1}^{\infty}\frac{\delta^n}{n!}\frac{\mathrm{dS}_n^{<}}{\mathrm{dy}}\right]\right\}.$$

In terms of the function $\mathrm{F}(\hat{\mathrm{x}})$, the coordinate transformation F^- can be expressed as:

$$\mathrm{F}^- = \frac{\hat{\mathrm{x}}-1}{\hat{\mathrm{x}}}\left[1-\frac{\tilde{\varepsilon}}{4}\left(\mathrm{F}(\hat{\mathrm{x}})+\frac{2\hat{\mathrm{x}}-1}{\hat{\mathrm{x}}^2(\hat{\mathrm{x}}-1)}\right)\right]. \tag{5.184}$$

Notice that all these expressions are well defined around the $\mathrm{y}=1$ and $\hat{\mathrm{x}}=1$ hypersurfaces

5.3.4 The end-state of black hole evolution

In the previous subsection, we obtained an evaporating black hole solution generated by collapsing matter. In this subsection, we examine the final state of the black hole's evolution. We adopt the approach described in Sec. 3.4.1. We first determine the apparent horizon, then analyze the curvature and locate the singularity. Their intersection specifies the end-point of the evaporation. At the conclusion of this subsection, we compute the total energy radiated away from the black hole during its evolution. The apparent horizon is defined by $\partial_+ e^{-2\phi}=0$, which is equivalent to $\mathrm{x}\partial_+\mathrm{x}=0$. Employing formula (5.114), a straightforward calculation gives:

$$\mathrm{x} = 1+\frac{\varepsilon}{4(\lambda a)^2}\left[\ln\delta+4-(\mathrm{x}-2)\ln\mathrm{x}-\frac{3}{2\mathrm{x}}+\frac{2}{\mathrm{x}^2}-\frac{5\mathrm{x}}{2}+\frac{\mathrm{x}-1}{2}\sum_{n=1}^{\infty}\frac{\delta^n}{n!}\left(\frac{\mathrm{x}-1}{\mathrm{x}}\frac{d\mathrm{S}_n}{d\mathrm{x}}-n\mathrm{S}_n\right)\right]. \tag{5.185}$$

Solving Eq. (5.185) perturbatively, by choosing ansatz $\mathrm{x}_{AH}=\mathrm{x}^{(0)}_{AH}+\varepsilon\mathrm{x}^{(1)}_{AH}$, we obtain:

$$\mathrm{x}_{AH} = 1+\frac{\varepsilon}{4(\lambda a)^2}\left(2+\ln\delta\right). \tag{5.186}$$

As time elapses, δ becomes progressively smaller, which correspondingly decreases the apparent horizon. This is precisely the outcome we anticipate. Observe that in computing $\partial_+\mathrm{x}$ we have employed expression (5.151). The same expression for the apparent horizon can also be obtained using formula (5.150), given that $\mathrm{x}^{(0)}_{AH}=1$. Adopting the new notation introduced in Sec. 5.3.3, and setting expression (5.157) equal to zero, the apparent horizon is determined by

$$\mathrm{y}_{AH} = \sqrt{1+\frac{\varepsilon}{(\lambda a)^2}}. \tag{5.187}$$

It is straightforward to verify that this relation reproduces the same result as in Eq. (5.186). Making use of formula (5.179), the dependence of the apparent horizon on $\hat{\mathrm{x}}(\delta)$ is

$$\hat{\mathrm{x}}_{AH} = 1+\frac{\varepsilon}{4(\lambda a)^2}\left[1+\left(1+\frac{\varepsilon}{4(\lambda a)^2}\ln\delta\right)^{\frac{4(\lambda a)^2}{\varepsilon}}\right]. \tag{5.188}$$

Taking the limit $\varepsilon\to 0$ of the expression inside the square brackets, and noting that this term is already of order $\mathcal{O}(\varepsilon)$, we arrive at the following simplified expression for the apparent horizon in the $(\hat{\mathrm{x}},\delta)$ coordinates:

$$\hat{\mathrm{x}}_{AH}(\delta) = 1+\frac{\varepsilon}{4(\lambda a)^2}(1+\delta). \tag{5.189}$$

The next step is to determine the line of the singularity. To achieve this, we must first compute the scalar curvature (3.3). Employing the equations of motion (5.45-5.46), the curvature can be written in terms of the first derivatives of the dilaton field:

$$R = \frac{2}{a^2}\frac{1+4a^2e^{-2\rho}\partial_+\mathrm{x}\partial_-\mathrm{x}}{\mathrm{x}^2-\frac{\varepsilon}{(\lambda a)^2}}. \tag{5.190}$$

At first glance, Eq. (5.190) appears to shift the singularity from $\mathrm{x}_S = 0$ to $\mathrm{x}_S = \frac{\sqrt{\varepsilon}}{\lambda a}$ once quantum corrections are taken into account. If this were indeed the case, it could signal a potential problem for the perturbative treatment. Making use of expression (5.190) together with the recurrence relation (5.108), the scalar curvature can be recast as

$$R = \frac{2}{a^2\mathrm{x}^3}\left\{1 + \frac{\varepsilon}{8(\lambda a)^2}\left[2\ln\mathrm{x} - 3 - \frac{2}{\mathrm{x}} + \frac{15}{\mathrm{x}^2} + 2\mathrm{x} + 2\ln\delta + \frac{(\mathrm{x}-1)^2}{\mathrm{x}}\sum_{n=1}^{\infty}\frac{\delta^n}{n!}\frac{\mathrm{dS}_n(\mathrm{x})}{\mathrm{dx}}\right]\right\}. \tag{5.191}$$

We first examine the beginning of evaporation, $\delta = 1$. Applying the relation (5.126), we obtain

$$R = \frac{2}{a^2\mathrm{x}^3}\left(1 + \frac{3\varepsilon}{2(\lambda a)^2}\frac{1}{\mathrm{x}^2}\right). \tag{5.192}$$

From Eq. (5.192), we find that the singularity line admits two distinct solutions:

$$\mathrm{x}_S = 0 \;\text{ and }\; \mathrm{x}_S \approx \sqrt{\frac{3\varepsilon}{2(\lambda a)^2}}. \tag{5.193}$$

Neither of these two solutions matches the expected result $\mathrm{x}_S = \frac{\sqrt{\varepsilon}}{\lambda a}$. This discrepancy may stem from the use of the perturbative approach. Fortunately, one can obtain a non-perturbative expression for the scalar curvature at the beginning of the evaporation. To this end, we solve the equations of motion on the hypersurface $\sigma^+ = \sigma_0^+ + \epsilon,\ \ \epsilon \to 0$. On this hypersurface, the metric is fixed by $e^{2\rho} = 1$, and the dilaton field is given by $\mathrm{x} = \frac{\sigma_0^+ - \sigma^-}{2a}$. This follows from the continuity conditions imposed across the hypersurface. From Eq. (5.113) we then find:

$$\mathrm{x}\partial_+\mathrm{x} + \frac{\varepsilon}{(\lambda a)^2}\partial_+\rho = \frac{\mathrm{x}-1}{2a}. \tag{5.194}$$

Using Eq. (5.194), one readily verifies that Eq. (5.46) holds. Combining Eq. (5.45) with Eq. (5.194) yields the following differential equation for $\partial_+\rho = f(\mathrm{x}(\sigma^-))$:

$$\frac{\mathrm{d}f}{\mathrm{dx}} = -\frac{1}{2a}\frac{1 + 2a\frac{\varepsilon}{(\lambda a)^2}f}{\mathrm{x}\left(\mathrm{x}^2 - \frac{\varepsilon}{(\lambda a)^2}\right)}. \tag{5.195}$$

The solution of Eq. (5.195) is given by:

$$f(\mathrm{x}) = \frac{\lambda^2 a}{2\varepsilon}\left(\frac{Q\mathrm{x}}{\sqrt{\mathrm{x}^2 - \frac{\varepsilon}{(\lambda a)^2}}} - 1\right), \tag{5.196}$$

where Q is an integration constant. By directly comparing Eq. (5.196) with the expression for $\partial_+\rho$ obtained from Eq. (5.151) in the case $\delta = 1$, we infer that $Q = 1$. Consequently, the solutions for $\partial_\pm\rho$ and $\partial_\pm\mathrm{x}$, together with the condition $\sigma^+ = \sigma_0^+$, take the form:

$$\partial_+\mathrm{x} = \frac{1}{2a}\left(1 - \frac{1}{\sqrt{\mathrm{x}^2 - \frac{\varepsilon}{(\lambda a)^2}}}\right), \qquad \partial_-\mathrm{x} = -\frac{1}{2a}, \tag{5.197}$$

$$\partial_+\rho = \frac{\lambda^2 a}{2\varepsilon}\left(\frac{\mathrm{x}}{\sqrt{\mathrm{x}^2 - \frac{\varepsilon}{(\lambda a)^2}}} - 1\right), \qquad \partial_-\rho = 0. \tag{5.198}$$

The scalar curvature is then given by:

$$R = \frac{2}{a^2} \frac{1}{\left(\mathrm{x}^2 - \frac{\varepsilon}{(\lambda a)^2}\right)^{\frac{3}{2}}}. \tag{5.199}$$

We therefore conclude that, at the beginning of the evaporation, the singularity forms at

$$\mathrm{x}_S = \frac{\sqrt{\varepsilon}}{\lambda a}, \tag{5.200}$$

as anticipated. Restoring all physical constants, this corresponds to $\varphi_S = \sqrt{\frac{\hbar G}{12\pi c^3}}$, which is of the order of the Planck length.

Next, we determine the quantum-corrected expression for the line of singularity given in Eq. (5.42). In the y coordinates (defined in Sec. 5.3.3), the singularity takes the form

$$\mathrm{y}_S = \frac{\sqrt{\varepsilon}}{\lambda a} \frac{1}{1 + \frac{\varepsilon}{4(\lambda a)^2} \ln \delta_S}. \tag{5.201}$$

Substituting Eq. (5.201) into Eq. (5.176) and expanding the result up to terms of order $\mathcal{O}(\varepsilon)$ yields the following condition for the singularity:

$$\left(1 + \frac{9\varepsilon}{8(\lambda a)^2}\right) \ln \delta_S + \frac{\varepsilon}{8(\lambda a)^2} \sum_{n=1}^{\infty} \frac{\delta_S^n}{n!} \mathrm{S}_n^<(0) = \hat{\mathrm{x}}_S + \ln |\hat{\mathrm{x}}_S - 1| - \frac{\varepsilon}{8(\lambda a)^2} \mathrm{S}_0^>(\hat{\mathrm{x}}_S). \tag{5.202}$$

Thus, Eq. (5.202) shows that the singularity (5.42) acquires a quantum correction of order $\mathcal{O}(\varepsilon)$.

The end-point of the evaporation

According to the cosmic censorship conjecture [106], a naked singularity cannot result from gravitational collapse. In contrast, the two hypersurfaces $\mathrm{y}_{AH}(\delta)$ (5.187) and $\mathrm{y}_S(\delta)$ (5.201) intersect at a finite value of the coordinate δ, determined by $\tilde{a}_E = \frac{\sqrt{\varepsilon}}{\lambda a}$. The corresponding point marks the end-point of evaporation, and is given by:

$$\sigma_E^+ = \sigma_0^+ + \frac{8a(\lambda a)^2}{\varepsilon} \left(1 - \frac{\sqrt{\varepsilon}}{\lambda a}\right). \tag{5.203}$$

If we now substitute all constants, expression (5.203) can be rewritten as

$$\sigma_E^+ = \sigma_0^+ + \frac{768\pi M^3 G^2}{\hbar \lambda^4} \left(1 - \frac{\lambda}{4M} \sqrt{\frac{\hbar}{3\pi G}}\right). \tag{5.204}$$

Eq. (5.204) shows that the leading contribution to the black hole evaporation time scales as M^3, which agrees with the standard thermodynamic estimate and coincides with the result obtained in [115]. It is convenient to rewrite the evaporation end-point in terms of the δ coordinate:

$$\delta_E = e^{-\frac{4(\lambda a)^2}{\varepsilon}\left(1 - \frac{\sqrt{\varepsilon}}{\lambda a}\right)}. \tag{5.205}$$

The quantity (5.205) is extremely small, $\delta_E \ll \frac{\varepsilon}{4(\lambda a)^2}$. Conversely, $\ln \delta_E$ is very large, scaling as $1/\varepsilon$. This indicates that the perturbative expansion ceases to be reliable at this stage.

Nevertheless, by proceeding with care we can still extract meaningful information. To determine the exact location of the evaporation end-point, besides δ_E we must also compute $\hat{\mathrm{x}}_E$. From $\mathrm{y}_E = \mathrm{y}_{AH} = 1 + \frac{\varepsilon}{2(\lambda a)^2}$, we infer that $\hat{\mathrm{x}}_E = 1 + \mathcal{O}(\varepsilon)$. Employing Eq. (5.180), the second coordinate of the evaporation end-point is

$$\hat{\mathrm{x}}_E = 1 + \frac{\varepsilon}{4(\lambda a)^2}\left[1 + e^{-\frac{4(\lambda a)^2}{\varepsilon}\left(1-\frac{\sqrt{\varepsilon}}{\lambda a}\right)}\right]. \tag{5.206}$$

Formula (5.206) can equivalently be obtained by using Eq. (5.189) and setting $\delta = \delta_E$. Observe that the end-point exhibits the same type of singular behavior as in the BPP model (4.124).

Finally, we discuss the location of the black hole's event horizon, which is determined by $\hat{\mathrm{x}} = \hat{\mathrm{x}}_E$. We expect it to form for $\mathrm{x} < 1$, but initially to lie very close to the $\mathrm{x} = 1$ hypersurface at the beginning of the evaporation. Subsequently, it should gradually move inward until it meets the singularity. To obtain the horizon curve $\mathrm{y}_H(\delta)$, we return to Eq. (5.179), which yields

$$\mathrm{y}_H = 1 + \frac{\varepsilon}{4(\lambda a)^2}\left[1 + \left(\frac{\tilde{a}_E}{\tilde{a}_H}\right)^{\frac{4(\lambda a)^2}{\varepsilon}}\right]. \tag{5.207}$$

Observe that in the limit $\tilde{a}_H \to \tilde{a}_E$, expression (5.207) simplifies to $\mathrm{y}_H = \mathrm{y}_{AH}$, as anticipated. It is now straightforward to determine x_H, which is given by

$$\mathrm{x}_H = \left(1 + \frac{\varepsilon}{4(\lambda a)^2}\ln\delta_H\right)\left[1 + \frac{\varepsilon}{4(\lambda a)^2}\left(1 + \frac{\delta_E}{\delta_H}\right)\right]. \tag{5.208}$$

Using Eq. (5.190) along the apparent horizon hypersurface, we obtain the non-perturbative expression for the scalar curvature:

$$R_{AH} = \frac{2}{a^2}\frac{1}{\mathrm{x}^2 - \frac{\varepsilon}{(\lambda a)^2}}. \tag{5.209}$$

A perturbative counterpart of this result can also be derived starting from Eq. (5.191), which can be recast as

$$R = \frac{2}{a^2}\frac{1}{\mathrm{x}^2 - \frac{\varepsilon}{(\lambda a)^2}}\frac{1}{\sqrt{\mathrm{y}^2 - \frac{\varepsilon}{(\lambda a)^2}}}\left\{1 + \frac{\varepsilon}{4(\lambda a)^2}\left[\ln\mathrm{y} + \frac{(\mathrm{y}^2-1)(2\mathrm{y}-3)}{2\mathrm{y}^2} + \frac{(\mathrm{y}-1)^2}{2\mathrm{y}}\sum_{n=1}^{\infty}\frac{\delta^n}{n!}\frac{\mathrm{dS}_n^<}{\mathrm{dy}}\right]\right\}, \tag{5.210}$$

and, upon inserting Eq. (5.187), this expression reduces to Eq. (5.209), as required.

The radiated energy

We now evaluate the total energy radiated by the black hole over its entire lifetime. It is given by Eq. (3.115):

$$E_{rad} = -\frac{\varepsilon}{G}\int_{-\infty}^{\sigma_E^-}\frac{d\sigma^-}{\mathrm{F}^-}t_-(\hat{\sigma}^-) = -\frac{\varepsilon}{8aG}\mathrm{F}(\hat{\mathrm{x}}_E). \tag{5.211}$$

Because the Schwarzschild radius λa scales linearly with the mass, it can serve as an energy measure. Accordingly, we can associate the quantity $\lambda a_{rad} = \frac{2E_{rad}G}{\lambda}$ with the radiated energy. Thus, λa_{rad} takes the form:

$$\lambda a_{rad} = -\frac{\varepsilon}{4\lambda a}\mathrm{F}(\hat{\mathrm{x}}_E). \tag{5.212}$$

The function $\mathrm{F}(\hat{\mathrm{x}})$ becomes ill-defined in the limit $\hat{\mathrm{x}} \to 1$. This is precisely the kind of issue discussed in Sec. 5.3.3. To address it, one needs to compute the first-order correction to $\mathrm{F}(\hat{\mathrm{x}})$:

$$\mathrm{F}(\hat{\mathrm{x}}) = -2\frac{\mathrm{dF}^-}{\mathrm{d}\hat{\mathrm{x}}} + \int \frac{\mathrm{d}\hat{\mathrm{x}}}{\mathrm{F}^-}\left(\frac{\mathrm{dF}^-}{\mathrm{d}\hat{\mathrm{x}}}\right)^2. \tag{5.213}$$

Using Eq. (5.176), we find:

$$\frac{1}{\mathrm{F}^-} = \frac{\mathrm{d}\mathcal{J}}{\mathrm{d}\hat{\mathrm{x}}} - \frac{\varepsilon}{8(\lambda a)^2}\left(\frac{2\hat{\mathrm{x}}}{\hat{\mathrm{x}}-1}\ln\hat{\mathrm{x}} + \frac{3}{\hat{\mathrm{x}}} + 7\right), \tag{5.214}$$

$$\frac{\mathrm{dF}^-}{\mathrm{d}\hat{\mathrm{x}}} = -\mathrm{F}^{-2}\left[\frac{\mathrm{d}^2\mathcal{J}}{\mathrm{d}\hat{\mathrm{x}}^2} + \frac{\varepsilon}{8(\lambda a)^2}\left(\frac{3}{\hat{\mathrm{x}}^2} + 2\frac{\ln\hat{\mathrm{x}}-1}{\hat{\mathrm{x}}-1}\right)\right]. \tag{5.215}$$

Since the terms of order $\mathcal{O}(\varepsilon)$ remain regular as $\hat{\mathrm{x}} \to 1$, they can be discarded. After changing variables to z (as defined in Eq. (5.164)), the upper integration limit becomes 1, while the lower limit becomes $\mathrm{z}_E = \mathrm{z}_1^+ + \left(\frac{\sqrt{\varepsilon}}{\lambda a}\right)^3 \frac{\delta_E}{4}$, where z_1^+ is given in Eq. (5.171). The integral now extends over a narrow interval around $\mathrm{z} = 1$, which allows us to set $\mathrm{z} = 1$ wherever this does not affect the well-definedness of the integrand. The integral then takes the form:

$$\int_\infty^{\hat{\mathrm{x}}_E} \frac{\mathrm{d}\hat{\mathrm{x}}}{\mathrm{F}^-}\left(\frac{\mathrm{dF}^-}{\mathrm{d}\hat{\mathrm{x}}}\right)^2 = -\frac{4(\lambda a)^4}{\varepsilon^2}\int_{\mathrm{z}_E}^1 \frac{(1-\mathrm{z})^4\mathrm{dz}}{(\mathrm{z}-\mathrm{z}_1^+)(\mathrm{z}-\mathrm{z}_2^+)^2}. \tag{5.216}$$

A straightforward evaluation up to order $\mathcal{O}(1)$ yields the following expression for $\mathrm{F}(\hat{\mathrm{x}}_E)$:

$$\mathrm{F}(\hat{\mathrm{x}}_E) = -\frac{4(\lambda a)^2}{\varepsilon} + \frac{8(\lambda a)}{\sqrt{\varepsilon}} + \ln\frac{\varepsilon}{4(\lambda a)^2} + \frac{3}{2}. \tag{5.217}$$

Hence, the radiated energy (5.211) is:

$$E_{rad} = Mc^2\left[1 - \sqrt{\frac{\hbar c}{12\pi M^2 G_N}} - \frac{\hbar c}{192\pi M^2 G_N}\left(\ln\frac{\hbar c}{192\pi M^2 G_N} + \frac{3}{2}\right) + o\left(\frac{\hbar c}{M^2 G_N}\right)\right], \tag{5.218}$$

where we have reinstated all physical constants. Eq. (5.218) shows that, during evaporation, nearly the entire initial mass of the black hole is radiated away, leaving only a small remnant of order $\sqrt{\varepsilon}$. This agrees with the results obtained in the RST and BPP dilaton gravity models [23, 24, 25].

5.3.5 The end-state geometry

Having already determined both the evaporation end-point and the total radiated energy in the previous subsection, the final element from Sec. 3.4.1 that remains to be examined is the geometry of region III of the spacetime (see Fig. 3.3). As in the BPP model, analyzing the late-time geometry within the perturbative scheme is difficult because the approximation fails close to the evaporation end-point. Nevertheless, we can still attempt to extract useful information by rewriting the Schwarzschild radius in terms of the $\hat{\mathrm{x}}$ coordinate, rather than the δ coordinate, following the procedure outlined in Sec. 3.4.1.

We start by evaluating $\mathrm{F}(\hat{\mathrm{x}})$, as defined in formula (5.100), in terms of x and δ. Applying the same procedure as in theorem 1, we obtain

$$\mathrm{F}(\hat{\mathrm{x}}) = \mathrm{F}(\mathrm{x}) + \sum_{n=1}^{\infty}\frac{(\delta-1)^n}{n!}\frac{\partial^n \mathrm{F}(\hat{\mathrm{x}})}{\partial\delta^n}\bigg|_{\delta=1}. \tag{5.219}$$

Following the method used in theorem 5, we derive

$$\left.\frac{\partial^n \mathrm{F}(\hat{\mathrm{x}})}{\partial \delta^n}\right|_{\delta=1} = e^{n\mathrm{x}}(\mathrm{x}-1)^n \left(\frac{e^{-\mathrm{x}}}{\mathrm{x}}\frac{\mathrm{d}}{\mathrm{dx}}\right)^{n-1} \frac{e^{-\mathrm{x}}}{\mathrm{x}}\frac{\mathrm{dF}(\mathrm{x})}{\mathrm{dx}}. \tag{5.220}$$

Independently, one can show by induction that the following identity holds:

$$\left.\frac{\partial^n \mathrm{F}(\hat{\mathrm{x}})}{\partial \delta^n}\right|_{\delta=1} = (-1)^n \left[\frac{1}{2}\frac{(\mathrm{x}-1)^2}{\mathrm{x}}\frac{\mathrm{dS}_n^>(\mathrm{x})}{\mathrm{dx}} - (n-1)!\right]. \tag{5.221}$$

The inductive step reduces to the recurrence relation for the functions $\mathrm{S}_n^>(\mathrm{x})$ given in Eq. (5.108). Substituting this form of $\frac{\partial^n \mathrm{F}(\hat{\mathrm{x}})}{\partial \delta^n}|_{\delta=1}$ into the series (5.219), we obtain:

$$\mathrm{F}(\hat{\mathrm{x}}) = \mathrm{F}(\mathrm{x}) + \ln\delta + \frac{(\mathrm{x}-1)^2}{2\mathrm{x}}\sum_{n=1}^{\infty}\frac{(1-\delta)^2}{n!}\frac{\mathrm{dS}_n^>(\mathrm{x})}{\mathrm{dx}}. \tag{5.222}$$

Using Eq. (5.222), we remove the $\ln\delta$ contribution from the expressions for the metric (5.150) and for the tortoise coordinate $\hat{\sigma}$ (5.152), which leads to:

$$\begin{aligned}
\mathrm{F}^+\mathrm{F}^-e^{2\rho} = \frac{1+\frac{\varepsilon}{4(\lambda a)^2}\mathrm{F}(\hat{\mathrm{x}})}{\mathrm{x}} - 1 + \frac{\varepsilon}{4(\lambda a)^2}\Bigg[&\frac{\mathrm{x}-2}{\mathrm{x}}\ln\frac{\mathrm{x}-1}{\mathrm{x}} + \frac{1}{\mathrm{x}} - \frac{3}{2}\frac{1}{\mathrm{x}^2} + \frac{2}{\mathrm{x}^3} \\
&+\frac{\mathrm{x}-1}{2\mathrm{x}}\sum_{n=1}^{\infty}\frac{(1-\delta)^n}{n!}\Big(\mathrm{S}_{n+1}^>(\mathrm{x}) - n\mathrm{S}_n^>(\mathrm{x}) + z_{n+1} - nz_n\Big)\Bigg],
\end{aligned} \tag{5.223}$$

$$\begin{aligned}
\frac{\hat{\sigma}}{a} = \mathrm{x} &+ \left(1+\frac{\varepsilon}{4(\lambda a)^2}\mathrm{F}(\hat{\mathrm{x}})\right)\ln\left(\frac{\mathrm{x}}{1+\frac{\varepsilon}{4(\lambda a)^2}\mathrm{F}(\hat{\mathrm{x}})} - 1\right) \\
&- \frac{\varepsilon}{8(\lambda a)^2}\left[\mathrm{S}_0^>(\mathrm{x}) - \frac{\pi^2}{3} - 2 - 2\left(\frac{\mathrm{x}}{\mathrm{x}-1} - \ln(\mathrm{x}-1)\right)\mathrm{F}(\mathrm{x}) - 9\ln\delta\right] \\
&+ \frac{\varepsilon}{8(\lambda a)^2}\sum_{n=1}^{\infty}\frac{(1-\delta)^n}{n!}\left[\mathrm{S}_n^>(\mathrm{x}) + z_n + \frac{(\mathrm{x}-1)^2}{\mathrm{x}}\left(\frac{\mathrm{x}}{\mathrm{x}-1} - \ln(\mathrm{x}-1)\right)\frac{\mathrm{dS}_n^>(\mathrm{x})}{\mathrm{dx}}\right].
\end{aligned} \tag{5.224}$$

In Eqs. (5.223) and (5.224), the factor $\varphi/\lambda a$ has, to zeroth order in ε, been replaced by $\varphi/\left(\lambda a + \frac{\varepsilon}{4\lambda a}\mathrm{F}(\hat{\mathrm{x}})\right)$. We now introduce a new running Schwarzschild radius, depending on the coordinate σ^-:

$$\lambda\hat{a}(\hat{\mathrm{x}}) = \lambda a + \frac{\varepsilon}{4\lambda a}\mathrm{F}(\hat{\mathrm{x}}). \tag{5.225}$$

To first order in ε, $\lambda\hat{a}$ coincides with λa, which means that in all expressions for the metric and dilaton we may replace λa by $\lambda\hat{a}$.

To analyze the final state of evaporation, we must first determine the behavior along the hypersurface $\hat{\mathrm{x}} = \hat{\mathrm{x}}_E$ for $\delta < \delta_E$. On this hypersurface, $\lambda\hat{a}(\hat{\mathrm{x}}_E)$ is fixed. Since $\mathrm{F}(\hat{\mathrm{x}}_E) \sim \ln\delta_E$, Eq. (5.217) leads to $\lambda\hat{a} = \mathcal{O}(\sqrt{\varepsilon})$, which, within first-order perturbation theory, effectively gives $\lambda\hat{a} = 0$. Taking this limit is analogous to the $\mathrm{x}\to\infty$ limit discussed in the previous subsection. From the behavior of $\mathrm{S}_n^>(\mathrm{x})$ given in Eq. (5.130), we obtain:

$$\mathrm{S}_n^>(\mathrm{x}) = (n-1)!\mathrm{S}_1^>(\mathrm{x}) - z_n + \mathcal{O}((\lambda\hat{a})^4). \tag{5.226}$$

In the metric Eq. (5.223), the first-order correction then vanishes in the limit $\lambda\hat{a}\to 0$, because the sum scales as $\mathcal{O}((\lambda\hat{a})^2)$, while the δ–independent part is of order $\mathcal{O}(\lambda\hat{a})$. We next consider the first-order term in ε in the dilaton Eq. (5.224) and again take the $\lambda\hat{a} \to 0$ limit. In this regime, the δ–dependent contribution becomes

$$\frac{\lambda\hat{a}\ln\delta}{(\lambda\hat{a})^2}\left[\mathrm{S}_1^> + \frac{(\mathrm{x}-1)^2}{\mathrm{x}}\left(\frac{\mathrm{x}}{\mathrm{x}-1} - \ln(\mathrm{x}-1)\right)\frac{d\mathrm{S}_1^>}{d\mathrm{x}} - 9\right]. \tag{5.227}$$

This term also disappears in the $\lambda\hat{a} \to 0$ limit, which can be seen by expanding in powers of $\lambda\hat{a}$ and then sending $\lambda\hat{a} \to 0$. A crucial point is that $\ln\delta$ scales as $1/\lambda\hat{a}$, so that the product $\lambda\hat{a}\ln\delta$ remains finite. The δ–independent terms vanish in essentially the same manner as in the $\mathrm{x} \to \infty$ limit. Performing this limit yields the following final results:

$$\mathrm{F}^+\mathrm{F}^- e^{2\rho} = \frac{\lambda\hat{a}_E}{\varphi} - 1, \tag{5.228}$$

$$\varphi + \lambda\hat{a}_E \ln\left(\frac{\varphi}{\lambda\hat{a}_E}\right) = \lambda\hat{\sigma}. \tag{5.229}$$

Since $\lambda\hat{a}_E = \lambda\hat{a}(\hat{\mathrm{x}}_E)$ is of order $\mathcal{O}(\sqrt{\varepsilon})$, Eqs. (5.228) and (5.229) describe a quantum-corrected Minkowski spacetime, as discussed in Sec. 5.2.2. This is encouraging, because we expect the final state to be free of energy fluxes at infinity. The next task is to smoothly match this solution to the vacuum solution along $\hat{\mathrm{x}} = \hat{\mathrm{x}}_E$. This matching has to be performed so that no new coordinate discontinuities are introduced, which implies that the final solution has the form $(\mathrm{F}^+, \mathrm{F}^-, a_f)$, where $\mathrm{F}^\pm$ agree with the coordinate transformations of the evaporating black hole, and a_f is a new constant. Further details are provided in Sec. 3.4.1.

By analogy with the BPP and RST models of dilaton gravity discussed in Chap. 4, one might anticipate the appearance of a shockwave at the end-point of the evaporation known as a thunderpop. To determine whether such a feature arises in the DREH model, one must smoothly join regions II and III (Fig. 3.3) across the $\sigma^- = \sigma_E^-$ hypersurface by integrating the "$--$" component of Eq. (5.44):

$$e^{-2\rho}\partial_-\varphi_> - e^{-2\rho}\partial_-\varphi_< = -\frac{\lambda}{2\mathrm{F}^-}\lambda a_0\varphi^{-1}e^{-2\rho} - \varepsilon(\partial_-\rho_> - \partial_-\rho_<)\varphi^{-1}e^{-2\rho}, \tag{5.230}$$

where $\lambda a_0 = \frac{2\Delta MG}{\lambda}$ denotes the mass carried by the shockwave at the end of evaporation, the symbol "$<$" refers to the portion of spacetime with $\sigma^- < \sigma_E^-$, and "$>$" to the portion with $\sigma^- > \sigma_E^-$. The derivatives in Eq. (5.230) are readily obtained from Eqs. (5.150) and (5.152) in the region $\sigma^+ < \sigma_0^+$. They are:

$$\partial_-\varphi_< = -\frac{\lambda}{2\mathrm{F}^-}\left\{1 - \frac{\lambda\hat{a}(\hat{\mathrm{x}})}{\sqrt{\varphi^2-\varepsilon}}\left[1 - \frac{\varepsilon}{4(\lambda a)^2}\left((2-\mathrm{x})\mathrm{F}(\mathrm{x}) - \frac{2}{\mathrm{x}} + \frac{3}{\mathrm{x}^2}\right)\right]\right\}, \tag{5.231}$$

$$\partial_-\rho_< = -\frac{1}{2}\partial_-\ln\mathrm{F}^- - \frac{\lambda}{4\mathrm{F}^-}\frac{\lambda\hat{a}(\hat{\mathrm{x}})}{\varphi^2}\left[1 - \frac{\varepsilon}{2(\lambda a)^2}\mathrm{F}(\mathrm{x})\right]. \tag{5.232}$$

Using the expressions (5.70) and (5.71) for the static configuration analyzed in Sec. 5.2.2, we compute the derivatives in the domain $\sigma^- > \sigma_E^-$. These derivatives match Eqs. (5.231-5.232) upon replacing $\hat{a}$ with a_f. This supports the conclusion that the final state is precisely the static solution presented in Sec. 5.2.2. In direct analogy with Eqs. (5.224-5.223), for $\hat{\mathrm{x}} = \hat{\mathrm{x}}_E$ we take the limit $\lambda\hat{a} \to 0$ to first order in perturbation theory. Under this limit, Eqs. (5.231-5.232) simplify to:

$$\partial_-\varphi_< = -\frac{\lambda}{2\mathrm{F}^-}\left(1 - \frac{\lambda\hat{a}_E}{\varphi}\right), \tag{5.233}$$

$$\partial_-\rho_< = -\frac{1}{2}\partial_-\ln\mathrm{F}^- - \frac{\lambda}{4\mathrm{F}^-}\frac{\lambda\hat{a}_E}{\varphi^2}, \tag{5.234}$$

whereas in the region $\sigma^- > \sigma_E^-$ we find:

$$\partial_- \varphi_> = -\frac{\lambda}{2\mathrm{F}^-}\left(1 - \frac{\lambda a_f}{\varphi}\right), \tag{5.235}$$

$$\partial_- \rho_> = -\frac{1}{2}\partial_- \ln \mathrm{F}^- - \frac{\lambda}{4\mathrm{F}^-}\frac{\lambda a_f}{\varphi^2}. \tag{5.236}$$

Substituting Eqs. (5.233-5.236) into Eq. (5.230) yields the following energy-balance relation:

$$\lambda a_{rad} = \lambda(a - a_f) - \lambda a_0, \tag{5.237}$$

where, using Eq. (5.211), we identify $\lambda a_{rad} = \frac{2E_{rad}G}{\lambda} = -\frac{\varepsilon}{4\lambda a}\mathrm{F}(\hat{\mathrm{x}}_E)$. It is thus evident that energy is conserved: the initial mass of the infalling matter, λa, equals the sum of the radiated energy λa_{rad}, the mass of the residual spacetime λa_f, and the energy carried by the thunderpop λa_0.

Since no further coordinate transformation is permitted as the $\hat{\mathrm{x}} = \hat{\mathrm{x}}_E$ hypersurface is crossed, continuity of the metric and the dilaton field, enforced by Eqs. (5.228-5.229), implies that the mass parameter of the final geometry must satisfy $\lambda a_f = \lambda \hat{a}_E$. When this is combined with the energy balance condition (5.237), it follows that there is no thunderpop at the end-point of the evaporation process, i.e. $\lambda a_0 = 0$. This result is valid within a perturbative analysis to first order in ε.

Another important issue to emphasize is that the asymptotically flat solution described in Sec. 5.2.2 develops a curvature singularity already at first order in the perturbative expansion. This behavior is similar to what occurs in the BPP and RST models (Sec. 4.3.3). As in those cases, one must therefore impose reflective boundary conditions at the hypersurface where the singularity appears.

In conclusion, the final geometry coincides with one of the static, quantum-corrected Minkowski vacuum configurations from Sec. 5.2.2, specified by $t_\pm(\hat{\sigma}^\pm) = 0$. Thus, even though the asymptotically flat coordinates remain continuous across the $\hat{\mathrm{x}} = \hat{\mathrm{x}}_E$ hypersurface and no thunderpop arises at the end of evaporation, the quantum state still undergoes a transition from $|0, \sigma\rangle$ to $|0, \hat{\sigma}\rangle$.

It should be emphasized that we do not know the exact structure of the ε correction to the metric in the $\lambda \hat{a}_E$ term in Eq. (5.228), because at this stage perturbation theory ceases to be reliable and higher-order contributions may affect the first-order terms. In particular, there may be an extra contribution beyond $-\frac{\varepsilon}{4\lambda a}\mathrm{F}(\hat{\mathrm{x}}_E)$. The presence of such a term would generate a non-vanishing thunderpop. To clarify this issue, one would require either a non-perturbative solution that captures the end-point of evaporation, or a numerical analysis of the equations of motion (5.44–5.46). However, this uncertainty does not affect the derivation of the energy balance relation (5.237).

Chapter 6

Dimensionally-reduced 5DCS gravity: Riemannian sector

In this chapter, we study the Riemannian sector of the dimensionally-reduced theory of five-dimensional Chern–Simons gravity (DR5DCS). Our analysis follows the same methodological framework as that employed for the CGHS model in Chap. 4 and for the DREH model in Chap. 5. Analogously to the DREH model, we demonstrate that the DR5DCS model does not admit exactly solvable equations of motion once quantum corrections are included. Thus, we resort to the perturbative treatment like in the analysis of the DREH model. The action in the Riemannian sector is obtained in Sec. 2.2.2 and is explicitly presented in Eq. (2.25). For convenience, we rewrite it here:

$$\begin{aligned} S_{\mathrm{DR5DCS-R}} =& \frac{k\pi^2}{(\lambda l)^3}\int \mathrm{d}x^2\sqrt{-g}e^{-3\phi}\Big[R\left(1+3(\lambda l)^2 e^{2\phi}\right) \\ &+6\left((\nabla\phi)^2+\lambda^2 e^{2\phi}\right)+\frac{6}{l^2}+3l^2(\nabla\phi)^2\left(\Box\phi-(\nabla\phi)^2\right)\Big]-\frac{1}{2}\int d^2x\sqrt{-g}\left(\nabla f\right)^2, \end{aligned} \tag{6.1}$$

For simplicity, we introduce the constant prefactor of the action as $a=\frac{k\pi^2}{(\lambda l)^3}$. The first term in Eq. (5.1) encodes the gravitational action, denoted by S_g, whereas the second term accounts for the matter sector, modeled here as a single scalar field, labeled S_m. The key difference here is the emergence of terms containing four derivatives of the dilaton field, which originate from the Gauss–Bonnet contribution in the full five-dimensional theory.

The chapter is organized into three sections. In the first Sec. 6.1, we examine the classical theory and demonstrate that the most general vacuum solution of the classical equations of motion corresponds to the dimensionally reduced BTZ black hole. We then analyze the classical gravitational collapse and determine how the spacetime mass depends on the integration constants appearing in the general solution. In the final subsection, we construct in detail the Penrose diagram corresponding to this collapse scenario.

The following Sec. 6.2 introduces the quantum corrections via the Polyakov-Liouville action. Since the resulting equations of motion cannot be solved exactly, we adopt the perturbative approach outlined in Sec. 3.4.1, derive the general quantum-corrected solution, and examine the static configurations that mimic the empty AdS spacetime. As in the BPP model, the AdS vacuum ceases to be a fluxless solution once the quantum corrections are included, so we obtain the quantum-corrected AdS spacetime. The final subsection then explores the eternal black hole scenario.

The final Sec. 6.3 addresses the evaporating black hole scenario. We construct the quantum-corrected collapse model by matching the quantum-corrected AdS spacetime to the evaporating black hole solution. Next, we determine the final state of the evaporation and analyze the geometry of the final spacetime. We demonstrate that it is once again a quantum-corrected AdS spacetime with a particular mass constant. Within first-order perturbation theory the thunderpop does not appear; however, when the solution is computed to higher orders in $\hbar$, one should obtain a non-vanishing mass for the thunderpop.

6.1 Classical equations of motion and their solutions

In this section, we examine the equations of motion, derive and analyze their solutions, and discuss selected thermodynamic properties within the Riemannian sector of the full theory of dimensionally-reduced 5DCS theory. We begin by deriving the general vacuum solution. It is found that the vacuum sector exhibits two distinct branches. We demonstrate that one branch corresponds to the dimensionally-reduced BTZ black hole [78, 116], whereas the other branch yields a family of solutions characterized by an arbitrary function. Consequently, the solution within the first branch is analogous to the Birkhoff-type configuration discussed in Chap. 5, in the sense that the most general solution in this branch is static. At the end of this section, we formulate the classical gravitational collapse scenario.

We begin by varying the the gravitational part of action (6.1) with respect to the metric:

$$\begin{aligned}\delta^{(g)}S_g = a\int \mathrm{d}^2x\sqrt{-g}e^{-3\phi}\Big\{&3\left[2+l^2\left(\Box\phi-2\left(\nabla\phi\right)^2\right)\right]\nabla_\mu\phi\nabla_\nu\phi\delta g^{\mu\nu}+3l^2\left(\nabla\phi\right)^2\nabla_\mu\nabla_\nu\phi\delta g^{\mu\nu}\\&-3\left[\left(\left(\nabla\phi\right)^2+\lambda^2e^{2\phi}\right)+\frac{1}{l^2}+\frac{l^2}{2}(\nabla\phi)^2\left(\Box\phi-(\nabla\phi)^2\right)\right]g_{\mu\nu}\delta g^{\mu\nu}\\&+\underbrace{\left(1+3(\lambda l)^2e^{2\phi}\right)g^{\mu\nu}\delta R_{\mu\nu}}_{A}-\underbrace{3l^2\left(\nabla\phi\right)^2g^{\mu\nu}\partial_\rho\phi\delta\Gamma^{\rho}_{\mu\nu}}_{B}\Big\}.\end{aligned}\tag{6.2}$$

The only remaining terms to be varied in Eq. (6.2) are A and B in the last line. The term A has the same form as in the CGHS case and is therefore obtained from Eq. (4.9) by performing the replacement $e^{-2\phi}\mapsto e^{-3\phi}+3(\lambda l)^2e^{-\phi}$, namely:

$$A = a\int \mathrm{d}^2x\sqrt{-g}\Big[-\nabla_\mu\nabla_\nu\left(e^{-3\phi}+3(\lambda l)^2e^{-\phi}\right)+g_{\mu\nu}\Box\left(e^{-3\phi}+3(\lambda l)^2e^{-\phi}\right)\Big]\delta g^{\mu\nu}.\tag{6.3}$$

To compute the term B in Eq. (6.2) we move to the locally-flat reference frame (LFRF) defined in Eq. (4.7):

$$\begin{aligned}B\Big|_{LFRF} &= -\frac{3al^2}{2}\int \mathrm{d}^2xe^{-3\phi}(\partial\phi)^2\eta^{\mu\nu}\partial_\rho\phi\eta^{\lambda\rho}\Big[\partial_\mu\left(\delta g_{\lambda\nu}\right)+\partial_\nu\left(\delta g_{\lambda\mu}\right)-\partial_\lambda\left(\delta g_{\mu\nu}\right)\Big]\\&= -\frac{3al^2}{2}\int \mathrm{d}^2xe^{-3\phi}(\partial\phi)^2\partial_\rho\phi\Big[2\eta^{\gamma\alpha}\eta^{\rho\beta}-\eta^{\alpha\beta}\eta^{\rho\gamma}\Big]\partial_\gamma\left(\delta g_{\alpha\beta}\right)\\&= -3al^2\int \mathrm{d}^2x\Big[\partial_\mu\left(e^{-3\phi}(\partial\phi)^2\partial_\nu\phi\right)-\frac{1}{2}\eta_{\mu\nu}\partial_\rho\left(e^{-3\phi}(\partial\phi)^2\partial^\rho\phi\right)\Big]\delta g^{\mu\nu}.\end{aligned}\tag{6.4}$$

Once more, by applying the identification (4.7), we lift the term B from the locally flat reference frame (6.4) back to a general Riemannian manifold. The resulting expression is:

$$B = -3al^2\int \mathrm{d}^2x\sqrt{-g}\Big[\nabla_\mu\left(e^{-3\phi}(\nabla\phi)^2\nabla_\nu\phi\right)-\frac{1}{2}\eta_{\mu\nu}\nabla_\rho\left(e^{-3\phi}(\nabla\phi)^2\nabla^\rho\phi\right)\Big]\delta g^{\mu\nu}.\tag{6.5}$$

After substituting both terms A and B from Eqs. (6.3) and (6.5), respectively, and performing algebraic manipulations, we obtain the following equation of motion for the metric field:

$$\begin{aligned}&\left[1+(\lambda l)^2e^{2\phi}-l^2\left(\Box\phi+(\nabla\phi)^2\right)\right]\nabla_\mu\phi\nabla_\nu\phi-\left[1+(\lambda l)^2e^{2\phi}\right]\nabla_\mu\nabla_\nu\phi\\&\quad+\frac{l^2}{2}\left[\nabla_\mu\phi\nabla_\nu\left(\nabla\phi\right)^2+\nabla_\nu\phi\nabla_\mu\left(\nabla\phi\right)^2\right]+\left[\Box\phi-2(\nabla\phi)^2+\lambda^2e^{2\phi}+\frac{1}{l^2}\right]g_{\mu\nu}\\&\quad+l^2\left[(\nabla\phi)^4+\left(\Box\phi-(\nabla\phi)^2\right)\lambda^2e^{2\phi}-\frac{1}{2}\nabla_\rho\phi\nabla^\rho\left(\nabla\phi\right)^2\right]=-\frac{(\lambda l)^3}{6k\pi^2}T_{\mu\nu}e^{3\phi},\end{aligned}\tag{6.6}$$

where $T_{\mu\nu}=\frac{-2}{\sqrt{-g}}\frac{\delta S_{\mathrm{mat}}}{\delta g^{\mu\nu}}$ is the energy-momentum tensor of matter fields. Next, we vary the action (6.1) with respect to the dilaton field:

$$\begin{aligned}\delta^{(\phi)}S_g=-3a\int\mathrm{d}^2x\sqrt{-g}e^{-3\phi}\Bigg\{&\left[R\left(1+(\lambda l)^2e^{2\phi}\right)+6(\nabla\phi)^2+2\lambda^2e^{2\phi}+\frac{6}{l^2}\right]\delta\phi\\&+3l^2(\nabla\phi)^2\left(\Box\phi-(\nabla\phi)^2\right)\delta\phi-l^2(\nabla\phi)^2\Box(\delta\phi)\\&-\left[2+l^2\left(\Box\phi-(\nabla\phi)^2\right)\right]\delta\left((\nabla\phi)^2\right)\Bigg\}.\end{aligned}\tag{6.7}$$

Using $\delta\left((\nabla\phi)^2\right)=2g^{\mu\nu}\nabla_\nu\phi\nabla_\mu(\delta\phi)$ and $\Box(\delta\phi)=g^{\mu\nu}\nabla_\nu\nabla_\mu(\delta\phi)$, and performing an integration by parts, Eq. (6.7) can, after some algebraic manipulation, be simplified to:

$$\begin{aligned}&3(\nabla\phi)^2-2\Box\phi+l^2\left[\left(2(\nabla\phi)^2-\Box\phi\right)\Box\phi+\left(\nabla_\mu\nabla_\nu\phi+4\nabla_\mu\phi\nabla_\nu\phi\right)\nabla^\mu\nabla^\nu\phi\right]\\&\qquad-3l^2\nabla_\mu\phi\nabla^\mu\left((\nabla\phi)^2\right)=\lambda^2e^{2\phi}+\frac{3}{l^2}+\frac{1}{2}R\left[1+(\lambda l)^2e^{2\phi}-l^2(\nabla\phi)^2\right].\end{aligned}\tag{6.8}$$

After changing to the reduced field x, defined in Eq. (2.46) the metric Equation of motion (6.6) becomes:

$$\begin{aligned}&(\mathrm{x}^2+1)\nabla_\mu\nabla_\nu\mathrm{x}+l^2\Box\mathrm{x}\nabla_\mu\mathrm{x}\nabla_\nu\mathrm{x}-\frac{l^2}{2}\left(\nabla_\mu\mathrm{x}\nabla_\nu\left(\nabla\mathrm{x}\right)^2+\nabla_\nu\mathrm{x}\nabla_\mu\left(\nabla\mathrm{x}\right)^2\right)\\&\quad-g_{\mu\nu}\left[(\mathrm{x}^2+1)\Box\mathrm{x}-\frac{\mathrm{x}}{l^2}\left(\mathrm{x}^2+1-l^2\left(\nabla\mathrm{x}\right)^2\right)-\frac{l^2}{2}\nabla^\alpha\mathrm{x}\nabla_\alpha\left(\nabla\mathrm{x}\right)^2\right]=-\frac{1}{6k\pi^2}T_{\mu\nu},\end{aligned}\tag{6.9}$$

It turns out that Eq. (6.9) can be simplified even further, using the following identity:

$$\begin{aligned}&(\nabla\mathrm{x})^2\nabla_\mu\nabla_\nu\mathrm{x}+\Box\mathrm{x}\nabla_\mu\mathrm{x}\nabla_\nu\mathrm{x}-\frac{1}{2}\left(\nabla_\mu\mathrm{x}\nabla_\nu\left(\nabla\mathrm{x}\right)^2+\nabla_\nu\mathrm{x}\nabla_\mu\left(\nabla\mathrm{x}\right)^2\right)\\&\qquad=\left[(\nabla\mathrm{x})^2\Box\mathrm{x}-\frac{1}{2}\nabla_\alpha\mathrm{x}\nabla^\alpha\left(\nabla\mathrm{x}\right)^2\right]g_{\mu\nu},\end{aligned}\tag{6.10}$$

where the two identities involving the Levi-Civita tensor (A.16) and (A.17), have been extensively used. The resulting expressions for the equations of motion of both the metric and the dilaton field take the following form:

$$\left(\mathrm{x}^2+1-l^2(\nabla\mathrm{x})^2\right)\left[\nabla_\mu\nabla_\nu\mathrm{x}-g_{\mu\nu}\left(\Box\mathrm{x}-\frac{\mathrm{x}}{l^2}\right)\right]=-\frac{1}{6k\pi^2}T_{\mu\nu},\tag{6.11}$$

$$\left(\mathrm{x}^2+1-l^2\left(\nabla\mathrm{x}\right)^2\right)\left(\mathrm{R}+\frac{2}{l^2}\right)+\frac{4\mathrm{x}^2}{l^2}-4\mathrm{x}\Box\mathrm{x}=2l^2\left(\nabla_\mu\nabla_\nu\mathrm{x}\nabla^\nu\nabla^\mu\mathrm{x}-(\Box\mathrm{x})^2\right),\tag{6.12}$$

where we have used the identity (6.10) to simplify the metric equation.

6.1.1 General vacuum solution

In this section, we address the equations of motion (6.11-6.12) in the absence of matter fields, i.e., in the regime where the energy–momentum tensor $T_{\mu\nu}$ vanishes. The metric Eq. (6.11) factorizes into the product of two independent terms, thereby giving rise to two distinct branches of solutions. We begin by examining the branch defined by:

$$\nabla_\mu \nabla_\nu \mathrm{x} = g_{\mu\nu} \left(\Box \mathrm{x} - \frac{\mathrm{x}}{l^2} \right). \tag{6.13}$$

Taking the trace of this equation yields $l^2 \Box \mathrm{x} = 2\mathrm{x}$. Combining this result with the dilaton Eq. (6.12) leads to the following system of differential equations in the conformal gauge (3.2):

$$\partial_\pm \left(e^{-2\rho} \partial_\pm \mathrm{x} \right) = 0 \quad \Longrightarrow \quad \partial_\pm \mathrm{x} = \frac{1}{2l} \mathrm{F}^\mp e^{2\rho}, \tag{6.14}$$

$$l^2 \Box \mathrm{x} = 2\mathrm{x} \quad \Longrightarrow \quad \partial_\pm \left(\mathrm{F}^+ \mathrm{F}^- e^{2\rho} + \mathrm{x}^2 \right) = 0, \tag{6.15}$$

$$R + \frac{2}{l^2} = 0. \tag{6.16}$$

From Eq. (6.14), it follows directly that the derivatives of the dilaton field take the static ansatz form Eq. (3.13) with $\mathcal{D} = 1$. Eq. (6.15) implies that the quantity Λ is indeed static $\Lambda = -(\mathrm{x}^2 - \mu)$, where μ denotes an arbitrary integration constant. The final Eq. (6.16) is fulfilled automatically. Consequently, the general solution in the first branch can be written as:

$$\begin{aligned} \mathrm{d}s^2 &= -(\mathrm{x}^2 - \mu)\mathrm{d}t^2 + \frac{l^2 \mathrm{d}\mathrm{x}^2}{\mathrm{x}^2 - \mu}, \\ \mathrm{x} &= \begin{cases} \sqrt{\mu} \tanh \left[\dfrac{\sqrt{\mu}}{2l} \left(\displaystyle\int \frac{\mathrm{d}x^+}{\mathrm{F}^+} + \int \frac{\mathrm{d}x^-}{\mathrm{F}^-} \right) \right], & 0 < \mathrm{x} < \sqrt{\mu}, \\ \sqrt{\mu} \coth \left[\dfrac{\sqrt{\mu}}{2l} \left(\displaystyle\int \frac{\mathrm{d}x^+}{\mathrm{F}^+} + \int \frac{\mathrm{d}x^-}{\mathrm{F}^-} \right) \right], & \mathrm{x} > \sqrt{\mu}, \end{cases} \end{aligned} \tag{6.17}$$

where the second equation follows directly from the definition of the tortoise coordinate (3.18). There are two coordinate charts that overlap across the $\mathrm{x} = \sqrt{\mu}$ hypersurface. We conclude that the general vacuum solution within the first branch is the two-dimensional BTZ black hole solution [78]. It is defined by two arbitrary function $\mathrm{F}^\pm$ and one constant μ, in other words $\mathrm{RI}(\mathrm{F}^+, \mathrm{F}^-, \mu)$. It represents a static solution and is expressed in the form described in Sec. 3.1.

The second branch reduces to only one equation, namely:

$$l^2 (\nabla \mathrm{x})^2 = \mathrm{x}^2 + 1. \tag{6.18}$$

This equation directly solves the metric equations of motion. However, with some algebraic transformation, one can verify that it also satisfies the dilaton Eq. (6.12). Therefore, the general vacuum solution within the second brunch is given by:

$$\mathrm{d}s^2 = 4l^2 \frac{\partial_+ \mathrm{x} \partial_- \mathrm{x}}{\mathrm{x}^2 + 1} \mathrm{d}x^+ \mathrm{d}x^-, \tag{6.19}$$

where the dilaton field $\mathrm{x} = \mathrm{x}(x^+, x^-)$ is an arbitrary function. This arbitrariness can be attributed to the residual freedom in the five-dimensional gauge transformations. We therefore infer that, in this branch, the solution does not have to be static, and the dilaton field remains an unconstrained function.

Upon applying the static ansatz from Sec. 3.1, Eq. (6.18) reduces to $\mathrm{x}^2+1+\Lambda\mathcal{D}^2=0$. Since this is the sole requirement, the most general static vacuum solution in the second branch, expressed in the form Eqs. (3.18-3.19), is given by:

$$
\begin{aligned}
\mathrm{d}s^2 &= \Lambda(\mathrm{x})\mathrm{d}t^2 + \frac{l^2\mathrm{dx}^2}{\mathrm{x}^2+1}, \\
\int \frac{\mathrm{dx}}{\sqrt{-\Lambda(\mathrm{x})(\mathrm{x}^2+1)}} &= -\frac{1}{2l}\left(\int \frac{\mathrm{d}x^+}{\mathrm{F}^+} + \int \frac{\mathrm{d}x^-}{\mathrm{F}^-}\right),
\end{aligned} \tag{6.20}
$$

Thus, the most general static solution within this sector can be written as $\mathrm{RII}(\mathrm{F}^+,\mathrm{F}^-,\Lambda(\mathrm{x}))$, where the functions $\mathrm{F}^\pm$ are arbitrary and encode the coordinate transformations, and $\Lambda=\Lambda(\mathrm{x})$ is an arbitrary function of the dilaton field.

One can readily verify that both solutions RI (6.17) and RII (6.19) fulfill the five-dimensional Chern-Simons equations of motion (2.30). The first branch represents a dimensionally reduced BTZ black hole [116]. The event horizon is determined by $\mathrm{x}_H=\sqrt{\mu}$. It is linked to the mass of the black hole—on which we will elaborate later—as well as to the surface gravity and, in turn, to the black hole's temperature:

$$
\kappa = \frac{1}{2l}\left|\mathcal{D}\frac{\mathrm{d}\Lambda}{\mathrm{dx}}\right|_H = \frac{\sqrt{\mu}}{l}. \tag{6.21}
$$

6.1.2 General static equations of motion

Let us first examine the metric Eq. (6.11). By inserting the ansatz (3.8), (3.13) and employing Eqs. (3.31) and (3.32), we obtain:

$$
\left(\mathrm{x}^2+1+\Lambda\mathcal{D}^2\right)\Lambda^2\mathcal{D}\frac{\mathrm{d}\mathcal{D}}{\mathrm{dx}} = -\frac{2l^2}{3k\pi^2}\mathrm{F}^{\pm 2}T_{\pm\pm}, \tag{6.22}
$$

$$
\left(\mathrm{x}^2+1+\Lambda\mathcal{D}^2\right)\left(\mathcal{D}\frac{\mathrm{d}}{\mathrm{dx}}\left(\Lambda\mathcal{D}\right)+2\mathrm{x}\right) = -\frac{l^2}{6k\pi^2}T, \tag{6.23}
$$

where T is the trace of the energy-momentum tensor. Recasting these two equations with the rank-two tensor ansatz (3.14) for the EMT, together with the identities (3.33) and (3.34), leads to:

$$
\frac{\mathrm{d}}{\mathrm{dx}}\left(\mathrm{x}^2+1+\Lambda\mathcal{D}^2\right)^2 = -\frac{2l^2}{3k\pi^2}\Lambda T^{\parallel\parallel}, \tag{6.24}
$$

$$
\left(\mathrm{x}^2+1+\Lambda\mathcal{D}^2\right)\left(\mathcal{D}^2\frac{\mathrm{d}\Lambda}{\mathrm{dx}}+2\mathrm{x}\right) = \frac{l^2}{3k\pi^2}\Lambda T^{\perp\perp}, \tag{6.25}
$$

$$
T^{\perp\parallel} = T^{\parallel\perp} = 0. \tag{6.26}
$$

Next, the dilaton field Eq. (6.12) reduces to:

$$
\left(\mathrm{x}^2+1+\Lambda\mathcal{D}^2\right)\left[\mathcal{D}\frac{\mathrm{d}}{\mathrm{dx}}\left(\mathcal{D}\frac{\mathrm{d}\Lambda}{\mathrm{dx}}\right)+2\right]+4\mathrm{x}^2+4\mathrm{x}\mathcal{D}\frac{\mathrm{d}\left(\Lambda\mathcal{D}\right)}{\mathrm{dx}}+\mathcal{D}^2\frac{\mathrm{d}\Lambda}{\mathrm{dx}}\frac{\mathrm{d}\left(\Lambda\mathcal{D}^2\right)}{\mathrm{dx}} = 0. \tag{6.27}
$$

By subtracting Eqs. (6.22) and (6.23), then differentiating the resulting expression and employing Eq. (6.27), we obtain the following condition for the EMT components:

$$
\frac{\mathrm{d}}{\mathrm{dx}}\left(4\mathrm{F}^{\pm 2}T_{\pm\pm}\right) = \Lambda\frac{\mathrm{d}T}{\mathrm{dx}} \quad\Longrightarrow\quad \left(T^{\parallel\parallel}+3T^{\perp\perp}\right)\frac{\mathrm{d}\Lambda}{\mathrm{dx}}+2\Lambda\frac{T^{\perp\perp}}{\mathrm{dx}} = 0. \tag{6.28}
$$

The final Eq. (6.28) expresses the conservation law for the Riemannian EMT of the matter fields, namely $\nabla_\mu T^{\mu\nu} = 0$, as previously introduced in Eq. (3.68).

It is possible to eliminate $\mathcal{D}$ from Eqs. (6.24-6.27) and derive one second-order differential equation for the metric function Λ. However, this equation cannot, in general, be solved exactly for arbitrary matter fields, even in the particular case where the EMT is traceless. For this reason, we do not present it here. When the matter is comprised of the massless real scalar fields, the EMT is traceless and satisfies Eq. (4.34). In contrast to the Secs. 4.1.4 and 5.1.2 where the solution with charged scalar matter is presented in the BPP and DREH models respectively, in case of the DR5DCS model there is no closed form for the charged scalar matter solution.

6.1.3 Conformal diagram of the maximally extended BTZ black hole

In this subsection, we construct the conformal diagram of the BTZ black hole, which corresponds to the most general vacuum solution of the equations of motion in the DR5DCS model. The metric in the static coordinates and the tortoise coordinate are given in Eq. (6.17). For convenience, we reproduce it here:

$$\Lambda = -\left(\mathrm{x}^2 - \mu\right), \qquad \frac{\sigma}{l} = \frac{1}{2\sqrt{\mu}} \ln \left| \frac{\mathrm{x} - \sqrt{\mu}}{\mathrm{x} + \sqrt{\mu}} \right|. \tag{6.29}$$

We work in the Eddington–Finkelstein gauge, so the solution is characterized by $(-1, 1, \mu)$. The first step toward obtaining the maximally extended geometry is to introduce Kruskal coordinates (see App. C.3 for the Schwarzschild case). These coordinates are regular at the horizons and are therefore defined using the surface gravity (6.21), as explained in App. D.5. The Kruskal coordinates are then given by

$$|\kappa x^{\pm}| = e^{\pm\kappa\sigma^{\pm}}, \qquad \kappa l = \sqrt{\mu}, \tag{6.30}$$

where the choice of sign depends on the spacetime quadrant indicated in Fig. 4.1. We now directly perform the conformal coordinate transformation that compactifies the spacetime, yielding the Penrose conformal diagram:

$$\mathrm{x}^+ = \arctan\left(\kappa x^+\right) \quad \wedge \quad \mathrm{x}^- = \arctan\left(\kappa x^-\right). \tag{6.31}$$

We start by identifying the event horizon in the diagram. As already noted, it is determined by the condition $\Lambda = 0$, or equivalently $\mathrm{x_H} = \sqrt{\mu}$. Hence, we obtain:

$$\Lambda = 0 \quad \Longrightarrow \quad \mathrm{x_H} = \sqrt{\mu} \quad \Longrightarrow \quad \sigma_{\mathrm{H}} \to -\infty \quad \Longrightarrow \quad x^{\pm} = 0 \quad \Longrightarrow \quad \mathrm{x}^{\pm} = 0. \tag{6.32}$$

We now focus on isolating the first quadrant, where $x^+ > 0$ and $x^- < 0$. As in the usual case, this region describes the exterior of the black hole, or the outer universe. However, the AdS asymptotics modify the standard structure of this spacetime patch. From Eq. (6.30) we infer that spatial infinity $\mathrm{x} \to \infty$ is now associated with $\sigma = 0$, in contrast to the conventional case where $\sigma \to \infty$. This significantly alters the conformal diagram:

$$\sigma = 0 \quad \Longrightarrow \quad \kappa^2 x^+ x^- = -1 \quad \Longrightarrow \quad \tan\left(\mathrm{x}^+\right)\tan\left(\mathrm{x}^-\right) = -1 \quad \Longrightarrow \quad \mathrm{x}^+ - \mathrm{x}^- = \frac{\pi}{2}. \tag{6.33}$$

Consequently, instead of being represented by a single point on the conformal diagram, spatial infinity i^0 becomes a time-like hypersurface. This is the key characteristic of an asymptotically AdS spacetime. Constant-time hypersurfaces appear as straight lines emanating from the bifurcation point $(0,0)$, while lines of constant x correspond to hyperbolae in the Kruskal coordinates:

$$t = const. \quad \Longrightarrow \quad \frac{x^+}{x^-} = const. \quad \wedge \quad \mathrm{x} = const. \quad \Longrightarrow \quad x^+x^- = const. \tag{6.34}$$

With this, region I is completely specified. Region II, defined by $x^+ > 0$ and $x^- > 0$, contains the singularity at $\mathrm{x} = 0$, and therefore corresponds to the black hole interior. From Eq. (6.30) we also obtain $\sigma = 0$. Hence, we have:

$$\sigma = 0 \quad \Longrightarrow \quad \kappa^2 x^+ x^- = 1 \quad \Longrightarrow \quad \tan\left(\mathrm{x}^+\right)\tan\left(\mathrm{x}^-\right) = 1 \quad \Longrightarrow \quad \mathrm{x}^+ + \mathrm{x}^- = \frac{\pi}{2}. \tag{6.35}$$

Because this region corresponds to $\Lambda < 0$ once the horizon has been crossed, time and space interchange their roles. In this case, constant-time slices are described by hyperbolae, whereas constant-x hypersurfaces are represented by straight lines emanating from the bifurcation point in the Kruskal diagram.

To fully construct the maximally extended solution, we must also analyze regions III and IV in Fig. 4.1. By following an analogous procedure, we recover the standard behavior. Region III represents the second exterior universe, while region IV corresponds to the white-hole region. It is worth emphasizing that the curvature invariants remain finite at the $\mathrm{x} = 0$ singularity. This singularity is present only from the perspective of the dilaton field, which must obey $\mathbf{x} > 0$. Therefore, without the dilaton argument, the BTZ black hole represents a specific patch of the AdS_2.

The full Penrose diagram is displayed in Fig. 6.1. In this figure, constant-time slices are drawn in red, whereas hypersurfaces of constant x are shown in blue. Spatial infinity and the event horizons are indicated by green lines, and the singularity is represented by a wavy black line. Thus, the entire causal structure is readily visualized.

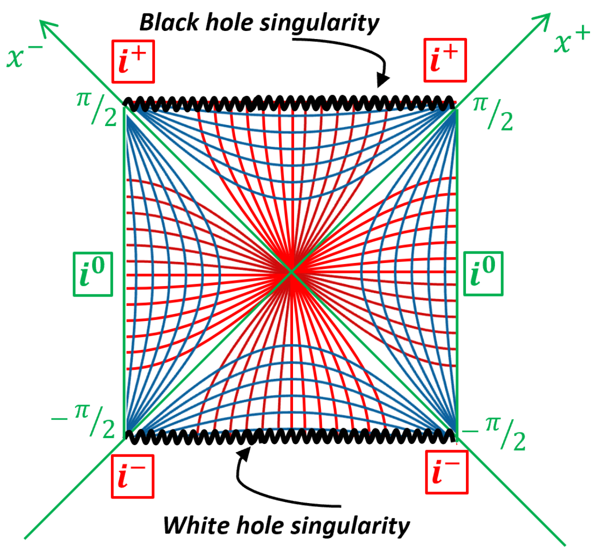

Figure 6.1: Penrose diagram for the BTZ black hole.

One can immediately see that null rays reach the asymptotic boundary in a finite time. We now demonstrate this explicitly:

$$\mathrm{d}s^2 = 0 \quad \Longrightarrow \quad \frac{\mathrm{dt}}{\mathrm{dx}} = \frac{1}{\mathrm{x}^2 - \mu} \quad \Longrightarrow \quad \Delta t = \frac{1}{2\sqrt{\mu}} \ln\left|\frac{\mathrm{x}_0 + \sqrt{\mu}}{\mathrm{x}_0 - \sqrt{\mu}}\right|, \tag{6.36}$$

where x_0 denotes the point from which the light ray is emitted. This behavior is a characteristic property of AdS-asymptotic spacetimes. Consequently, one typically imposes reflective boundary conditions at the asymptotic boundary for all fields, which effectively confines the particles to a box. From the standpoint of Hawking radiation, however, this setup is problematic, since the radiation should be able to escape to infinity. To resolve this, one introduces flat bath regions and replaces the reflective boundary conditions with transparent ones, allowing the Hawking quanta to propagate into the thermal bath regions. Additional discussion of this construction is provided in Sec. 11.1.

6.1.4 Classical collapse scenario

Here, we investigate the classical collapse scenario. We strictly follow Sec. 3.4 where it was first described. The matter fields are incorporated as an ingoing shockwave of massless particles along the $x^+ = x_0^+$ hypersurface, with the EMT given in Eq. (3.99). This shockwave divides the spacetime into two distinct regions, as illustrated in Fig. 3.2. Subsequently, one has to join these regions smoothly by imposing the continuity conditions (3.102) and (3.104).

We start by rewriting the "++" equation of motion (6.11) in the form (3.103). It is given by:

$$\left(\mathrm{x}^2 + 1 - l^2 (\nabla \mathrm{x})^2\right) \partial_+ \left(e^{-2\rho} \partial_+ \mathrm{x}\right) = \frac{M}{6k\pi^2 \mathrm{F}^+} \delta\left(x^+ - x_0^+\right) e^{-2\rho}. \tag{6.37}$$

Next, we integrate Eq. (6.37) with respect to the x^+ coordinate over the interval from $x_0^+ - \epsilon$ to $x_0^+ + \epsilon$, and then take the limit $\epsilon \to 0$. We assume that x, ∂_-x, ρ and $\partial_-\rho$ are continuous functions, whereas ∂_+x, $\partial_+\rho$, $\partial_+\partial_-$x, and $\partial_+\partial_-\rho$ are allowed to exhibit discontinuities across the hypersurface $x^+ = x_0^+$. Under these conditions, the integration yields:

$$\left(\mathrm{x}^2 + 1 - \frac{1}{2} l^2 (\nabla \mathrm{x})^2\right) \partial_+ \mathrm{x}\Big|_<^> = \frac{M}{6k\pi^2 \mathrm{F}^+}\Big|_{x^+ = x_0^+}, \tag{6.38}$$

where ">" ("<") corresponds to the region of the spacetime where $x^+ > x_0^+$ ($x^+ < x_0^+$). Using the static ansatz (3.8) and (3.13), Eq. (6.38) becomes:

$$\left(\mathrm{x}^2 + 1 + \frac{1}{2}\Lambda \mathcal{D}^2\right) \Lambda \mathcal{D}\Big|_<^> = \frac{Ml}{3k\pi^2}, \tag{6.39}$$

which coincides with the form given in Eq. (3.104). We now continuously connect two solutions $\mathrm{RI}(\mathrm{F}_\mathrm{I}^+, \mathrm{F}_\mathrm{I}^-, \mu_\mathrm{I})$ and $\mathrm{RI}(\mathrm{F}_\mathrm{II}^+, \mathrm{F}_\mathrm{II}^-, \mu_\mathrm{II})$. Upon inserting the expression (6.17) into Eq. (6.39), the latter simplifies to:

$$\mu_\mathrm{II}\left(\mu_\mathrm{II} + 2\right) - \mu_\mathrm{I}\left(\mu_\mathrm{I} + 2\right) = \frac{2Ml}{3k\pi^2}. \tag{6.40}$$

Requiring the continuity of metric gives the jump in F^- coordinate transformation:

$$\frac{\mathrm{F}^+ \mathrm{F}_\mathrm{II}^- e^{2\rho}}{\mathrm{F}^+ \mathrm{F}_\mathrm{I}^- e^{2\rho}} = \frac{\mathrm{F}_\mathrm{II}^-}{\mathrm{F}_\mathrm{I}^-} = \frac{\mathrm{x}^2 - \mu_\mathrm{II}}{\mathrm{x}^2 - \mu_\mathrm{I}}\Big|_{x^+ = x_0^+}. \tag{6.41}$$

Finally, one has to verify whether the continuity condition for the dilaton field holds. Since Eq. (6.40) requires $\mu_\mathrm{II} > \mu_\mathrm{I}$, we must distinguish three separate cases: $0 < \mathrm{x} < \sqrt{\mu_\mathrm{I}}$, $\sqrt{\mu_\mathrm{I}} < \mathrm{x} < \sqrt{\mu_\mathrm{II}}$, and $\mathrm{x} > \sqrt{\mu_\mathrm{II}}$. These intervals correspond to two coordinate charts that together form the atlas of the BTZ solution (6.17) in both spacetime regions. Thus, we obtain:

$$\sqrt{\frac{\mu_\mathrm{I}}{\mu_\mathrm{II}}} = \begin{cases} \dfrac{\tanh\left(\frac{\sqrt{\mu_\mathrm{II}}}{2l}\left(\sigma_0^+ - \hat{\sigma}^-\right)\right)}{\tanh\left(\frac{\sqrt{\mu_\mathrm{I}}}{2l}\left(\sigma_0^+ - \sigma^-\right)\right)}, & 0 < \mathrm{x} < \sqrt{\mu_\mathrm{I}}, \\ \dfrac{\tanh\left(\frac{\sqrt{\mu_\mathrm{II}}}{2l}\left(\sigma_0^+ - \hat{\sigma}^-\right)\right)}{\coth\left(\frac{\sqrt{\mu_\mathrm{I}}}{2l}\left(\sigma_0^+ - \sigma^-\right)\right)}, & \sqrt{\mu_\mathrm{I}} < \mathrm{x} < \sqrt{\mu_\mathrm{II}}, \\ \dfrac{\coth\left(\frac{\sqrt{\mu_\mathrm{II}}}{2l}\left(\sigma_0^+ - \hat{\sigma}^-\right)\right)}{\coth\left(\frac{\sqrt{\mu_\mathrm{I}}}{2l}\left(\sigma_0^+ - \sigma^-\right)\right)}, & \mathrm{x} > \sqrt{\mu_\mathrm{II}}, \end{cases} \tag{6.42}$$

where $\hat{\sigma}^{\pm}$ denote Eddington–Finkelstein-like coordinates in region II of the spacetime. One can readily verify that Eqs. (6.41) and (6.42) are mutually consistent. Moreover, Eq. (6.42) serves as the defining relation for the $\hat{\sigma}^{-}$ coordinate, while the other coordinate remains unchanged, $\hat{\sigma}^{+} = \sigma^{+}$. Therefore, we conclude that the solution in region II takes the form:

$$\begin{cases} \mathrm{RI}\left(\mathrm{F}_{\mathrm{I}}^{+}, \mathrm{F}_{\mathrm{I}}^{-}\left[1+\frac{\mu_{\mathrm{II}}-\mu_{\mathrm{I}}}{\mu_{\mathrm{I}}}\cosh^2\left(\frac{\sqrt{\mu_{\mathrm{I}}}}{2l}\left(\sigma_0^{+}-\sigma^{-}\right)\right)\right], \sqrt{\left(\mu_{\mathrm{I}}+1\right)^2+\frac{2Ml}{3k\pi^2}}-1\right), & \mathrm{x}<\sqrt{\mu_{\mathrm{I}}}, \\ \mathrm{RI}\left(\mathrm{F}_{\mathrm{I}}^{+}, \mathrm{F}_{\mathrm{I}}^{-}\left[1-\frac{\mu_{\mathrm{II}}-\mu_{\mathrm{I}}}{\mu_{\mathrm{I}}}\sinh^2\left(\frac{\sqrt{\mu_{\mathrm{I}}}}{2l}\left(\sigma_0^{+}-\sigma^{-}\right)\right)\right], \sqrt{\left(\mu_{\mathrm{I}}+1\right)^2+\frac{2Ml}{3k\pi^2}}-1\right), & \mathrm{x}>\sqrt{\mu_{\mathrm{I}}}. \end{cases} \tag{6.43}$$

Eq. (6.43) describes how the spacetime is modified when an infalling shockwave with mass M is introduced. To obtain a genuine gravitational collapse setup, region I must be described by a massless AdS spacetime. There are two possible values of the parameter μ that yield AdS: $\mu = 0$ and $\mu = -1$. The appropriate choice in this context is $\mu = 0$. This follows from the fact that, for μ in the range between -1 and 0, there are several naked singularities [78, 117], which are forbidden by the cosmic censorship conjecture [106]. Consequently, the classical collapse scenario corresponds to the situation in which the initial spacetime is described by $\mathrm{RI}(-1, 1, 0)$. Taking the limit $\mu \to 0$ in the solution (6.17) one obtains:

$$\mathrm{d}s^2 = -\mathrm{x}^2\mathrm{d}t^2 + \frac{l^2\mathrm{dx}^2}{\mathrm{x}^2}, \qquad \frac{1}{\mathrm{x}} = \frac{1}{2l}\left(\int\frac{\mathrm{d}x^{+}}{\mathrm{F}^{+}} + \int\frac{\mathrm{d}x^{-}}{\mathrm{F}^{-}}\right), \tag{6.44}$$

where we have used only the second chart, corresponding to $\mathrm{x} > \sqrt{\mu}$, and set $\mu = 0$. One can readily verify that this metric indeed describes AdS spacetime in Poincaré coordinates. Under the coordinate transformation $\mathrm{x} = -1/\mathrm{z}$, the metric is immediately brought into the standard Poincaré patch form, namely

$$\mathrm{d}s^2 = \frac{-\mathrm{d}t^2 + l^2\mathrm{dz}^2}{\mathrm{z}^2}, \qquad -\frac{1}{\mathrm{x}} = \mathrm{z} = -\frac{1}{2l}\left(\int\frac{\mathrm{d}x^{+}}{\mathrm{F}^{+}} + \int\frac{\mathrm{d}x^{-}}{\mathrm{F}^{-}}\right). \tag{6.45}$$

Having established that $\mu = 0$ corresponds to empty AdS spacetime, taking this limit in (6.43) yields the following solution in region II of the spacetime:

$$\mathrm{RI}\left(-1, 1-\mu\left(\frac{\sigma_0^{+}-\sigma^{-}}{2l}\right)^2, \sqrt{1+\frac{2Ml}{3k\pi^2}}-1\right). \tag{6.46}$$

The $\hat{\sigma}^{\pm}$ coordinates following the collapse are therefore:

$$\hat{\sigma}^{+} = \sigma^{+}, \tag{6.47}$$

$$\hat{\sigma}^{-} = \sigma_0^{+} - \frac{l}{\sqrt{\mu}}\ln\left|\frac{1+\frac{\sqrt{\mu}}{2l}\left(\sigma_0^{+}-\sigma^{-}\right)}{1-\frac{\sqrt{\mu}}{2l}\left(\sigma_0^{+}-\sigma^{-}\right)}\right|. \tag{6.48}$$

Then, the solution in region II of the spacetime is given by:

$$\begin{aligned} \frac{1}{2\sqrt{\mu}}\ln\left|\frac{\mathrm{x}-\sqrt{\mu}}{\mathrm{x}+\sqrt{\mu}}\right| &= -\ln\delta + \frac{1}{2\sqrt{\mu}}\ln\left|\frac{1+\hat{\mathrm{x}}\sqrt{\mu}}{1-\hat{\mathrm{x}}\sqrt{\mu}}\right|, \\ \mathrm{F}^{+}\mathrm{F}^{-}e^{2\rho} &= -\mathrm{x}^2 + \mu, \end{aligned} \tag{6.49}$$

where we have used the collapse-adapted coordinates $(\delta, \hat{\mathrm{x}})$ defined in Eq. (3.107). In these coordinates the coordinate transformations take the form:

$$\mathrm{F}^{+} = 1 \quad \wedge \quad \mathrm{F}^{-} = 1 - \mu\hat{\mathrm{x}}^{2}. \tag{6.50}$$

Note that, on the shockwave hypersurface $\delta = 1$, equations reduce to the solution (6.44). The horizon and the singularity remain $\mathrm{x_H} = \sqrt{\mu}$ and $\mathrm{x_S} = 0$, respectively, or in terms of the $\sigma^{\pm}$ coordinates:

$$\hat{\mathrm{x}}_{\mathrm{H}} = -\frac{1}{\sqrt{\mu}}, \qquad \ln \delta_{\mathrm{S}/i^0} = \frac{1}{2\sqrt{\mu}} \ln \left| \frac{1 + \hat{\mathrm{x}}_{\mathrm{S}/i^0}\sqrt{\mu}}{1 - \hat{\mathrm{x}}_{\mathrm{S}/i^0}\sqrt{\mu}} \right|. \tag{6.51}$$

Observe that these two hypersurfaces intersect at infinity, that is $\sigma^{+}_{\mathrm{E}} = +\infty$, which is consistent with the absence of quantum corrections in the classical setting. Another important point is that the two limits, $\mathrm{x} \to 0$ (corresponding to the singularity) and $\mathrm{x} \to +\infty$ (corresponding to spatial infinity i^0), are described by the same formula in Eq. (6.51). The logarithmic term admits two distinct branches. The singularity is characterized by the branch where $\hat{\mathrm{x}}_{\mathrm{S}} < -1/\sqrt{\mu}$, whereas spatial infinity is associated with the interval $-1/\sqrt{\mu} < \hat{\mathrm{x}}_{\mathrm{B}} < 0$.

Fig. 6.2 depicts the classical collapse setup in the $(\delta, \hat{\mathrm{x}})$ coordinates (3.107). The ingoing shockwave at $\delta = 1$, shown in red, divides the spacetime into two distinct regions, labeled region I and region II. Through the relation $\mathrm{x} = -1/\mathrm{z}$, spatial infinity is identified with $\mathrm{z} = 0$, while the spacetime boundary at $\mathrm{x} = 0$ is mapped to $\mathrm{z} \to -\infty$. As a result, the ingoing shockwave intersects the spacetime boundary only at infinity, and it is exactly at this location that the singularity forms. In Fig. 6.2, this singularity is shown as the wavy black line. The event horizon, dashed purple line, links the singularity to spatial infinity at future time infinity i^+, which is located at coordinates $(0, -1/\sqrt{\mu})$. The explicit forms of these hypersurfaces are given in Eq. (6.51), and the spacetime metric with the corresponding tortoise coordinate is given in Eq. (6.49).

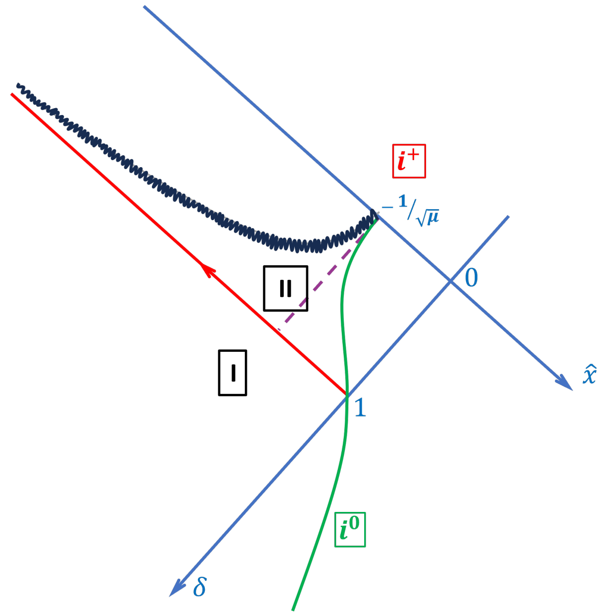

Figure 6.2: Classical gravitational collapse scenario for the BTZ black hole in $(\delta, \hat{\mathrm{x}})$ coordinates.

Next, we turn to the analysis of solutions of type RII. Since $\partial_{-}\mathrm{x}_{<} = \partial_{-}\mathrm{x}_{>}$, the function $\mathcal{D}$ is continuous across the hypersurface $x^{+} = x^{+}_{0}$, which in turn implies that Λ is also continuous. We therefore conclude that, within this framework of gravitational collapse, solutions of type RII cannot be continuously connected.

Finally, one needs to investigate what happens if the solution in one spacetime region is of type RI, while the solution in the other region is of type RII. As before, the continuity condition for the $\mathcal{D}$ function has to be applied. Because the RI solution satisfies $\mathcal{D} = 1$, the remaining portion of the spacetime corresponds to an AdS patch. Consequently, the problem reduces to that of matching two RI-type solutions, with the caveat that one of them has $\mu = -1$, which, as previously noted, is unphysical.

Observe that Eq. (6.46) implies the proper relation between the mass of a BTZ black hole and the parameter μ is:

$$\mu = \sqrt{1 + \frac{2Ml}{3k\pi^2}} - 1. \tag{6.52}$$

This outcome agrees with the result obtained in [118]. It can likewise be reproduced using the ADM formalism [119], or by employing the holographic framework together with the boundary stress-energy tensor [120].

6.1.5 Conformal diagram depicting the classical collapse scenario

In this section, we construct the conformal diagram for the classical gravitational collapse scenario, illustrated in Fig. 6.2. Region I represents the massless BTZ black hole, whose metric and tortoise coordinate are given in Eq. (6.44). We have seen that, by performing the substitution $\mathrm{x} = -1/\mathrm{z}$, one obtains the Poincaré patch of the two-dimensional AdS spacetime, as defined in Eq. (6.45). Because $\mathrm{x} > 0$ implies $\mathrm{z} < 0$, the spacetime of region I corresponds to a part of the left Poincaré patch. We now define the conformal coordinates as:

$$\mathrm{x}^+ = \arctan\left(\frac{\sqrt{\mu}}{2l}\left(\sigma^+ - \sigma_0^+\right)\right), \quad \wedge \quad \mathrm{x}^- = \arctan\left(\frac{\sqrt{\mu}}{2l}\left(\sigma^- - \sigma_0^+\right)\right). \tag{6.53}$$

Then, the spatial infinity i^0, characterized by $\mathrm{x} \to \infty$ prior to the shockwave corresponds to $\mathrm{z} = 0$, or $\sigma_+ = \sigma_-$. In terms of the conformal coordinates (6.53), this condition becomes $\mathrm{x}^+ = \mathrm{x}^-$. Conversely, the spacetime boundary at $\mathrm{x} = 0$ corresponds to the limit $\mathrm{z} \to -\infty$. As a result, it consists of two distinct hypersurfaces:

$$\begin{aligned} \sigma^+ \to -\infty \quad &\Longrightarrow \quad \mathrm{x}^+ = -\frac{\pi}{2}, \\ \sigma^- \to \infty \quad &\Longrightarrow \quad \mathrm{x}^- = \frac{\pi}{2}, \end{aligned} \tag{6.54}$$

In the absence of the shockwave, we simply recover the left Poincaré patch of AdS spacetime. Once the infalling matter is introduced, the region I terminates at the shockwave hypersurface, which slices through the left Poincaré patch along $\sigma^+ = \sigma_0^+$. In terms of the conformal coordinates, this corresponds to $\mathrm{x}^+ = 0$. Consequently, region II occupies the part of the spacetime characterized by $\mathrm{x}^+ > 0$.

In region II, spatial infinity is again located at $\mathrm{z} = 0$. Due to the change in the asymptotic coordinates, however, this hypersurface becomes curved. Its form is determined by Eq. (6.51), which can be written as:

$$\hat{\mathrm{x}}_{i^0}\sqrt{\mu} = \frac{\delta_{i^0}^{2\sqrt{\mu}} - 1}{\delta_{i^0}^{2\sqrt{\mu}} + 1} = \tanh(\sqrt{\mu}\ln\delta_{i^0}) \quad \Longrightarrow \quad \mathrm{x}_{i^0}^- = \arctan\left(\tanh\left(\tan\mathrm{x}_{i^0}^+\right)\right), \tag{6.55}$$

in the conformal coordinates (6.53). The other branch of Eq. (6.51) defines the singularity hypersurface generated by the gravitational collapse. The singularity is given by:

$$\hat{\mathrm{x}}_{\mathrm{S}}\sqrt{\mu} = \frac{\delta_{\mathrm{S}}^{2\sqrt{\mu}} + 1}{\delta_{\mathrm{S}}^{2\sqrt{\mu}} - 1} = \coth(\sqrt{\mu}\ln\delta_{\mathrm{S}}) \quad \Longrightarrow \quad \mathrm{x}_{\mathrm{S}}^- = \arctan\left(\coth\left(\tan\mathrm{x}_{\mathrm{S}}^+\right)\right), \tag{6.56}$$

in the conformal coordinates (6.53). Finally, the horizon becomes:

$$\hat{\mathrm{x}}_{\mathrm{H}}\sqrt{\mu} = -1 \quad \Longrightarrow \quad \mathrm{x}_{\mathrm{H}}^- = \frac{\pi}{4}. \tag{6.57}$$

These three hypersurfaces (6.55), (6.56), and (6.57) intersect at future time infinity i^+. The coordinates of the future time infinity point i^+ and the past time infinity point i^- are:

$$i^+ = \left(\frac{\pi}{4}, \frac{\pi}{2}\right), \quad \wedge \quad i^- = \left(-\frac{\pi}{2}, -\frac{\pi}{2}\right). \tag{6.58}$$

respectively, in the format $(\mathrm{x}^-, \mathrm{x}^+)$. The conformal diagram is shown in Fig. 6.3.

Fig. 6.3 shows the Penrose diagram for the classical gravitational collapse scenario within the dimensionally-reduced five-dimensional Chern-Simons gravity. Both region I, prior to the collapse, and region II, following the collapse, are clearly displayed. Region I corresponds to the part of the left Poincaré patch of AdS spacetime discussed above. It is separated from the other region by the ingoing shockwave hypersurface, depicted in red. The spacetime boundary at $\mathrm{x} = 0$ is shown as the black line within region I of the diagram. It extends into region II of spacetime, where it represents the black hole singularity (illustrated by the wavy black line), which is concealed behind the event horizon, drawn as the dashed purple line. The spatial infinity i^0 appears as a smooth green line which extends in both regions. The figure also displays both future time infinity i^+ and past time infinity i^-.

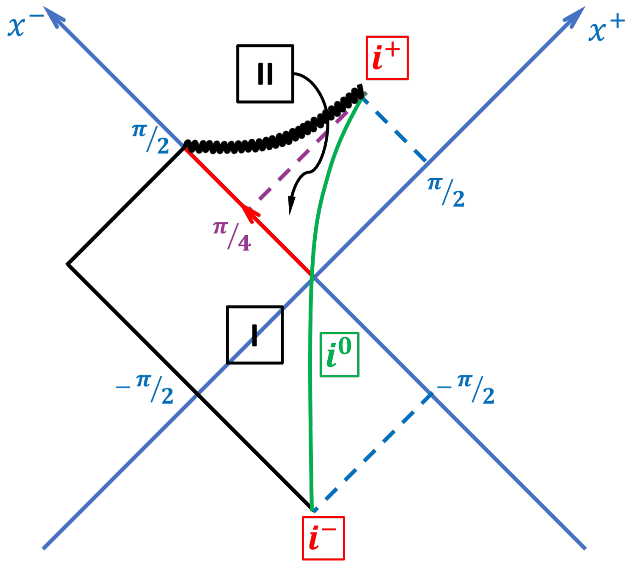

Figure 6.3: Penrose diagram of the classical gravitational collapse for the BTZ black hole.

6.2 Adding quantum corrections

In this section, we incorporate quantum corrections into the classical DR5DCS action (6.1). These corrections are included via the Polyakov–Liouville action (3.72), in the same manner as in the BPP and DREH models. As in the DREH model, equations cannot be solved exactly, so we adopt the perturbative method presented in Sec. 3.3. Because no counterterms are added, the dilaton Equation of motion (6.12) remains unchanged. In contrast, the metric equation of motion (6.11) is modified by the EMT of the quantum fields (3.77). We now directly express the metric equation in the conformal gauge (3.2):

$$\left(\mathrm{x}^2 + 1 - l^2(\nabla \mathrm{x})^2\right)\partial_\pm \left(e^{-2\rho}\partial_\pm \mathrm{x}\right) = \varepsilon\left[(\partial_\pm\rho)^2 - \partial_\pm^2\rho + t_\pm(x^\pm)\right]e^{-2\rho}, \tag{6.59}$$

$$\left(\mathrm{x}^2 + 1 - l^2(\nabla \mathrm{x})^2\right)\left(\frac{2\mathrm{x}}{l^2} - \Box \mathrm{x}\right) = -\frac{\varepsilon}{2}R, \tag{6.60}$$

where, in the second line, we have made use of the trace anomaly of the scalar-field EMT, namely $\langle \Delta T^{(f)}\rangle = \frac{\hbar}{24\pi}R$. Moreover, we introduce a natural perturbative parameter $\varepsilon = \frac{\hbar}{72k\pi^3}$. We then evaluate the quantum-corrected solution corresponding to the first branch (6.17). The derivatives of the dilaton field and of the metric take the form:

$$\partial_\pm \mathrm{x} = -\frac{\mathrm{x}^2 - \mu}{2l\mathrm{F}^\pm} \quad \wedge \quad \partial_\pm\rho = -\frac{\mathrm{x}}{2l\mathrm{F}^\pm} - \frac{1}{2}\partial_\pm \ln \mathrm{F}^\pm. \tag{6.61}$$

The first step in the perturbative treatment of these equations is to expand the fields to first order in ε using Eq. (3.108), i.e. $\mathrm{x} \mapsto \mathrm{x} + \varepsilon\theta$ and $\rho \mapsto \rho + \varepsilon\alpha$. Since both $\partial_\pm(e^{-2\rho}\partial_\pm \mathrm{x})$ and $\frac{2\mathrm{x}}{l^2} - \Box\mathrm{x}$ are already of first order in ε, quantity $\mathrm{x}^2 + 1 - l^2(\nabla\mathrm{x})^2$ is evaluated at zeroth order. The same reasoning applies to the EMT components. A straightforward calculation based on Eq. (6.61) gives:

$$\mathrm{x}^2 + 1 - l^2(\nabla\mathrm{x})^2 = \mu + 1, \quad R = -\frac{2}{l^2}, \quad (\partial_\pm\rho)^2 - \partial_\pm^2\rho + t_\pm(x^\pm) = \frac{t_\pm(\sigma^\pm)}{\mathrm{F}^{\pm 2}} + \frac{\mu}{4l^2\mathrm{F}^{\pm 2}}. \tag{6.62}$$

Upon substituting Eq. (6.62), the equations of motion (6.59) and (6.60) take the form (3.109), which reads:

$$\partial_\pm\left(e^{-2\rho}\partial_\pm\theta - \frac{\alpha}{l}\mathrm{F}^\mp\right) = \frac{1}{\mu+1}\left[\frac{t_\pm(\sigma^\pm)}{\mathrm{F}^{\pm 2}} + \frac{\mu}{4l^2\mathrm{F}^{\pm 2}}\right], \tag{6.63}$$

$$2\theta + 4l^2 e^{-2\rho}\partial_+\partial_-\theta + 4\mathrm{x}\alpha = \frac{1}{\mu+1}. \tag{6.64}$$

The next step is to integrate Eq. (6.63) and derive the closed-form expressions for the derivatives of θ, as outlined in Eq. (3.110). These expressions are given by:

$$\partial_\pm\theta = \frac{1}{2l}\mathrm{F}^\mp\left[\mathcal{D}_1 + 2\alpha + \frac{\mathrm{G}^\mp}{\mathrm{F}^\mp}\right]e^{2\rho} - \frac{1}{\mu+1}\mathrm{F}^\mp e^{2\rho}\int\frac{\mathrm{d}x^\pm}{\mathrm{F}^\pm}\frac{t_\pm(\sigma^\pm)}{\mathrm{x}^2-\mu} \tag{6.65}$$

where the function $\mathcal{D}_1$ is defined through:

$$\frac{\mathrm{d}\mathcal{D}_1}{\mathrm{dx}} = \frac{1}{\mu+1}\frac{\mu}{(\mathrm{x}^2-\mu)^2}. \tag{6.66}$$

Next, we need to remove the function α from Eq. (6.65). This can be achieved by employing Eq. (6.64). As a result, we obtain two first-order differential equations for θ: one involving $\partial_+\theta$ and the other involving $\partial_-\theta$. These equations can be solved, leading to:

$$\begin{aligned}\mathrm{x}\theta = \mathrm{H}^\mp + \frac{1}{2}\left(\mathrm{x}^2-\mu\right)\left[\frac{\mathrm{G}^-}{\mathrm{F}^-} + \frac{\mathrm{G}^+}{\mathrm{F}^+} + 2\alpha + \mathcal{D}_1\right] + \frac{\mathrm{x}}{2(\mu+1)} + \int\mathrm{dx}\mathcal{D}_1\mathrm{x} \\ + \frac{1}{\mu+1}\int\frac{\mathrm{d}x^\pm}{\mathrm{F}^\pm}\mathrm{x}\left(\mathrm{x}^2-\mu\right)\int\frac{\mathrm{d}x^\pm}{\mathrm{F}^\pm}\frac{t_\pm(\sigma^\pm)}{\mathrm{x}^2-\mu} - l\frac{\mathrm{x}^2-\mu}{\mu+1}\int\frac{\mathrm{d}x^\mp}{\mathrm{F}^\mp}\frac{t_\mp(\sigma^-)}{\mathrm{x}^2-\mu},\end{aligned} \tag{6.67}$$

where $\mathrm{H}^\mp$ represent another set of arbitrary functions. Furthermore, by using Eq. (6.65) we have removed the remaining derivative term $\partial_\mp\theta$, which reintroduces the function α. Requiring that the two equations in Eq. (6.67) coincide then imposes the following consistency condition on the functions $\mathrm{H}^\mp$:

$$\mathrm{H}^- - \frac{l}{\mu+1}\int\frac{\mathrm{d}x^-}{\mathrm{F}^-}t_-(\sigma^-) = \mathrm{H}^+ - \frac{l}{\mu+1}\int\frac{\mathrm{d}x^+}{\mathrm{F}^+}t_+(\sigma^+) = C, \tag{6.68}$$

where we have included an integration constant C. It may be interpreted as the integration constant of $\int\mathrm{dx}\mathcal{D}\mathrm{x}$. Consequently, by eliminating the $\mathrm{H}^\mp$ functions, we obtain:

$$\mathrm{x}\theta = \frac{1}{2}\left(\mathrm{x}^2-\mu\right)\left[\frac{\mathrm{G}^-}{\mathrm{F}^-} + \frac{\mathrm{G}^+}{\mathrm{F}^+} + 2\alpha + \mathcal{D}_1\right] + \frac{\mathrm{x}}{2(\mu+1)} + \int\mathrm{dx}\mathcal{D}_1\mathrm{x} + \frac{\mathrm{I}'_+ + \mathrm{I}'_-}{2(\mu+1)}, \tag{6.69}$$

where the integrals $\mathrm{I}'_\pm$ are defined as follows:

$$\mathrm{I}'_\pm = 2\int\frac{\mathrm{d}x^\pm}{\mathrm{F}^\pm}\mathrm{x}\left(\mathrm{x}^2-\mu\right)\int\frac{\mathrm{d}x^\pm}{\mathrm{F}^\pm}\frac{t_\pm(\sigma^\pm)}{\mathrm{x}^2-\mu}. \tag{6.70}$$

By following the method outlined in Sec. 3.4.1, a final integration remains to be carried out. Isolating α from Eq. (6.65) and substituting it into Eq. (6.69) transforms Eq. (6.69) into a first-order differential equation for θ. As before, there are two such equations, depending on whether the derivative $\partial_\pm\theta$ appears. Solving these equations introduces two additional arbitrary functions, which are then determined by imposing mutual consistency of the two solutions. In this way, one ultimately obtains the following expression for the final solution of θ:

$$\frac{\theta}{\mathrm{x}^2-\mu}=\frac{1}{2l}\left(\int \mathrm{d}x^+\frac{\mathrm{G}^+}{\mathrm{F}^{+2}}+\int \mathrm{d}x^-\frac{\mathrm{G}^-}{\mathrm{F}^{-2}}\right)-\int\frac{\mathrm{dx}}{\left(\mathrm{x}^2-\mu\right)^2}\left[\frac{\mathrm{x}}{\mu+1}+2\int \mathrm{dx}\mathcal{D}_1\mathrm{x}\right]+\frac{\mathrm{I}_++\mathrm{I}_-}{\mu+1}, \tag{6.71}$$

where we have introduced another set of integrals:

$$\mathrm{I}_\pm=\int\frac{\mathrm{d}x^\pm}{\mathrm{F}^\pm}\frac{1}{\mathrm{x}^2-\mu}\int\frac{\mathrm{d}x^\pm}{\mathrm{F}^\pm}t_\pm(\sigma^\pm). \tag{6.72}$$

The final step consists in reverting to the quantum-corrected quantities (3.113). We begin by examining the quantum-corrected metric:

$$\begin{aligned}\mathrm{F}^+\mathrm{F}^-e^{2\rho}&=-\left(\mathrm{x}^2-\mu\right)\left[1+\varepsilon\left(\frac{\mathrm{G}^-}{\mathrm{F}^-}+\frac{\mathrm{G}^+}{\mathrm{F}^+}+2\alpha\right)\right]\\&=-\mathrm{x}^2+\mu-2\varepsilon\mathrm{x}\theta+\varepsilon\left[\frac{\mathrm{x}}{\mu+1}+2\int\mathrm{dx}\mathcal{D}_1\mathrm{x}+\left(\mathrm{x}^2-\mu\right)\mathcal{D}_1\right]+\frac{\varepsilon}{\mu+1}\left(\mathrm{I}'_++\mathrm{I}'_-\right)\\&=-\left(\mathrm{x}+\varepsilon\theta\right)^2+\mu+\varepsilon\left[\frac{\mathrm{x}}{\mu+1}+2\int\mathrm{dx}\mathcal{D}_1\mathrm{x}+\left(\mathrm{x}^2-\mu\right)\mathcal{D}_1\right]+\frac{\varepsilon}{\mu+1}\left(\mathrm{I}'_++\mathrm{I}'_-\right),\end{aligned} \tag{6.73}$$

where Eq. (6.69) has been applied. We now determine the quantum-corrected tortoise coordinate by making use of Eq. (6.71):

$$\begin{aligned}\frac{1}{2\sqrt{\mu}}\ln\left|\frac{\mathrm{x}-\sqrt{\mu}}{\mathrm{x}+\sqrt{\mu}}\right|+\frac{\varepsilon\theta}{\mathrm{x}^2-\mu}+\varepsilon\int\frac{\mathrm{dx}}{\left(\mathrm{x}^2-\mu\right)^2}\left[\frac{\mathrm{x}}{\mu+1}+2\int\mathrm{dx}\mathcal{D}_1\mathrm{x}\right]-\frac{\varepsilon}{\mu+1}\left(\mathrm{I}_++\mathrm{I}_-\right)\\=-\frac{1}{2l}\left[\int\frac{\mathrm{d}x^+}{\mathrm{F}^+}\left(1-\varepsilon\frac{\mathrm{G}^+}{\mathrm{F}^+}\right)+\int\frac{\mathrm{d}x^-}{\mathrm{F}^-}\left(1-\varepsilon\frac{\mathrm{G}^-}{\mathrm{F}^-}\right)\right].\end{aligned} \tag{6.74}$$

From this equation, it is evident that $\mathrm{G}^\pm$ indeed encode the quantum corrections to the coordinate transformations. The only remaining task is to explicitly evaluate all integrals over x that appear in Eqs. (6.73) and (6.74). These are:

$$\mathcal{D}_1=-\frac{1}{2(\mu+1)}\left[\frac{1}{2\sqrt{\mu}}\ln\left|\frac{\mathrm{x}-\sqrt{\mu}}{\mathrm{x}+\sqrt{\mu}}\right|+\frac{\mathrm{x}}{\mathrm{x}^2-\mu}\right], \tag{6.75}$$

$$\frac{\mathrm{x}}{\mu+1}+2\int\mathrm{dx}\mathcal{D}_1\mathrm{x}+\left(\mathrm{x}^2-\mu\right)\mathcal{D}_1=-\frac{\mathrm{x}^2}{\mu+1}\frac{1}{2\sqrt{\mu}}\ln\left|\frac{\mathrm{x}-\sqrt{\mu}}{\mathrm{x}+\sqrt{\mu}}\right|+C, \tag{6.76}$$

$$\int\frac{\mathrm{dx}}{\left(\mathrm{x}^2-\mu\right)^2}\left[\frac{\mathrm{x}}{\mu+1}+2\int\mathrm{dx}\mathcal{D}_1\mathrm{x}\right]=\frac{1}{\mu+1}\frac{1}{4\sqrt{\mu}}\frac{\mathrm{x}}{\mathrm{x}^2-\mu}\ln\left|\frac{\mathrm{x}-\sqrt{\mu}}{\mathrm{x}+\sqrt{\mu}}\right|+C\frac{\mu+1}{\mu}\mathcal{D}_1. \tag{6.77}$$

Finally, as anticipated, the integration constant C is understood as the quantum correction to the constant μ. In other words, we make the replacement $\mu+\varepsilon C\mapsto\mu$. This removes C from both of the final Eqs. (6.73) and (6.74). Consequently, the general quantum-corrected solution takes the form:

$$\mathrm{F}^{+}\mathrm{F}^{-}e^{2\rho} = -\mathrm{x}^2 + \mu - \frac{\varepsilon}{\mu+1}\left[\frac{\mathrm{x}^2}{2\sqrt{\mu}}\ln\left|\frac{\mathrm{x}-\sqrt{\mu}}{\mathrm{x}+\sqrt{\mu}}\right| - \mathrm{I}'\right], \tag{6.78}$$

$$\frac{1}{2\sqrt{\mu}}\ln\left|\frac{\mathrm{x}-\sqrt{\mu}}{\mathrm{x}+\sqrt{\mu}}\right| + \frac{\varepsilon}{\mu+1}\left[\frac{\mathrm{x}}{\mathrm{x}^2-\mu}\frac{1}{4\sqrt{\mu}}\ln\left|\frac{\mathrm{x}-\sqrt{\mu}}{\mathrm{x}+\sqrt{\mu}}\right| - \mathrm{I}\right] = -\frac{1}{2l}\left(\int\frac{\mathrm{d}x^+}{\mathrm{F}^+} + \int\frac{\mathrm{d}x^-}{\mathrm{F}^-}\right). \tag{6.79}$$

We therefore find that the general quantum-corrected branch-one solution, which is continuously connected to the dimensionally reduced BTZ black hole at the classical level, is defined by $(\mathrm{F}^+, \mathrm{F}^-, \mu, t_+(\sigma^+), t_-(\sigma^-))$. The integrals (6.70) and (6.72) can be evaluated once the quantum state is chosen, because they depend on the functions $t_\pm(\sigma^\pm)$. In particular, the quantum state $|0, x\rangle$ is characterized by $t_\pm(x^\pm) = 0$ (see Sec. 3.3). We have adopted the shorthand notation $\mathrm{I} = \mathrm{I}_+ + \mathrm{I}_-$ and $\mathrm{I}' = \mathrm{I}'_+ + \mathrm{I}'_-$. Note that these two integrals are not independent; they are related through the equations of motion, so once the quantum state is fixed, only one of them actually needs to be computed. A key property of the solution (6.78-6.79) is that, in contrast to the DREH model (see Sec. 5.2), Eq. (6.79) is not transcendental, and thus x can be written in terms of the coordinates using elementary functions.

Note that we have not addressed the dilaton equation of motion (6.12) explicitly. This equation is automatically fulfilled once the solution (6.78-6.79) is substituted, because it is equivalent to the metric equation combined with the EMT conservation law, which is obeyed by the quantum-corrected EMT (3.75).

For completeness one could also consider the quantum-corrected branch-two solution. Yet this solution is not continuously connected to a well-behaved BTZ black hole and involves an arbitrary function, which likely originates from unfixed five-dimensional gauge transformations. Consequently, it does not constitute a physically meaningful solution. Therefore, we will not examine it further here.

6.2.1 General static quantum-corrected solution

In this subsection, we employ the static ansatz from Sec. 3.1 for the quantum-corrected equations of motion (6.24-6.26). Upon substituting the explicit expressions for the components of the EMT describing the quantum corrections (3.79), the metric equation of motion simplifies to:

$$T^{\perp\parallel} = T^{\parallel\perp} = 0 \quad \Longrightarrow \quad t_+(\sigma^+) = t_-(\sigma^-) = \frac{1}{4l^2}\Xi, \tag{6.80}$$

$$\frac{\Lambda}{2}\frac{\mathrm{d}}{\mathrm{dx}}\left(\mathrm{x}^2 + 1 + \Lambda\mathcal{D}^2\right)^2 = \varepsilon\left[\Xi + \frac{1}{4}\left(\mathcal{D}\frac{\mathrm{d}\Lambda}{\mathrm{dx}}\right)^2 - \Lambda\mathcal{D}\frac{\mathrm{d}}{\mathrm{dx}}\left(\mathcal{D}\frac{\mathrm{d}\Lambda}{\mathrm{dx}}\right)\right], \tag{6.81}$$

$$\Lambda\left(\mathrm{x}^2 + 1 + \Lambda\mathcal{D}^2\right)\left(\mathcal{D}^2\frac{\mathrm{d}\Lambda}{\mathrm{dx}} + 2\mathrm{x}\right) = -\varepsilon\left[\Xi + \frac{1}{4}\left(\mathcal{D}\frac{\mathrm{d}\Lambda}{\mathrm{dx}}\right)^2\right], \tag{6.82}$$

where Ξ is a constant related to the state of the quantum fields. To complete this system, we must also include the dilaton equation of motion (6.27). Since both the left-hand side and the right-hand side are of order ε, we can directly insert the classical static solution (6.17). The system of Eqs. (6.81) and (6.82) then takes the form:

$$\frac{\mathrm{d}\left(\Lambda\mathcal{D}^2\right)}{\mathrm{dx}} = -2\mathrm{x} - \frac{\varepsilon}{\mu+1}\left(\frac{\Xi+\mu}{\mathrm{x}^2-\mu} - 1\right), \tag{6.83}$$

$$\mathcal{D}^2\frac{\mathrm{d}\Lambda}{\mathrm{dx}} = -2\mathrm{x} + \frac{\varepsilon}{\mu+1}\left(\frac{\Xi+\mu}{\mathrm{x}^2-\mu} + 1\right). \tag{6.84}$$

Subtracting Eq. (6.84) from Eq. (6.83) gives the following solution for the function $\mathcal{D}$:

$$\frac{\mathrm{d}\mathcal{D}^2}{\mathrm{dx}} = \frac{2\varepsilon}{\mu+1}\frac{\Xi+\mu}{\mathrm{x}^2-\mu} = 2\varepsilon\left(\frac{\Xi}{\mu}+1\right)\frac{\mathrm{d}\mathcal{D}_1}{\mathrm{dx}} \quad \Longrightarrow \quad \mathcal{D}^2 = 1 + 2\varepsilon\left(\frac{\Xi}{\mu}+1\right)\mathcal{D}_1, \tag{6.85}$$

where we have employed Eq. (6.66) to rewrite the solution for $\mathcal{D}$ in terms of the function $\mathcal{D}_1$, presented in Eq. (6.75). Upon substituting this expression for $\mathcal{D}$ into Eq. (6.84) and performing the integration, the metric function Λ takes the form:

$$\Lambda = -\mathrm{x}^2 + \mu + \varepsilon\left(\frac{\Xi}{\mu}+1\right)\left[\frac{\mathrm{x}}{\mu+1} + 2\int \mathrm{dx}\mathcal{D}_1\mathrm{x} + \left(\mathrm{x}^2-\mu\right)\mathcal{D}_1\right] - \frac{\varepsilon}{\mu+1}\frac{\Xi}{\mu}\left(\mathrm{x}-\sqrt{\mu}\right). \tag{6.86}$$

Finally, we determine the tortoise coordinate using Eq. (3.18), which gives:

$$\begin{aligned}\frac{\sigma}{l} = \frac{1}{2\sqrt{\mu}}\ln\left|\frac{\mathrm{x}-\sqrt{\mu}}{\mathrm{x}+\sqrt{\mu}}\right| &+ \varepsilon\left(\frac{\Xi}{\mu}+1\right)\int\frac{\mathrm{dx}}{\left(\mathrm{x}^2-\mu\right)^2}\left[\frac{\mathrm{x}}{\mu+1} + 2\int \mathrm{dx}\mathcal{D}_1\mathrm{x}\right] \\ &- \frac{\varepsilon\Xi}{4\mu^2(\mu+1)}\left(\ln\left|\frac{\mathrm{x}-\sqrt{\mu}}{\mathrm{x}+\sqrt{\mu}}\right| - \frac{\mathrm{x}-\sqrt{\mu}}{\mathrm{x}+\sqrt{\mu}}\right).\end{aligned} \tag{6.87}$$

The solutions (6.85), (6.86), and (6.87) are expressed through the integrals (6.66-6.77). By substituting these expressions, we obtain the following final solution:

$$\begin{aligned}\mathcal{D} &= 1 - \frac{\varepsilon}{2(\mu+1)}\left(\frac{\Xi}{\mu}+1\right)\left[\frac{1}{2\sqrt{\mu}}\ln\left|\frac{\mathrm{x}-\sqrt{\mu}}{\mathrm{x}+\sqrt{\mu}}\right| + \frac{\mathrm{x}}{\mathrm{x}^2-\mu}\right], \\ \Lambda &= -\mathrm{x}^2 + \mu - \frac{\varepsilon}{\mu+1}\left(\frac{\Xi}{\mu}+1\right)\frac{\mathrm{x}^2}{2\sqrt{\mu}}\ln\left|\frac{\mathrm{x}-\sqrt{\mu}}{\mathrm{x}+\sqrt{\mu}}\right| - \frac{\varepsilon}{\mu+1}\frac{\Xi}{\mu}\left(\mathrm{x}-\sqrt{\mu}\right), \\ \frac{\sigma}{l} &= \frac{1}{2\sqrt{\mu}}\ln\left|\frac{\mathrm{x}-\sqrt{\mu}}{\mathrm{x}+\sqrt{\mu}}\right| + \frac{\varepsilon}{\mu+1}\left(\frac{\Xi}{\mu}+1\right)\frac{\mathrm{x}}{\mathrm{x}^2-\mu}\frac{1}{4\sqrt{\mu}}\ln\left|\frac{\mathrm{x}-\sqrt{\mu}}{\mathrm{x}+\sqrt{\mu}}\right| \\ &\quad - \frac{\varepsilon\Xi}{4\mu^2(\mu+1)}\left(\ln\left|\frac{\mathrm{x}-\sqrt{\mu}}{\mathrm{x}+\sqrt{\mu}}\right| - \frac{\mathrm{x}-\sqrt{\mu}}{\mathrm{x}+\sqrt{\mu}}\right).\end{aligned} \tag{6.88}$$

6.2.2 Solution without energy flux at the asymptotic infinity

In this section, we derive the quantum-corrected AdS vacuum solution. By definition, it is a static configuration with no energy flux at asymptotic infinity. The corresponding vacuum state is the Boulware state (3.96), which is implemented by choosing $t_\pm(\sigma^\pm) = 0$. Equivalently, this means that the EMT of the quantum fields is normal-ordered with respect to the Eddington–Finkelstein coordinates. The general static solution (6.88) depends on the constant Ξ, which is fixed by the choice of vacuum through Eq. (6.80). Setting $\Xi = 0$ selects the Boulware state. In this case, the solution simplifies to:

$$\begin{aligned}\mathcal{D} &= 1 - \frac{\varepsilon}{2(\mu+1)}\left[\frac{1}{2\sqrt{\mu}}\ln\left|\frac{\mathrm{x}-\sqrt{\mu}}{\mathrm{x}+\sqrt{\mu}}\right| + \frac{\mathrm{x}}{\mathrm{x}^2-\mu}\right],\\ \Lambda &= -\mathrm{x}^2+\mu-\frac{\varepsilon}{\mu+1}\frac{\mathrm{x}^2}{2\sqrt{\mu}}\ln\left|\frac{\mathrm{x}-\sqrt{\mu}}{\mathrm{x}+\sqrt{\mu}}\right|,\\ \frac{\sigma}{l} &= \frac{1}{2\sqrt{\mu}}\ln\left|\frac{\mathrm{x}-\sqrt{\mu}}{\mathrm{x}+\sqrt{\mu}}\right| + \frac{\varepsilon}{\mu+1}\frac{\mathrm{x}}{\mathrm{x}^2-\mu}\frac{1}{4\sqrt{\mu}}\ln\left|\frac{\mathrm{x}-\sqrt{\mu}}{\mathrm{x}+\sqrt{\mu}}\right|.\end{aligned} \tag{6.89}$$

This solution can be obtained directly from the general solution of the quantum-corrected equations of motion (6.78-6.79). It is specified by $(\mathrm{F}^+, \mathrm{F}^-, \mu, 0, 0)$, which corresponds to the vanishing integrals (6.70) and (6.72). Once these integrals are set to zero, the two solutions coincide.

The important feature of the fluxless solution in the DREH model is that, in the limit of vanishing mass, it remains smoothly connected to the Minkowski vacuum solution (see Sec. 5.2.2). This feature does not hold in the BPP model. As demonstrated in Sec. 4.3.1, the linear dilaton vacuum in the BPP framework carries energy flux at both past and future null infinity. Solution (6.89) displays analogous behavior. Although the limit $\mu \to 0$ is well defined, it does not reproduce the AdS vacuum solution. Instead, in this limit the configuration approaches the quantum-corrected AdS spacetime, given by:

$$\mathcal{D} = 1, \quad \Lambda = -\mathrm{x}^2 + \varepsilon\mathrm{x} + \varepsilon C, \quad \frac{\sigma}{l} = -\frac{1}{\mathrm{x}} - \frac{\varepsilon}{2\mathrm{x}^2} - \frac{\varepsilon C}{3\mathrm{x}^3}, \tag{6.90}$$

where we have retained the quantum correction C to the μ constant. It is worth emphasizing that, even in the limit $C \to 0$, the solution does not reduce to pure AdS spacetime.

In Secs. 4.3.3 and 5.2.2 we show that the fluxless solutions are horizonless in both BPP and DREH models. The same logic follows here as well. Trying to find the horizon reduces to demanding that the norm of the Killing vector vanishes, i.e. $\Lambda = 0$. Solving this equation in a perturbative expansion yields $\mathrm{x}_{\mathrm{H}} = \sqrt{\mu} + \mathcal{O}(\varepsilon)$. At first sight, this suggests the presence of a quantum-corrected horizon. Nevertheless, this solution is not well defined within the perturbative framework, because the quantum correction to Λ vanishes when evaluated on the classical horizon. Consequently, there is actually no horizon within the first-order of the perturbation theory.

Another issue that needs to be addressed is whether the solution (6.89) develops any singularities. In both the BPP and DREH models, the scalar curvature diverges on a certain hypersurface, which must therefore be identified as the boundary of the spacetime. A straightforward calculation of the scalar curvature reveals that it does not receive any quantum corrections within the first order in ε, i.e.:

$$R = -\frac{2}{l^2}. \tag{6.91}$$

From this analysis, we infer that no curvature singularities arise at first order in perturbation theory. Nonetheless, one must keep in mind that $\mathrm{x} > 0$, so within the DR5DCS framework we are still required to impose the reflective boundary conditions (4.117) on the hypersurface at $\mathrm{x} = 0$.

6.2.3 Eternal black hole scenario

In this section, we present the eternal black hole scenario. It describes a black hole in equilibrium with its environment. Consequently, it corresponds to a static configuration and must be specified by choosing a particular value of the constant Ξ within the general static solution (6.88). Because this is a black hole solution, it must possess a well-defined event horizon [106]. The event horizon is specified by the condition $\Lambda = 0$, so the classical location of the horizon is $\mathrm{x_H} = \sqrt{\mu}$. As long as the solution contains a term of the form $\ln|\mathrm{x} - \sqrt{\mu}|$, the quantum correction diverges at the classical horizon, just as in the fluxless solution discussed in the previous section. There is a unique value of Ξ that eliminates the logarithmic contribution in Λ, namely:

$$\Xi = -\mu. \tag{6.92}$$

Substituting this value of Ξ into the general solution (6.88), we obtain the following eternal black hole solution:

$$\begin{aligned} \mathcal{D} &= 1, \\ \Lambda &= -\mathrm{x}^2 + \mu + \frac{\varepsilon}{\mu+1}(\mathrm{x} - \sqrt{\mu}), \\ \frac{\sigma}{l} &= \frac{1}{2\sqrt{\mu}} \ln\left|\frac{\mathrm{x}-\sqrt{\mu}}{\mathrm{x}+\sqrt{\mu}}\right| + \frac{\varepsilon}{4\mu(\mu+1)}\left(\ln\left|\frac{\mathrm{x}-\sqrt{\mu}}{\mathrm{x}+\sqrt{\mu}}\right| - \frac{\mathrm{x}-\sqrt{\mu}}{\mathrm{x}+\sqrt{\mu}}\right) \end{aligned} \tag{6.93}$$

We can now straightforwardly determine the event horizon by solving $\Lambda = 0$. One observes that the integration constant in the Ξ-dependent term of Eq. (6.88) is fixed such that the quantum-corrected horizon coincides with the classical one, $\mathrm{x_H} = \sqrt{\mu}$. We then proceed to evaluate the curvature. A direct calculation gives:

$$R = \frac{1}{l^2}\frac{\mathrm{d}^2\Lambda}{\mathrm{dx}^2} = -\frac{2}{l^2} \quad \Longrightarrow \quad \mathrm{x_S} = 0. \tag{6.94}$$

Thus, the singularity does not acquire any quantum corrections as well. The surface gravity is given by:

$$\kappa = \frac{1}{2l}\left|\mathcal{D}\frac{\mathrm{d}\Lambda}{\mathrm{dx}}\right|_{\mathrm{H}} = \frac{\sqrt{\mu}}{l}\left[1 - \frac{\varepsilon}{2(\mu+1)\sqrt{\mu}}\right]. \tag{6.95}$$

To confirm that the solution (6.93) indeed describes an eternal black hole, we must verify that the quantum fields are prepared in the Hartle-Hawking state (3.97). This requirement means that the EMT is normal-ordered in Kruskal coordinates, which are obtained by exponentiating the Eddington-Finkelstein coordinates (see App. D.5), using the surface gravity (6.95). Employing the definition of Ξ (6.80) together with the transformation law for the quantum-corrected EMT (3.83), we find:

$$\frac{1}{4l^2}\Xi = t_\pm(\sigma^\pm) = \left(\frac{\mathrm{d}x^\pm}{\mathrm{d}\sigma^\pm}\right)^2\left[\cancelto{0}{t_\pm}(x^\pm) - \frac{1}{2}D_{x^\pm}[\sigma^\pm]\right] = -\frac{\kappa^2}{4} \quad \Longrightarrow \quad \Xi = -(\kappa l)^2 = -\mu. \tag{6.96}$$

Since this matches Eq. (6.92), the solution (6.93) indeed describes an eternal black hole. We now examine the singular behavior of the tortoise coordinate. Using the surface gravity in Eq. (6.95) leads to:

$$\sigma = \frac{1}{2\kappa}\left[\ln\left|\frac{\mathrm{x}-\sqrt{\mu}}{\mathrm{x}+\sqrt{\mu}}\right| - \frac{\varepsilon}{2(\mu+1)\sqrt{\mu}}\frac{\mathrm{x}-\sqrt{\mu}}{\mathrm{x}+\sqrt{\mu}}\right]. \tag{6.97}$$

In the general static quantum-corrected solution (6.88), the Ξ-dependent term in the tortoise coordinate is chosen so that there is a single logarithmic pole exactly at the quantum-corrected event horizon $\mathrm{x_H} = \sqrt{\mu}$, where the quantum correction vanishes.

The same solution can be derived from the general quantum-corrected configuration (6.78-6.79) by explicitly evaluating the integrals I and I′. In this setting, the solution is given by $(\mathrm{F}^+, \mathrm{F}^-, \mu, -\frac{\mu}{4l^2}, -\frac{\mu}{4l^2})$. Care is required, since these integrals are defined only up to arbitrary functions, which must be fixed by substituting the solution back into the original equations of motion. An analogous analysis for the DREH model appears in Sec. 5.2.3.

6.3 Evaporating black hole scenario

The evaporating black hole scenario covers both the gravitational collapse forming the black hole and its later Hawking-radiation-driven evaporation. We use the framework of Sec. 3.4, adapted to an asymptotically AdS spacetime.

In Sec. 6.1.4, we studied purely classical gravitational collapse, and in Sec. 6.1.5 we constructed its conformal diagram. We now extend this to the quantum-corrected case. Including the back-reaction of quantum fields on the classical geometry yields an evaporating black hole. As in the BPP model—and unlike the DREH model—the initial spacetime cannot be the AdS vacuum. We therefore use the quantum-corrected AdS spacetime defined in Eq. (6.90). For an evaporating black hole, the relevant vacuum is the Unruh state (3.98), defined by $t_\pm(\sigma^\pm) = 0$. Although the initial spacetime has zero energy flux at infinity, a nonzero flux appears at future null infinity after the black hole forms, due to the change in asymptotic coordinates (see Sec. 3.4).

The quantum-corrected collapse scenario is shown in Fig. 6.4. Before black hole formation, we use the Eddington–Finkelstein gauge, i.e., the $\sigma^\pm$ coordinates of solution (6.90), for which the solution is $(-1, 1, \varepsilon C_0, 0, 0)$. In region II, where an evaporating black hole is present, we use Eddington–Finkelstein coordinates $\hat{\sigma}^\pm$, and the solution is $(-1, \mathrm{F}^-, \mu, 0, t_-(\hat{\sigma}^-))$. We must therefore determine $t_\pm(\hat{\sigma}^\pm)$ via the transformation law (3.83). Since the coordinate transformation (3.6) is written in terms of the functions $\mathrm{F}^\pm$, defined in Eq. (6.50), this amounts to computing the Schwarzian derivative. The final result is expressed in terms of the coordinate $\hat{\mathrm{x}}$:

$$t_+(\hat{\sigma}^+) = 0, \quad t_-(\hat{\sigma}^-) = -\frac{\mu}{4l^2}. \tag{6.98}$$

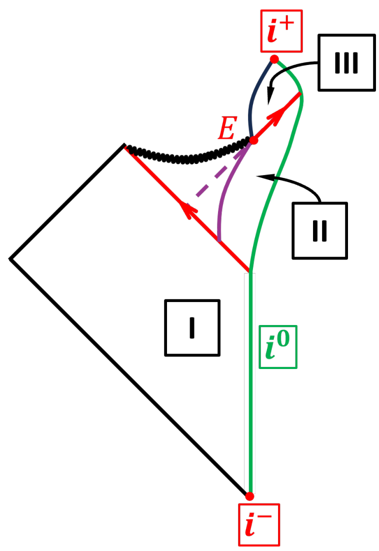

Figure 6.4: Penrose diagram of the quantum-corrected gravitational collapse for the BTZ black hole.

When the back-reaction is included, the classical spacetime depicted in Fig. 6.3 acquires a third region as illustrated in Fig. 6.4. This additional region represents the static remanent spacetime created as a consequence of the black hole evaporation. It is characterized by the end-state geometry. With all necessary ingredients specified, the next task is to determine θ, whose general expression is given in Eq. (6.71). This solution, however, is only fixed up to the integral I in Eq. (6.72). The problem therefore reduces to computing these integrals for the particular choice (6.98). Because $t_+ = 0$, the integral I_+ vanishes, leaving us solely with the integral I_-:

$$\mathrm{I} = \int \frac{\mathrm{d}\sigma^-}{\mathrm{F}^-} \frac{1}{\mathrm{x}^2 - \mu} \int \frac{\mathrm{d}\sigma^-}{\mathrm{F}^-} t_-(\hat{\sigma}^-). \tag{6.99}$$

We begin by computing the inner integral. Upon applying the substitution in (6.50), the resulting integral evaluates to:

$$\int \frac{\mathrm{d}\sigma^-}{\mathrm{F}^-} t_-(\hat{\sigma}^-) = \frac{\sqrt{\mu}}{4l} \ln \left| \frac{1 + \hat{\mathrm{x}}\sqrt{\mu}}{1 - \hat{\mathrm{x}}\sqrt{\mu}} \right| \equiv \frac{1}{4l} \mathrm{F}(\hat{\mathrm{x}}), \tag{6.100}$$

where we have defined an additional function $\mathrm{F}(\hat{\mathrm{x}})$. Unlike in the DREH model, $\hat{\mathrm{x}}$ can be expressed in terms of the elementary functions of x and δ. As a result, the integral I simplifies to:

$$\mathrm{I} = \frac{\mathrm{x}}{\mathrm{x}^2 - \mu} \frac{1}{4\sqrt{\mu}} \ln \left| \frac{\mathrm{x} - \sqrt{\mu}}{\mathrm{x} + \sqrt{\mu}} \right| + \frac{1}{16\mu} \ln^2 \left| \frac{\mathrm{x} - \sqrt{\mu}}{\mathrm{x} + \sqrt{\mu}} \right| + \frac{1}{4} \frac{1}{\mathrm{x}^2 - \mu} - (\mu + 1)\mathcal{D}_1(\mathrm{x}) \ln \delta, \tag{6.101}$$

where the function $\mathcal{D}_1$ is defined in Eq. (6.75). Plugging this expression into the solution for θ in Eq. (6.71) yields:

$$\begin{aligned} \frac{\theta}{\mathrm{x}^2 - \mu} = \frac{1}{2l} \left(\int \mathrm{d}\sigma^+ \frac{\mathrm{G}^+}{\mathrm{F}^{+2}} + \int \mathrm{d}\sigma^- \frac{\mathrm{G}^-}{\mathrm{F}^{-2}} \right) + \frac{1}{4(\mu + 1)} \left[\frac{1}{4\mu} \ln^2 \left| \frac{\mathrm{x} - \sqrt{\mu}}{\mathrm{x} + \sqrt{\mu}} \right| + \frac{1}{\mathrm{x}^2 - \mu} \right] \\ - \mathcal{D}_1(\mathrm{x}) \left(\ln \delta + C \frac{\mu + 1}{\mu} \right). \end{aligned} \tag{6.102}$$

The metric correction α can be obtained directly from the Equation of motion (6.64). The resulting expression is:

$$(\mathrm{x}^2 - \mu) \left[2\alpha + \frac{\mathrm{G}^+}{\mathrm{F}^+} + \frac{\mathrm{G}^-}{\mathrm{F}^-} \right] - 2\mathrm{x}\theta = \frac{1}{2(\mu + 1)} \left[\frac{\mathrm{x}^2 - \mu}{2\sqrt{\mu}} \ln \left| \frac{\mathrm{x} - \sqrt{\mu}}{\mathrm{x} + \sqrt{\mu}} \right| - \mathrm{x} \right] - \frac{\mu}{\mu + 1} \ln \delta - C. \tag{6.103}$$

Eqs. (6.102) and (6.103) describe the quantum modifications of the tortoise coordinate and of the metric solutions, respectively. Hence, the final form of the solution can be written as:

$$\mathrm{F}^+\mathrm{F}^- e^{2\rho} = -\mathrm{x}^2 + \mu - \frac{\varepsilon}{\mu + 1} \left[\frac{\mathrm{x}^2 - \mu}{4\sqrt{\mu}} \ln \left| \frac{\mathrm{x} - \sqrt{\mu}}{\mathrm{x} + \sqrt{\mu}} \right| - \frac{\mathrm{x}}{2} \right] + \varepsilon \left(\frac{\mu}{\mu + 1} \ln \delta + C \right), \tag{6.104}$$

$$\frac{\hat{\sigma}}{l} = \frac{1}{2\sqrt{\mu}} \ln \left| \frac{\mathrm{x} - \sqrt{\mu}}{\mathrm{x} + \sqrt{\mu}} \right| - \frac{\varepsilon}{4(\mu + 1)} \left[\frac{1}{4\mu} \ln^2 \left| \frac{\mathrm{x} - \sqrt{\mu}}{\mathrm{x} + \sqrt{\mu}} \right| + \frac{1}{\mathrm{x}^2 - \mu} \right] + \varepsilon \mathcal{D}_1 \left(\ln \delta + C \frac{\mu + 1}{\mu} \right). \tag{6.105}$$

Eqs. (6.104) and (6.105) describe a family of evaporating black hole solutions specified by a constant C and by the coordinate transformation F^-. The transformation F^+ cannot vary across the ingoing shockwave hypersurface. The values of C and F^- are uniquely determined once the continuity conditions (3.102) and (3.104) are enforced.

6.3.1 Evaporating black hole solution

In this subsection, we identify the specific solution among (6.104-6.105) that remains continuously connected to the quantum-corrected AdS vacuum solution across the ingoing shockwave hypersurface. In region I, the solution is provided by Eq. (6.90). For clarity, we rewrite it here:

$$e^{2\rho} = \mathrm{x}^2 - \varepsilon \mathrm{x} - \varepsilon C_0, \qquad -\frac{1}{\mathrm{x}} - \frac{\varepsilon}{2\mathrm{x}^2} - \frac{\varepsilon C_0}{3\mathrm{x}^3} = -\ln\delta + \hat{\mathrm{x}}, \tag{6.106}$$

where we have retained the constant C_0, which is linked to the mass of the spacetime in region I. We keep this constant as a diagnostic tool to monitor the energy balance in the model. Nonetheless, from a physical standpoint we must set $C_0 = 0$, because the initial spacetime is required to be massless. Let us now determine the metric and the dilaton field along the ingoing shockwave, that is, on the $\delta = 1$ hypersurface. They are given by:

$$e^{2\rho}\Big|_{\delta=1} = \frac{1}{\hat{\mathrm{x}}^2} - \frac{\varepsilon C_0}{3}, \qquad \mathrm{x}\Big|_{\delta=1} = -\frac{1}{\hat{\mathrm{x}}}\left[1 - \frac{\varepsilon}{2}\hat{\mathrm{x}} + \frac{\varepsilon C_0}{3}\hat{\mathrm{x}}^2\right]. \tag{6.107}$$

The coordinate transformation F^- can now be straightforwardly determined by imposing continuity of the metric across the $\delta = 1$ hypersurface. In this limit, Eq. (6.104) reduces to:

$$\mathrm{F}^- e^{2\rho} = \mathrm{x}^2 - \mu - \varepsilon C + \frac{\varepsilon}{\mu+1}\left[\frac{\mathrm{x}^2-\mu}{4\sqrt{\mu}}\ln\left|\frac{\mathrm{x}-\sqrt{\mu}}{\mathrm{x}+\sqrt{\mu}}\right| - \frac{\mathrm{x}}{2}\right]. \tag{6.108}$$

After inserting Eq. (6.107), we arrive at the explicit expression for $\mathrm{F}^- = \mathrm{F}^-(\hat{\mathrm{x}})$:

$$\mathrm{F}^- = 1 - \left(\mu + \varepsilon(C - C_0)\right)\hat{\mathrm{x}}^2 - \varepsilon\hat{\mathrm{x}} - \frac{\varepsilon\mu C_0}{3}\hat{\mathrm{x}}^4 + \frac{\varepsilon}{\mu+1}\left[\frac{1-\mu\hat{\mathrm{x}}^2}{4\sqrt{\mu}}\ln\left|\frac{1+\hat{\mathrm{x}}\sqrt{\mu}}{1-\hat{\mathrm{x}}\sqrt{\mu}}\right| + \frac{\hat{\mathrm{x}}}{2}\right]. \tag{6.109}$$

Next, we enforce the "++" equation condition (3.104), which in the DR5DCS model takes the form:

$$\left[\left(\mathrm{x}^2 + 1 - \frac{1}{2}l^2\left(\nabla\mathrm{x}\right)^2\right)\partial_+\mathrm{x} + \varepsilon\partial_+\rho\right]\Bigg|_<^> = -\frac{M}{6k\pi^2}\Bigg|_{x^+=x_0^+}, \tag{6.110}$$

where $>$ and $<$ refer to the sides of region II and region I relative to the $\delta = 1$ hypersurface. Upon substituting solution (6.106) in region I and solutions (6.104-6.105) in region II, Eq. (6.110) simplifies to:

$$\mu(\mu+2) + 2\varepsilon\left((\mu+1)C - C_0\right) = \frac{2Ml}{3k\pi^2}. \qquad \Longrightarrow \qquad C = \frac{C_0}{\mu+1}, \tag{6.111}$$

where we have employed the classical relation (6.52) connecting the mass to the parameter μ. Now that both F^- and C are fixed, we proceed to evaluate the $\hat{\sigma}^-$ coordinate. A straightforward integration gives:

$$\begin{aligned}\frac{\sigma_0^+ - \hat{\sigma}^-}{2l} = \frac{1}{2\sqrt{\mu}}\ln\left|\frac{1+\hat{\mathrm{x}}\sqrt{\mu}}{1-\hat{\mathrm{x}}\sqrt{\mu}}\right| - \frac{\varepsilon}{4(\mu+1)}\left[\frac{1}{4\mu}\ln^2\left|\frac{1+\hat{\mathrm{x}}\sqrt{\mu}}{1-\hat{\mathrm{x}}\sqrt{\mu}}\right| + \frac{\hat{\mathrm{x}}^2}{1-\mu\hat{\mathrm{x}}^2}\right] + \frac{\varepsilon}{2}\frac{\hat{\mathrm{x}}^2}{1-\mu\hat{\mathrm{x}}^2} \\ + \frac{\varepsilon C_0}{3\mu}\left[(1-2\mu)\mathcal{D}_1\left(-\frac{1}{\hat{\mathrm{x}}}\right) - \frac{1}{2\sqrt{\mu}}\ln\left|\frac{1+\hat{\mathrm{x}}\sqrt{\mu}}{1-\hat{\mathrm{x}}\sqrt{\mu}}\right| + \hat{\mathrm{x}}\right].\end{aligned} \tag{6.112}$$

Hence, the solution describing an evaporating black hole can be written as:

$$\mathrm{F}^+\mathrm{F}^- e^{2\rho} = -\mathrm{x}^2 + \mu + \frac{\varepsilon}{\mu+1}\left[\mu \ln\delta + C_0 - \frac{\mathrm{x}^2-\mu}{4\sqrt{\mu}}\ln\left|\frac{\mathrm{x}-\sqrt{\mu}}{\mathrm{x}+\sqrt{\mu}}\right| + \frac{\mathrm{x}}{2}\right], \tag{6.113}$$

$$\begin{aligned}\frac{1}{2\sqrt{\mu}}\ln\left|\frac{\mathrm{x}-\sqrt{\mu}}{\mathrm{x}+\sqrt{\mu}}\right| - \frac{\varepsilon}{4(\mu+1)}\left[\frac{1}{4\mu}\ln^2\left|\frac{\mathrm{x}-\sqrt{\mu}}{\mathrm{x}+\sqrt{\mu}}\right| + \frac{1}{\mathrm{x}^2-\mu}\right] + \frac{\varepsilon}{\mu}\left(\mu\ln\delta + C_0\right)\mathcal{D}_1(\mathrm{x}) \quad (6.114)\\ = -\ln\delta + \frac{1}{2\sqrt{\mu}}\ln\left|\frac{1+\hat{\mathrm{x}}\sqrt{\mu}}{1-\hat{\mathrm{x}}\sqrt{\mu}}\right| - \frac{\varepsilon}{4(\mu+1)}\left[\frac{1}{4\mu}\ln^2\left|\frac{1+\hat{\mathrm{x}}\sqrt{\mu}}{1-\hat{\mathrm{x}}\sqrt{\mu}}\right| + \frac{\hat{\mathrm{x}}^2}{1-\mu\hat{\mathrm{x}}^2}\right] + \frac{\varepsilon}{2}\frac{\hat{\mathrm{x}}^2}{1-\mu\hat{\mathrm{x}}^2}\\ + \frac{\varepsilon C_0}{3\mu}\left[(1-2\mu)\mathcal{D}_1\left(-\frac{1}{\hat{\mathrm{x}}}\right) - \frac{1}{2\sqrt{\mu}}\ln\left|\frac{1+\hat{\mathrm{x}}\sqrt{\mu}}{1-\hat{\mathrm{x}}\sqrt{\mu}}\right| + \hat{\mathrm{x}}\right].\end{aligned}$$

The solution takes the form $\left(-1, \mathrm{F}^-, \sqrt{1+\frac{2Ml}{3k\pi^2}} - 1 + \frac{\varepsilon C_0}{\mu+1}, 0, -\frac{\mu}{4l^2}\right)$, where F^- is defined in Eq. (6.109). One can readily verify that Eq. (6.114) remains valid on the $\delta = 1$ hypersurface. Substituting the expression for x from Eq. (6.107) and expanding the left-hand side in powers of ε, we find that it coincides with the right-hand side, viewed as a function of $\hat{\mathrm{x}}$.

6.3.2 Evaporation adapted form of the solution

In this subsection, we follow the approach of Sec. 5.3.3, where the solution in the DREH model was recast into a form that is manifestly well defined on the classical horizon. The metric in Eq. (6.113) is already well defined at the horizon. The tortoise coordinate (6.114), however, does not display the well behavior there. It should exhibit a pole along a well defined hypersurface, but in its current form of the solution, one cannot readily find that hypersurface. Our goal in this section is to resolve this issue. For convenience, we set $C_0 = 0$. We begin by evaluating the derivatives of the dilaton field, which are:

$$\partial_+\mathrm{x} = \frac{1}{2l}\left[\mathrm{x}^2 - \tilde{\mu} - \frac{\varepsilon}{\mu+1}\mathrm{x}\right], \tag{6.115}$$

$$\partial_-\mathrm{x} = -\frac{1}{2l\mathrm{F}^-}\left[\mathrm{x}^2 - \tilde{\mu} + \frac{\varepsilon}{\mu+1}\left(\frac{\mathrm{x}^2-\mu}{4\sqrt{\mu}}\ln\left|\frac{\mathrm{x}-\sqrt{\mu}}{\mathrm{x}+\sqrt{\mu}}\right| - \frac{\mathrm{x}}{2}\right)\right], \tag{6.116}$$

where we have defined the reduced parameter $\tilde{\mu}$ as follows:

$$\tilde{\mu} = \mu + \frac{\varepsilon}{\mu+1}\Big(\mu\ln\delta + C_0\Big). \tag{6.117}$$

Next, we define a new constant $\mathrm{y} = \mathrm{x}/\sqrt{\tilde{\mu}}$. Our goal is to determine a function $\mathcal{J}(\mathrm{y})$ such that $\mathcal{J}(\mathrm{y})/\sqrt{\tilde{\mu}} = \frac{\sigma^+}{2l}$. Differentiating this relation with respect to σ^+ and inserting expression (6.115), we obtain the following first-order differential equation for $\mathcal{J}$:

$$\left[\mathrm{y}^2 - 1 - \frac{\varepsilon}{2(\mu+1)\sqrt{\mu}}\mathrm{y}\right]\frac{\mathrm{d}\mathcal{J}}{\mathrm{dx}} + \frac{\varepsilon}{2(\mu+1)\sqrt{\mu}}\mathcal{J} = 1. \tag{6.118}$$

The general form of the solution to this equation of motion is given by:

$$\mathcal{J}(\mathrm{y}) = \frac{2(\mu+1)\sqrt{\mu}}{\varepsilon}\left(1 - e^{-f(\mathrm{y})}\right) + Se^{-f(\mathrm{y})}, \tag{6.119}$$

where S denotes an arbitrary constant, and the function $f(\mathrm{y})$ is defined as:

$$f(\mathrm{y}) = \frac{\varepsilon}{2(\mu+1)\sqrt{\mu}} \int \frac{\mathrm{dy}}{\mathrm{y}^2 - 1 - \frac{\varepsilon}{2(\mu+1)\sqrt{\mu}}\mathrm{y}} = \frac{\varepsilon}{2(\mu+1)\sqrt{\mu}} \frac{1}{\mathrm{y}_+ - \mathrm{y}_-} \ln\left|\frac{\mathrm{y}-\mathrm{y}_+}{\mathrm{y}-\mathrm{y}_-}\right|, \tag{6.120}$$

where $\mathrm{y}_\pm$ are solutions of the following quadratic equation:

$$\mathrm{y}^2 - 1 - \frac{\varepsilon}{2(\mu+1)\sqrt{\mu}}\mathrm{y} = 0 \quad \Longrightarrow \quad \mathrm{y}_\pm = \pm 1 + \frac{\varepsilon}{4(\mu+1)\sqrt{\mu}}. \tag{6.121}$$

We have expanded the roots of the given quadratic equation to first order in ε. For the consistency check, we expand the function $\mathcal{J}$ (6.119) to first order in y:

$$\begin{aligned}
f(\mathrm{y}) &= \frac{\varepsilon}{4(\mu+1)\sqrt{\mu}}\left[\ln\left|\frac{\mathrm{y}-1}{\mathrm{y}+1}\right| - \frac{\varepsilon}{2(\mu+1)\sqrt{\mu}}\frac{1}{\mathrm{y}^2-1}\right],\\
\mathcal{J}(\mathrm{y}) &= \frac{2(\mu+1)\sqrt{\mu}}{\varepsilon}\left(f(\mathrm{y}) - \frac{1}{2}f^2(\mathrm{y})\right) + S\left(1 - f(\mathrm{y})\right),\\
&= \frac{1}{2}\ln\left|\frac{\mathrm{y}-1}{\mathrm{y}+1}\right| - \frac{\varepsilon}{4(\mu+1)\sqrt{\mu}}\left[\frac{1}{4}\ln^2\left|\frac{\mathrm{y}-1}{\mathrm{y}+1}\right| + \frac{1}{\mathrm{y}^2-1}\right] + S\left[1 - \frac{\varepsilon}{4(\mu+1)\sqrt{\mu}}\ln\left|\frac{\mathrm{y}-1}{\mathrm{y}+1}\right|\right],\\
\frac{\mathcal{J}(\mathrm{y})}{\sqrt{\tilde{\mu}}} &= \frac{1}{2\sqrt{\mu}}\ln\left|\frac{\mathrm{x}-\sqrt{\mu}}{\mathrm{x}+\sqrt{\mu}}\right| - \frac{\varepsilon}{4(\mu+1)}\left[\frac{1}{4\mu}\ln^2\left|\frac{\mathrm{x}-\sqrt{\mu}}{\mathrm{x}+\sqrt{\mu}}\right| + \frac{1}{\mathrm{x}^2-\mu}\right] + \frac{\varepsilon}{\mu}\left(\mu\ln\delta + C_0\right)\mathcal{D}_1(\mathrm{x})\\
&\quad + S\left[1 - \frac{\varepsilon}{4\mu(\mu+1)}\ln\left|\frac{\mathrm{x}-\sqrt{\mu}}{\mathrm{x}+\sqrt{\mu}}\right|\right].
\end{aligned} \tag{6.122}$$

We therefore find that the functional $\mathcal{J}$ correctly reproduces the left-hand side of the solution (6.114) for the dilaton field in the case $S = 0$. Next, we impose $C_0 = 0$ and likewise recast the right-hand side of that equation:

$$\frac{1}{\sqrt{\tilde{\mu}}}\mathcal{J}\left(\frac{\mathrm{x}}{\sqrt{\tilde{\mu}}}\right) = -\ln\delta + \frac{1}{\sqrt{\mu}}\mathcal{J}\left(-\frac{1}{\hat{\mathrm{x}}\sqrt{\tilde{\mu}}}\right), \qquad \tilde{\mu} = \mu\left(1 + \varepsilon\hat{\mathrm{x}}\right). \tag{6.123}$$

Thus, the appropriate pole in the dilaton solution is determined by the pole of the $\mathcal{J}$ function, namely $\mathrm{y} = \mathrm{y}_+ = 1 + \frac{\varepsilon}{4(\mu+1)\sqrt{\mu}}$, expanded to first order in ε. We now examine the behavior of the solution in the vicinity of the classical horizon, that is, for $\mathrm{y} = 1 + \frac{\varepsilon}{4(\mu+1)\sqrt{\mu}}\eta$ and $-\frac{1}{\hat{\mathrm{x}}\sqrt{\tilde{\mu}}} = 1 + \frac{\varepsilon}{4(\mu+1)\sqrt{\mu}}\vartheta$. Eq. (6.123) can be recast in the following form:

$$\frac{\mu}{\tilde{\mu}}e^{-2f(\mathrm{y})} = e^{-2f(-1/(\sqrt{\tilde{\mu}}\hat{\mathrm{x}}))} \quad \Longrightarrow \quad \left(\frac{\tilde{\mu}}{\mu}\right)^{\frac{2(\mu+1)\sqrt{\mu}}{\varepsilon}}\left|\frac{\mathrm{y}-\mathrm{y}_+}{\mathrm{y}-\mathrm{y}_-}\right| = \left|\frac{-\frac{1}{\hat{\mathrm{x}}\sqrt{\tilde{\mu}}} - \mathrm{y}_+}{-\frac{1}{\hat{\mathrm{x}}\sqrt{\tilde{\mu}}} - \mathrm{y}_-}\right|, \tag{6.124}$$

where the implication follows after raising the equation to the power $-\frac{2(\mu+1)\sqrt{\mu}}{\varepsilon}$. This relation is valid for all values of y and $\hat{\mathrm{x}}$. We now examine the behavior in the vicinity of the classical horizon. Because both sides of the equation are already of order ε, we can safely take the limit $\varepsilon \to 0$ in the remaining parts of the equation. This leads to:

$$\left|\frac{\vartheta-1}{\eta-1}\right| = \left(1 + \frac{\varepsilon}{\mu+1}\ln\delta\right)^{\frac{2(\mu+1)\sqrt{\mu}}{\varepsilon}} \quad \Longrightarrow \quad \left|\frac{\vartheta-1}{\eta-1}\right| = \delta^{2\sqrt{\mu}}. \tag{6.125}$$

Here, the final result arises from taking the limit $\varepsilon \to 0$ on the left-hand side of the equation.

6.3.3 The end-state of black hole evolution

In the previous subsections evaporating black hole has been found, which resides in region II of the spacetime illustrated in Fig. 6.4. The final state of black hole evaporation characterizes both the quantum matter fields in region III and the ultimate geometry of region III. To investigate this end-state, we must first establish that region III indeed exists. As discussed in Sec. 3.4.1, evaporation terminates when the singularity intersects the apparent horizon. Consequently, we must first identify the hypersurfaces corresponding to the apparent horizon and the singularity. The apparent horizon is specified by the condition $\partial_+ e^{-3\phi} = 0$. Employing Eq. (6.115), we obtain:

$$\mathrm{x}^2 - \mu - \frac{\varepsilon}{\mu+1}\left(\mu \ln\delta + C_0\right) - \frac{\varepsilon}{\mu+1}\mathrm{x} = 0 \quad\Longrightarrow\quad \mathrm{x}_{\mathrm{AH}}^2 = \mu\left[1 + \frac{\varepsilon}{\mu+1}\left(\ln\delta + \frac{C_0}{\mu} + \frac{1}{\sqrt{\mu}}\right)\right]. \tag{6.126}$$

For $\delta \approx 1$, the apparent horizon lies close to the classical horizon. As δ decreases, however, $\ln\delta$ becomes more negative, which in turn reduces the radius of the apparent horizon. Consequently, at late times (corresponding to smaller values of δ), it approaches the classical singularity. This is the desired behavior from the standpoint of black hole evaporation, as it indicates that the black hole shrinks over time. Because the apparent horizon initially coincides with the classical horizon at the onset of evaporation, it is more conveniently described in the y coordinate:

$$\mathrm{y}_{\mathrm{AH}} = \sqrt{1 + \frac{\varepsilon}{(\mu+1)\sqrt{\mu}}}. \tag{6.127}$$

We observe that, in this y coordinate, the apparent horizon remains at a fixed value. As demonstrated in the preceding subsection, the y coordinate is well defined throughout the evaporation process, so we may extend our analysis to any time.

Next, we express the apparent horizon in terms of the $\hat{\mathrm{x}}$ coordinate. For this purpose, we employ Eq. (6.125), noting that both y and $-1/(\hat{\mathrm{x}}\sqrt{\mu})$ lie close to the classical horizon. After some algebraic manipulation, we obtain:

$$-\frac{1}{\hat{\mathrm{x}}_{\mathrm{AH}}} = \sqrt{\mu} - \frac{\varepsilon}{2} + \frac{\varepsilon}{4(\mu+1)}\left(1 + \delta_{\mathrm{AH}}^{2\sqrt{\mu}}\right), \tag{6.128}$$

where we have used the fact that $\eta = 2$ for y_{AH}.

To identify the singularity line, we first calculate the scalar curvature. A detailed analysis reveals that the scalar curvature receives no quantum corrections, so we have $R = -2/l^2$. Consequently, the singularity remains located at $\mathrm{x}_{\mathrm{S}} = 0$, or, equivalently, at $\mathrm{y}_{\mathrm{S}} = 0$. Inserting $\mathrm{y}_{\mathrm{S}} = 0$ into Eq. (6.124) gives:

$$\sqrt{\mu}\hat{\mathrm{x}}_{\mathrm{S}} = \hat{\mathrm{x}}_{\mathrm{S}}\sqrt{\mu} + \frac{\varepsilon}{\sqrt{\mu}}\hat{\mathrm{x}}_{\mathrm{S}}^2 = \frac{\mathrm{y}_+\left(1 + \frac{\varepsilon}{\mu+1}\ln\delta_{\mathrm{S}}\right)^{\frac{2(\mu+1)\sqrt{\mu}}{\varepsilon}} + \mathrm{y}_+^{-1}}{\left(1 + \frac{\varepsilon}{\mu+1}\ln\delta_{\mathrm{S}}\right)^{\frac{2(\mu+1)\sqrt{\mu}}{\varepsilon}} - 1}, \tag{6.129}$$

where y_+ is defined in Eq. (6.121). In the limit $\varepsilon \to 0$, the singular line reduces to the classical one given in Eq. (6.56). This provides a straightforward consistency test of our perturbative method. An analogous statement holds for the quantum-corrected spatial infinity hypersurface i^0, which is given by:

$$\sqrt{\mu}\hat{\mathrm{x}}_{i^0} = \hat{\mathrm{x}}_{i^0}\sqrt{\mu} + \frac{\varepsilon}{\sqrt{\mu}}\hat{\mathrm{x}}_{i^0}^2 = \frac{\mathrm{y}_+\left(1 + \frac{\varepsilon}{\mu+1}\ln\delta_{i^0}\right)^{\frac{2(\mu+1)\sqrt{\mu}}{\varepsilon}} - \mathrm{y}_+^{-1}}{\left(1 + \frac{\varepsilon}{\mu+1}\ln\delta_{i^0}\right)^{\frac{2(\mu+1)\sqrt{\mu}}{\varepsilon}} + 1}. \tag{6.130}$$

The end-point of the evaporation

The cosmic censorship conjecture [106] rules out the occurrence of naked singularities. In the present context, the singularity becomes naked once it intersects the apparent horizon hypersurface. The intersection point is referred to as the end-point of the evaporation. By setting Eq. (6.126) equal to Eq. (6.129), we obtain:

$$\ln \delta_{\mathrm{E}} = -\frac{\mu+1}{\varepsilon} - \frac{C_0}{\mu} - \frac{1}{\sqrt{\mu}}. \tag{6.131}$$

Next, we determine the remaining coordinate. Substituting $\ln \delta_{\mathrm{E}}$ directly into (6.128) gives:

$$\delta_{\mathrm{E}} = e^{-\frac{\mu+1}{\varepsilon}-\frac{1}{\sqrt{\mu}}} \quad \wedge \quad \hat{\mathrm{x}}_{\mathrm{E}} = -\frac{1}{\sqrt{\mu}}\left[1 + \frac{\varepsilon}{2\sqrt{\mu}} - \frac{\varepsilon}{4(\mu+1)\sqrt{\mu}} e^{-\frac{\mu+1}{\varepsilon}-\frac{1}{\sqrt{\mu}}}\right]. \tag{6.132}$$

Therefore, the evaporation end-point shows the same type of singular behavior in the limit $\varepsilon \to 0$ as in both the BPP model (4.124) and the DREH model (5.205-5.206). The event horizon is determined by the condition $\hat{\mathrm{x}}_{\mathrm{H}} = \hat{\mathrm{x}}_{\mathrm{E}}$. Employing Eq. (6.125), we can express the y-coordinate of the event horizon in terms of δ as follows:

$$\mathrm{y}_{\mathrm{H}} = 1 + \frac{\varepsilon}{4(\mu+1)\sqrt{\mu}}\left(1 + \frac{\delta_{\mathrm{E}}}{\delta_{\mathrm{H}}}\right). \tag{6.133}$$

The horizon may also be expressed as a dependence of the dilaton field on the δ coordinate:

$$\mathrm{x}_{\mathrm{H}}^2 = \mu\left[1 + \frac{\varepsilon}{\mu+1}\left(\ln \delta_{\mathrm{H}} + \frac{1}{2\sqrt{\mu}}\left(1 + \frac{\delta_{\mathrm{E}}}{\delta_{\mathrm{H}}}\right)\right)\right]. \tag{6.134}$$

At the beginning of the evaporation the event horizon appears near the classical horizon, because in this regime one has $\delta_{\mathrm{E}} \ll \frac{\varepsilon}{\mu+1} \ll 1$. In this case, it is simply displaced from the classical horizon by $\frac{\varepsilon}{4(\mu+1)}$. As δ evolves towards the end-point of the evaporation, x_{H} tends to zero. We thus deduce that, at the evaporation end-point, all three hypersurfaces—the apparent horizon (6.126), the event horizon (6.134), and the singularity $\mathrm{x}_{\mathrm{S}} = 0$ intersect at the end-point of the evaporation. We now proceed to evaluate the evaporation time, whose leading contribution is:

$$\Delta t_{\mathrm{E}} = \frac{72\pi^3 klc^2}{\hbar}\sqrt{1 + \frac{2ML}{3k\pi^2c^2}}, \tag{6.135}$$

where we have returned all physical constants. It follows that, in large mass limit, the evaporation time in the DR5DCS model scales as $\sqrt{M}$. Observe that all hypersurfaces were evaluated in the limit $C_0 = 0$, because Eq. (6.123) is valid only in this case. We therefore conclude that the behavior of all relevant hypersurfaces coincides with that found in the DREH model. Further discussion can be found in Sec. 5.3.

The radiated energy

The subsequent step is to evaluate the total energy which has been evaporated from the black hole via Hawking radiation, following the procedure outlined in Sec. 3.4.1. Nonetheless, expression (3.115) is not applicable for an asymptotically AdS spacetime, since the metric diverges near the asymptotic boundary. Consequently, the conventional definition of energy also becomes divergent. We are therefore required to renormalize the energy expression in light of this behavior. The dilaton field scales as $\mathrm{x} = 1/\epsilon$ with $\epsilon \to 0$. In this limit, the metric assumes the following form:

$$ds^2 = -e^{2\rho}\mathrm{d}\sigma^+\mathrm{d}\sigma^- \approx \frac{1}{\epsilon^2}\frac{\mathrm{d}\sigma^+}{\mathrm{d}\hat{\mathrm{x}}}\frac{2l}{\mathrm{F}^-}\mathrm{d}\hat{\mathrm{x}}^2 \equiv -\frac{\mathrm{d}\tau^2}{\epsilon^2}, \tag{6.136}$$

where we have defined the parameter τ along the hypersurface at spatial infinity, as specified in Eq. (6.130). The total energy is therefore:

$$\begin{aligned}
E_{rad} &= \int_{\tau_0}^{\tau_{\mathrm{E}}} \mathrm{d}\tau \langle \Delta T_{\tau\tau}^{(f)}\rangle \\
&= 2l\int_0^{\hat{\mathrm{x}}_{\mathrm{E}}}\frac{\mathrm{d}\hat{\mathrm{x}}}{\mathrm{F}^-}\left[\left(\frac{\mathrm{d}\sigma^+}{\mathrm{d}\tau}\right)^2\langle\Delta T_{++}^{(f)}\rangle + \left(\frac{\mathrm{d}\sigma^-}{\mathrm{d}\tau}\right)^2\cancelto{0}{\langle\Delta T_{--}^{(f)}\rangle} + 2\left(\frac{\mathrm{d}\sigma^+}{\mathrm{d}\tau}\right)\left(\frac{\mathrm{d}\sigma^-}{\mathrm{d}\tau}\right)\cancelto{0}{\langle\Delta T_{+-}^{(f)}\rangle}\right] \\
&= 2l\int_0^{\hat{\mathrm{x}}_{\mathrm{E}}}\frac{\mathrm{d}\hat{\mathrm{x}}}{\mathrm{F}^-}\langle\Delta T_{++}^{(f)}\rangle = -\frac{\hbar\mu}{24\pi l}\int_0^{\hat{\mathrm{x}}_{\mathrm{E}}}\frac{\mathrm{d}\hat{\mathrm{x}}}{\mathrm{F}^-} = -\frac{3k\pi^2}{l}\mu\varepsilon\int_0^{\hat{\mathrm{x}}_{\mathrm{E}}}\frac{\mathrm{d}\hat{\mathrm{x}}}{\mathrm{F}^-} = -\frac{3k\pi^2}{l}\mu\varepsilon\frac{\sigma_0^+ - \hat{\sigma}_{\mathrm{E}}^-}{2l} \\
&= -\frac{3k\pi^2}{2l}\varepsilon\sqrt{\mu}\ln\left|\frac{1+\hat{\mathrm{x}}_{\mathrm{E}}\sqrt{\mu}}{1-\hat{\mathrm{x}}_{\mathrm{E}}\sqrt{\mu}}\right| \quad \Longrightarrow \quad \mu_{rad}(\mu_{rad}+2) = -\varepsilon\sqrt{\mu}\ln\left|\frac{1+\hat{\mathrm{x}}_{\mathrm{E}}\sqrt{\mu}}{1-\hat{\mathrm{x}}_{\mathrm{E}}\sqrt{\mu}}\right|,
\end{aligned} \tag{6.137}$$

where we have introduced a μ-parameter associated with the radiated energy. In the second line, we use the fact that the only nonvanishing component of the quantum-corrected EMT is the "++" component. There, we substitute its explicit expression, $\langle\Delta T_{++}^{(f)}\rangle = -\frac{\mu}{4l^2}$, and observe that the integral simplifies to the definition of the $\hat{\sigma}^-$ coordinate. The third line provides the first-order solution to the integral.

6.3.4 The end-state geometry

As outlined in Sec. 3.4.1, the final step of formulating the quantum-corrected gravitational collapse scenario is to specify the geometry of region III of the spacetime shown in Fig. 6.4. In what follows, we retain the constant C_0, as our goal is to examine how the energy balance is modified throughout the evaporation process. We start by expressing the evaporating black hole solution (6.113-6.114) in terms of the dilaton field and the $\hat{\mathrm{x}}$ coordinate:

$$\mathrm{F}^+\mathrm{F}^-e^{2\rho} = -\mathrm{x}^2 + \hat{\mu} + \frac{\varepsilon C_0}{\mu+1} - \frac{\varepsilon}{\hat{\mu}+1}\left[\frac{\mathrm{x}^2+\hat{\mu}}{4\sqrt{\hat{\mu}}}\ln\left|\frac{\mathrm{x}-\sqrt{\hat{\mu}}}{\mathrm{x}+\sqrt{\hat{\mu}}}\right| - \frac{\mathrm{x}}{2}\right], \tag{6.138}$$

$$\begin{aligned}
\frac{\hat{\sigma}}{l} &= \frac{1}{2\sqrt{\hat{\mu}}}\ln\left|\frac{\mathrm{x}-\sqrt{\hat{\mu}}}{\mathrm{x}+\sqrt{\hat{\mu}}}\right| - \frac{\varepsilon}{4(\hat{\mu}+1)}\left[\frac{1}{4\hat{\mu}}\ln^2\left|\frac{\mathrm{x}-\sqrt{\hat{\mu}}}{\mathrm{x}+\sqrt{\hat{\mu}}}\right| + \frac{1}{\mathrm{x}^2-\hat{\mu}}\right] \\
&\quad + \varepsilon\left(\frac{C_0}{\hat{\mu}} - \frac{1}{2\sqrt{\hat{\mu}}}\ln\left|\frac{\mathrm{x}-\sqrt{\hat{\mu}}}{\mathrm{x}+\sqrt{\hat{\mu}}}\right|\right)\mathcal{D}_1(\mathrm{x}),
\end{aligned} \tag{6.139}$$

where we have introduced a running μ-parameter:

$$\hat{\mu} = \mu\left(1 + \frac{\varepsilon}{2(\mu+1)\sqrt{\mu}}\ln\left|\frac{1+\hat{\mathrm{x}}\sqrt{\mu}}{1-\hat{\mathrm{x}}\sqrt{\mu}}\right|\right). \tag{6.140}$$

Next, we evaluate this parameter on the hypersurface $\hat{\mathrm{x}} = \hat{\mathrm{x}}_{\mathrm{E}}$. Observing that the ε-dependent contribution is proportional to the $\hat{\sigma}^-$ coordinate, and employing Eq. (6.123), we obtain:

$$\begin{aligned}
\hat{\mu}_{\mathrm{E}} &= \mu\left[1 + \frac{\varepsilon}{\mu+1}\frac{1}{\sqrt{\mu}}\mathcal{J}\left(-\frac{1}{\hat{\mathrm{x}}_{\mathrm{E}}\sqrt{\mu}}\right)\right] = \mu\left[1 + \frac{\varepsilon}{\mu+1}\left(\ln\delta_{\mathrm{E}} + \frac{1}{\sqrt{\tilde{\mu}}_{\mathrm{E}}}\mathcal{J}(0)\right)\right] \\
&= -\frac{\varepsilon}{\mu+1}\left(C_0 + \sqrt{\mu}\right),
\end{aligned} \tag{6.141}$$

where we have used $f(0) = \frac{1}{2}\left(\frac{\varepsilon}{2(\mu+1)\sqrt{\mu}}\right)^2$, which implies $\mathcal{J}(0) = \frac{\varepsilon}{4(\mu+1)\sqrt{\mu}} = \mathcal{O}(\varepsilon)$. Consequently, $\mathcal{J}(0)$ can be discarded as it only contributes at order $\mathcal{O}(\varepsilon)$. In the second line we substitute the expression for $\delta_{\rm E}$ from Eq. (6.131). It follows that $\hat{\mu}_{\rm E}$ is a first-order quantity in the perturbation theory. Hence, within the first-order contributions of Eqs. (6.138-6.139) evaluated on the hypersurface $\hat{\rm x} = \hat{\rm x}_{\rm E}$—which separates regions II and III in Fig. 6.4—we may safely take the limit $\hat{\mu}_{\rm E} \to 0$. Implementing this limit gives:

$$\begin{aligned} \mathrm{F}^+\mathrm{F}^- e^{2\rho} &= -\mathrm{x}^2 + \varepsilon \mathrm{x} + \hat{\mu}_{\rm E} + \frac{\varepsilon C_0}{\mu+1}, \\ \frac{\hat{\sigma}}{l} &= -\frac{1}{\mathrm{x}} - \frac{\varepsilon}{2\mathrm{x}^2} - \frac{\hat{\mu}_{\rm E} + \frac{\varepsilon C_0}{\mu+1}}{3\mathrm{x}^3}. \end{aligned} \tag{6.142}$$

Since no further coordinate transformation such as the $\hat{\rm x} = \hat{\rm x}_{\rm E}$ hypersurface is traversed, the geometry in region III is described by the solution (6.142). We can directly observe that this corresponds to the quantum-corrected AdS vacuum solution (6.90) for a particular choice of the constant C_f:

$$\varepsilon C_f = \hat{\mu}_{\rm E} + \frac{\varepsilon C_0}{\mu+1} = -\frac{\varepsilon\sqrt{\mu}}{\mu+1} \quad \Longrightarrow \quad C_f = -\frac{\varepsilon\sqrt{\mu}}{\mu+1}. \tag{6.143}$$

Consequently, in direct analogy with the BPP model (see Sec. 4.3.4), the resulting geometry is independent of the particular choice of the initial geometry. We emphasize that we have not taken the limit $\mu \to 0$ in the terms containing the constant C_0. This is because C_0 contributes to the constant C in region II (6.111), and therefore must remain fixed.

Finally, we need to determine whether a thunderpop emerging from the end-point of the evaporation. To this end, we consider the "$--$" Equation from Eqs. (6.59). Integrating it across the dividing hypersurface $\hat{\rm x} = \hat{\rm x}_{\rm E}$ yields:

$$\left[\left(\mathrm{x}^2 + 1 - \frac{1}{2}l^2 \left(\nabla \mathrm{x}\right)^2\right) \partial_- \mathrm{x} + \varepsilon \partial_- \rho\right] \Bigg|_<^> = \frac{\Delta M}{6k\pi^2 \mathrm{F}^-}\Bigg|_{\hat{\rm x} = \hat{\rm x}_{\rm E}}, \tag{6.144}$$

where ">" designates region III, while "<" designates region II. The shockwave mass is represented by ΔM. Inserting the solutions (6.113-6.114) and (6.142) gives:

$$\begin{aligned} -\hat{\mu}_{\rm E}\left(\hat{\mu}_{\rm E} + 2\right) + 2\varepsilon(C_f - C_0) + \varepsilon\sqrt{\hat{\mu}_{\rm E}} \ln\left|\frac{\mathrm{x} - \sqrt{\hat{\mu}_{\rm E}}}{\mathrm{x} + \sqrt{\hat{\mu}_{\rm E}}}\right| \\ + \frac{\varepsilon}{\hat{\mu}_{\rm E} + 1}(\mathrm{x}^2 + \hat{\mu}_{\rm E} + 2)\left[\frac{\mathrm{x}^2 - \hat{\mu}_{\rm E}}{4\sqrt{\hat{\mu}_{\rm E}}} \ln\left|\frac{\mathrm{x} - \sqrt{\hat{\mu}_{\rm E}}}{\mathrm{x} + \sqrt{\hat{\mu}_{\rm E}}}\right| + \frac{\mathrm{x}}{2}\right] = \frac{2\Delta M l}{3k\pi^2}. \end{aligned} \tag{6.145}$$

By taking the limit $\hat{\mu}_{\rm E} \to 0$ in the x-dependent terms, this equation simplifies to:

$$-\hat{\mu}_{\rm E}\left(\hat{\mu}_{\rm E} + 2\right) + 2\varepsilon(C_f - C_0) = \frac{2\Delta M l}{3k\pi^2}. \tag{6.146}$$

A direct calculation, carried out strictly to first order in the perturbative parameter, yields the following result:

$$\hat{\mu}_{\rm E}\left(\hat{\mu}_{\rm E} + 2\right) = \mu(\mu+2) + \varepsilon\sqrt{\mu} \ln\left|\frac{1 + \hat{\rm x}_{\rm E}\sqrt{\mu}}{1 - \hat{\rm x}_{\rm E}\sqrt{\mu}}\right| = \mu(\mu+2) - \mu_{rad}(\mu_{rad} + 2), \tag{6.147}$$

where we have employed the expression (6.137) for the radiated energy. Consequently, we verify that the black hole has lost nearly all of its mass by the time the evaporation process reaches its end-point. Substituting this relation into Eq. (6.146) yields the following energy balance equation:

$$\mu(\mu+2) = \mu_{rad}(\mu_{rad}+2) + 2\varepsilon(C_f - C_0) - \frac{2\Delta M l}{3k\pi^2}. \tag{6.148}$$

The mass of the initial shockwave, $M \sim \mu(\mu+2)$, together with the mass constant of the pre-collapse geometry, $2\varepsilon C_0$, is equal to the sum of the radiated energy, $E_{\mathrm{rad}} \sim \mu_{\mathrm{rad}}(\mu_{\mathrm{rad}}+2)$, the mass constant of the final geometry, $2\varepsilon C_f$, and the small amount of negative energy, ΔM, carried away by the outgoing shockwave (thunderpop) that appears at the end-point of the evaporation. Therefore, we infer that energy is conserved in the dimensionally reduced model of 5D Chern–Simons gravity.

Substituting the expression for C_f from Eq. (6.143) into the energy balance Eq. (6.148) yields the following formula for the energy of the thunderpop:

$$\Delta M = -\frac{3k\pi^2}{2l}\left(\frac{2\varepsilon\mu C_0}{\mu+1} + \hat{\mu}_{\mathrm{E}}^2\right). \tag{6.149}$$

The first term is proportional to the mass constant of the initial spacetime, which we set to be $C_0 = 0$ for physical reasons. Since $\hat{\mu}_{\mathrm{E}}$ is a quantity of $\mathcal{O}(\varepsilon)$ order, the second term in Eq. (6.149) is not reliable within the first-order perturbative expansion. This implies that there is no thunderpop within the first order, the same result as in the DREH model (5.237). However, we expect that Eq. (6.146) should be of non-perturbative origin, Since Eqs. (6.111) and (6.143) imply that the mass constant of the spacetime is inherited after each discontinuity is crossed, it should also be of non-perturbative origin. This two together give a non-vanishing thunderpop energy but only in higher orders of the perturbation theory.

In summary, the resulting geometry matches one of the static, quantum-corrected AdS vacuum solutions (6.90), characterized by $t_\pm(\hat{\sigma}^\pm) = 0$. Therefore, although there is no discontinuity in the coordinate transformations across $\hat{\mathrm{x}} = \hat{\mathrm{x}}_E$, the quantum state nonetheless transitions from $|0,\sigma\rangle$ to $|0,\hat{\sigma}\rangle$.

Chapter 7

Full dimensionally reduced theory of 5DCS gravity

In this chapter, we study the full dimensionally-reduced theory of five-dimensional Chern–Simons gravity (DR5DCS). The action is obtained in Sec. 2.3 and written explicitly in Eq. (2.47). For convenience, we rewrite it here:

$$
\begin{aligned}
S_{\mathrm{DRCS}_5} =& \frac{k\pi^2}{(\lambda l)^3}\int \mathrm{d}^2x\sqrt{-g}e^{-3\phi}\Bigg\{\left(1+\frac{3}{\mathrm{x}^2}\left(1-\Phi^2-\theta^2\right)\right)\left[\mathrm{R}+2\varepsilon^{\alpha\beta}\partial_\alpha \mathrm{K}_\beta+\frac{2}{l^2}\right] \\
&+\frac{4}{l^2}+\frac{6}{l\mathrm{x}^3}\theta^2\nabla_\alpha\phi^\alpha+\frac{6}{l\mathrm{x}}\left(1+\frac{1}{\mathrm{x}^2}\left(1-\Phi^2-\theta^2\right)\right)\left[\nabla_\alpha\phi^\alpha-\varepsilon^{\alpha\beta}\phi_\alpha \mathrm{K}_\beta\right] \\
&-\frac{6}{\mathrm{x}^2}\left[\nabla_\alpha\phi^\beta\nabla_\beta\phi^\alpha-\nabla_\alpha\phi^\alpha\nabla_\beta\phi^\beta-\varepsilon^{\alpha\beta}\mathrm{K}_\alpha\nabla_\beta\Phi^2\right]\Bigg\}+S_{\mathrm{mat}},
\end{aligned}
\tag{7.1}
$$

where ϕ^μ and θ denote fields originating from the five-dimensional spin-connection, $\mathrm{x} = e^{-\phi}$ is the reduced dilaton field, $\varepsilon^{\alpha\beta}$ is the Levi–Civita tensor, $g_{\mu\nu}$ is the metric, and K_μ is the two-dimensional contorsion. Furthermore, $\Phi^2 = \phi_\mu\phi^\mu$. It is immediately apparent that the field θ plays the role of a Lagrange multiplier, thereby imposing a constraint on the system of equations. Consequently, when $\theta \neq 0$, an additional equation arises, which substantially restricts the phase space of admissible solutions. This property is particularly advantageous when attempting to solve the equations of motion.

The chapter is divided into four sections. In Sec. 7.1, we derive the equations of motion and impose the symmetric ansatz introduced in Sec. 3.1. We then solve the vacuum equations and demonstrate that their most general solution is the BTZ black hole with non-zero θ torsion. Consequently, this solution is directly inherited from the parent 5DCS theory.

The following Sec. 7.2 focuses on general solutions in the presence of non-vanishing matter fields. The matter sector is strictly two-dimensional, meaning that the only sources in the theory are the matter energy-momentum tensor and the contorsion current, obtained by varying the matter action with respect to the metric and the contorsion, respectively. In this part, the θ-field constraint is heavily used to solve equations of motion for the additional fields, including the two-dimensional contorsion, and to derive the resulting source equations in terms of the metric function Λ, the dilaton field, and their derivatives. A variety of distinct cases arise in the course of solving the equations, and these are summarized in Tab. 7.1.

The penultimate Sec. 7.3 explores explicit solutions once the form of matter minimally coupled to gravity is specified in the $\theta \neq 0$ sector of the theory; for $\theta = 0$ the model reduces to its Riemannian sector, which was analyzed in the preceding chapter. Several types of field theories are considered. We first introduce matter as a real scalar field and obtain cosmological solutions. Next, we examine the general solutions of the equations of motion coupled to pure electrodynamics. In this setting, we show that no solutions with $\theta \neq 0$ exist; however, there is a well-defined charged black hole solution when the theory is restricted to the Riemannian sector. The subsequent subsection studies the coupling to a spinor field, where we identify a fermionic star soliton solution together with a well-defined phase transition mechanism. We then analyze gravity coupled to scalar electrodynamics, for which the general solution is again of cosmological type. The section concludes with the case where the matter content is given by an ideal fluid.

In the final Sec. 7.4 we incorporate quantum corrections. There, we demonstrate that the $\theta \neq 0$ case requires a very specific solution characterized by two non-extremal singular horizons at which both torsion and curvature diverge. This behavior results from the condensation of quanta, since the EMT associated with the quantum corrections also diverges at those locations. The singularity is hidden behind both horizons, and the resulting geometry is therefore reminiscent of the rotating BTZ black hole of [78].

7.1 Equation of motion and the symmetric ansatz

In this section we derive the equations of motion for the complete dimensionally-reduced 5DCS theory defined by the action (7.1). Since we do not impose vanishing torsion from the outset, the full set of independent fields is $\{g_{\mu\nu}, \mathrm{K}^\mu, \phi, \phi^\mu, \theta\}$. We start by varying the action with respect to the metric. The corresponding field equation is:

$$\begin{aligned}
&(\mathrm{x}^2+1)\nabla_\mu\nabla_\nu \mathrm{x} - \frac{1}{l}\nabla_\alpha\phi^\alpha\phi_\mu\phi_\nu + \frac{1}{2l}\left(\phi_\mu\nabla_\nu\Phi^2 + \phi_\nu\nabla_\mu\Phi^2\right) - \nabla_\mu\nabla_\nu\left(\mathrm{x}\theta^2\right) \\
&\quad - 2\varepsilon^{\alpha\beta}\left(\nabla_\alpha \mathrm{x} + \frac{1}{l}\phi_\alpha\right)\mathrm{K}_\beta\phi_\mu\phi_\nu - \left[\left(\nabla_\mu \mathrm{x} + \frac{1}{l}\phi_\mu\right)\nabla_\nu\Phi^2 + \left(\nabla_\nu \mathrm{x} + \frac{1}{l}\phi_\nu\right)\nabla_\mu\Phi^2\right] \\
&\quad + \left(\nabla^\alpha \mathrm{x} + \frac{1}{l}\phi^\alpha\right) A^\sigma\varepsilon^{\rho\delta}\nabla_\delta\phi^\lambda\left[\varepsilon_{\lambda\alpha}\Big(g_{\mu\sigma}g_{\nu\rho} + g_{\nu\sigma}g_{\mu\rho}\Big) + \varepsilon_{\sigma\rho}\Big(\varepsilon_{\mu\alpha}\varepsilon_{\nu\lambda} + \varepsilon_{\nu\alpha}\varepsilon_{\mu\lambda}\Big)\right] \\
&\quad + 2\mathrm{x}\left(\nabla_\mu \mathrm{x} + \frac{1}{l}\phi_\mu\right)\left(\nabla_\nu \mathrm{x} + \frac{1}{l}\phi_\nu\right) + \frac{1}{2l}\varepsilon^{\rho\sigma}\nabla_\rho\phi_\sigma\Big(\phi_\mu\varepsilon_{\nu\alpha} + \phi_\nu\varepsilon_{\mu\alpha}\Big)\phi^\alpha \\
&\quad - \frac{1}{2}\Phi^2\left[\nabla_\mu\left(\nabla_\nu \mathrm{x} + \frac{1}{l}\phi_\nu\right) + \nabla_\nu\left(\nabla_\mu \mathrm{x} + \frac{1}{l}\phi_\mu\right)\right] + g_{\mu\nu}\left(\Box\left(\mathrm{x}\theta^2\right) - \frac{\mathrm{x}\theta^2}{l^2}\right) \\
&\quad + g_{\mu\nu}\left[2\left(\nabla^\alpha \mathrm{x} + \frac{1}{l}\phi^\alpha\right)\nabla_\alpha\left(\Phi^2 - \frac{1}{2}\mathrm{x}^2\right) + \Phi^2\nabla_\alpha\left(\nabla^\alpha \mathrm{x} + \frac{1}{l}\phi^\alpha\right)\right] \\
&\quad - g_{\mu\nu}\left[(\mathrm{x}^2+1)\Box \mathrm{x} - \frac{\mathrm{x}}{l^2}\Big(\mathrm{x}^2 + 1 - \Phi^2\Big) + \frac{1}{2l}\phi^\alpha\nabla_\alpha\Phi^2\right] = -\frac{1}{6k\pi^2}T_{\mu\nu},
\end{aligned} \tag{7.2}$$

where we have already eliminated the original dilaton ϕ in favor of the reduced dilaton field x defined in Eq. (2.46). Notice that only a single term involves the two-dimensional contorsion. Varying the action with respect to the contorsion then gives:

$$\Big(\mathrm{x}^2 + 1 - \theta^2 - \Phi^2\Big)\left(\nabla_\mu \mathrm{x} + \frac{1}{l}\phi_\mu\right) - \mathrm{x}\nabla_\mu\theta^2 = \frac{1}{6k\pi^2}\varepsilon_{\mu\nu}T^\nu_{\mathrm{K}}, \tag{7.3}$$

where we have introduced the contorsion current $T^\mu_{\mathrm{K}} = -\frac{1}{\sqrt{-g}}\frac{\delta S_{\mathrm{mat}}}{\delta \mathrm{K}_\mu}$. In an analogous manner, variation with respect to the scalar field associated with the five-dimensional torsion function,

θ, yields:

$$\mathrm{x}\theta\left[\mathrm{R}+2\varepsilon^{\alpha\beta}\partial_\alpha\mathrm{K}_\beta+\frac{2}{l^2}-\frac{2}{l\mathrm{x}}\varepsilon^{\alpha\beta}\phi_\alpha\mathrm{K}_\beta\right]=-\frac{1}{6k\pi^2}T_{(\theta)},\tag{7.4}$$

with $T_{(\theta)}=-\frac{1}{\sqrt{-g}}\frac{\delta S_{\text{mat}}}{\delta\theta}$. It is worth emphasizing that in the limit of vanishing contorsion this equation turns into a constraint which, for $\theta\neq 0$, fixes the scalar curvature to the constant AdS value. This is why we interpret the field θ as playing the role of a Lagrange multiplier in the action. Finally, varying the action (7.1) with respect to the vector field ϕ^μ and the dilaton field ϕ gives:

$$\varepsilon_\sigma{}^\nu\left[\varepsilon_{\rho\mu}\nabla^\sigma\phi^\rho-\phi_\mu\mathrm{K}^\sigma-\frac{\mathrm{x}}{l}\varepsilon_\mu{}^\sigma\right]\left(\nabla_\nu\mathrm{x}+\frac{1}{l}\phi_\nu\right)-\frac{1}{2l}\left(\mathrm{x}^2+1-\theta^2-\Phi^2\right)\varepsilon_{\mu\nu}\mathrm{K}^\nu=\frac{1}{12k\pi^2\lambda l}T^{(\phi)}_\mu,\tag{7.5}$$

$$\begin{aligned}\left(\mathrm{x}^2+1-\theta^2-\Phi^2\right)\left[\mathrm{R}+2\varepsilon^{\alpha\beta}\partial_\alpha\mathrm{K}_\beta+\frac{2}{l^2}\right]+\frac{4\mathrm{x}^2}{l^2}+\frac{4\mathrm{x}}{l}\left(\nabla_\alpha\phi^\alpha-\varepsilon^{\alpha\beta}\phi_\alpha\mathrm{K}_\beta\right)&\\-2\left(\nabla_\mu\phi_\nu\nabla^\nu\phi^\mu-\nabla_\mu\phi^\mu\nabla_\nu\phi^\nu-\varepsilon^{\alpha\beta}\mathrm{K}_\alpha\nabla_\beta\Phi^2\right)=-\frac{1}{3k\pi^2}\frac{1}{\mathrm{x}}T^{(\phi)},&\end{aligned}\tag{7.6}$$

where the matter sources for ϕ^μ and ϕ are defined as $T^{(\phi)}_\mu=-\frac{1}{\sqrt{-g}}\frac{\delta S_{\text{mat}}}{\delta\phi^\mu}$ and $T^{(\phi)}=-\frac{1}{\sqrt{-g}}\frac{\delta S_{\text{mat}}}{\delta\phi}$, respectively.

All equations of motion (7.2-7.6) are explicitly written so that, upon imposing $\phi_\mu=-l\nabla_\mu\phi$, $\mathrm{K}_\mu=0$ and $\theta=0$, they reduce to the Riemannian sector of the theory (6.11-6.12). Using Eqs. (7.3-7.6), the metric Eq. (7.2) can be further recast in the following form:

$$\begin{aligned}\left(\mathrm{x}^2+1-\theta^2-\Phi^2\right)\Bigg\{\nabla_\mu\phi_\nu+\nabla_\nu\phi_\mu-\frac{1}{\mathrm{x}}\left(\phi_\mu\nabla_\nu\mathrm{x}+\phi_\nu\nabla_\mu\mathrm{x}\right)-\frac{2}{l\mathrm{x}}\phi_\mu\phi_\nu+(\phi_\mu\varepsilon_{\nu\sigma}+\phi_\nu\varepsilon_{\mu\sigma})\mathrm{K}^\sigma&\\-2g_{\mu\nu}\left[\nabla_\alpha\phi^\alpha-\frac{1}{\mathrm{x}}\phi^\alpha\nabla_\alpha\mathrm{x}-\frac{1}{l\mathrm{x}}\Phi^2+\frac{\mathrm{x}}{l}\right]\Bigg\}=\frac{l}{3k\pi^2}\bar{T}_{\mu\nu},&\end{aligned}\tag{7.7}$$

where we have introduced a reduced EMT, which incorporates contributions from additional sources beyond the standard EMT, and is defined as

$$\begin{aligned}\bar{T}_{\mu\nu}=T_{\mu\nu}-\frac{1}{2l\mathrm{x}}\left(\phi_\mu\varepsilon_{\nu\sigma}+\phi_\nu\varepsilon_{\mu\sigma}\right)T^\sigma_{\mathrm{K}}+\frac{1}{2}\left(g_{\mu\sigma}\varepsilon_{\nu\rho}+g_{\nu\sigma}\varepsilon_{\mu\rho}\right)\nabla^\sigma T^\rho_{\mathrm{K}}-g_{\mu\nu}\varepsilon^{\alpha\beta}\left(\nabla_\alpha T^{\mathrm{K}}_\beta-\frac{1}{l\mathrm{x}}\phi_\alpha T^{\mathrm{K}}_\beta\right)&\\-\frac{1}{2\lambda l}\left(\phi_\mu T^{(\phi)}_\nu+\phi_\nu T^{(\phi)}_\mu\right).&\end{aligned}\tag{7.8}$$

In this representation, the equation makes it manifest that, even in the presence of non-zero torsion, the enhanced symmetry of the 5DCS theory ensures the appearance of the simple prefactor $\mathrm{x}^2+1-\theta^2-\Phi^2$, in complete analogy with the Riemannian sector (6.11).

Because the full theory's equations of motion are extremely complicated, we restrict our analysis to solutions that admit at least one Killing vector. When this vector is time-like, we focus on static, black-hole-type configurations. Conversely, if it is space-like, the resulting solutions describe cosmological spacetimes. Consequently, we proceed directly to implementing the symmetric ansatz introduced in Sec. 3.1. Employing Eqs. (3.12), (3.13), and (3.19), we obtain the following ansatz for ϕ_μ, K_μ, $\nabla_\mu\mathrm{x}$, and the metric:

$$\phi_\mu=\phi^{\parallel}(\mathrm{x})\xi_\mu+\phi^{\perp}(\mathrm{x})\varepsilon_{\mu\nu}\xi^\nu,\;\;\mathrm{K}_\mu=\mathrm{K}^{\parallel}(\mathrm{x})\xi_\mu+\mathrm{K}^{\perp}(\mathrm{x})\varepsilon_{\mu\nu}\xi^\nu,\;\;\nabla_\mu\mathrm{x}=\frac{1}{l}\mathcal{D}(\mathrm{x})\varepsilon_{\mu\nu}\xi^\nu,\;\;\xi^2=\Lambda(\mathrm{x}).\tag{7.9}$$

Using Eq. (7.9) equations of motion (7.3-7.7) can be rewritten in the following form:

$$\Lambda^2\left(\mathrm{x}^2+1-\theta^2-\Phi^2\right)\left\{\mathcal{D}\frac{\mathrm{d}\phi^\perp}{\mathrm{dx}}-\frac{1}{\mathrm{x}}\left(\phi^{\parallel 2}+\phi^\perp\left(\phi^\perp+\mathcal{D}\right)\right)+l\left(\phi^\parallel\mathrm{K}^\perp+\phi^\perp\mathrm{K}^\parallel\right)\right.$$
$$\left.\mp\left[\mathcal{D}\frac{\mathrm{d}\phi^\parallel}{\mathrm{dx}}-\frac{1}{\mathrm{x}}\phi^\parallel\left(2\phi^\perp+\mathcal{D}\right)+l\left(\phi^\parallel\mathrm{K}^\parallel+\phi^\perp\mathrm{K}^\perp\right)\right]\right\}=\frac{2l^2}{3k\pi^2}\mathrm{F}^{\pm 2}\bar{T}_{\pm\pm}, \quad (7.10)$$

$$\left(\mathrm{x}^2+1-\theta^2-\Phi^2\right)\left[\mathcal{D}\frac{\mathrm{d}}{\mathrm{dx}}\left(\Lambda\phi^\perp\right)+\frac{1}{\mathrm{x}}\Lambda\left(\phi^{\parallel 2}-\phi^\perp\left(\phi^\perp+\mathcal{D}\right)\right)-2\mathrm{x}\right.$$
$$\left.+l\Lambda\left(\phi^\parallel\mathrm{K}^\perp-\phi^\perp\mathrm{K}^\parallel\right)\right]=\frac{l^2}{6k\pi^2}\bar{T}, \quad (7.11)$$

$$\Lambda\left(\mathrm{x}^2+1-\theta^2-\Phi^2\right)\phi^\parallel=\frac{l}{6k\pi^2}\varepsilon^{\mu\nu}\xi_\mu T_\nu^{\mathrm{K}}, \quad (7.12)$$

$$\Lambda\left[\left(\mathrm{x}^2+1-\theta^2-\Phi^2\right)\left(\phi^\perp+\mathcal{D}\right)-\mathrm{x}\mathcal{D}\frac{\mathrm{d}\theta^2}{\mathrm{dx}}\right]=\frac{l}{6k\pi^2}\xi^\mu T_\mu^{\mathrm{K}}, \quad (7.13)$$

$$\mathrm{x}\theta\left[\mathcal{D}\frac{\mathrm{d}}{\mathrm{dx}}\left(\mathcal{D}\frac{\mathrm{d}\Lambda}{\mathrm{dx}}-2l\Lambda\mathrm{K}^\parallel\right)+2+\frac{2}{\mathrm{x}}l\Lambda\left(\phi^\perp\mathrm{K}^\parallel-\phi^\parallel\mathrm{K}^\perp\right)\right]=-\frac{l^2}{6k\pi^2}T^{(\theta)}, \quad (7.14)$$

$$\phi^\parallel\left[\mathcal{D}\left(2\Lambda\frac{\mathrm{d}\phi^\perp}{\mathrm{dx}}+\left(2\phi^\perp+\mathcal{D}\right)\frac{\mathrm{d}\Lambda}{\mathrm{dx}}\right)-2\mathrm{x}+2l\Lambda\left(\phi^\parallel\mathrm{K}^\perp-\left(\phi^\perp+\mathcal{D}\right)\mathrm{K}^\parallel\right)\right]$$
$$-l\left(\mathrm{x}^2+1-\theta^2-\Phi^2\right)\mathrm{K}^\perp=\frac{l}{6k\pi^2\lambda}\frac{\xi^\mu T_\mu^{(\phi)}}{\Lambda}, \quad (7.15)$$

$$\mathcal{D}\left[2\Lambda\phi^\parallel\frac{\mathrm{d}\phi^\parallel}{\mathrm{dx}}+\left(\phi^{\parallel 2}+\phi^\perp\left(\phi^\perp+\mathcal{D}\right)\right)\frac{\mathrm{d}\Lambda}{\mathrm{dx}}\right]-2\mathrm{x}\left(\phi^\perp+\mathcal{D}\right)+2l\Lambda\phi^\perp\left(\phi^\parallel\mathrm{K}^\perp-\left(\phi^\perp+\mathcal{D}\right)\mathrm{K}^\parallel\right)$$
$$-l\left(\mathrm{x}^2+1-\theta^2-\Phi^2\right)\mathrm{K}^\parallel=\frac{l}{6k\pi^2\lambda}\frac{\varepsilon^{\mu\nu}\xi_\mu T_\nu^{(\phi)}}{\Lambda}, \quad (7.16)$$

$$\left(\mathrm{x}^2+1-\theta^2-\Phi^2\right)\left[\mathcal{D}\frac{\mathrm{d}}{\mathrm{dx}}\left(\mathcal{D}\frac{\mathrm{d}\Lambda}{\mathrm{dx}}-2l\Lambda\mathrm{K}^\parallel\right)+2\right]+4\mathrm{x}^2-4\mathrm{x}\mathcal{D}\frac{\mathrm{d}\left(\Lambda\phi^\perp\right)}{\mathrm{dx}}$$
$$-\mathcal{D}\frac{\mathrm{d}\Phi^2}{\mathrm{dx}}\left(\mathcal{D}\frac{\mathrm{d}\Lambda}{\mathrm{dx}}-2l\Lambda\mathrm{K}^\parallel\right)-4l\mathrm{x}\Lambda(\phi^\parallel\mathrm{K}^\perp-\phi^\perp\mathrm{K}^\parallel)=-\frac{l^2}{3k\pi^2}\frac{1}{\mathrm{x}}T^{(\phi)}. \quad (7.17)$$

The first pair of Eqs. (7.10-7.11) describe, respectively, the "$\pm\pm$" component and the trace of the metric equation of motion (7.7). The following two Eqs. (7.12-7.13) give the parallel and normal components of the contorsion Eq. (7.3). The equation of motion for the θ field (7.4) simplifies to Eq. (7.14) once the symmetric ansatz is imposed. Eqs. (7.15-7.16) represent the normal and parallel components of the Eq. (7.5) for the vector field ϕ^μ. Finally, the last Eq. (7.17) is equivalent to Eq. (7.6) for the dilaton field.

Within this chapter, we restrict ourselves to theories whose matter content is strictly two-dimensional, which implies

$$T^{(\phi)}=T_\mu^{(\phi)}=T^{(\theta)}=0. \quad (7.18)$$

Thus, the only non-vanishing sources are the EMT, $T_{\mu\nu}\neq 0$, and the contorsion current, $T_\mu^{\mathrm{K}}\neq 0$. Since Eqs. (7.14-7.17) contain no sources, they act as constraints inherited from the five-dimensional theory and, as such, are analyzed later. We first turn to the Eqs. (7.10-7.11), rewriting them in terms of the symmetric ansatz components of the EMT. Employing

Eqs. (3.33) and (3.34), they take the form:

$$\left(\mathrm{x}^2+1-\theta^2-\Phi^2\right)\left[\mathcal{D}\frac{\mathrm{d}\phi^{\perp}}{\mathrm{dx}}-\frac{1}{\mathrm{x}}\left(\phi^{\parallel 2}+\phi^{\perp}\left(\phi^{\perp}+\mathcal{D}\right)\right)+l\left(\phi^{\parallel}\mathrm{K}^{\perp}+\phi^{\perp}\mathrm{K}^{\parallel}\right)\right]$$
$$=\frac{l^2}{6k\pi^2}\left(T^{\parallel\parallel}+T^{\perp\perp}\right)+\frac{l}{6k\pi^2}\left[\mathcal{D}\frac{\mathrm{d}T^{\parallel}_{\mathrm{K}}}{\mathrm{dx}}-\frac{1}{\mathrm{x}}\left(\phi^{\parallel}T^{\perp}_{\mathrm{K}}+\phi^{\perp}T^{\parallel}_{\mathrm{K}}\right)\right], \tag{7.19}$$

$$\left(\mathrm{x}^2+1-\theta^2-\Phi^2\right)\left[\mathcal{D}\frac{\mathrm{d}\phi^{\parallel}}{\mathrm{dx}}-\frac{1}{\mathrm{x}}\phi^{\parallel}\left(2\phi^{\perp}+\mathcal{D}\right)+l\left(\phi^{\parallel}\mathrm{K}^{\parallel}+\phi^{\perp}\mathrm{K}^{\perp}\right)\right]$$
$$=\frac{l^2}{3k\pi^2}T^{\parallel\perp}+\frac{l}{6k\pi^2}\left[\mathcal{D}\frac{\mathrm{d}T^{\perp}_{\mathrm{K}}}{\mathrm{dx}}-\frac{1}{\mathrm{X}}\left(\phi^{\parallel}T^{\parallel}_{\mathrm{K}}+\phi^{\perp}T^{\perp}_{\mathrm{K}}\right)\right], \tag{7.20}$$

$$\left(\mathrm{x}^2+1-\theta^2-\Phi^2\right)\left[\mathcal{D}\frac{\mathrm{d}}{\mathrm{dx}}\left(\Lambda\phi^{\perp}\right)+\frac{\Lambda}{\mathrm{x}}\left(\phi^{\parallel 2}-\phi^{\perp}\left(\phi^{\perp}+\mathcal{D}\right)\right)-2\mathrm{x}+l\Lambda\left(\phi^{\parallel}\mathrm{K}^{\perp}-\phi^{\perp}\mathrm{K}^{\parallel}\right)\right]$$
$$=\frac{l^2\Lambda}{6k\pi^2}\left(T^{\parallel\parallel}-T^{\perp\perp}\right)+\frac{l}{6k\pi^2}\left[\mathcal{D}\frac{\mathrm{d}\left(\Lambda T^{\parallel}_{\mathrm{K}}\right)}{\mathrm{dx}}+\frac{\Lambda}{\mathrm{x}}\left(\phi^{\parallel}T^{\perp}_{\mathrm{K}}-\phi^{\perp}T^{\parallel}_{\mathrm{K}}\right)\right]. \tag{7.21}$$

Using Eqs. (7.13-7.12) together with Eqs. (7.15-7.16), Eq. (7.19) reduces to

$$\left(\mathrm{x}^2+1-\theta^2-\Phi^2\right)\phi^{\parallel}2l\Lambda\mathrm{K}^{\parallel}=\frac{l^2}{3k\pi^2}T^{\parallel\perp}. \tag{7.22}$$

If one multiplies Eq. (7.19) by Λ and subtracts it from Eq. (7.21), one finds:

$$\left(\mathrm{x}^2+1-\theta^2-\Phi^2\right)\left[\mathcal{D}\phi^{\perp}\frac{\mathrm{d}\Lambda}{\mathrm{dx}}-2\mathrm{x}-2l\Lambda\phi^{\perp}\mathrm{K}^{\parallel}\right]=-\frac{l^2}{3k\pi^2}\Lambda T^{\perp\perp}+\frac{l}{6k\pi^2}\mathcal{D}\frac{\mathrm{d}\Lambda}{\mathrm{dx}}T^{\parallel}_{\mathrm{K}}. \tag{7.23}$$

Conversely, adding instead of subtracting yields:

$$\left(\mathrm{x}^2+1-\theta^2-\Phi^2\right)\left[2\Lambda\left(\mathcal{D}\frac{\mathrm{d}\phi^{\perp}}{\mathrm{dx}}-\frac{1}{\mathrm{x}}\phi^{\perp}\left(\phi^{\perp}+\mathcal{D}\right)\right)+\mathcal{D}\phi^{\perp}\frac{\mathrm{d}\Lambda}{\mathrm{dx}}-2\mathrm{x}+2l\Lambda\phi^{\parallel}\mathrm{K}^{\perp}\right]$$
$$=\frac{l}{6k\pi^2}\left[2l\Lambda T^{\parallel\parallel}+\mathcal{D}\left(\frac{\mathrm{d}\Lambda}{\mathrm{dx}}T^{\parallel}_{\mathrm{K}}+2\Lambda\frac{\mathrm{d}T^{\parallel}_{\mathrm{K}}}{\mathrm{dx}}\right)-\frac{2}{\mathrm{x}}\Lambda\phi^{\perp}T^{\parallel}_{\mathrm{K}}\right]. \tag{7.24}$$

The relations (7.13-7.12) admit no substantial further simplification and read:

$$\left(\mathrm{x}^2+1-\theta^2-\Phi^2\right)\phi^{\parallel}=\frac{l}{6k\pi^2}T^{\perp}_{\mathrm{K}}, \tag{7.25}$$

$$\left(\mathrm{x}^2+1-\theta^2-\Phi^2\right)\left(\phi^{\perp}+\mathcal{D}\right)-\mathrm{x}\mathcal{D}\frac{\mathrm{d}\theta^2}{\mathrm{dx}}=\frac{l}{6k\pi^2}T^{\parallel}_{\mathrm{K}}. \tag{7.26}$$

For later convenience, we now define the following auxiliary source-dependent functions:

$$\begin{aligned}
\tilde{T}^{\perp\perp}&=\frac{l}{6k\pi^2}\left(2l\Lambda T^{\perp\perp}-T^{\parallel}_{\mathrm{K}}\frac{\mathrm{d}\Lambda}{\mathrm{d}\bar{\mathrm{x}}}\right),\\
\tilde{T}^{\parallel\parallel}&=\frac{l}{6k\pi^2}\left(2l\Lambda T^{\parallel\parallel}+T^{\parallel}_{\mathrm{K}}\frac{\mathrm{d}\Lambda}{\mathrm{d}\bar{\mathrm{x}}}+2\Lambda\frac{\mathrm{d}T^{\parallel}_{\mathrm{K}}}{\mathrm{d}\bar{\mathrm{x}}}\right),\\
\tilde{T}^{\parallel\perp}&=\frac{l}{6k\pi^2}2l\Lambda T^{\parallel\perp},\ \ \tilde{T}^{\parallel/\perp}=\frac{l}{6k\pi^2}T^{\parallel/\perp},
\end{aligned} \tag{7.27}$$

and, analogously, we introduce auxiliary functions for the fields:

$$\mathcal{Z}=\mathrm{x}^2+1-\theta^2-\Phi^2, \tag{7.28}$$

$$\mathcal{S}=\frac{\mathrm{d}\Lambda}{\mathrm{d}\bar{\mathrm{x}}}-2l\Lambda\mathrm{K}^{\parallel}. \tag{7.29}$$

The complete symmetric system of equations of motion is represented by the equations containing the sources: the EMT (7.22-7.24) and the contorsion current (7.25-7.26). In addition to this set, four constraints (7.14-7.17) must be imposed. These constraints originate from the dimensional reduction procedure. Further details can be found in Sec. 2.3.

7.1.1 General symmetric vacuum solutions

In this section we derive the most general solution of the vacuum equations of motion (7.10–7.17) that admits at least one Killing vector. In the vacuum case, all source terms vanish, i.e. $T_{\mu\nu} = T^{\mu}_{\mathrm{K}} = T^{\mu}_{(\phi)} = T^{(\theta)} = T^{(\phi)} = 0$. As in the Riemannian sector discussed in Sec. 6.1.1, the complete theory again splits into two distinct branches of solutions. We first analyze the branch characterized by $\mathrm{x}^2 + 1 - \theta^2 - \Phi^2 \neq 0$.

From Eq. (7.12), we infer $\phi^{\parallel} = 0$. Then, using Eq. (7.15) we obtain $\mathrm{K}^{\perp} = 0$. Next, combining Eq. (7.10) with Eq. (7.11) and inserting the resulting expression into Eq. (7.16) leads to $\mathrm{K}^{\parallel} = 0$. Thus, the remaining nontrivial equations reduce to

$$\mathcal{D}\frac{\mathrm{d}\phi^{\perp}}{\mathrm{dx}} = \frac{1}{\mathrm{x}}\phi^{\perp}\left(\phi^{\perp} + \mathcal{D}\right), \tag{7.30}$$

$$\mathcal{D}\phi^{\perp}\frac{\mathrm{d}\Lambda}{\mathrm{dx}} = 2\mathrm{x}, \tag{7.31}$$

$$\mathrm{x}\mathcal{D}\frac{\mathrm{d}\theta^2}{\mathrm{dx}} = \left(\mathrm{x}^2 + 1 - \theta^2 + \Lambda\phi^{\perp 2}\right)\left(\phi^{\perp} + \mathcal{D}\right), \tag{7.32}$$

$$\theta\left[\mathcal{D}\frac{\mathrm{d}}{\mathrm{dx}}\left(\mathcal{D}\frac{\mathrm{d}\Lambda}{\mathrm{dx}}\right) + 2\right] = 0. \tag{7.33}$$

We now change to the coordinate $\bar{\mathrm{x}}$ as introduced in Eq. (3.20). Eq. (7.30) can be integrated directly, yielding $\bar{\mathrm{x}} = -\frac{\mathrm{x}}{\phi^{\perp}}$. Substituting this relation into Eq. (7.31) and integrating gives the metric function $\Lambda = -(\bar{\mathrm{x}}^2 - \mu)$, where μ is an integration constant. With this form of Λ, Eq. (7.33) is automatically fulfilled. The remaining Eq. (7.32) can then be integrated to obtain the θ field:

$$\theta^2 = 1 + \frac{1}{3}\phi^{\perp 2} + \frac{\eta}{\phi^{\perp}}, \tag{7.34}$$

where η is another integration constant. A straightforward check confirms that Eq. (7.5) is satisfied as well.

Hence, the solution is specified by two arbitrary coordinate transformations $\mathrm{F}^{\pm}$, an arbitrary function of the dilaton $\phi^{\perp}(\mathrm{x})$, and the constants μ and η, which we collectively denote by $\mathrm{RCI}(\mathrm{F}^+, \mathrm{F}^-, \phi^{\perp}(\bar{\mathrm{x}}), \mu, \eta)$:

$$\begin{aligned}
&\mathrm{d}s^2 = -(\bar{\mathrm{x}}^2 - \mu)\mathrm{d}t^2 + \frac{l^2\mathrm{d}\bar{\mathrm{x}}^2}{\bar{\mathrm{x}}^2 - \mu},\\
&\bar{\mathrm{x}} = \begin{cases} \sqrt{\mu}\tanh\left[\frac{\sqrt{\mu}}{2l}\left(\int\frac{\mathrm{d}x^+}{\mathrm{F}^+} + \int\frac{\mathrm{d}x^-}{\mathrm{F}^-}\right)\right], & 0 < \bar{\mathrm{x}} < \sqrt{\mu},\\ \sqrt{\mu}\coth\left[\frac{\sqrt{\mu}}{2l}\left(\int\frac{\mathrm{d}x^+}{\mathrm{F}^+} + \int\frac{\mathrm{d}x^-}{\mathrm{F}^-}\right)\right], & \bar{\mathrm{x}} > \sqrt{\mu}, \end{cases}\\
&\phi^{\parallel} = 0,\ \mathrm{K}^{\parallel} = 0,\ \mathrm{K}^{\perp} = 0,\ \mathrm{x} = -\bar{\mathrm{x}}\phi^{\perp}(\bar{\mathrm{x}}),\\
&\theta^2 = 1 + \frac{1}{3}\mu\phi^{\perp 2}(\bar{\mathrm{x}}) + \frac{\eta}{\phi^{\perp}(\bar{\mathrm{x}})}.
\end{aligned} \tag{7.35}$$

Choosing $\phi^{\perp} = -1$ and $\theta = 0$, which corresponds to fixing $\eta = 1 + \mu/3$, brings this solution back to the generic branch-one solution in the Riemannian sector of the theory (6.17), as anticipated.

The other branch is defined by $\mathrm{x}^2 + 1 - \theta^2 - \Phi^2 = 0$. Consequently, Eqs. (7.10-7.12) are satisfied identically. From Eq. (7.13) it follows that $\theta^2 = \theta_0^2 = \text{const}$. After some straightforward algebra, one finds that Eqs. (7.15-7.16) reduce to the dilaton Eq. (7.17). Therefore, the system effectively boils down to the following two equations:

$$\theta_0 \left[\mathcal{D} \frac{\mathrm{d}}{\mathrm{dx}} \left(\mathcal{D} \frac{\mathrm{d}\Lambda}{\mathrm{dx}} - 2l\Lambda \mathrm{K}^{\parallel} \right) + 2 + \frac{2}{\mathrm{x}} l\Lambda \left(\phi^{\perp}\mathrm{K}^{\parallel} - \phi^{\parallel}\mathrm{K}^{\perp} \right) \right] = 0, \tag{7.36}$$

$$\mathcal{D} \left[2\Lambda \frac{\mathrm{d}\phi^{\perp}}{\mathrm{dx}} + \left(2\phi^{\perp} + \mathcal{D} \right) \frac{\mathrm{d}\Lambda}{\mathrm{dx}} \right] - 2\mathrm{x} + 2l\Lambda \left(\phi^{\parallel}\mathrm{K}^{\perp} - \left(\phi^{\perp} + \mathcal{D} \right) \mathrm{K}^{\parallel} \right) = 0. \tag{7.37}$$

Inspection of Eqs. (7.36-7.37) shows that the case $\theta_0 = 0$ is somewhat special, because only a single differential equation, namely Eq. (7.37), remains. In this situation, the solution is specified by two coordinate transformations $\mathrm{F}^{\pm}$ and four arbitrary functions of the coordinate $\bar{\mathrm{x}}$. The field $\mathrm{K}^{\perp}$ is then determined from Eq. (7.37), whereas $\phi^{\parallel}$ is obtained from the constraint $\mathrm{x}^2 + 1 = \Lambda \left(\phi^{\parallel 2} - \phi^{\perp 2} \right)$. The coordinate $\bar{\mathrm{x}}$ is fixed by evaluating the integral (3.18). We denote this family of solutions by $\mathrm{RCIIB}(\mathrm{F}^+, \mathrm{F}^-\Lambda(\bar{\mathrm{x}}), \phi^{\perp}(\bar{\mathrm{x}}), \mathrm{K}^{\parallel}(\bar{\mathrm{x}}), \mathrm{x}(\bar{\mathrm{x}}))$.

By imposing $\phi^{\parallel} = \mathrm{K}^{\perp} = \mathrm{K}^{\parallel} = 0$ and $\phi^{\perp} = -\mathcal{D}$, the single Eq. (7.37) is automatically fulfilled, provided that the condition $\mathrm{x}^2 + 1 + \Lambda\mathcal{D}^2 = 0$ holds. Consequently, only one arbitrary function, $\Lambda(\mathrm{x})$, remains undetermined. Hence, this solution effectively coincides with the general branch-two solution of the Riemannian sector equations of motion (6.20).

The case with $\theta_0 \neq 0$ is genuinely Riemann–Cartan. Both differential equations are still present, so the solution now depends on one fewer arbitrary function and on two additional constants, θ_0 and C. We denote this solution by $\mathrm{RCIIA}(\mathrm{F}^+, \mathrm{F}^-\Lambda(\bar{\mathrm{x}}), \phi^{\perp}(\bar{\mathrm{x}}), \mathrm{x}(\bar{\mathrm{x}}), \theta_0, C)$. It is explicitly given by

$$\begin{aligned} \mathrm{x}^2 + 1 - \theta_0^2 &= \Lambda \left(\phi^{\parallel 2} - \phi^{\perp 2} \right), \ \theta = \theta_0, \\ l\Lambda\mathrm{K}^{\parallel} &= \frac{1}{2}\frac{\mathrm{d}\Lambda}{\mathrm{d}\bar{\mathrm{x}}} - \frac{C - \Lambda\phi^{\perp}}{\mathrm{x}}, \\ l\Lambda\phi^{\parallel}\mathrm{K}^{\perp} &= \mathrm{x} + \phi^{\perp} \left[\frac{1}{2}\frac{\mathrm{d}\Lambda}{\mathrm{d}\bar{\mathrm{x}}} - \frac{C - \Lambda\phi^{\perp}}{\mathrm{x}} \right] + \mathrm{x}\frac{\mathrm{d}}{\mathrm{d}\bar{\mathrm{x}}} \left(\frac{C - \Lambda\phi^{\perp}}{\mathrm{x}} \right). \end{aligned} \tag{7.38}$$

In this regime, the contorsion is completely determined by the metric, the dilaton field, and the vector field ϕ^{μ}. These fields themselves, however, remain arbitrary, subject only to the brunch condition.

A straightforward substitution confirms that all three solution families, RCI (7.35), RCIIA (7.38), and RCIIB, also satisfy the five-dimensional equations of motion (2.30). In addition, the five-dimensional BTZ black hole with torsion (2.31–2.32) remains a valid solution of this dimensionally-reduced 5DCS theory, within the first branch. The presence of some of the arbitrary functions in the branch-two solutions is an artifact of the unfixed five-dimensional gauge symmetries. To verify if this solutions are stable, one should see how they change when small perturbations of the sources are introduces. A further comment on this issue is given in Sec. 7.2.4.

7.1.2 Classical gravitational collapse

The objective of this subsection is to determine which geometries can arise from classical gravitational collapse in the presence of non-vanishing torsion. To address this, we first need to derive the junction condition across an infalling matter shockwave. Unlike the previous analyses in Secs. 4.1.5, 5.1.3, and 6.1.4, where the matter shockwave was allowed to carry only mass, we now have to consider additional possible charges associated with various fields that either originate from 5D torsion or represent intrinsic 2D torsion.

We take the ingoing shockwave to lie at $x^+ = x_0^+$, implying that all sources are proportional to a Dirac δ-function supported at this specific spacetime point. In what follows, we derive more general junction conditions by allowing the sources associated with the fields arising from 5D torsion and the dilaton to be non-zero. Since the unique tangent vector along this hypersurface must be of the form $n^\mu = (0, c)$, the EMT and any vector field A^μ that is localized on the shockwave are consequently constrained to take the form:

$$T_{\mu\nu} = \mathcal{E} n_\mu n_\nu, \;\; A_\mu = \mathcal{A} n_\mu \quad \Longrightarrow \quad T_{++}, \;\; A_+ \neq 0, \tag{7.39}$$

are the only non-vanishing components. In other words, we have:

$$T_{++}, \;\; T_+^{\mathrm{K}}, \;\; T_+^{(\phi)}, \;\; T^{(\phi)}, \;\; T^{(\theta)} \propto \delta(x^+ - x_0^+). \tag{7.40}$$

We require that the metric ρ and the dilaton field x remain continuous across the shockwave. Since, at the shockwave, they are well-defined functions of x^-, their derivatives with respect to x^- cannot exhibit discontinuities and must therefore also be continuous. This, in turn, ensures the continuity of F^+, which is a component of the time-like Killing vector orthogonal to the ingoing shockwave. Furthermore, for static solutions, the function $\mathcal{D}(\mathrm{x})$ must likewise be continuous. On the other hand, Eq. (7.3) shows that the only field allowed to have a discontinuity, due to the non-zero contorsion current on the shockwave hypersurface, is the θ field. Consequently, we do not impose continuity on θ, even though it is a scalar field. We justify this by noting that it is actually a component of the five-dimensional torsion.

We begin by integrating Eq. (7.3), which was obtained by varying the action with respect to the contorsion, from $x_0^+ - \epsilon$ to $x_0^+ + \epsilon$, with $\epsilon > 0$, and then taking the limit $\epsilon \to 0$. Because ϕ_+ and $\partial_+ \mathrm{x}$ possess only a finite number of discontinuities, we find:

$$\mathrm{x}\theta^2 \Big|_<^> = \frac{1}{6k\pi^2} \lim_{\epsilon\to 0} \int_{x_0^+ - \epsilon}^{x_0^+ + \epsilon} T_+^{\mathrm{K}} \, \mathrm{d}x^+, \tag{7.41}$$

where the symbol ">" ("<") denotes the region of spacetime after (before) the collapse. The "$-$" component of Eq. (7.3) is automatically satisfied. We now turn to Eq. (7.5), for which both components must be analyzed. After carrying out the integration and carefully examining the behavior of each term, we obtain two additional constraints:

$$\left(\partial_- \mathrm{x} + \frac{1}{2l}\phi_-\right)\phi_- \Big|_<^> = 0, \tag{7.42}$$

$$\lim_{\epsilon\to 0} \int_{x_0^+ - \epsilon}^{x_0^+ + \epsilon} \left(\partial_- \mathrm{x} + \frac{1}{l}\phi_-\right) \partial_+ \left(e^{-2\rho}\phi_+\right) \mathrm{d}x^+ = -\frac{1}{24k\pi^2\lambda l} \lim_{\epsilon\to 0} \int_{x_0^+ - \epsilon}^{x_0^+ + \epsilon} T_+^{(\phi)} \, \mathrm{d}x^+. \tag{7.43}$$

Observe that Eq. (7.42) does not directly enforce continuity of ϕ_-. A straightforward evaluation of the "$+-$" component of Eq. (7.7) gives:

$$\left[\mathrm{x}^2 + 1 - \theta^2 + 4l\, e^{-2\rho}\phi_+ \left(\partial_- \mathrm{x} + \frac{1}{l}\phi_-\right)\right]\phi_- \Big|_<^> = \frac{l}{6k\pi^2} \lim_{\epsilon\to 0} \int_{x_0^+ - \epsilon}^{x_0^+ + \epsilon} \partial_- T_+^{\mathrm{K}} \, \mathrm{d}x^+, \tag{7.44}$$

which becomes identically satisfied once Eqs. (7.41) and (7.3) are taken into account. The "$--$" component of the metric equation does not introduce any further conditions, so only the "$++$" component remains. Integrating this component, we obtain:

$$\left(\mathrm{x}^2+1-\theta^2-\Phi^2\right)e^{-2\rho}\phi_+\Big|_<^> + \lim_{\epsilon\to 0}\int_{x_0^+-\epsilon}^{x_0^++\epsilon}\mathrm{d}x^+\left[\partial_+\Phi^2-4\left(l\partial_-\mathrm{x}+\phi_-\right)\partial_+\left(e^{-2\rho}\phi_+\right)\right]e^{-2\rho}\phi_+$$
$$=\frac{l}{6k\pi^2}\lim_{\epsilon\to 0}\int_{x_0^+-\epsilon}^{x_0^++\epsilon}\mathrm{d}x^+\left[T_{++}e^{-2\rho}-\partial_+\left(e^{-2\rho}T_+^{\mathrm{K}}\right)\right], \quad (7.45)$$

which, upon using Eq. (7.43), simplifies to:

$$\left(\mathrm{x}^2+1-\theta^2-2l\,e^{-2\rho}\phi_+\partial_-\mathrm{x}\right)e^{-2\rho}\phi_+\Big|_<^> = \frac{l}{6k\pi^2}\lim_{\epsilon\to 0}\int_{x_0^+-\epsilon}^{x_0^++\epsilon}T_{++}e^{-2\rho}\,\mathrm{d}x^+, \quad (7.46)$$

where we have used $e^{-2\rho}T_+^{\mathrm{K}}\big|_>^< = 0$, since T_+^{K} is nonzero only precisely on the shockwave hypersurface. Next, we integrate the θ equation, Eq. (7.4), obtaining:

$$\mathrm{x}e^{-2\rho}\mathrm{K}_-\Big|_<^> = \frac{1}{24k\pi^2}\lim_{\epsilon\to 0}\int_{x_0^+-\epsilon}^{x_0^++\epsilon}\mathrm{d}x^+\,T^{(\theta)}. \quad (7.47)$$

Finally, applying Eq. (7.6) for the dilaton field yields the remaining condition:

$$\left[\left(\mathrm{x}^2+1-\theta^2-\Phi^2\right)\mathrm{K}_-+\frac{2\mathrm{x}}{l}\phi_--4e^{-2\rho}\phi_-\partial_-\phi_+-4l\partial_-\left(\partial_-\mathrm{x}e^{-2\rho}\phi_+\right)\right]\Big|_<^>$$
$$=\frac{1}{12k\pi^2}\lim_{\epsilon\to 0}\int_{x_0^+-\epsilon}^{x_+^++\epsilon}\mathrm{d}x^+\left[\frac{1}{\mathrm{x}}T^{(\phi)}e^{2\rho}-\frac{2}{\mathrm{x}}\mathrm{K}_-T_+^{\mathrm{K}}-\frac{2}{\lambda}\partial_-T_+^{(\phi)}\right]. \quad (7.48)$$

We now restrict our analysis to situations in which the matter sector is strictly two-dimensional, implying $T_+^{(\phi)}=T^{(\phi)}=T^{(\theta)}=0$. From Eq. (7.47) it follows immediately that K_- must be continuous across the shockwave. Inspecting Eq. (7.43), we see right away that ϕ_- and ϕ_+ cannot both be discontinuous: if they were, the integrand would no longer be well defined as a distribution, since it would involve a product of two distributions. To study that kind of behavior one would need to abandon the idealization of the infalling matter as an infinitely thin shell. Because our goal is to formulate junction conditions precisely in the limit of an infinitely thin shell, we must therefore restrict ourselves to cases in which ϕ_- and ϕ_+ are not both discontinuous. This leads to three distinct possibilities:

- ϕ_--discontinuous: In this case, Eq. (7.43) enforces the continuity of ϕ_+. Consequently, the full set of junction conditions becomes:

$$\begin{aligned}&\phi_-^> = -\phi_-^< - 2l\partial_-\mathrm{x}, \quad \phi_+^> = \phi_+^<,\\ &\mathrm{x}\theta^2\Big|_<^> = \frac{1}{6k\pi^2}\lim_{\epsilon\to 0}\int_{x_0^+-\epsilon}^{x_+^++\epsilon}T_+^{\mathrm{K}}\mathrm{d}x^+, \quad \lim_{\epsilon\to 0}\int_{x_0^+-\epsilon}^{x_+^++\epsilon}\mathrm{d}x^+\left[\phi_+T_+^{\mathrm{K}}+l\mathrm{x}T_{++}\right]=0,\\ &\mathrm{K}_- = \partial_-\ln\phi_+-\frac{1}{2l}\frac{\mathrm{x}}{\phi_+}e^{2\rho}.\end{aligned} \quad (7.49)$$

- ϕ_--continuous and $\phi_- \neq -l\partial_- \mathrm{x}$: Here, Eq. (7.43) again implies that ϕ_+ must be continuous. Then Eq. (7.48) yields $\mathrm{K}_- = 0$, so the junction conditions are:

$$\begin{aligned}
&\phi_\mu^> = \phi_\mu^<, \\
&\mathrm{x}\theta^2\Big|_<^> = \frac{1}{6k\pi^2}\lim_{\epsilon\to 0}\int_{x_0^+-\epsilon}^{x_+^++\epsilon} T_+^{\mathrm{K}}\mathrm{d}x^+, \quad \lim_{\epsilon\to 0}\int_{x_0^+-\epsilon}^{x_+^++\epsilon}\mathrm{d}x^+\left[\phi_+T_+^{\mathrm{K}} + l\mathrm{x}T_{++}\right] = 0, \\
&\mathrm{K}_- = 0.
\end{aligned} \tag{7.50}$$

- $\phi_- = -l\partial_-\mathrm{x}$: This is the most general physically relevant case, since the mass is no longer tied to the discontinuity in the θ field as it was in the previous two scenarios. Now ϕ_+ is allowed to be discontinuous, and we obtain the following junction conditions:

$$\begin{aligned}
&\phi_- = -l\partial_-\mathrm{x}, \\
&\left(\mathrm{x}^2 + 1 - \theta^2 - 2le^{-2\rho}\phi_+\partial_-\mathrm{x}\right)e^{-2\rho}\phi_+\Big|_<^> = \frac{l}{6k\pi^2}\lim_{\epsilon\to 0}\int_{x_0^+-\epsilon}^{x_+^++\epsilon} T_{++}e^{-2\rho}\mathrm{d}x^+, \\
&\mathrm{x}\theta^2\Big|_<^> = \frac{1}{6k\pi^2}\lim_{\epsilon\to 0}\int_{x_0^+-\epsilon}^{x_+^++\epsilon} T_+^{\mathrm{K}}\mathrm{d}x^+, \quad \mathrm{K}_- = -\partial_-\ln\left(e^{-2\rho}\partial_-\mathrm{x}\right).
\end{aligned} \tag{7.51}$$

Gravitational collapse into a BTZ black hole with torsion

We do not impose junction conditions on solutions of type RCIIA and RCIIB, because they involve numerous undetermined functions associated with unfixed gauge symmetries. For the type RCI solutions given in Eq. (7.35), we find that the junction conditions (7.49) and (7.50) do not describe a gravitational collapse, as anticipated. Only the junction conditions in Eq. (7.51) yield a genuine gravitational collapse.

$$\phi_- = -l\partial_-\mathrm{x} \quad\Longrightarrow\quad \phi^\perp + \mathcal{D} = 0 \quad\Longrightarrow\quad \phi^\perp = -\mathcal{D} = -1 \tag{7.52}$$

The condition enforcing vanishing contorsion is now satisfied automatically, since it reduces to $\mathrm{K}_- = -\partial_-\ln\mathcal{D} = 0$. The mass relation then becomes:

$$\left(\mu + 1 - \theta^2\right)\Big|_<^> + 2\mathrm{x}^2\theta^2\Big|_<^> = \frac{2lM}{3k\pi^2}. \tag{7.53}$$

This expression immediately implies that θ^2 must be continuous across the junction, which in turn gives $T_\mu^{\mathrm{K}} = 0$. Consequently, the mass is determined by:

$$\frac{2Ml}{3k\pi^2} = \left(\mu + 1 - \theta^2\right)^2 - \left(1 - \theta^2\right), \tag{7.54}$$

where we have again taken the initial spacetime to be the AdS vacuum with $\mu = 0$, as in the Riemannian analysis of Sec. 6.1.4. It is now clear that this mass formula reduces to Eq. (6.52) in the limit $\theta \to 0$, in agreement with the fact that the theory then collapses to its purely Riemannian sector. The requirement that the metric and the dilaton field be continuous yields the same discontinuity in the function F^- as in the Riemannian case, given by Eq. (6.43) for an arbitrary initial constant $\mu_<$ and by Eq. (6.46) for gravitational collapse from the AdS vacuum.

To conclude, we observe that gravitational collapse fixes the unphysical gauge freedom of the function $\phi^\perp$, as one would anticipate. Moreover, this implies $\mathcal{D} = 1$ and $\bar{\mathrm{x}} = \mathrm{x}$, so that the dilaton once again serves as the coordinate in which the black-hole metric takes its standard form, defined in Eq. (3.20). Finally, the θ function becomes a fundamental constant of the spacetime, which cannot be altered by gravitational collapse between vacuum configurations. This matches the conclusion of [89]. Nevertheless, this does not imply that once specific matter fields are included, θ cannot change as a consequence of dynamical gravitational collapse. We do not explore this route here.

7.2 General solutions with non-vanishing matter fields

In this section, we analyze the gravity equations of motion in the presence of matter. As our focus excludes the vacuum solutions, at least one component of the EMT and/or the contorsion current must be non-vanishing. The main aim is to find solutions for the additional field content, i.e. the contorsion K^μ, vector field ϕ^μ and θ in terms of the dilaton field x and the metric function Λ, and subsequently express the remaining equations in terms of the sources and Λ.

One of the equations of motion (7.14) is inherently satisfied when $\theta = 0$, significantly altering both the form of the equations of motion and their corresponding solutions. Moreover, since the function $\mathcal{Z}$ appears as a prefactor in most equations, whether it vanishes or not gives rise to additional distinct cases. Further special instances require individual consideration. Therefore, we provide Tab. 7.1, which summarizes all these cases. The initial column of the table indicates the non-zero source, whereas the subsequent three columns outline the conditions that specify the solution. The axillary function $\mathcal{J}$ appearing in Tab. 7.1 varies from case to case, and for that reason it is defined for each particular case, while P is an integration constant relevant to some cases. Using the axillary functions of the sources (7.27), the conservation laws for the EMT (3.66) and (3.67) can be rewritten in the following form:

$$
\begin{aligned}
&2\Lambda\frac{\mathrm{d}\tilde{T}^{\perp\perp}}{\mathrm{d}\bar{\mathrm{x}}}+\frac{\mathrm{d}\Lambda}{\mathrm{d}\bar{\mathrm{x}}}\left(\tilde{T}^{\shortparallel\shortparallel}+\tilde{T}^{\perp\perp}\right)=4l\Lambda\mathrm{K}^{\perp}\frac{\mathrm{d}}{\mathrm{d}\bar{\mathrm{x}}}\left(\Lambda\tilde{T}^{\perp}_{\mathrm{K}}\right)-2\Lambda\tilde{T}^{\shortparallel}_{\mathrm{K}}\frac{\mathrm{d}\mathcal{S}}{\mathrm{d}\bar{\mathrm{x}}},\\
&\tilde{T}^{\shortparallel\perp}=2l\Lambda\mathrm{K}^{\shortparallel}\tilde{T}^{\perp}_{\mathrm{K}}+\frac{const.}{\Lambda},
\end{aligned}
\tag{7.55}
$$

where within our model the constant in the second equation vanishes. The second condition is automatically satisfied on Eqs. (7.22) and (7.25). It is straight-forward to check that the first conservation law is satisfied in each case separately.

It turns out that any free, minimally-coupled matter field theory possesses an identically vanishing contorsion current. For scalar and vector fields this is straightforward. The subtlety arises for spinor fields, where the contorsion appears explicitly in the action. Even so, when one varies the action with respect to the contorsion, the ensuing contorsion current manifestly vanishes. A non-zero value for this current occurs only once non-minimal couplings are introduced. Consequently, we focus in particular on setups where the energy-momentum tensor is the only non-vanishing source. In such a situation we automatically obtain $\phi^{\shortparallel} = \mathrm{K}^{\perp} = 0$, as well as $T^{\shortparallel\perp} = 0$. There are for configurations with non-vanishing θ field. In all these configurations the solution is determined by three integration constants η, P, and D, and is most conveniently expressed in the z coordinate (3.21). On the other hand, if one allows the θ field to vanish, the theory collapses to the purely Riemannian sector analyzed in the preceding chapter.

The case when the parallel component of the contorsion current together with the EMT does not vanish is of great importance when there is non-minimal coupling of the matter fields only to the curvature of the spacetime. In the two-dimensional case, terms linear in curvature have the following form:

$$S_{int} \propto \int \varepsilon_{ab} R^{ab} F = - \int \mathrm{d}^2 x \sqrt{-g} \left(\mathrm{R} + 2\varepsilon^{\alpha\beta} \nabla_\alpha \mathrm{K}_\beta \right) F, \tag{7.56}$$

where F denotes a scalar function related to the field content within the theory. The second equality comes from expression (2.42). The second term in expression (7.56) is significant for the purpose of our argument. Varying with respect to K_μ leads to the following expression for the source of contorsion:

$$T^\mu_{\mathrm{K}} \propto \varepsilon^{\mu\nu} \nabla_\nu F = \frac{\mathcal{D}}{l} \frac{\mathrm{d}F}{\mathrm{dx}} \xi^\mu, \tag{7.57}$$

implying that only a parallel component of the contorsion current exists. Even adding a quadratic term in the Riemann-Cartan curvature, or any function of R, leads to an identical outcome. Since $T^\perp_{\mathrm{K}} = 0$, once again $\phi^\parallel = 0$ and $\mathrm{K}^\perp = 0$, as well as $T^{\parallel\perp} = 0$.

In this situation, the solutions reduce to those of the previous case when one takes the limit in which the contorsion current vanishes. However, for $\theta \neq 0$ there are five distinct solutions, in contrast to the earlier case. The presence of a non-zero parallel component of the contorsion current yields a BTZ-like solution with non-vanishing EMT, together with an arbitrary $\phi^\perp$ function and constants P and η. In contrast with the preceding case, when $\theta = 0$ the non-vanishing $T^\parallel_{\mathrm{K}}$ leads to a much richer spectrum of solutions, which can display a non-zero two-dimensional torsion, as shown in Tab. 7.1. Finally, only in this scenario can a vanishing $\mathcal{Z}$ function be imposed. This provides an additional perspective on the stability of the vacuum solutions RCIIA (7.38) and RCIIB.

Finally, the most general case arises when the normal component of the contorsion current does not vanish. This situation occurs only in the presence of a non-minimal coupling of the matter action to the two-dimensional torsion. The solutions in the $\theta \neq 0$ sector are then characterized by two constants, η and P, whereas the $\theta = 0$ sector resembles the previous case and reduces to it in the limit where the normal component of the contorsion current goes to zero.

In what follows, we do not organize this section according to which component of the contorsion current vanishes. Instead, we directly solve the equations and thereby explain why the various cases appear. The discussion is structured around three main scenarios: two scenarios with $\mathcal{Z} \neq 0$, distinguished by whether θ is present or absent, and a third scenario with $\mathcal{Z} = 0$. Moreover, when $\mathcal{Z} \neq 0$, we further distinguish three cases according to which components of the contorsion current are non-vanishing. Throughout all of these cases, we assume that both the dilaton field and the metric are non-zero, i.e., $\mathrm{x} \neq 0$ and $\Lambda \neq 0$.

7.2.1 Solutions when $\mathcal{Z} \neq 0$ and $\theta \neq 0$

We begin by analyzing the constraint equations. Since $\theta \neq 0$, condition (7.14) is satisfied, and consequently the dilaton field Eq. (7.17) becomes considerably simpler, as the scalar curvature term drops out. After additionally substituting Eqs. (7.15) and (7.16) into Eq. (7.17), we obtain:

$$\begin{aligned} \frac{4}{\mathrm{x}} l \left(\mathrm{x}^2 - \Phi^2\right) \varepsilon^{\alpha\beta} \phi_\alpha \mathrm{K}_\beta = \frac{2}{\mathrm{x}} \Lambda \phi^\perp \mathcal{D} \frac{\mathrm{d}}{\mathrm{dx}} \left(\mathrm{x}^2 - \Phi^2\right) + \frac{4}{\mathrm{x}} \left(\mathrm{x}^2 - \Phi^2\right) \left(\mathrm{x} - \mathcal{D} \frac{\mathrm{d}\left(\Lambda \phi^\perp\right)}{\mathrm{dx}} \right) \\ - \mathcal{D} \left(\frac{\mathrm{d}\Phi^2}{\mathrm{dx}} - \frac{2}{\mathrm{x}} \Phi^2 \right) \left(\mathcal{D} \frac{\mathrm{d}\Lambda}{\mathrm{dx}} - 2l\Lambda \mathrm{K}^\parallel \right). \end{aligned} \tag{7.58}$$

Source	Condition 1	Condition 2	Condition 3	Condition 4
$T^{\mathrm{K}}_{\mu} = 0$	$\theta \neq 0 \ \wedge \ \mathcal{Z} \neq 0$	$\Lambda > 0$	$\mathrm{x}^2 + \Lambda\phi^{\perp 2} > 0$	/
		$\Lambda < 0$	$\mathrm{x}^2 + \Lambda\phi^{\perp 2} > 0$	/
			$\mathrm{x}^2 + \Lambda\phi^{\perp 2} < 0$	/
			$\mathrm{x}^2 + \Lambda\phi^{\perp 2} = 0$	/
	$\theta = 0 \ \wedge \ \mathcal{Z} \neq 0$	$\phi^{\perp} \neq 0$	$\mathcal{S}^2 + 4\Lambda \neq 0 \ \wedge \ \mathcal{J} \neq 0$	$\mathcal{S}' + 2 = 0$
				$\mathcal{S}' + 2 \neq 0$
			$\mathcal{S}^2 + 4\Lambda \neq 0 \ \wedge \ \mathcal{J} = 0$	/
			$\mathcal{S}^2 + 4\Lambda = 0$	/
		$\phi^{\perp} = 0$	/	/
$T^{\perp}_{\mathrm{K}} = 0$	$\theta \neq 0 \ \wedge \ \mathcal{Z} \neq 0$	$\mathcal{S}\phi^{\perp} \neq 2\mathrm{x}$	$\Lambda > 0$	$\mathrm{x}^2 + \Lambda\phi^{\perp 2} > 0$
			$\Lambda < 0$	$\mathrm{x}^2 + \Lambda\phi^{\perp 2} > 0$
				$\mathrm{x}^2 + \Lambda\phi^{\perp 2} < 0$
				$\mathrm{x}^2 + \Lambda\phi^{\perp 2} = 0$
		$\mathcal{S}\phi^{\perp} = 2\mathrm{x}$	/	/
	$\theta = 0 \ \wedge \ \mathcal{Z} \neq 0$	$\phi^{\perp} \neq 0 \ \wedge \ \mathcal{D} \neq 0$	$\mathcal{S}^2 + 4\Lambda \neq 0 \ \wedge \ \mathcal{J} \neq 0$	$\tilde{T}^{\perp\perp} \neq 0$
				$\tilde{T}^{\perp\perp} = 0$
			$\mathcal{S}^2 + 4\Lambda \neq 0 \ \wedge \ \mathcal{J} = 0$	$\mathcal{Z} \neq 2/3$
				$\mathcal{Z} = 2/3$
			$\mathcal{S}^2 + 4\Lambda = 0$	$\tilde{T}^{\perp\perp} \neq 0$
				$\tilde{T}^{\perp\perp} = 0$
		$\mathcal{D} = 0$	/	/
		$\phi^{\perp} = 0$	/	/
	$\mathcal{Z} = 0$	/	/	/
$T^{\perp}_{\mathrm{K}} \neq 0$	$\theta \neq 0 \ \wedge \ \mathcal{Z} \neq 0$	$\Phi^2 \neq \mathrm{x}^2 \ \wedge \ \phi^{\perp} \neq 0$	$P \neq 0$	$\mathcal{S}^2 + 4\Lambda \notin \{0, P^2\}$
				$\mathcal{S}^2 + 4\Lambda = P^2$
				$\mathcal{S}^2 + 4\Lambda = 0$
			$P = 0$	$\mathcal{S}^2 + 4\Lambda \neq 0$
				$\mathcal{S}^2 + 4\Lambda = 0$
		$\Phi^2 = \mathrm{x}^2 \ \wedge \ \phi^{\perp} \neq 0$	$\mathcal{S}^2 + 4\Lambda \neq 0$	/
			$\mathcal{S}^2 + 4\Lambda = 0$	/
		$\phi^{\perp} = 0$	/	/
	$\theta = 0 \ \wedge \ \mathcal{Z} \neq 0$	$\phi^{\perp} \neq 0 \ \wedge \ \mathcal{D} \neq 0$	$\mathcal{S}^2 + 4\Lambda \neq 0 \ \wedge \ \mathcal{J} \neq 0$	$\tilde{T}^{\perp\perp} \neq 0$
				$\tilde{T}^{\perp\perp} = 0$
			$\mathcal{S}^2 + 4\Lambda \neq 0 \ \wedge \ \mathcal{J} = 0$	$\mathcal{Z} \neq 2/3$
				$\mathcal{Z} = 2/3$
			$\mathcal{S}^2 + 4\Lambda = 0$	$\tilde{T}^{\perp\perp} \neq 0$
				$\tilde{T}^{\perp\perp} = 0$
		$\mathcal{D} = 0$	/	/
		$\phi^{\perp} = 0$	/	/

Table 7.1: Classification of the solutions to the equations of motion

Observe that Eq. (7.58) is identically fulfilled when $\Phi^2 = \mathrm{x}^2$, indicating that this special case must be treated independently. Accordingly, the subsection is split into five parts, distinguished by which components of the contorsion current vanish and by whether the condition $\Phi^2 = \mathrm{x}^2$ holds.

Completely vanishing contorsion current

Here we solve the equations of motion in the case where $T_{\mathrm{K}}^{\shortparallel} = T_{\mathrm{K}}^{\perp} = 0$. Because $\mathcal{Z} \neq 0$, Eq. (7.25) enforces $\phi^{\shortparallel} = 0$, which in turn simplifies Eq. (7.15) to $\mathrm{K}^{\perp} = 0$. From Eq. (7.22) we further obtain $T^{\shortparallel\perp} = 0$. Consequently, the system of equations simplifies to:

$$\mathcal{Z}\left[\phi^{\perp}\frac{\mathrm{d}\Lambda}{\mathrm{d}\bar{\mathrm{x}}} - 2\mathrm{x} - 2l\Lambda\phi^{\perp}\mathrm{K}^{\shortparallel}\right] = -\tilde{T}^{\perp\perp}, \tag{7.59}$$

$$\mathcal{Z}\left[2\Lambda\left(\frac{\mathrm{d}\phi^{\perp}}{\mathrm{d}\bar{\mathrm{x}}} - \frac{1}{\mathrm{x}}\phi^{\perp}\left(\phi^{\perp} + \mathcal{D}\right)\right) + \phi^{\perp}\frac{\mathrm{d}\Lambda}{\mathrm{d}\bar{\mathrm{x}}} - 2\mathrm{x}\right] = \tilde{T}^{\shortparallel\shortparallel}, \tag{7.60}$$

$$\mathcal{Z}\left(\phi^{\perp} + \mathcal{D}\right) = \mathrm{x}\frac{\mathrm{d}\theta^2}{\mathrm{d}\bar{\mathrm{x}}}, \tag{7.61}$$

$$\left(\phi^{\perp} + \mathcal{D}\right)\left[\phi^{\perp}\frac{\mathrm{d}\Lambda}{\mathrm{d}\bar{\mathrm{x}}} - 2\mathrm{x} - 2l\Lambda\phi^{\perp}\mathrm{K}^{\shortparallel}\right] = l\mathcal{Z}\mathrm{K}^{\shortparallel}, \tag{7.62}$$

$$\frac{\mathrm{d}}{\mathrm{d}\bar{\mathrm{x}}}\left(\frac{\mathrm{d}\Lambda}{\mathrm{d}\bar{\mathrm{x}}} - 2l\Lambda\mathrm{K}^{\shortparallel}\right) + 2 + \frac{2}{\mathrm{x}}l\Lambda\phi^{\perp}\mathrm{K}^{\shortparallel} = 0, \tag{7.63}$$

$$\left[2\Lambda\left(\frac{\mathrm{d}\phi^{\perp}}{\mathrm{d}\bar{\mathrm{x}}} - \frac{1}{\mathrm{x}}\phi^{\perp}\left(\phi^{\perp} + \mathcal{D}\right)\right) + \phi^{\perp}\frac{\mathrm{d}\Lambda}{\mathrm{d}\bar{\mathrm{x}}} - 2\mathrm{x}\right]\left[\phi^{\perp}\frac{\mathrm{d}\Lambda}{\mathrm{d}\bar{\mathrm{x}}} - 2\mathrm{x} - 2l\Lambda\phi^{\perp}\mathrm{K}^{\shortparallel}\right] = 0. \tag{7.64}$$

By imposing that the second bracket in Eq. (7.64) vanishes, the EMT is set to zero, implying $T^{\shortparallel\shortparallel} = T^{\perp\perp} = 0$, and the resulting solution coincides exactly with Eq. (7.35). This case is not of particular interest, since we are focusing on configurations where at least one EMT component is non-zero. Consequently, the first bracket in Eq. (7.64) must vanish, which leads to

$$\frac{\mathrm{d}}{\mathrm{d}\bar{\mathrm{x}}}\left(\Lambda\phi^{\perp 2} + \mathrm{x}^2\right) = \frac{2}{\mathrm{x}}\left(\Lambda\phi^{\perp 2} + \mathrm{x}^2\right)\left(\phi^{\perp} + \mathcal{D}\right). \tag{7.65}$$

Taken together with Eq. (7.60), this condition also eliminates the parallel component of the EMT, i.e. $T^{\shortparallel\shortparallel} = 0$, while the normal component remains non-zero. Depending on the signs of Λ and $\Lambda\phi^{\perp 2} + \mathrm{x}^2$, four distinct cases must be considered. In all of these cases, the coordinate z, defined by Eq. (3.21), is employed.

- $\underline{\Lambda > 0}$: Integrating Eq. (7.65) results into the following solution for $\phi^{\perp}$:

$$\phi^{\perp} = \frac{\mathrm{x}}{\sqrt{\Lambda}}\tan\mathrm{z}. \tag{7.66}$$

Using this solution as well as the definition of the z coordinate (3.21), Eq. (7.61) can be integrated resulting in a solution for the θ field:

$$\theta^2 = 1 + \frac{1}{3}\left(\frac{\mathrm{x}}{\cos\mathrm{z}}\right)^2 + \eta\frac{\cos\mathrm{z}}{\mathrm{x}}, \tag{7.67}$$

where η is an integration constant. Next, direct integration of Eq. (7.63) results into:

$$2l\Lambda\mathrm{K}^{\shortparallel} = \frac{\mathrm{d}\Lambda}{\mathrm{d}\bar{\mathrm{x}}} + 2\sqrt{\Lambda}\tan\mathrm{z} - \frac{P}{\cos\mathrm{z}}, \tag{7.68}$$

where P is another integration constant. Using the solutions (7.66-7.68) makes Eq. (7.62) integrable, giving the following solution for the dilaton field:

$$\frac{2}{3}\left(\frac{\mathrm{x}}{\cos \mathrm{z}}\right)^3 = \frac{D\cos \mathrm{z}}{\sqrt{\Lambda} - \frac{P}{2}\sin \mathrm{z}} + \eta, \tag{7.69}$$

where D is the final integration constant. Placing solutions (7.66-7.69) in the last remaining Eq. (7.59) gives a condition for the EMT:

$$T^{\perp\perp} = \frac{6k\pi^2 D}{l^2}\frac{1}{\Lambda^{3/2}}. \tag{7.70}$$

- $\underline{\Lambda < 0 \ \wedge \ \mathrm{x}^2 + \Lambda\phi^{\perp 2} > 0}$: In this case, the solution to the Eq. (7.65) is given by the following expression:

$$\phi^{\perp} = \frac{\mathrm{x}}{\sqrt{-\Lambda}}\tanh \mathrm{z}. \tag{7.71}$$

Integrating Eqs. (7.61) and (7.63) yields:

$$\theta^2 = 1 + \frac{1}{3}\left(\frac{\mathrm{x}}{\cosh \mathrm{z}}\right)^2 + \eta\frac{\cosh \mathrm{z}}{\mathrm{x}}, \tag{7.72}$$

$$2l\Lambda \mathrm{K}^{\parallel} = \frac{\mathrm{d}\Lambda}{\mathrm{d}\bar{\mathrm{x}}} - 2\sqrt{-\Lambda}\tanh \mathrm{z} - \frac{P}{\cosh \mathrm{z}}, \tag{7.73}$$

respectively. The solution to Eq. (7.62) and the constraint on the perpendicular component of the EMT are given by:

$$\frac{2}{3}\left(\frac{\mathrm{x}}{\cosh \mathrm{z}}\right)^3 = \frac{D\cosh \mathrm{z}}{\sqrt{-\Lambda} - \frac{P}{2}\sinh \mathrm{z}} + \eta, \tag{7.74}$$

$$T^{\perp\perp} = -\frac{6k\pi^2 D}{l^2}\frac{1}{(-\Lambda)^{3/2}}. \tag{7.75}$$

Similarly to the previous case, the solution depends on three constants η, P and D.

- $\underline{\Lambda < 0 \ \wedge \ \mathrm{x}^2 + \Lambda\phi^{\perp 2} < 0}$: Eq. (7.65) gives the following solution:

$$\phi^{\perp} = \frac{\mathrm{x}}{\sqrt{-\Lambda}}\coth \mathrm{z}. \tag{7.76}$$

Eqs. (7.61) and (7.63) reduce to:

$$\theta^2 = 1 - \frac{1}{3}\left(\frac{\mathrm{x}}{\sinh \mathrm{z}}\right)^2 + \eta\frac{\sinh \mathrm{z}}{\mathrm{x}}, \tag{7.77}$$

$$2l\Lambda \mathrm{K}^{\parallel} = \frac{\mathrm{d}\Lambda}{\mathrm{d}\bar{\mathrm{x}}} - 2\sqrt{-\Lambda}\coth \mathrm{z} - \frac{P}{\sinh \mathrm{z}}, \tag{7.78}$$

respectively. The answer to Eq. (7.62) along with the condition on the perpendicular component of the EMT is expressed as:

$$\frac{2}{3}\left(\frac{\mathrm{x}}{\sinh \mathrm{z}}\right)^3 = \frac{D\sinh \mathrm{z}}{\sqrt{-\Lambda} + \frac{P}{2}\cosh \mathrm{z}} - \eta, \tag{7.79}$$

$$T^{\perp\perp} = -\frac{6k\pi^2 D}{l^2}\frac{1}{(-\Lambda)^{3/2}}. \tag{7.80}$$

In a manner akin to the earlier situations, the solution relies on three constants: η, P, and D.

- $\underline{\Lambda < 0 \wedge \mathrm{x}^2 + \Lambda\phi^{\perp 2} = 0}$: The specific condition in this case automatically satisfies Eq. (7.65) and implies:

$$\phi^{\perp} = \pm\frac{\mathrm{x}}{\sqrt{-\Lambda}} \tag{7.81}$$

It is straight-forward to integrate both Eqs. (7.61) and (7.63). The solution is given by:

$$\theta^2 = 1 + \frac{\eta}{\mathrm{x}}e^{\pm \mathrm{z}}. \tag{7.82}$$

$$2l\Lambda\mathrm{K}^{\shortparallel} = \frac{\mathrm{d}\Lambda}{\mathrm{d}\bar{\mathrm{x}}} \mp 2\sqrt{-\Lambda} + 2Pe^{\mp\mathrm{z}}. \tag{7.83}$$

In this instance, solving the integral of Eq. (7.62) results in:

$$\frac{2}{3}\left(\mathrm{x}e^{\mp\mathrm{z}}\right)^3 = \frac{\eta}{P}\left[\left(\pm\sqrt{-\Lambda} - \frac{P}{2}e^{\mp\mathrm{z}}\right)e^{\mp\mathrm{z}} + D\right], \tag{7.84}$$

while the constraint imposed on the EMT is given by:

$$T^{\perp\perp} = \pm\frac{6k\pi^2\eta P}{l^2}\frac{1}{(-\Lambda)^{3/2}}. \tag{7.85}$$

We conclude that, in this final case, the solution once again depend on three constants η, P and D.

Non-vanishing parallel component of contorsion current

In this section, we assume that $T_{\mathrm{K}}^{\shortparallel} \neq 0$ while $T_{\mathrm{K}}^{\perp} = 0$. Due to analogous reasons presented in the preceding section, it holds that $\phi^{\shortparallel} = \mathrm{K}^{\perp} = T^{\shortparallel\perp} = 0$. Consequently, we have the following system of equations remaining:

$$\mathcal{Z}\left[\phi^{\perp}\frac{\mathrm{d}\Lambda}{\mathrm{d}\bar{\mathrm{x}}} - 2\mathrm{x} - 2l\Lambda\phi^{\perp}\mathrm{K}^{\shortparallel}\right] = -\tilde{T}^{\perp\perp}, \tag{7.86}$$

$$\mathcal{Z}\left[2\Lambda\left(\frac{\mathrm{d}\phi^{\perp}}{\mathrm{d}\bar{\mathrm{x}}} - \frac{1}{\mathrm{x}}\phi^{\perp}\left(\phi^{\perp} + \mathcal{D}\right)\right) + \phi^{\perp}\frac{\mathrm{d}\Lambda}{\mathrm{d}\bar{\mathrm{x}}} - 2\mathrm{x}\right] = \tilde{T}^{\shortparallel\shortparallel} - \frac{2}{\mathrm{x}}\Lambda\phi^{\perp}\tilde{T}_{\mathrm{K}}^{\shortparallel}, \tag{7.87}$$

$$\mathcal{Z}\left(\phi^{\perp} + \mathcal{D}\right) - \mathrm{x}\frac{\mathrm{d}\theta^2}{\mathrm{d}\bar{\mathrm{x}}} = \tilde{T}_{\mathrm{K}}^{\shortparallel}, \tag{7.88}$$

$$\left(\phi^{\perp} + \mathcal{D}\right)\left[\phi^{\perp}\frac{\mathrm{d}\Lambda}{\mathrm{d}\bar{\mathrm{x}}} - 2\mathrm{x} - 2l\Lambda\phi^{\perp}\mathrm{K}^{\shortparallel}\right] = l\mathcal{Z}\mathrm{K}^{\shortparallel}, \tag{7.89}$$

$$\frac{\mathrm{d}}{\mathrm{d}\bar{\mathrm{x}}}\left(\frac{\mathrm{d}\Lambda}{\mathrm{d}\bar{\mathrm{x}}} - 2l\Lambda\mathrm{K}^{\shortparallel}\right) + 2 + \frac{2}{\mathrm{x}}l\Lambda\phi^{\perp}\mathrm{K}^{\shortparallel} = 0, \tag{7.90}$$

$$\left[2\Lambda\left(\frac{\mathrm{d}\phi^{\perp}}{\mathrm{d}\bar{\mathrm{x}}} - \frac{1}{\mathrm{x}}\phi^{\perp}\left(\phi^{\perp} + \mathcal{D}\right)\right) + \phi^{\perp}\frac{\mathrm{d}\Lambda}{\mathrm{d}\bar{\mathrm{x}}} - 2\mathrm{x}\right]\left[\phi^{\perp}\frac{\mathrm{d}\Lambda}{\mathrm{d}\bar{\mathrm{x}}} - 2\mathrm{x} - 2l\Lambda\phi^{\perp}\mathrm{K}^{\shortparallel}\right] = 0. \tag{7.91}$$

In contrast to the previous section, setting the second bracket in Eq. (7.91) to zero does not lead to the EMT disappearing, as $T_{\mathrm{K}}^{\shortparallel}$ remains non-zero. Then Eqs. (7.89) and (7.86) reduce to $\mathrm{K}^{\shortparallel} = 0$ and $\tilde{T}^{\perp\perp} = 0$, respectively. The metric function Λ is completely determined from Eq. (7.90), that is:

$$\Lambda = -\left(\bar{\mathrm{x}}^2 - \mu\right), \tag{7.92}$$

where μ is an integration constant. Using this solution (7.92) together with Eq. (7.91) results in the following:

$$\mathrm{x} = -\bar{\mathrm{x}}\phi^{\perp}(\bar{\mathrm{x}}). \tag{7.93}$$

Putting Eq. (7.92) and Eq. (7.93) into Eq. (7.87) results into a condition for the EMT, given by:

$$\tilde{T}^{\shortparallel\shortparallel} + \frac{2}{\bar{\mathrm{x}}}\Lambda\tilde{T}^{\shortparallel}_{\mathrm{K}} = 0. \tag{7.94}$$

The last Eq. (7.88) can be directly integrated giving a solution for the θ filed:

$$\theta^2 = 1 + \frac{1}{3}\mu\phi^{\perp 2} + \frac{1}{\phi^{\perp}}\left(\eta + \int \frac{\mathrm{d}\bar{\mathrm{x}}}{\bar{\mathrm{x}}}\tilde{T}^{\shortparallel}_{\mathrm{K}}\right), \tag{7.95}$$

where η is the integration constant.

Choosing the first bracket in Eq. (7.91) to vanish we arrive at the same Eq. (7.65) as in the case when the entire contorsion current vanishes, namely:

$$\frac{\mathrm{d}}{\mathrm{d}\bar{\mathrm{x}}}\left(\Lambda\phi^{\perp 2} + \mathrm{x}^2\right) = \frac{2}{\mathrm{x}}\left(\Lambda\phi^{\perp 2} + \mathrm{x}^2\right)\left(\phi^{\perp} + \mathcal{D}\right). \tag{7.96}$$

To proceed further, we must examine four separate cases due to the varying options for the signs of Λ and $\mathrm{x}^2 + \Lambda\phi^{\perp 2}$.

- $\underline{\Lambda > 0}$: Similarly to the previous section, Eqs. (7.96), (7.87) and (7.90) reduce to the following:

$$\phi^{\perp} = \frac{\mathrm{x}}{\sqrt{\Lambda}}\tan\mathrm{z}, \tag{7.97}$$

$$\tilde{T}^{\shortparallel\shortparallel} = 2\sqrt{\Lambda}\tilde{T}^{\shortparallel}_{\mathrm{K}}\tan\mathrm{z}, \tag{7.98}$$

$$2l\Lambda\mathrm{K}^{\shortparallel} = \frac{\mathrm{d}\Lambda}{\mathrm{d}\bar{\mathrm{x}}} + 2\sqrt{\Lambda}\tan\mathrm{z} - \frac{P}{\cos\mathrm{z}}, \tag{7.99}$$

where P is the standard integration constant related to the parallel component of the contorsion. Eq. (7.88) can be directly integrated using Eq. (7.97) resulting in:

$$\theta^2 = 1 + \frac{1}{3}\left(\frac{\mathrm{x}}{\cos\mathrm{z}}\right)^2 + \frac{\cos\mathrm{z}}{\mathrm{x}}\left(\eta + I\right), \tag{7.100}$$

where η is another constant and $I = -\int \frac{\mathrm{d}\mathrm{z}\sqrt{\Lambda}}{\cos\mathrm{z}}\tilde{T}^{\shortparallel}_{\mathrm{K}}$. Eq. (7.86) gives the solution for x in the following form:

$$\frac{2}{3}\left(\frac{\mathrm{x}}{\cos\mathrm{z}}\right)^3 = \frac{\tilde{T}^{\perp\perp}\sqrt{\Lambda}}{2}\frac{\cos\mathrm{z}}{\sqrt{\Lambda} - \frac{P}{2}\sin\mathrm{z}} + \eta + I, \tag{7.101}$$

The final Eq. (7.89) gives another condition for the EMT:

$$\frac{\mathrm{d}}{\mathrm{d}\mathrm{z}}\left(\sqrt{\Lambda}\tilde{T}^{\perp\perp}\right) + \frac{2\sqrt{\Lambda}\tilde{T}^{\shortparallel}_{\mathrm{K}}}{\cos\mathrm{z}}\frac{\sqrt{\Lambda} - \frac{P}{2}\sin\mathrm{z}}{\cos\mathrm{z}} = 0. \tag{7.102}$$

- $\underline{\Lambda < 0 \ \wedge \ \mathrm{x}^2 + \Lambda\phi^{\perp 2} > 0}$: Analogues to the previous case, integration of Eqs. (7.96), (7.87) and (7.90) results into:

$$\phi^{\perp} = \frac{\mathrm{x}}{\sqrt{-\Lambda}}\tanh\mathrm{z}, \tag{7.103}$$

$$\tilde{T}^{\shortparallel\shortparallel} = -2\sqrt{-\Lambda}\tilde{T}^{\shortparallel}_{\mathrm{K}}\tanh\mathrm{z}, \tag{7.104}$$

$$2l\Lambda\mathrm{K}^{\shortparallel} = \frac{\mathrm{d}\Lambda}{\mathrm{d}\bar{\mathrm{x}}} - 2\sqrt{-\Lambda}\tanh\mathrm{z} - \frac{P}{\cosh\mathrm{z}}. \tag{7.105}$$

The other three equations provide solutions for the θ and x fields, along with an additional constraint for the EMT:

$$\theta^2 = 1 + \frac{1}{3}\left(\frac{\mathrm{x}}{\cosh \mathrm{z}}\right)^2 + \frac{\cosh \mathrm{z}}{\mathrm{x}}\left(\eta + I\right), \tag{7.106}$$

$$\frac{2}{3}\left(\frac{\mathrm{x}}{\cosh \mathrm{z}}\right)^3 = \frac{\tilde{T}^{\perp\perp}\sqrt{-\Lambda}}{2}\frac{\cosh \mathrm{z}}{\sqrt{-\Lambda} - \frac{P}{2}\sinh \mathrm{z}} + \eta + I, \tag{7.107}$$

$$\frac{\mathrm{d}}{\mathrm{dz}}\left(\sqrt{-\Lambda}\tilde{T}^{\perp\perp}\right) + \frac{2\sqrt{-\Lambda}\tilde{T}^{\parallel}_{\mathrm{K}}}{\cosh \mathrm{z}}\frac{\sqrt{-\Lambda} - \frac{P}{2}\sinh \mathrm{z}}{\cosh \mathrm{z}} = 0, \tag{7.108}$$

where the integral I is given by:

$$I = \int \frac{\mathrm{dz}\sqrt{-\Lambda}}{\cosh \mathrm{z}}\tilde{T}^{\parallel}_{\mathrm{K}}. \tag{7.109}$$

- $\underline{\Lambda < 0 \ \wedge \ \mathrm{x}^2 + \Lambda\phi^{\perp 2} < 0}$: Solving Eqs. (7.96), (7.87) and (7.90) yileds:

$$\phi^{\perp} = \frac{\mathrm{x}}{\sqrt{-\Lambda}}\coth \mathrm{z}, \tag{7.110}$$

$$\tilde{T}^{\parallel\parallel} = -2\sqrt{-\Lambda}\tilde{T}^{\parallel}_{\mathrm{K}}\coth \mathrm{z}, \tag{7.111}$$

$$2l\Lambda \mathrm{K}^{\parallel} = \frac{\mathrm{d}\Lambda}{\mathrm{d}\bar{\mathrm{x}}} - 2\sqrt{-\Lambda}\coth \mathrm{z} - \frac{P}{\sinh \mathrm{z}}. \tag{7.112}$$

Once again, the remaining equations reduce to the expected solutions:

$$\theta^2 = 1 - \frac{1}{3}\left(\frac{\mathrm{x}}{\sinh \mathrm{z}}\right)^2 + \frac{\sinh \mathrm{z}}{\mathrm{x}}\left(\eta + I\right), \tag{7.113}$$

$$\frac{2}{3}\left(\frac{\mathrm{x}}{\sinh \mathrm{z}}\right)^3 = \frac{\tilde{T}^{\perp\perp}\sqrt{-\Lambda}}{2}\frac{\sinh \mathrm{z}}{\sqrt{-\Lambda} + \frac{P}{2}\cosh \mathrm{z}} - (\eta + I), \tag{7.114}$$

$$\frac{\mathrm{d}}{\mathrm{dz}}\left(\sqrt{-\Lambda}\tilde{T}^{\perp\perp}\right) - \frac{2\sqrt{-\Lambda}\tilde{T}^{\parallel}_{\mathrm{K}}}{\sinh \mathrm{z}}\frac{\sqrt{-\Lambda} + \frac{P}{2}\cosh \mathrm{z}}{\sinh \mathrm{z}} = 0, \tag{7.115}$$

where the integral I is given by:

$$I = \int \frac{\mathrm{dz}\sqrt{-\Lambda}}{\sinh \mathrm{z}}\tilde{T}^{\parallel}_{\mathrm{K}}. \tag{7.116}$$

- $\underline{\Lambda < 0 \ \wedge \ \mathrm{x}^2 + \Lambda\phi^{\perp 2} = 0}$: According to the condition defining this case, Eq. (7.96) is solved, resulting in:

$$\phi^{\perp} = \pm\frac{\mathrm{x}}{\sqrt{-\Lambda}}. \tag{7.117}$$

The solutions to Eqs. (7.87) and (7.90) have the standard form:

$$\tilde{T}^{\parallel\parallel} = \mp 2\sqrt{-\Lambda}\tilde{T}^{\parallel}_{\mathrm{K}}, \tag{7.118}$$

$$2l\Lambda \mathrm{K}^{\parallel} = \frac{\mathrm{d}\Lambda}{\mathrm{d}\bar{\mathrm{x}}} \mp 2\sqrt{-\Lambda} + 2Pe^{\mp \mathrm{z}}. \tag{7.119}$$

Integrating Eq. (7.88) yields:

$$\theta^2 = 1 + \frac{e^{\pm \mathrm{z}}}{\mathrm{x}}\left(\eta + I\right), \tag{7.120}$$

where $I=\int \mathrm{dz}\sqrt{-\Lambda}\tilde{T}^{\parallel}_{\mathrm{K}}e^{\mp \mathrm{z}}$. Eq. (7.86) reduces to a constraint for the $T^{\perp\perp}$, that is:

$$\frac{1}{2}\sqrt{-\Lambda}\tilde{T}^{\perp\perp}\pm P(\eta+I)=0, \tag{7.121}$$

while the final Eq. (7.89) gives the following solution for x:

$$\frac{2}{3}P\left(\mathrm{x}e^{\mp \mathrm{z}}\right)^{3}=(\eta+I)\left(\pm\sqrt{-\Lambda}-\frac{P}{2}e^{\mp \mathrm{z}}\right)e^{\mp \mathrm{z}}+\eta D-\int \mathrm{dz}\sqrt{-\Lambda}\tilde{T}^{\parallel}_{\mathrm{K}}\left(\pm\sqrt{-\Lambda}-\frac{P}{2}e^{\mp \mathrm{z}}\right)e^{\mp 2\mathrm{z}}. \tag{7.122}$$

We conclude that if a non-zero parallel component of the contorsion current is present, the solutions depend on three integration constants η, P, and D similar to those in the prior section. Moreover, by taking the limit $T^{\parallel}_{\mathrm{K}}\to 0$, these solutions align with those derived earlier.

Non-vanishing normal component of contorsion current when $\Phi^2\neq \mathrm{x}^2$ and $\phi^{\perp}\neq 0$

Here, we derive the most general solution to the equations of motion (7.10-7.17). In the previous two sections, the condition $\phi^{\perp}\neq 0$ was assumed, which does not automatically hold when $T^{\perp}_{\mathrm{K}}\neq 0$. This particular situation is analyzed independently in the following sections.

After multiplying Eq. (7.14) by $\mathrm{x}^2-\Phi^2$ and substituting Eq. (7.58) into this modified equation, we reach an integrable form. Upon integration, the resulting expression is as follows:

$$\frac{\mathrm{d}\Lambda}{\mathrm{d}\bar{\mathrm{x}}}+\frac{2}{\mathrm{x}}\Lambda\phi^{\perp}-2l\Lambda\mathrm{K}^{\parallel}=\frac{P}{\mathrm{x}}\sqrt{|\mathrm{x}^2-\Phi^2|}, \tag{7.123}$$

where P is an arbitrary integration constant. We use a following convention:

$$\mathrm{x}^2-\Phi^2=\pm\left|\mathrm{x}^2-\Phi^2\right|. \tag{7.124}$$

Placing Eq. (7.123) in Eq. (7.58) we arrive at the following expression for $\mathrm{K}^{\perp}$:

$$\begin{aligned}2l\Lambda\phi^{\parallel}\mathrm{K}^{\perp}=P&\left[\frac{\mathrm{d}}{\mathrm{d}\bar{\mathrm{x}}}\sqrt{|\mathrm{x}^2-\Phi^2|}-\frac{1}{\mathrm{x}}\left(\phi^{\perp}+\mathcal{D}\right)\sqrt{|\mathrm{x}^2-\Phi^2|}\right]\\&-\left[2\Lambda\left(\frac{\mathrm{d}\phi^{\perp}}{\mathrm{d}\bar{\mathrm{x}}}-\frac{1}{\mathrm{x}}\phi^{\perp}\left(\phi^{\perp}+\mathcal{D}\right)\right)+\phi^{\perp}\frac{\mathrm{d}\Lambda}{\mathrm{d}\bar{\mathrm{x}}}-2\mathrm{x}\right].\end{aligned} \tag{7.125}$$

Substituting solutions for $\mathrm{K}^{\parallel}$ (7.123) and $\mathrm{K}^{\perp}$ (7.125) in Eqs. (7.15) and (7.16) gives:

$$l\mathcal{Z}\mathrm{K}^{\parallel}=P\phi^{\perp}\frac{\mathrm{d}}{\mathrm{d}\bar{\mathrm{x}}}\sqrt{|\mathrm{x}^2-\Phi^2|}-\frac{\mathrm{d}}{\mathrm{d}\bar{\mathrm{x}}}\left(\mathrm{x}^2-\Phi^2\right), \tag{7.126}$$

$$l\mathcal{Z}\mathrm{K}^{\perp}=P\phi^{\parallel}\frac{\mathrm{d}}{\mathrm{d}\bar{\mathrm{x}}}\sqrt{|\mathrm{x}^2-\Phi^2|}. \tag{7.127}$$

Eq. (7.22), together with Eq. (7.25), implies that the parallel component of the contorsion, as well as the variable $\mathcal{S}$, as defined in Eq. (7.29), are fully specified by the sources and the metric function Λ, leading to:

$$\mathrm{K}^{\parallel}=\frac{T^{\parallel\perp}}{T^{\perp}_{\mathrm{K}}},\qquad \mathcal{S}=\frac{\mathrm{d}\Lambda}{\mathrm{d}\bar{\mathrm{x}}}-2l\Lambda\frac{T^{\parallel\perp}}{T^{\perp}_{\mathrm{K}}} \tag{7.128}$$

Eqs. (7.123) and (7.125) can be regarded as solutions for $\mathrm{K}^{\parallel}$ and $\mathrm{K}^{\perp}$, respectively, in terms of the metric and ϕ^{μ} vector field. Using these, contorsion is removed from the equations of motion, leading to the following set of equations:

$$\mathcal{Z}\left(\mathcal{S}\phi^{\perp}-2\mathrm{x}\right)=-\tilde{T}^{\perp\perp}, \tag{7.129}$$

$$\mathcal{Z}P\left[\frac{\mathrm{d}}{\mathrm{d}\bar{\mathrm{x}}}-\frac{1}{\mathrm{x}}\left(\phi^{\perp}+\mathcal{D}\right)\right]\sqrt{|\mathrm{x}^2-\Phi^2|}=\tilde{T}^{\parallel\parallel}-\frac{2}{\mathrm{x}}\Lambda\phi^{\perp}\tilde{T}^{\parallel}_{\mathrm{K}}, \tag{7.130}$$

$$\mathcal{Z}\phi^{\parallel}=\tilde{T}^{\perp}_{\mathrm{K}}, \tag{7.131}$$

$$\mathcal{Z}\left(\phi^{\perp}+\mathcal{D}\right)-\mathrm{x}\frac{\mathrm{d}\theta^2}{\mathrm{d}\bar{\mathrm{x}}}=\tilde{T}^{\parallel}_{\mathrm{K}}, \tag{7.132}$$

$$\frac{\mathcal{Z}}{2\Lambda}\left(\frac{\mathrm{d}\Lambda}{\mathrm{d}\bar{\mathrm{x}}}-\mathcal{S}\right)=P\phi^{\perp}\frac{\mathrm{d}}{\mathrm{d}\bar{\mathrm{x}}}\sqrt{|\mathrm{x}^2-\Phi^2|}-\frac{\mathrm{d}}{\mathrm{d}\bar{\mathrm{x}}}\left(\mathrm{x}^2-\Phi^2\right), \tag{7.133}$$

$$\mathcal{Z}\left(\frac{\mathrm{d}\mathcal{S}}{\mathrm{d}\bar{\mathrm{x}}}+2\right)=2P\mathrm{x}\frac{\mathrm{d}}{\mathrm{d}\bar{\mathrm{x}}}\sqrt{|\mathrm{x}^2-\Phi^2|}-\mathcal{S}\frac{\mathrm{d}}{\mathrm{d}\bar{\mathrm{x}}}\left(\mathrm{x}^2-\Phi^2\right), \tag{7.134}$$

$$\mathcal{S}\mathrm{x}+2\Lambda\phi^{\perp}=P\sqrt{|\mathrm{x}^2-\Phi^2|}. \tag{7.135}$$

Eqs. (7.129-7.132) are analogous to the initial Eqs. (7.23-7.26); Eq. (7.135) is a reformulation of expression (7.123). Moreover, Eq. (7.133) corresponds to Eq. (7.126), whereas Eq. (7.134) is obtained by subtracting Eq. (7.126), multiplied by $\phi^{\perp}$, from Eq. (7.127).

All fields can be expressed in terms of $\sqrt{|\mathrm{x}^2-\Phi^2|}$, $\mathcal{Z}$ and sources. By concurrently solving Eqs. (7.129) and (7.135) with respect to x and $\phi^{\perp}$, we obtain:

$$\left(\mathcal{S}^2+4\Lambda\right)\phi^{\perp}=\sqrt{|\mathrm{x}^2-\Phi^2|}\left[2P-\frac{\mathcal{S}\tilde{T}^{\perp\perp}}{\mathcal{Z}\sqrt{|\mathrm{x}^2-\Phi^2|}}\right], \tag{7.136}$$

$$\left(\mathcal{S}^2+4\Lambda\right)\mathrm{x}=\sqrt{|\mathrm{x}^2-\Phi^2|}\left[P\mathcal{S}+\frac{2\Lambda\tilde{T}^{\perp\perp}}{\mathcal{Z}\sqrt{|\mathrm{x}^2-\Phi^2|}}\right], \tag{7.137}$$

while $\phi^{\parallel}$ is determined from Eq. (7.131):

$$\phi^{\parallel}=\frac{\tilde{T}^{\perp}_{\mathrm{K}}}{\mathcal{Z}}. \tag{7.138}$$

Next, we examine expression (7.135) by taking its square. After multiplication by $\mathcal{Z}^2$ and substitution of Eqs. (7.129) and (7.131) we arrive at:

$$\left(\mathcal{S}^2+4\Lambda\mp P^2\right)\mathcal{Z}^2\left(\mathrm{x}^2-\Phi^2\right)=\Lambda\left(\tilde{T}^{\perp\perp2}-\left(\mathcal{S}^2+4\Lambda\right)\tilde{T}^{\perp2}_{\mathrm{K}}\right), \tag{7.139}$$

where we have used the convention defined in Eq. (7.124). Eqs. (7.133) and (7.134) are transformed into the following equivalent set of equations:

$$\frac{\mathcal{Z}}{2}\frac{\mathrm{d}}{\mathrm{d}\bar{\mathrm{x}}}\left(\mathcal{S}^2+4\Lambda\right)=-\left(\mathcal{S}^2+4\Lambda\mp P^2\right)\frac{\mathrm{d}}{\mathrm{d}\bar{\mathrm{x}}}\left(\mathrm{x}^2-\Phi^2\right), \tag{7.140}$$

$$\frac{\mathcal{Z}^2}{2\Lambda}\left[\mathcal{S}^2+4\Lambda+2\Lambda\frac{\mathrm{d}\mathcal{S}}{\mathrm{d}\bar{\mathrm{x}}}-\mathcal{S}\frac{\mathrm{d}\Lambda}{\mathrm{d}\bar{\mathrm{x}}}\right]=P\tilde{T}^{\perp\perp}\frac{\mathrm{d}}{\mathrm{d}\bar{\mathrm{x}}}\sqrt{|\mathrm{x}^2-\Phi^2|}. \tag{7.141}$$

with the help of expression (7.135). Observe that these two equations are identical when $\mathcal{S}^2+4\Lambda=0$, which indicates that we need to revisit the original set of equations in this scenario. Observing this new set of Eqs. (7.136-7.141), together with Eqs. (7.130) and (7.132), we conclude that the solving procedure branches depending on whether $\mathcal{S}^2+4\Lambda\in\{0,\pm P^2\}$ and whether constant P vanishes. Let us first examine the cases where $P\neq 0$.

- $\underline{P \neq 0}$: Combining Eqs. (7.130) and (7.132) leads to an integrable equation, the solution of which is given by:
$$\theta^2 = 1 + \frac{1}{3}\left(\mathrm{x}^2 - \Phi^2\right) + \frac{1}{P}\frac{\eta + I}{\sqrt{|\mathrm{x}^2 - \Phi^2|}}, \tag{7.142}$$
where η is an integration constant, while integral I is defined as:
$$I = -\int \mathrm{d}\bar{\mathrm{x}} \left(\tilde{T}^{\shortparallel\shortparallel} + \mathcal{S}\tilde{T}^{\shortparallel}_{\mathrm{K}}\right). \tag{7.143}$$
Now, we have also expressed $\mathcal{Z}$ solely in terms of $|\mathrm{x}^2 - \Phi^2|$ and the sources. Here, we have another branching of the solution depending on whether the quantity $\mathcal{S}^2 + 4\Lambda \mp P^2$ and/or $\mathcal{S}^2 + 4\Lambda$ is non-zero.

  ⋆ $\underline{\mathcal{S}^2 + 4\Lambda \mp P^2 \neq 0 \ \wedge \ \mathcal{S}^2 + 4\Lambda \neq 0}$: From Eq. (7.139) we get a solution for $|\mathrm{x}^2 - \Phi^2|$:
$$\pm\frac{2}{3}\left|\mathrm{x}^2 - \Phi^2\right|^{\frac{3}{2}} = \mathcal{J} + \frac{\eta + I}{P}, \tag{7.144}$$
  where we have introduced a function $\mathcal{J}$ of the source fields, given by:
$$\mathcal{J} = \pm'\sqrt{\frac{\pm\Lambda\left(\tilde{T}^{\perp\perp 2} - \left(\mathcal{S}^2 + 4\Lambda\right)\tilde{T}^{\perp 2}_{\mathrm{K}}\right)}{\mathcal{S}^2 + 4\Lambda \mp P^2}}, \tag{7.145}$$
  with additional sign choice denoted by $\pm'$. The remaining three Eqs. (7.140), (7.141) and (7.132) reduce to the constraints placed upon the sources, given by:
$$\tilde{T}^{\shortparallel\shortparallel} + \mathcal{S}\tilde{T}^{\shortparallel}_{\mathrm{K}} = \frac{P}{2}\mathcal{J}\frac{\mathrm{d}}{\mathrm{d}\bar{\mathrm{x}}}\ln\left|\Lambda\left(\tilde{T}^{\perp\perp 2} - \left(\mathcal{S}^2 + 4\Lambda\right)\tilde{T}^{\perp 2}_{\mathrm{K}}\right)\right|, \tag{7.146}$$
$$\mathcal{S}^2 + 4\Lambda + 2\Lambda\frac{\mathrm{d}\mathcal{S}}{\mathrm{d}\bar{\mathrm{x}}} - \mathcal{S}\frac{\mathrm{d}\Lambda}{\mathrm{d}\bar{\mathrm{x}}} = \mp\frac{P\Lambda\tilde{T}^{\perp\perp}}{2\mathcal{J}}\frac{\mathrm{d}}{\mathrm{d}\bar{\mathrm{x}}}\ln\left|\mathcal{S}^2 + 4\Lambda \mp P^2\right|, \tag{7.147}$$
$$\tilde{T}^{\shortparallel}_{\mathrm{K}} \pm \frac{P\mathcal{S}}{2\mathcal{J}}\frac{\frac{\mathrm{d}}{\mathrm{d}\bar{\mathrm{x}}}\left(\Lambda\tilde{T}^{\perp 2}_{\mathrm{K}}\right)}{\mathcal{S}^2 + 4\Lambda \mp P^2} = \frac{2\Lambda\frac{\mathrm{d}\tilde{T}^{\perp\perp}}{\mathrm{d}\bar{\mathrm{x}}} + \tilde{T}^{\perp\perp}\frac{\mathrm{d}\Lambda}{\mathrm{d}\bar{\mathrm{x}}}}{\mathcal{S}^2 + 4\Lambda}\left[1 \pm \frac{P\mathcal{S}}{2\mathcal{J}}\frac{\tilde{T}^{\perp\perp}}{\mathcal{S}^2 + 4\Lambda \mp P^2}\right]. \tag{7.148}$$
  Lastly, the perpendicular component of contorsion is expressed as follows:
$$l\mathrm{K}^{\perp} = \mp\frac{P\tilde{T}^{\perp}_{\mathrm{K}}}{4\mathcal{J}}\frac{\mathrm{d}}{\mathrm{d}\bar{\mathrm{x}}}\ln\left|\mathcal{S}^2 + 4\Lambda \mp P^2\right|. \tag{7.149}$$

  ⋆ $\underline{\mathcal{S}^2 + 4\Lambda = \pm P^2}$: From Eq. (7.139) we have a condition for the sources:
$$\tilde{T}^{\perp\perp 2} = \pm P^2\tilde{T}^{\perp 2}_{\mathrm{K}}, \tag{7.150}$$
  which implies that $\mathrm{x}^2 > \Phi^2$, meaning the plus sign is applicable in this case. Eq. (7.140) is automatically solved. Eq. (7.132) gives fourth, and final, condition for the sources, i.e.
$$4\Lambda\tilde{T}^{\shortparallel}_{\mathrm{K}} = 2\frac{\mathrm{d}}{\mathrm{d}\bar{\mathrm{x}}}\left(\Lambda\tilde{T}^{\perp\perp}\right) - \mathcal{S}\tilde{T}^{\perp\perp} + \mathcal{S}\tilde{T}^{\shortparallel\shortparallel}. \tag{7.151}$$
  Unfortunately, within this scenario, equation for $\mathcal{J} = \mathcal{Z}\sqrt{|\mathrm{x}^2 - \Phi^2|}$ cannot be solved in general. It is given by:
$$\frac{\mathrm{d}\mathcal{J}}{\mathrm{d}\bar{\mathrm{x}}} = \frac{P}{2\Lambda\tilde{T}^{\perp\perp}}\left(\frac{\mathrm{d}\mathcal{S}}{\mathrm{d}\bar{\mathrm{x}}} + 2\right)\mathcal{J}^2 + \frac{1}{P}\left(\tilde{T}^{\shortparallel\shortparallel} + \mathcal{S}\tilde{T}^{\shortparallel}_{\mathrm{K}}\right). \tag{7.152}$$

- $\star$ $\underline{\mathcal{S}^2+4\Lambda=0}$: In this scenario, Eq. (7.141) still holds, implying that:

$$\sqrt{|\mathrm{x}^2-\Phi^2|}=Q=const. \tag{7.153}$$

This outcome annuls the right-hand side of both Eqs. (7.133) and (7.134), leading to:

$$\mathcal{S}=-2\bar{\mathrm{x}},\;\;\Lambda=-\bar{\mathrm{x}}^2. \tag{7.154}$$

Simultaneously solving Eqs. (7.129), (7.131) and (7.135) yields a solution for the fields x and ϕ^μ in terms of the sources, as well as one condition for the EMT:

$$\mathrm{x}=\frac{Q\bar{\mathrm{x}}}{P}\left(\frac{P^2\tilde{T}_{\mathrm{K}}^{\perp 2}}{\tilde{T}^{\perp\perp 2}}\mp 1\right)-\frac{PQ}{4\bar{\mathrm{x}}}, \tag{7.155}$$

$$\phi^\perp=-\frac{Q}{P}\left(\frac{P^2\tilde{T}_{\mathrm{K}}^{\perp 2}}{\tilde{T}^{\perp\perp 2}}\mp 1\right)-\frac{PQ}{4\bar{\mathrm{x}}^2}, \tag{7.156}$$

$$\phi^{\shortparallel}=-\frac{PQ}{\bar{\mathrm{x}}}\frac{\tilde{T}_{\mathrm{K}}^{\perp}}{\tilde{T}^{\perp\perp}}, \tag{7.157}$$

$$\pm\frac{2}{3}Q^3=-\frac{\bar{\mathrm{x}}}{P}\tilde{T}^{\perp\perp}+\frac{\eta+I}{P}. \tag{7.158}$$

Since $\mathcal{S}$ and Λ have a form given by Eq. (7.153), the contorsion vanishes entirely, i.e.

$$\mathrm{K}^{\shortparallel}=\mathrm{K}^{\perp}=T^{\shortparallel\perp}=0. \tag{7.159}$$

The last remaining Eq. (7.132) reduces to another condition for the sources:

$$\tilde{T}_{\mathrm{K}}^{\shortparallel}=\left[\frac{\bar{\mathrm{x}}}{P^2}\left(\frac{P^2\tilde{T}_{\mathrm{K}}^{\perp 2}}{\tilde{T}^{\perp\perp 2}}\pm 1\right)+\frac{1}{4\bar{\mathrm{x}}}\right]\frac{\mathrm{d}}{\mathrm{d}\bar{\mathrm{x}}}\left(\bar{\mathrm{x}}\tilde{T}^{\perp\perp}\right)-\frac{1}{\tilde{T}^{\perp\perp}}\frac{\mathrm{d}}{\mathrm{d}\bar{\mathrm{x}}}\left(\bar{\mathrm{x}}^2\tilde{T}_{\mathrm{K}}^{\perp 2}\right). \tag{7.160}$$

- $\underline{P=0}$: Now, Eq. (7.130) gives a condition for the parallel component of the EMT:

$$\tilde{T}^{\shortparallel\shortparallel}=\frac{2}{\mathrm{x}}\Lambda\phi^\perp\tilde{T}_{\mathrm{K}}^{\shortparallel}. \tag{7.161}$$

In addition, from Eq. (7.125) we conclude that:

$$\mathrm{K}^\perp=0. \tag{7.162}$$

We further consider two separate cases, depending on whether $\mathcal{S}^2+4\Lambda$ vanishes or not.

- $\star$ $\underline{\mathcal{S}^2+4\Lambda\neq 0}$: Under the condition $P\to 0$, the Eqs. (7.136-7.138) remain valid, providing corresponding solutions for ϕ^μ and x. Meanwhile, Eqs. (7.130), (7.132) and (7.141) simplify to the same constraints on sources as given by Eqs. (7.146-7.148) in the limit $P\to 0$. Consequently, Eq. (7.139) yields the solution for θ:

$$\theta^2=1+\mathrm{x}^2-\Phi^2+\frac{\mathcal{J}}{\sqrt{|\mathrm{x}^2-\Phi^2|}}, \tag{7.163}$$

where $\mathcal{J}$ is given by:

$$\mathcal{J}=\pm'\sqrt{\pm\left(\frac{\Lambda\tilde{T}^{\perp\perp 2}}{\mathcal{S}^2+4\Lambda}-\Lambda\tilde{T}_{\mathrm{K}}^{\perp 2}\right)}. \tag{7.164}$$

Using the function $\mathcal{J}$, the integration of the final Eq. (7.140) becomes straightforward, resulting in:

$$\pm\frac{2}{3}\left|\mathrm{x}^2-\Phi^2\right|^{\frac{3}{2}} = D - \frac{1}{2}\int \mathrm{d}\bar{\mathrm{x}}\mathcal{J}\frac{\mathrm{d}}{\mathrm{d}\bar{\mathrm{x}}}\ln\left|\mathcal{S}^2+4\Lambda\right|, \tag{7.165}$$

where D is an integration constant. Furthermore, condition (7.147) allows us to determine $\mathcal{S}$ purely as a function of the metric. The solution is expressed as follows:

$$\mathcal{S} = \begin{cases} -2\sqrt{\Lambda}\tan\mathrm{z}; & \Lambda>0 \\ 2\sqrt{-\Lambda}\coth\mathrm{z}; & \Lambda<0,\ \mathcal{S}^2+4\Lambda>0 \\ 2\sqrt{-\Lambda}\tanh\mathrm{z}; & \Lambda<0,\ \mathcal{S}^2+4\Lambda<0 \end{cases}, \tag{7.166}$$

where we have used the z coordinate defined in Eq. (3.21).

⋆ $\underline{\mathcal{S}^2+4\Lambda=0}$: The condition defining this case, can be rewritten in the following form:

$$\mathcal{S} = \pm 2\sqrt{-\Lambda}. \tag{7.167}$$

From Eq. (7.161) we have:

$$\tilde{T}^{\shortparallel\shortparallel} + \mathcal{S}\tilde{T}^{\shortparallel}_{\mathrm{K}} = 0. \tag{7.168}$$

Eqs. (7.129) together with Eq. (7.135) gives the fourth condition for the sources:

$$\tilde{T}^{\perp\perp} = 0. \tag{7.169}$$

Eqs. (7.133) and (7.134) are equivalent in this case. With the help of Eq. (7.134), Eq. (7.132) becomes integrable, giving the following expression for x (and $\phi^{\perp}$ through Eq. (7.129)):

$$\mathcal{Z}\mathrm{x} = \frac{S\mathcal{Z}\phi^{\perp}}{2} = \frac{e^{\pm 2\mathrm{z}}}{\sqrt{-\Lambda}}\left(\eta + \int \mathrm{dz}\Lambda\tilde{T}^{\shortparallel}_{\mathrm{K}}e^{\mp 2\mathrm{z}}\right), \tag{7.170}$$

where the $\pm$ notation is defined by Eq. (7.167). Direct calculation yields:

$$\theta^2 = 1 + \mathrm{x}^2 - \Phi^2 \pm' \frac{\sqrt{-\Lambda}\tilde{T}^{\perp}_{\mathrm{K}}}{\sqrt{\mathrm{x}^2-\Phi^2}}, \tag{7.171}$$

where another sign convection $\pm'$ is defined. The last Eq. (7.133) can be directly integrated, resulting into:

$$\frac{2}{3}\left(\mathrm{x}^2-\Phi^2\right)^{\frac{3}{2}} = D \pm' \frac{1}{4}\int \mathrm{dz}\mathcal{S}\tilde{T}^{\shortparallel}_{\mathrm{K}}\left(\frac{\mathrm{d}\mathcal{S}}{\mathrm{d}\bar{\mathrm{x}}}+2\right). \tag{7.172}$$

Non-vanishing normal component of contorsion current when $\Phi^2 = \mathrm{x}^2$ and $\phi^{\perp}\neq 0$

The defining condition gives a solution for $\phi^{\shortparallel}$ in terms of $\phi^{\perp}$ and x:

$$\phi^{\shortparallel} = \pm\sqrt{\frac{\mathrm{x}^2+\Lambda\phi^{\perp 2}}{\Lambda}} \tag{7.173}$$

In this case, Eq. (7.58) is solved. It is easy to see that the components of the contorsion satisfy the following condition:

$$\phi^{\shortparallel}\mathrm{K}^{\shortparallel} = \phi^{\perp}\mathrm{K}^{\perp}. \tag{7.174}$$

This equation, together with Eq. (7.14) gives the solution for the contorsion K^μ in terms of ϕ^μ and x:

$$l\mathrm{K}^{\parallel} = \frac{\phi^{\perp}}{2\mathrm{x}}\left(\frac{\mathrm{d}\mathcal{S}}{\mathrm{d}\bar{\mathrm{x}}}+2\right), \quad l\mathrm{K}^{\perp} = \frac{\phi^{\parallel}}{2\mathrm{x}}\left(\frac{\mathrm{d}\mathcal{S}}{\mathrm{d}\bar{\mathrm{x}}}+2\right), \tag{7.175}$$

where $\mathcal{S}$ is given by:

$$\mathcal{S} = \frac{\mathrm{d}\Lambda}{\mathrm{d}\bar{\mathrm{x}}} - 2l\Lambda\frac{T^{\parallel\perp}}{T_{\mathrm{K}}^{\perp}}. \tag{7.176}$$

The full system of equations now simplifies to:

$$\left(1-\theta^2\right)\left(\mathcal{S}\phi^{\perp}-2\mathrm{x}\right) = -\tilde{T}^{\perp\perp}, \tag{7.177}$$

$$\left(1-\theta^2\right)\left[\frac{\mathrm{d}}{\mathrm{d}\bar{\mathrm{x}}}-\frac{1}{\mathrm{x}}\left(\phi^{\perp}+\mathcal{D}\right)\right]\left(2\Lambda\phi^{\perp}+\mathcal{S}\mathrm{x}\right) = \tilde{T}^{\parallel\parallel}-\frac{2}{\mathrm{x}}\Lambda\phi^{\perp}\tilde{T}_{\mathrm{K}}^{\parallel}, \tag{7.178}$$

$$\left(1-\theta^2\right)\sqrt{\frac{\mathrm{x}^2+\Lambda\phi^{\perp 2}}{\Lambda}} = \pm\tilde{T}_{\mathrm{K}}^{\perp}, \tag{7.179}$$

$$\left(1-\theta^2\right)\left(\phi^{\perp}+\mathcal{D}\right)-\mathrm{x}\frac{\mathrm{d}\theta^2}{\mathrm{d}\bar{\mathrm{x}}} = \tilde{T}_{\mathrm{K}}^{\parallel}, \tag{7.180}$$

$$\left(1-\theta^2\right)\left(\frac{\mathrm{d}\mathcal{S}}{\mathrm{d}\bar{\mathrm{x}}}+2\right) = 2\mathrm{x}\frac{\mathrm{d}}{\mathrm{d}\bar{\mathrm{x}}}\left(2\Lambda\phi^{\perp}+\mathcal{S}\mathrm{x}\right), \tag{7.181}$$

$$\left(\frac{\mathrm{d}\Lambda}{\mathrm{d}\bar{\mathrm{x}}}-\mathcal{S}\right) = \frac{1}{\mathrm{x}}\Lambda\phi^{\perp}\left(\frac{\mathrm{d}\mathcal{S}}{\mathrm{d}\bar{\mathrm{x}}}+2\right), \tag{7.182}$$

where $\phi^{\parallel}$ and K^μ have been entirely removed from the original equations by employing Eqs. (7.173) and (7.175), respectively. Expressing $\mathcal{D}$ from Eq. (7.180) and substituting it into the Eq. (7.178), followed by integration, yields:

$$\left(1-\theta^2\right)\left(2\Lambda\phi^{\perp}+\mathcal{S}\mathrm{x}\right) = \eta + I, \tag{7.183}$$

where η is an integration constant, and integral I is defined by:

$$I = \int \mathrm{d}\bar{\mathrm{x}}\left(\tilde{T}^{\parallel\parallel}+\mathcal{S}\tilde{T}_{\mathrm{K}}^{\parallel}\right). \tag{7.184}$$

Solving Eqs. (7.177) and (7.183) in terms of $\phi^{\perp}$ and x yields:

$$\left(\mathcal{S}+4\Lambda\right)\mathcal{Z}\phi^{\perp} = 2(\eta+I)-\mathcal{S}\tilde{T}^{\perp\perp}, \tag{7.185}$$

$$\left(\mathcal{S}+4\Lambda\right)\mathcal{Z}\mathrm{x} = \mathcal{S}(\eta+I)+2\Lambda\tilde{T}^{\perp\perp}. \tag{7.186}$$

Once again, a special case emerges when $\mathcal{S}^2+4\Lambda=0$, which is analyzed separately.

- $\underline{\mathcal{S}^2+4\Lambda\neq 0}$: Eqs. (7.185) and (7.186) define a solution for $\mathcal{Z}\phi^{\perp}$ and $\mathcal{Z}\mathrm{x}$. Next, after substituting this solution into Eqs. (7.179) and (7.182) we arrive at two conditions for the sources, given by:

$$(\eta+I)^2 = \left(\mathcal{S}^2+4\Lambda\right)\Lambda\tilde{T}_{\mathrm{K}}^{\perp 2}-\Lambda\tilde{T}^{\perp\perp 2}, \tag{7.187}$$

$$(\eta+I)\left[\mathcal{S}^2+4\Lambda+2\Lambda\frac{\mathrm{d}\mathcal{S}}{\mathrm{d}\bar{\mathrm{x}}}-\mathcal{S}\frac{\mathrm{d}\Lambda}{\mathrm{d}\bar{\mathrm{x}}}\right] = \frac{1}{2}\Lambda\tilde{T}^{\perp\perp}\frac{\mathrm{d}}{\mathrm{d}\bar{\mathrm{x}}}\left(\mathcal{S}^2+4\Lambda\right). \tag{7.188}$$

  Using Eqs. (7.185), (7.186) as well as condition (7.188), Eq. (7.180) becomes the following constraint for the sources:

$$4\Lambda\tilde{T}_{\mathrm{K}}^{\parallel} = 2\Lambda\frac{\mathrm{d}\tilde{T}^{\perp\perp}}{\mathrm{d}\bar{\mathrm{x}}}+\left(\frac{\mathrm{d}\Lambda}{\mathrm{d}\bar{\mathrm{x}}}-\mathcal{S}\right)\tilde{T}^{\perp\perp}+\mathcal{S}\tilde{T}^{\parallel\parallel}-\left(\frac{\mathrm{d}\mathcal{S}}{\mathrm{d}\bar{\mathrm{x}}}+2\right)(\eta+I). \tag{7.189}$$

The last remaining unknown function $\mathcal{Z}$ is determined by solving Eq. (7.181). The solution is as follows:

$$\frac{2}{3}\left(\frac{\eta+I}{\mathcal{Z}}\right)^3 = D + \int \frac{\mathrm{d}\bar{\mathrm{x}}\,(\eta+I)^2}{\mathcal{S}\,(\eta+I)+2\Lambda\tilde{T}^{\perp\perp}}\left(\frac{\mathrm{d}\mathcal{S}}{\mathrm{d}\bar{\mathrm{x}}}+2\right). \tag{7.190}$$

Note that $\theta^2 = 1-\mathcal{Z}$.

- $\underline{\mathcal{S}^2+4\Lambda=0}$: This scenario resembles the related situation where $\mathrm{x}^2 \neq \Phi^2$ and $P \neq 0$. We begin by examining Eq. (7.182), which can be rewritten in the following way:

$$\left(2\Lambda\phi^{\perp}+\mathcal{S}\mathrm{x}\right)\left(\frac{\mathrm{d}\mathcal{S}}{\mathrm{d}\bar{\mathrm{x}}}+2\right)=0. \tag{7.191}$$

The first bracket in Eq. (7.191) cannot be zero because this would lead to $\tilde{T}^{\perp}_{\mathrm{K}} = 0$, contradicting the primary assumption. Then, Eq. (7.191) gives the following solution for the metric:

$$\Lambda = -\bar{\mathrm{x}}^2, \;\; \mathcal{S} = -2\bar{\mathrm{x}}. \tag{7.192}$$

Consequentially, Eq. (7.181) implies:

$$2\Lambda\phi^{\perp}+\mathcal{S}\mathrm{x} = Q, \tag{7.193}$$

where $Q \neq 0$ is a constant. Then, simultaneously solving Eqs. (7.179) and (7.193) yields:

$$\mathrm{x} = Q\left[\frac{\bar{\mathrm{x}}\tilde{T}^{\perp 2}_{\mathrm{K}}}{\tilde{T}^{\perp\perp 2}}-\frac{1}{4\bar{\mathrm{x}}}\right], \tag{7.194}$$

$$\phi^{\perp} = -Q\left[\frac{\bar{\mathrm{x}}\tilde{T}^{\perp 2}_{\mathrm{K}}}{\tilde{T}^{\perp\perp 2}}+\frac{1}{4\bar{\mathrm{x}}}\right]. \tag{7.195}$$

From Eq. (7.177) we have the following solution for the θ-field:

$$\theta^2 = 1+\frac{\bar{\mathrm{x}}}{Q}\tilde{T}^{\perp\perp}. \tag{7.196}$$

Eqs. (7.183) and (7.180) reduce to two constraints placed upon the EMT and contorsion current, given by:

$$\bar{\mathrm{x}}\tilde{T}^{\perp\perp} = \eta + I, \tag{7.197}$$

$$\tilde{T}^{\parallel}_{\mathrm{K}} = \left[\frac{\bar{\mathrm{x}}\tilde{T}^{\perp 2}_{\mathrm{K}}}{\tilde{T}^{\perp\perp 2}}+\frac{1}{4\bar{\mathrm{x}}}\right]\frac{\mathrm{d}}{\mathrm{d}\bar{\mathrm{x}}}\left(\bar{\mathrm{x}}\tilde{T}^{\perp\perp}\right)-\frac{1}{\tilde{T}^{\perp\perp}}\frac{\mathrm{d}}{\mathrm{d}\bar{\mathrm{x}}}\left(\bar{\mathrm{x}}^2\tilde{T}^{\perp 2}_{\mathrm{K}}\right). \tag{7.198}$$

Non-vanishing normal component of contorsion current when $\phi^{\perp} = 0$

If the normal component of the contorsion current is zero, the equations of motion necessitate a non-zero $\phi^{\perp}$. Conversely, the presence of a non-vanishing $T^{\perp}_{\mathrm{K}}$ alters this condition. In the last two sections, we considered $\phi^{\perp}$ to be non-zero, hence the scenario where $\phi^{\perp}$ equals zero requires a separate analysis. It is easy to express all fields in terms of $\mathcal{Z}$, the EMT, and the contorsion current.

$$\mathrm{x} = \frac{\tilde{T}^{\perp\perp}}{2\mathcal{Z}},\ \phi^{\parallel} = \frac{\tilde{T}^{\perp}_{\mathrm{K}}}{\mathcal{Z}},\ \phi^{\perp} = 0, \tag{7.199}$$

$$2l\Lambda\mathrm{K}^{\parallel} = \frac{\tilde{T}^{\parallel\perp}}{\tilde{T}^{\perp}_{\mathrm{K}}},\ 2l\Lambda\mathrm{K}^{\perp} = \frac{\tilde{T}^{\parallel\parallel} + \tilde{T}^{\perp\perp}}{\tilde{T}^{\perp}_{\mathrm{K}}}, \tag{7.200}$$

$$\theta^2 = \left(\frac{\tilde{T}^{\perp\perp}}{2\mathcal{Z}}\right)^2 + 1 - \frac{\Lambda\tilde{T}^{\perp 2}_{\mathrm{K}}}{\mathcal{Z}^2} - \mathcal{Z}. \tag{7.201}$$

These expressions directly solve Eqs. (7.22-7.25). Eqs. (7.16) and (7.14) become conditions for the sources given by:

$$2\tilde{T}^{\parallel}_{\mathrm{K}} = \frac{\mathrm{d}\tilde{T}^{\perp\perp}}{\mathrm{d}\bar{\mathrm{x}}} + \frac{\tilde{T}^{\perp\perp}}{2\Lambda}\left(\frac{\mathrm{d}\Lambda}{\mathrm{d}\bar{\mathrm{x}}} - \mathcal{S}\right), \tag{7.202}$$

$$\tilde{T}^{\parallel\parallel} = \frac{1}{2}\tilde{T}^{\perp\perp}\frac{\mathrm{d}\mathcal{S}}{\mathrm{d}\bar{\mathrm{x}}}, \tag{7.203}$$

where $\mathcal{S}$ defined by Eq. (7.29) is expressed in terms of the sources as well:

$$\mathcal{S} = \frac{\mathrm{d}\Lambda}{\mathrm{d}\bar{\mathrm{x}}} - 2l\Lambda\frac{T^{\parallel\perp}}{T^{\perp}_{\mathrm{K}}}, \tag{7.204}$$

the same as in the previous two sections. The remaining three equations read:

$$\mathcal{Z}^3\frac{\tilde{T}^{\parallel\parallel} + \tilde{T}^{\perp\perp}}{2\Lambda\tilde{T}^{\perp 2}_{\mathrm{K}}} = \frac{1}{2}\mathcal{S}\tilde{T}^{\perp\perp}\frac{\mathrm{d}}{\mathrm{d}\bar{\mathrm{x}}}\ln\left(\frac{\tilde{T}^{\perp\perp}}{\mathcal{Z}}\right) + \tilde{T}^{\parallel\parallel}, \tag{7.205}$$

$$\mathcal{Z}\left(\frac{\mathrm{d}\mathcal{S}}{\mathrm{d}\bar{\mathrm{x}}} + 2\right) = \frac{\tilde{T}^{\parallel\parallel}\tilde{T}^{\perp\perp}}{\mathcal{Z}^2} + \mathcal{S}\frac{\mathrm{d}}{\mathrm{d}\bar{\mathrm{x}}}\left(\frac{\Lambda\tilde{T}^{\perp 2}_{\mathrm{K}}}{\mathcal{Z}^2}\right), \tag{7.206}$$

$$2\tilde{T}^{\parallel}_{\mathrm{K}} = \frac{\mathrm{d}\tilde{T}^{\perp\perp}}{\mathrm{d}\bar{\mathrm{x}}} - \frac{1}{6}\frac{\mathrm{d}}{\mathrm{d}\bar{\mathrm{x}}}\left(\frac{\tilde{T}^{\perp\perp}}{\mathcal{Z}}\right)^3 + \frac{\tilde{T}^{\perp\perp}}{\mathcal{Z}}\frac{\mathrm{d}}{\mathrm{d}\bar{\mathrm{x}}}\left(\frac{\Lambda\tilde{T}^{\perp 2}_{\mathrm{K}}}{\mathcal{Z}^2}\right). \tag{7.207}$$

Combining all three Eqs. (7.205-7.207) we obtain an integrable equation, the solution of which is given by the following expression:

$$\Lambda\tilde{T}^{\perp 2}_{\mathrm{K}} = \frac{1}{4}\tilde{T}^{\perp\perp 2}\left(1 - \frac{\mathcal{S}^2}{P^2}\right), \tag{7.208}$$

where $P \in \mathbb{R}\cup\{\infty\}$ represents a constant of integration. Note that when P takes on an infinite value, it corresponds to the scenario previously encountered where $\mathrm{x}^2 = \Phi^2$. Substituting Eq. (7.208) into Eq. (7.207) eliminates $\mathcal{Z}$ form the equation, giving another constraint on the sources:

$$2\tilde{T}^{\parallel}_{\mathrm{K}} = \frac{\mathrm{d}\tilde{T}^{\perp\perp}}{\mathrm{d}\bar{\mathrm{x}}} - \frac{\mathcal{S}}{2P^2}\frac{\mathrm{d}\mathcal{S}}{\mathrm{d}\bar{\mathrm{x}}}. \tag{7.209}$$

In conclusion, the integration of Eq. (7.206) allows us to directly determine the unknown variable $\mathcal{Z}$, which is represented by the subsequent expression:

$$\frac{1}{6}\left(\frac{\mathcal{S}\tilde{T}^{\perp\perp}}{\mathcal{Z}}\right)^3 = D + \int \mathrm{d}\bar{\mathrm{x}}\frac{P^2\mathcal{S}^2}{P^2 - \mathcal{S}^2}\left(\frac{\mathrm{d}\mathcal{S}}{\mathrm{d}\bar{\mathrm{x}}} + 2\right)\tilde{T}^{\perp\perp}. \tag{7.210}$$

Note that the case corresponding to $P \to \infty$ results in the vanishing parallel component of contorsion. This can be easily seen by comparing Eqs. (7.202) and (7.209).

7.2.2 Solutions when $\mathcal{Z} \neq 0$, $\theta = 0$ and $\phi^{\perp} \neq 0$

In this section, we investigate the solutions to the equations of motion when $\theta = 0$. This is a rather special case, since Eq. (7.14) is trivially solved. We solve equations by expressing all fields in terms of $\mathcal{Z}$ and the sources, and then we solve the equation for $\mathcal{Z}$, defined in Eq. (7.28). The multiplication of Eq. (7.15) by $\phi^{\perp}$ followed by subtraction of Eq. (7.16) results in the following equation:

$$l\phi^{\perp}\mathrm{K}^{\perp} = \phi^{\shortparallel}\left[l\mathrm{K}^{\shortparallel} + \frac{\mathrm{d}}{\mathrm{d}\bar{\mathrm{x}}}\ln\mathcal{Z}\right]. \tag{7.211}$$

Expression (7.211) represents a way to remove the orthogonal component of the contorsion from other equations. The $\phi^{\shortparallel}$ is easily obtained form Eq. (7.25):

$$\phi^{\shortparallel} = \frac{\tilde{T}^{\perp}_{\mathrm{K}}}{\mathcal{Z}}. \tag{7.212}$$

Eq. (7.22), as in previous sections, represents a constraint for the sources, that is:

$$\left(\frac{\mathrm{d}\Lambda}{\mathrm{d}\bar{\mathrm{x}}} - \mathcal{S}\right)\tilde{T}^{\perp}_{\mathrm{K}} = \tilde{T}^{\shortparallel\perp}. \tag{7.213}$$

where we have used the definition for $\mathcal{S}$ (7.29) to eliminate $\mathrm{K}^{\shortparallel}$ in the last step. Multiplying Eq. (7.16) by $\mathcal{Z}^2$ and employing original Eqs. (7.22) and (7.26), as well as Eqs. (7.211) and (7.212) we arrive at:

$$-\tilde{T}^{\perp\perp}\tilde{T}^{\shortparallel}_{\mathrm{K}} + \frac{\mathrm{d}}{\mathrm{d}\bar{\mathrm{x}}}\left(\Lambda\tilde{T}^{\perp 2}_{\mathrm{K}}\right) = \frac{\mathcal{Z}^3 - 2\Lambda\tilde{T}^{\perp 2}_{\mathrm{K}}}{2\Lambda}\left(\frac{\mathrm{d}\Lambda}{\mathrm{d}\bar{\mathrm{x}}} - \mathcal{S}\right). \tag{7.214}$$

Eq. (7.24) is transformed into the following form:

$$\mathcal{Z}^2\frac{\mathrm{d}\mathcal{Z}}{\mathrm{d}\bar{\mathrm{x}}} + \tilde{T}^{\perp\perp}\tilde{T}^{\shortparallel}_{\mathrm{K}} + \frac{\mathcal{Z}^3}{2\Lambda}\left(\frac{\mathrm{d}\Lambda}{\mathrm{d}\bar{\mathrm{x}}} - \mathcal{S}\right) = 2\tilde{T}^{\shortparallel}_{\mathrm{K}}\mathcal{Z}\mathrm{x} + \tilde{T}^{\shortparallel\shortparallel}\mathcal{Z}\phi^{\perp}. \tag{7.215}$$

upon utilizing Eqs. (7.26), (7.211), and (7.214). We rewrite Eqs. (7.23) and (7.26) in full:

$$\mathcal{Z}\left(\mathcal{S}\phi^{\perp} - 2\mathrm{x}\right) = -\tilde{T}^{\perp\perp}, \tag{7.216}$$

$$\mathcal{Z}\left(\phi^{\perp} + \mathcal{D}\right) = \tilde{T}^{\shortparallel}_{\mathrm{K}}. \tag{7.217}$$

Employing the quartet of equations obtained earlier (7.214-7.217), we reformulate the final Eq. (7.17) as:

$$2\Lambda\frac{\mathrm{d}\tilde{T}^{\perp\perp}}{\mathrm{d}\bar{\mathrm{x}}} + \frac{\mathrm{d}\Lambda}{\mathrm{d}\bar{\mathrm{x}}}\left(\tilde{T}^{\perp\perp} + \tilde{T}^{\shortparallel\shortparallel}\right) + 2\Lambda\tilde{T}^{\shortparallel}_{\mathrm{K}}\frac{\mathrm{d}\mathcal{S}}{\mathrm{d}\bar{\mathrm{x}}} = 2\frac{\frac{1}{2\Lambda}\left(\frac{\mathrm{d}\Lambda}{\mathrm{d}\bar{\mathrm{x}}} - \mathcal{S}\right) + \frac{\mathrm{d}}{\mathrm{d}\bar{\mathrm{x}}}\ln\mathcal{Z}}{\mathcal{Z}\phi^{\perp}}\frac{\mathrm{d}}{\mathrm{d}\bar{\mathrm{x}}}\left(\Lambda\tilde{T}^{\perp}_{\mathrm{K}}\right)^2. \tag{7.218}$$

Note that this equation is the conservation law for the EMT given by Eq. (3.66) rewritten using redefined EMT components $\tilde{T}_{\mu\nu}$. These five Eqs. (7.214-7.218), together with the definition of $\mathcal{Z} = \mathrm{x}^2 + 1 - \Phi^2$, form a complete set of equations that are analyzed in this section. Substituting x from Eq. (7.216) into the definition for $\mathcal{Z}$, we derive a quadratic equation for $\mathcal{Z}\phi^{\perp}$:

$$\left(\mathcal{S}^2 + 4\Lambda\right)\left(\mathcal{Z}\phi^{\perp}\right)^2 + 2\mathcal{S}\tilde{T}^{\perp\perp}\left(\mathcal{Z}\phi^{\perp}\right) + \tilde{T}^{\perp\perp 2} - 4\Lambda\tilde{T}^{\perp 2}_{\mathrm{K}} - 4\mathcal{Z}^2\left(\mathcal{Z} - 1\right) = 0. \tag{7.219}$$

Upon examining Eq. (7.219), it becomes clear that the scenario where $\mathcal{S}^2 + 4\Lambda = 0$ requires independent examination. The solutions for x and $\phi^{\perp}$ are given by:

$$\mathcal{Z}\mathrm{x} = \begin{cases} \mathcal{M}\tilde{T}^{\perp\perp} \pm \sqrt{\mathcal{J}}, & \mathcal{S}^2 + 2\Lambda \neq 0, \\ \frac{1}{4}\tilde{T}^{\perp\perp} + \frac{\Lambda \tilde{T}^{\perp}_{\mathrm{K}} + \mathcal{Z}^2 (\mathcal{Z} - 1)}{\tilde{T}^{\perp\perp}}, & \mathcal{S}^2 + 4\Lambda = 0, \end{cases} \tag{7.220}$$

$$\mathcal{S}\mathcal{Z}\phi^{\perp} = \begin{cases} (2\mathcal{M} - 1)\,\tilde{T}^{\perp\perp} \pm 2\sqrt{\mathcal{J}}, & \mathcal{S}^2 + 2\Lambda \neq 0, \\ -2\tilde{T}^{\perp\perp}\left[\frac{1}{4} - \frac{\Lambda \tilde{T}^{\perp}_{\mathrm{K}} + \mathcal{Z}^2 (\mathcal{Z} - 1)}{\tilde{T}^{\perp\perp 2}}\right], & \mathcal{S}^2 + 2\Lambda = 0 \end{cases} \tag{7.221}$$

where, we have defined two more axillary quantities:

$$\mathcal{J} = (2\mathcal{M} - 1)\left[\frac{1}{2}\mathcal{M}\tilde{T}^{\perp\perp 2} - \Lambda \tilde{T}^{\perp 2}_{\mathrm{K}} - \mathcal{Z}^2 (\mathcal{Z} - 1)\right], \tag{7.222}$$

$$\mathcal{M} = \frac{2\Lambda}{\mathcal{S}^2 + 4\Lambda}. \tag{7.223}$$

This section is divided into three parts, akin to the previous section, contingent on which components of the contorsion current are non-zero. Each part has three distinctive cases depending on whether $\mathcal{S}^2 + 4\Lambda$ or $\mathcal{J}$ vanish.

Completely vanishing contorsion current

From Eq. (7.212), we deduce $\phi^{\parallel} = 0$ because $\tilde{T}^{\perp}_{\mathrm{K}} = 0$. Subsequently, using Eqs. (7.211) and (7.213), it follows that $\mathrm{K}^{\perp} = 0$ and $T^{\parallel\perp} = 0$, respectively. Additionally, since $\tilde{T}^{\parallel}_{\mathrm{K}}$ is zero, Eq. (7.214), implies:

$$\frac{\mathrm{d}\Lambda}{\mathrm{d}\bar{\mathrm{x}}} = \mathcal{S},\ \mathrm{K}^{\parallel} = 0. \tag{7.224}$$

We now arrive at the following system of equations:

$$\mathcal{Z}^2 \frac{\mathrm{d}\mathcal{Z}}{\mathrm{d}\bar{\mathrm{x}}} = \tilde{T}^{\parallel\parallel}\mathcal{Z}\phi^{\perp}, \tag{7.225}$$

$$\phi^{\perp} + \mathcal{D} = 0, \tag{7.226}$$

$$2\Lambda \frac{\mathrm{d}\tilde{T}^{\perp\perp}}{\mathrm{d}\bar{\mathrm{x}}} + \frac{\mathrm{d}\Lambda}{\mathrm{d}\bar{\mathrm{x}}}\left(\tilde{T}^{\perp\perp} + \tilde{T}^{\parallel\parallel}\right) = 0, \tag{7.227}$$

In this case $\tilde{T}^{\perp\perp} \neq 0$, since otherwise it follows from Eq. (7.227) that $\tilde{T}^{\parallel\parallel} = 0$, and the whole EMT vanishes.

- $\underline{\mathcal{S}^2 + 4\Lambda \neq 0 \ \wedge \ \mathcal{J} \neq 0}$: After making use of all the equations, Eq. (7.226) can be rewritten as:

$$\mathcal{Z}^3 \left(\frac{\mathrm{d}\mathcal{S}}{\mathrm{d}\bar{\mathrm{x}}} + 2\right) = \tilde{T}^{\perp\perp}\tilde{T}^{\parallel\parallel} \tag{7.228}$$

  and we must now distinguish two separate subcases:

  - ⋆ $\underline{\mathcal{S}' + 2 = 0}$: Since $\mathcal{S} = \frac{\mathrm{d}\Lambda}{\mathrm{d}\bar{\mathrm{x}}}$, this condition implies that the metric exactly coincides with that of the BTZ black hole:

$$\Lambda = -\left(\bar{\mathrm{x}}^2 - \mu\right), \tag{7.229}$$

where μ is a constant. From Eq. (7.228) we immediately obtain:

$$\tilde{T}^{\parallel\parallel} = 0, \tag{7.230}$$

as a necessary condition for the EMT. The remaining two field equations can then be straightforwardly integrated, giving:

$$\mathcal{Z} = const. \quad \tilde{T}^{\perp\perp} = \frac{D}{\bar{\mathrm{x}}}, \tag{7.231}$$

where D is another integration constant.

⋆ $\underline{\mathcal{S}' + 2 \neq 0}$: In this case, $\mathcal{Z}$ is determined by Eq. (7.228), namely:

$$\mathcal{Z}^3 = \frac{\tilde{T}^{\perp\perp}\tilde{T}^{\parallel\parallel}}{\frac{\mathrm{d}\mathcal{S}}{\mathrm{d}\bar{\mathrm{x}}} + 2}. \tag{7.232}$$

Substituting this expression into Eq. (7.225) leads to the following constraint on the EMT:

$$\frac{1}{3}\frac{\mathrm{d}}{\mathrm{d}\bar{\mathrm{x}}}\left(\frac{\tilde{T}^{\perp\perp}\tilde{T}^{\parallel\parallel}}{\frac{\mathrm{d}\mathcal{S}}{\mathrm{d}\bar{\mathrm{x}}} + 2}\right)^3 = \tilde{T}^{\parallel\parallel}\left[(2\mathcal{M} - 1)\,\tilde{T}^{\perp\perp} \pm 2\sqrt{\mathcal{J}}\right], \tag{7.233}$$

where $\mathcal{J}$, after inserting Eq. (7.232), becomes a function solely of the EMT components. The remaining Eq. (7.227) is already in the form of a covariant conservation law for the EMT.

- $\underline{\mathcal{S}^2 + 4\Lambda \neq 0 \ \wedge \ \mathcal{J} = 0}$: Condition $\mathcal{J} = 0$ reduces to:

$$\Lambda\tilde{T}^{\perp\perp 2} = \mathcal{Z}^2\,(\mathcal{Z} - 1)\left(\mathcal{S}^2 + 4\Lambda\right). \tag{7.234}$$

Using Eq. (7.234), Eq. (7.227) takes the form:

$$\mathcal{Z}^3\left(\frac{\mathrm{d}\mathcal{S}}{\mathrm{d}\bar{\mathrm{x}}} + 2\right) = \tilde{T}^{\perp\perp}\tilde{T}^{\parallel\parallel} \tag{7.235}$$

and Eq. (7.226) can be recast as:

$$(3\mathcal{Z} - 2)\,\tilde{T}^{\parallel\parallel} = 0. \tag{7.236}$$

Taken together with Eqs. (7.225) and (7.235), Eq. (7.236) implies that both the metric and the EMT are completely fixed:

$$\Lambda = -\left(\bar{\mathrm{x}}^2 - \mu\right), \ \tilde{T}^{\parallel\parallel} = 0, \ \Lambda\tilde{T}^{\perp\perp 2} = 4\mu\mathcal{Z}^2\,(\mathcal{Z} - 1), \tag{7.237}$$

with μ and $\mathcal{Z}$ constant.

- $\underline{\mathcal{S}^2 + 4\Lambda = 0}$: This relation, together with $\frac{\mathrm{d}\Lambda}{\mathrm{d}\bar{\mathrm{x}}} = \mathcal{S}$, immediately leads to:

$$\Lambda = -\bar{\mathrm{x}}^2, \ \ \mathcal{S} = -2\bar{\mathrm{x}}. \tag{7.238}$$

Under this condition, Eq. (7.226) simplifies to:

$$\tilde{T}^{\parallel\parallel} = 0, \tag{7.239}$$

while the remaining Eqs. (7.225) and (7.227) yield:

$$\tilde{T}^{\perp\perp} = \frac{D}{\bar{\mathrm{x}}}, \ \mathcal{Z} = const, \tag{7.240}$$

where D is another constant.

Non-vanishing parallel component of contorsion current

Given that $\tilde{T}^{\perp}_{\mathrm{K}} = 0$, we immediately deduce $\phi^{\parallel} = \mathrm{K}^{\perp} = T^{\parallel\perp} = 0$. The system of equations then reduces to:

$$\mathcal{Z}^2 \frac{\mathrm{d}\mathcal{Z}}{\mathrm{d}\bar{\mathrm{x}}} = \tilde{T}^{\parallel}_{\mathrm{K}} \tilde{T}^{\perp\perp} + \mathcal{Z}\phi^{\perp}\left(\tilde{T}^{\parallel\parallel} + \mathcal{S}\tilde{T}^{\parallel}_{\mathrm{K}}\right), \tag{7.241}$$

$$\mathcal{Z}\left(\phi^{\perp} + \mathcal{D}\right) = \tilde{T}^{\parallel}_{\mathrm{K}}, \tag{7.242}$$

$$\frac{\mathcal{Z}^3}{2\Lambda}\left(\frac{\mathrm{d}\Lambda}{\mathrm{d}\bar{\mathrm{x}}} - \mathcal{S}\right) = -\tilde{T}^{\perp\perp}\tilde{T}^{\parallel}_{\mathrm{K}}, \tag{7.243}$$

$$2\Lambda \frac{\mathrm{d}\tilde{T}^{\perp\perp}}{\mathrm{d}\bar{\mathrm{x}}} + \frac{\mathrm{d}\Lambda}{\mathrm{d}\bar{\mathrm{x}}}\left(\tilde{T}^{\perp\perp} + \tilde{T}^{\parallel\parallel}\right) + 2\Lambda\tilde{T}^{\parallel}_{\mathrm{K}}\frac{\mathrm{d}\mathcal{S}}{\mathrm{d}\bar{\mathrm{x}}} = 0. \tag{7.244}$$

- $\underline{\mathcal{S}^2 + 4\Lambda \neq 0 \ \wedge \ \mathcal{J} \neq 0}$: Exploiting the full set of equations, Eq. (7.242) can be recast in the form:

$$0 = \left[(2\mathcal{M}-1)\,\tilde{T}^{\perp\perp} \pm 2\sqrt{\mathcal{J}}\right]\left[\mathcal{S}\tilde{T}^{\parallel}_{\mathrm{K}} - \left((2\mathcal{M}-1)\,\tilde{T}^{\perp\perp} \pm 2\sqrt{\mathcal{J}}\right)\right] \times \left[\frac{\Lambda\tilde{T}^{\parallel}_{\mathrm{K}}}{\mathcal{M}}\left(2 + \frac{\mathcal{S}\frac{\mathrm{d}\mathcal{M}}{\mathrm{d}\bar{\mathrm{x}}}}{2\mathcal{M}-1}\right) + \left(\frac{\mathrm{d}\Lambda}{\mathrm{d}\bar{\mathrm{x}}} - \mathcal{S}\right)\left(\tilde{T}^{\parallel\parallel} + \mathcal{S}\tilde{T}^{\parallel}_{\mathrm{K}}\right)\right]. \tag{7.245}$$

  The first factor in Eq. (7.245) cannot vanish, as it is proportional to $\phi^{\perp} \neq 0$. Consequently, the solution splits into two distinct branches, depending on which of the remaining factors is set to zero.

  - ⋆ $\underline{\mathrm{x} = const}$: This case arises when the middle bracket is set to zero. Then we obtain $\tilde{T}^{\parallel}_{\mathrm{K}} = \mathcal{Z}\phi^{\perp}$, which in turn implies $\mathcal{D} = 0$, or equivalently $\mathrm{x} = const$. Solving Eq. (7.244) for $\tilde{T}^{\parallel\parallel}$ and employing Eq. (7.243) together with the defining condition of this class, one verifies that Eq. (7.241) is fulfilled. In terms of x and $\mathcal{Z}$, all fields can now be written as:

$$\phi^{\perp} = \pm\sqrt{\frac{\mathcal{Z} - (\mathrm{x}^2+1)}{\Lambda}}, \tag{7.246}$$

$$\tilde{T}^{\perp\perp} = \mathcal{Z}\left[2\mathrm{x} \mp \mathcal{S}\sqrt{\frac{\mathcal{Z} - (\mathrm{x}^2+1)}{\Lambda}}\right], \tag{7.247}$$

$$\tilde{T}^{\parallel}_{\mathrm{K}} = \pm\mathcal{Z}\sqrt{\frac{\mathcal{Z} - (\mathrm{x}^2+1)}{\Lambda}}, \tag{7.248}$$

    where we have adopted a new sign convention. Eq. (7.244) now acts as a constraint on the sources, while the remaining Eq. (7.243) turns into an algebraic equation that fixes $\mathcal{Z}$:

$$\left(\frac{\mathrm{d}\Lambda}{\mathrm{d}\bar{\mathrm{x}}} - 3\mathcal{S}\right)^2 \mathcal{Z}^2 + 4\left(\mathrm{x}^2+1\right)\left[\left(\mathrm{x}^2+1\right)\mathcal{S}^2 + 4\mathrm{x}^2\Lambda\right] + 4\left[\mathcal{S}\left(\mathrm{x}^2+1\right)\left(\frac{\mathrm{d}\Lambda}{\mathrm{d}\bar{\mathrm{x}}} - 3\mathcal{S}\right) - 4\mathrm{x}^2\Lambda\right]\mathcal{Z} = 0. \tag{7.249}$$

  - ⋆ $\underline{\mathrm{x} \neq const. \ \wedge \ \tilde{T}^{\perp\perp} \neq 0}$: In this situation, the third bracket in Eq. (7.245) must vanish, which yields the following reduced system of equations:

$$\left(\frac{\mathrm{d}\Lambda}{\mathrm{d}\bar{\mathrm{x}}}-\mathcal{S}\right)\left(\tilde{T}^{\shortparallel\shortparallel}+\mathcal{S}\tilde{T}^{\shortparallel}_{\mathrm{K}}\right)=-\frac{\Lambda\tilde{T}^{\shortparallel}_{\mathrm{K}}}{\mathcal{M}}\left(2+\frac{\mathcal{S}\frac{\mathrm{d}\mathcal{M}}{\mathrm{d}\bar{\mathrm{x}}}}{2\mathcal{M}-1}\right), \tag{7.250}$$

$$\Lambda\tilde{T}^{\shortparallel}_{\mathrm{K}}\tilde{T}^{\perp\perp}\frac{\mathrm{d}}{\mathrm{d}\bar{\mathrm{x}}}\left(\mathcal{S}^2+4\Lambda\right)=\left(\frac{\mathrm{d}\Lambda}{\mathrm{d}\bar{\mathrm{x}}}-\mathcal{S}\right)\frac{\mathrm{d}}{\mathrm{d}\bar{\mathrm{x}}}\left(\Lambda\tilde{T}^{\perp\perp2}\right), \tag{7.251}$$

$$\mathcal{Z}^3\frac{\mathrm{d}}{\mathrm{d}\bar{\mathrm{x}}}\left(\mathcal{S}^2+4\Lambda\right)=-2\frac{\mathrm{d}}{\mathrm{d}\bar{\mathrm{x}}}\left(\Lambda\tilde{T}^{\perp\perp2}\right), \tag{7.252}$$

$$\frac{\mathrm{d}}{\mathrm{d}\bar{\mathrm{x}}}\ln\left[\mathcal{Z}^2\left(\mathcal{S}^2+4\Lambda\right)\right]=\pm\frac{4\sqrt{\mathcal{J}}}{\mathcal{S}\mathcal{M}\tilde{T}^{\perp\perp}}\left[1+\frac{\mathcal{S}\frac{\mathrm{d}\mathcal{M}}{\mathrm{d}\bar{\mathrm{x}}}}{2\left(2\mathcal{M}-1\right)}\right]. \tag{7.253}$$

Since $\tilde{T}^{\perp\perp}\neq 0$, it follows that $\frac{\mathrm{d}\Lambda}{\mathrm{d}\bar{\mathrm{x}}}\neq\mathcal{S}$. Eq. (7.252) can be solved for $\mathcal{Z}$, while the other three equations impose constraints on the sources.

⋆ $\underline{\mathrm{x}\neq \mathit{const.}\ \wedge\ \tilde{T}^{\perp\perp}=0}$: In this final case, the last bracket in Eq. (7.245) vanishes. Using Eq. (7.88), one obtains $\frac{\mathrm{d}\Lambda}{\mathrm{d}\bar{\mathrm{x}}}=\mathcal{S}$. Inserting this result into Eq. (7.245) gives $\frac{\mathrm{d}\mathcal{S}}{\mathrm{d}\bar{\mathrm{x}}}+2=0$. Taken together, these relations yield the following metric:

$$\Lambda=-\left(\bar{\mathrm{x}}^2-\mu\right),\ \mathcal{S}=-2\bar{\mathrm{x}}, \tag{7.254}$$

where μ is an integration constant. Integrating Eq. (7.241) under these conditions leads to:

$$\phi^{\perp}+\frac{1}{3}\mu\phi^{\perp3}=\eta-\int\frac{\mathrm{d}\bar{\mathrm{x}}}{\bar{\mathrm{x}}}\tilde{T}^{\shortparallel}_{\mathrm{K}}, \tag{7.255}$$

with η another integration constant. The dilaton then follows directly from Eq. (7.216):

$$\mathrm{x}=-\bar{\mathrm{x}}\phi^{\perp}. \tag{7.256}$$

Under these assumptions, Eq. (7.244) reduces to the following condition on the sources:

$$\tilde{T}^{\shortparallel\shortparallel}=-\frac{2\Lambda}{\bar{\mathrm{x}}}\tilde{T}^{\shortparallel}_{\mathrm{K}}. \tag{7.257}$$

• $\underline{\mathcal{S}^2+4\Lambda\neq 0\ \wedge\ \mathcal{J}=0}$: Substituting Eq. (7.241) into Eq. (7.244) transforms Eq. (7.244) as follows:

$$\left[\mathcal{S}\left(3\mathcal{Z}-2\right)-\mathcal{Z}\frac{\mathrm{d}\Lambda}{\mathrm{d}\bar{\mathrm{x}}}\right]\frac{\mathrm{d}}{\mathrm{d}\bar{\mathrm{x}}}\left[\mathcal{Z}^2\left(\mathcal{S}^2+4\Lambda\right)\right]=0. \tag{7.258}$$

Imposing that the derivative term in Eq. (7.258) vanishes and using Eq. (7.242) yields

$$\left(3\mathcal{Z}-2\right)\left[\frac{2}{\mathcal{S}}\left(2\mathcal{M}-1\right)+\frac{\mathrm{d}\mathcal{M}}{\mathrm{d}\bar{\mathrm{x}}}\right]=0. \tag{7.259}$$

This leads to a new branching of the solution space.

⋆ $\underline{\mathcal{Z}\sqrt{\mathcal{S}^2+4\Lambda}=\pm\sqrt{Q}\ \wedge\ \mathcal{Z}\neq 2/3}$: In this branch, $\mathcal{Z}$ is completely fixed. Consequently, Eqs. (7.221) and (7.220) already provide the final forms of $\phi^{\perp}$ and x, and Eq. (7.258) is automatically fulfilled. The remaining Eqs. (7.241) and (7.243), together with $\mathcal{J}=0$, impose the following constraints on the sources:

$$\tilde{T}^{\shortparallel\shortparallel}+\mathcal{S}\tilde{T}^{\shortparallel}_{\mathrm{K}}=0, \tag{7.260}$$

$$\tilde{T}^{\shortparallel}_{\mathrm{K}}=\frac{1}{2}\frac{\tilde{T}^{\perp\perp}}{\mathcal{S}^2+4\Lambda}\frac{\frac{\mathrm{d}\Lambda}{\mathrm{d}\bar{\mathrm{x}}}-\mathcal{S}}{\pm\sqrt{\frac{\mathcal{S}^2+4\Lambda}{Q}}-1}, \tag{7.261}$$

$$\Lambda\tilde{T}^{\perp\perp2}=Q\left(\pm\sqrt{\frac{Q}{\mathcal{S}^2+4\Lambda}}-1\right), \tag{7.262}$$

respectively. Finally, Eq. (7.259) determines $\mathcal{S}$ in terms of the metric:

$$\mathcal{S} = \begin{cases} -2\sqrt{\Lambda}\tan \mathrm{z}; & \Lambda > 0 \\ 2\sqrt{-\Lambda}\coth \mathrm{z}; & \Lambda < 0,\ \mathcal{S}^2 + 4\Lambda > 0 \\ 2\sqrt{-\Lambda}\tanh \mathrm{z}; & \Lambda < 0,\ \mathcal{S}^2 + 4\Lambda < 0 \end{cases} . \tag{7.263}$$

- ⋆ $\underline{\mathcal{Z}\sqrt{\mathcal{S}^2 + 4\Lambda} = \sqrt{Q}\ \wedge\ \mathcal{Z} = 2/3}$: In this case, Eqs. (7.258) and (7.259) are again identically satisfied, and $\mathcal{Z}$ is fully fixed, which in turn determines x and $\phi^{\perp}$. Under these two conditions, $\mathcal{S}$ can be written entirely in terms of Λ as:

$$\mathcal{S}^2 = \frac{9Q}{4} - 4\Lambda. \tag{7.264}$$

The leftover equations, (7.241) and (7.243), together with $\mathcal{J} = 0$, become:

$$\mathcal{S}\tilde{T}^{\shortparallel\shortparallel} = 4\Lambda\tilde{T}^{\shortparallel}_{\mathrm{K}}, \tag{7.265}$$

$$\tilde{T}^{\shortparallel}_{\mathrm{K}} = \frac{4\tilde{T}^{\perp\perp}}{9Q}\left(\frac{\mathrm{d}\Lambda}{\mathrm{d}\bar{\mathrm{x}}} - \mathcal{S}\right), \tag{7.266}$$

$$\Lambda\tilde{T}^{\perp\perp 2} = -\frac{Q}{3}, \tag{7.267}$$

respectively.

- ⋆ $\underline{\mathcal{S}\left(3\mathcal{Z} - 2\right) = \mathcal{Z}\frac{\mathrm{d}\Lambda}{\mathrm{d}\bar{\mathrm{x}}}}$: Inserting this relation into Eq. (7.88) and imposing $\mathcal{J} = 0$ gives:

$$\tilde{T}^{\shortparallel}_{\mathrm{K}} = -\frac{\mathcal{S}\tilde{T}^{\perp\perp}}{\mathcal{S}^2 + 4\Lambda}. \tag{7.268}$$

Comparing with Eq. (7.221), we infer $\tilde{T}^{\shortparallel}_{\mathrm{K}} = \mathcal{Z}\phi^{\perp}$, which implies $\mathcal{D} = 0$, i.e. $\mathrm{x} = const$. Combining $\mathcal{J} = 0$ with Eq. (7.220), we find:

$$\mathcal{Z} = 1 + \frac{\mathrm{x}^2}{2\mathcal{M}}. \tag{7.269}$$

The remaining equations then impose the following conditions on the EMT and the contorsion current:

$$\tilde{T}^{\perp\perp} = \frac{\mathrm{x}}{\mathcal{M}}\left(1 + \frac{\mathrm{x}^2}{2\mathcal{M}}\right), \tag{7.270}$$

$$2\Lambda\tilde{T}^{\shortparallel}_{\mathrm{K}} = -\mathrm{x}\mathcal{S}\left(1 + \frac{\mathrm{x}^2}{2\mathcal{M}}\right), \tag{7.271}$$

$$\tilde{T}^{\shortparallel\shortparallel} = \frac{\mathrm{x}\Lambda}{\mathcal{S}\mathcal{M}^2}\left(1 + \frac{\mathrm{x}^2}{2\mathcal{M}}\right)\left[\frac{\mathrm{d}\mathcal{M}}{\mathrm{d}\bar{\mathrm{x}}} - \frac{2\mathcal{S}\mathcal{M}^2}{\Lambda}\right], \tag{7.272}$$

$$\frac{\mathrm{d}\Lambda}{\mathrm{d}\bar{\mathrm{x}}} = \mathcal{S}\frac{2\mathcal{M} + 3\mathrm{x}^2}{2\mathcal{M} + \mathrm{x}^2}. \tag{7.273}$$

- $\underline{\mathcal{S}^2 + 4\Lambda = 0}$: This is the final case for $\tilde{T}^{\perp}_{\mathrm{K}} = 0$. We begin by examining Eq. (7.242), which can be rewritten as:

$$\left(\frac{1}{4} - \frac{\mathcal{Z}^2\left(\mathcal{Z} - 1\right)}{\tilde{T}^{\perp\perp 2}}\right)\left[2\Lambda\tilde{T}^{\shortparallel}_{\mathrm{K}} - \mathcal{S}\tilde{T}^{\perp\perp}\left(\frac{1}{4} - \frac{\mathcal{Z}^2\left(\mathcal{Z} - 1\right)}{\tilde{T}^{\perp\perp 2}}\right)\right]\left(\tilde{T}^{\shortparallel\shortparallel} + \mathcal{S}\tilde{T}^{\shortparallel}_{\mathrm{K}}\right) = 0. \tag{7.274}$$

The first factor in Eq. (7.274) cannot vanish because it is proportional to $\phi^{\perp}$, which leaves two possible subclasses of solutions.

- ⋆ $\underline{\mathrm{x} = const}$: This subclass corresponds to imposing that the middle factor in Eq. (7.274) is zero. Comparing with Eq. (7.221), one deduces $\tilde{T}^{\parallel}_{\mathrm{K}} = \mathcal{Z}\phi^{\perp}$, implying $\mathcal{D} = 0$ and, consequently, that x is constant. Eq. (7.244) then remains as the EMT conservation law, whereas Eq. (7.241) is automatically satisfied for a constant dilaton. All fields are determined in terms of $\mathcal{Z}$. In this situation, the solution coincides with the one obtained for $\mathcal{S}^2 + 4\Lambda \neq 0 \ \wedge \ \mathcal{J} \neq 0$, further restricted by the condition $\mathcal{S}^2 + 4\Lambda = 0$.
- ⋆ $\underline{\mathrm{x} \neq const \ \wedge \ \tilde{T}^{\perp\perp} \neq 0}$: In this case, Eq. (7.274) yields:

$$\tilde{T}^{\parallel\parallel} + \mathcal{S}\tilde{T}^{\parallel}_{\mathrm{K}} = 0, \tag{7.275}$$

which, combined with Eq. (7.244), provides an EMT expressed via the metric:

$$\tilde{T}^{\perp\perp} = \frac{D}{\sqrt{-\Lambda}}. \tag{7.276}$$

Together with Eq. (7.241), this leads to a solution for $\mathcal{Z}$:

$$\mathcal{Z} = \frac{\eta}{\sqrt{-\Lambda}} e^{\pm \mathrm{z}}, \tag{7.277}$$

where the coordinate z is defined by Eq. (3.21). The last condition follows from Eq. (7.243):

$$\tilde{T}^{\parallel}_{\mathrm{K}} = -\frac{\eta^3}{3D}\frac{\mathrm{d}}{\mathrm{dz}}\left(\frac{e^{\mp 3\mathrm{z}}}{(-\Lambda)^{\frac{3}{2}}}\right). \tag{7.278}$$

Thus, this family of solutions is characterized by the two constants η and D.
- ⋆ $\underline{\mathrm{x} \neq const \ \wedge \ \tilde{T}^{\perp\perp} = 0}$: From Eq. (7.243) we obtain the metric:

$$\Lambda = -\bar{\mathrm{x}}^2, \ \mathcal{S} = -2\bar{\mathrm{x}}. \tag{7.279}$$

The remaining equations then become:

$$\tilde{T}^{\parallel\parallel} = 2\bar{\mathrm{x}}\tilde{T}^{\parallel}_{\mathrm{K}}, \tag{7.280}$$

$$\phi^{\perp} = \eta - \int \frac{\mathrm{d}\bar{\mathrm{x}}}{\bar{\mathrm{x}}}\tilde{T}^{\parallel}_{\mathrm{K}}, \tag{7.281}$$

$$\mathrm{x} = -\bar{\mathrm{x}}\left[\eta - \int \frac{\mathrm{d}\bar{\mathrm{x}}}{\bar{\mathrm{x}}}\tilde{T}^{\parallel}_{\mathrm{K}}\right]. \tag{7.282}$$

Non-vanishing normal component of contorsion current

The system of equations defining this case is given by:

$$\mathcal{Z}^2\frac{\mathrm{d}\mathcal{Z}}{\mathrm{d}\bar{\mathrm{x}}} = -\frac{\mathcal{Z}^3}{2\Lambda}\left(\frac{\mathrm{d}\Lambda}{\mathrm{d}\bar{\mathrm{x}}} - \mathcal{S}\right) + \mathcal{Z}\phi^{\perp}\left(\tilde{T}^{\parallel\parallel} + \mathcal{S}\tilde{T}^{\parallel}_{\mathrm{K}}\right), \tag{7.283}$$

$$\mathcal{Z}\left(\phi^{\perp} + \mathcal{D}\right) = \tilde{T}^{\parallel}_{\mathrm{K}}, \tag{7.284}$$

$$-\tilde{T}^{\perp\perp}\tilde{T}^{\parallel}_{\mathrm{K}} + \frac{\mathrm{d}}{\mathrm{d}\bar{\mathrm{x}}}\left(\Lambda\tilde{T}^{\perp 2}_{\mathrm{K}}\right) = \frac{\mathcal{Z}^3 - 2\Lambda\tilde{T}^{\perp 2}_{\mathrm{K}}}{2\Lambda}\left(\frac{\mathrm{d}\Lambda}{\mathrm{d}\bar{\mathrm{x}}} - \mathcal{S}\right), \tag{7.285}$$

$$2\Lambda\frac{\mathrm{d}\tilde{T}^{\perp\perp}}{\mathrm{d}\bar{\mathrm{x}}} + \frac{\mathrm{d}\Lambda}{\mathrm{d}\bar{\mathrm{x}}}\left(\tilde{T}^{\perp\perp} + \tilde{T}^{\parallel\parallel}\right) + 2\Lambda\tilde{T}^{\parallel}_{\mathrm{K}}\frac{\mathrm{d}\mathcal{S}}{\mathrm{d}\bar{\mathrm{x}}} = 2\frac{\frac{1}{2\Lambda}\left(\frac{\mathrm{d}\Lambda}{\mathrm{d}\bar{\mathrm{x}}} - \mathcal{S}\right) + \frac{\mathrm{d}}{\mathrm{d}\bar{\mathrm{x}}}\ln\mathcal{Z}}{\mathcal{Z}\phi^{\perp}}\frac{\mathrm{d}}{\mathrm{d}\bar{\mathrm{x}}}\left(\Lambda\tilde{T}^{\perp}_{\mathrm{K}}\right)^2, \tag{7.286}$$

together with the solutions for $\phi^{\perp}$ and x, given by Eqs. (7.221) and (7.220) respectively. The method of solving of these equations mirrors that of the earlier section, with identical scenarios arising.

- $\underline{\mathcal{S}^2+4\Lambda\neq 0\ \wedge\ \mathcal{J}\neq 0}$: Once again starting from Eq. (7.284) we get:

$$0=\left[(2\mathcal{M}-1)\,\tilde{T}^{\perp\perp}\pm 2\sqrt{\mathcal{J}}\right]\left[\mathcal{S}\tilde{T}^{\shortparallel}_{\mathrm{K}}-\left((2\mathcal{M}-1)\,\tilde{T}^{\perp\perp}\pm 2\sqrt{\mathcal{J}}\right)\right]\times \left[2+\frac{\mathcal{S}}{2\mathcal{M}-1}\frac{\mathrm{d}\mathcal{M}}{\mathrm{d}\bar{\mathrm{x}}}-\frac{2\mathcal{M}\tilde{T}^{\perp\perp}}{\mathcal{Z}^3}\left(\tilde{T}^{\shortparallel\shortparallel}+\mathcal{S}\tilde{T}^{\shortparallel}_{\mathrm{K}}\right)\right]. \tag{7.287}$$

The first bracket in Eq. (7.287) cannot be equal to zero, since it is proportional to $\phi^{\perp}\neq 0$. The solution branches into two potential outcomes based on the selection of the vanishing bracket.

  - ⋆ $\underline{\mathrm{x}=const}$: This scenario occurs when the middle bracket is set to zero. This indicates that $\tilde{T}^{\shortparallel}_{\mathrm{K}}=\mathcal{Z}\phi^{\perp}$, which consequently leads to $\mathcal{D}=0$, or $\mathrm{x}=const$. Employing all other eequations yields:

$$\begin{gathered}\theta=0,\ \ \mathrm{x}=const.\\ \phi^{\perp}=\pm\sqrt{\frac{\mathcal{Z}-(\mathrm{x}^2+1)}{\Lambda}+\frac{\tilde{T}^{\perp 2}_{\mathrm{K}}}{\mathcal{Z}^2}},\ \ \phi^{\shortparallel}=\frac{\tilde{T}^{\perp}_{\mathrm{K}}}{\mathcal{Z}},\\ l\mathrm{K}^{\shortparallel}=\frac{1}{2\Lambda}\left(\frac{\mathrm{d}\Lambda}{\mathrm{d}\bar{\mathrm{x}}}-\mathcal{S}\right),\ \ l\mathrm{K}^{\perp}=\frac{\tilde{T}^{\perp}_{\mathrm{K}}}{\mathcal{Z}^3}\left(\tilde{T}^{\shortparallel\shortparallel}+\mathcal{S}\tilde{T}^{\shortparallel}_{\mathrm{K}}\right),\end{gathered} \tag{7.288}$$

  where $\mathcal{Z}$ is the solution of the following algebraic equation:

$$\mathcal{Z}^3\left(\frac{\mathrm{d}\Lambda}{\mathrm{d}\bar{\mathrm{x}}}-3\mathcal{S}\right)+2\mathcal{S}\left(\mathrm{x}^2+1\right)\mathcal{Z}^2=2\frac{\mathrm{d}}{\mathrm{d}\bar{\mathrm{x}}}\left(\Lambda\tilde{T}^{\perp}_{\mathrm{K}}\right)^2\mp 4\mathrm{x}\Lambda\mathcal{Z}^2\sqrt{\frac{\mathcal{Z}-(\mathrm{x}^2+1)}{\Lambda}+\frac{\tilde{T}^{\perp 2}_{\mathrm{K}}}{\mathcal{Z}^2}}. \tag{7.289}$$

  Finally, conditions that the sources must satisfy are as follows:

$$\begin{gathered}\tilde{T}^{\perp\perp}=\mathcal{Z}\left[2\mathrm{x}\mp\mathcal{S}\sqrt{\frac{\mathcal{Z}-(\mathrm{x}^2+1)}{\Lambda}+\frac{\tilde{T}^{\perp 2}_{\mathrm{K}}}{\mathcal{Z}^2}}\right],\qquad \tilde{T}^{\shortparallel}_{\mathrm{K}}=\pm\mathcal{Z}\sqrt{\frac{\mathcal{Z}-(\mathrm{x}^2+1)}{\Lambda}+\frac{\tilde{T}^{\perp 2}_{\mathrm{K}}}{\mathcal{Z}^2}},\\ 2\Lambda\frac{\mathrm{d}\tilde{T}^{\perp\perp}}{\mathrm{d}\bar{\mathrm{x}}}+\frac{\mathrm{d}\Lambda}{\mathrm{d}\bar{\mathrm{x}}}\tilde{T}^{\perp\perp}+\frac{\Lambda\mathcal{S}\tilde{T}^{\shortparallel}_{\mathrm{K}}}{\mathcal{M}(2\mathcal{M}-1)}\frac{\mathrm{d}\mathcal{M}}{\mathrm{d}\bar{\mathrm{x}}}=\left[\frac{2}{\mathcal{Z}^3}\frac{\mathrm{d}}{\mathrm{d}\bar{\mathrm{x}}}\left(\Lambda\tilde{T}^{\perp}_{\mathrm{K}}\right)^2-\frac{\mathrm{d}\Lambda}{\mathrm{d}\bar{\mathrm{x}}}\right]\left(\tilde{T}^{\shortparallel\shortparallel}+\mathcal{S}\tilde{T}^{\shortparallel}_{\mathrm{K}}\right).\end{gathered} \tag{7.290}$$

  Notice that taking the limit $T^{\perp}_{\mathrm{K}}\to 0$ results into the equivalent solution of the previous section.

  - ⋆ $\underline{\mathrm{x}\neq const.\ \wedge\ \tilde{T}^{\perp\perp}\neq 0}$: Here, the third bracket in Eq. (7.287) must vanish, leading to the following reduced set of equations:

$$\begin{gathered}\mathcal{Z}^3\frac{\mathrm{d}}{\mathrm{d}\bar{\mathrm{x}}}\left(\mathcal{S}^2+4\Lambda\right)=2\frac{\mathrm{d}}{\mathrm{d}\bar{\mathrm{x}}}\left[-\Lambda\tilde{T}^{\perp\perp 2}+\Lambda\tilde{T}^{\perp 2}_{\mathrm{K}}\left(\mathcal{S}^2+4\Lambda\right)\right],\\ \frac{\mathrm{d}}{\mathrm{d}\bar{\mathrm{x}}}\ln\left[\mathcal{Z}^2\left(\mathcal{S}^2+4\Lambda\right)\right]=\pm\frac{4\sqrt{\mathcal{J}}}{\mathcal{S}\mathcal{M}\tilde{T}^{\perp\perp}}\left[1+\frac{\mathcal{S}\frac{\mathrm{d}\mathcal{M}}{\mathrm{d}\bar{\mathrm{x}}}}{2\left(2\mathcal{M}-1\right)}\right],\\ 2\Lambda\tilde{T}^{\perp\perp}\tilde{T}^{\shortparallel}_{\mathrm{K}}=\mathcal{M}\frac{\mathrm{d}}{\mathrm{d}\bar{\mathrm{x}}}\left(\Lambda\tilde{T}^{\perp\perp 2}\right)\mathcal{S}\left[1+\frac{\mathcal{S}\frac{\mathrm{d}\mathcal{M}}{\mathrm{d}\bar{\mathrm{x}}}}{2\left(2\mathcal{M}-1\right)}\right]\left(\mathcal{Z}^3-2\Lambda\tilde{T}^{\perp 2}_{\mathrm{K}}\right),\\ \mathcal{M}\tilde{T}^{\perp\perp}\left(\tilde{T}^{\shortparallel\shortparallel}+\mathcal{S}\tilde{T}^{\shortparallel}_{\mathrm{K}}\right)=\mathcal{Z}^3\left[1+\frac{\mathcal{S}\frac{\mathrm{d}\mathcal{M}}{\mathrm{d}\bar{\mathrm{x}}}}{2\left(2\mathcal{M}-1\right)}\right].\end{gathered} \tag{7.291}$$

This is the most general solution to the full set of equations of motion when $\theta = 0$. Note that $\tilde{T}^{\perp\perp} \neq 0$ implies that $\frac{\mathrm{d}\Lambda}{\mathrm{d}\bar{\mathrm{x}}} \neq \mathcal{S}$. The first equation can be interpreted as a solution for $\mathcal{Z}$, while the remaining three are then the conditions for the sources.

⋆ $\underline{\mathrm{x} \neq \mathit{const.} \wedge \tilde{T}^{\perp\perp} = 0}$: This case corresponds to setting the third bracket in Eq. (7.287) as well. The remaining equations reduce to the following set:

$$\begin{aligned}
&\frac{\mathcal{Z}^3 - 2\Lambda\tilde{T}_{\mathrm{K}}^{\perp 2}}{2\Lambda}\left(\frac{\mathrm{d}\Lambda}{\mathrm{d}\bar{\mathrm{x}}} - \mathcal{S}\right) = \frac{\mathrm{d}}{\mathrm{d}\bar{\mathrm{x}}}\left(\Lambda\tilde{T}_{\mathrm{K}}^{\perp 2}\right), \ \tilde{T}^{\perp\perp} = 0, \\
&\left(\mathcal{S}^2 + 4\Lambda\right)\tilde{T}_{\mathrm{K}}^{\shortparallel} = \frac{\mathcal{S}}{\mathcal{Z}^3}\left(\mathcal{Z}^3 - 2\Lambda\tilde{T}_{\mathrm{K}}^{\perp 2}\right)\left(\tilde{T}^{\shortparallel\shortparallel} + \mathcal{S}\tilde{T}_{\mathrm{K}}^{\shortparallel}\right), \\
&\mathcal{Z}^2\frac{\mathrm{d}\mathcal{Z}}{\mathrm{d}\bar{\mathrm{x}}} + \frac{\mathcal{Z}^3}{2\Lambda}\left(\frac{\mathrm{d}\Lambda}{\mathrm{d}\bar{\mathrm{x}}} - \mathcal{S}\right) = \pm 2\left(\tilde{T}^{\shortparallel\shortparallel} + \mathcal{S}\tilde{T}_{\mathrm{K}}^{\shortparallel}\right)\sqrt{\frac{\Lambda\tilde{T}_{\mathrm{K}}^{\perp 2} + \mathcal{Z}^2(\mathcal{Z}-1)}{\mathcal{S}^2 + 4\Lambda}},
\end{aligned} \tag{7.292}$$

where the first equation represents a solution for $\mathcal{Z}$. The other axillary function $\mathcal{S}$ is given by:

$$\mathcal{S} = \begin{cases} -2\sqrt{\Lambda}\tan\mathrm{z}; & \Lambda > 0 \\ 2\sqrt{-\Lambda}\coth\mathrm{z}; & \Lambda < 0, \ \mathcal{S}^2 + 4\Lambda > 0 \\ 2\sqrt{-\Lambda}\tanh\mathrm{z}; & \Lambda < 0, \ \mathcal{S}^2 + 4\Lambda < 0 \end{cases}. \tag{7.293}$$

- $\underline{\mathcal{S}^2 + 4\Lambda \neq 0 \wedge \mathcal{J} = 0}$: Applying Eqs. (7.283–7.285) to rewrite Eq. 7.287 yields:

$$\left[\mathcal{Z}^2(\mathcal{Z}-1) + \Lambda\tilde{T}_{\mathrm{K}}^{\perp 2} + \frac{\Lambda}{\mathcal{S}}\tilde{T}^{\perp\perp}\tilde{T}_{\mathrm{K}}^{\shortparallel}\right]\frac{\mathrm{d}}{\mathrm{d}\bar{\mathrm{x}}}\left[\mathcal{Z}^2\left(\mathcal{S}^2 + 4\Lambda\right)\right] = 0. \tag{7.294}$$

Imposing that the derivative term in Eq. (7.294) vanishes and using Eq. (7.284) leads to:

$$(3\mathcal{Z} - 2)\left[\frac{2}{\mathcal{S}}(2\mathcal{M} - 1) + \frac{\mathrm{d}\mathcal{M}}{\mathrm{d}\bar{\mathrm{x}}}\right] = 0, \tag{7.295}$$

which is identical to Eq. (7.259). Hence, we obtain an additional branch of solutions.

⋆ $\underline{\mathcal{Z}\sqrt{\mathcal{S}^2 + 4\Lambda} = \pm\sqrt{Q} \wedge \mathcal{Z} \neq 2/3}$: In this case, $\mathcal{Z}$ is fully fixed, so Eqs. (7.221) and (7.220) already provide the final solutions for $\phi^{\perp}$ and x. Eq. (7.294) is then automatically fulfilled. The remaining Eqs. (7.283) and (7.285), together with $\mathcal{J} = 0$, reduce to the following constraints on the sources:

$$\begin{aligned}
&\tilde{T}^{\shortparallel\shortparallel} + \mathcal{S}\tilde{T}_{\mathrm{K}}^{\shortparallel} = 0, \\
&\tilde{T}^{\perp\perp}\tilde{T}_{\mathrm{K}}^{\shortparallel} = \frac{\mathrm{d}}{\mathrm{d}\bar{\mathrm{x}}}\left(\Lambda\tilde{T}_{\mathrm{K}}^{\perp 2}\right) - \frac{\mathcal{Z}^3 - 2\Lambda\tilde{T}_{\mathrm{K}}^{\perp 2}}{2\Lambda}\left(\frac{\mathrm{d}\Lambda}{\mathrm{d}\bar{\mathrm{x}}} - \mathcal{S}\right), \\
&\Lambda\tilde{T}^{\perp\perp 2} = \Lambda\tilde{T}_{\mathrm{K}}^{\perp 2}\left(\mathcal{S}^2 + 4\Lambda\right) + Q\left(\pm\sqrt{\frac{Q}{\mathcal{S}^2 + 4\Lambda}} - 1\right).
\end{aligned} \tag{7.296}$$

Here, the auxiliary function $\mathcal{S}$ is completely determined by the metric as:

$$\mathcal{S} = \begin{cases} -2\sqrt{\Lambda}\tan\mathrm{z}; & \Lambda > 0 \\ 2\sqrt{-\Lambda}\coth\mathrm{z}; & \Lambda < 0, \ \mathcal{S}^2 + 4\Lambda > 0 \\ 2\sqrt{-\Lambda}\tanh\mathrm{z}; & \Lambda < 0, \ \mathcal{S}^2 + 4\Lambda < 0 \end{cases} \tag{7.297}$$

Note that in the limit $T_{\mathrm{K}}^{\perp} \to 0$, this solution reduces to the corresponding solution obtained in the previous section.

- ⋆ $\underline{\mathcal{Z}\sqrt{\mathcal{S}^2+4\Lambda} = \pm\sqrt{Q} \ \wedge \ \mathcal{Z} = 2/3}$: Under these conditions, Eqs. (7.294) and (7.295) are again trivially satisfied, which fully fixes $\mathcal{Z}$ and therefore also x and $\phi^{\perp}$. Incorporating these conditions, $\mathcal{S}$ can be expressed solely in terms of Λ as:

$$\mathcal{S}^2 = \frac{9Q}{4} - 4\Lambda. \tag{7.298}$$

The remaining equations simplify to the following constraints that the sources must obey:

$$\begin{aligned} &\tilde{T}^{\perp\perp}\left(\tilde{T}^{\parallel\parallel} + \mathcal{S}\tilde{T}^{\parallel}_{\mathrm{K}}\right) = -\frac{Q}{3\Lambda\mathcal{S}}\left(\frac{\mathrm{d}\Lambda}{\mathrm{d}\bar{\mathrm{x}}} - \mathcal{S}\right), \\ &\tilde{T}^{\perp\perp}\tilde{T}^{\parallel}_{\mathrm{K}} = \frac{\mathrm{d}}{\mathrm{d}\bar{\mathrm{x}}}\left(\Lambda\tilde{T}^{\perp 2}_{\mathrm{K}}\right) - \frac{\frac{8}{27} - 2\Lambda\tilde{T}^{\perp 2}_{\mathrm{K}}}{2\Lambda}\left(\frac{\mathrm{d}\Lambda}{\mathrm{d}\bar{\mathrm{x}}} - \mathcal{S}\right), \\ &\Lambda\tilde{T}^{\perp\perp 2} = \Lambda\tilde{T}^{\perp 2}_{\mathrm{K}}\left(\mathcal{S}^2 + 4\Lambda\right) - \frac{Q}{3}, \end{aligned} \tag{7.299}$$

In the limit $T^{\perp}_{\mathrm{K}} \to 0$, this branch likewise reduces to the corresponding solution of the preceding section.

- ⋆ $\underline{\mathcal{S}\left(\mathcal{Z}^2(\mathcal{Z}-1) + \Lambda\tilde{T}^{\perp 2}_{\mathrm{K}}\right) + \Lambda\tilde{T}^{\perp\perp}\tilde{T}^{\parallel}_{\mathrm{K}} = 0}$: This case corresponds to choosing the first bracket in Eq. (7.294) to vanish. Using $\mathcal{J} = 0$, one readily finds that this condition simplifies to:

$$\mathcal{S}\tilde{T}^{\parallel}_{\mathrm{K}} = (2\mathcal{M} - 1)\tilde{T}^{\perp\perp}, \tag{7.300}$$

which further implies $\tilde{T}^{\parallel}_{\mathrm{K}} = \mathcal{Z}\phi^{\perp}$. From Eq. (7.284) we then infer that x = const. Consequently, this corresponds to the special case of the general solution with constant x discussed at the beginning of this section.

- $\underline{\mathcal{S}^2 + 4\Lambda = 0}$: This is the final scenario when $\tilde{T}^{\perp}_{\mathrm{K}} \neq 0$. We begin by examining Eq. (7.284), which can be recast in the form:

$$\left(\frac{1}{4} - \frac{\mathcal{Z}^2\left(\mathcal{Z}-1\right) + \Lambda\tilde{T}^{\perp 2}_{\mathrm{K}}}{\tilde{T}^{\perp\perp 2}}\right)\left[2\Lambda\tilde{T}^{\parallel}_{\mathrm{K}} - \mathcal{S}\tilde{T}^{\perp\perp}\left(\frac{1}{4} - \frac{\mathcal{Z}^2\left(\mathcal{Z}-1\right) + \Lambda\tilde{T}^{\perp 2}_{\mathrm{K}}}{\tilde{T}^{\perp\perp 2}}\right)\right]\left(\tilde{T}^{\parallel\parallel} + \mathcal{S}\tilde{T}^{\parallel}_{\mathrm{K}}\right) = 0. \tag{7.301}$$

The first factor in Eq. (7.301) cannot vanish, since it is proportional to $\phi^{\perp}$, leaving us with two distinct possibilities:

  - ⋆ $\underline{\mathrm{x} = \mathit{const}}$: In this situation, the middle factor in Eq. (7.301) is set to zero. Comparing with Eq. (7.221), one obtains $\tilde{T}^{\parallel}_{\mathrm{K}} = \mathcal{Z}\phi^{\perp}$, implying that $\mathcal{D} = 0$ and thus that x is constant. Consequently, this case is just a particular instance of the first scenario analyzed in this section.

  - ⋆ $\underline{\mathrm{x} \neq \mathit{const} \ \wedge \ \tilde{T}^{\perp\perp} \neq 0}$: In this case Eq. (7.301) simplifies to:

$$\tilde{T}^{\parallel\parallel} + \mathcal{S}\tilde{T}^{\parallel}_{\mathrm{K}} = 0, \tag{7.302}$$

which, in combination with Eqs. (7.283) and (7.286), yields the following expressions for the EMT and the auxiliary function $\mathcal{Z}$ in terms of the metric:

$$\tilde{T}^{\perp\perp} = \frac{D}{\sqrt{-\Lambda}}, \qquad \mathcal{Z} = \frac{\eta}{\sqrt{-\Lambda}}e^{\pm \mathrm{z}}, \tag{7.303}$$

where z is the coordinate introduced in Eq. (3.21). The remaining constraint follows from Eq. (7.285) and reads:

$$\tilde{T}_{\mathrm{K}}^{\shortparallel}=-\frac{\eta^{3}}{3D}\frac{\mathrm{d}}{\mathrm{dz}}\left(\frac{e^{\mp3\mathrm{z}}}{(-\Lambda)^{\frac{3}{2}}}\right)-\frac{e^{\pm2\mathrm{z}}}{D\Lambda^{2}}\frac{\mathrm{d}}{\mathrm{dz}}\left(\Lambda^{3}\tilde{T}_{\mathrm{K}}^{\perp2}e^{\mp2\mathrm{z}}\right), \tag{7.304}$$

so this branch of solutions is characterized by two parameters, η and D. In the limit $T_{\mathrm{K}}^{\perp}\to0$ one recovers the corresponding solution from the previous section.

⋆ $\underline{\mathrm{x}\neq const\ \wedge\ \tilde{T}^{\perp\perp}=0}$: This is the last possibility considered here. The fields take the form:

$$\begin{aligned}\phi^{\perp}&=\pm\frac{\mathrm{x}}{\sqrt{-\Lambda}},\quad\phi^{\shortparallel}=\frac{\sqrt{-\Lambda}\tilde{T}_{\mathrm{K}}^{\perp}}{\eta}e^{\mp\mathrm{z}},\\ \mathrm{K}^{\perp}&=0,\quad2l\Lambda\mathrm{K}^{\shortparallel}=\frac{\mathrm{d}\Lambda}{\mathrm{d}\bar{\mathrm{x}}}\mp2\sqrt{-\Lambda},\\ \mathrm{x}&=\frac{e^{\pm\mathrm{z}}}{\eta}\left[D+\int\mathrm{dz}\Lambda\tilde{T}_{\mathrm{K}}^{\shortparallel}e^{\mp2\mathrm{z}}\right],\quad\theta=0,\end{aligned} \tag{7.305}$$

while the sources are constrained by:

$$\begin{aligned}&\tilde{T}^{\shortparallel\shortparallel}+\mathcal{S}\tilde{T}_{\mathrm{K}}^{\shortparallel}=0,\quad\tilde{T}^{\perp\perp}=0,\\ &\Lambda\tilde{T}_{\mathrm{K}}^{\perp2}+\mathcal{Z}^{2}\left(\mathcal{Z}-1\right)=0.\end{aligned} \tag{7.306}$$

The auxiliary function $\mathcal{Z}$ is again:

$$\mathcal{Z}=\frac{\eta}{\sqrt{-\Lambda}}e^{\pm\mathrm{z}}. \tag{7.307}$$

Here D is an integration constant.

7.2.3 Solutions when $\mathcal{Z}\neq0$, $\theta=0$ and $\phi^{\perp}=0$

The same way as in Sec. 7.2.1 all fields can be expressed in terms of the sources, that is:

$$\mathrm{x}=\frac{\tilde{T}^{\perp\perp}}{2\mathcal{Z}},\quad\phi^{\shortparallel}=\frac{\tilde{T}_{\mathrm{K}}^{\perp}}{\mathcal{Z}},\quad\phi^{\perp}=0, \tag{7.308}$$

$$2l\Lambda\mathrm{K}^{\shortparallel}=\frac{\tilde{T}^{\shortparallel\perp}}{\tilde{T}_{\mathrm{K}}^{\perp}},\quad2l\Lambda\mathrm{K}^{\perp}=\frac{\tilde{T}^{\shortparallel\shortparallel}+\tilde{T}^{\perp\perp}}{\tilde{T}_{\mathrm{K}}^{\perp}}, \tag{7.309}$$

while the solution for θ (7.201) becomes a condition given by:

$$\frac{1}{4}\tilde{T}^{\perp\perp2}=\Lambda\tilde{T}_{\mathrm{K}}^{\perp2}+\mathcal{Z}^{2}\left(\mathcal{Z}-1\right). \tag{7.310}$$

The remaining equations have the same form as in Sec. 7.2.1, given by:

$$2\tilde{T}_{\mathrm{K}}^{\shortparallel}=\frac{\mathrm{d}\tilde{T}^{\perp\perp}}{\mathrm{d}\bar{\mathrm{x}}}+\frac{\tilde{T}^{\perp\perp}}{2\Lambda}\left(\frac{\mathrm{d}\Lambda}{\mathrm{d}\bar{\mathrm{x}}}-\mathcal{S}\right) \tag{7.311}$$

$$\mathcal{Z}^{3}\frac{\tilde{T}^{\shortparallel\shortparallel}+\tilde{T}^{\perp\perp}}{2\Lambda\tilde{T}_{\mathrm{K}}^{\perp2}}=\frac{1}{2}\mathcal{S}\tilde{T}^{\perp\perp}\frac{\mathrm{d}}{\mathrm{d}\bar{\mathrm{x}}}\ln\left(\frac{\tilde{T}^{\perp\perp}}{\mathcal{Z}}\right)+\tilde{T}^{\shortparallel\shortparallel}, \tag{7.312}$$

$$\mathcal{Z}\left(\frac{\mathrm{d}\mathcal{S}}{\mathrm{d}\bar{\mathrm{x}}}+2\right)=\frac{\tilde{T}^{\shortparallel\shortparallel}\tilde{T}^{\perp\perp}}{\mathcal{Z}^{2}}+\mathcal{S}\frac{\mathrm{d}}{\mathrm{d}\bar{\mathrm{x}}}\left(\frac{\Lambda\tilde{T}_{\mathrm{K}}^{\perp2}}{\mathcal{Z}^{2}}\right), \tag{7.313}$$

$$2\tilde{T}_{\mathrm{K}}^{\shortparallel}=\frac{\mathrm{d}\tilde{T}^{\perp\perp}}{\mathrm{d}\bar{\mathrm{x}}}-\frac{1}{6}\frac{\mathrm{d}}{\mathrm{d}\bar{\mathrm{x}}}\left(\frac{\tilde{T}^{\perp\perp}}{\mathcal{Z}}\right)^{3}+\frac{\tilde{T}^{\perp\perp}}{\mathcal{Z}}\frac{\mathrm{d}}{\mathrm{d}\bar{\mathrm{x}}}\left(\frac{\Lambda\tilde{T}_{\mathrm{K}}^{\perp2}}{\mathcal{Z}^{2}}\right). \tag{7.314}$$

As in previous sections, we investigate three distinct scenarios, depending on which components of contorsion current vanish.

- $T_{\mathrm{K}}^{\mu} = 0$: In this case, as always, we have $\phi^{\parallel} = \mathrm{K}^{\perp} = T^{\parallel\perp} = 0$. From Eq. (7.26) we get $\mathcal{D} = 0$, which indicates $\mathrm{x} = const$. Since $\mathcal{Z} = \mathrm{x}^2 + 1$, from Eq. (7.23) we conclude that $\tilde{T}^{\perp\perp}$ is also constant:
$$\tilde{T}^{\perp\perp} = -\tilde{T}^{\parallel\parallel} = 2\mathrm{x}\left(\mathrm{x}^2 + 1\right), \tag{7.315}$$
where we have also used Eq. (7.24). The remaining equations are then solved by the following metric:
$$\Lambda = -\left[\frac{3\mathrm{x}^2 + 1}{\mathrm{x}^2 + 1}\bar{\mathrm{x}}^2 - \mu\right], \tag{7.316}$$
where μ is a constant. Finally, this metric implies a vanishing parallel component of the contorsion.

- $T_{\mathrm{K}}^{\perp} = 0$: In this scenario, $\tilde{T}_{\mathrm{K}}^{\parallel}$ is not equal to zero, but the condition of vanishing normal component of the contorsion current still implies $\phi^{\parallel} = \mathrm{K}^{\perp} = T^{\parallel\perp} = 0$. It resembles the earlier case, with the sole difference being that the dilaton, and subsequently the EMT, is not required to remain constant. The dilaton is found as a solution of $2\mathrm{x}\left(\mathrm{x}^2+1\right) = \tilde{T}^{\perp\perp}$ as a function $\mathrm{x} = f(\tilde{T}^{\perp\perp})$. Then, all other fields can be expressed in terms of f, that is:
$$l\mathrm{K}^{\parallel} = -\frac{2ff'}{1+f^2}\frac{\mathrm{d}\tilde{T}^{\perp\perp}}{\mathrm{d}\bar{\mathrm{x}}}, \tag{7.317}$$
$$\tilde{T}_{\mathrm{K}}^{\parallel} = \left(f^2+1\right)f'\frac{\mathrm{d}\tilde{T}^{\perp\perp}}{\mathrm{d}\bar{\mathrm{x}}}, \tag{7.318}$$
$$\frac{\mathrm{d}\mathcal{S}}{\mathrm{d}\bar{\mathrm{x}}} = -2\frac{3f^2+1}{f^2+1}, \tag{7.319}$$
$$\tilde{T}^{\parallel\parallel} = -\tilde{T}^{\perp\perp}. \tag{7.320}$$

- $T_{\mathrm{K}}^{\perp} \neq 0$: This is the most general case. Using Eq. (7.310), normal component of contorsion current is removed from the system of equations. Also, $\tilde{T}^{\parallel\parallel}$ is eliminated using Eq. (7.313). After this, we are left with three equations which cannot be further simplified at this point.

7.2.4 Solutions when $\mathcal{Z} = 0$

This is the final special scenario, corresponding to a vacuum solutions of type RCIIA (7.38) and RCIIB. Eqs. (7.22-7.26) reduce to a following set of conditions:

$$\tilde{T}^{\perp\perp} = \tilde{T}^{\parallel\perp} = \tilde{T}_{\mathrm{K}}^{\perp} = \tilde{T}^{\parallel\parallel} - \frac{2}{\mathrm{x}}\Lambda\phi^{\perp}\tilde{T}_{\mathrm{K}}^{\parallel} = 0, \tag{7.321}$$
$$\tilde{T}_{\mathrm{K}}^{\parallel} = -\mathrm{x}\frac{\mathrm{d}\theta^2}{\mathrm{d}\bar{\mathrm{x}}}. \tag{7.322}$$

These equations imply that $\theta^2 \neq const.$ since otherwise all sources vanish. Using the condition $\mathcal{Z} = 0$, the remaining four Eqs. (7.14-7.17) are rewritten in the following form:

$$\frac{\mathrm{d}}{\mathrm{d}\bar{\mathrm{x}}}\left(\frac{\mathrm{d}\Lambda}{\mathrm{d}\bar{\mathrm{x}}} - 2l\Lambda\mathrm{K}^{\parallel}\right) + 2 + \frac{2}{\mathrm{x}}l\Lambda\left(\phi^{\perp}\mathrm{K}^{\parallel} - \phi^{\parallel}\mathrm{K}^{\perp}\right) = 0, \tag{7.323}$$

$$\phi^{\parallel}\mathcal{A} = 0, \tag{7.324}$$

$$\phi^{\perp}\mathcal{A} = \frac{\mathrm{d}\theta^2}{\mathrm{d}\bar{\mathrm{x}}}, \tag{7.325}$$

$$2\mathrm{x}\mathcal{A} = \frac{\mathrm{d}\theta^2}{\mathrm{d}\bar{\mathrm{x}}}\left(\frac{\mathrm{d}\Lambda}{\mathrm{d}\bar{\mathrm{x}}} - 2l\Lambda\mathrm{K}^{\parallel}\right), \tag{7.326}$$

where $\mathcal{A}$ is a function of the fields and their derivatives given by:

$$\begin{aligned}\mathcal{A} = \left(\phi^{\perp} + \mathcal{D}\right)\left(\frac{\mathrm{d}\Lambda}{\mathrm{d}\bar{\mathrm{x}}} - 2l\Lambda\mathrm{K}^{\parallel}\right) + 2\Lambda\frac{\mathrm{d}\phi^{\perp}}{\mathrm{d}\bar{\mathrm{x}}} + \phi^{\perp}\frac{\mathrm{d}\Lambda}{\mathrm{d}\bar{\mathrm{x}}} \\ - 2\mathrm{x} + 2l\Lambda\phi^{\parallel}\mathrm{K}^{\perp}.\end{aligned} \tag{7.327}$$

Given that θ is not a constant, Eq. (7.325) indicates $\mathcal{A} \neq 0$, consequently leading to $\phi^{\parallel} = 0$. The nullification of $\phi^{\parallel}$ removes $\mathrm{K}^{\perp}$ from the equations entirely, thus making it an arbitrary function. By applying Eqs. (7.326) and (7.325) and substituting the resultant form into Eq. (7.323), we derive an integrable equation, presented with the subsequent solution:

$$\Lambda = -\left(\frac{\mathrm{x}^2}{\phi^{\perp 2}} - \mu\right), \tag{7.328}$$

where μ is the integration constant. The parallel component of contorsion is then given by:

$$2l\Lambda\mathrm{K}^{\parallel} = \frac{\mathrm{d}\Lambda}{\mathrm{d}\bar{\mathrm{x}}} \mp 2\sqrt{\mu - \Lambda}. \tag{7.329}$$

The last remaining equation of the four is automatically satisfied by the condition $\mathcal{Z} = 0$. The solutions for x and θ are as follows:

$$\theta^2 = 1 + \mu\phi^{\perp 2}, \tag{7.330}$$

$$\mathrm{x} = \pm\phi^{\perp}\sqrt{\Lambda - \mu}. \tag{7.331}$$

Finally, integrating Eq. (7.322) results in the solution for $\phi^{\perp}$:

$$\phi^{\perp 3} = \eta \mp \frac{3}{2\mu}\int\frac{\mathrm{d}\bar{\mathrm{x}}}{\sqrt{\mu - \Lambda}}\tilde{T}^{\parallel}_{\mathrm{K}}. \tag{7.332}$$

We conclude that this special case is dependent on two constants μ and η, and an arbitrary function $\mathrm{K}^{\perp}$ and can only manifest itself when $T^{\parallel}_{\mathrm{K}} \neq 0$ and $T^{\perp}_{\mathrm{K}} = 0$. Thus, we can see that the corresponding vacuum solutions are stable only when there is a non-vanishing parallel component of the contorsion current.

7.3 Adding matter minimally coupled to gravity

In this section, we examine how various matter fields couple to gravity. The fields are assumed to be minimally coupled, which means that the quantities $\tau_\mu = 0$ and $\varrho = 0$ introduced in Eq. (3.51), and therefore the matter Lagrangian takes the form $\mathcal{L}_{\mathrm{M}} = \mathcal{L}_{\mathrm{M}}\left(g^{\mu\nu}, \omega_\mu, \phi_r, \tilde{\nabla}_\mu\phi_r\right)$. The set ϕ_r denotes the complete matter sector of the theory. The notation used for each type of matter field follows the conventions summarized in Tab. 7.2.

Field	Label	Additional fields
R-scalars	F	/
C-scalars	f	$f \equiv Fe^{i\gamma}$
U(1) gauge	$\mathcal{A}$	$\mathcal{F}_{\mu\nu} \equiv \partial_\mu\mathcal{A}_\nu - \partial_\nu\mathcal{A}_\mu$
Spinors	ψ	$\psi = \begin{pmatrix}\varphi e^{i\alpha} & \chi e^{i\beta}\end{pmatrix}^T$
Fluids	u^μ	ρ, p, μ

Table 7.2: Field content

We begin by examining configurations in which a single field is present. Next, we consider the localization of the $U(1)$ symmetry, which leads to scalar and spinor electrodynamics. We then turn to ideal fluid hydrodynamics. In all of these cases, the contorsion current T^μ_{K} vanishes, so the energy-momentum tensor (EMT) is the only remaining source. When θ is set to zero, the theory reduces to its purely Riemannian sector, as described in the previous section. Since Riemannian solutions were the focus of the preceding chapter, we do not study them here and instead confine our analyzes to configurations with a non-vanishing θ field. Consequently, the relevant solutions of the gravitational equations of motion are characterized by $T^\mu_{\mathrm{K}} = 0$, $\theta \neq 0$, and $\mathcal{Z} \neq 0$ (corresponding to the first four entries in Tab. 7.1). After eliminating the additional gravity-related fields, the full set of gravitational equations of motion simplifies to:

$$\begin{cases} T^{\perp\perp} = \dfrac{6k\pi^2 D}{l^2}\dfrac{1}{\Lambda^{3/2}}, & T^{\parallel\parallel} = T^{\parallel\perp} = 0, \qquad \Lambda > 0, \\ T^{\perp\perp} = -\dfrac{6k\pi^2 D}{l^2}\dfrac{1}{(-\Lambda)^{3/2}}, & T^{\parallel\parallel} = T^{\parallel\perp} = 0, \quad \Lambda < 0. \end{cases} \tag{7.333}$$

Hence, the EMT is entirely determined in terms of the single metric function Λ. To obtain a complete description, these equations must be supplemented by the equations of motion for the matter fields. Another key point to emphasize is that $\mathrm{K}^{\parallel} \neq 0$, because if it were zero, then D would also be zero and the EMT would vanish.

7.3.1 Real scalar field theory

It turns out that the massless scalars directly imply the vanishing θ field. For that reason we investigate a more general theory with an arbitrary scalar potential. In other words, we investigate the interacting scalar field theories within this subsection. Therefore, the action for the real scalar field, minimally-coupled to gravity, is given by:

$$S_{\mathrm{RSF}} = -\int \mathrm{d}^2x\sqrt{-g}\left[\frac{1}{2}\left(\nabla F\right)^2 + V[F]\right], \tag{7.334}$$

where $V[F]$ is the scalar potential. The variation with respect to the metric gives the following energy-momentum tensor:

$$T_{\mu\nu} = \partial_\mu F\partial_\nu F - \left[\frac{1}{2}\left(\nabla F\right)^2 + V[F]\right]g_{\mu\nu}, \tag{7.335}$$

which, after applying the Symmetric ansatz of Sec. 3.1, more precisely Eq. (3.14), reduces to:

$$l^2 T^{\perp\perp} = \frac{1}{2}\left(\frac{\mathrm{d}F}{\mathrm{d}\bar{\mathrm{x}}}\right)^2 + \frac{l^2}{\Lambda}V[F], \tag{7.336}$$

$$l^2 T^{\Vert\Vert} = \frac{1}{2}\left(\frac{\mathrm{d}F}{\mathrm{d}\bar{\mathrm{x}}}\right)^2 - \frac{l^2}{\Lambda}V[F], \tag{7.337}$$

where we have employed the $\bar{\mathrm{x}}$ coordinate defined in Eq. (3.20). The equation of motion for the scalar field is:

$$\Box F = \frac{\mathrm{d}V}{\mathrm{d}F} \equiv V'[F] \quad \Longrightarrow \quad \frac{\mathrm{d}}{\mathrm{d}\bar{\mathrm{x}}}\left(\Lambda\frac{\mathrm{d}F}{\mathrm{d}\bar{\mathrm{x}}}\right) + l^2 V'[F] = 0. \tag{7.338}$$

Using the conditions for sources (7.333) together with the expressions (7.336) and (7.337) we arrive at the following two equations:

$$V[F] = \frac{3k\pi^2 D}{l^2}\frac{1}{\sqrt{|\Lambda|}}, \quad \left(\frac{\mathrm{d}F}{\mathrm{d}\bar{\mathrm{x}}}\right)^2 = \frac{6k\pi^2 D}{\Lambda}\frac{1}{\sqrt{|\Lambda|}}. \tag{7.339}$$

It is obvious that $V = 0$ implies $D = 0$, in other words, the complete vanishing of the EMT. For that reason we must have a non-vanishing scalar potential. Using Eq. (7.339), Eq. (7.338) is automatically satisfied. With the help of these equations, all relevant physical quantities are expressed in terms of F as follows:

$$\begin{aligned} &\mathrm{d}s^2 = \frac{1}{V}\left[\left(\frac{3k\pi^2 D}{l^2}\right)^2\frac{\mathrm{d}t^2}{|V|} - \frac{1}{2}\mathrm{d}F^2\right], \quad \mathrm{z} = \pm\int\frac{\mathrm{d}F}{\sqrt{2l^2 V}}, \\ &R = 8V\sqrt{|V|}\frac{\mathrm{d}^2}{\mathrm{d}F^2}\left(\frac{1}{\sqrt{|V|}}\right), \quad \kappa = \sqrt{2}\frac{6k\pi^2|D|}{l^2}\left|\frac{\mathrm{d}}{\mathrm{d}F}\left(\frac{1}{\sqrt{|V|}}\right)\right|_H. \end{aligned} \tag{7.340}$$

The last equation in Eq. (7.340) represents an expression for surface gravity if the horizon exists. From the first expression, we conclude that, if the horizon exists, it is given by $V[F_H] = 0$. Now, we look into some specific choices of the scalar potential. Firstly, the free real scalar field theory is analyzed, i.e. $V[F] = \frac{1}{2}m^2F^2$. Since $\Lambda > 0$, we redefine coordinate (3.21) by taking $\tau = l\mathrm{z}$ as the new time coordinate, and defining the spatial coordinate as $r = 2mlt$. The solution is a de Sitter space-time:

$$\Lambda = (2ml)^2 e^{4m\tau}, \;\; F = \pm\sqrt{\frac{3k\pi^2 D}{(ml)^3}}e^{-m\tau}. \tag{7.341}$$

The curvature is $R = 8m^2$, meaning that the de Sitter radius is $1/(2m)$. After placing Eq. (7.341) into Eq. (7.333) we arrive at the following final solution for the free scalar field theory:

$$\begin{aligned} &\mathrm{d}s^2 = -\mathrm{d}\tau^2 + e^{4m\tau}\mathrm{d}r^2, \quad \mathrm{x} = \cos\frac{\tau}{l}\left[\frac{3}{2}\left(\frac{D\cos\frac{\tau}{l}}{2mle^{2m\tau} - \frac{P}{2}\sin\frac{\tau}{l}} + \eta\right)\right]^{\frac{1}{3}}, \\ &\theta^2 = 1 + \frac{1}{3}\left(\frac{\mathrm{x}}{\cos\frac{\tau}{l}}\right)^2 + \eta\frac{\cos\frac{\tau}{l}}{\mathrm{x}}, \quad l\mathrm{K}^{\Vert} = \left[1 + \frac{1}{2ml}\tan\frac{\tau}{l} - \frac{P}{8(ml)^2}\frac{e^{-2m\tau}}{\cos\frac{\tau}{l}}\right]e^{-2m\tau}, \\ &\phi^{\Vert} = \mathrm{K}^{\perp} = 0, \quad \phi^{\perp} = \frac{\mathrm{x}}{2ml}\tan\frac{\tau}{l}e^{-2m\tau}, \quad F = \pm\sqrt{\frac{3k\pi^2 D}{(ml)^3}}e^{-m\tau}. \end{aligned} \tag{7.342}$$

Note that the parallel component of contorsion exhibits many poles in time, in particular whenever $\tau_n = (2n+1)\frac{\pi}{2}l$ the $\cos\frac{\tau}{l}$ vanishes leading to a divergence. All other functions exhibit a well defined behavior at all finite values of τ. This situation can be interpreted as a sequence of sudden singularities, in which the scale factor stays fixed while certain fields may blow up. Specifically, in this setup the parallel component of the contorsion becomes divergent. Solutions of this kind are well known and have been extensively analyzed in various gravitational theories [92, 93].

7.3.2 Pure electrodynamics

The action for pure electrodynamics is formulated in terms of the $U(1)$ gauge potential $\mathcal{A} = \mathcal{A}_\mu \mathrm{d}x^\mu$ and depends solely on the field strength tensor $\mathcal{F} = \mathrm{d}\mathcal{A}$. Because the exterior derivative is insensitive to torsion, the action keeps exactly the same form as in the Riemannian sector, namely:

$$S_{\mathrm{ED}} = -\frac{1}{4}\int \mathrm{d}x^2 \sqrt{-g}\, \mathcal{F}_{\mu\nu}\mathcal{F}^{\mu\nu}. \tag{7.343}$$

Varying this action with respect to the metric and the gauge field leads to the following EMT and Maxwell equation:

$$T_{\mu\nu} = \mathcal{F}_{\mu\rho}\mathcal{F}_\nu{}^\rho - \frac{1}{4}g_{\mu\nu}\mathcal{F}_{\alpha\beta}\mathcal{F}^{\alpha\beta} \quad \wedge \quad \nabla_\mu \mathcal{F}^{\mu\nu} = 0. \tag{7.344}$$

In two spacetime dimensions, any rank-2 antisymmetric tensor must be proportional to the Levi-Civita tensor. Consequently, Eq. (7.344) simplifies to

$$\mathcal{F}_{\mu\nu} = \mathcal{F}\varepsilon_{\mu\nu} \quad \Longrightarrow \quad T_{\mu\nu} = -\frac{1}{2}\mathcal{F}^2 g_{\mu\nu}, \quad \wedge \quad \partial_\mu \mathcal{F} = 0. \tag{7.345}$$

Hence, the scalar function $\mathcal{F}$ must be constant. Interpreting this constant as the electric charge, we denote it by $\mathcal{F} = Q$. Implementing the symmetric ansatz of Sec. 3.1 yields

$$T_{\mu\nu} = -\frac{Q^2}{2\Lambda}\left(\xi_\mu\xi_\nu - \varepsilon_{\mu\rho}\varepsilon_{\nu\sigma}\xi^\rho\xi^\sigma\right) \quad \Longrightarrow \quad \Lambda T^{\perp\perp} = -\Lambda T^{\shortparallel\shortparallel} = \frac{Q^2}{2}, \tag{7.346}$$

$$\mathcal{F}_{\mu\nu} = \frac{1}{l}\frac{\mathrm{d}}{\mathrm{d}\bar{\mathrm{x}}}\left(\Lambda\mathcal{A}^{\shortparallel}\right)\varepsilon_{\mu\nu}, \tag{7.347}$$

where we have used expression (3.26) in the second line. On the other hand, the constraints (7.333) enforce $T^{\shortparallel\shortparallel} = 0$, which immediately leads to $T^{\perp\perp} = 0$. We thus infer that no solution exists for $\theta \neq 0$, and the theory collapses to its purely Riemannian branch. This mirrors the situation for a scalar field: the massless case admits no solution, whereas introducing a non-vanishing scalar potential allows one to recover a solution. By analogy, a massive vector field might also support solutions; however, since a mass term explicitly breaks the $U(1)$ gauge symmetry, we do not pursue that possibility here.

Note that the field strength tensor in Eq. (7.347) is independent of the perpendicular component of the electromagnetic field. Consequently, this component merely specifies a gauge choice and therefore does not carry any physical degrees of freedom.

Charged black hole in the Riemannian sector

When the theory is restricted to its Riemannian sector, one obtains a charged black hole solution. Inserting the EMT components from Eq. (7.346) into the general static field Eqs. (6.24-6.25) of the Riemannian theory yields

$$\frac{\mathrm{d}}{\mathrm{dx}}\left(\mathrm{x}^2+1+\Lambda\mathcal{D}^2\right)^2=\frac{l^2Q^2}{3k\pi^2}, \tag{7.348}$$

$$\left(\mathrm{x}^2+1+\Lambda\mathcal{D}^2\right)\left(\mathcal{D}^2\frac{\mathrm{d}\Lambda}{\mathrm{dx}}+2\mathrm{x}\right)=\frac{l^2Q^2}{6k\pi^2}. \tag{7.349}$$

If we multiply the second equation by 2 and subtract it from the first, we obtain $\mathcal{D}=1$. The metric function Λ is then determined by integrating the first equation, giving

$$\Lambda=-\left(\mathrm{x}^2+1-\sqrt{(\mu+1)^2+\frac{Q^2l^2}{3k\pi^2}\mathrm{x}}\right). \tag{7.350}$$

This form is chosen so that, in the limit $Q\to 0$, the solution reduces to the vacuum configuration (6.17). To evaluate the tortoise coordinate (3.18), one should compute the integral $-\int\frac{\mathrm{dx}}{\Lambda}$. However, this integral cannot be represented in terms of elementary functions in a convenient form, and we therefore do not determine the tortoise coordinate here.

To check whether the singularity shifts away from the hypersurface $\mathrm{x}=0$, we calculate the scalar curvature:

$$l^2R=\frac{\mathrm{d}^2\Lambda}{\mathrm{dx}^2}=-2-\left(\frac{Q^2l^2}{6k\pi^2}\right)^2\left((\mu+1)^2+\frac{Q^2l^2}{3k\pi^2}\mathrm{x}\right)^{-\frac{3}{2}}<0. \tag{7.351}$$

Hence, the geometry is not a patch of AdS spacetime, but the curvature remains strictly negative, indicating that the singularity stays at $\mathrm{x_S}=0$ once the black hole is charged.

To locate the horizon, we solve $\Lambda=0$. This equation admits two real roots, one negative and one positive. Because we restrict to $\mathrm{x}>0$, only the positive root is physically relevant, so there is a single horizon. This is in contrast to the Reissner–Nordström charged black hole, which possesses two horizons—an inner and an outer one [106]. Finally, we evaluate the surface gravity:

$$\kappa=\frac{1}{2l}\left|\frac{\mathrm{d}\Lambda}{\mathrm{dx}}\right|_{\mathrm{H}}=\frac{1}{l}\left[\mathrm{x_H}-\frac{Q^2l^2}{12k\pi^2}\left((\mu+1)^2+\frac{Q^2l^2}{3k\pi^2}\mathrm{x_H}\right)^{-\frac{1}{2}}\right]. \tag{7.352}$$

As equation $\Lambda=0$ is a quartic equation for $\mathrm{x_H}$, a closed-form expression for the horizon location does exist, but we do not present it here because it is an extremely cumbersome combination of nested radicals.

7.3.3 Spinor field theory

In this subsection, we investigate how matter composed of Dirac spinor fields influences the gravitational equations of motion. We employ the symmetric Dirac action presented in App. A and defined in Eq. (A.24). For convenience we rewrite it here:

$$S_D=-\int\mathrm{d}^2x\sqrt{-g}\left[\frac{1}{2}\bar{\psi}\gamma^\mu\tilde{\nabla}_\mu\psi-\frac{1}{2}\tilde{\nabla}_\mu\bar{\psi}\gamma^\mu\psi-V\left[\sigma\right]\right], \tag{7.353}$$

where $V[\sigma]$ denotes the spinor potential, and we denote the bilinear invariant by $\sigma = \bar{\psi}\psi$. For a free massive spinor field one has $V[\bar{\psi}\psi] = m\bar{\psi}\psi$, while the Lorentz-covariant derivatives take the form:

$$\tilde{\nabla}_\mu \psi = \left(\partial_\mu + \omega_\mu \frac{\sigma_3}{2}\right)\psi, \quad \tilde{\nabla}_\mu \bar{\psi} = \partial_\mu \bar{\psi} - \bar{\psi}\frac{\sigma_3}{2}\omega_\mu. \tag{7.354}$$

Further details regarding the spinor conventions are provided in App. A. Since $\omega_\mu = \Delta_\mu + \mathrm{K}_\mu$, the action depends explicitly on the contorsion. Varying the action with respect to the contorsion yields:

$$T^\mu_{\mathrm{K}} = \frac{1}{2}\bar{\psi}\left\{\frac{\sigma_3}{2}, \gamma^\mu\right\}\psi \quad \Longrightarrow \quad T^\mu_{\mathrm{K}} = 0, \tag{7.355}$$

where the anticommutator manifestly vanishes because $\gamma^\mu \in \{\sigma_1, \sigma_2\}$. Consequently, the contorsion current is zero even in the presence of minimally coupled Dirac spinors, in agreement with the statement made at the beginning of this section. Variation with respect to the metric and the Dirac field then produces the following EMT of the Dirac field and the usual Dirac equation of motion:

$$\begin{aligned} T_{\mu\nu} =& \frac{1}{4}\left[\bar{\psi}\gamma_\mu \tilde{\nabla}_\nu \psi + \bar{\psi}\gamma_\nu \tilde{\nabla}_\mu \psi - \left(\tilde{\nabla}_\mu \bar{\psi}\right)\gamma_\nu \psi - \left(\tilde{\nabla}_\nu \bar{\psi}\right)\gamma_\mu \psi\right], \\ &\left(\gamma^\mu \tilde{\nabla}_\mu - V'[\sigma]\right)\psi = 0. \end{aligned} \tag{7.356}$$

Note that the EMT displays the same qualitative behavior as the contorsion current (7.355). In particular, all spin-connection contributions collect into anticommutator terms that identically vanish. Consequently, it depends only on ordinary partial derivatives. We now implement the symmetric spinor ansatz from Eq. (3.17). As a first step, we recast the energy-momentum tensor:

$$T_{\mu\nu} = \frac{1}{l\sqrt{-\Lambda}}\left(\varphi^2 \frac{\mathrm{d}\alpha}{\mathrm{d}\bar{\mathrm{x}}} - \chi^2 \frac{\mathrm{d}\beta}{\mathrm{d}\bar{\mathrm{x}}}\right)\varepsilon_{\mu\rho}\varepsilon_{\nu\sigma}\xi^\rho\xi^\sigma + \frac{1}{2l\sqrt{-\Lambda}}\left(\varphi^2 \frac{\mathrm{d}\alpha}{\mathrm{d}\bar{\mathrm{x}}} + \chi^2 \frac{\mathrm{d}\beta}{\mathrm{d}\bar{\mathrm{x}}}\right)(\varepsilon_{\mu\rho}\xi_\nu + \varepsilon_{\nu\rho}\xi_\mu)\,\xi^\rho. \tag{7.357}$$

Next, the Dirac equation in Eq. (7.356) simplifies, upon separating its real and imaginary parts, to the following four equations:

$$\frac{\mathrm{d}}{\mathrm{d}\bar{x}} \ln\left(\varphi(-\Lambda)^{\frac{1}{4}}\right) - \frac{l}{2}\mathrm{K}^{\shortparallel} = \frac{lV'[\sigma]}{\sqrt{-\Lambda}}\frac{\chi}{\varphi}\sin(\beta - \alpha), \tag{7.358}$$

$$\frac{\mathrm{d}}{\mathrm{d}\bar{x}} \ln\left(\chi(-\Lambda)^{\frac{1}{4}}\right) - \frac{l}{2}\mathrm{K}^{\shortparallel} = \frac{lV'[\sigma]}{\sqrt{-\Lambda}}\frac{\varphi}{\chi}\sin(\beta - \alpha), \tag{7.359}$$

$$\frac{\mathrm{d}\alpha}{\mathrm{d}\bar{\mathrm{x}}} = -\frac{lV'[\sigma]}{\sqrt{-\Lambda}}\frac{\chi}{\varphi}\cos(\beta - \alpha), \tag{7.360}$$

$$\frac{\mathrm{d}\beta}{\mathrm{d}\bar{\mathrm{x}}} = \frac{lV'[\sigma]}{\sqrt{-\Lambda}}\frac{\varphi}{\chi}\cos(\beta - \alpha). \tag{7.361}$$

It is immediately evident that, in the massless case $V = 0$, the derivatives of both phases α and β vanish. As a consequence, the entire EMT in Eq. (7.357) is zero. Hence, no solution with $\theta \neq 0$ exists, and the theory collapses to its purely Riemannian sector. We therefore reach the same conclusion as in the real scalar field case: a non-vanishing spinor potential is required in order to obtain a solution with $\theta \neq 0$. Expressing this system in terms of the coordinate z from Eq. (3.21), we obtain:

$$\frac{\mathrm{d}\alpha}{\mathrm{dz}} = lV'[\sigma]\frac{\chi}{\varphi}\cos(\beta-\alpha), \tag{7.362}$$

$$\frac{\mathrm{d}\beta}{\mathrm{dz}} = -lV'[\sigma]\frac{\varphi}{\chi}\cos(\beta-\alpha), \tag{7.363}$$

$$\frac{\mathrm{d}}{\mathrm{dz}}\left(\frac{\varphi}{\chi}\right) = lV'[\sigma]\left[\left(\frac{\varphi}{\chi}\right)^2 - 1\right]\sin(\beta-\alpha), \tag{7.364}$$

$$\frac{\mathrm{d}}{\mathrm{dz}}\ln\left(\varphi\chi\sqrt{-\Lambda}\right) + l\sqrt{-\Lambda}\mathrm{K}^{\parallel} = -lV'[\sigma]\left(\frac{\varphi}{\chi}+\frac{\chi}{\varphi}\right)\sin(\beta-\alpha), \tag{7.365}$$

where the last two relations follow from subtracting and adding Eqs. (7.358) and (7.359), respectively. The first three equations constitute a closed subsystem for α, β, and the ratio $\frac{\varphi}{\chi}$, with $V'[\sigma]$ left arbitrary. Nonetheless, this subsystem can be integrated to express the phases in terms of $\frac{\varphi}{\chi}$, yielding:

$$\begin{aligned} \cos(\beta-\alpha) &= \frac{\omega}{2}\left(\frac{\varphi}{\chi}-\frac{\chi}{\varphi}\right), \\ \alpha+\beta &= -\arcsin\left[\frac{1}{2}\frac{\omega}{\sqrt{1+\omega^2}}\left(\frac{\varphi}{\chi}+\frac{\chi}{\varphi}\right)\right] + \gamma_0, \end{aligned} \tag{7.366}$$

where ω and γ_0 are integration constants. Substituting this solution into Eq. (7.365) and eliminating the phase dependence via Eq. (7.364), we arrive at:

$$\frac{\mathrm{d}}{\mathrm{dz}}\ln\left[\varphi\chi\sqrt{-\Lambda}\left(\frac{\varphi}{\chi}-\frac{\chi}{\varphi}\right)\right] + l\sqrt{-\Lambda}\mathrm{K}^{\parallel} = 0 \quad\Longrightarrow\quad \frac{\mathrm{d}}{\mathrm{dz}}\ln\left(\sigma\sqrt{-\Lambda}\right) + l\sqrt{-\Lambda}\mathrm{K}^{\parallel} = 0, \tag{7.367}$$

where we used $\sigma = \bar{\psi}\psi = -2\varphi\chi\cos(\beta-\alpha)$ together with the solution (7.366).

We now proceed to impose the conditions (7.333). The constraint $T^{\parallel\parallel} = 0$ is trivially fulfilled, because the EMT (7.357) does not have a parallel component. Imposing $T^{\parallel\perp} = 0$ is equivalent to simultaneously enforcing Eqs. (7.360) and (7.361). The remaining condition, associated with the perpendicular component of the EMT, simplifies to

$$\frac{3k\pi^2 D}{l\Lambda} = -\frac{lV'[\sigma]}{\sqrt{-\Lambda}}\varphi\chi\cos(\beta-\alpha) \quad\Longrightarrow\quad \sigma V'[\sigma] = -\frac{6k\pi^2 D}{l^2\sqrt{-\Lambda}}, \tag{7.368}$$

where we have once again employed the definition of σ. Eq. (7.368) is interpreted as an equation determining the function σ in terms of the metric function Λ once the spinor potential is specified. Thus, expressing σ as a function of Λ via Eq. (7.368) and substituting this relation into Eq. (7.367) yields a first-order differential equation for Λ. Solving this equation fixes both Λ and σ. Subsequently, the remaining Eq. (7.364) becomes explicitly integrable. Its solution can be written as

$$\varphi = \chi\sqrt{\frac{e^{2s}+\frac{1}{4}(\omega^2+1)e^{-2s}+1}{e^{2s}+\frac{1}{4}(\omega^2+1)e^{-2s}-1}}, \qquad s = l\int V'[\sigma]\mathrm{dz}. \tag{7.369}$$

The overall problem therefore reduces to solving Eq. (7.367), once the algebraic equation for σ in Eq. (7.368) has been resolved.

All of these equations hold for both $\Lambda > 0$ and $\Lambda < 0$ by analytic continuation. For a black hole solution to exist, there must be an event horizon. Since it is defined by $\Lambda = 0$, such a horizon can arise only if the function $\sigma V'[\sigma]$ has a pole in $\mathbb{R}\cup\{\pm\infty\}$. In that case, one can analytically match the two coordinate patches corresponding to opposite signs of the metric function Λ, thereby constructing a black hole geometry: the interior region is described on a chart with $\Lambda > 0$, and the exterior region on a chart with $\Lambda < 0$, as usual. We now turn to a discussion of particular choices for the spinor potential $V[\sigma]$.

- $\underline{V[\sigma] = 0}$: This choice corresponds to a theory of massless spinors. As discussed above, this condition leads to a vanishing EMT, so within this framework there is no nontrivial solution.

- $\underline{V[\sigma] = m\sigma}$: For massless spinors, we have $V'[\sigma] = m$, a constant. Therefore, Eq. (7.368) implies $\sigma\sqrt{-\Lambda} = \text{const.}$, and Eq. (7.367) reduces to $\mathrm{K}^{\parallel} = 0$. Consequently, even the massive Dirac field admits no solution, since $\mathrm{K}^{\parallel} = 0$ again causes the EMT to vanish on the gravitational side of the field equations.

- $\underline{V[\sigma] = -b\ln|\sigma|}$: For this potential we obtain $V'[\sigma] = -b/\sigma$. Substituting into Eq. (7.368) yields a flat spacetime:

$$\Lambda_0 = -\left(\frac{6k\pi^2 D}{bl^2}\right)^2. \tag{7.370}$$

When $\Lambda < 0$, three distinct cases arise. Without loss of generality, we present only the case in which $\mathrm{K}^{\parallel}$ is given by Eq. (7.73). Integrating Eq. (7.367) then gives:

$$\sigma = \frac{\sigma_0}{\sinh \mathrm{z}} \exp\left(-\frac{P}{2\sqrt{-\Lambda_0}} \arctan(\sinh \mathrm{z})\right), \tag{7.371}$$

while s, defined in Eq. (7.369), can be written in terms of the hypergeometric function as follows:

$$s = \frac{4ilb}{\sigma_0(2-ia)} \left(\frac{1+i\sinh(\mathrm{z})}{2}\right)^{1-\frac{ia}{2}} {}_2F_1\left(1-\frac{ia}{2}, -\frac{ia}{2}; 2-\frac{ia}{2}; \frac{1+i\sinh(\mathrm{z})}{2}\right) + s_0, \tag{7.372}$$

where $a = \frac{P}{2\sqrt{-\Lambda_0}}$.

- $\underline{V[\sigma] = m\sigma - \frac{g}{2}\sigma^2}$: Taking the derivative yields $V'[\sigma] = m - g\sigma$. For convenience, we now restrict to the massless case. Solving Eq. (7.368) for σ then gives

$$\sigma = Q(-\Lambda)^{-\frac{1}{4}}, \qquad D = \frac{gl^2Q^2}{6k\pi^2}. \tag{7.373}$$

The metric follows by directly integrating Eq. (7.367). We evaluate it in each of the four distinct cases introduced in the previous section:

$$\sqrt{|\Lambda|} = \begin{cases} \frac{P}{2}\sin\bar{\mathrm{z}} + \left(\frac{P}{2}\ln|\sec\bar{\mathrm{z}} + \tan\bar{\mathrm{z}}| + \mu\right)\cos^2\bar{\mathrm{z}}, & \Lambda > 0, \\ \frac{P}{2}\sinh \mathrm{z} + \left(\frac{P}{2}\arctan(\sinh \mathrm{z}) + \mu\right)\cosh^2 \mathrm{z}, & \Lambda < 0,\ \mathrm{x}^2 + \Lambda\phi^{\perp 2} > 0, \\ -\frac{P}{2}\cosh \mathrm{z} + \left(\mu - \frac{P}{2}\ln\left|\tanh\frac{\mathrm{z}}{2}\right|\right)\sinh^2 \mathrm{z}, & \Lambda < 0,\ \mathrm{x}^2 + \Lambda\phi^{\perp 2} < 0, \\ \pm\frac{2}{3}Pe^{\mp \mathrm{z}} + \mu e^{\pm 2\mathrm{z}}, & \Lambda < 0,\ \mathrm{x}^2 + \Lambda\phi^{\perp 2} = 0, \end{cases} \tag{7.374}$$

where μ denotes an integration constant. We now determine the scalar curvature in each of these regimes to examine whether the resulting spacetimes develop curvature singularities:

$$R = -\frac{4}{l^2}\begin{cases} 1-\tan^2\bar{\mathrm{z}}+\dfrac{P\sin\bar{\mathrm{z}}}{2\sqrt{\Lambda}\cos^2\bar{\mathrm{z}}}, & \Lambda>0, \\ 1+\tanh^2\mathrm{z}+\dfrac{P\sinh\mathrm{z}}{2\sqrt{-\Lambda}\cosh^2\mathrm{z}}, & \Lambda<0,\ \mathrm{x}^2+\Lambda\phi^{\perp 2}>0, \\ 1+\coth^2\mathrm{z}+\dfrac{P\cosh\mathrm{z}}{2\sqrt{-\Lambda}\sinh^2\mathrm{z}}, & \Lambda<0,\ \mathrm{x}^2+\Lambda\phi^{\perp 2}<0, \\ 2\mp\dfrac{P}{\sqrt{-\Lambda}}e^{\mp\mathrm{z}}, & \Lambda<0,\ \mathrm{x}^2+\Lambda\phi^{\perp 2}=0. \end{cases} \tag{7.375}$$

Finally, we obtain the surface gravity for these geometries whenever a horizon is present. It takes the form

$$\kappa = \frac{1}{l}\begin{cases} \dfrac{P}{\cosh\mathrm{z_H}}, & \Lambda<0,\ \mathrm{x}^2+\Lambda\phi^{\perp 2}>0, \\ \dfrac{P}{\sinh\mathrm{z_H}}, & \Lambda<0,\ \mathrm{x}^2+\Lambda\phi^{\perp 2}<0, \\ -2Pe^{\mp\mathrm{z_H}}, & \Lambda<0,\ \mathrm{x}^2+\Lambda\phi^{\perp 2}=0. \end{cases} \tag{7.376}$$

We observe that the parameter P is directly tied to the surface gravity: once P is set to zero, κ vanishes as well.

We first consider the case $\Lambda>0$. Setting $P=0$, the solution simplifies to $\sqrt{\Lambda}=\mu\cos^2\bar{\mathrm{z}}$, and the metric takes the form

$$\mathrm{d}s^2 = -\mathrm{d}\tau^2+\mu l^2\cos^4\frac{\tau}{l}\mathrm{dr}^2, \tag{7.377}$$

where we have introduced the rescaled time coordinate $\tau=l\bar{\mathrm{z}}$. The corresponding curvature becomes divergent at $\tau=(2n+1)\frac{\pi}{2}l$, with $n\in\mathbb{Z}$. This describes a cosmological spacetime oscillating through a succession of big bang and big crunch events.

For $P\neq 0$, this basic pattern persists: curvature singularities still occur at $\tau=\pm(2n+1)\frac{\pi}{2}l$. However, in this case the scale factor remains finite at those points, so these singularities correspond to a sequence of sudden singularities [92, 93]. In addition, there now appears another series of curvature singularities at the zeros of the scale factor, where $\Lambda=0$, located at $\tau=\tau_{\mathrm{S}}+2n\pi l$, with $\tau_{\mathrm{S}}\in\left(-\frac{\pi}{2},\frac{\pi}{2}\right)l$. Consequently, the $P\neq 0$ solution can be understood as an oscillatory universe evolving between the big bang and the big crunch events with two additional sudden curvature singularities occurring between each such pair of events.

We now turn to the cases with $\Lambda<0$. The first question to address, when considering a spacetime that possesses a time-like Killing vector, is whether a Killing horizon exists [106], characterized by $\Lambda=0$. Let us determine under which conditions this equation admits a solution. We begin with the case $\mathrm{x}^2+\Lambda\phi^{\perp 2}>0$ and introduce the variable $u=\sinh\mathrm{z}$. With this substitution, the equation becomes:

$$f(u)=\frac{u}{1+u^2}+\arctan(u)=-\frac{2\mu}{P} \quad\Longrightarrow\quad f'(u)=\frac{2}{(u^2+1)^2}>0. \tag{7.378}$$

Hence, $f(u)$ is a monotonically increasing and its range is confined to the interval $(-\frac{\pi}{2},\frac{\pi}{2})$. Consequently, there is always a unique solution precisely when:

$$\left|\frac{\mu}{P}\right|<\frac{\pi}{4}. \tag{7.379}$$

If no horizon is present, i.e. when $\left|\frac{\mu}{P}\right| > \frac{\pi}{4}$, then there is likewise no curvature singularity. In this regime, the solution describes the ground state of a stable fermionic soliton star spacetime that is globally regular. The gravitational attraction, mediated by the dilaton/metric, is exactly counterbalanced by the repulsive spin–torsion coupling. As the system tends to contract (which would drive Λ to zero), the spin–torsion interaction energy increases more rapidly than the gravitational potential energy, thereby preventing the emergence of an event horizon. The value $\left|\frac{\mu}{P}\right| = \frac{\pi}{4}$ marks a critical mass and signals a phase transition. For $\left|\frac{\mu}{P}\right| < \frac{\pi}{4}$, the gravitational attraction dominates over the spin–torsion repulsion, and a horizon is formed. This horizon simultaneously generates a curvature singularity at the same spacetime location, rendering it a singular horizon.

If P does not vanish, then the surface gravity (7.376) is finite and non-zero, implying that the horizon is non-extremal. Consequently, this stationary, naked, finite-temperature singular horizon is viewed as an idealized but unstable classical background. In practice, the horizon acts like a usual bifurcate Killing horizon, except that the curvature singularity lies precisely on it. In analogy with the Reissner–Nordström solution, this horizon plays the role of the inner Cauchy horizon, which is subject to blueshift instability and gives rise to classical mass inflation.

Next, we analyze the solution corresponding to $\mathrm{x}^2 + \Lambda\phi^{\perp 2} < 0$. In the limit $P \to 0$, this reduces to a configuration that still possesses a horizon at $\mathrm{z_H} = 0$. Yet, for $P = 0$ the surface gravity is zero, so the solution represents a completely stable extremal ground state. We then study how the horizon position changes when $P \neq 0$. Defining $u = \tanh \frac{\mathrm{z}}{2}$, the condition $\Lambda = 0$ becomes

$$f(u) = \frac{1}{4}\left(u^2 - \frac{1}{u^2}\right) + \ln|u| = \frac{2\mu}{P}. \tag{7.380}$$

Since $|u| < 1$, it follows that $f(u) > 0$, implying the existence of a two symmetric horizons at $\pm\mathrm{z_H}$, whenever $\mu P > 0$. As before, these horizons are singular, just as in the previous case, and the same line of reasoning applies. However, inspecting the curvature (7.375) now reveals an additional singularity between the two singular horizons at $\mathrm{z_S} = 0$, which cannot be removed by any means. The remaining case, $\mathrm{x}^2 + \Lambda\phi^{\perp 2} = 0$, displays qualitatively the same behavior as the one just discussed. The difference is that the limit $P \to 0$ now yields AdS spacetime, because the scalar curvature is a negative constant.

We argue that these configurations are still viable solutions of the coupled Dirac–Chern–Simons theory. The origin of the singular horizon in all these examples is directly tied to a blow up in the fermionic density function σ at the horizon, since σ is inversely proportional to the metric function Λ. Consequently, the phase transition—most clearly visible in the first case—can be understood as a condensation process of the fermion mass at the singular horizon. In this sense, the mechanism behind the formation of the singular horizon is understood, and it should no longer be regarded as a naked singularity. Instead, it signifies a spacetime locus at which the fermionic star soliton solution condenses. Because an infinite amount of fermion mass accumulates at this horizon, the geometry must react with a curvature singularity. One may anticipate that incorporating quantum corrections would smooth out this singularity, while preserving a maximum of the fermionic density function in the lower phase at the same spacetime position. Another open question is whether taking into account the fermion mass m in the spinor potential can in any way remove or regularizes this singular horizon.

To further clarify the nature of this fermionic star solution, we may fix the boundary of the star and smoothly match it to the general vacuum solution of Sec. 7.1.1. In doing so, the fermionic star soliton is interpreted as a compact object embedded in a larger spacetime. The open question is where exactly to place the star's boundary: right at the singular horizon where the fermions condense, or outside of it?

In contrast, the hard singularity that appears in the last two families of solutions is a direct consequence of the coupling to torsion, as the torsion itself diverges at $z_S = 0$, independently of the choice of matter fields. We expect that, once the Polyakov–Liouville-type quantum corrections (3.72) are taken into account, the singular behavior of the horizon will be resolved, yet a maximum of the fermionic density function will remain there. In this interpretation, the singular horizon acts as a massive barrier that prevents anything from reaching the genuine singularity at $z_S = 0$. Alternatively, one can regard this singularity as a strong-coupling region between the torsion and the metric, where quantum gravity effects become essential, in close analogy with the CGHS model discussed in Chap. 4. In that case, this region should be removed from the classical spacetime description by imposing reflective boundary conditions on the singular horizon hypersurface, thereby effectively turning it into a reflective spacetime boundary.

7.3.4 Scalar electrodynamics

Here we study how a $U(1)$-localized complex scalar field theory modifies the gravitational equations of motion. Accordingly, the matter action is

$$S_{\text{mat}} = -\int \mathrm{d}^2x\sqrt{-g}\left[(D_\mu f)^* D^\mu f + V\left[|f|\right] + \frac{1}{4}\mathcal{F}_{\mu\nu}\mathcal{F}^{\mu\nu}\right], \tag{7.381}$$

where $V[|f|]$ denotes the potential of the scalar field, and the $U(1)$-covariant derivative is defined in the usual way as $D_\mu f = \nabla_\mu f + iq\mathcal{A}_\mu f$, with q the electric charge carried by the complex scalar field particles. We begin by examining the electromagnetic sector. Varying the action with respect to the gauge field leads to

$$\nabla_\nu \mathcal{F}^{\mu\nu} = iq\Big(f^* D^\mu f - f\left(D^\mu f\right)^*\Big) \equiv J^\mu, \tag{7.382}$$

from which we recover the standard $U(1)$ current associated with the scalar field. Implementing the symmetric ansatz of Sec. 3.1, this equation becomes

$$\left[\frac{\mathrm{d}^2}{\mathrm{d}\bar{\mathrm{x}}^2}\left(\Lambda\mathcal{A}^{\shortparallel}\right) + 2(ql)^2F^2\mathcal{A}^{\shortparallel}\right]\xi_\mu + 2qlF^2\left[\frac{\mathrm{d}\gamma}{\mathrm{d}\bar{\mathrm{x}}} + ql\mathcal{A}^{\perp}\right]\varepsilon_{\mu\nu}\xi^\nu = 0, \tag{7.383}$$

where we use the notation introduced in Tab. 7.2 for the complex scalar field. As in Sec. 7.3.2, the component of Eq. (7.383) normal to ξ_μ shows that $\mathcal{A}^\perp$ serves as a gauge choice, since the phase γ of the complex scalar field remains arbitrary until the gauge is fixed. Consequently, only the parallel component of this equation provides a nontrivial equation of motion. We now vary the action with respect to the scalar field and obtain:

$$D_\mu D^\mu F = V'\left[F\right] \quad\Longrightarrow\quad \frac{\mathrm{d}}{\mathrm{d}\bar{\mathrm{x}}}\left(\Lambda\frac{\mathrm{d}F}{\mathrm{d}\bar{\mathrm{x}}}\right) + (ql)^2\Lambda\mathcal{A}^{\shortparallel 2}F + \frac{l^2}{2}V'\left[F\right] = 0. \tag{7.384}$$

We now turn to the gravitational sector of the theory. The EMT of the matter fields is

$$T_{\mu\nu} = (D_\mu f)^* D_\nu f + (D_\nu f)^* D_\mu f - g_{\mu\nu}\Big((D_\alpha f)^* D^\alpha f + V[F] + \frac{1}{2}\mathcal{F}^2\Big), \tag{7.385}$$

where we have employed the reduced form of the electromagnetic EMT obtained in Eq. (7.345). Implementing the symmetric ansatz yields

$$\begin{aligned} l^2\Lambda T_{\mu\nu} = &\left[\Lambda\left(\left(\frac{\mathrm{d}F}{\mathrm{d}\bar{\mathrm{x}}}\right)^2 + (ql)^2F^2\mathcal{A}^{\shortparallel 2}\right) - l^2V[F] - \frac{1}{2}\left(\frac{\mathrm{d}\left(\Lambda\mathcal{A}^{\shortparallel}\right)}{\mathrm{d}\bar{\mathrm{x}}}\right)^2\right]\xi_\mu\xi_\nu \\ &+\left[\Lambda\left(\left(\frac{\mathrm{d}F}{\mathrm{d}\bar{\mathrm{x}}}\right)^2 + (ql)^2F^2\mathcal{A}^{\shortparallel 2}\right) + l^2V[F] + \frac{1}{2}\left(\frac{\mathrm{d}\left(\Lambda\mathcal{A}^{\shortparallel}\right)}{\mathrm{d}\bar{\mathrm{x}}}\right)^2\right]\varepsilon_{\mu\rho}\varepsilon_{\nu\sigma}\xi^\rho\xi^\sigma \end{aligned} \tag{7.386}$$

Imposing the constraints (7.333) on the energy–momentum tensor (7.386) leads to the following pair of equations:

$$\Lambda\left(\left(\frac{\mathrm{d}F}{\mathrm{d}\bar{\mathrm{x}}}\right)^2 + (ql)^2F^2\mathcal{A}^{\shortparallel 2}\right) = l^2V[F] + \frac{1}{2}\left(\frac{\mathrm{d}\left(\Lambda\mathcal{A}^{\shortparallel}\right)}{\mathrm{d}\bar{\mathrm{x}}}\right)^2, \tag{7.387}$$

$$\frac{6k\pi^2D}{\sqrt{|\Lambda|}} = \Lambda\left(\left(\frac{\mathrm{d}F}{\mathrm{d}\bar{\mathrm{x}}}\right)^2 + (ql)^2F^2\mathcal{A}^{\shortparallel 2}\right) + l^2V[F] + \frac{1}{2}\left(\frac{\mathrm{d}\left(\Lambda\mathcal{A}^{\shortparallel}\right)}{\mathrm{d}\bar{\mathrm{x}}}\right)^2. \tag{7.388}$$

Combining Eqs. (7.387) and (7.388), one finds that the remaining two Eqs. (7.383) and (7.384) become identical. Consequently, the system of equations simplifies to:

$$\left(\frac{\mathrm{d}F}{\mathrm{d}\bar{\mathrm{x}}}\right)^2 = \frac{3k\pi^2D}{\Lambda}\frac{1}{\sqrt{|\Lambda|}} - (ql)^2F^2\mathcal{A}^{\shortparallel 2}, \tag{7.389}$$

$$\left(\frac{\mathrm{d}\left(\Lambda\mathcal{A}^{\shortparallel}\right)}{\mathrm{d}\bar{\mathrm{x}}}\right)^2 = \frac{6k\pi^2D}{\sqrt{|\Lambda|}} - 2l^2V[F], \tag{7.390}$$

$$\frac{3k\pi^2D}{|\Lambda|^{3/2}}\frac{\mathrm{d}|\Lambda|}{\mathrm{d}\bar{\mathrm{x}}} = 4(ql)^2F^2\mathcal{A}^{\shortparallel}\frac{\mathrm{d}\left(\Lambda\mathcal{A}^{\shortparallel}\right)}{\mathrm{d}\bar{\mathrm{x}}} - l^2V'[F]\frac{\mathrm{d}F}{\mathrm{d}\bar{\mathrm{x}}}. \tag{7.391}$$

This system of equations can in principle be solved numerically. Nonetheless, we confine our subsequent analysis to the simplest, massless case with $V[F] = 0$. From Eq. (7.387) it follows that $\Lambda > 0$, and Eq. (7.388) further requires $D > 0$. Consequently, we are looking for cosmological solutions. Expressing the system in terms of the z coordinate (3.21) and introducing a new constant Q via $6k\pi^2D = Q^2$, we obtain:

$$\frac{\mathrm{d}\left(\Lambda\mathcal{A}^{\shortparallel}\right)}{\mathrm{d}\tau} = Q\Lambda^{1/4}, \quad \frac{\mathrm{d}\Lambda}{\mathrm{d}\tau} = \frac{8(ql)^2}{Q}F^2\Lambda\mathcal{A}^{\shortparallel}\Lambda^{3/4}, \quad \Lambda\left(\frac{\mathrm{d}F}{\mathrm{d}\tau}\right)^2 + (ql)^2F^2\left(\Lambda\mathcal{A}^{\shortparallel}\right)^2 = \frac{Q^2}{2}\sqrt{\Lambda}. \tag{7.392}$$

This system is invariant under scale transformations, which implies that all relevant fields can be expressed as power laws. A straightforward calculation leads to the solution:

$$\Lambda = \left(\frac{Qql}{3\sqrt{2}}\right)^4\mathrm{z}^8, \quad \Lambda\mathcal{A}^{\shortparallel} = \frac{Q^2ql}{9\sqrt{2}}\mathrm{z}^3, \quad F = \frac{\sqrt{3}}{ql}\mathrm{z}^{-1}. \tag{7.393}$$

Since the gauge potential itself is not directly physical, we instead determine the electric field. The resulting physical configuration of fields is

$$\mathrm{d}s^2 = -\mathrm{d}\tau^2 + \left(\frac{Qq}{3l\sqrt{2}}\right)^4\tau^8l^2\mathrm{d}r^2, \quad \mathcal{F} = \frac{3\sqrt{2}}{q}\tau^{-2}, \quad F = \frac{\sqrt{3}}{q}\tau^{-1}, \tag{7.394}$$

where we have introduced the time coordinate $\tau = lz$. The remaining fields are specified in Eqs. (7.66-7.69) and are the same as in the case of the real scalar field (7.342). The cosmological singularity occurs at $\tau = 0$, where the spatial section collapses to a point, and both the electric field and the scalar field become divergent. Analogously to the case of a real scalar field, the parallel component of the contorsion displays a sequence of sudden singularities [92, 93].

Note that this does not represent the general solution of system (7.392). The system can be recast as a single first-order, second-kind Abel differential equation, which does not admit an exact closed-form solution. The solution provided here corresponds to an exact singular fixed point within the parameter space of solutions. Any other choice of initial conditions leads to phase-space trajectories that spiral around or away from this exact analytical solution, their behavior being fully determined by the aforementioned Abel differential equation.

7.3.5 Ideal fluid dynamics

In this subsection, we examine how the geometry responds to the matter content described by the energy–momentum tensor of an ideal fluid, namely:

$$T_{\mu\nu} = (p+\rho)u_\mu u_\nu + p g_{\mu\nu}. \tag{7.395}$$

Expressing this using the symmetric ansatz introduced in Sec. 3.1, we obtain:

$$T_{\mu\nu} = \left[(p+\rho)u^{\shortparallel 2} + \frac{p}{\Lambda}\right]\xi_\mu\xi_\nu + (p+\rho)u^{\shortparallel}u^{\perp}\left(\varepsilon_{\mu\rho}\xi_\nu + \varepsilon_{\nu\rho}\xi_\mu\right)\xi^\rho + \left[(p+\rho)u^{\perp 2} - \frac{p}{\Lambda}\right]\varepsilon_{\mu\rho}\varepsilon_{\nu\sigma}\xi^\rho\xi^\sigma. \tag{7.396}$$

To the Eqs. (7.333), we must supplement a condition on the four–velocity, namely:

$$u_\mu u^\mu = -1 \quad \Longrightarrow \quad \Lambda\left(u^{\shortparallel 2} - u^{\perp 2}\right) = -1. \tag{7.397}$$

We first impose the condition $T^{\shortparallel\perp} = 0$. This leads to the conclusion that either $u^{\shortparallel} = 0$ or $u^{\perp} = 0$, since the choice $p + \rho = 0$ would cause the entire EMT to vanish identically.

- $\underline{u^{\shortparallel} = 0}$: In this case, the condition $T^{\shortparallel\perp} = 0$ is automatically fulfilled. From Eq. (7.397) we obtain the normal component of the four-velocity:

  $$u^{\perp} = \pm\frac{1}{\sqrt{\Lambda}}, \tag{7.398}$$

  which requires $\Lambda > 0$. Thus, we are dealing with the cosmological solution. The vanishing of the parallel component of the EMT imposes $p = 0$, while its normal component yields the density as a function of the metric function Λ:

  $$p = 0 \quad \wedge \quad \rho = \frac{6k\pi^2 D}{l^2\sqrt{\Lambda}}. \tag{7.399}$$

- $\underline{u^{\perp} = 0}$: In an analogous way, the condition $T^{\shortparallel\perp} = 0$ is again satisfied, and Eq. (7.397) now provides the parallel component of the four-velocity:

  $$u^{\shortparallel} = \pm\frac{1}{\sqrt{-\Lambda}}, \tag{7.400}$$

  which enforces $\Lambda < 0$. Consequently, we are considering the static star solution, once the stellar boundary is specified and the metric is matched across this boundary to one of the general vacuum solutions of Sec. 7.1.1. Unlike the previous case, the constraint $T^{\shortparallel\shortparallel} = 0$ implies $\rho = 0$, and from the normal component of the EMT we obtain the pressure as a function of Λ:

$$p = -\frac{6k\pi^2 D}{l^2\sqrt{-\Lambda}}, \quad \wedge \quad \rho = 0. \tag{7.401}$$

Note that in both branches the metric function Λ remains arbitrary. This reflects the gauge freedom inherited from the underlying five-dimensional Chern–Simons theory. Consequently, any choice of metric solves the full set of equations of motion. One might say that an additional thermodynamic relation $p = p(\rho)$ is missing. However, the equations of motion already enforce that either the pressure or the density must vanish, so there is no room to introduce an extra independent equation into the system.

Conversely, one would typically prefer a setup where the spacetime metric is dynamically determined. This is only possible once an additional field is incorporated into the matter sector. For instance, including an electromagnetic field merely shifts the EMT by $T^{ED}_{\mu\nu} = -\frac{Q^2}{2} g_{\mu\nu}$ (see Sec. 7.3.2). In this case, the equations reduce to:

$$\begin{cases} p = \dfrac{Q^2}{2} \quad \wedge \quad \rho = \dfrac{6k\pi^2 D}{l^2\sqrt{\Lambda}} - \dfrac{Q^2}{2}, \qquad u^{\shortparallel} = 0, \\ p = -\dfrac{6k\pi^2 D}{l^2\sqrt{-\Lambda}} + \dfrac{Q^2}{2}, \quad \wedge \quad \rho = -\dfrac{Q^2}{2}, \quad u^{\perp} = 0. \end{cases} \tag{7.402}$$

At this stage it becomes consistent to impose an additional thermodynamic relation $p = p(\rho)$. Yet p and ρ are already fully determined in terms of the metric, so enforcing this relation restricts the solution to flat Minkowski spacetime, where both the pressure and the density of the ideal fluid turn out to be constant. If we then continuously match the $u^{\perp} = 0$ solution to a generic vacuum configuration from Sec. 7.1.1, the result is a perfectly homogeneous torsion star, with both the two-dimensional torsion and the θ-component of the five-dimensional torsion remaining non-zero in a BTZ background endowed with θ torsion.

Including a massless real scalar field leads to the same outcome: the equations of motion still only admit flat Minkowski spacetime with torsion. However, once a non-trivial scalar potential is introduced, the equations of motion become genuinely dynamical, and one obtains a non-constant pressure, density, and metric.

Finally, it would be worthwhile to explore the role of the Polyakov–Liouville quantum corrections (3.72) in this ideal-fluid thermodynamic framework. We anticipate that the quantum-corrected solution will select a definite metric function Λ once the condition $p = p(\rho)$ is imposed, because the Polyakov–Liouville EMT (3.79) depends explicitly on derivatives of Λ.

7.4 Adding quantum fluctuations

In this section, we incorporate Polyakov–Liouville quantum corrections. We focus exclusively on the eternal black hole configuration with scalar matter. Because the Polyakov–Liouville action (3.72) does not involve any contorsion terms, this setup still corresponds to the situation in which the only non-vanishing source is the EMT, given in Eq. (3.79). The EMT must satisfy the same constraints as in all the theories considered in the previous section, namely those in Eq. (7.333). Hence, the following two equations must hold:

$$\Lambda\frac{\mathrm{d}^2\Lambda}{\mathrm{d}\bar{\mathrm{x}}^2}-\frac{1}{4}\left(\frac{\mathrm{d}\Lambda}{\mathrm{d}\bar{\mathrm{x}}}\right)^2=\Xi, \tag{7.403}$$

$$\frac{6k\pi^2 D}{\sqrt{|\Lambda|}}=-\frac{\hbar}{24\pi\Lambda}\left[\Xi+\frac{1}{4}\left(\frac{\mathrm{d}\Lambda}{\mathrm{d}\bar{\mathrm{x}}}\right)^2\right], \tag{7.404}$$

where $t_\pm(\sigma^\pm)=\frac{1}{4l^2}\Xi$ is a constant that, as usual, characterizes the quantum vacuum state. For the Hartle–Hawking state (3.97), we have $t_\pm(\sigma^\pm)=-\frac{\kappa^2}{4}$, which implies $\Xi=-(\kappa l)^2$. Upon differentiation, Eq. (7.403) simplifies to the second equation, Eq. (7.404), whose solution in terms of the z coordinate (3.21) takes the form

$$\sqrt{|\Lambda|}=\begin{cases}\dfrac{D}{2\varepsilon}\left[(\mathrm{z}-\mathrm{z}_0)^2-\left(\dfrac{\varepsilon\kappa l}{D}\right)^2\right], & \Lambda<0,\\[2ex] \dfrac{D}{2\varepsilon}\left[\left(\dfrac{\varepsilon\kappa l}{D}\right)^2-(\mathrm{z}-\mathrm{z}_0)^2\right], & \Lambda>0,\end{cases} \tag{7.405}$$

with z_0 an integration constant and $\varepsilon=\frac{\hbar}{72k\pi^3}$. From this expression, it is immediately evident that two Killing horizons are present. They are determined by the condition $\Lambda=0$, and thus located at

$$\mathrm{z}_\pm=\mathrm{z}_0\pm\frac{\varepsilon\kappa l}{D}. \tag{7.406}$$

Since $\varepsilon\to 0$, the separation between the two horizons is extremely small. Moreover, these horizons are singular and non-extremal, because $\kappa\neq 0$ and $R\to\infty$ at the horizon locations. Consequently, the solution is unstable. Nonetheless, we proceed to examine it in more detail.

Without loss of generality, we fix $D>0$. Consequently, $\Lambda>0$ between the two horizons, i.e. for $\mathrm{z}\in(\mathrm{z}_-,\mathrm{z}_+)$, while $\Lambda<0$ for $\mathrm{z}<\mathrm{z}_-$ or $\mathrm{z}>\mathrm{z}_+$. A straightforward calculation of the tortoise coordinate yields

$$\frac{\sigma}{l}=\frac{1}{\kappa l}\ln\left|\frac{\mathrm{z}-\mathrm{z}_+}{\mathrm{z}-\mathrm{z}_-}\right|. \tag{7.407}$$

To obtain the maximally extended geometry (see App. C.3 for the Schwarzschild case), we introduce Kruskal coordinates using the surface gravity:

$$|\kappa x^\pm|=e^{\kappa x^\pm}, \tag{7.408}$$

where the overall sign is chosen according to the quadrant of spacetime covered by the coordinates. Further details are provided in App. D.5. We begin by examining the region $\mathrm{z}>\mathrm{z}_+$, which corresponds to the exterior of the black hole. In this domain, the Kruskal coordinates are defined as

$$\kappa x^+=e^{\kappa\sigma^+}\qquad\wedge\qquad\kappa x^-=-e^{-\kappa\sigma^-}. \tag{7.409}$$

In the limit $\mathrm{z} \to \mathrm{z}_+$, we find $\sigma \to -\infty$, so that $x^+ \to 0$ and $x^- \to 0$. Hence, this hypersurface indeed corresponds to the horizon. Conversely, taking $\mathrm{z} \to \infty$ leads to $\sigma \to 0$, which implies $\kappa^2 x^+ x^- = -1$. This hypersurface is associated with spatial infinity i^0. Therefore, the region $\mathrm{z} > \mathrm{z}_+$ exhibits a Poincaré-patch-like structure, even though the underlying geometry is not that of pure AdS spacetime.

To access the region located between the two horizons, i.e., $\mathrm{z}_- < \mathrm{z} < \mathrm{z}_+$, one must first cross the outer horizon at $\mathrm{z} = \mathrm{z}_+$. Consequently, this intermediate region lies in the second quadrant of Fig. 4.1. Within it, both $x^+ > 0$ and $x^- > 0$ hold. Approaching the inner horizon $\mathrm{z} = \mathrm{z}_-$ drives $\sigma \to +\infty$, which in turn implies $x^+ \to \infty$ and $x^- \to \infty$. The intersection of the corresponding hypersurfaces defines the second bifurcation point. Since we have not yet entered the $\mathrm{z} > \mathrm{z}_-$ domain, we introduce a redefined tortoise coordinate in Eq. (7.407), now adapted to a new set of Kruskal coordinates centered at this second bifurcation point (in direct analogy with the Reissner–Nordström case [106, 121]):

$$\frac{\sigma'}{l} = \frac{1}{\kappa l} \ln \left| \frac{\mathrm{z} - \mathrm{z}_-}{\mathrm{z} - \mathrm{z}_+} \right| \quad \Longrightarrow \quad |\kappa x'^{\pm}| = \pm e^{\pm \sigma'^{\pm}}, \tag{7.410}$$

because the fourth quadrant relative to the second bifurcation point is equivalent to the second quadrant of the first bifurcation point. In this coordinate system, the limit $\sigma' \to -\infty$—or, equivalently, $x'^+ = 0$ or $x'^- = 0$ in Kruskal coordinates—identifies the inner horizon $\mathrm{z} = \mathrm{z}_-$. Passing through this horizon takes us into the black hole interior characterized by $\mathrm{z} < \mathrm{z}_-$, which, as seen from the second bifurcation point, lies in quadrant III. In the limit $\mathrm{z} \to -\infty$, we obtain $\sigma' = 0$, or in in terms of Kruskal coordinates $\kappa^2 x^+ x^- = -1$, signaling the approach to the second spatial infinity region. To construct the maximally extended solution, this procedure is replicated in all remaining quadrants. This generates two further bifurcation points, and iterating the construction indefinitely yields an infinite tower–like global structure, analogous to that of the Reissner–Nordström spacetime [121] and closely resembling that of the rotating three-dimensional BTZ black hole [78].

At first sight, there appears to be no singularity other than the singular horizons. This is not correct, however. Because the theory contains several distinct fields, one must check whether any of them become divergent, and in particular determine the hypersurface on which the dilaton field vanishes. For $\Lambda < 0$ there are three possible cases. We focus our detailed analysis on the regime $\mathrm{x}^2 + \Lambda \phi^\perp > 0$. We start by studying the behavior of the dilaton field, whose form is given in Eq. (7.74):

$$\frac{2}{3} \left(\frac{\mathrm{x}}{\cosh \mathrm{z}} \right)^3 = \frac{2\varepsilon \cosh \mathrm{z}}{(\mathrm{z} - \mathrm{z}_+)(\mathrm{z} - \mathrm{z}_-) - \frac{\varepsilon P}{D} \sinh \mathrm{z}} + \eta. \tag{7.411}$$

This quantity diverges when $(\mathrm{z} - \mathrm{z}_+)(\mathrm{z} - \mathrm{z}_-) - \frac{\varepsilon P}{D} \sinh \mathrm{z} = 0$. That equation admits at most three roots. For $P > 0$, the denominator is negative as $\mathrm{z} \to \infty$ and positive as $\mathrm{z} \to -\infty$. When $P \ll 1/\varepsilon$, there is always at least one solution with $\mathrm{z} > \mathrm{z}_+$. Since we require $\mathrm{x} > 0$, this forces us to choose $P < 0$. Taking the limit $\mathrm{z} \to \infty$ in Eq. (7.411) yields $\frac{2}{3} \left(\frac{\mathrm{x}}{\cosh \mathrm{z}} \right)^3 \to -\frac{2D}{P} + \eta > 0$, which implies $\eta > \frac{2D}{P}$. On the other hand, for $\mathrm{z} \approx 0$, the expression (7.411) can be made arbitrarily small while remaining positive, which leads to $\eta > -\mathcal{O}(\varepsilon)$. Since we do not expect η to be of order $\mathcal{O}(\varepsilon)$, we infer that $\eta > 0$. Consequently, $\mathrm{x} \to \infty$ along a particular hypersurface defined by $\mathrm{z} = \mathrm{z}_S$ with $\mathrm{z}_S < \mathrm{z}_-$. Approaching this hypersurface from the other side gives $\mathrm{x} \to -\infty$, so it represents a genuine singularity. With the specific choices $P < 0$ and $\eta > 0$, this singular hypersurface lies inside the black hole region, secluded by both horizons.

The behavior of the function in Eq. (7.411) as a function of the z coordinate for various negative values of P ($P < 0$) is shown in Fig. 7.1. As $\mathrm{z} \to \infty$, the function asymptotically approaches the value $-\frac{2D}{P}$. Moreover, the divergence at $\mathrm{z} = \mathrm{z}_S$ is clearly visible. For all $\mathrm{z} > \mathrm{z}_\mathrm{S}$, the function remains positive and is well-defined. A nonzero η merely shifts the graph vertically along the y-axis. Consequently, negative η are excluded, since they would yield negative x. The function clearly feels a bounce (local maximum) in the vicinity of the horizon region, and this effect becomes more pronounced for smaller values of P.

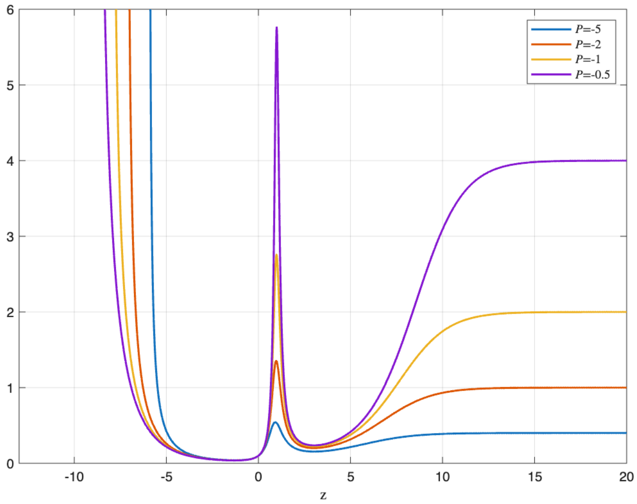

Figure 7.1: Plot of function in Eq. (7.411) for different values of P and $\varepsilon = 0.05$, $\eta = 0$, $D = 1$ and $\mathrm{z}_0 = 1$.

Using Eqs. (7.71) and (7.72), we infer that the remaining field invariants, θ^2 and $\Phi^2 = \Lambda\phi^{\perp 2}$, diverge exclusively at $\mathrm{z} = \mathrm{z}_\mathrm{S}$. In contrast, Eq. (7.73) shows that the torsion invariant $T_\mu T^\mu = \Lambda \mathrm{K}^{\parallel 2}$ diverges at the singular horizons.

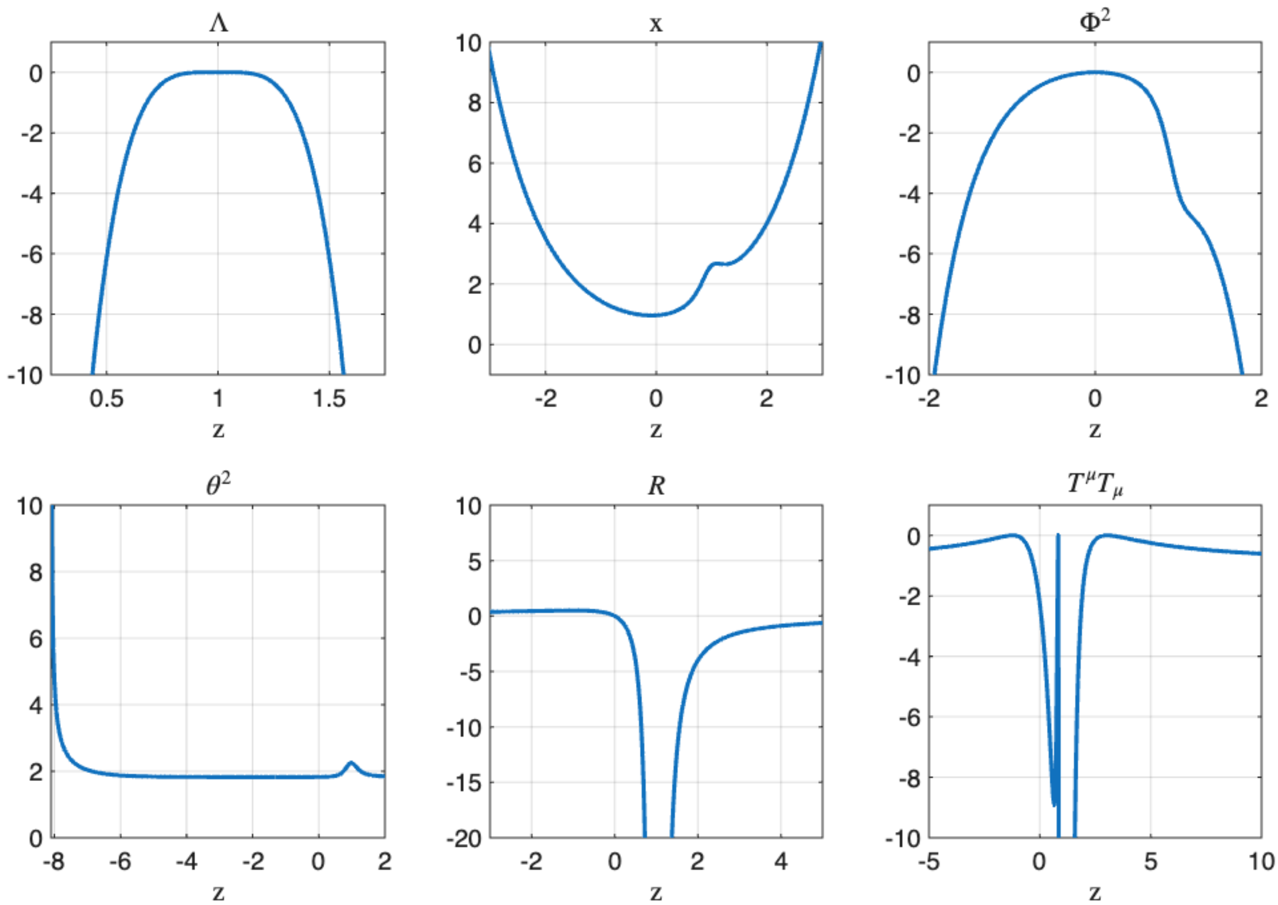

Figure 7.2: Plot of the behavior of field content with respect to the z coordinate, when $\mathrm{x}^2 + \Lambda\phi^{\perp 2} > 0$.

The asymptotic and near-horizon behavior of all relevant fields is shown in Fig. 7.2. It is evident that the curvature and torsion invariants blow up at both the inner and outer horizons, whereas the fields themselves exhibit a sort of bounce in the vicinity of the horizons. The singularity is located at approximately $\mathrm{z_S} \approx -8$. In contrast, at the singularity, the fields diverge, while the curvature and torsion invariants remain finite. Asymptotically, the curvature goes to zero, whereas the torsion invariant stays non-vanishing. The θ field approaches a finite value, while the remaining fields diverge, with the dilaton diverging as expected. The figure corresponds to the following choice of constants: $P = -1$, $D = 1$, $\eta = 1$, $\mathrm{z}_0 = 1$, $\varepsilon = 0.05$, $\kappa l = 1$, and $l = 1$.

We now turn to the remaining configurations of the field content. For $\Lambda\phi^{\perp 2} + \mathrm{x}^2 < 0$, there is a genuine (hard) singularity at $\mathrm{z} = 0$. At this point the torsion diverges, while the curvature stays finite. At the same time, the dilaton field vanishes at $\mathrm{z} = 0$, making this point the natural candidate for the singularity. All other field invariants remain regular there. The behavior of the dilaton should again be analyzed analogously to the discussion in the previous case. The counterpart of Eq. (7.411) reads:

$$\frac{2}{3}\left(\frac{\mathrm{x}}{\sinh \mathrm{z}}\right)^3 = \frac{2\varepsilon \sinh \mathrm{z}}{(\mathrm{z}-\mathrm{z}_+)(\mathrm{z}-\mathrm{z}_-) + \frac{\varepsilon P}{D}\cosh \mathrm{z}} - \eta. \tag{7.412}$$

For $\mathrm{z} > 0$, $P > 0$, and $\eta < 0$, this function is manifestly positive, provided that P is not of the same order as ε. Its limit at spatial infinity is $\frac{2}{3}\left(\frac{\mathrm{x}}{\sinh \mathrm{z}}\right)^3 \to \frac{2D}{P} - \eta$, and the function exhibits a small bounce in the vicinity of the horizon. The same qualitative behavior appears in all other relevant functions. Consequently, this case is effectively analogous to the previous one: it shows identical asymptotic and near-horizon features, with the only difference that the singularity is now strictly localized at $\mathrm{z_S} = 0$. The final case, $\Lambda\phi^{\perp} + \mathrm{x}^2 = 0$, displays similar qualitative properties to the first two and will therefore not be discussed in more detail here.

We thus infer that the apparent singularity on the horizons arises as an artifact of non-vanishing torsion. Moreover, the EMT associated with the quantum corrections diverges along the horizons, indicating that the quanta condense at these locations, in close analogy with the behavior found for fermionic soliton stars in Sec. 7.3.3.

The extremal limit is obtained by taking $\kappa \to 0$. In this limit, the two horizons collapse onto each other, forming a single horizon located at $\mathrm{z} = \mathrm{z}_0$. This horizon remains singular, because $R \to \infty$ as $\Lambda \to 0$. Nevertheless, an extremal singular horizon represents a well-defined and stable configuration. The analysis of the field content proceeds in the same way as in the non-extremal case, and we reach the same conclusion of the singularity located at $\mathrm{z} = \mathrm{z_S}$ behind the horizon.

The Penrose diagrams for the non-extremal and extremal cases are presented in Figs. 7.3 and 7.4 respectively. As already mentioned, both diagrams display a characteristic tower-like pattern. In the non-extremal configuration, one finds an infinite sequence of bifurcation points labeled B_n and B'_n. The points B_n are associated with the outer horizon, while the B'_n correspond to the inner horizon. Each B_n bifurcation point partitions the spacetime into four distinct regions. Two of these regions represent the outer universes containing the spatial infinity i^0, while the remaining two describe the inter-horizon domains where $\Lambda > 0$ and the roles of space and time are interchanged. The B'_n bifurcation points, in turn, separate spacetime into two singular sectors and two inter-horizon regions. Unlike the usual case with space-like singularities, these singularities are time-like. Because these singular sectors correspond to $\Lambda < 0$, the usual distinction between space and time is preserved there. In the extremal case, the inter-horizon regions disappear and the two distinct bifurcation points merge into one, so that crossing the horizon leads directly into the singular region. Spatial infinities, horizons, and bifurcation points are drawn in green, whereas the singularities are indicated by wavy black lines. Constant-time slices are shown in red, and hypersurfaces of constant z are drawn in blue.

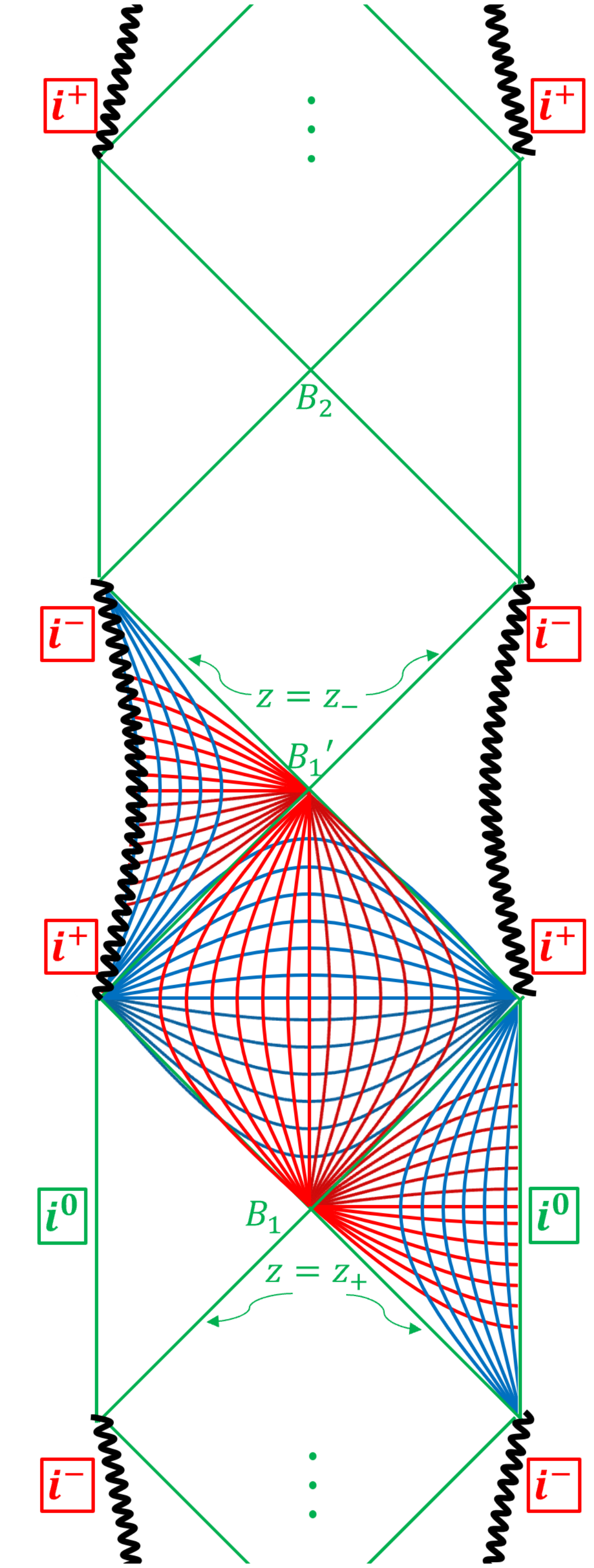

Figure 7.3: Penrose diagram depicting the causal structure of the non-extremal eternal black hole within the Full DR5DCS model.

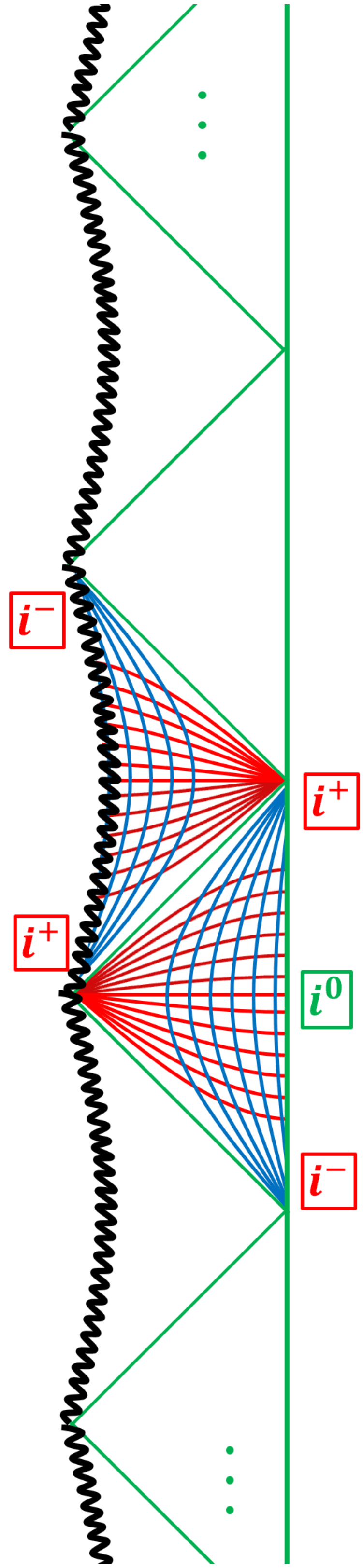

Figure 7.4: Penrose diagram depicting the causal structure of the extremal eternal black hole within the Full DR5DCS model.

Chapter 8

Entanglement entropy in gravitational systems

In the preceding chapters, we examined various two-dimensional gravity models with the goal of describing both eternal and evaporating black hole scenarios and subsequently studying their associated fine-grained thermodynamic properties. The coarse-grained aspects of black holes are already well established and have been thoroughly explored ever since Hawking demonstrated that black holes behave as thermal objects [13]. In contrast, the fine-grained properties appear to imply non-unitary time evolution and an inevitable loss of information. The purpose of this chapter is therefore to revisit the old notions of the fine-grained entropy in gravitational systems and to review the more recent Maldacena–Lewkowycz prescription [33], which yields the island-rule formula (1.6). This framework refines the computation of fine-grained entropy in such a way that unitarity is maintained, thereby preparing the ground for an explicit derivation of the Page curve in concrete 2D dilaton gravity models, which will be analyzed in the subsequent chapters.

In this chapter, we obtain explicit formulas for various notions of entropy that arise in gravitational systems. As a preliminary step, we highlight the distinction between fine–grained and coarse–grained entropy [8, 26]. These concepts are standard in statistical physics and information theory and are not inherently specific to gravity. In the first Sec. 8.1 of this chapter, we clarify their interpretation and importance in gravitational contexts.

In the subsequent Sec. 8.2, we evaluate the fine–grained entropy in several particular configurations introduced earlier. We begin with the case of a uniformly accelerated observer in the Minkowski vacuum. Such an observer detects a thermal spectrum of particles with a temperature proportional to their proper acceleration, a phenomenon known as the Unruh effect [122, 123, 124]. We then generalize this treatment to a broader class of observers, in both flat and curved spacetime backgrounds [26], and finally examine the entropy in spacetimes that contain a reflective boundary.

In Sec. 8.3, we turn to the analysis of coarse–grained entropy in gravitational settings. We start by examining matter in a coherent state, along with the quantum–corrected entropy of a black hole [26], working within the BPP model. Modeling the collapsing matter as a coherent state is physically well motivated, since in many condensed matter systems the ground state is accurately described by a coherent state. It is therefore natural to assume that the matter responsible for forming the singularity is in its ground state. We end this section by formulating a precise version of what we call the Hawking information loss paradox.

In the final Sec. 8.4, starting from our main working assumption—the central dogma—which states that a black hole behaves like an ordinary quantum system up to a certain boundary surface, we sketch the derivation of the central formula on which this work is founded: the formula for the fine–grained entropy in gravitational systems [1]. We close the chapter with several comments on unresolved aspects of the black hole information paradox, focusing in particular on the remaining difficulties associated with reconstructing the causal diamond (entanglement wedge reconstruction), following the discussion in [1].

8.1 Coarse–grained and fine–grained entropy

As already emphasized, this section is not directly concerned with gravitational effects; rather, it deals with general notions in physics. In broad terms, a fine-grained description of a system offers a detailed microscopic account of all its degrees of freedom. In contrast, a coarse-grained description is obtained by averaging or integrating over these microscopic variables, so that only a smaller set of macroscopic or effective variables is kept. In what follows, we clarify this distinction through a specific example built around the concept of entropy.

The primary quantity employed in thermodynamics is the von Neumann (Gibbs) entropy. In classical mechanics, it is defined as a functional of the probability distribution over phase space, $\rho(\vec{p}, \vec{q})$, that characterizes the occupied states:

$$S_{FG}[\rho] = -k_B \int \left(\prod_{i=1}^{n} dp_i dq_i \right) \rho \ln \rho, \tag{8.1}$$

where k_B is the Boltzmann constant and n denotes the dimension of configuration space. This quantity is fine–grained, since it is constructed directly from the microscopic distribution function ρ. As a result, it contains the full microscopic information about the system. In particular, it is well defined at every point in phase space. Furthermore, Liouville's theorem implies that $\frac{d\rho}{dt} = 0$ along Hamiltonian trajectories, so the corresponding entropy is exactly conserved in time. Hence, this entropy—commonly associated with the von Neumann (or Gibbs) entropy in the classical limit—cannot serve as thermodynamic entropy, because it does not exhibit temporal growth.

Gibbs proposed a systematic method for obtaining a coarse–grained quantity from the fine–grained distribution ρ. The idea is to divide phase space into a set of cells and, within each cell, to perform a local averaging of ρ. This averaging defines the coarse–grained distribution $\bar{\rho}$. In this way, the difference between "coarse–grained" and "fine–grained" descriptions becomes clear: the former is a smoothed, cell-averaged version of the latter. On this basis, one can introduce a coarse–grained entropy in direct analogy with the von Neumann entropy, but now expressed in terms of the coarse–grained distribution $\bar{\rho}$:

$$S_{CG}[\bar{\rho}] = -k_B \int \left(\prod_{i=1}^{n} dp_i dq_i \right) \bar{\rho} \ln \bar{\rho}, \tag{8.2}$$

$$\bar{\rho}(x) = \sum_{C} p_\rho(C) \rho_C(x), \quad p_\rho(C) = \int_C \rho(x) \left(\prod_{i=1}^{n} dp_i dq_i \right). \tag{8.3}$$

In this construction, the macroscopic properties are extracted from ρ and are fully encoded in the coarse–grained distribution $\bar{\rho}$. This coarse–graining step is exactly what the entropy is meant to capture. With this definition, the entropy built from $\bar{\rho}$ is compatible with, and in fact obeys, the second law of thermodynamics. There is, however, another route to clarifying the difference between these notions of entropy. For quantum systems, the fine–grained (von Neumann) entropy is defined as

$$S_{FG} = -k_B \operatorname{Tr}\{\hat{\rho} \ln \hat{\rho}\} \quad \text{and} \quad \langle \hat{A} \rangle_\rho = \operatorname{Tr}\left\{\hat{\rho}\hat{A}\right\}, \ \forall \hat{A}, \tag{8.4}$$

where $\hat{\rho}$ denotes the density matrix of the system. For a system in a pure state, this entropy vanishes. Thus, it measures how far the state is from being pure, i.e., the amount of statistical uncertainty (or missing information) about the system's state. The crucial feature of the density matrix — which contains the maximal microscopic information that can be obtained about the system — is embodied in the second relation above: it shows that, given $\hat{\rho}$, one can determine the expectation value of any observable of the system.

In realistic scenarios, one usually does not access the full set of observables of a system. Instead, attention is limited to those observables that are relevant at the macroscopic level, hereafter referred to as coarse–grained quantities. We denote this chosen family of observables by $\{\hat{A}_i\}$. Now consider the set of all density operators $\tilde{\rho}$ that fulfill

$$\operatorname{Tr}\left\{\tilde{\rho}\hat{A}_i\right\} = \operatorname{Tr}\left\{\hat{\rho}\hat{A}_i\right\}, \ \forall \hat{A}_i, \tag{8.5}$$

and evaluate the von Neumann entropy for each such $\tilde{\rho}$. Among these, select the density operator that maximizes the entropy. This entropy–maximizing state, denoted by $\bar{\rho}$, is defined as the coarse–grained density matrix. The corresponding maximal entropy is then interpreted as the thermodynamic entropy. This prescription reproduces the standard coarse–graining construction familiar from classical statistical mechanics.

From these definitions, one immediately obtains that the fine–grained entropy never exceeds the coarse–grained entropy, i.e., $S_{\mathrm{FG}} \leqslant S_{\mathrm{CG}}$. The reason is that we can always pick $\tilde{\rho} = \hat{\rho}$, which in general does not maximize the entropy, while the optimal $\tilde{\rho}$ by definition does. Equivalently, S_{CG} can be viewed as quantifying the effective total number of degrees of freedom available to the system, thereby furnishing an upper bound on the entanglement that the system can share with an external system.

8.1.1 Fine-grained entropy in gravitation

Up to this point, we have discussed entropy in a broad, largely abstract framework. We now focus on its concrete consequences for gravitational systems. Our primary goal is to clarify the physical interpretation of von Neumann entropy in a gravitational context—most prominently for quantum fields on curved spacetime backgrounds, such as those giving rise to Hawking radiation—and to identify and describe the coarse–grained notion of entropy naturally associated with a black hole.

When we ask for the entropy of the radiation outside the black hole, we are necessarily working with a fine–grained entropy. This is because it pertains to only a subsystem of the full quantum–gravitational configuration: effectively, the internal degrees of freedom of the black hole have been traced out. To make this more explicit, consider a stationary observer positioned asymptotically far from the black hole. From this observer's viewpoint, there exists a finite region of spacetime that is causally out of reach. This region is bounded by the black hole's apparent horizon, as no light rays can escape from within it. Consequently, there are degrees of freedom located behind the event horizon that are inaccessible to the external observer.

If the black hole arises from the gravitational collapse of matter initially prepared in a pure quantum state, then the state of the combined system—comprising both the black hole and its Hawking radiation—remains pure at all times and can be denoted by $|\psi\rangle$. However, as emphasized above, the stationary observer cannot probe all the degrees of freedom associated with this global state. The density operator describing the complete system is $\hat{\rho} = |\psi\rangle\langle\psi|$. Since the Hawking radiation observable at infinity is quantum–mechanically entangled with the degrees of freedom inside the black hole, the density matrix actually accessible to the observer is obtained by tracing over the interior degrees of freedom lying behind the apparent horizon:

$$\hat{\rho}_{out} = \mathrm{Tr}_{in}\{|\psi\rangle\langle\psi|\}. \tag{8.6}$$

The full information about the Hawking radiation measured by an observer at infinity is encoded in this density matrix. From it, one can extract both the radiation temperature and any correlations that may be present in the radiation. The next step is to compute the entropy of the radiation. We define it as the von Neumann entropy expressed in terms of the density matrix $\hat{\rho}_{out}$:

$$S_{FG} = -k_B\,\mathrm{Tr}\{\hat{\rho}_{out}\ln\hat{\rho}_{out}\}. \tag{8.7}$$

In evaluating this trace, we explicitly assume that the relevant spacetime region lies within the portion that contains the Hawking radiation. Consequently, to evaluate this quantity one must first choose a spacelike hypersurface Σ (i.e., a constant-time slice, $t = \text{const.}$). This hypersurface specifies the moment at which the entropy is measured. In this manner, an explicit time dependence is introduced directly into the expression for S_{FG}. Next, we define the spatial region A' containing the degrees of freedom accessible to the observer as the causal diamond associated with some portion of the hypersurface Σ. The remainder of Σ then determines one or more causal diamonds whose degrees of freedom are inaccessible to the observer; we denote this region by A. In the computation of S_{FG}, we trace over the degrees of freedom belonging to region A. Since the total quantum state on $A \cup A'$ is pure, the von Neumann entropy S_{VN} for region A is equal to the corresponding S_{VN} for region A' [8, 26].

For a black hole, the region A is taken to be the causal diamond associated with the portion of the hypersurface Σ that lies inside the apparent horizon. This prescription was long regarded as the appropriate way to define fine-grained entropy in gravitational systems. Nevertheless, it turns out to be incompatible with the unitarity of quantum mechanics, leading to a conceptual inconsistency. This tension is resolved by introducing islands [1], which we describe in greater detail in Sec. 8.4. Consequently, the entropy defined in this manner is now interpreted as the von Neumann entropy rather than the genuine fine-grained entropy of a gravitational system. It is still crucial, as it constitutes a part of the formula for the fine-grained entropy in gravitational systems.

In Sec. 8.2, we compute the von Neumann entropy $S_{VN}(\Sigma)$ for several different choices of the region A. We begin with the Unruh effect, where A is taken to be the entire left Rindler wedge of Minkowski spacetime. We then extend this analysis to a general region in Minkowski spacetime. After that, we further generalize the results to curved spacetimes. Finally, we study the case in which the spacetime has a boundary with reflective boundary conditions, corresponding to a dynamical evaporating black hole scenario.

In Fig. 8.1, an arbitrary region $A = [x_1^+, x_2^+] \times [x_1^-, x_2^-]$ is shown shaded in red. The spacelike hypersurface Σ is represented by the green line and passes through the points (x_1^+, x_2^-) and (x_2^+, x_1^-). Yet, regardless of which hypersurface we choose, as long as it intersects these two points, the von Neumann entropy takes the same value. This follows from the fact that the entropy depends solely on the spacetime separation of these points, that is, on the area of the corresponding causal diamond [1]. Consequently, we regard the entropy as a property of the causal diamond rather than of the constant-time slice Σ.

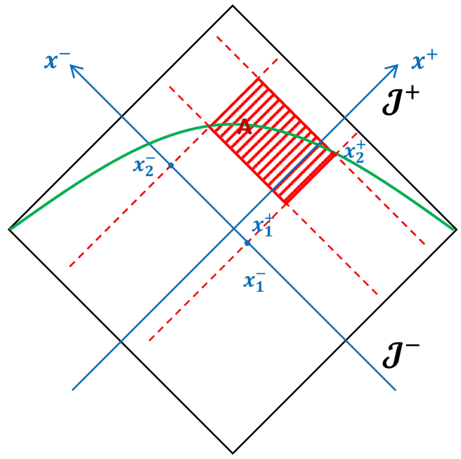

Figure 8.1: Arbitrary region A that contains the inaccessible degrees of freedom.

In the preceding chapters, we examined various gravitational models where the matter was always represented by massless scalar fields. Now we see why this was important, i.e., how much it simplifies the calculation of entropy. Namely, the Klein–Gordon equation $\Box\phi = 0$ reduces to $\partial_+\partial_-\phi = 0$, as we saw in Sec. 3.3 when discussing the transformation properties of the energy–momentum tensor. The solution to this equation is as follows:

$$\phi(x^+, x^-) = \phi_+(x^+) + \phi_-(x^-). \tag{8.8}$$

Consequently, the left–propagating modes are completely decoupled from the right–propagating modes. This also allows us to compute the entropy independently, i.e., first determine the entropy arising due to the right–propagating modes, and then add the contribution associated with the left–propagating modes, therefore obtaining the total entropy. However, this is no longer true when one investigates the gravitational collapse, because in that case there is a boundary with reflective boundary conditions. In such a situation the modes cease to be independent, and it becomes necessary to analyze separately what occurs in this case.

8.2 Von Neumann entropy in gravity

In this section, we compute the von Neumann entropy (8.7) for various configurations of the region A that is inaccessible to an asymptotic observer. We begin with a review of the Unruh effect, namely the phenomenon whereby a uniformly accelerated observer perceives a thermal particle spectrum, even though an inertial Minkowski observer regards the state as vacuum. The coordinates adapted to such uniformly accelerated observers are the Rindler coordinates. Their derivation, along with the explicit relation to the worldlines of uniformly accelerated observers, is provided in App. D.3. We then extend the method developed for the Rindler observer to more general observers in curved spacetime.

Throughout the discussion, we first focus on right-moving modes. The contribution from left-moving modes is later added in an analogous manner, since their respective contributions to the entropy are independent. We denote by $x^\pm$ the coordinates in which the quantum vacuum is defined, and by $\sigma^\pm$ the coordinates natural to the observer. In this section, we consistently employ the results summarized in App. D, which concern quantum field theory in curved spacetime.

8.2.1 Minkowski vacuum and a region of type: $A = (-\infty, 0] \times [0, +\infty)$

The choice of the region A associated with a uniformly accelerated observer is illustrated in Fig. 8.2. In this context, we employ Unruh's method to compute the Bogoliubov coefficients (see App. D.3 and [124]). The key point we rely on is that the entropy is independent of the particular choice of basis functions in the Hilbert space. Consequently, we are free to select modes in whichever coordinates are most convenient. Since we are dealing with a Rindler observer, we adopt Rindler coordinates. The Rindler coordinates are given by the following relation:

$$\sigma^-_{out} = -\frac{1}{a}\ln\left(-ax^-\right) \;\;\wedge\;\; \sigma^-_{in} = -\frac{1}{a}\ln\left(ax^-\right).$$

For more details on the derivation of this transformation see App. D.3.

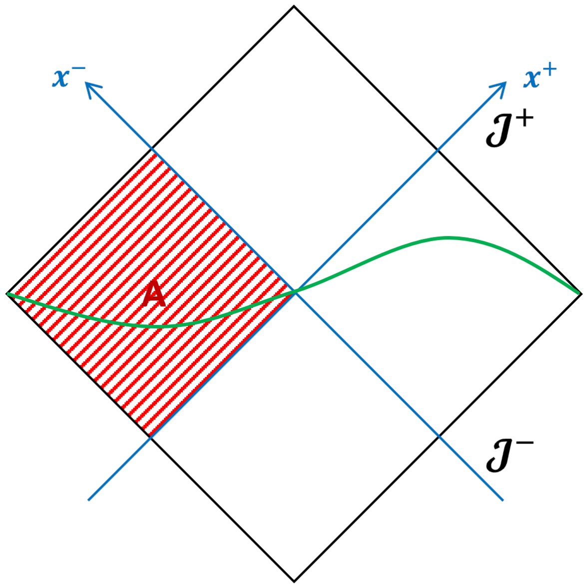

Figure 8.2: Region A that contains the inaccessible degrees of freedom in a case of the Rindler observer.

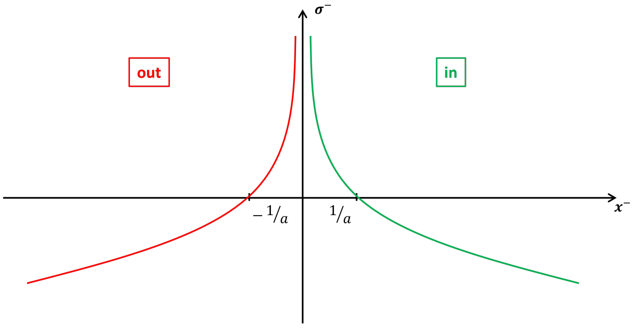

Figure 8.3: Function $\sigma^- = \sigma^-(x^-)$ for the case of a Rindler observer.

The constant a denotes the acceleration of the Rindler observer. We observe that the expressions for the Rindler coordinates in different wedges of the spacetime can be merged by introducing the absolute value:

$$\sigma^- = -\frac{1}{a}\ln\left|ax^-\right|. \tag{8.9}$$

Fig. 8.3 presents the graph illustrating the behavior of this function. The *in* region is depicted in green, whereas the *out* region is shown in red.

We start by identifying the positive–frequency modes. For right–propagating waves in region A', we have:

$$\partial_t\phi^\omega = -i\omega\phi^\omega \quad\Longrightarrow\quad \frac{d\phi^\omega_{out}}{d\sigma^-_{out}} = -i\omega\phi^\omega_{out} \quad\Longrightarrow\quad \phi^\omega_{out} = \frac{1}{\sqrt{4\pi\omega}}\theta(-x^-)e^{-i\omega\sigma^-_{out}}, \tag{8.10}$$

In the left Rindler wedge, corresponding to region A, the timelike Killing vector that we use to define the modes points in the opposite direction. Consequently, the sign on the right–hand side of the defining equation for the modes is reversed and there is no explicit "−":

$$\partial_{-t}\phi^\omega = -i\omega\phi^\omega \quad\Longrightarrow\quad \frac{d\phi^\omega_{in}}{d\sigma^-_{in}} = i\omega\phi^\omega_{in} \quad\Longrightarrow\quad \phi^\omega_{in} = \frac{1}{\sqrt{4\pi\omega}}\theta(x^-)e^{i\omega\sigma^-_{in}}. \tag{8.11}$$

From Sec. 3.3, we recall that the normalization constant is $\frac{1}{\sqrt{4\pi\omega}}$ (see Eq. (3.86)). Hence, the field can be written as an expansion in these modes as follows:

$$\phi_- = \int_0^\infty d\omega\left[a_{out}(\omega)\phi^\omega_{out} + a_{in}(\omega)\phi^\omega_{in} + a^\dagger_{out}(\omega)\phi^{\omega*}_{out} + a^\dagger_{in}(\omega)\phi^{\omega*}_{in}\right]. \tag{8.12}$$

The appropriate procedure at this point would be to work directly with the Minkowski modes and compute the Bogoliubov coefficients, as outlined in App. D.2. Since this calculation is quite involved, we instead employ the Unruh trick [124]. Our goal is to rewrite the Rindler modes using the Minkowski light-cone coordinates $x^{\pm}$ and then analytically continue these expressions to the full spacetime. If this can be done, we obtain a family of mutually orthogonal modes that are defined on all of Minkowski spacetime and written in Minkowski coordinates. In other words, we construct a basis in Minkowski coordinates. This basis must also correspond to the Minkowski vacuum, and therefore the resulting modes are precisely the Minkowski modes. We start from the ϕ^{ω}_{out} mode and attempt to analytically extend it to the entire spacetime:

$$
\begin{aligned}
\phi^{\omega}_{out} &= \frac{1}{\sqrt{4\pi\omega}}\theta(-x^-)e^{-i\omega\sigma^-_{out}} = \frac{1}{\sqrt{4\pi\omega}}\theta(-x^-)\left(-ax^-\right)^{\frac{i\omega}{a}}, \\
\phi^{\omega}_{in} &= \frac{1}{\sqrt{4\pi\omega}}\theta(x^-)e^{i\omega\sigma^-_{in}} = \frac{1}{\sqrt{4\pi\omega}}\theta(x^-)\left(ax^-\right)^{-\frac{i\omega}{a}}, \\
\phi^{\omega*}_{in} &= \frac{1}{\sqrt{4\pi\omega}}\theta(x^-)\left(ax^-\right)^{\frac{i\omega}{a}} = \frac{1}{\sqrt{4\pi\omega}}\theta(x^-)\left(-e^{-i\pi}ax^-\right)^{\frac{i\omega}{a}} = \frac{1}{\sqrt{4\pi\omega}}e^{\frac{\pi\omega}{a}}\theta(x^-)\left(-ax^-\right)^{\frac{i\omega}{a}}, \\
\phi^{\omega*}_{out} &= \frac{1}{\sqrt{4\pi\omega}}\theta(-x^-)\left(-ax^-\right)^{-\frac{i\omega}{a}} = \frac{1}{\sqrt{4\pi\omega}}\theta(-x^-)\left(e^{i\pi}ax^-\right)^{-\frac{i\omega}{a}} = \frac{1}{\sqrt{4\pi\omega}}e^{\frac{\pi\omega}{a}}\theta(-x^-)\left(ax^-\right)^{-\frac{i\omega}{a}},
\end{aligned}
$$

$$
\Longrightarrow \phi^{\omega}_{out} + e^{-\frac{\pi\omega}{a}}\phi^{\omega*}_{in} = \frac{1}{\sqrt{4\pi\omega}}\left[\theta(-x^-)+\theta(x^-)\right]\left(-ax^-\right)^{\frac{i\omega}{a}} = \frac{1}{\sqrt{4\pi\omega}}\left(-ax^-\right)^{\frac{i\omega}{a}} \propto \phi^{\omega}_{1}, \tag{8.13}
$$

$$
\Longrightarrow \phi^{\omega}_{in} + e^{-\frac{\pi\omega}{a}}\phi^{\omega*}_{out} = \frac{1}{\sqrt{4\pi\omega}}\left[\theta(-x^-)+\theta(x^-)\right]\left(ax^-\right)^{-\frac{i\omega}{a}} = \frac{1}{\sqrt{4\pi\omega}}\left(ax^-\right)^{-\frac{i\omega}{a}} \propto \phi^{\omega}_{2}. \tag{8.14}
$$

We observe that, by adding the term proportional to $\phi^{\omega*}_{\text{in}}$ to $\phi^{\omega}_{\text{out}}$, we obtain a mode that is well defined everywhere in Minkowski spacetime. It remains to explain why, in the third line, we chose the branch $-1 = e^{-i\pi}$, while in the fourth line we used $-1 = e^{i\pi}$. The key point is that we require the Minkowski modes to be globally well defined under analytic continuation of x^- into the complex plane.

To see this, let us consider the analyticity condition for the mode $f^{\omega}_{-} \propto e^{-i\omega x^-}$ in the limit $x^- \to \infty$. In terms of real and imaginary parts, we have

$$
f^{\omega}_{-} \propto e^{i\omega\,\mathrm{Re}\left\{x^-\right\}+\omega\,\mathrm{Im}\left\{x^-\right\}},
$$

which implies that we must have $\mathrm{Im}\{x^-\} < 0$ for the mode to remain bounded. In the third line we analytically continue from x^- to $-x^-$ in the complex plane. Since $\mathrm{Im}\{x^-\} < 0$, these two points must be connected through the lower half–plane, corresponding to a rotation by $-\pi$ and thus a phase factor $e^{-i\pi}$, which is the negative mathematical direction.

In the fourth line, we go back from $-x^-$ to x^-, again through the lower half–plane, which now corresponds to a rotation by $+\pi$ and therefore contributes the phase $e^{i\pi}$, the positive mathematical direction. This whole discussion is equivalent to imposing the condition that, for the Minkowski modes to be analytic over the full complex plane, the branch cut of the power function must lie in the upper half–plane. The next step is to normalize the modes $\phi^{\omega}_{1,2}$:

$$
\begin{aligned}
(\phi^{\omega}_{1,2}, \phi^{\omega'}_{1,2}) &= C^{\omega}_{1,2}C^{\omega' *}_{1,2}\left[(\phi^{\omega}_{out,in}, \phi^{\omega'}_{out,in}) + e^{-\frac{2\pi\omega}{a}}(\phi^{\omega*}_{in,out}, \phi^{\omega' *}_{in,out})\right] \\
&= \left|C^{\omega}_{1,2}\right|\left(1+e^{-\frac{2\pi\omega}{a}}\right)\delta(\omega-\omega').
\end{aligned} \tag{8.15}
$$

Hence, the Minkowski modes (annihilation operators) can be written in terms of the Rindler modes (annihilation operators) as follows:

$$\begin{aligned}
\phi_1^\omega &= \frac{1}{\sqrt{2\sinh\frac{\pi\omega}{a}}}\left[\phi_{out}^\omega e^{\frac{\pi\omega}{2a}} + \phi_{in}^{\omega *} e^{-\frac{\pi\omega}{2a}}\right], \;\; a_1(\omega) = \frac{1}{\sqrt{2\sinh\frac{\pi\omega}{a}}}\left[a_{out}(\omega) e^{\frac{\pi\omega}{2a}} - a_{in}^\dagger(\omega) e^{-\frac{\pi\omega}{2a}}\right], \\
\phi_2^\omega &= \frac{1}{\sqrt{2\sinh\frac{\pi\omega}{a}}}\left[\phi_{in}^\omega e^{\frac{\pi\omega}{2a}} + \phi_{out}^{\omega *} e^{-\frac{\pi\omega}{2a}}\right], \;\; a_2(\omega) = \frac{1}{\sqrt{2\sinh\frac{\pi\omega}{a}}}\left[a_{in}(\omega) e^{\frac{\pi\omega}{2a}} - a_{out}^\dagger(\omega) e^{-\frac{\pi\omega}{2a}}\right].
\end{aligned} \tag{8.16}$$

Therefore, the Bogoliubov coefficients are fully determined. The set of modes $\{\phi_1^\omega, \phi_2^\omega \,|\, \omega \in \mathbb{R}_0^+\}$ forms a complete basis of the Hilbert space of fields in Minkowski spacetime. Consequently, the annihilation operators appearing in Eq. (8.16) must annihilate the Minkowski vacuum. This construction is commonly known as the Unruh trick. Its main objective is to represent the Minkowski vacuum $|0_M\rangle$ as a superposition of Fock states supported in the left and right Rindler wedges. In full generality, this expansion can be written in the following way:

$$|0_M\rangle = \sum_{n_1,\ldots,n_s=0}^{\infty} \sum_{m_1,\ldots,m_s=0}^{\infty} A_{n_1 n_2 \ldots n_s}^{m_1 m_2 \ldots m_s} |n_1, n_2, \ldots, n_s, out\rangle \otimes |m_1, m_2, \ldots, m_s, in\rangle, \tag{8.17}$$

where $\{|n, in/out\rangle \,|\, n \in \{1, 2, \ldots, s\}\}$ denotes a basis of the single–particle state space in the in/out sector, and $A_{n_1 n_2 \ldots n_s}^{m_1 m_2 \ldots m_s}$ are the expansion coefficients to be determined. We fix the dimension of this single–particle state space to be s, without assuming s to be finite. The associated Fock basis, built from Slater permanents, is then

$$|n_1, n_2, \ldots, n_s, in/out\rangle = \frac{\left(a_{in/out}^\dagger(\omega_1)\right)^{n_1} \ldots \left(a_{in/out}^\dagger(\omega_s)\right)^{n_s}}{\sqrt{n_1! n_2! \ldots n_s!}} \left|0_{in/out}\right\rangle, \tag{8.18}$$

where $\{\omega_n \,|\, n \in \{1, 2, \ldots, s\}\}$ are the single–particle energies associated with the eigenstates $\{|n\rangle \,|\, n \in \{1, 2, \ldots, s\}\}$. The Minkowski vacuum is defined as the state annihilated by all Minkowski annihilation operators, i.e.

$$(\forall k \in \{1, 2, .., s\}) \;\; a_1(\omega_k) |0_M\rangle = 0, \tag{8.19}$$

$$a_2(\omega_k) |0_M\rangle = 0. \tag{8.20}$$

Solving the system of equations imposed by these two conditions, and using the standard action of creation and annihilation operators on the Fock basis, one finds the following recursion relations for the expansion coefficients:

$$(\forall k \in \{1, 2, \ldots, s\}) \;\; A_{n_1 n_2 \ldots n_s}^{m_1 m_2 \ldots m_s} = \sqrt{\frac{m_k}{n_k}} e^{-\frac{\pi\omega_k}{a}} A_{n_1 \ldots n_k - 1 \ldots n_s}^{m_1 \ldots m_k - 1 \ldots m_s} \tag{8.21}$$

$$A_{n_1 n_2 \ldots n_s}^{m_1 m_2 \ldots m_s} = \sqrt{\frac{n_k}{m_k}} e^{-\frac{\pi\omega_k}{a}} A_{n_1 \ldots n_k - 1 \ldots n_s}^{m_1 \ldots m_k - 1 \ldots m_s}. \tag{8.22}$$

Relation (8.21) follows from Eq. (8.19), while Eq. (8.22) is derived from Eq. (8.20). From these equations we immediately deduce that $n_k = m_k$ for all k, allowing us to write

$$A_{n_1 n_2 \ldots n_s}^{m_1 m_2 \ldots m_s} = \alpha_{n_1 n_2 \ldots n_s} \delta_{n_1 m_1} \delta_{n_2 m_2} \ldots \delta_{n_s m_s}, \tag{8.23}$$

$$\alpha_{n_1 n_2 \ldots n_s} = e^{-\frac{\pi\omega_k}{a}} \alpha_{n_1 \ldots n_k - 1 \ldots n_s}, \;\; \forall k. \tag{8.24}$$

By repeatedly lowering the occupation number n_k down to zero, one acquires n_k factors of $e^{-\frac{\pi\omega_k}{a}}$. Reducing all occupation numbers to zero and denoting $\alpha_{00\ldots0} = C$, we obtain

$$|0_M\rangle = C \sum_{n_1, n_2, \ldots, n_s = 0}^{\infty} e^{-\frac{\pi}{a}\sum_{k=1}^{s} n_k \omega_k} |n_1, n_2, \ldots, n_s, out\rangle \otimes |n_1, n_2, \ldots, n_s, in\rangle. \tag{8.25}$$

Here it is clear that C is a normalization constant. To determine it, we impose

$$1 = \langle 0_M | 0_M \rangle = |C|^2 \left(\sum_{n_1=0}^{\infty} e^{-\frac{2\pi n_1 \omega_1}{a}} \right) \left(\sum_{n_2=0}^{\infty} e^{-\frac{2\pi n_2 \omega_2}{a}} \right) ... \left(\sum_{n_s=0}^{\infty} e^{-\frac{2\pi n_s \omega_s}{a}} \right). \tag{8.26}$$

Thus the normalized Minkowski vacuum can be written as

$$|0_M\rangle = \sqrt{\prod_{k=1}^{s} \left(1 - e^{-\frac{2\pi\omega_k}{a}}\right)} \sum_{n_1,...,n_s=0}^{\infty} e^{-\frac{\pi}{a}\sum_{k=1}^{s} n_k \omega_k} |n_1, ..., n_s, out\rangle \otimes |n_1, ..., n_s, out\rangle . \tag{8.27}$$

This expression can be cast into a more compact form by rewriting the vacuum as an explicitly expanded Fock-state exponential. After a straightforward computation, we arrive at

$$|0_M\rangle = \sqrt{\prod_{k=1}^{s} \left(1 - e^{-\frac{2\pi\omega_k}{a}}\right)} \exp\left\{ \sum_{k=1}^{s} e^{-\frac{\pi\omega_k}{a}} a^{\dagger}_{out}(\omega_k) \otimes a^{\dagger}_{in}(\omega_k) \right\} |0_{out}\rangle \otimes |0_{in}\rangle . \tag{8.28}$$

The next task is to determine the density matrix as perceived by a uniformly accelerated observer, assuming that an inertial observer in Minkowski spacetime measures no particle flux, i.e., that the quantum state is the Minkowski vacuum given in Eq. (8.28). This density matrix is constructed by taking the partial trace, as defined in Eq. (8.6), over the degrees of freedom corresponding to the inaccessible region A:

$$\begin{aligned} \hat{\rho}_{out} &= \mathrm{Tr}_{in}\{|0_M\rangle \langle 0_M|\} \\ &= \sum_{n_1,n_2,...,n_s=0}^{\infty} \langle n_1, ..., n_s, in|0_M|n_1, ..., n_s, in|0_M\rangle \langle 0_M|n_1, ..., n_s, in|0_M|n_1, ..., n_s, in\rangle . \end{aligned} \tag{8.29}$$

By substituting Eq. (8.28) directly and carrying out the resulting algebra, we obtain:

$$\hat{\rho}_{out} = \left[\prod_{k=1}^{s} \left(1 - e^{-\frac{2\pi\omega_k}{a}}\right) \right] \sum_{n_1,...,n_s=0}^{\infty} e^{-\frac{2\pi}{a}\sum_{k=1}^{s} n_k \omega_k} |n_1, ..., n_s, out\rangle \langle n_1, ..., n_s, out| . \tag{8.30}$$

Our first observation is that the resulting density matrix is diagonal. Furthermore, since the energy of the state $|n_1, n_2, \ldots, n_s, out\rangle$ is given by $\sum_{k=1}^{s} n_k\omega_k$, it follows that the emitted radiation is described by a thermal state. The overall prefactor in Eq. (8.30) can therefore be interpreted as the inverse partition function, and the associated temperature is readily obtained:

$$\hat{\rho}_{out} = \frac{1}{\mathcal{Z}} e^{-\beta H} \quad \Longrightarrow \quad \mathcal{Z} = \prod_{k=1}^{s} \frac{1}{1 - e^{-\frac{2\pi\omega_k}{a}}} \quad \wedge \quad T = \frac{a}{2\pi}. \tag{8.31}$$

Thus, we have explicitly recovered the Bose–Einstein distribution for a one–dimensional ideal gas [8]. As a consequence, we have demonstrated that a uniformly accelerated observer measures a thermal flux of particles with a temperature proportional to the observer's proper acceleration, cf. Eq. (8.31). The remaining task in this section is to compute the von Neumann entropy of the radiation as perceived by the Rindler observer (we work in units where $k_B = 1$):

$$\begin{aligned}
S_{VN} &= -\operatorname{Tr}\{\hat{\rho}_{out}\ln\hat{\rho}_{out}\} = -C^2 \sum_{n_1,n_2,\dots n_s=0}^{\infty} e^{-\frac{2\pi}{a}\sum_{k=1}^{s} n_k\omega_k} \ln\left(C^2 e^{-\frac{2\pi}{a}\sum_{k=1}^{s} n_k\omega_k}\right) \\
&= -\ln C^2 + \frac{2\pi}{a}C^2 \sum_{n_1,n_2,\dots,n_s=0}^{\infty} e^{-\frac{2\pi}{a}\sum_{k=1}^{s} n_k\omega_k}(n_1\omega_1 + n_2\omega_2 + \dots + n_s\omega_s) \\
&= -\ln C^2 + \frac{2\pi}{a}C^2 \left[\left(\sum_{n_1=0}^{\infty} e^{-\frac{2\pi n_1\omega_1}{a}} n_1\omega_1\right)\left(\sum_{n_2=0}^{\infty} e^{-\frac{2\pi n_2\omega_2}{a}}\right)\dots\left(\sum_{n_s=0}^{\infty} e^{-\frac{2\pi n_s\omega_s}{a}}\right) + \dots\right] \\
&= -\ln C^2 + \frac{2\pi}{a}\sum_{k=1}^{s}\frac{\sum_{n=0}^{\infty} e^{-\frac{2\pi n\omega_k}{a}} n\omega_k}{\sum_{n=0}^{\infty} e^{-\frac{2\pi n\omega_k}{a}}} = -\sum_{k=1}^{s}\ln\left(1 - e^{-\frac{2\pi\omega_k}{a}}\right) + \frac{2\pi}{a}\sum_{k=1}^{s}\frac{\omega_k}{e^{\frac{2\pi\omega_k}{a}} - 1} \\
&= -\frac{L}{2\pi}\int_0^{\infty} d\omega \ln\left(1 - e^{-\frac{2\pi\omega}{a}}\right) + \frac{L}{a}\int_0^{\infty}\frac{\omega d\omega}{e^{\frac{2\pi\omega}{a}} - 1} \\
&= \frac{L}{2\pi}\left[-\omega\ln\left(1 - e^{-\frac{2\pi\omega}{a}}\right)\Big|_0^{\infty} + \int_0^{\infty}\frac{\omega d\omega}{1 - e^{-\frac{2\pi\omega}{a}}}\left(-e^{-\frac{2\pi\omega}{a}}\right)\left(-\frac{2\pi}{a}\right)\right] + \frac{L}{a}\int_0^{\infty}\frac{\omega d\omega}{e^{\frac{2\pi\omega}{a}} - 1}
\end{aligned} \tag{8.32}$$

In the fifth line we replaced the discrete sum over modes by a continuous integral. Here, L denotes the dimension of spacetime expressed in the σ^- coordinate, which is naturally adapted to the Rindler observer. In the final line we performed an integration by parts. The boundary term vanishes, and the two remaining contributions are identical. Proceeding with the evaluation leads to:

$$S_{VN} = \frac{2L}{a}\int_0^{\infty}\frac{\omega d\omega}{e^{\frac{2\pi\omega}{a}} - 1} = \frac{2L}{a}\left(\frac{a}{2\pi}\right)^2\int_0^{\infty}\frac{\xi d\xi}{e^{\xi} - 1} = \frac{aL}{2\pi^2}\frac{\pi^2}{6} = \frac{aL}{12} \Longrightarrow S_{VN} = \frac{\pi LT}{6}. \tag{8.33}$$

Thus, we have derived the entropy of a one–dimensional gas [8], in agreement with the expected result. The only remaining step is to determine the length L. This quantity corresponds to the length of the interval in the σ^-_{out} coordinate. However, this interval is unbounded, since $\sigma^-_{out} \in (-\infty, \infty)$. Consequently, we must introduce an ultraviolet (UV) cut-off $X^-_{\min}$ and an infrared (IR) cut-off $X^-_{\max}$ [26]. We define these cut-offs in globally flat coordinates, i.e. in terms of x^-. Hence,

$$S_{VN} = \frac{aL}{12} = \frac{a}{12}\left[\max\{\sigma^-_{in}\} - \min\{\sigma^-_{in}\}\right] = \frac{\cancel{a}}{12}\frac{1}{\cancel{a}}\ln\frac{X^-_{\max}}{X^-_{\min}} = \frac{1}{12}\ln\frac{X^-_{\max}}{X^-_{\min}}. \tag{8.34}$$

Besides characterizing the acceleration of the Rindler observer, the parameter a also specifies the observer's trajectory (see App. D.3). We see that the final expression does not depend on the detailed shape of the trajectory, i.e. on the particular hypersurface that intersects the endpoints of region A, but only on those endpoints themselves. In this framework, the UV cut-off encodes arbitrarily small length scales around $x^- = 0$. For this reason, it is often referred to as the short–distance parameter and denoted by δ^-.

To obtain the full entropy of the radiation detected by a Rindler observer, we must include both right–moving and left–moving modes. Incorporating the left–moving sector simply introduces the additional cut-offs $X^+_{\max\,/\,\min}$, so that the total entropy is [26]:

$$S_{VN} = \frac{1}{12}\ln\frac{X^+_{max}X^-_{max}}{\delta^2}. \tag{8.35}$$

Here, we have defined the short–distance parameter $\delta = \sqrt{\delta^+\delta^-}$, which is Lorentz invariant, unlike the individual quantities $\delta^\pm$, which are the components of a vector. The divergence near $x^- = 0$ stems from the entanglement between field modes localized infinitesimally to the left of this point and those localized infinitesimally to the right. Consequently, the parameter δ is always present, even when region A is of finite size. This is not problematic, since δ is invariant under all spacetime symmetries and therefore does not influence any physical observable or any intermediate step in the calculation; it effectively plays the role of an integration constant. One may also regularize the entropy to handle this divergence explicitly. Finally, the logarithmic dependence of the entropy is anticipated, as it reflects the invariance of the entropy under rescalings of the vacuum fluctuations of a massless scalar field.

Finally, it is necessary to analyze several properties of the transformation $\sigma^- = \sigma^-(x^-)$, shown in Fig. 8.3, to enable its extension to more general forms of the inaccessible region A:

- The mappings $\sigma^-_{out}(x^-)$ and $\sigma^-_{in}(x^-)$ are bijective on their respective domains and therefore each possesses a well-defined inverse.
- In both regions, the coordinate σ^- ranges over the entire real axis, $(-\infty, +\infty)$.
- The time coordinate associated with σ^- runs in opposite directions in regions A and A'. This is a consequence of the differing monotonicity properties of the functions σ_{in} and σ_{out}.
- At the interface between A and A', both functions approach the same limiting value (in this example, $+\infty$). This allows one to define an analytic continuation across the boundary.

In the remainder of this section, we adopt the derivations given in [26].

8.2.2 Minkowski vacuum and a region of type: $A = [x_1^+, x_2^+] \times [x_1^-, x_2^-]$

We now generalize the results obtained in the previous section to an arbitrary finite region A. As shown earlier, the key step is to introduce a suitable coordinate system that meets the conditions specified at the end of the preceding section, thereby enabling a clear and unambiguous distinction between the regions A and A'. In Fig. 8.4, a generic region A is illustrated. The constant a that appears here should not be interpreted as an acceleration; it is introduced purely to maintain dimensional consistency. This parameter determines the precise shape of the trajectory within region A [125]. For a region A of this type, an appropriate coordinate transformation is:

$$\sigma^-_{in} = -\frac{1}{a}\ln\frac{x^- - x_1^-}{x_2^- - x^-}, \quad \sigma^-_{out} = -\frac{1}{a}\ln\frac{x_1^- - x^-}{x_2^- - x^-}. \tag{8.36}$$

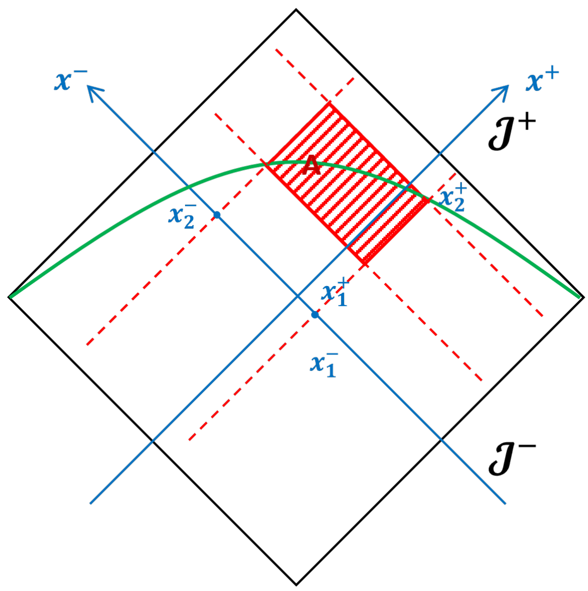

Figure 8.4: Arbitrary region A that contains the inaccessible degrees of freedom.

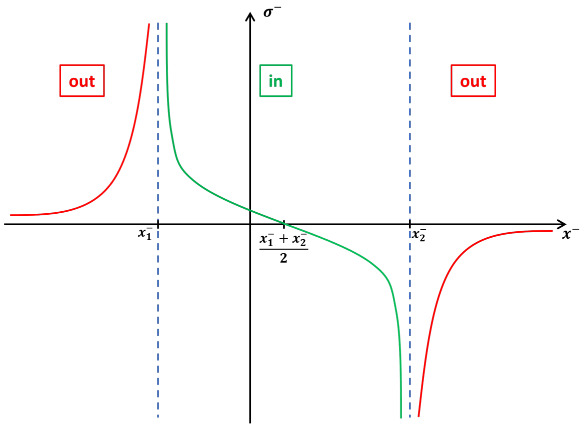

Figure 8.5: Function $\sigma^- = \sigma^-(x^-)$ for the case of an arbitrary region A.

We immediately notice that the expressions in Eq. (8.36) can be rewritten in terms of an absolute value, yielding

$$\sigma^- = -\frac{1}{a}\ln\left|\frac{x^- - x_1^-}{x_2^- - x^-}\right|, \tag{8.37}$$

which is directly analogous to the Unruh case shown in Eq. (8.9). The behavior of this function in the *in* region (green) and the *out* region (red) of the spacetime is illustrated in Fig. 8.5. In particular, the function displays behavior analogous to the coordinate transformation that yields Rindler coordinates.

From the construction above, it immediately follows that the functions σ_{in}^- and σ_{out}^-, defined in this way, are monotonic on their respective domains, although each exhibits a different type of monotonicity. In addition, on their domains both functions take all real values in the interval $(-\infty, +\infty)$. Hence, σ_{in}^- and σ_{out}^- are both bijections. We therefore confirm that all four conditions established in the previous chapter are fulfilled.

Let us now interpret the meaning of these newly defined coordinates. Introducing $\sigma^\pm = \tau \pm \sigma$ and rewriting the metric in terms of these variables, we find:

$$ds^2 = a^2(x_2^- - x_1^-)(x_2^+ - x_1^+)\frac{-d\tau^2 + d\sigma^2}{4\left(\cosh\left(a\tau\right) + \cosh\left(a\sigma\right)\right)^2}. \tag{8.38}$$

To understand what the $\sigma =$ const. curves represent, we introduce the constant $c = e^{2a\sigma}$, which labels a specific trajectory, and determine the corresponding curve in the (t, x) coordinates. This yields:

$$\left(x - \frac{c(x_2^+ - x_1^-) + x_2^- - x_1^+}{2(c-1)}\right)^2 - \left(t - \frac{c(x_2^+ + x_1^-) - x_2^- - x_1^+}{2(c-1)}\right)^2 = \frac{c(x_2^- - x_1^-)(x_2^+ - x_1^+)}{(c-1)^2}. \tag{8.39}$$

It is clear that this equation describes a hyperbola, analogous to the case of Rindler coordinates, presented in App. D.3. This is precisely the curve passing through the boundary points of the region A, and at the same time it corresponds to a segment of the worldline of a Rindler observer whose proper acceleration is proportional to the inverse of the area of the region A. Thus, we see that we have indeed constructed a direct generalization of the Rindler coordinates to a finite inaccessible region A.

We now follow a procedure fully analogous to that used for the Rindler observer. We first introduce the *in* and *out* modes in a completely analogous fashion:

$$\begin{aligned}
\phi_{in}^\omega &= \frac{1}{\sqrt{4\pi\omega}}\left[\theta(x^- - x_1^-) - \theta(x_2^- - x^-)\right] e^{i\omega\sigma_{in}^-}, \\
\phi_{out}^\omega &= \frac{1}{\sqrt{4\pi\omega}}\left[\theta(x^- - x_2^-) + \theta(x_1^- - x^-)\right] e^{-i\omega\sigma_{out}^-}.
\end{aligned} \tag{8.40}$$

The subsequent steps in the entropy computation are identical and thus lead to the same intermediate expression as in Eq. (8.34), namely:

$$S_{VN} = \frac{a}{12}\left[\sigma_{in}^-(x_1^- + \delta_1^-) - \sigma_{in}^-(x_2^- - \delta_2^-)\right] = \frac{1}{12}\left[\ln\frac{x_2^- - x_1^-}{\delta_2^-} - \ln\frac{\delta_1^-}{x_2^- - x_1^-}\right]. \tag{8.41}$$

Here, we subtract in the opposite order because $\sigma_{in}^{-}(x^{-})$ is a monotonically decreasing function. Note also that we have again introduced a short–distance cut–off. We now clarify the meaning of the parameters $\delta^{\pm}$. As anticipated, UV divergences arise at the boundaries of region A, where short–wavelength modes become highly entangled. To regularize these divergences, we introduce the short–distance cut–off δ. One may interpret this as follows: we consider all admissible spacelike hypersurfaces and assign to each of them a layer of thickness δ at the boundary of the inaccessible region A. In this sense, δ specifies a particular foliation of spacetime.

In order to obtain the full expression for the entropy, we must also include the contribution from the left–propagating modes, which yields

$$S_{VN} = \frac{1}{12} \ln \frac{(x_2^{+} - x_1^{+})^2 (x_2^{-} - x_1^{-})^2}{\delta_1^{+} \delta_1^{-} \delta_2^{+} \delta_2^{-}}. \tag{8.42}$$

This result admits an alternative interpretation: it can be written as the sum of two Rindler–like contributions, each term associated with one of the boundaries of the region A. In this picture, the squared spacetime separation effectively plays the role of the IR cutoff parameter introduced in Eq. (8.35).

However, Eq. (8.42) does not capture the full entropy. In particular, there is an extra contribution that must be included, originating from the exclusion of the $\omega = 0$ mode in the previous analysis. This contribution cannot be ignored, because it corresponds to an infinite set of quantum states. Inside region A this mode is constant, but outside A it can decay in infinitely many distinct ways. Let us first clarify which modes were actually incorporated in the derivation of Eq. (8.42). We have included those modes that are narrow compared to the size of the interval $[x_1^{-}, x_2^{-}]$, i.e., modes with short wavelengths. Consequently, such modes cross either the boundary at $x^{-} = x_1^{-}$ or the boundary at $x^{-} = x_2^{-}$. We therefore interpret Eq. (8.42) as representing the sum of the contributions to the entropy arising from the entanglement between states localized near one boundary of the interval and states localized near the opposite boundary. The modes that were omitted are those that span the entire interval, namely the long-wavelength modes. One can demonstrate that these long-wavelength modes are maximally entangled with the spatially constant mode within the interval [26], so that the vacuum can be written as

$$|0_M\rangle = |\text{short}\rangle \otimes |\text{long}\rangle \otimes |\text{uncorrelated}\rangle \,. \tag{8.43}$$

Here, $|\text{short}\rangle$ denotes the short-wavelength modes, whose effect is already accounted for in Eq. (8.42), while $|\text{uncorrelated}\rangle$ represents modes that are sharply localized, either fully inside the interval or fully outside it. Finally, $|\text{long}\rangle$ corresponds to modes with wavelengths larger than the width of the interval, whose contribution is still missing. We anticipate that the long-wavelength sector can be expanded as:

$$|\text{long}\rangle \propto \prod_{k=0}^{\max} \sum_{n_k=0}^{\infty} |n_k, R\rangle \otimes |n_k, L\rangle \otimes |n_k, in\rangle \,. \tag{8.44}$$

Since all these modes have wavelengths larger than the size of the interval, we can regard the k-th mode as having an effective width $2^k(x_2^{-} - x_1^{-})$, i.e. it extends over a region that is 2^k times wider than the interval itself; n_k labels the occupation number of this mode. The states $|n_k, R\rangle$ describe the portion of the k-th mode that lies to the right of the interval, meaning $x^{-} > x_2^{-}$, while the states $|n_k, L\rangle$ describe the portion of the k-th mode that lies to the left of the interval, i.e., $x^{-} < x_1^{-}$. The remaining states, denoted $|n_k, in\rangle$, correspond to the part of the k-th mode that is supported within the interval. This is precisely the contribution associated with the $\omega = 0$ mode. Because this component is maximally entangled with both $|n_k, R\rangle$ and $|n_k, L\rangle$ (as follows from Eq. (8.44)), tracing out $|n_k, in\rangle$ yields the same reduced state as tracing out $|n_k, L\rangle \otimes |n_k, in\rangle$ (or equivalently, $|n_k, R\rangle \otimes |n_k, in\rangle$). We are thus led to conclude that the construction of the density matrix for the $\omega = 0$ mode is equivalent to tracing over either the left-hand part or the right-hand part of the interval. Consequently, in this situation as well, we may employ the same entropy formula as in the Rindler case, namely the one given in Eq. (8.35).

In Fig. 8.6, a single long-wavelength mode is depicted. The argument can be formulated as follows: because the mode remains constant over the interval $[x_1^-, x_2^-]$, compressing this interval does not alter the result in any essential way. If we shrink the interval length to zero, we clearly recover the Rindler case. Consequently, the interval width can be interpreted as the thickness of the hypersurface at $x^- = 0$, which corresponds to introducing a short-distance cuto-ff parameter. Thus, we identify $\delta = x_2^- - x_1^-$.

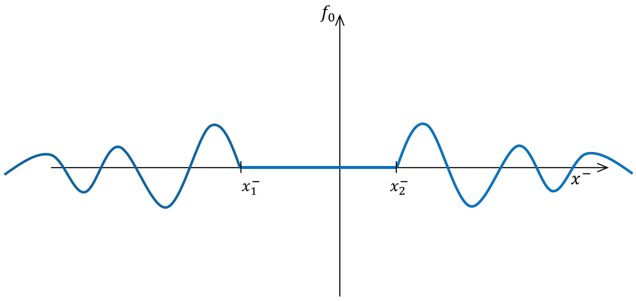

Figure 8.6: Representation of the behavior of the single long–wavelength mode.

It is now evident that the length of the interval acts as the UV cut-off. Naturally, an IR cut-off is also required, just as in the Rindler setup in Eq. (8.35). In this case, the contribution of the long–wavelength modes to the entropy takes the form

$$S_{VN,\text{long}} = \frac{1}{12} \ln \frac{X^-_{\text{max}}}{x_2^- - x_1^-}. \tag{8.45}$$

Including the left–moving modes and combining this with the short–wavelength contribution previously obtained in Eq. (8.42), we arrive at the following expression for the entropy associated with a general inaccessible region A:

$$S_{VN} = \frac{1}{6} \ln \frac{(x_2^+ - x_1^+)(x_2^- - x_1^-)}{\delta_1 \delta_2} + \frac{1}{12} \ln \frac{X^+_{\text{max}} X^-_{\text{max}}}{(x_2^+ - x_1^+)(x_2^- - x_1^-)}. \tag{8.46}$$

Here we introduce the shorthand notation $\delta_1 = \sqrt{\delta_1^+ \delta_1^-}$ and $\delta_2 = \sqrt{\delta_2^+ \delta_2^-}$, which we once more express in a Lorentz–invariant form. The Minkowski interval $(x_2^+ - x_1^+)(x_2^- - x_1^-)$ is itself Lorentz invariant, and therefore the complete expression for the von Neumann entropy is Lorentz invariant as well. It is also crucial that δ be independent of the spacetime point, since we require the foliation to be uniform throughout spacetime. This condition will play an important role in the extension to the curved spacetime discussed in the following section. Finally, it should be emphasized that the contribution from the $\omega = 0$ mode is irrelevant for the applications to black hole thermodynamics.

8.2.3 Generalization to the curved spacetime

In this subsection, we extend the results of the previous section to the case of curved spacetime, focusing in particular on Eq. (8.42). Before doing so, we first generalize the discussion to an arbitrary quantum state defined on Minkowski spacetime. This state need not coincide with the Minkowski vacuum; instead, it may be the vacuum associated with some other choice of coordinates. The only essential requirement is that a globally inertial coordinate system exists, i.e. the underlying spacetime is still Minkowski.

Assume now that an observer associated with the coordinates $y^{\pm} = y^{\pm}(x^{\pm})$ detects no particle flux and therefore perceives the vacuum. In this description the quantum state is not the Minkowski vacuum $|0, x\rangle$, but rather $|\psi\rangle = |0, y\rangle$. We can then repeat precisely the same construction as in the Unruh case, but carried out in the $y^{\pm}$ coordinate system. Since the logic is unchanged, we can immediately write that the von Neumann entropy associated with the right–moving modes is:

$$S_{VN} = \frac{1}{12} \ln \frac{(y_2^- - y_1^-)^2}{\hat{\delta}_1^- \hat{\delta}_2^-}, \tag{8.47}$$

which constitutes a straightforward generalization of Eq. (8.41). Here we have again discarded the contribution from the zero mode. It should in principle be treated separately, but as it does not play a role in our black–hole analysis, we omit it. What becomes apparent, however, is that the short–distance cut–off now depends on the position in spacetime. Since at the end of the previous section we argued that such position dependence is undesirable, we must express it in terms of Minkowski coordinates. Interpreting it as a vector of length dimension, we obtain:

$$\hat{\delta}^{\mu} = \frac{\partial y^{\mu}}{\partial x^{\nu}} \delta^{\nu} \quad \Longrightarrow \quad \hat{\delta}^- = \frac{\mathrm{d}y^-}{\mathrm{d}x^-}\delta^- \;\wedge\; \hat{\delta}^+ = \frac{\mathrm{d}y^+}{\mathrm{d}x^+}\delta^+, \tag{8.48}$$

where the quantities $\delta^{\pm}$ are indeed constants throughout the entire spacetime. Consequently, the straightforward generalization of Eq. (8.42) takes the form:

$$S_{VN} = \frac{1}{12} \ln \frac{(y_2^+ - y_1^+)^2 (y_2^- - y_1^-)^2}{y_1^{+'} y_1^{-'} y_2^{+'} y_2^{-'} \delta_1^+ \delta_1^- \delta_2^+ \delta_2^-}. \tag{8.49}$$

Since $\delta^{\pm}_{1,2}$ are now specified in globally inertial coordinates, the above expression is indeed Lorentz invariant. In two dimensions we can always adopt the conformal gauge of Eq. (3.2). The mapping between the $y^{\pm}$ and $x^{\pm}$ coordinates is itself conformal, so we obtain:

$$ds^2 = -dx^+dx^- = -\frac{\mathrm{d}x^+}{\mathrm{d}y^+}\frac{\mathrm{d}x^-}{\mathrm{d}y^-}\mathrm{d}y^+\mathrm{d}y^- = -e^{2\rho}\mathrm{d}y^+\mathrm{d}y^- \quad \Longrightarrow \quad y^{+'} y^{-'} = e^{-2\rho}. \tag{8.50}$$

Using this relation, we arrive at the main result of this section:

$$S_{VN} = \frac{1}{12} \ln \frac{(y_2^+ - y_1^+)^2 (y_2^- - y_1^-)^2}{\delta^4 e^{-2\rho_1} e^{-2\rho_2}} \quad \wedge \quad ds^2 = -e^{2\rho} dy^+ dy^-. \tag{8.51}$$

This expression is significant because it also extends to curved spacetime. In that setting, we may again define the vacuum with respect to some coordinates $y^{\pm}$. The only subtlety in the previous reasoning concerns whether δ can be treated as a constant and what that notion means in curved spacetime. Although we lack globally inertial coordinates in curved spacetime, we do possess locally inertial frames. The framework remains self-consistent provided that δ is defined in locally flat coordinates at the relevant spacetime points, which we are always free to do. Consequently, the von Neumann entropy is invariant under local Lorentz transformations. In addition, we may still perform an arbitrary $SL(2, \mathbb{C})$ transformation on the $y^{\pm}$ coordinates, reflecting the symmetries of the quantum vacuum. Therefore the action of the $SL(2, \mathbb{C})$ group must leave the von Neumann entropy unchanged, and this requirement is indeed fulfilled.

We must also introduce a further condition on ρ, namely that the conformal factor $e^{2\rho}$ remain approximately constant throughout the layer of thickness δ. This requirement guarantees that the spacetime foliation is both well defined and physically meaningful within that region. We now proceed to extend the Rindler expression in Eq. (8.35) to the case of curved spacetime. The extension is straightforward:

$$S_{VN} = \frac{1}{12}\ln\frac{Y^+_{\max}Y^-_{\max}}{\hat{\delta}^+_P\hat{\delta}^-_P} = \frac{1}{12}\ln\frac{Y^+_{\max}Y^-_{\max}}{y^{+'}_P y^{-'}_P\delta^+_P\delta^-_P} \implies S_{VN} = \frac{1}{12}\ln\frac{Y^+_{\max}Y^-_{\max}}{\delta^2 e^{-2\rho_P}}. \tag{8.52}$$

Here, P denotes an arbitrary point that splits spacetime into left and right quadrants. In the original Unruh derivation, this point corresponded to $x^- = 0$.

8.2.4 Spacetime with the reflective boundary conditions

So far, the left- and right-moving modes have been treated as independent, which is appropriate when studying an eternal black hole, where spatial infinity i^0 is the only spacetime boundary. In contrast, for an evaporating black hole, the spacetime—besides having the spatial infinity i^0—also develops a boundary at a finite location. In this situation, one must impose reflective boundary conditions at that finite boundary. Because of these conditions, the left- and right-moving modes cease to be independent; they become correlated, and these correlations must be incorporated when computing the von Neumann entropy. In this subsection, we analyze several distinct setups. We begin with the case in which the boundary is specified by a simple relation between the coordinates, and subsequently extend the discussion to a more general configuration. Finally, we give a comment on possible interference of the wave packets along the constant-time slice.

The spacetime manifold illustrated in Fig. 8.7 is bounded on one side by an idealized, perfectly reflecting mirror, defined by the condition $y^+ = y^-$, and on the other side by future and past null infinity. As a first step, we introduce the coordinate y^+, which parametrizes the left–moving modes on $\mathcal{J}^-$. Next, we define the coordinate y^- in such a way that the relation $y^+ = y^-$ holds precisely on the mirror itself. In Fig. 8.7 clearly displays how the right–moving modes are reflected upon reaching the spacetime boundary. We see that, after reflection, they behave identically to the left–moving modes in the interval $y^+ \in [y_2^-, y_1^-]$ on $\mathcal{J}^-$. Therefore, performing the partial trace over the left– and right–moving modes in the inaccessible region A is equivalent to taking the trace over the interval $A = [y_2^-, y_1^-] \cup [y_1^+, y_2^+]$ on $\mathcal{J}^-$, involving only the left–moving modes.

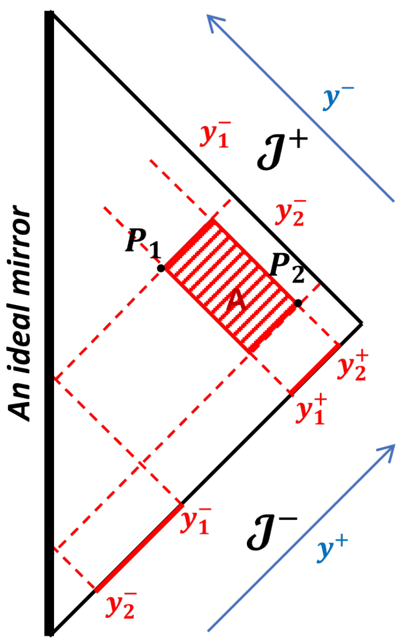

Figure 8.7: Region A that contains the inaccessible degrees of freedom in a spacetime with a boundary represented by an ideal mirror.

In the general scenario shown in Fig. 8.7, one must compute the trace over a region made up of two disconnected intervals. The calculation involved in this case is substantially more complicated, and a full analysis is deferred to the subsequent subsection. Consider instead a spacelike hypersurface Σ and a point P lying on it, as depicted in Fig. 8.8. The causal diamond located above the segment of the hypersurface stretching from point P to the mirror defines the inaccessible region A. In this setup, the two separate intervals effectively coalesce into a single one: $y^+ \in [y_P^-, y_P^+]$. This configuration has already been thoroughly studied in the previous subsection, allowing us to directly write:

$$S_{VN} = \frac{1}{12} \ln \frac{(y_P^+ - y_P^-)^2}{\delta^2 e^{-2\rho_P}}, \tag{8.53}$$

which represents the extension of the Unruh result to the curved spacetime case given in Eq. (8.52).

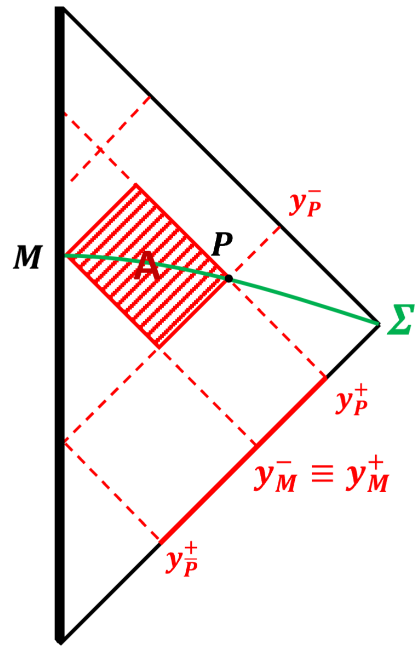

Figure 8.8: Region A that contains the inaccessible degrees of freedom in the spacetime with a boundary.

In the collapse models analyzed in this dissertation, the boundary is not specified by such a relation, but rather by one of the type

$$y^+ - y^- = \text{const.} \tag{8.54}$$

This does not pose any difficulty, because we can apply the same mapping procedure, sending the point P to a single interval on $\mathcal{J}^-$. We then denote its image as the point $\bar{P}$. The corresponding interval on $\mathcal{J}^-$ is given by $y^+ \in [y_{\bar{P}}^+, y_P^+]$. Furthermore, we observe that $\hat{\delta}_{\bar{P}}^+ = \hat{\delta}_P^-$, which implies that $\hat{\delta}_{\bar{P}}^+ \hat{\delta}_P^+ = \delta^2 e^{-2\rho_P}$. Consequently, the generalized expression in the case of a spacetime with reflective boundary conditions and a boundary defined by Eq. (8.54) takes the form:

$$S_{VN} = \frac{1}{12} \ln \frac{(y_P^+ - y_{\bar{P}}^+)^2}{\delta^2 e^{-2\rho_P}}. \tag{8.55}$$

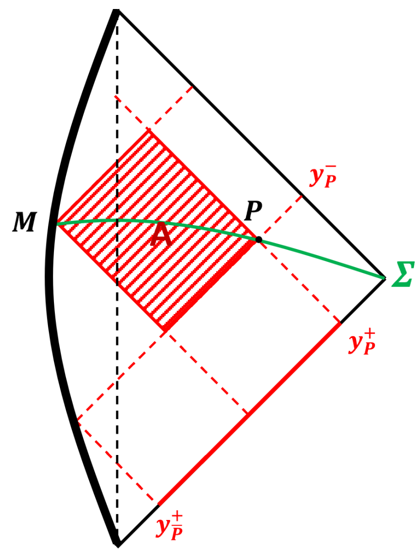

Figure 8.9: Region A that contains the inaccessible degrees of freedom in spacetime with a curved boundary.

It turns out that a small mistake was made in the course of this analysis. Consider two wave packets localized within the interval $y^+ \in [y_{\bar{P}}^+, y_P^+]$ and entangled with modes lying outside this interval. What can occur is that these two wave packets interfere with each other on the hypersurface Σ, and this interference can be destructive. Let us assume that this is exactly what happens. Even though each wave packet is individually entangled with modes outside the interval, their coherent superposition is not entangled with the modes in the A' region on the hypersurface Σ, as a consequence of the destructive interference.

This means that we are effectively assuming a stronger correlation than is actually present. Fig. 8.10 depicts an example of such a scenario. When considering modes whose wavelengths are much smaller than the width of the interval, the resulting error is negligible. As the wavelength of the mode grows, however, the corresponding error increases as well. From dimensional analysis, one finds that this error appears in the formula as a dimensionless constant of order $\mathcal{O}(1)$. Therefore, it is independent of the UV and IR cut–offs and can be absorbed into the short–distance cut–off δ. Moreover, in the context of the island formula (1.6), this constant drops out when determining the island, since that procedure involves the extremization of the fine-grained entropy.

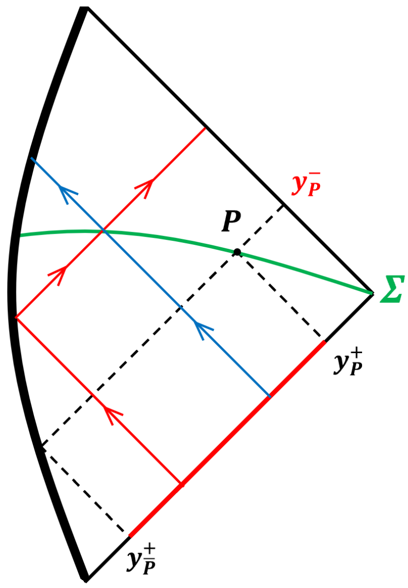

Figure 8.10: Penrose diagram which illustrate the interference of the wave packets.

8.2.5 Case of the two disconnected regions

In this section, we compute the von Neumann entropy for the case of two disjoint intervals, specifically $A = \left([x_1^+, x_2^+] \times [x_1^-, x_2^-]\right) \cup \left([x_3^+, x_4^+] \times [x_3^-, x_4^-]\right)$. This result is crucial for the subsequent study of the island rule in Eq. (1.6) and for deriving the expression of the fine–grained entropy in gravitational systems. In Fig. 8.11, we display the corresponding Penrose diagram, where the disconnected region A is highlighted in red and the constant-time slice is shown in green.

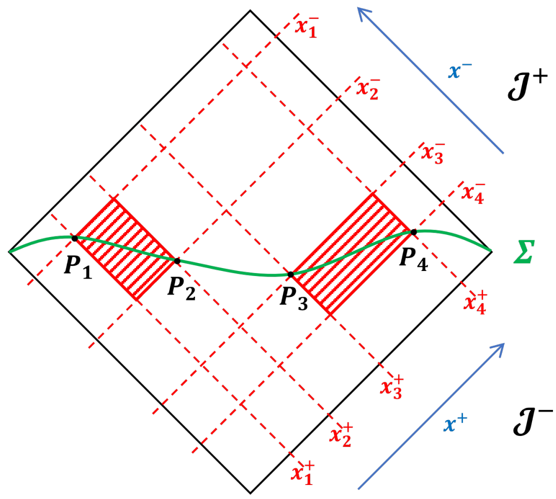

Figure 8.11: Region A, which contains the inaccessible degrees of freedom, in the case where it consists of two disconnected intervals.

A natural first step is to introduce new coordinates obtained by adding the contributions from the two single-interval configurations, and then analyze whether these coordinates satisfy the desired properties.

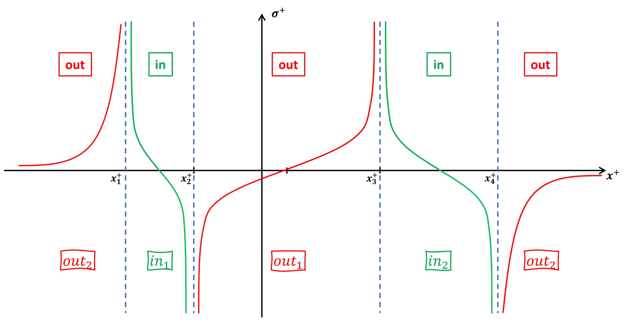

Figure 8.12: Function $\sigma^- = \sigma^-(x^-)$ for a case of a disconnected region A.

By directly summing the contributions in Eq. (8.37) corresponding to the two regions considered here, we obtain

$$\sigma^- = -\frac{1}{a} \ln \left| \frac{x^- - x_1^-}{x_2^- - x^-} \frac{x^- - x_3^-}{x_4^- - x^-} \right|. \tag{8.56}$$

We immediately observe that almost all the necessary conditions are satisfied. The subtlety is that, in this situation, the maps $\sigma^-_{\text{in/out}}$ are not bijective.

Since there are two disconnected regions, in_1 and in_2, in Fig. 8.11, the mapping $\sigma^-_{in}(x^-)$ is in fact a 1–2 mapping rather than a bijection. To address this issue, we introduce the functions $\sigma^-_{in,1}$, $\sigma^-_{in,2}$, $\sigma^-_{out,1}$, and $\sigma^-_{out,2}$, each defined on its respective domain as depicted in Fig. 8.12. In this way, we obtain a bijective correspondence, guaranteeing a one-to-one mapping between the relevant sets. As a result, we identify four distinct types of positive-frequency modes:

$$\begin{aligned}
\phi^\omega_{in,1} &= \frac{1}{\sqrt{4\pi\omega}}\left[\theta(x^- - x_1^-) - \theta(x_2^- - x^-)\right] e^{i\omega\sigma^-_{in,1}}, \\
\phi^\omega_{in,2} &= \frac{1}{\sqrt{4\pi\omega}}\left[\theta(x^- - x_3^-) - \theta(x_4^- - x^-)\right] e^{i\omega\sigma^-_{in,2}}, \\
\phi^\omega_{out,1} &= \frac{1}{\sqrt{4\pi\omega}}\left[\theta(x^- - x_2^-) - \theta(x_3^- - x^-)\right] e^{-i\omega\sigma^-_{out,1}}, \\
\phi^\omega_{out,2} &= \frac{1}{\sqrt{4\pi\omega}}\left[\theta(x^- - x_4^-) + \theta(x_1^- - x^-)\right] e^{-i\omega\sigma^-_{out,2}}.
\end{aligned} \tag{8.57}$$

Upon performing the analytic continuation, the argument of the logarithm becomes positive in both *in* regions and negative in both *out* regions. Hence, the same Bogoliubov coefficient appears as the prefactor of both *in* modes. We therefore infer that the *in*-modes are maximally entangled with one another, allowing us to take suitable linear combinations of these solutions and interpret the result as a new “in"-mode that is consistently defined across both regions. A completely analogous construction applies to the *out*-modes:

$$\phi^\omega_{in} = \phi^\omega_{in,1} + \phi^\omega_{in,2} \quad \wedge \quad \phi^\omega_{out} = \phi^\omega_{out,1} + \phi^\omega_{out,2}. \tag{8.58}$$

Effectively, the problem reduces to that of two regions, *in* and *out*. Consequently, as in all previous cases, we can invoke the result from the Rindler setup in Eq. (8.34), namely:

$$\begin{aligned}
S_{VN} &= -\frac{a}{12}\left[\sigma^-_{in}(x_2^- - \delta_2^-) - \sigma^-_{in}(x_1^- + \delta_1^-) + \sigma^-_{in}(x_4^- - \delta_4^-) - \sigma^-_{in}(x_3^- + \delta_3^-)\right] \\
&= \frac{1}{12}\ln\left|\frac{x_2^- - x_1^-}{\delta_2^-}\frac{x_2^- - x_3^-}{x_4^- - x_2^-}\frac{x_2^- - x_1^-}{\delta_1^-}\frac{x_4^- - x_1^-}{x_1^- - x_3^-}\frac{x_4^- - x_1^-}{x_2^- - x_4^-}\frac{x_4^- - x_3^-}{\delta_4^-}\frac{x_2^- - x_3^-}{x_3^- - x_1^-}\frac{x_4^- - x_3^-}{\delta_3^-}\right| \\
&= \frac{1}{12}\ln\frac{(x_2^- - x_1^-)^2(x_3^- - x_2^-)^2(x_4^- - x_1^-)^2(x_4^- - x_3^-)^2}{(x_4^- - x_2^-)^2(x_3^- - x_1^-)^2\delta_1^-\delta_2^-\delta_3^-\delta_4^-}.
\end{aligned} \tag{8.59}$$

The next step in the analysis is to include the left–moving modes and then to extend the result to curved spacetime. In direct analogy with the earlier sections, this part of the derivation proceeds without difficulty. The final expression is:

$$S_{VN} = \frac{1}{6}\ln\frac{d_{12}^2 d_{23}^2 d_{14}^2 d_{34}^2}{\delta^4 d_{24}^2 d_{13}^2 e^{-\rho_1}e^{-\rho_2}e^{-\rho_3}e^{-\rho_4}}, \text{ with } d_{ij}^2 = (x_i^+ - x_j^+)(x_i^- - x_j^-). \tag{8.60}$$

Here, d_{ij} denote the Minkowski separations between the endpoints of the regions illustrated in Fig. 8.11. As in the previous discussion, the $\omega = 0$ mode requires a separate treatment. We do not address this issue here, since it is not directly relevant to the study of Hawking radiation from black holes. If one of the endpoints lies at infinity, the corresponding d_{ij} factors must be replaced using appropriate IR cut–offs, and the formula continues to hold in those situations as well. Eq. (8.60) thus provides the most general form of the Von Neumann entropy for quantum fields on a fixed classical spacetime background needed to evaluate the fine-grained entropy in gravitational systems, as specified in Eq. (1.6).

It remains to examine the scenario in which the spacetime manifold includes a spacetime boundary obeying reflective boundary conditions, while the opposite endpoint of the region A does not coincide with this boundary. This configuration is relevant for an evaporating black hole. We have previously shown that it corresponds to a setup with two disconnected intervals on $\mathcal{J}^-$, namely $A = [y_{\bar{2}}^+, y_{\bar{1}}^+] \cup [y_1^+, y_2^+]$. This situation is depicted in Fig. 8.13; the inaccessible region A is shaded in red, while the constant-time slice is illustrated in green as usual. We should also emphasize that there is a residual error due to the destructive interference of the wave packets; however, this term can again be consistently absorbed into the UV cut–off. It is a constant contribution and therefore does not affect the extremization procedure associated with the island formula in Eq. (1.6). The formula follows directly from Eq. (8.59):

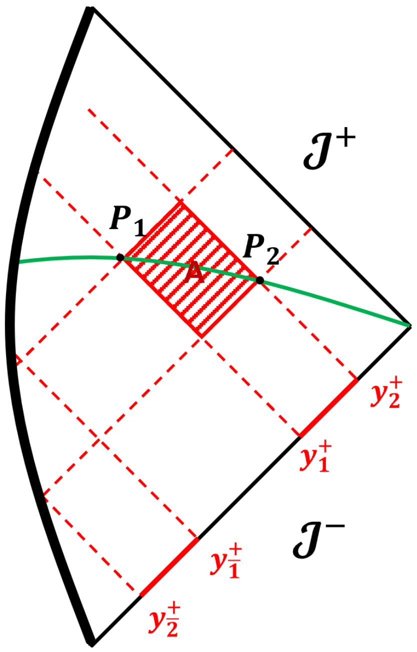

Figure 8.13: Region A that contains the inaccessible degrees of freedom in the case of the spacetime with reflective boundary conditions.

$$S_{VN} = \frac{1}{12} \ln \frac{(x_1^+ - x_2^+)^2 (x_{\bar{1}}^+ - x_{\bar{2}}^+)^2 (x_{\bar{1}}^+ - x_1^+)^2 (x_{\bar{2}}^+ - x_2^+)^2}{\delta^4 (x_{\bar{2}}^+ - x_1^+)^2 (x_{\bar{1}}^+ - x_2^+)^2 e^{-2\rho_1} e^{-2\rho_2}}. \tag{8.61}$$

To conclude this section, we emphasize that Eqs. (8.60) and (8.61) constitute the central results of this section. They are essential for evaluating the fine–grained entropy in gravitational systems (1.6) when an island is present, and thereby for reproducing the Page curve.

8.3 Quantum states and the black hole entropy

So far, we have determined the semi-classical component of the island formula (1.6). Before turning to a detailed explanation of this formula in Sec. 8.4, we now examine the area term in the fine-grained entropy. In many situations, this term can be treated using the purely classical Bekenstein–Hawking expression (1.4). Nevertheless, in certain cases it must be supplemented by a quantum correction.

This section is divided into three subsections. In the first, we introduce the notion of coherent states. This discussion is especially important, since coherent states provide a canonical reference state for a broad class of physical systems found in nature. We then turn to the coarse-grained entropy of the black hole, with the aim of determining the quantum correction to the Bekenstein–Hawking entropy formula. In these two subsections, we continue to follow the framework of [26]. Finally, we investigate the entropy carried by Hawking radiation and formulate the Hawking information paradox (in the sense of [1]), which constitutes the main subject of the present study.

8.3.1 Matter in coherent state

Up to this point, the quantum state of the scalar field has always been taken to be a vacuum state in some choice of coordinates. The only operation we have performed is a change of coordinates with respect to which this vacuum is defined. In contrast, for the quantum state describing matter, one typically expects a coherent state. The aim of this subsection is to demonstrate that the von Neumann entropy of a coherent state constructed on top of a given vacuum is equal to the von Neumann entropy of that vacuum itself. To this end, we introduce a simple model that captures the essential features of the situation.

Our model consists of two decoupled linear harmonic oscillators with annihilation operators a_1 and a_2. This is equivalent to a bosonic system with two levels. We now perform the most general Bogoliubov transformation that preserves the canonical commutation relations, as outlined in App. D.2, and define the new annihilation operators by:

$$a_1(\gamma) = \frac{1}{\sqrt{1-\gamma^2}}\left(a_1 - \gamma a_2^\dagger\right) \quad \wedge \quad a_2(\gamma) = \frac{1}{\sqrt{1-\gamma^2}}\left(a_2 - \gamma a_1^\dagger\right), \tag{8.62}$$

where $\gamma \in \mathbb{R}$ with $|\gamma| < 1$. By following the same steps used to construct the Minkowski vacuum, we can also construct the corresponding vacuum in this setting and write it in terms of the product vacuum of the two uncoupled oscillators:

$$|0_\gamma\rangle = \sqrt{1-\gamma^2}\, e^{\gamma a_1^\dagger \otimes a_2^\dagger} |0_1\rangle \otimes |0_2\rangle = \sqrt{1-\gamma^2} \sum_{n=0}^{\infty} \gamma^n |n,1\rangle \otimes |n,2\rangle\,. \tag{8.63}$$

As in the Minkowski-vacuum case, we can obtain the reduced density matrix associated with the first mode by tracing out the degrees of freedom of the second mode:

$$\rho_1^\gamma = \mathrm{Tr}_2\{|0_\gamma\rangle\langle 0_\gamma|\} = (1-\gamma^2)\sum_{n=0}^{\infty}\gamma^{2n}|n,1\rangle\langle n,1|\,. \tag{8.64}$$

We recognize this as a thermal density matrix, with an effective temperature defined through $e^{-\beta\omega} = \gamma^2$, where ω is the frequency of the first oscillator. We now construct the corresponding coherent state, defined as a simultaneous eigenstate of the transformed annihilation operators:

$$a_1(\gamma)|\gamma,\alpha_1,\alpha_2\rangle = \alpha_1|\gamma,\alpha_1,\alpha_2\rangle \quad \wedge \quad a_2(\gamma)|\gamma,\alpha_1,\alpha_2\rangle = \alpha_2|\gamma,\alpha_1,\alpha_2\rangle\,. \tag{8.65}$$

A general state in this basis can be expanded as:

$$|\gamma,\alpha_1,\alpha_2\rangle = \sum_{n_1,n_2=0}^{\infty} A_{n_1 n_2}|n_1,n_2\rangle\,, \tag{8.66}$$

with $A_{n_1 n_2}$ unknown coefficients. Substituting this expansion into the eigenvalue equations above and using the standard action of the annihilation operators on Fock states, we obtain the following recursion relations for the coefficients:

$$A_{n_1 n_2} = \frac{\alpha_1}{\sqrt{n_1}}A_{n_1-1,n_2} \;\wedge\; A_{n_1 n_2} = \frac{\alpha_2}{\sqrt{n_2}}A_{n_1,n_2-1} \quad \Longrightarrow \quad A_{n_1 n_2} = \frac{\alpha_1^{n_1}\alpha_2^{n_2}}{\sqrt{n_1!n_2!}}C, \tag{8.67}$$

where C is a normalization factor. We determine C from the normalization condition:

$$1 = \langle\gamma,\alpha_1,\alpha_2|\gamma,\alpha_1,\alpha_2\rangle = |C|^2\sum_{n_1,n_2=0}^{\infty}\frac{|\alpha_1|^{2n_1}|\alpha_2|^{2n_2}}{n_1!n_2!} = |C|^2 e^{|\alpha_1|^2+|\alpha_2|^2}. \tag{8.68}$$

Consequently, the normalized coherent state takes the form:

$$|\gamma, \alpha_1, \alpha_2\rangle = e^{-\frac{1}{2}\left(|\alpha_1|^2+|\alpha_2|^2\right)} e^{\alpha_1 a_1^\dagger(\gamma)+\alpha_2 a_2^\dagger(\gamma)} |0_\gamma\rangle \,. \tag{8.69}$$

Having constructed the coherent state, we now proceed to evaluate the entropy associated with it. To this end, we first introduce shifted annihilation operators:

$$\hat{a}_1(\gamma) = a_1(\gamma) - \alpha_1 \;\wedge\; \hat{a}_2(\gamma) = a_2(\gamma) - \alpha_2 \implies \hat{a}_1(\gamma)\,|\gamma, \alpha_1, \alpha_2\rangle = \hat{a}_2(\gamma)\,|\gamma, \alpha_1, \alpha_2\rangle = 0. \tag{8.70}$$

In this way, we define the operators $\hat{a}_{1,2}(\gamma)$, which annihilate the coherent state; in other words, the coherent state plays the role of the vacuum for these operators. We now investigate whether it is possible to similarly shift the original operators $a_{1,2}$ to new operators $\hat{a}_{1,2} = a_{1,2} - b_{1,2}$, such that they are related to $a_{1,2}(\gamma)$ by the same Bogoliubov transformation, namely:

$$a_1(\gamma) = \frac{1}{\sqrt{1-\gamma^2}}\left(\hat{a}_1 - \gamma \hat{a}_2^\dagger\right) + \frac{b_1 - \gamma b_2^*}{\sqrt{1-\gamma^2}} = \hat{a}_1(\gamma) + \alpha_1 \qquad \Longrightarrow \qquad \alpha_1 = \frac{b_1 - \gamma b_2^*}{\sqrt{1-\gamma^2}}. \tag{8.71}$$

Applying the same reasoning to the second mode yields an analogous relation. We thus obtain a system of two linear equations for the two unknowns b_1 and b_2. Solving this system, we find:

$$b_1 = \frac{\alpha_1 + \gamma \alpha_2^*}{\sqrt{1-\gamma^2}} \qquad \wedge \qquad b_2 = \frac{\alpha_2 + \gamma \alpha_1^*}{\sqrt{1-\gamma^2}}. \tag{8.72}$$

Consequently, we have demonstrated that the same Bogoliubov relations connect $\hat{a}_{1,2}$ and $\hat{a}_{1,2}(\gamma)$ as those that connect $a_{1,2}$ and $a_{1,2}(\gamma)$. We are therefore justified in writing:

$$|\gamma, \alpha_1, \alpha_2\rangle = \sqrt{1-\gamma^2} e^{\gamma \hat{a}_1^\dagger \otimes \hat{a}_2^\dagger} \left|\hat{0}_1\right\rangle \otimes \left|\hat{0}_2\right\rangle \quad \wedge \quad \rho_1^{\gamma'} = (1-\gamma^2) \sum_{n=0}^{\infty} \gamma^{2n} \left|\hat{n}, 1\right\rangle \left\langle \hat{n}, 1\right| . \tag{8.73}$$

We note that the density matrices ρ_1^γ from Eq. (8.64) and $\rho_1^{\gamma'}$ from Eq. (8.73) have exactly the same structure. The only difference lies in the choice of basis used to represent them. This clearly leaves both their eigenvalues and the associated entropies unchanged. Consequently, the entropy of a coherent state coincides with that of the vacuum state upon which the coherent state is built.

Considering each mode separately, we find that the Bogoliubov transformation is identical to that obtained for the Minkowski vacuum, with the only caveat that now $\gamma = e^{-\pi\omega}$. The general Minkowski coherent state can be written as:

$$|\vec{\alpha}, 0_M\rangle \propto \prod_j \left(e^{\alpha_{1j} a_1^\dagger(\omega_j) + \alpha_{2j} a_{\omega_j}^\dagger} \,|0_M, j\rangle \right), \tag{8.74}$$

where $|0_M, j\rangle$ is the vacuum annihilated by $a_1(\omega_j)$ and $a_2(\omega_j)$. This expression may equivalently be recast as the tensor product:

$$|\vec{\alpha}, 0_M\rangle \propto \bigotimes_j \left|\gamma_j = e^{-\pi\omega_j}, \alpha_{out,j}, \alpha_{in,j}\right\rangle . \tag{8.75}$$

From this form, it is clear that our earlier result extends straightforwardly to both the Minkowski vacuum and Minkowski coherent states. If we now take a vacuum defined with respect to coordinates $y^\pm = y^\pm(x^\pm)$, obtained from Minkowski coordinates via a conformal transformation, the previous conclusions continue to apply without alteration. The extension to curved spacetime is direct. Hence, we have established that the following statement holds: the formula for the fine-grained entropy is the same when the quantum state of matter is a vacuum state (in either flat or curved spacetime) and when it is a coherent state constructed on that vacuum.

8.3.2 Black hole entropy

In this subsection, we derive the expression for the coarse-grained entropy of the black hole. Our main aim is to obtain the quantum correction to the Bekenstein–Hawking entropy in the setting of the classical CGHS model, as derived in Sec. 4.5. There, we found:

$$M = \frac{\lambda}{\pi G} e^{-2\phi_H} \quad \wedge \quad S = \frac{2}{G} e^{-2\phi_H} \quad \wedge \quad T = \frac{\lambda}{2\pi}. \tag{8.76}$$

Our goal now is to compute the quantum-corrected entropy in the BPP model and to again express it in terms of the value of the dilaton at the horizon, ϕ_H. The sole modification appears in the functional dependence $M = M(\phi_H)$, since it is known that the temperature remains unchanged once quantum fluctuations are taken into account.

Let us consider a black hole in equilibrium with surrounding radiation inside a finite cavity. We now adiabatically send in a small amount of left-moving matter with energy ΔM. This process corresponds to an evolution through a family of equilibrium states, so the relevant quantum state is the Hartle–Hawking vacuum at all times. Eventually, this matter crosses below the apparent horizon. When this occurs, the apparent horizon moves outward due to the increase in the black hole mass, which in turn changes the black hole entropy by an amount ΔS_{BH}. Simultaneously, as the horizon expands, some of the radiation outside becomes enclosed by the horizon, resulting in a change in the entropy of the exterior matter, ΔS_{mat}. Hence, the total change in entropy is given by:

$$\Delta S_{BH} + \Delta S_{mat} = \frac{\Delta M}{T}. \tag{8.77}$$

For a black hole in thermal equilibrium, the relevant state is the Hartle–Hawking state, and the metric components are given by Eq. (4.104), which we rewrite here:

$$e^{-2\rho} = e^{-2\phi} = -\lambda^2 x^+ (x^- + \Delta) + \frac{\pi G M}{\lambda}. \tag{8.78}$$

The location of the apparent horizon is determined by $\partial_+ e^{-2\phi} = 0$, implying $x_H^- = -\Delta$. Consequently, on the horizon we obtain $\Delta e^{-2\phi_H} = \frac{\pi G \Delta M}{\lambda}$. Moreover, it is important to stress that the collapse of the additional mass ΔM leads to a shift in the parameter Δ, so that x_H^- moves to more negative values. As expected, this corresponds to a displacement of the horizon that can be interpreted as an expansion of the black hole. Thus we find:

$$\frac{\Delta M}{T} = \frac{2}{G} \Delta e^{-2\phi_H}. \tag{8.79}$$

We must now determine how the entropy of matter outside the horizon changes. One way to define this quantity is to use the von Neumann entropy S_{VN} of the quantum fields restricted to the region exterior to the horizon. At first glance this may appear peculiar, since we are computing a coarse-grained entropy while expressing the entropy of the external fields in terms of their fine-grained entropy. Our rationale is that the matter fields outside the horizon are highly entangled with those inside, such that the coarse-grained entropy of the exterior fields is approximately equal to their fine-grained entropy.

Fig. 8.14 shows the inaccessible region A in the case of an eternal black hole. Since this region is defined as lying outside the apparent horizon, the setup is directly identified with the curved-spacetime extension of the Rindler result. Consequently, we employ the expression in Eq. (8.52) for the entropy of the matter fields:

$$S_{VN} = \frac{N}{6}\left[\rho_H + \frac{1}{2}\ln\frac{-X^+_{\max}X^-_{\max}}{\delta^2}\right]. \quad (8.80)$$

The overall factor of N reflects the presence of N matter fields in the BPP model. We now focus on the IR-divergent contribution to this expression, as it provides the following leading behavior:

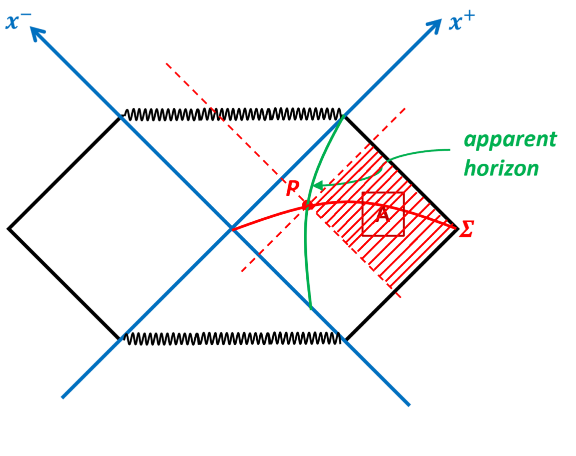

Figure 8.14: Region A that contains the inaccessible degrees of freedom in the eternal black hole setting.

$$S_{VN} \approx \frac{N}{12}\ln\left(-X^+_{\max}X^-_{\max}\right) = \frac{N}{12}2\lambda\sigma_{\max} = 2N\frac{\pi}{6}TL, \quad (8.81)$$

where L denotes the linear dimension of the cavity, i.e., $L = \sigma_{\max}$. We have recovered $2N$ times the standard expression for the thermodynamic entropy of a one-dimensional gas. The factor of two arises from the contributions of left- and right-moving modes, while the factor of N reflects the presence of N distinct scalar field species within the BPP model. This supports our claim that the choice of ΔS_{mat} is appropriate. In this expression, the only quantity that varies is ρ_H, so we obtain

$$\Delta S_{mat} = \frac{N}{6}\Delta\rho_H = \frac{N}{6}\Delta\phi_H, \quad (8.82)$$

where we have used the Kruskal condition $\phi = \rho$. By combining the expressions in Eqs. (8.79) and (8.82), we arrive at the following quantum-corrected version of the Bekenstein–Hawking entropy formula:

$$\Delta S_{BH} = \frac{\Delta M}{T} - \Delta S_{mat} = \Delta\left(\frac{2}{G}e^{-2\phi_H} - \frac{N}{6}\phi_H\right) \implies S_{BH} = \frac{2}{G}e^{-2\phi_H} - \frac{N}{6}\phi_H. \quad (8.83)$$

The expression in Eq. (8.83) is determined only up to an additive integration constant, which is not particularly significant for our purposes. It can be viewed as the area term $\frac{A}{4G}$ that appears in the island formula (1.6), now including the quantum correction to the area A. We next compute the precise ratio between this quantum correction and the classical Bekenstein–Hawking entropy:

$$\frac{\Delta S_{BH}}{S^{(0)}_{BH}} = -\frac{N\hbar G}{12c^3}\phi_H e^{2\phi_H} = \frac{N\hbar\lambda}{24\pi cM}\ln\frac{\pi GM}{\lambda c^2}, \quad (8.84)$$

where all relevant physical constants have been restored. Hence, this correction is of the order $\hbar$, and therefore can be consistently regarded as a genuine quantum correction.

8.3.3 Hawking information loss paradox

We conclude this section by presenting a precise statement of the Hawking information loss paradox [16]. This paradox is the main subject of the present work and was first introduced and qualitatively discussed in the introductory chapter. In the 1970s, Stephen Hawking made a landmark contribution to gravitational theory by showing that black holes behave as thermal objects. In particular, they possess a well-defined temperature and are expected to emit radiation. He further demonstrated that this radiation is purely thermal and lacks correlations. The full result is derived within the framework of quantum field theory in curved spacetime, using a method that is essentially the same as the one employed to obtain the Unruh effect in Sec. 8.2.1.

If we assume that the black hole originates from the collapse of matter initially in a pure state, more specifically in a coherent state, it is puzzling to find that, once the evaporation process is complete, the final state is a thermal ensemble, i.e., a mixed state. The thermal properties emerge because we effectively partition the vacuum, or the coherent state (see Sec. 4.3.1), into two regions: the interior of the black hole and the exterior. As is well known, in quantum field theory the vacuum is an entangled state. Thus, while the global vacuum is pure, its degrees of freedom exhibit short-distance entanglement. Consequently, when we restrict our attention to only one portion of spacetime, we obtain a mixed state. We have already encountered this in Sec. 8.2, where we derived the expressions for the von Neumann entropy in a gravitational context. The physical picture can be described as follows: the vacuum continually creates and annihilates particle–antiparticle pairs, with each pair's constituents being mutually entangled. It may happen that one member of the pair is produced just inside the horizon and falls toward the singularity, while the other is created just outside the horizon and escapes to asymptotic infinity. The escaping particle is what we observe as Hawking radiation.

In Fig. 8.15, an example of such a process is shown. The infalling matter that gives rise to the singularity is indicated in green, the event horizon is represented by a red line, and the entangled particle pair is shown in blue. In this scenario, the two particles together form a pure (entangled) state. Yet, if we restrict our attention to just one of them, say particle a, which belongs to the exterior region, we find that it is described by a mixed state, which effectively appears as a thermal state at the Hawking temperature. We have already seen an analogous situation for the Rindler observer in App. D.3. The method is essentially the same: first, one computes the Bogoliubov coefficients and then performs a partial trace over the degrees of freedom confined within the black hole, yielding the reduced density matrix that characterizes the degrees of freedom accessible to an observer outside the black hole.

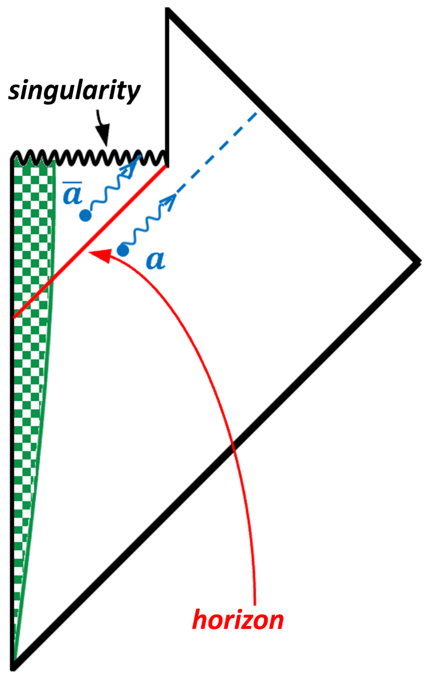

Figure 8.15: Penrose diagram depicting an entangled pair of particles.

This observation indicates that, at early times, the entropy carried by the radiation grows monotonically, in agreement with the usual expectations for the time evolution of entropy in any quantum system. The difficulty appears once the entropy of the radiation exceeds the Bekenstein–Hawking entropy, which characterizes the coarse-grained entropy of the black hole. From that point on, the radiation can no longer remain entangled with the black hole's internal degrees of freedom, because the black hole now has a smaller thermodynamic entropy, and thus fewer degrees of freedom, than the radiation. This is also evident from the fact that the fine-grained entropy is always bounded above by the coarse-grained entropy. We are therefore led to the following conclusion: if the black hole is assumed to form from a pure state, then the combined state of the black hole plus Hawking radiation must remain pure at all times. It follows that the entropy of the radiation must coincide with the fine-grained entropy of the black hole, which in turn must be smaller than its coarse-grained entropy, namely the Bekenstein–Hawking entropy.

However, what is found instead is that the entropy of the radiation reaches the Bekenstein–Hawking entropy and then continues to grow beyond that point. This implies that the state of the overall system can no longer be pure and must instead be described as a mixed state. This has two consequences:

1. *Violation of unitarity:* We begin with a pure state and end with a mixed state. Hawking interpreted this as an intrinsic feature of quantum gravity and therefore maintained that a black hole cannot be treated as an ordinary quantum system, since time evolution in quantum mechanics is required to be unitary.

2. Regardless of how intricate the initial state is that collapses to form the black hole, by the time the evaporation process is complete, one is left only with a thermal ensemble devoid of correlations. Such a state clearly cannot contain as much information as the original pure state from which the black hole formed.

From this we are led to the conclusion that a black hole destroys information. This is known as the Hawking information loss paradox. As already noted, Hawking himself did not regard this as a paradox, but rather as a fundamental characteristic of quantum gravity [16]. If, on the contrary, we insist on treating the black hole as a conventional quantum system, then at the moment when the entropy of the radiation becomes equal to the Bekenstein–Hawking entropy, the entropy of the radiation must start to decrease, eventually reaching zero at the end-point of evaporation. At that stage only the radiation remains, and it must be in a pure state in order to preserve unitarity.

To fix this non-unitary behavior, Don Page proposed a curve for the fine-grained entropy of radiation that preserves unitarity [17, 18], illustrated in Fig. 8.16. At early times, the entropy follows Hawking's prediction (red curve), increasing until it reaches a maximum. After this Page time, the entropy decreases to zero by the end of evaporation, so the radiation returns to a pure state and unitarity is restored. The full Page curve is shown in green, with the late-time asymptotic behavior indicated in blue.

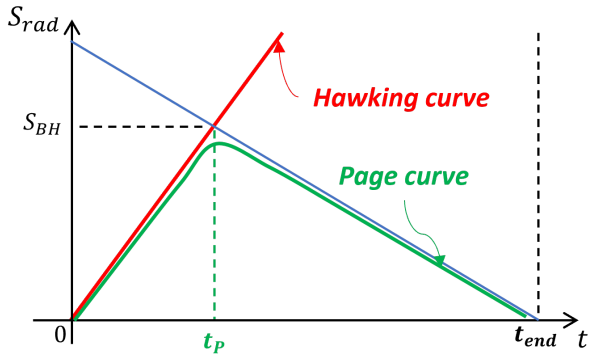

Figure 8.16: Page curve visualization.

We close with several additional remarks:

- As the black hole evaporates, its mass steadily decreases. This effect is known as the backreaction of Hawking radiation on the black hole, and we have already incorporated it into our analysis. It does not, however, resolve the problem.
- Near the end of the black hole's lifetime, its linear size becomes comparable to the Planck length. At that stage, we expect significant quantum-gravitational effects to appear, and the semiclassical framework we are using breaks down. This, too, fails to address the problem, because at the Page time the black hole is still macroscopically large.
- Since the issue is tied to the very definition of fine-grained entropy—a macroscopic quantity—small modifications to the Hamiltonian and/or to the quantum states in the vicinity of the horizon cannot fix it. Consequently, the paradox persists to all orders in perturbation theory, and any genuine resolution must be non-perturbative in the gravitational constant G.
- One might have anticipated that an observable such as fine-grained entropy would not be captured exactly by the semiclassical approximation. Indeed, it was long believed that, once a complete theory of quantum gravity was available, the semiclassical result would receive corrections. The current view, however, is the opposite: the semiclassical formula is now regarded as giving the entropy of the exact quantum state of the radiation.
- To genuinely solve the problem, it is therefore necessary to modify the very definition of fine-grained entropy. We examine this point in detail in the following section.

8.4 Fine-grained entropy formula in gravitational systems

The preceding two sections focused on the two individual contributions that appear in the island formula (1.6). We began by examining the entropy of the quantum fields, followed by an analysis of the area term. In this section, we bring these two ingredients together and demonstrate how the new formula for the fine-grained entropy in gravitational systems [29, 34, 33] succeeds in reproducing the Page curve. Consequently, this section is devoted to the main formula of this work. Its importance is substantial, as it provides the mechanism by which the Page curve is correctly obtained, which is the central goal of this study.

The section is divided into four subsections. We start by stating and discussing the main working assumption, which we will refer to as the central dogma [1]. Next, we examine the formula for the fine-grained entropy in detail. We explain how it allows us to reconstruct the Page curve, first for the fine-grained entropy of the black hole and then for the fine-grained entropy of the radiation. In the third subsection, we outline the derivation of the formula itself. Finally, in the fourth subsection, we consider the questions related to the information paradox that remain unresolved. Throughout, we follow the analysis presented in [1].

8.4.1 Central dogma

In the previous section, we introduced the notion of the information paradox. We now turn to its resolution. Our central hypothesis is as follows: from the perspective of an external observer, the black hole behaves as a conventional quantum system with $\frac{A}{4G}$ degrees of freedom that undergo unitary evolution. In what follows, we explore the implications of this assumption and show how it leads to a modification of the fine-grained entropy formula in gravitational settings, thereby obtaining the island rule in Eq. (1.6).

The black hole, along with the full spacetime region bounded by a certain hypersurface, can be effectively described as the quantum system proposed by the central dogma. The exact position of this hypersurface is not yet fixed, and we will refer to it as the cut-off surface. In Fig. 8.17, this is represented by a blue dashed line.

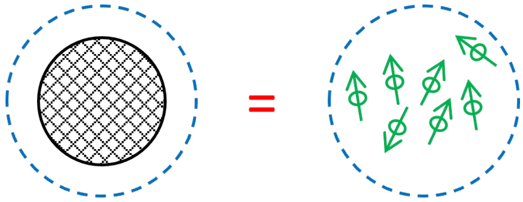

Figure 8.17: Visualization of the black hole as an ordinary quantum system.

It is well established that entropy can be written as $S = \ln W$, where W denotes the number of available microstates. This is the definition used in the microcanonical ensemble. In quantum mechanics, W corresponds to the dimension of the Hilbert space of states. We first emphasize that the Hilbert space associated with the system is taken to be finite-dimensional. The difficulty then stems from the fact that these microscopic degrees of freedom are not visible in the gravitational description, where a black hole is specified only by a limited set of macroscopic parameters (mass, spin, charge, etc.). In addition, another subtlety must be addressed. Assuming that time evolution is unitary, there must exist a Hamiltonian operator that generates this unitary evolution. This Hamiltonian also does not appear explicitly in the gravitational framework. Instead, what one finds in the gravitational theory is the Hamiltonian constraint, which is a global condition imposed on the whole spacetime. According to the central dogma, it should be possible to isolate only the part corresponding to the exterior region, but a standard procedure for doing so has not yet been established.

We now add some clarifying comments about the cut-off surface. This surface acts as a reflective boundary that encloses the system we identify as the black hole, which is assumed to evolve unitarily. In an asymptotically flat spacetime, however, the precise location of this hypersurface is unclear. We draw an imaginary surface well outside the event horizon (at least several Schwarzschild radii away), and designates everything inside it as the black hole. The corresponding quantum system is then coupled to the degrees of freedom lying outside this region. The exterior of this boundary surface is treated as a quantum system propagating on a fixed spacetime background, i.e., as semiclassical. In this outer region, we neglect large metric fluctuations but still include weakly interacting gravitons. The full evolution of both regions together should be unitary. This leads us to the following perspective: the gravitational response is to be compared with that of a quantum system, defined on an imaginary cut-off surface and coupled to degrees of freedom localized far from the black hole.

We now turn to analyzing how entropy is formulated for gravitational systems. As a starting point, we examine the physical meaning of the coarse-grained entropy associated with the combined system consisting of the black hole and its surrounding radiation. Hawking has shown that this entropy is given by the generalized entropy, which takes the form

$$S_{gen} = \frac{A}{4G} + S_{outside}, \tag{8.85}$$

where the first term is the Bekenstein–Hawking entropy, and the second term represents the contribution from the quantum fields outside the black hole horizon. This quantity obeys the second law of thermodynamics, $\Delta S_{gen} \geqslant 0$, and can thus be interpreted as a coarse-grained entropy [13, 16]. Hawking derived this expression using the Euclidean gravitational path integral [32]:

$$
\begin{aligned}
\mathcal{Z} &= \int \mathcal{D}g_{\mu\nu}\mathcal{D}\phi\, e^{-\frac{1}{\hbar}S_E[g_{\mu\nu},\phi]} \\
&= \int \mathcal{D}g_{\mu\nu}\mathcal{D}\phi \exp\left\{-\frac{1}{\hbar}\left[S_E[g^{(0)}_{\mu\nu},\phi^{(0)}] + \cancelto{0}{\left.\frac{\delta S_E}{\delta\phi}\right|_{(0)}}\delta\phi + \frac{1}{2}\left.\frac{\delta^2 S_E}{\delta\phi^2}\right|_{(0)}(\delta\phi)^2 + \ldots\right]\right\} \\
&= e^{-\frac{1}{\hbar}S_E[g^{(0)}_{\mu\nu},\phi^{(0)}]}\int \mathcal{D}g_{\mu\nu}\mathcal{D}\phi \exp\left\{-\frac{1}{2\hbar}\left.\frac{\delta^2 S_E}{\delta\phi^2}\right|_{(0)}(\delta\phi)^2 + \ldots\right\} = e^{-\frac{1}{\hbar}S_E[g^{(0)}_{\mu\nu},\phi^{(0)}]}\mathcal{Z}_{quantum}. \qquad (8.86)
\end{aligned}
$$

In this expression, we perform an expansion around the saddle point of the integrand, determined by the classical equations of motion (denoted by the superscript (0)). As a result, the term linear in the fluctuation vanishes, and the leading correction is quadratic. The partition function therefore receives contributions both from the geometry and from the quantum matter fields. The gravitational contribution is obtained by evaluating the action on the classical solution, whereas the quantum contribution is computed with the background geometry held fixed (the semiclassical approximation). The geometry is required to be regular at the horizon. This condition reflects the fact that a freely falling observer experiences no singular physical effect when crossing the event horizon, as discussed in App. D.5. To extract the entropy and energy from the partition function, we employ the usual thermodynamic relations:

$$
S = (1-\beta\partial_\beta)\ln\mathcal{Z} \quad \wedge \quad E = -\partial_\beta \ln\mathcal{Z}. \qquad (8.87)
$$

Using these mathematical expressions, Hawking arrived at the generalized-entropy formula presented in Eq. (8.85). The first term represents the surface contribution, whereas the second term describes the quantum contribution to the partition function. When evaluated at the horizon, this formula gives the coarse-grained entropy of the combined system of the black hole and its Hawking radiation. In this setup, $S_{outside}$ serves as the fine-grained entropy of the radiation, which in turn implies a non-unitary time evolution. Our aim is to enforce unitary evolution; therefore, this formula must be suitably modified. One can demonstrate that the new formula can be derived in an equivalent way from the generalized-entropy expression. The only change is that we now choose a different boundary surface on which to evaluate the generalized entropy. Instead of the event horizon, we focus on the surface that extremizes the generalized-entropy functional, namely the surface where the generalized entropy assumes its minimum. We now explain more precisely what this entails. Consider a surface X that is genuinely two-dimensional within spacetime, meaning that it is not a hypersurface but rather an embedded spatial surface. In other words, it is localized in one spatial direction and in time. We define this surface as the one that minimizes the generalized-entropy functional and refer to it as the quantum extremal surface (QES). More specifically, it minimizes the entropy along the spatial direction while maximizing it along the temporal direction. If multiple such surfaces exist, we must choose the one that yields the global minimum. The procedure for determining it can thus be summarized as follows: first, select a spacelike hypersurface given by a constant-time slice ($t = \text{const.}$). On this hypersurface, find the surface that minimizes the generalized-entropy functional. Then consider the full family of such spacelike hypersurfaces and pick the one for which the associated minimizing surface produces the largest value of the generalized entropy.

Accordingly, the expression for the fine-grained entropy in gravitational systems takes the form

$$S_{FG} = \min_X \left\{ \operatorname*{ext}_X \left[\frac{A[X]}{4G} + S_{\text{semi-cl}}\left(\Sigma_X\right) \right] \right\}. \tag{8.88}$$

In this formula, X denotes the surface of interest, and Σ_X is the segment of a spacelike hypersurface bounded on one side by X and on the other by the cut-off surface that defines the quantum system under investigation. This setup identifies the causal diamond that encloses the portion of spacetime where the degrees of freedom associated with the chosen quantum system are localized. The von Neumann entropy of the quantum fields on Σ_X is denoted by $S_{semi-cl}(\Sigma_X)$. We employ this notation to emphasize that all calculations are performed within the semiclassical regime. This relation is central to our discussion and was originally obtained by Maldacena and Lewkowycz [33]. In typical scenarios, the surface X lies inside the black hole, i.e., behind the event horizon. The essential idea is as follows: we begin by selecting a trial surface X located outside the black hole's event horizon. We then smoothly deform and extend this surface across the horizon into the interior region to identify the configuration that yields the required minimal value.

Since the QES is located inside the black hole, the entropy must therefore depend on features of the black hole's interior. The surprising aspect is that it does not depend on the full interior, but only on a limited portion of that region. The entire construction follows from the Euclidean gravitational path integral, through a technique analogous to the one Hawking employed to obtain the expression for the generalized entropy in Eq. (8.85). An outline of this derivation is provided in Sec. 8.4.3. We must now refine what is meant by a "quantum extremal surface" in reference to the surface X. Geometrically, X is an ordinary surface; it is termed quantum because it encloses the region in which the quantum fields reside. Fig. 8.18 depicts the deformation of X, starting from the cut-off hypersurface, passing through the event horizon (dashed purple line), and continuing into the interior until the QES is reached.

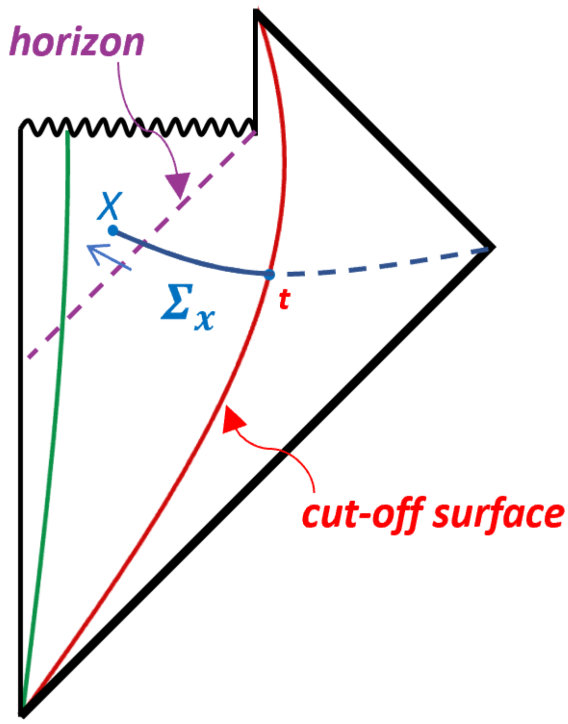

Figure 8.18: Penrose diagram showing the quantum extremal surface.

8.4.2 Reproducing the Page curve for the black hole sector

We now apply the fine-grained entropy formula for gravitational systems, viewing the black hole as a quantum subsystem. At the moment of black hole formation, no Hawking quanta have escaped. Consequently, for any surface X located inside the event horizon, no QES appears, and the associated construction continues all the way out to the asymptotic boundary of spacetime. In this regime, the surface contribution is absent, leaving only $S_{semi-cl}(\Sigma_X)$, which evaluates to zero. In this way, one recovers Hawking's original result.

As time goes on, the first quanta escape from the black-hole region, causing the fine-grained entropy S_{FG} to increase, driven by the growth of the second term in Eq. (8.88). At time t_1, the entropy is still below the Bekenstein–Hawking value S_{BH}. By time t_2, however, the fine-grained entropy has risen above S_{BH}. This behavior matches Hawking's original semiclassical result: the entropy keeps growing monotonically with time, increasing steadily until the black hole has fully evaporated. This situation is known as the vanishing QES case and is illustrated in Fig. 8.19.

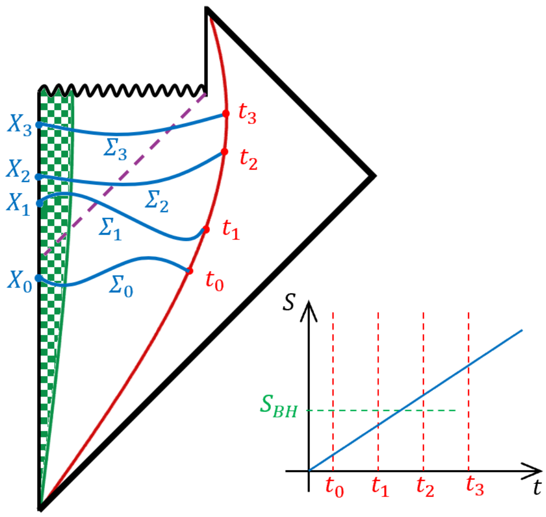

Figure 8.19: Penrose diagram depicting to the zero QES phase.

Shortly after Hawking radiation begins to leave the black-hole region, an additional QES appears. The position of this surface depends on how much radiation has escaped and therefore varies explicitly with time. The formula for the generalized entropy in Eq. (8.88) now acquires a surface contribution. Furthermore, this surface term dominates over the semiclassical term, because at this early stage only a small fraction of radiation has escaped and the QES lies very close to the horizon. Consequently, the contribution from this nontrivial QES is much larger than that from the vanishing QES configuration, thus the global minimum in Eq. (8.88) is still given by the vanishing QES. This situation, referred to as the nonzero QES case, is presented in Fig. 8.20.

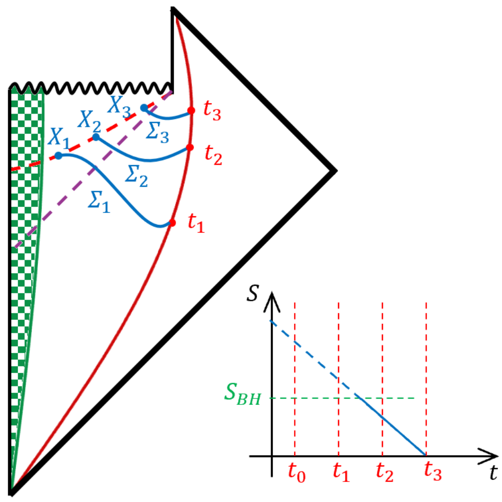

Figure 8.20: Penrose diagram depicting to the non-zero QES phase.

From these observations, we infer that at early times in the evaporation process, the global minimum of the entropy is determined by the trivial (vanishing) QES. As time increases and the black hole evaporates, the horizon area shrinks, which in turn reduces the contribution from the nonzero QES. At some point between t_1 and t_2, this decreasing contribution falls below the increasing contribution associated with the vanishing QES, since the non-vanishing QES is located closely to the horizon. Since S_{FG} is computed using the QES that yields the smallest value, the relevant QES switches at that moment, and the entropy begins to decrease. We interpret this change as a phase transition. This behavior is depicted in Fig. 8.21.

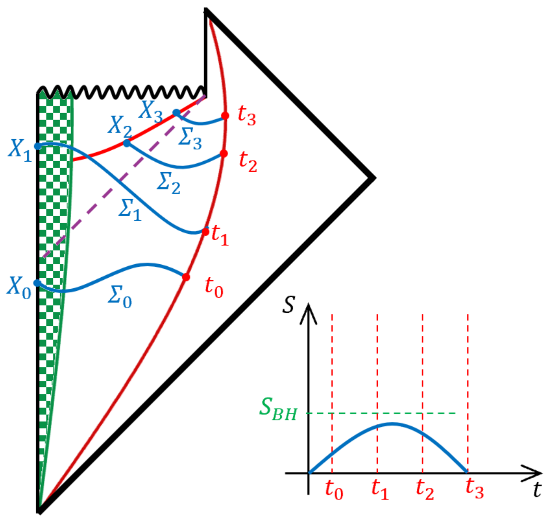

Figure 8.21: Penrose diagram depicting the phase transition.

At the phase transition, the previously dominant contribution coming from the vanishing QES remains smaller than the Bekenstein–Hawking entropy S_{BH}. As a result, the entanglement entropy displays the characteristic behavior of the Page curve. This is because the entropy associated with the non-vanishing QES follows the thermodynamic entropy of the black hole. The key point is that this QES lies very close to the event horizon, which is precisely the surface at which the thermodynamic entropy is evaluated. Since the entropy does not exceed S_{BH}—the QES being situated inside the horizon—the entropy at the intersection point cannot be above the value S_{BH}. This moment corresponds to the Page time.

We therefore find that the Page curve is correctly reproduced, assuming that a nonzero QES does in fact lie inside the black hole horizon. One must then establish the presence of a surface with saddle-point characteristics: namely, a surface such that small spatial displacements away from a given point cause the entropy to increase, while small temporal displacements from that same point cause the entropy to decrease. We do not present a rigorous proof of this here. Instead, we offer an intuitive argument suggesting that such a surface should exist, based on analyzing the behavior along the direction of left-moving waves.

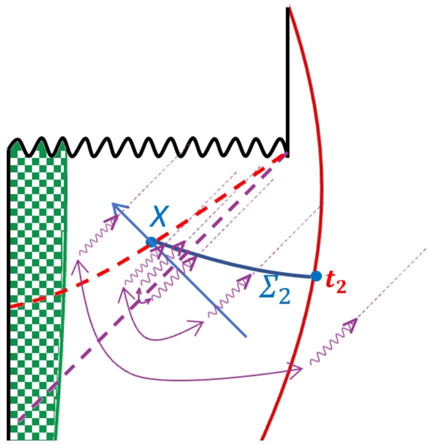

Figure 8.22: Penrose diagram which demonstrates of the existence of a non-zero QES.

What is firmly established is that the surface term decreases as we approach the point $r = 0$. The remaining issue is how the quantity $S_{\text{semi-cl}}(\Sigma_X)$ behaves in this limit. Consider the following process: the hypersurface X is first exactly placed at the event horizon and then slowly, adiabatically, moved below the horizon, following the trajectory of the left-moving modes, as depicted in Fig. 8.22. As X is shifted inward, the additional quanta that appear on the hypersurface Σ_X are entangled with those quanta that previously lay on Σ_X in the region between the horizon and the cut-off surface. Consequently, by carrying out this procedure we are purifying the quantum state along Σ_X, since we are now including both members of each entangled pair. This purification continues until we have captured all quanta that are entangled with the degrees of freedom supported on the portion of Σ_X located to the right of the horizon. At that stage, the state along Σ_X has become maximally purified.

Throughout this part of the evolution, the entropy $S_{\text{semi}-\text{cl}}(\Sigma_X)$ decreases, tracking the gradual purification of the system's state. Once we push X further inward, however, we start to pick up quanta that are entangled with partners that have already escaped the black hole region, i.e., that lie outside the cut-off surface. From this point on, the entropy $S_{\text{semi}-\text{cl}}(\Sigma_X)$ begins to increase again. We therefore infer that, along this direction in configuration space, $S_{\text{semi}-\text{cl}}(\Sigma_X)$ possesses a local minimum. Because the surface term is strictly decreasing, this also implies the existence of a local minimum for S_{FG}.

We thus arrive at the following picture of an evaporating black hole: two distinct QESs emerge. One is the original Hawking saddle, situated at the asymptotic boundary of spacetime, which gives an entropy contribution that grows monotonically with time. The second QES lies just below the event horizon and contributes an entropy that decreases monotonically with time. At each moment, the fine-grained entropy of the radiation is determined by taking the smaller of these two contributions, and in this way one recovers the characteristic Page curve behavior.

8.4.3 Reproducing the Page curve for the Hawking radiation sector

In the previous section, we introduced a method for evaluating the fine-grained entropy of the black hole subsystem and showed that it correctly reproduces the expected behavior of the Page curve. We now turn to the fine-grained entropy of the radiation subsystem. In earlier treatments, this entropy was expressed solely through the von Neumann entropy of the quantum fields. Within that approach, the entropy increases monotonically throughout the evaporation process and ultimately exceeds the Bekenstein–Hawking entropy of the black hole, thus violating the unitarity. This discrepancy signals that the standard expression for the entropy of Hawking radiation must be modified or supplemented by additional terms. As before, we aim to use the fine-grained entropy formula for gravitational systems given in Eq. (1.6). Yet, this requires justification, because the radiation resides in a region where the gravitational field is extremely weak, and one would normally not expect a gravitational entropy formula to be applicable there. The justification is that the quantum state of the radiation is still generated within the underlying theory of gravity.

Until now, we have applied the formula to a specific gravitational system, such as a black hole. However, the radiation region itself contains no black hole. Moreover, we have thus far assumed the hypersurface Σ_X was simply connected. We now relax this and allow Σ_X to have disconnected components. This increases the boundary area and thus the area term in Eq. (1.6). To compensate, the generalized entropy must change by decreasing $S_{\text{semi-cl}}(\Sigma_X)$. This is achieved by including part of the black hole interior that contains the entangled partners of quanta outside the cut-off surface, thereby purifying the state. This added portion is the island region, and its boundary is the island or island boundary, so that $\Sigma_X = \Sigma_I \cup \Sigma_{\text{rad}}$. In this framework, the island coincides with the quantum extremal surface, and the fine-grained entropy is given by the island-rule entropy formula:

$$S_{FG} = \min_{I} \left\{ \operatorname*{\mathbf{ext}}_{I} \left[\frac{A[I]}{4G} + S_{\text{semi-cl}} \left(\Sigma_I \cup \Sigma_{rad} \right) \right] \right\}. \tag{8.89}$$

It is important to stress that this quantity represents the fine-grained entropy of the precise quantum state of the radiation. However, the precise quantum state itself remains unknown; only its entropy can be determined within the semiclassical approximation. This setup is depicted schematically in Fig. 8.23. The island I lies behind the black hole horizon in the interior region, as previously discussed. The cut-off hypersurface is indicated in red, and the separate region containing the radiation degrees of freedom is shown in blue. We therefore infer that the mechanism underlying Eq. (8.89) is precisely the same as for the black hole subsystem. Consequently, the resulting entropy evolution reproduces the Page curve, exactly as in the black hole case.

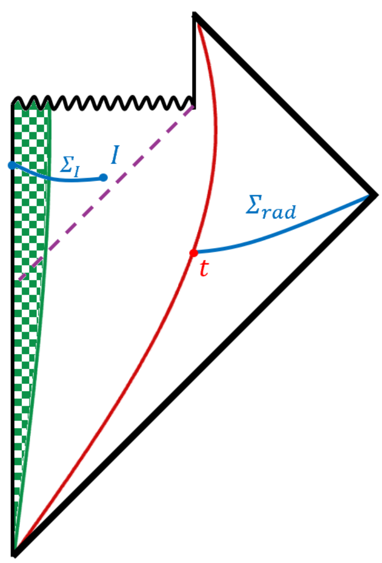

Figure 8.23: Penrose diagram depicting the island and the radiation hypersurfaces.

As in the black hole case, at the beginning of the evaporation process there is no QES (island). As a result, the entropy (8.89) is fully determined by its semiclassical term, which is initially zero because no radiation quanta have yet escaped the black hole. As time goes on, quanta of radiation start to emerge from the black hole region, causing the quantity $S_{\text{semi-cl}}(\Sigma_{rad})$ to increase. As before, this quantity extremizes the generalized entropy at each moment of the evaporation, although it need not represent the global minimum at all times. This portion of the discussion reproduces Hawking's conclusion that the fine-grained entropy of the radiation grows monotonically throughout the evaporation process.

As before, the island (a non-vanishing QES) that extremizes the generalized entropy emerges shortly after the evaporation process begins and lies close to the horizon. Consequently, the entropy obtained from this QES is initially very large and therefore does not correspond to the global minimum. As time goes on, however, the horizon shrinks, which in turn reduces this entropy contribution until it eventually becomes the global minimum, signaling a phase transition. From that point onward, throughout the remaining evolution, we evaluate S_{FG} using the configuration that includes the island. This yields an entropy that decreases monotonically and ultimately goes to zero at the end of the evaporation process. We thus find that the Page curve is reproduced once more, now for the case of Hawking radiation. This behavior is illustrated in Fig. 8.24.

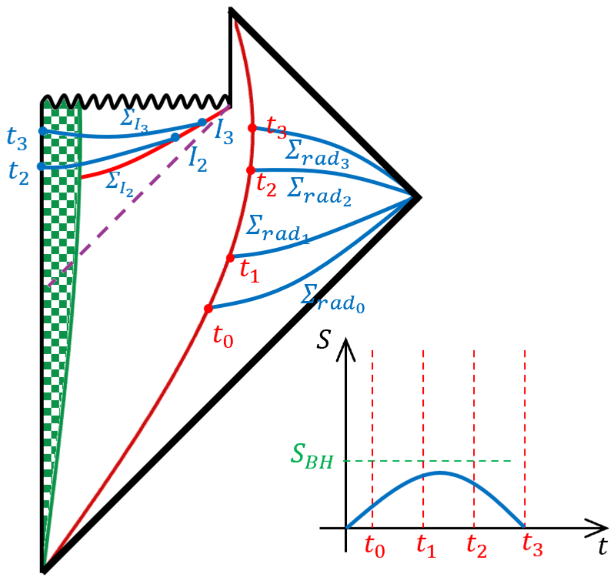

Figure 8.24: Penrose diagram depicting the phase transition for the radiation entropy.

If the black hole forms from a pure state, the fine-grained entropies of the black hole and Hawking radiation subsystems match at all times. This occurs because, for the black hole subsystem, the quantum extremal surface coincides with the island, so the area terms in the entropy are identical in the two descriptions. On the Cauchy slice $\Sigma_I \cup \Sigma_X \cup \Sigma_{rad}$, the von Neumann entropy in Eq. (8.88) for Σ_X must equal that in Eq. (8.89) for $\Sigma_I \cup \Sigma_{rad}$, since the total state on the full Cauchy surface is pure. Hence $S_{\text{semi-cl}}(\Sigma_X) = S_{\text{semi-cl}}(\Sigma_I \cup \Sigma_{rad})$. Because we extremize the same functional in both descriptions, the entropies necessarily coincide. Thus, the fine-grained entropies of the black hole and Hawking radiation subsystems are equal throughout evaporation, reproducing the characteristic Page curve.

The key reason this construction successfully reproduces the Page curve for the Hawking radiation subsystem is that the black hole interior is included when computing the fine-grained entropy of the Hawking radiation. Furthermore, it is quite natural to recover the Page curve once the interior is taken into account, since its inclusion purifies the quantum state of the emitted radiation. At first, it may appear that we have simply added the interior in an ad hoc manner, without any physical underpinning. However, as emphasized at the beginning of this section, the fine-grained entropy formula for gravitational systems can be derived from the Euclidean gravitational path integral. This derivation employs the replica wormholes technique, which we describe in the following subsection.

8.4.4 Replica wormholes method

In this section, we sketch the derivation of the formula for the fine-grained entropy in gravitational systems [33, 34, 38, 126, 127, 128]. We focus on the situation in which the black hole has fully evaporated. The detailed physics in the immediate neighborhood of the evaporation end-point is omitted, because in that regime strong quantum-gravitational effects play a crucial role and the semiclassical approximation is no longer applicable.

From the perspective of entropy calculations, the relevant geometric setup is illustrated in Fig. 8.25. Our starting point is the unnormalized pure state $|\psi\rangle$, which characterizes the collapsing matter that eventually forms the singularity. The aim is to evolve this state into some final radiation state $|j\rangle$ via the gravitational path integral. In doing so, we obtain the transition amplitude from the initial state $|\psi\rangle$ to the final state $|j\rangle$, namely $\langle j|\psi\rangle$. Fig. 8.25 provides a depiction of this transition amplitude: the ocher line indicates the evolution from the interior state $|\psi\rangle$ to the exterior radiation state $|j\rangle$.

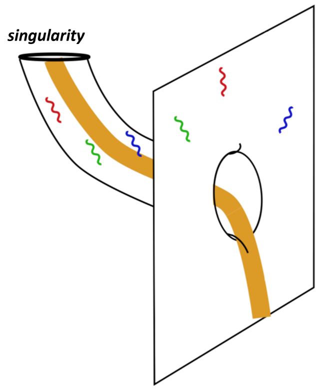

Figure 8.25: The diagram representing the transition amplitude: $\langle j|\psi\rangle$, taken from [1].

Our central question is whether the post-evaporation state $\hat{\rho}$ is pure or mixed. For this purpose, we use the standard purity criterion for a quantum state:

$$\mathrm{Tr}\left\{\hat{\rho}^2\right\} = \left(\mathrm{Tr}\{\hat{\rho}\}\right)^2 . \tag{8.90}$$

If this condition holds, the state is pure; if it fails, the state is mixed. To check this, we adopt a diagrammatic method. We first draw a diagram representing the trace, i.e.,

$$\mathrm{Tr}\{\hat{\rho}\} = \sum_i \langle i|\psi\rangle \langle\psi|i\rangle . \tag{8.91}$$

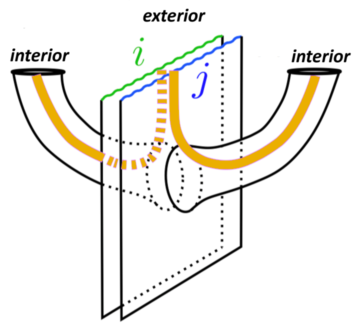

Figure 8.26: The diagram representing the matrix element: ρ_{ij}, taken from [1].

Starting from the state $|\psi\rangle$, we construct the density matrix $\hat{\rho} = |\psi\rangle\langle\psi|$. In Fig. 8.26, we depict a diagram corresponding to the matrix element of this density operator in the Hilbert-space basis of the final radiation: $\rho_{ij} = \langle i|\psi\rangle\langle\psi|j\rangle$. In this diagram, there are two interior regions associated with $|\psi\rangle$, which are identified with each other, and two exterior regions containing the final radiation states $|i\rangle$ and $|j\rangle$. This configuration can be interpreted as the product of two diagrams of the type shown in Fig. 8.25, differing only in the choice of the exterior final states.

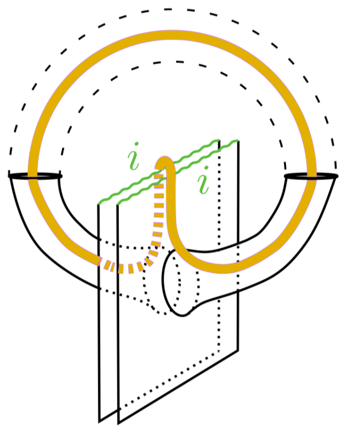

Figure 8.27: The diagram representing: $\mathrm{Tr}\{\hat{\rho}\}$, taken from [1].

To compute the trace in Eq. (8.91), we must also identify the exterior regions and then sum over all possible exterior states $|i\rangle$. This procedure produces a closed loop in the diagram representing the trace, as illustrated in Fig. 8.27.

To verify the relation in Eq. (8.90), it is necessary to additionally express:

$$\mathrm{Tr}\{\hat{\rho}^2\} = \sum_{i,j} \langle i|\psi\rangle \langle\psi|j\rangle \langle j|\psi\rangle \langle\psi|i\rangle \,. \tag{8.92}$$

From the summation it is evident how the final (exterior) states are identified; however, we must also identify the interior regions so that the sum runs over both i and j. There are two distinct ways to connect these interior parts and obtain a closed loop.

In the first option, we connect the interior of the matrix element $\langle i|\psi\rangle$ with that of $\langle j|\psi\rangle$, and then do the same for the remaining pair. This construction yields a single large loop, as depicted in Fig. 8.28. In the second option, we instead connect the interiors of the two matrix elements $\langle i|\psi\rangle$ with each other, and similarly connect the interiors of the two $\langle j|\psi\rangle$ matrix elements. In this configuration, the diagram clearly splits into two separate loops, as shown in Fig. 8.29.

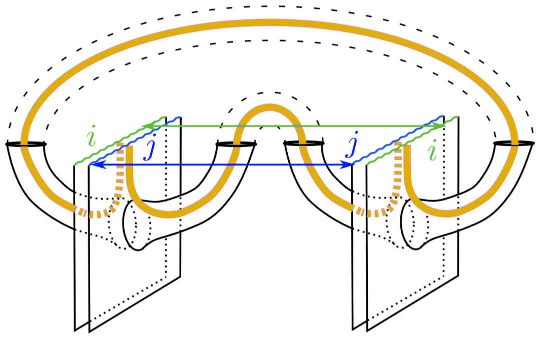

Figure 8.28: The diagram representing: $\mathrm{Tr}\{\hat{\rho}^2\}$ - Hawking saddle point, taken from [1].

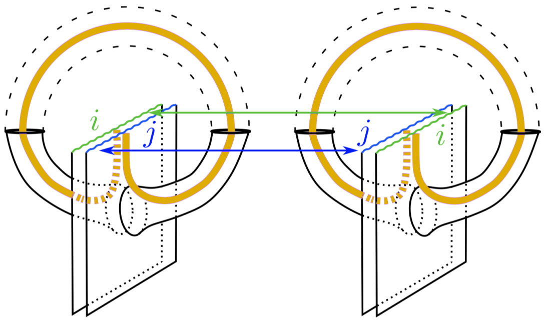

Figure 8.29: The diagram representing: $\mathrm{Tr}\{\hat{\rho}^2\}$ - replica wormhole saddle point, taken from [1].

In quantum mechanics—and likewise in the present setting—it is a basic requirement that one sums over all possible configurations. Here, this means summing over all allowed geometric topologies, i.e., over all distinct ways of connecting the interior regions. The contribution depicted in Fig. 8.28 cannot be decomposed into two independent loops and corresponds to Hawking's saddle point of the gravitational path integral. By contrast, the second diagram in Fig. 8.29 manifestly splits into two loops, showing that it represents the product of two diagrams associated with $\mathrm{Tr}\{\hat{\rho}\}$. This term is linked to the saddle-point configuration of replica wormholes and implies that the final state $\hat{\rho}$ after evaporation is pure, since it obeys the purity condition (8.90). Because the entropy of a pure state vanishes, the second diagram gives the leading contribution in the saddle-point approximation to the Euclidean gravitational path integral, namely:

$$\mathcal{Z} = \int \mathcal{D}g_{\mu\nu}\mathcal{D}\phi \, e^{-S_E[g_{\mu\nu},\phi]} \approx e^{-S_{E,RW}} + e^{-S_{E,H}} = 1 + e^{-S_{E,H}} \approx 1. \tag{8.93}$$

We therefore infer that the dominant contribution guarantees unitarity. A potential concern that remains is the persistence of Hawking's saddle point. Its effect is exponentially suppressed, so we expect it not to cause any substantial difficulty once the full quantum theory of gravity is taken into account. With this understanding, we have demonstrated that the final state after black hole evaporation is a pure state. Nonetheless, one must still determine the entropy of either subsystem at each instant throughout the evaporation process. To obtain the fine-grained entropy formula for gravitational systems at every moment in time, we make use of the replica trick:

$$S_{FG} = (1 - n\partial_n)\,\mathrm{Tr}\{\hat{\rho}^n\}\Big|_{n=1}. \tag{8.94}$$

Here, $\hat{\rho}$ denotes the density matrix associated with one of the two subsystems. When computing $\mathrm{Tr}\{\hat{\rho}^n\}$, the interiors admit many possible ways of being connected, which significantly complicates the calculation. After evaluating $\mathrm{Tr}\{\hat{\rho}^n\}$ for arbitrary $n \in \mathbb{N}$, we analytically continue to $n \in \mathbb{R}$ and then take the limit $\lim\limits_{n\to 1}$. Out of all possible configurations, we must choose the one yielding the smallest contribution. Under this analytic continuation, it turns out that this prescription is exactly equivalent to identifying the quantum extremal surface, as discussed in the previous subsections. A rigorous proof of this equivalence is not provided here; however, its validity should be clear on intuitive grounds. We now conclude with several further remarks:

- In principle, reconstructing the exact quantum state of the emitted radiation requires performing a path integral over the full space of geometries, including all nonperturbative effects. Currently, no existing formulation of quantum gravity allows us to carry out this procedure explicitly. Within our present framework, what is actually under control is the semiclassical state. Using this semiclassical state, we compute the fine-grained entropy of the radiation. Furthermore, it is known that the fine-grained entropy obtained from the semiclassical state coincides with the value that would be derived from the exact quantum state. For sufficiently simple observables, the semiclassical state provides an adequate description. For more intricate observables, however, this approximation breaks down, and the full exact quantum state of the system becomes necessary.

- Because the quantum state of the radiation encodes information about the black hole interior, sufficiently elaborate measurements on the radiation's degrees of freedom can modify the spacetime geometry by generating wormholes that connect to the interior of the black hole [127, 129, 130]. We elaborate on this point in the following subsection.

- We compute the quantity S_{FG} using the Euclidean gravitational path integral. This object is not a well-defined quantity. In particular, it is not clear which saddle points should be included in the sum and which should be discarded. It is conceivable that some theories might select Hawking's saddle instead of the replica wormhole saddle. We expect any such theories to be ultimately inconsistent. A further ambiguity arises in the choice of integration contour for evaluating the gravitational path integral.

- A further conceptual challenge concerns how to choose the cut-off hypersurface that specifies the boundary of the quantum subsystem associated with the black hole. It is unclear whether the fine-grained entropy formula in gravitational settings remains valid when this boundary surface is not taken to lie at infinity.

8.4.5 Entanglement wedge reconstruction

At first glance, reconstructing the Page curve seems to resolve the black hole information paradox. Nonetheless, this conclusion is not entirely warranted, and several key issues remain open. Within the central dogma, we introduced the degrees of freedom used to describe the black hole from the perspective of an observer outside it. The natural question is: which region of the black hole interior do these degrees of freedom actually encode? To address this, consider the formula for the fine-grained entropy in gravitational systems (1.6). It depends on the interior of the black hole only up to the quantum extremal surface. We are thus led to the following statement: the degrees of freedom appearing in the central dogma describe the geometry only up to the quantum extremal surface. Since the entropy is tied to the full causal diamond, we can interpret it as characterizing that entire causal diamond.

This causal diamond is known as the entanglement wedge of the black hole [70, 71, 72], because it contains precisely the degrees of freedom that describe the black hole. There are three relevant regimes, which occur successively in time. The first regime corresponds to times $t < t_p$ and describes the era before the phase transition, as shown in Fig. 8.30. In this regime, there is no QES, and therefore the full interior is captured by the black hole degrees of freedom. The second regime covers the interval $t_p < t < t_{end}$, where t_{end} is the time at which evaporation is complete; this is depicted in Fig. 8.31. Here, the phase transition has already occurred, so a QES exists. Consequently, the black hole degrees of freedom are associated only with the part of the interior up to the QES, while the rest of the interior belongs to the island, which is part of the radiation region. Thus, after the Page time, some of the radiation's degrees of freedom are located inside the black hole interior. The third regime corresponds to times after evaporation has ended, $t > t_{end}$, as illustrated in Fig. 8.32. The region inside the cut-off surface is then simply flat space, while the entire region that lay below the event horizon is part of the island, i.e. it is encoded in the radiation degrees of freedom.

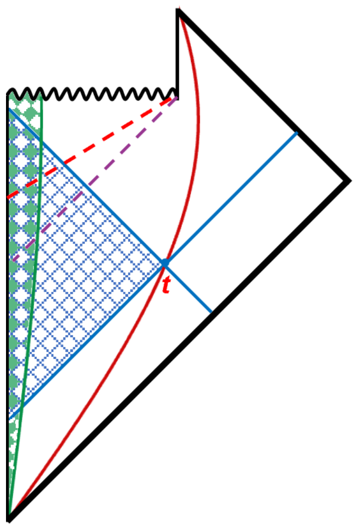

Figure 8.30: Penrose diagram corresponding to the spacetime before the critical point, i.e. $t < t_p$.

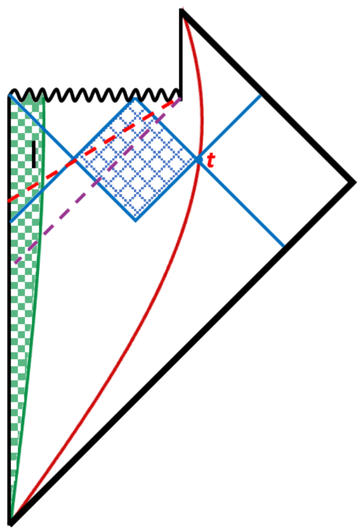

Figure 8.31: Penrose diagram corresponding to the spacetime at the critical point, i.e. $t_p < t < t_{end}$.

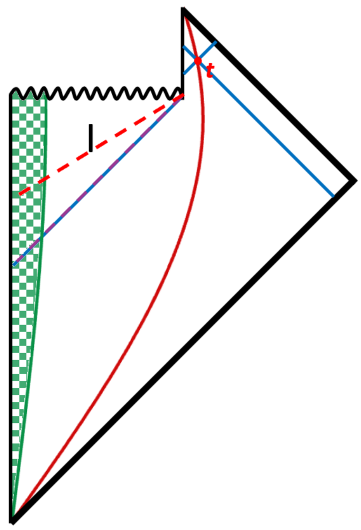

Figure 8.32: Penrose diagram corresponding to the spacetime after the critical point, i.e. $t > t_{end}$.

We therefore infer that once the Page time is surpassed, most of the microscopic degrees of freedom that were initially confined within the event horizon are no longer stored in the remaining black hole, but instead are encoded in the outgoing Hawking radiation. By the time the evaporation process is complete, all of the degrees of freedom that had resided inside the horizon have been completely transferred to, and are fully captured by, the radiation.

Let us now examine the situation in which most of the degrees of freedom located inside the black hole horizon are carried by radiation. In this case, the action of semiclassical operators supported in the region behind the horizon changes the entropy of the outgoing radiation, in agreement with the standard formula for fine-grained entropy in gravitational systems. Throughout this discussion, we take this entropy to coincide with the entropy of the exact quantum state of the radiation. It then follows that semiclassical operators acting behind the horizon of the black hole necessarily modify the exact quantum state of that radiation. [131, 132, 133] General theorems in quantum information theory further imply that there exists a reconstruction map, commonly known as the Petz map, which allows one to recover information about this exact quantum state. [134, 135] For simple gravitational theories, this map can be constructed explicitly using the gravitational path integral, employing the replica wormhole technique. It should be stressed, however, that the quantum measurements required on the radiation degrees of freedom are extraordinarily intricate: their complexity grows exponentially with the Bekenstein–Hawking entropy of the black hole. [136, 137] A fully general formulation of this method, applicable to arbitrary situations and theories, has not yet been obtained.

When we speak of the degrees of freedom of a black hole, we typically refer to the quantum fields that live in the region beneath the event horizon. These are clearly distinct from the degrees of freedom invoked in the central dogma, where what matters are the black hole's degrees of freedom as seen by an asymptotic observer. We know that the degrees of freedom defined by quantum fields inside the horizon can lie on either side of the quantum extremal surface. By "black hole degrees of freedom" we mean specifically those that lie to the right of the quantum extremal surface. Thus, these constitute only a subset of all the degrees of freedom present inside the horizon.

Building on this observation, we have thus addressed another paradox originally posed by Wheeler in 1964 [138]. He noted that there are classical geometries that from the outside look like black holes, yet behind the horizon the entropy can be arbitrarily large—far exceeding one quarter of the horizon area. He referred to such configurations as bags of gold. The resolution of this puzzle is similar: if the entropy contained in the interior exceeds the area of the throat (the horizon), then the causal diamond associated with the degrees of freedom of the black hole captures only that part of the interior that excludes this arbitrarily large entropy.

Fig. 8.33 displays an example of a bag-of-gold geometry. We note that the spacetime of the evaporating black hole analyzed in the previous section (and in the current one) evolves, after the Page time, into a configuration that is effectively equivalent to a bag-of-gold geometry. The key point is that the degrees of freedom of the black hole are associated with only a small fraction of the total degrees of freedom located behind the black hole horizon.

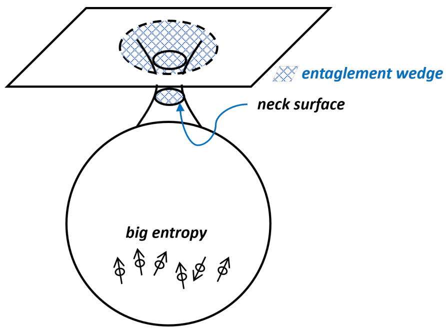

Figure 8.33: Visualization of the bag-of-gold geometry.

In this section, we bring our examination of entropy in gravitational systems to a close. In the following chapters, we present a detailed and explicit reconstruction of the Page curve within concrete, well-specified models of two-dimensional dilaton gravity. This objective is achieved by applying the formula for fine-grained entropy in gravitational systems (1.6), whose derivation and thorough analysis have been the central focus of the present chapter.

Chapter 9

Page curve in the BPP model

In this chapter, we illustrate how the Page curve is reproduced within the BPP model of two-dimensional dilaton gravity introduced in Sec. 4.3. As already shown in Chap. 4.3, the BPP model is exactly solvable. This allows for an exact semi-classical evaluation of the Page curve up to the end-point of the evaporation process, beyond which the corrections from the full theory of quantum gravity will become relevant [1]. We now demonstrate how Eq. (1.6) is applied to compute the Page curve for both eternal and evaporating black hole scenarios in the BPP model. The chapter is organized into two sections.

In the first Sec. 9.1, we reproduce the Page curve for the eternal black hole studied in Sec. 4.3.2. Our analysis follows the derivations in [41] and [57]. We begin with the no–island configuration, in which we recover the standard Hawking result: the Page curve increases monotonically with time [16]. We then apply the fine–grained entropy formula for gravitational systems (1.6), which allows us to obtain the Page curve for this setup.

A crucial point is that, for an eternal black hole, we do not expect the entropy of radiation to decrease at late times. Instead, it should asymptotically approach and then remain at the value $2S_{BH}$. This behavior is due to the fact that the black hole is in thermal equilibrium, so the flux of Hawking radiation it emits is balanced by the flux it absorbs. Consequently, the entropy grows monotonically until it reaches its maximum value, namely $2S_{BH}$, defined in Eq. (1.4). The factor of two arises because an eternal black hole has two asymptotically flat regions. Moreover, since S_{BH} is the coarse–grained black hole entropy, the fine–grained entropy of the radiation cannot exceed this bound (see Sec. 8.1).

In the second part, i.e Sec. 9.2, we then reconstruct the Page curve for an evaporating black hole in the BPP model introduced in Sec. 4.3.4, again following the derivation of [41]. As before, we start by analyzing the setup without including an island, which reproduces the standard Hawking result [16]. We then demonstrate how the inclusion of an island at late times in the evaporation process (i.e., after the Page time) resolves the paradox. The Page curve is computed in two coordinate systems: we first locate the island in asymptotically flat coordinates, and subsequently repeat the analysis in Kruskal coordinates, obtaining, of course, identical results. Unlike the eternal black hole case, the Page curve here decreases and eventually goes to zero at the end-point of the evaporation.

9.1 Page curve in the eternal black hole scenario

In this section, we compute the fine-grained entropy of Hawking radiation for the eternal black hole in the BPP model introduced in Sec. 4.3.2. The discussion is divided into two parts. First, we study the configuration without an island and reproduce Hawking's original result. Next, we perform the full entropy calculation using the fine-grained entropy formula for gravitational systems (1.6). In the late stages of evaporation, we demonstrate the emergence of an island region outside the horizon that contributes to the constant term in the entanglement entropy. This contribution causes the Page curve to saturate at $2S_{BH}$, thereby recovering the purity of the initial quantum state at the end of evaporation. Throughout this section, we follow the derivation presented in [57].

9.1.1 No-island configuration

In the absence of an island in the spacetime, the formula (1.6) simplifies to just the second term, namely $S_{semi-cl}(\Sigma_{rad})$. Because the region containing the degrees of freedom that are inaccessible to the asymptotic observer is simply connected, and there is no spacetime boundary on which reflective boundary conditions are imposed, the appropriate expression for the entanglement entropy of quantum fields in curved spacetime is given by Eq. (8.51). For convenience, we rewrite it here:

$$S_{FG} = \frac{N}{12} \ln \frac{(x_R^+ - x_L^+)^2 (x_R^- - x_L^-)^2}{\delta^4 e^{-2\rho_R} e^{-2\rho_L}}, \tag{9.1}$$

where we have included an overall factor of N in Eq. (8.51) because the BPP model contains N distinct scalar field species. In addition, the expression is written in Kruskal coordinates (4.41), as we are focusing on the eternal black hole setup.

Fig. 9.1 depicts the region A that is inaccessible to an asymptotic observer (as defined in Fig. 8.1) for the case of an eternal black hole. The two asymptotically flat regions are denoted by R and L in both Fig. 9.1 and Eq. (9.1). In each of these regions, we introduce a cut-off surface at $\sigma = b$. Since we are interested in evaluating the entropy at a fixed time t, we consider the hypersurface $t =$ const. in the right wedge. The segment of this hypersurface that supports the radiation degrees of freedom, Σ_{rad}, extends from spatial infinity i^0 to the cut-off surface.

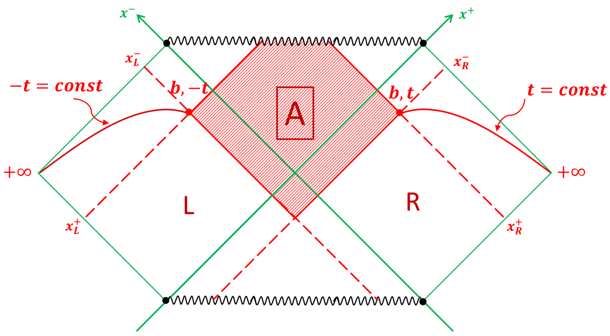

Figure 9.1: Penrose diagram illustrating the no-island setup for an eternal black hole in the BPP model

In the left asymptotically flat region, radiation exits the black hole region along the x^-–axis. At the same time, the Killing vector reverses its direction, implying that the time coordinate t in the right asymptotically flat region corresponds to the time coordinate $-t$ in the left asymptotically flat region. Because of these two effects, the boundary point of region A in the left asymptotically flat region appears as the mirror reflection of the corresponding boundary point in the right asymptotically flat region, as illustrated in Fig. 9.1.

Since Killing time is defined in Eddington–Finkelstein coordinates, we first need to rewrite the Kruskal coordinates $x^{\pm}_{L/R}$ in terms of the asymptotically flat coordinates $\sigma^{\pm}$, and therefore in terms of t and b, using the transformation law (4.41). Doing so gives:

$$\lambda x_R^+ = e^{\lambda(t+b)}, \quad \lambda x_R^- = -e^{-\lambda(t-b)}, \quad \lambda x_L^+ = -e^{\lambda(-t+b)}, \quad \lambda x_L^- = e^{-\lambda(-t-b)}. \tag{9.2}$$

We now proceed to evaluate the fine–grained entropy (9.1). As a first step, we compute the differences $(x_R^\pm - x_L^\pm)$ by substituting Eq. (9.2):

$$\begin{aligned} \lambda\left(x_R^+ - x_L^+\right) &= e^{\lambda(t+b)} + e^{\lambda(b-t)} = e^{\lambda b}\left(e^{\lambda t} + e^{-\lambda t}\right) = 2e^{\lambda b}\cosh(\lambda t), \\ \lambda\left(x_R^- - x_L^-\right) &= -e^{\lambda(b-t)} - e^{\lambda(t+b)} = -e^{\lambda b}\left(e^{-\lambda t} + e^{\lambda t}\right) = -2e^{\lambda b}\cosh(\lambda t). \end{aligned} \tag{9.3}$$

The left-right symmetry requires $\rho_L = \rho_R$. Consequently, for the metric (4.104) evaluated at the boundaries of the region A (see Fig. 9.1) we find:

$$e^{-2\rho_R} = e^{-2\rho_L} = -\lambda^2 x_R^+ x_R^- + \frac{\pi G M}{\lambda} = e^{2\lambda b} + \frac{\pi G M}{\lambda} = -\lambda^2 x_L^+ x_L^- + \frac{\pi G M}{\lambda}. \tag{9.4}$$

Inserting Eqs. (9.3) and (9.4) into the original expression for the entanglement entropy (9.1) leads to:

$$S_{FG} = \frac{N}{6}\ln\frac{4\cosh^2(\lambda t)}{(\lambda\delta)^2\left(1 + \frac{\pi G M}{\lambda}e^{-2\lambda b}\right)}. \tag{9.5}$$

Let us now analyze the behavior of this function at the beginning of the evaporation process. Recall that S_{FG} is defined only up to a renormalization constant (because of the divergence $\ln\delta$ as $\delta \to 0$). We can therefore choose this constant so that $S_{FG} = 0$ at $t = 0$. For $t = 0$ we have $\cosh(\lambda t) = 1$, and the expression simplifies to:

$$S_{FG} = \frac{N}{6}\ln\frac{4}{(\lambda\delta)^2\left(1 + \frac{\pi G M}{\lambda}e^{-2\lambda b}\right)} = 0 \quad \Longrightarrow \quad S_{FG} = \frac{N}{3}\ln\Big[\cosh(\lambda t)\Big]. \tag{9.6}$$

Expanding this expression around $t = 0$, we obtain:

$$S_{FG} = \frac{N}{6}(\lambda t)^2. \tag{9.7}$$

Thus, near $t = 0$ the entropy grows quadratically in time. We now turn to the late–time behavior of Eq. (9.5):

$$\cosh(\lambda t) = \frac{1}{2}\left(e^{\lambda t} + \cancelto{0}{e^{-\lambda t}}\right) \approx \frac{1}{2}e^{\lambda t} \quad \Longrightarrow \quad S_{FG} \approx \frac{N}{3}\lambda t - \frac{N}{3}\ln 2. \tag{9.8}$$

We thus arrive at the main conclusion of this section: in the setup without an island, the Page curve is not recovered. Instead, we reproduce the standard Hawking result [16], where the entropy increases monotonically with time. This monotonic growth is incompatible with unitarity, since beyond a certain time S_{FG} exceeds the bound set by the coarse–grained entropy $2S_{BH}$. The time at which this happens is the Page time, determined by:

$$S_{FG} = 2S_{BH} \quad \Longrightarrow \quad \frac{N}{3}\lambda c t_p = 2\frac{2c^3}{G\hbar}\frac{\pi G M}{\lambda c^2} \quad \Longrightarrow \quad t_p = \frac{12\pi M}{N\hbar\lambda^2}. \tag{9.9}$$

9.1.2 Island configuration

When the island is present, both the area contribution and the semi-classical entanglement entropy term in expression (1.6) for the fine-grained entropy are non-zero. Furthermore, the presence of the island implies that the region A in Fig. 9.2, which is inaccessible to the observer, is composed of two disconnected components. Consequently, the semi-classical part of the fine-grained entropy is given by Eq. (8.60), namely:

$$S_{semi-cl} = \frac{N}{6} \ln \frac{d_{12}^2 d_{23}^2 d_{14}^2 d_{34}^2}{\delta^4 d_{24}^2 d_{13}^2 e^{-\rho_1} e^{-\rho_2} e^{-\rho_3} e^{-\rho_4}}, \tag{9.10}$$

where $d_{ij}^2 = (x_i^+ - x_j^+)(x_i^- - x_j^-)$ represents the Minkowski distance between the corresponding points depicted in Fig. 9.2 in Kruskal coordinates. As before, we multiply expression (9.10) by N because the BPP model contains N species of scalar fields. We assign the indices i and j such that the identification $(1, 2, 3, 4) \longleftrightarrow (Ra, Rb, La, Lb)$ holds. As in the preceding section, R labels the right wedge and L the left wedge of the spacetime. Meanwhile, a designates the boundary of the island region, and b labels the cut-off hypersurface. All these hypersurfaces are explicitly marked in Fig. 9.2.

Fig. 9.2 shows the region A that an asymptotic observer cannot access (as defined in Fig. 8.1) for an eternal black hole in the presence of an island. The island, labeled by I, is highlighted in blue. For an eternal black hole, the non-zero QES is expected to appear very close to the quantum-corrected horizon, but still outside it. In the right asymptotically flat region, the island's coordinates are $(t', -a)$. We denote the spatial coordinate by $-a$ because the island should be located near the horizon, which is given by $\sigma_{\rm H} \to -\infty$ (4.39).

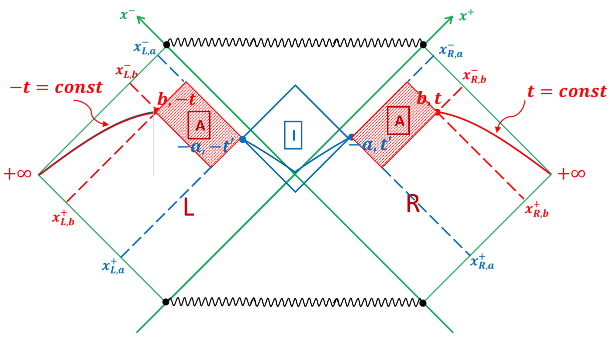

Figure 9.2: Penrose diagram illustrating the island setup for an eternal black hole in the BPP model

In direct analogy with the case without an island, we send the island's boundary point to the left asymptotically flat region by reflecting it across the time axis. In this way, its coordinates become $(-t', -a)$, which encodes the fact that the time-like Killing vector in the left wedge is oriented in the opposite direction. Note that we have not identified the island's time coordinate with the time coordinate on the cut-off surface. This choice is motivated by the requirement that the generalized entropy must be extremized with respect to both space and time: the entropy must be maximized along the temporal direction and minimized along the spatial direction.

The first step in evaluating the fine-grained entropy (9.10) is to express the Minkowski distances in the Kruskal coordinates in terms of the Eddington–Finkelstein coordinates, using Eq. (4.41). This yields

$$\begin{aligned} &\lambda x_{Rb}^+ = e^{\lambda(t+b)}, \quad \lambda x_{Rb}^- = -e^{-\lambda(t-b)}, \quad \lambda x_{Lb}^+ = -e^{\lambda(-t+b)}, \quad \lambda x_{Lb}^- = e^{-\lambda(-t-b)}, \\ &\lambda x_{Ra}^+ = e^{\lambda(t'-a)}, \quad \lambda x_{Ra}^- = -e^{-\lambda(t'+a)}, \quad \lambda x_{La}^+ = -e^{\lambda(-t'-a)}, \quad \lambda x_{La}^- = e^{-\lambda(-t'+a)}. \end{aligned} \tag{9.11}$$

Substituting Eq. (9.11), the Minkowski distances d_{ij}^2 can then be written in terms of t, t', a, and b as

$$\begin{aligned}
\lambda^2 d_{12}^2 &= (x_{Rb}^+ - x_{Ra}^+)(x_{Rb}^- - x_{Ra}^-) = \left(e^{\lambda(t+b)} - e^{\lambda(t'-a)}\right)\left(-e^{\lambda(b-t)} + e^{-\lambda(t'+a)}\right), \\
\lambda^2 d_{34}^2 &= (x_{Lb}^+ - x_{La}^+)(x_{Lb}^- - x_{La}^-) = \left(-e^{\lambda(b-t)} + e^{-\lambda(t'+a)}\right)\left(e^{\lambda(t+b)} - e^{\lambda(t'-a)}\right), \\
\lambda^2 d_{14}^2 &= (x_{Rb}^+ - x_{Lb}^+)(x_{Rb}^- - x_{Lb}^-) = \left(e^{\lambda(t+b)} + e^{-\lambda(t-b)}\right)\left(-e^{-\lambda(t-b)} - e^{\lambda(t+b)}\right), \\
\lambda^2 d_{23}^2 &= (x_{Ra}^+ - x_{La}^+)(x_{Ra}^- - x_{La}^-) = \left(e^{\lambda(t'-a)} + e^{-\lambda(t'+a)}\right)\left(-e^{-\lambda(t'+a)} - e^{\lambda(t'-a)}\right), \\
\lambda^2 d_{24}^2 &= (x_{Ra}^+ - x_{Lb}^+)(x_{Ra}^- - x_{Lb}^-) = \left(e^{\lambda(t'-a)} + e^{\lambda(b-t)}\right)\left(-e^{-\lambda(t'+a)} - e^{\lambda(t+b)}\right), \\
\lambda^2 d_{13}^2 &= (x_{Rb}^+ - x_{La}^+)(x_{Rb}^- - x_{La}^-) = \left(e^{\lambda(t+b)} + e^{-\lambda(t'+a)}\right)\left(-e^{\lambda(b-t)} - e^{\lambda(t'-a)}\right).
\end{aligned} \tag{9.12}$$

From these expressions we see that $d_{12}^2 = d_{34}^2$ and $d_{24}^2 = d_{13}^2$. Moreover,

$$\lambda^2 d_{14}^2 = -4e^{2\lambda b}\cosh^2(\lambda t), \qquad \lambda^2 d_{23}^2 = -4e^{-2\lambda a}\cosh^2(\lambda t'). \tag{9.13}$$

In the early phase of evaporation, the configuration without an island gives the minimal value of the fine-grained entropy (1.6), so we focus instead on the late-time regime, where the dominant configuration is expected to include an island. Consider, in the late-time limit $\lambda t \gg 1$ and $\lambda t' \gg 1$, the following ratio:

$$\frac{d_{23}^2 d_{14}^2}{d_{24}^2 d_{13}^2} = 16e^{2\lambda(b-a)}\frac{\cosh^2(\lambda t)\cosh^2(\lambda t')}{\left(e^{\lambda(t+b)} + e^{-\lambda(t'+a)}\right)^2\left(e^{\lambda(b-t)} + e^{\lambda(t'-a)}\right)^2} \sim 1, \quad t, t' \to \infty. \tag{9.14}$$

Since the logarithm of the quantity in Eq. (9.14) appears in the semi-classical entropy (9.10), this behavior implies that it can be ignored in the late-time limit. The other necessary ingredient is the eternal black hole metric (4.104), which, using left–right symmetry, takes the form

$$\begin{aligned}
e^{-2\rho_1} &= e^{-2\rho_4} = e^{2\lambda b} + \frac{\pi GM}{\lambda} \equiv e^{-2\rho_b}, \\
e^{-2\rho_2} &= e^{-2\rho_3} = e^{-2\lambda a} + \frac{\pi GM}{\lambda} \equiv e^{-2\rho_a}.
\end{aligned} \tag{9.15}$$

After substituting Eqs. (9.12) and (9.15), and using the late-time behavior of Eq. (9.14), the semi-classical entropy of the quantum fields becomes

$$S_{semi-cl} = \frac{N}{6}\ln\left(\frac{d_{12}^4}{\delta^4}e^{2\rho_a}e^{2\rho_b}\right) = \frac{N}{6}\ln\frac{\left(e^{\lambda(t+b)} - e^{\lambda(t'-a)}\right)^2\left(-e^{\lambda(b-t)} + e^{-\lambda(t'+a)}\right)^2}{(\lambda\delta)^2\left(e^{2\lambda b} + \frac{\pi GM}{\lambda}\right)\left(e^{-2\lambda a} + \frac{\pi GM}{\lambda}\right)}. \tag{9.16}$$

Now we extremize Eq. (9.16) with respect to the temporal coordinate. This can be done without including the surface contribution in Eq. (1.6), since that term depends only on the static black hole metric and is therefore time independent. Extremizing Eq. (9.16) gives the relation between the time at the island boundary and the time at the cut-off surface:

$$\partial_{t'} S_{gen} = \partial_{t'} S_{semi-cl} = \frac{N}{3}\frac{\partial_{t'} d_{12}^2}{d_{12}^2} = \frac{2N\lambda}{3d_{12}^2}e^{\lambda(b-a)}\sinh\left(\lambda(t-t')\right) = 0 \implies t' = t. \tag{9.17}$$

It is important to note that this relation between t and t' is valid only in the asymptotic late-time regime, $\lambda t \gg 1$ and $\lambda t' \gg 1$. This justifies imposing the condition $\lambda t' \gg 1$ simultaneously with $\lambda t \gg 1$. We can therefore rewrite Eq. (9.16) in the following static form:

$$S_{semi-cl} = \frac{N}{3}\rho_a + \frac{N}{3}\ln\frac{\left(e^{\lambda b} - e^{-\lambda a}\right)^2}{(\lambda\delta)^2\sqrt{e^{2\lambda b} + \frac{\pi GM}{\lambda}}}. \tag{9.18}$$

We choose the regularization of the UV cut-off so that the semi-classical entropy (9.18) is given by:

$$S_{semi-cl} = \frac{N}{3}\left(\rho_a - \rho_b\right) + \frac{2N}{3}\ln\left(e^{\lambda b} - e^{-\lambda a}\right) - \frac{2N}{3}\ln 2 - \frac{2N}{3}\lambda b. \tag{9.19}$$

Next, we examine the surface term in Eq. (1.6). It is not a priori obvious whether this contribution should be identified solely with the classical Bekenstein–Hawking entropy (1.4), or instead with its quantum-corrected counterpart (8.83) evaluated at the island boundary. Following [57], we adopt the quantum-corrected expression. An additional factor of 2 is required, as the geometry contains two asymptotically flat regions. The area term is therefore:

$$\frac{A[I]}{4G} = 2\left[\frac{2}{G\hbar}e^{-2\phi_a} - \frac{N}{6}\phi_a\right] + C = \frac{4}{G\hbar}\left[e^{-2\lambda a} + \frac{\pi GM}{\lambda}\right] + \frac{N}{6}\ln\left(e^{-2\lambda a} + \frac{\pi GM}{\lambda}\right) + C. \tag{9.20}$$

In Sec. 8.3.2 we pointed out that the quantum-corrected area term (8.83) is fixed only up to an additive constant C. This contribution is absent when the island is moved all the way down to the boundary of spacetime. However, this situation is not equivalent to imposing $\frac{A[I]}{4G} = 0$ in the limit $a \to \infty$, because in that case one recovers the Bekenstein–Hawking entropy (8.83), as $a \to \infty$ corresponds to the event horizon. A natural prescription for choosing the constant C is to require that at the moment of the black hole formation, i.e. in the combined limit $a \to \infty$ and $M \to 0$, the expression (9.20) goes to zero. It is important to emphasize that the order in which these limits are taken matters. With this prescription, the constant C is given by

$$C = -\frac{N}{6}\ln\frac{\pi GM}{\lambda}. \tag{9.21}$$

With this choice, the full expression for the generalized entropy, obtained by adding Eqs. (9.19) and (9.20), takes the form:

$$S_{gen} = \frac{4}{G\hbar}\left[e^{-2\lambda a} + \frac{\pi GM}{\lambda}\right] - \frac{N}{3}\rho_b + \frac{2N}{3}\ln\left(1 - e^{-\lambda(a+b)}\right) - \frac{2N}{3}\ln 2 - \frac{2N}{3}\lambda b + C, \tag{9.22}$$

where we have adopted the Kruskal gauge $\rho_a = \phi_a$ and inserted the metric solution (4.104). We now extremize this expression along the spatial direction, that is, with respect to the parameter a:

$$\partial_a S_{gen} = -\frac{8\lambda}{G\hbar}e^{-2\lambda a} + \frac{2N\lambda}{3}\frac{1}{e^{\lambda(a+b)} - 1} = 0 \quad \Longleftrightarrow \quad e^{2\lambda a} - \frac{12}{NG\hbar}e^{\lambda b}e^{\lambda a} + \frac{12}{NG\hbar} = 0. \tag{9.23}$$

Thus, we arrive at a quadratic equation in $e^{\lambda a}$. Its solutions are:

$$e^{\lambda a_\pm} = \frac{6}{NG\hbar}e^{\lambda b}\left[1 \pm \sqrt{1 - \frac{NG\hbar}{3}e^{-2\lambda b}}\right]. \tag{9.24}$$

Eq. (9.24) yields two quantum extremal surfaces. To identify which of these corresponds to the correct island boundary, we must determine which root gives the global minimum of Eq. (9.22). We begin by examining the expression under the square root in Eq. (9.24):

$$1 - \frac{NG\hbar}{3} e^{-2\lambda b} > 0 \quad \Longrightarrow \quad e^{2\lambda b} > \frac{NG\hbar}{3}. \tag{9.25}$$

Since both b and the black hole mass M are expected to be large, we consider the two limiting regimes $e^{2\lambda b} \gg \frac{NG\hbar}{3}$ and $\frac{\pi GM}{\lambda} \gg e^{2\lambda b}$. Implementing these approximations in (9.24) gives

$$e^{\lambda a_+} \approx \frac{12}{NG\hbar} e^{\lambda b} \quad \wedge \quad e^{\lambda a_-} \approx e^{-\lambda b}. \tag{9.26}$$

We first analyze the effect of substituting the a_- root into the generalized entropy (9.22). In this case we find

$$\frac{1}{G\hbar} e^{-2\lambda a} \to \frac{1}{G\hbar} e^{2\lambda b} \to \infty, \quad \ln\left(1 - e^{-\lambda(a+b)}\right) \to \ln\left(\frac{NG\hbar}{12} e^{-2\lambda b}\right) \to -\infty, \tag{9.27}$$

so that the generalized entropy diverges, $S_{gen} \to \infty$, in the limits under consideration. In contrast, using the a_+ root we obtain

$$e^{-2\lambda a} \to \left(\frac{NG\hbar}{12}\right)^2 e^{-2\lambda b} \to 0, \quad \ln\left(1 - e^{-\lambda(a+b)}\right) \to \ln\left(1 - \frac{NG\hbar}{12} e^{-2\lambda b}\right) \to -\frac{NG\hbar}{12} e^{-2\lambda b} \to 0. \tag{9.28}$$

Thus, the a_+ root leads to a finite, well-defined limit of the generalized entropy (9.22), and therefore corresponds to the global minimum. Consequently, the fine-grained entropy is obtained by inserting a_+ from Eq. (9.24) into Eq. (9.22), which yields

$$\begin{aligned} S_{FG} &= \frac{4}{G\hbar}\left[\left(\frac{NG\hbar}{12}\right)^2 e^{-2\lambda b} + \frac{\pi GM}{\lambda}\right] - \frac{N}{3}\rho_b - \frac{2N}{3}\frac{NG\hbar}{12} e^{-2\lambda b} - \frac{2N}{3}\ln 2 - \frac{2N}{3}\lambda b + C \\ &= \frac{4\pi M}{\lambda\hbar} + \frac{N}{6}\ln\left(e^{2\lambda b} + \frac{\pi GM}{\lambda}\right) - \frac{N^2 G\hbar}{18} e^{-2\lambda b} - \frac{2N}{3}\ln 2 - \frac{2N}{3}\lambda b + C \\ &\approx \frac{4\pi M}{\lambda\hbar} + \frac{N}{6}\ln\frac{\pi GM}{\lambda} + C = 2S_{BH}. \end{aligned} \tag{9.29}$$

It is evident that the global minimum corresponds to the a_+ root in Eq. (9.24). In the first line of Eq. (9.29) we employed the approximation $\frac{NG\hbar}{12} e^{-2\lambda b} \ll 1$. Next, in the second line we simplified the resulting expression. In the third line we assumed a very large mass, namely $\frac{\pi GM}{\lambda} \gg e^{2\lambda b}$, and inserted the Eq. (9.21) for the constant C. As a result, we find that the entropy we obtain is approximately equal to $2S_{BH}$, as expected. We therefore conclude that, within this model, we have successfully reproduced the Page curve, which is given by:

$$S_{FG} = \mathbf{min}\left\{\frac{N}{3}\lambda t, 2S_{BH}\right\}. \tag{9.30}$$

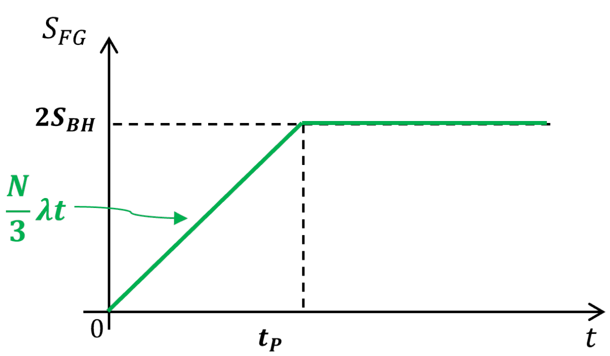

Figure 9.3: Page curve for an eternal black hole in the BPP model

9.2 Page curve in the evaporating black hole scenario

Here we study the entanglement entropy of the evaporating black hole solution in the BPP model introduced in Sec. 4.3.4. The discussion is organized into four subsections. In the first, we investigate the no-island configuration, which reproduces Hawking's original result and leads to information loss. We then consider the entanglement entropy in the presence of an island. In this case we demonstrate that the island forms behind the horizon, as expected, and that the Page curve is correctly obtained using the formula for the fine-grained entropy in gravitational systems (1.6). The third subsection is devoted to analyzing the Page time. The full computation is performed in asymptotically flat Eddington–Finkelstein coordinates, since these provide the time measured by an asymptotic stationary observer. In the final subsection, we repeat the calculation of the island location, now working in Kruskal coordinates (4.2). For most of this chapter we closely follow the derivation presented in [41].

9.2.1 No-island configuration

Unlike an eternal black hole, an evaporating black hole possesses a well-defined spacetime boundary on which reflective boundary conditions are imposed. Consequently, we must employ the expression (8.55) for the entanglement entropy of the quantum fields, which explicitly incorporates these reflective boundary conditions. In the no-island setup, the fine-grained entropy (1.6) therefore simplifies to the semiclassical contribution given by Eq. (8.55), namely:

$$S_{FG} = \frac{N}{12} \ln \frac{(\sigma^+_S - \sigma^+_{\bar{S}})^2}{\delta^2 e^{-2\rho_S(\sigma)}}. \tag{9.31}$$

Because we are considering an evaporating black hole, the relevant quantum state is the Unruh vacuum (3.98). The EMT is normal ordered with respect to the asymptotically flat coordinates defined before the collapse, namely the Eddington–Finkelstein coordinates $\sigma^\pm$. Thus entropy (9.31) is expressed in terms of these coordinates.

Fig. 9.4 depicts the evaporating black hole scenario. The constant-time slice supporting the radiation degrees of freedom is indicated in red. It stretches from spatial infinity i^0 and intersects the cut-off surface (dashed blue line) at a point with coordinates (t, b). The point S represents the projection of this intersection onto past null infinity $\mathcal{J}^-$, while the point $\bar{S}$ is obtained by reflecting (t, b) across the spacetime boundary and then projecting onto the $\mathcal{J}^-$ hypersurface. This explains the labels S and $\bar{S}$ used in Eq. (9.31). The region inaccessible to an asymptotic observer is shaded in red. The spacetime boundary is given by Eq. (4.115), namely $2\lambda\sigma_{cr} = \ln \frac{\varepsilon\pi G}{4}$. Hence, the reflective boundary conditions imply:

$$\sigma^+_{\bar{S}} = \sigma^-_{\bar{S}} + 2\sigma_{cr} = \sigma^-_S + 2\sigma_{cr}. \tag{9.32}$$

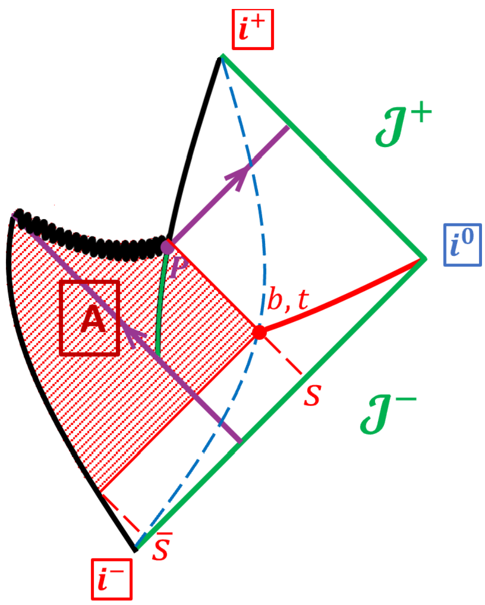

Figure 9.4: Penrose diagram illustrating the no-island setup for an evaporating black hole in the BPP model

The notion of time is specified using the asymptotically flat coordinates of region II (see Fig. 4.6), namely the $\hat{\sigma}^{\pm}$ coordinates introduced in Eq. (4.59). Consequently, in order to examine the time dependence of Eq. (9.31), we must rewrite it in terms of the $\hat{\sigma}^{\pm}$ coordinates. Implementing Eq. (9.32), the coordinate difference in Eq. (9.31) becomes

$$\sigma_S^+ - \sigma_{\bar{S}}^+ = \sigma_S^+ - \sigma_S^- - \frac{1}{\lambda}\ln\frac{\varepsilon\pi G}{4} = 2\sigma_S - \frac{1}{\lambda}\ln\frac{\varepsilon\pi G}{4}, \tag{9.33}$$

while the metric (4.119) can be written as

$$\begin{aligned}
e^{2\lambda b} &= -\lambda^2 x_S^+(x_S^- + \Delta) = e^{2\lambda\sigma_S} - \lambda\Delta e^{\lambda(t+b)} \implies \sigma_S = b + \frac{1}{2\lambda}\ln\left(1+\lambda\Delta e^{\lambda(t-b)}\right),\\
e^{-2\rho_S(\sigma)} &= \frac{d\sigma^+}{dx^+}\frac{d\sigma^-}{dx^-}e^{-2\rho_S(x)} = e^{-2\lambda\sigma_S}\left[-\lambda^2 x_S^+(x_S^-+\Delta) - \frac{\varepsilon\pi G}{4}\ln\left(-\lambda^2 x_S^+ x_S^-\right) + \frac{\pi G M}{\lambda} + C^*\right]\\
&= \frac{1-\left[\frac{\varepsilon\pi G}{4}\ln\left(1+\lambda\Delta e^{\lambda(t-b)}\right) + \frac{\varepsilon\pi G}{2}\lambda b - \frac{\pi G M}{\lambda} - C^*\right]e^{-2\lambda b}}{1+\lambda\Delta e^{\lambda(t-b)}}.
\end{aligned} \tag{9.34}$$

By inserting Eqs. (9.33) and (9.34) into the expression for the fine-grained entropy (9.31), we obtain:

$$S_{FG} = \frac{N}{12}\ln\frac{\left[2\lambda b + \ln\left(1+\lambda\Delta e^{\lambda(t-b)}\right) - \ln\frac{\varepsilon\pi G}{4}\right]^2\left(1+\lambda\Delta e^{\lambda(t-b)}\right)}{(\lambda\delta)^2\left[1-\left(\frac{\varepsilon\pi G}{4}\ln\left(1+\lambda\Delta e^{\lambda(t-b)}\right) + \frac{\varepsilon\pi G}{2}\lambda b - \frac{\pi G M}{\lambda} - C^*\right)e^{-2\lambda b}\right]}. \tag{9.35}$$

At the beginning of the evaporation process, this function is effectively linear, but with a highly nontrivial slope. We do not study this limiting behavior in detail. To regularize the UV divergence in Eq. (9.35), we impose that the fine-grained entropy vanishes at $t = 0$. This implies that $S_{FG}(t)$ is shifted to $S_{FG}(t) - S_{FG}(0)$. Denoting the expression in Eq. (9.35) by $S(t)$, the renormalized entropy becomes $S_{FG}(t) = S(t) - S(0)$. To determine whether information is lost, we must investigate the asymptotic behavior of Eq. (9.35) at late times, i.e., for $\lambda t \gg 1$. In this regime, we immediately obtain $\ln\left(1+\lambda\Delta e^{\lambda(t-b)}\right) \approx \ln(\lambda\Delta) + \lambda(t-b)$. Under this approximation, Eq. (9.35) takes the following form:

$$S_{FG} \approx \frac{N}{12}\ln\frac{\lambda\Delta e^{\lambda(t-b)}\left[\lambda(t+b) + \ln(\lambda\Delta) - \ln\frac{\varepsilon\pi G}{4}\right]^2}{(\lambda\delta)^2\left[1-\left(\frac{\varepsilon\pi G}{4}\ln(\lambda\Delta) + \frac{\varepsilon\pi G}{4}(t+b) - \frac{\pi G M}{\lambda} - C^*\right)e^{-2\lambda b}\right]} - S(0). \tag{9.36}$$

From this expression we identify a logarithmic term proportional to $\ln(\lambda t)$ as well as a term growing linearly with t. At late times, the linear contribution clearly dominates the entropy growth. Consequently, we obtain:

$$S_{FG} \approx \frac{N}{12}\lambda t. \tag{9.37}$$

Therefore, in the no-island configuration, the information is lost and the Page curve cannot be recovered. The behavior we find reproduces Hawking's original result [16], as anticipated. To achieve unitary evolution, one must include the island and evaluate the entropy using the island rule.

9.2.2 Island configuration

We now consider the situation in which an island region is present in the spacetime. In this case, both contributions in Eq. (1.6) are non-zero. As in the eternal black hole setup discussed in the previous subsection, reflective boundary conditions must be imposed at the spacetime boundary. Although the inaccessible region A is simply connected, these reflective boundary conditions imply that its projection onto the $\mathcal{J}^-$ hypersurface breaks up into two separate regions. Consequently, for this configuration we must employ a considerably more complicated formula for the semiclassical entropy in Eq. (1.6), namely the one given in Eq. (8.61):

$$S_{semi-cl} = \frac{N}{12} \ln \frac{(\sigma_I^+ - \sigma_S^+)^2(\sigma_{\bar{I}}^+ - \sigma_{\bar{S}}^+)^2(\sigma_I^+ - \sigma_{\bar{I}}^+)^2(\sigma_S^+ - \sigma_{\bar{S}}^+)^2}{\delta^4(\sigma_S^+ - \sigma_{\bar{I}}^+)^2(\sigma_I^+ - \sigma_{\bar{S}}^+)^2 e^{-2\rho_S(\sigma)} e^{-2\rho_I(\sigma)}}. \tag{9.38}$$

Here, the labels S and $\bar{S}$ denote, respectively, the projection of the intersection between the constant-time slice and the cut-off hypersurface, and the projection of its reflection on the spacetime boundary onto past null infinity $\mathcal{J}^-$. Similarly, I and $\bar{I}$ represent the projections of the island boundary location and of its reflection on the spacetime boundary onto the hypersurface $\mathcal{J}^-$, respectively.

Fig. 9.5 depicts how the configuration in Fig. 9.4 is modified once an island region is included. The island, denoted by I, is indicated in blue, while the inaccessible region A is highlighted in red. All relevant projections, namely S, $\bar{S}$, I, and $\bar{I}$, are explicitly displayed. The $\sigma^\pm$ coordinates corresponding to these projections are determined using the definition of the spacetime boundary hypersurface (4.115), and take the form

$$\begin{aligned} \sigma_{\bar{S}}^+ &= \sigma_{\bar{S}}^- + 2\sigma_{cr} = \sigma_S^- + \frac{1}{\lambda} \ln \frac{\varepsilon \pi G}{4}, \\ \sigma_{\bar{I}}^+ &= \sigma_{\bar{I}}^- + 2\sigma_{cr} = \sigma_I^- + \frac{1}{\lambda} \ln \frac{\varepsilon \pi G}{4}. \end{aligned} \tag{9.39}$$

Because our goal is to analyze the time dependence of the fine-grained entropy, and the time coordinate is defined in terms of the new asymptotically flat coordinates of region II given in Eq. (4.59), we must rewrite Eq. (9.38) in this coordinate system.

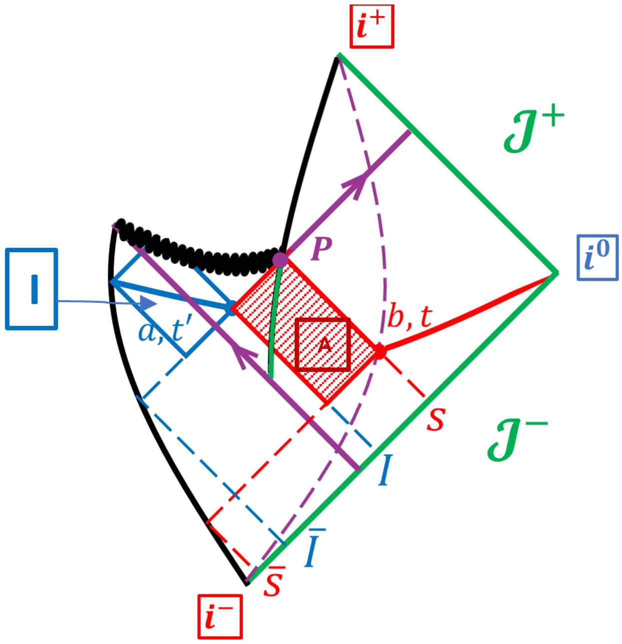

Figure 9.5: Penrose diagram illustrating the island setup for an evaporating black hole in the BPP model

We denote the island position by (t', a), whereas the coordinates on the cut–off surface are specified in the usual way as (t, b). In the large–mass limit, the horizon is located just below the hypersurface $x^- = -\Delta$ (see Sec. 4.3.4), implying that $x_I^- + \Delta$ is positive. Consequently, for the island coordinates, after using Eq. (4.59), we obtain:

$$\lambda x_I^+ = e^{\lambda(t'+a)} = e^{\lambda \sigma_I^+} \quad \wedge \quad \lambda(x_I^- + \Delta) = e^{-\lambda(t'-a)} = -e^{-\lambda \sigma_I^-} + \lambda\Delta. \tag{9.40}$$

Meanwhile, the coordinates on the cut-off surface are expressed as:

$$\lambda x_S^+ = e^{\lambda(t+b)} = e^{\lambda \sigma_S^+} \quad \wedge \quad \lambda(x_S^- + \Delta) = -e^{-\lambda(t-b)} = -e^{-\lambda \sigma_S^-} + \lambda\Delta. \tag{9.41}$$

By combining Eqs. (9.40) and (9.41) and employing the relations given in Eq. (9.39), the coordinate differences that appear in the expression (9.38) for the semiclassical entropy take the following form:

$$\begin{aligned}
&\sigma_I^+ - \sigma_S^+ = \hat{\sigma}_I^+ - \hat{\sigma}_S^+ = t' + a - (t+b),\\
&\sigma_{\bar{I}}^+ - \sigma_{\bar{S}}^+ = \sigma_I^- - \sigma_S^- = -\frac{1}{\lambda}\ln\left(\lambda\Delta - e^{-\lambda(t'-a)}\right) + \frac{1}{\lambda}\ln\left(\lambda\Delta + e^{-\lambda(t-b)}\right),\\
&\sigma_I^+ - \sigma_{\bar{I}}^+ = \sigma_I^+ - \sigma_I^- - \frac{1}{\lambda}\ln\frac{\varepsilon\pi G}{4} = t' + a + \frac{1}{\lambda}\ln\left(\lambda\Delta - e^{-\lambda(t'-a)}\right) - \frac{1}{\lambda}\ln\frac{\varepsilon\pi G}{4},\\
&\sigma_S^+ - \sigma_{\bar{S}}^+ = \sigma_S^+ - \sigma_S^- - \frac{1}{\lambda}\ln\frac{\varepsilon\pi G}{4} = t + b + \frac{1}{\lambda}\ln\left(\lambda\Delta + e^{-\lambda(t-b)}\right) - \frac{1}{\lambda}\ln\frac{\varepsilon\pi G}{4},\\
&\sigma_S^+ - \sigma_{\bar{I}}^+ = \sigma_S^+ - \sigma_I^- - \frac{1}{\lambda}\ln\frac{\varepsilon\pi G}{4} = t + b + \frac{1}{\lambda}\ln\left(\lambda\Delta - e^{-\lambda(t'-a)}\right) - \frac{1}{\lambda}\ln\frac{\varepsilon\pi G}{4},\\
&\sigma_I^+ - \sigma_{\bar{S}}^+ = \sigma_I^+ - \sigma_S^- - \frac{1}{\lambda}\ln\frac{\varepsilon\pi G}{4} = t' + a + \frac{1}{\lambda}\ln\left(\lambda\Delta + e^{-\lambda(t-b)}\right) - \frac{1}{\lambda}\ln\frac{\varepsilon\pi G}{4}.
\end{aligned} \tag{9.42}$$

In the early stages of the evaporation process, the configuration without an island yields the minimum of the fine-grained entropy. We now focus on the late-time regime, where the minimum is expected to switch to the spacetime configuration that includes an island. We start by analyzing the following quantity in the regime where $\lambda t \gg 1$ and $\lambda t' \gg 1$:

$$\begin{aligned}
&\frac{(\sigma_I^+ - \sigma_{\bar{I}}^+)(\sigma_S^+ - \sigma_{\bar{S}}^+)}{(\sigma_I^+ - \sigma_{\bar{S}}^+)(\sigma_S^+ - \sigma_{\bar{I}}^+)} \\
&= \frac{\left[t' + a + \frac{1}{\lambda}\ln\left(\lambda\Delta - e^{-\lambda(t'-a)}\right) - \frac{1}{\lambda}\ln\frac{\varepsilon\pi G}{4}\right]\left[t + b + \frac{1}{\lambda}\ln\left(\lambda\Delta + e^{-\lambda(t-b)}\right) - \frac{1}{\lambda}\ln\frac{\varepsilon\pi G}{4}\right]}{\left[t + b + \frac{1}{\lambda}\ln\left(\lambda\Delta - e^{-\lambda(t'-a)}\right) - \frac{1}{\lambda}\ln\frac{\varepsilon\pi G}{4}\right]\left[t' + a + \frac{1}{\lambda}\ln\left(\lambda\Delta + e^{-\lambda(t-b)}\right) - \frac{1}{\lambda}\ln\frac{\varepsilon\pi G}{4}\right]} \to 1.
\end{aligned} \tag{9.43}$$

Thus, in analogy with the no-island configuration, the contribution (9.43) can be neglected in the late-time limit of Eq. (9.38), yielding:

$$S_{semi-cl} = \frac{N}{6}\left(\rho_S(\sigma) + \rho_I(\sigma)\right) + \frac{N}{12}\ln\frac{(\sigma_I^+ - \sigma_S^+)^2(\sigma_{\bar{I}}^+ - \sigma_{\bar{S}}^+)^2}{\delta^4}. \tag{9.44}$$

In this late-time regime, the difference of the reflected coordinates in Eq. (9.44) may be further approximated as:

$$\sigma_{\bar{I}}^+ - \sigma_{\bar{S}}^+ = \frac{1}{\lambda}\left[\ln\left(1 + \frac{1}{\lambda\Delta}e^{-\lambda(t-b)}\right) - \ln\left(1 - \frac{1}{\lambda\Delta}e^{-\lambda(t'-a)}\right)\right] \approx \frac{1}{\lambda^2\Delta}\left(e^{-\lambda(t-b)} + e^{-\lambda(t'-a)}\right). \tag{9.45}$$

We emphasize that the UV divergences must be regularized in exactly the same manner as in the configuration without an island (or in the eternal black hole case). This affects the result only by an additive constant. Consequently, the semiclassical entropy formula (9.44) becomes:

$$S_{semi-cl} = \frac{N}{6}\left(\rho_S(\sigma) + \rho_I(\sigma)\right) + \frac{N}{6}\ln\frac{\left|\lambda(t + b - t' - a)\right|\left(e^{-\lambda(t-b)} + e^{-\lambda(t'-a)}\right)}{(\lambda\delta)^2(\lambda\Delta)} - S_0, \tag{9.46}$$

where we have subtracted the additive constant S_0. We now consider the surface term appearing in Eq. (1.6). As in the eternal black hole scenario, it is again given by Eq. (8.83). Thus, we obtain:

$$
\begin{aligned}
\frac{A[I]}{4G} &= \frac{2}{G\hbar}e^{-2\phi_I} - \frac{N}{6}\phi_I + C \\
&= \frac{2}{G\hbar}\left[-\lambda^2 x_I^+(x_I^- + \Delta) - \frac{\varepsilon\pi G}{4}\ln\left(-\lambda^2 x_I^+ x_I^-\right) + \frac{\pi G M}{\lambda} + C^*\right] - \frac{N}{6}\phi_I + C \\
&= \frac{2}{G\hbar}\left[-e^{2\lambda a} - \frac{\varepsilon\pi G}{4}\ln\left(-e^{2\lambda a} + \lambda\Delta e^{\lambda(t'+a)}\right) + \frac{\pi G M}{\lambda} + C^*\right] - \frac{N}{6}\phi_I + C \\
&= \frac{2}{G\hbar}\left[-e^{2\lambda a} - \frac{\varepsilon\pi G}{4}\lambda(t'+a) - \frac{\varepsilon\pi G}{4}\ln(\lambda\Delta) + \frac{\pi G M}{\lambda} + C^*\right] - \frac{N}{6}\phi_I + C,
\end{aligned}
\tag{9.47}
$$

where C is an arbitrary integration constant. For further details, see Sec. 8.3.2. In the second line we have inserted the metric (4.119). In the third line, we have used the island position (9.40). Finally, in the last line we have taken the large-t' limit. We now need to rewrite the dilaton field ϕ_I in terms of the metric function ρ_I. To do so, we use the fact that these two quantities coincide in Kruskal coordinates, and then transform them to the Eddington–Finkelstein coordinates of region II in Fig. 4.6. Concretely, we have

$$
e^{2\phi}\mathrm{d}x^+\mathrm{d}x^- = e^{2\rho(\sigma)}\mathrm{d}\sigma^+\mathrm{d}\sigma^- \quad \Longrightarrow \quad e^{2\phi_I} = \frac{\mathrm{d}\sigma^+}{\mathrm{d}x^+}\frac{\mathrm{d}\sigma^-}{\mathrm{d}x^-}e^{2\rho_I(\sigma)} = e^{-2\lambda\sigma_I}e^{2\rho_I(\sigma)}. \tag{9.48}
$$

This leads to the following form for the dilaton field:

$$
\phi_I = \rho_I(\sigma) - \lambda\sigma_I = \rho_I(\sigma) - \frac{1}{2}\ln\left(-e^{2\lambda a} + \lambda\Delta e^{\lambda(t'+a)}\right) = \rho_I(\sigma) - \frac{1}{2}\lambda(a+t') - \frac{1}{2}\ln(\lambda\Delta), \tag{9.49}
$$

where, in the last step, we have again employed the large-t' limit. Substituting this expression into Eq. (9.47), we obtain

$$
\frac{A[I]}{4G} = \frac{2}{G\hbar}\left[-e^{2\lambda a} + \frac{\varepsilon\pi G}{4}\lambda(a+t') + \frac{\varepsilon\pi G}{4}\ln(\lambda\Delta) + \frac{\pi G M}{\lambda} + C^*\right] - \frac{N}{6}\rho_I(\sigma) + C. \tag{9.50}
$$

The generalized entropy is then defined as the sum of the semiclassical contribution (9.46) and the area term (9.50). It is given by the following expression:

$$
\begin{aligned}
S_{gen} =& \frac{2}{G\hbar}\left[-e^{2\lambda a} + \frac{\varepsilon\pi G}{4}\lambda(a+t') + \frac{\pi G M}{\lambda} + C^*\right] + \frac{N}{6}\rho_S(\sigma) \\
&+ \frac{N}{6}\ln\frac{\left|\lambda(t+b-t'-a)\right|\left(e^{-\lambda(t-b)} + e^{-\lambda(t'-a)}\right)}{(\lambda\delta)^2(\lambda\Delta)^{3/4}} + C - S_0.
\end{aligned}
\tag{9.51}
$$

Next, we extremize this expression with respect to both the temporal coordinate t' and the spatial coordinate a:

$$
\partial_{t'}S_{gen} = 0 \quad \Longleftrightarrow \quad \frac{N}{24}\lambda + \frac{N}{6}\lambda\left[\frac{1}{\lambda(t'+a-t-b)} - \frac{1}{1+e^{\lambda(t'-t+b-a)}}\right] = 0, \tag{9.52}
$$

$$
\partial_a S_{gen} = 0 \quad \Longleftrightarrow \quad -\frac{4\lambda}{G\hbar}e^{2\lambda a} + \frac{N}{24}\lambda + \frac{N}{6}\lambda\left[\frac{1}{\lambda(t'+a-t-b)} + \frac{1}{1+e^{\lambda(t'-t+b-a)}}\right] = 0. \tag{9.53}
$$

After simplifying, this system of algebraic equations can be rewritten as:

$$\frac{1}{\lambda(t'+a-t-b)}+\frac{1}{1+e^{\lambda(t'-t+b-a)}}=-\frac{1}{4}+\frac{2}{\varepsilon\pi G}e^{2\lambda a}, \tag{9.54}$$

$$\frac{1}{\lambda(t'+a-t-b)}-\frac{1}{1+e^{\lambda(t'-t+b-a)}}=-\frac{1}{4}. \tag{9.55}$$

Subtracting these two equations yields a quadratic equation for $e^{\lambda a}$:

$$e^{2\lambda a}+e^{\lambda a}e^{\lambda(t'-t+b)}-\varepsilon\pi G=0 \quad\Longrightarrow\quad e^{\lambda a}=\frac{1}{2}e^{\lambda(t'-t+b)}\left[\sqrt{1+4\varepsilon\pi G e^{-2\lambda(t'-t+b)}}-1\right]. \tag{9.56}$$

Only one root is physically acceptable, as we must have $e^{\lambda a}>0$. This solution is very similar to the island location in the eternal black hole case, namely Eq. (9.24). However, here we still need to determine t' and a independently. To do so, we adopt the same approximation used for the eternal black hole, that is: $4\varepsilon\pi G e^{-2\lambda(t'-t+b)}\ll 1$. Under this approximation, the solution (9.56) simplifies to:

$$e^{\lambda a}=\varepsilon\pi G e^{-\lambda(t'-t+b)} \quad\Longrightarrow\quad e^{2\lambda a}=\varepsilon\pi G e^{-\lambda(t'-a+b-t)}=\varepsilon\pi G e^{-\mathrm{x}}, \tag{9.57}$$

where we introduced the auxiliary variable $\mathrm{x}=\lambda(t'-a+b-t)$. Adding Eqs. (9.54) and (9.55) gives:

$$\mathrm{x}=\frac{1}{-\frac{1}{4}+e^{-\mathrm{x}}}+2\lambda(b-a)=\frac{1}{-\frac{1}{4}+e^{-\mathrm{x}}}+2\lambda b-\ln(\varepsilon\pi G)+\mathrm{x}, \tag{9.58}$$

where, in the second equality, we have used the approximate expression (9.57). Solving this equation for x leads to:

$$e^{-\mathrm{x}}=\frac{1}{4}+\frac{1}{\ln\left(\varepsilon\pi G e^{-2\lambda b}\right)}. \tag{9.59}$$

Substituting this back into Eq. (9.57) yields:

$$e^{2\lambda a}=\frac{\varepsilon\pi G}{4}+\frac{\varepsilon\pi G}{\ln\left(\varepsilon\pi G e^{-2\lambda b}\right)}\approx\frac{\varepsilon\pi G}{4}, \tag{9.60}$$

where the last approximation follows from the condition $\varepsilon\pi G e^{-2\lambda b}\ll 1$, which renders the second term negligible. Consequently, in the late stages of black hole evaporation, extremizing the generalized entropy gives an island located at:

$$e^{2\lambda a}=\frac{\varepsilon\pi G}{4} \quad\wedge\quad \lambda t'=\lambda(t-b)+\frac{1}{2}\ln(4\varepsilon\pi G). \tag{9.61}$$

Within this approximation, we observe that t' becomes very large. This validates our initial assumption that we can take $\lambda t'\gg 1$ whenever $\lambda t\gg 1$. The remaining step is to determine the contribution of this island to the fine–grained entropy of the radiation, and to verify whether it reproduces the Page curve. Substituting Eq. (9.61) directly into the expression for the generalized entropy (9.51) gives:

$$
\begin{aligned}
S_{gen} &= \frac{2}{G\hbar}\left[\frac{\varepsilon\pi G}{4}\lambda(t-b)+\frac{\pi GM}{\lambda}+2C^{*}+\frac{\varepsilon\pi G}{4}\ln 2\right]+\frac{N}{6}\ln\frac{\frac{5}{4}\ln\left(\varepsilon\pi G e^{-2\lambda b}\right)}{(\lambda\delta)^2(\lambda\Delta)^{3/4}}+C-S_0\\
&\quad -\frac{N}{6}\lambda(t-b)+\frac{N}{12}\ln\frac{1+\lambda\Delta e^{\lambda(t-b)}}{1-\left[\frac{\varepsilon\pi G}{4}\ln\left(1+\lambda\Delta e^{\lambda(t-b)}\right)+\frac{\varepsilon\pi G}{2}\lambda b-\frac{\pi GM}{\lambda}-C^{*}\right]e^{-2\lambda b}}\\
&= -\frac{N}{24}\lambda t+\frac{2}{G\hbar}\left[\frac{\pi GM}{\lambda}+\frac{\varepsilon\pi G}{4}\lambda b+2C^{*}-\frac{\varepsilon\pi G}{4}\ln\left(\lambda\Delta\right)+\frac{\varepsilon\pi G}{4}\ln 2\right]\\
&\quad +\frac{N}{6}\ln\frac{\frac{5}{4}\left(\ln\left(\varepsilon\pi G\right)-2\lambda b\right)}{(\lambda\delta)^2\sqrt{1-\left[\frac{\varepsilon\pi G}{4}\ln\left(\lambda\Delta\right)+\frac{\varepsilon\pi G}{4}\lambda(t+b)-\frac{\pi GM}{\lambda}-C^{*}\right]e^{-2\lambda b}}}+C-S_0. \qquad (9.62)
\end{aligned}
$$

Note that, within the large-mass approximation, the constant term in this expression approaches the Bekenstein–Hawking entropy (1.4), provided the constants C and S_0 are chosen appropriately. Consequently, at the saddle point determined by the island, the generalized entropy becomes:

$$
S_{gen}=S_{BH}^{(0)}-\frac{N}{24}\lambda t \qquad\Longrightarrow\qquad S_{FG}=\mathbf{min}\left\{\frac{N}{12}\lambda t,\, S_{BH}^{(0)}-\frac{N}{24}\lambda t\right\}. \qquad (9.63)
$$

The first observation is that the island lies precisely where anticipated: just beneath the black hole's horizon. We can specify its location using Kruskal coordinates as

$$
\lambda^2 x_I^{+}(x_I^{-}+\Delta)=\frac{\varepsilon\pi G}{4}. \qquad (9.64)
$$

This shows that the island mirrors the apparent horizon across the hypersurface $x^{-}=-\Delta$, which almost exactly matches the horizon in large-mass limit.

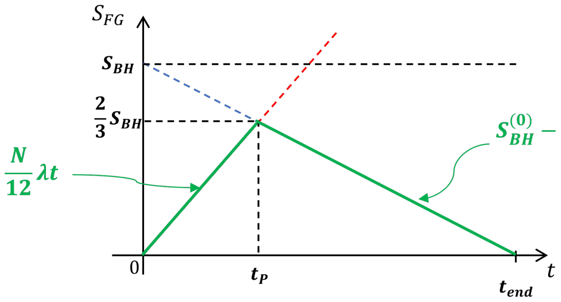

Figure 9.6: Page curve for an evaporating black hole in the BPP model

9.2.3 Page time and the validity of the Page curve

In this section, we examine the consistency of the solution obtained and determine several key parameters of the evaporation process, in particular the Page time. The Page time is defined as the moment when the phase transition in Eq. (9.63) takes place. Our first consistency check is to verify that the evaporation indeed terminates at the evaporation end-point (4.141). This follows immediately, since the fine-grained entropy (9.63) vanishes once we substitute Eq. (4.141). We now compute the Page time:

$$
\frac{N}{12}\lambda t_p=S_{BH}^{(0)}-\frac{N}{24}\lambda t_p \qquad\Longrightarrow\qquad t_p=\frac{16\pi M}{N\hbar\lambda^2}, \qquad (9.65)
$$

where we have used the classical expression for the Bekenstein–Hawking entropy of a black hole in the CGHS model. From this we infer that the phase transition occurs at one third of the total evaporation time, i.e. $t_p=\frac{t_{\text{end}}}{3}$. This is much earlier than the moment when quantum gravitational effects become significant, since the black hole remains macroscopically large at that time. Therefore, the semiclassical approximation is reliable at the Page time. It remains to evaluate the entropy at the Page time. We obtain:

$$
S_{FG,p}=\frac{N}{12}\lambda t_p=\frac{N}{12}\lambda\frac{8S_{BH}^{(0)}}{N\lambda} \qquad\Longrightarrow\qquad S_{FG,p}=\frac{2}{3}S_{BH}. \qquad (9.66)
$$

This is the maximum value attained by the fine-grained entropy of the radiation during black hole evaporation, and it is manifestly smaller than the Bekenstein–Hawking entropy of the black hole. We can thus conclude that unitarity is preserved. Consequently, the curve shown in Fig. 9.6 is indeed the Page curve.

As we know, throughout the entire black hole evaporation process the island remains located behind the event horizon. At some point, the trajectory traced by the island over time (9.64) intersects the singularity. We must verify that this intersection happens only at the very end of evaporation, because the Page curve description is valid only as long as such an intersection does not occur. To this end, we need to solve the following system of equations:

$$\lambda^2 x^+_{col}(x^-_{col}+\Delta) = \frac{\varepsilon\pi G}{4}, \tag{9.67}$$

$$-\lambda^2 x^+_{col}(x^-_{col}+\Delta) - \frac{\varepsilon\pi G}{4}\ln\left(-\lambda^2 x^+_{col}x^-_{col}\right) + \frac{\pi G M}{\lambda} + C^* = 0, \tag{9.68}$$

where the second equation specifies the singularity hypersurface (4.120). We previously solved an analogous system when determining where the apparent horizon meets the singularity in Sec. 4.3.4. The solution to the present system is as follows:

$$\lambda x^+_{col} = \frac{\varepsilon\pi G}{4\lambda\Delta}\left[1+e^{-2+\frac{4M}{\varepsilon\lambda}}\right] \quad \wedge \quad \lambda(x^-_{col}+\Delta) = \frac{\lambda\Delta}{1+e^{-2+\frac{4M}{\varepsilon\lambda}}}. \tag{9.69}$$

Consequently, the collision time is given by:

$$e^{2\lambda t_{col}} = \frac{x^+_{col}}{x^-_{col}+\Delta} = \frac{\varepsilon\pi G}{4(\lambda\Delta)^2}\left(1+e^{-2+\frac{4M}{\varepsilon\lambda}}\right)^2. \tag{9.70}$$

We now determine when this intersection takes place relative to the total evaporation time. Using Eq. (4.124), the end-time can be written as:

$$e^{2\lambda t_{end}} = \frac{\varepsilon\pi G}{4(\lambda\Delta)^2}\left(e^{\frac{4M}{\varepsilon\lambda}}-1\right)^2. \tag{9.71}$$

Subtracting the time defined in Eq. (9.69) from that in Eq. (9.71) yields:

$$\begin{aligned}\lambda\Delta t = \lambda(t_{end}-t_{col}) &= \ln\left(e^{\frac{4M}{\varepsilon\lambda}}-1\right) - \ln\left(e^{-2+\frac{4M}{\varepsilon\lambda}}+1\right)\\ &= \frac{4M}{\varepsilon\lambda} + \ln\left(1-e^{-\frac{4M}{\varepsilon\lambda}}\right) - \left(-2+\frac{4M}{\varepsilon\lambda}\right) - \ln\left(1-e^{2-\frac{4M}{\varepsilon\lambda}}\right) \approx 2. \end{aligned}\tag{9.72}$$

We observe that this time gap is $\lambda\Delta t \approx 2$, which is of order $\mathcal{O}(1)$. For a large initial mass this contribution is negligible. Hence, the intersection effectively occurs just before the very end of the black hole's lifetime. At that stage, the black hole has shrunk to a size of order the Planck length, so quantum gravitational effects become important and the semiclassical approximation is no longer reliable. In a full theory of quantum gravity, one may therefore expect that the island and the singularity never actually collide.

As we can see, this does not pose a problem either, and we conclude that our semiclassical approximation remains valid until the very end of the black hole evaporation process. Completely identical results are obtained in the RST model [40].

9.2.4 Position of the island in terms of the Kruskal coordinates

In this subsection we repeat the computation of the island position using Kruskal coordinates. To do this, we express the generalized entropy in terms of the Kruskal coordinates and then extremize it, following the procedure in [41]. In these coordinates we no longer need to guess where the island should lie, since the Kruskal coordinates $x^{\pm}$ are analytic throughout the whole spacetime. We avoided this route at first because the asymptotic observer's time is defined via the $\hat{\sigma}^{\pm}$ coordinates, which directly encode the time dependence of the entropy. For that reason, the earlier method is more convenient for giving a physical interpretation of black hole evaporation process.

We now go directly to the late–time limit of the evaporation. In this limit the quantity (9.43) approaches unity. The remaining differences can then be easily evaluated:

$$\sigma_I^+ - \sigma_S^+ = \frac{1}{\lambda}\ln\frac{x_I^+}{x_S^+} \quad \wedge \quad \sigma_I^+ - \sigma_{\bar{S}}^+ = \frac{1}{\lambda}\ln\frac{x_I^-}{x_S^-}. \tag{9.73}$$

Substituting Eq. (9.73) and the metric (4.119) into Eq. (9.38), the semi–classical entropy becomes

$$S_{semi-cl} = \frac{N}{12}\ln\frac{\ln^2\frac{x_I^+}{x_S^+}\ln^2\frac{x_I^-}{x_S^-}\left(-\lambda^2 x_I^+ x_I^-\right)e^{2\rho_S(\sigma)}}{(\lambda\delta)^4\left[-\lambda^2 x_I^+(x_I^- + \Delta) - \frac{\varepsilon\pi G}{4}\ln\left(-\lambda^2 x_I^+ x_I^-\right) + \frac{\pi G M}{\lambda} + C^*\right]} - S_0, \tag{9.74}$$

while the surface contribution (8.83) is

$$\begin{aligned}\frac{A[I]}{4G} &= \frac{2}{G\hbar}e^{-2\phi_I} - \frac{N}{6}\phi_I + C\\ &= \frac{2}{G\hbar}\left[-\lambda^2 x_I^+(x_I^- + \Delta) - \frac{\varepsilon\pi G}{4}\ln\left(-\lambda^2 x_I^+ x_I^-\right) + \frac{\pi G M}{\lambda} + C^*\right]\\ &\quad + \frac{N}{12}\ln\left\{-\lambda^2 x_I^+(x_I^- + \Delta) - \frac{\varepsilon\pi G}{4}\ln\left(-\lambda^2 x_I^+ x_I^-\right) + \frac{\pi G M}{\lambda} + C^*\right\} + C.\end{aligned} \tag{9.75}$$

Since we are interested only in the island position and not in the explicit closed form of the fine–grained entropy, we group all terms independent of $x_I^{\pm}$ into a single constant C_0. The generalized entropy can then be written as

$$S_{gen} = \frac{2}{G\hbar}\left[-\lambda^2 x_I^+(x_I^- + \Delta) - \frac{\varepsilon\pi G}{4}\ln\left(-\lambda^2 x_I^+ x_I^-\right)\right] + \frac{N}{12}\ln\left(-\lambda^2 x_I^+ x_I^- \ln^2\frac{x_I^+}{x_S^+}\ln^2\frac{x_I^-}{x_S^-}\right) + C_0. \tag{9.76}$$

We now extremize this expression with respect to x_I^+ and x_I^-, obtaining

$$\partial_+ S_{gen} = 0 \quad \Longleftrightarrow \quad \frac{2}{G\hbar}\left[-\lambda^2(x_I^- + \Delta) - \frac{\varepsilon\pi G}{4}\frac{1}{x_I^+}\right] + \frac{N}{12}\left[\frac{1}{x_I^+} + \frac{2}{\ln\frac{x_I^+}{x_S^+}}\frac{1}{x_I^+}\right] = 0, \tag{9.77}$$

$$\partial_- S_{gen} = 0 \quad \Longleftrightarrow \quad \frac{2}{G\hbar}\left[-\lambda^2 x_I^+ - \frac{\varepsilon\pi G}{4}\frac{1}{x_I^-}\right] + \frac{N}{12}\left[\frac{1}{x_I^-} + \frac{2}{\ln\frac{x_I^-}{x_S^-}}\frac{1}{x_I^-}\right] = 0. \tag{9.78}$$

Multiplying the first of these by x_I^+ and the second by x_I^- leads to

$$\lambda^2 x_I^+(x_I^- + \Delta) = \frac{\varepsilon\pi G}{4} + \frac{\varepsilon\pi G}{\ln\frac{x_I^+}{x_S^+}}, \tag{9.79}$$

$$\lambda^2 x_I^+ x_I^- = \frac{\varepsilon\pi G}{4} + \frac{\varepsilon\pi G}{\ln\frac{x_I^-}{x_S^-}}. \tag{9.80}$$

Consider now the second term in Eq. (9.79):

$$\frac{\varepsilon\pi G}{\ln\frac{x_I^+}{x_S^+}} = \frac{\varepsilon\pi G}{\ln x_I^+ - \ln x_S^+} = \frac{\varepsilon\pi G}{\ln x_I^+ - \lambda(t+b)} \to 0, \qquad \lambda(t+b) \gg 1. \tag{9.81}$$

In contrast, the second term in Eq. (9.80) does not vanish in this approximation. We now assume that we are located, if not exactly on $\mathcal{J}^+$, then at least very close to it. This implies $x_S^+ \to \infty$, while x_S^- remains finite. Under these conditions, the island position is determined by the same relation as in the preceding section:

$$\lambda^2 x_I^+(x_I^- + \Delta) = \frac{\varepsilon\pi G}{4}. \tag{9.82}$$

Chapter 10

Page curve in the DREH model

In this chapter, we demonstrate how the Page curve is recovered within the DREH model of two-dimensional dilaton gravity introduced in Chap. 5. The analysis parallels the derivation carried out for the BPP model in Chap. 9. In contrast to the BPP model, the DREH model contains the quantum-corrected Schwarzschild black hole solution, which has been experimentally tested. It is therefore not only qualitatively, but also quantitatively more relevant. For example, in Sec. 5.3, we show that the evaporation time obtained in this two-dimensional framework agrees with the four-dimensional thermodynamic expectations.

The key distinction between the BPP and DREH models is that, once quantum corrections are included, the DREH equations of motion are no longer analytically solvable and must be treated perturbatively, as in Sec. 5.2. Since the perturbative expansion fails near the end-point of evaporation, computing the Page curve there requires special care. Nevertheless, around this stage the effects of the full quantum gravity theory become significant [1], so the breakdown of perturbation theory is ultimately less concerning. In this chapter, we illustrate how Eq. (1.6) can be used to determine the Page curve for both eternal and evaporating black holes within the DREH model. The chapter is organized into three sections.

In the first Sec. 10.1, we analyze the eternal black hole solution in the DREH model, introduced in Sec. 5.2.3. We demonstrate that if the area term in Eq. (1.6) is omitted, one recovers only Hawking's original conclusion of information loss [16]. In contrast, once the area term is included, the correct Page curve emerges. The resulting Page curve is the quantum-corrected counterpart of the one obtained in [59]. This section essentially reviews the findings of [42].

The second Sec. 10.2 studies the Page curve in the setting of a classical collapse, presented in Sec. 5.1.3. We show that the fine-grained entropy always remains below the thermodynamic upper limit given by the Bekenstein–Hawking formula (1.4). Nevertheless, the entropy does not decrease after the Page phase transition; instead, it asymptotically approaches and then remains fixed at the value S_{BH} as time tends to infinity. This behavior is anticipated, since the post-shockwave region of spacetime still admits a timelike Killing vector; only the global spacetime is truly non-stationary.

To explicitly break time-translation invariance, quantum corrections to the classical DREH action must be taken into account. The corresponding evaporating black hole solution was derived in [111] and is reviewed in Sec. 5.3. The Page curve associated with this solution is discussed in the final Sec. 10.3 of the chapter. We show that, once quantum corrections are included, there appears a decreasing contribution to the fine-grained entropy, thereby reproducing the full Page curve. The analysis in these last two sections is based on [43].

10.1 Page curve in the eternal black hole scenario

In this section, we examine how the fine-grained entropy of Hawking radiation evolves in time in the eternal black hole setup, using the QES formula (1.6). The eternal black hole in the DREH model is presented in Sec. 5.2.3. Our analysis parallels the procedure used for the BPP model in Sec. 9.1. Accordingly, we study two distinct configurations: the no-island case, which recovers the conventional Hawking information loss result [16], and the island case, which yields the Page curve. Our derivation largely follows that of [42].

10.1.1 No-island configuration

Let us first consider the situation in which no island is present. In this case, we expect to reproduce Hawking's original result [16]. For an eternal black hole, the relevant quantum state is the Hartle–Hawking state (3.97). Therefore, the semi-classical entanglement entropy (1.6) must be expressed in the Kruskal coordinates. The corresponding expression is given in Eq. (8.51), namely:

$$S_{semi-cl} = \frac{1}{12} \ln \frac{(x_R^+ - x_L^+)^2 (x_R^- - x_L^-)^2}{\delta^4 e^{-2\rho_R} e^{-2\rho_L}}. \tag{10.1}$$

As usual, the subscripts R/L refer to the two wedges of the spacetime, depicted in Fig. 10.1. To obtain the correct time dependence of the fine-grained entropy, we switch to (t, r_*) coordinates, or equivalently (t, r), since $r_* = r_*(r)$. The parameter δ serves as a UV cutoff.

Coordinates on the cutoff surface can therefore be written as either (t, b) or (t, b_*). The $t =$ const. slice is drawn in red. Because the time-like Killing vector reverses direction when one moves from right wedge to the left wedge, the constant-time slice in the left wedge corresponds to the coordinate $-t$. Consequently, the region that an asymptotic observer cannot access is indicated by the shaded red area in Fig. 10.1. The black hole singularity is depicted by the wavy black curve, and the event horizon is shown as the green line.

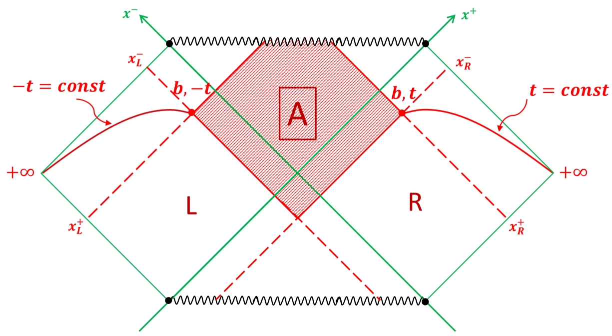

Figure 10.1: Penrose diagram depicting the no-island configuration for the eternal black hole in the DREH model.

To recover the time dependence of the fine-grained entropy S_{FG} along the cut-off surface, we switch to asymptotically flat Eddington–Finkelstein coordinates that incorporate the quantum-corrected surface gravity (5.89):

$$\kappa x_R^+ = e^{\kappa(t+b_*)}, \;\; \kappa x_R^- = -e^{-\kappa(t-b_*)}, \;\; \kappa x_L^+ = -e^{\kappa(-t+b_*)}, \;\; \kappa x_L^- = e^{-\kappa(-t-b_*)}. \tag{10.2}$$

For more details see App. D.5. In the absence of an island, the fine-grained entropy (1.6) simply reduces to the semi-classical contribution (10.1). Employing the metric (5.87), for which $\rho = \frac{1}{2}\ln\Lambda - \kappa r_*$, and inserting Eq. (10.2) into Eq. (10.1), we obtain:

$$S_{FG} = S_{semi-cl} = \frac{1}{6} \ln \frac{4\Lambda(b)\cosh^2(\kappa t)}{(\kappa\delta)^2}. \tag{10.3}$$

We regularize the UV divergence by imposing that the fine-grained entropy vanishes at the beginning of the evaporation, i.e. $S_{FG}(0) = 0$. Under this condition, Eq. (10.3) simplifies to:

$$S_{FG} = \frac{1}{3} \ln \Big[\cosh(\kappa t) \Big]. \tag{10.4}$$

We now distinguish two relevant regimes. At early times, near the beginning of evaporation, the entropy behaves as:

$$S_{FG} = \frac{1}{6} (\kappa t)^2. \tag{10.5}$$

In contrast, at late times $\kappa t \gg 1$, we find the anticipated linear growth:

$$S_{FG} \approx \frac{1}{3} \kappa t - \frac{1}{3} \ln 2, \tag{10.6}$$

which agrees with the behavior found in other dilaton gravity models [40, 41, 57, 58]. Therefore, the fine-grained entropy of the radiation increases monotonically, consistent with Hawking's original result. The crucial difference is that, unlike in the RST and BPP models, the DREH model predicts that the surface gravity receives a quantum correction.

10.1.2 Island configuration

In the presence of an island, the region that remains inaccessible to an asymptotic observer splits into two disconnected components, so we must employ formula (8.60):

$$S_{semi-cl} = \frac{1}{6} \ln \frac{d_{12}^2 d_{23}^2 d_{14}^2 d_{34}^2}{\delta^4 d_{24}^2 d_{13}^2 e^{-\rho_1} e^{-\rho_2} e^{-\rho_3} e^{-\rho_4}}, \tag{10.7}$$

where the Minkowski distances d_{ij} are defined as

$$d_{ij}^2 = (x_i^+ - x_j^+)(x_i^- - x_j^-). \tag{10.8}$$

As in the BPP model, we choose the labels i and j so that $(1, 2, 3, 4) \longleftrightarrow (Ra, Rb, La, Lb)$ holds. Here, R denotes the right wedge and L the left wedge of the spacetime.

Meanwhile, a denotes the boundary of the island region, and b indicates the cut-off hypersurface. All these hypersurfaces are explicitly shown in Fig. 10.2. The location of the island is specified by (t', a_*) in the asymptotically flat region on the right. In the left region, the corresponding point is obtained by reflection across the vertical axis. One can clearly see that the emergence of the island region I, highlighted in blue, inside the inaccessible region A of Fig. 10.1 splits A into two smaller, disconnected subregions.

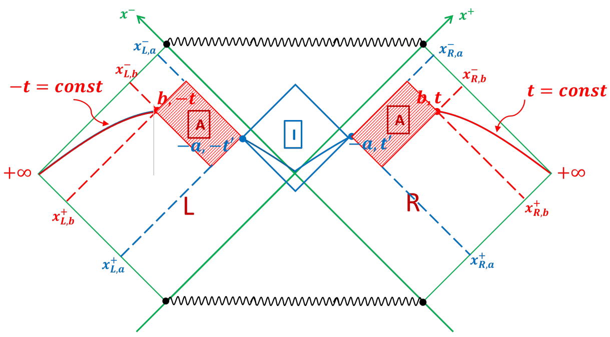

Figure 10.2: Penrose diagram depicting the island configuration for the eternal black hole in the DREH model.

In the asymptotically flat coordinates, the positions of the regions A and I in Fig. 10.4 are as follows:

$$\begin{aligned} &\kappa x^+_{Rb} = e^{\kappa(t+b_*)}, \quad \kappa x^-_{Rb} = -e^{-\kappa(t-b_*)}, \quad \kappa x^+_{Lb} = -e^{\kappa(-t+b_*)}, \quad \kappa x^-_{Lb} = e^{-\kappa(-t-b_*)}, \\ &\kappa x^+_{Ra} = e^{\kappa(t'+a_*)}, \quad \kappa x^-_{Ra} = -e^{-\kappa(t'-a_*)}, \quad \kappa x^+_{La} = -e^{\kappa(-t'+a_*)}, \quad \kappa x^-_{La} = e^{-\kappa(-t'-a_*)}. \end{aligned} \tag{10.9}$$

We now turn to the late-time regime of the evaporation process. In the limit of large times, one finds:

$$\frac{d_{23}^2 d_{14}^2}{d_{24}^2 d_{13}^2} = 16e^{2\kappa(b_*-a_*)}\frac{\cosh^2(\kappa t)\cosh^2(\kappa t')}{\left(e^{\kappa(t+b_*)}+e^{-\kappa(t'+a_*)}\right)^2\left(e^{\kappa(b_*-t)}+e^{\kappa(t'-a_*)}\right)^2} \approx 1;\ \ t,t' \to \infty. \tag{10.10}$$

Here we have used Eq. (10.9). In this regime it is straightforward to verify that $d_{12} = d_{34}$, $\rho_1 = \rho_4$, and $\rho_2 = \rho_3$. With these relations, Eq. (10.7) simplifies to:

$$S_{semi-cl} = \frac{1}{6}\ln\left(\frac{d_{12}^4}{\delta^4}e^{2\rho_1}e^{2\rho_2}\right). \tag{10.11}$$

Substituting the metric (5.87) and the Minkowski distances (10.8) into Eq. (10.11) yields:

$$S_{semi-cl} = \frac{1}{6}\ln\frac{\Lambda_I\Lambda_b\left(e^{\kappa(t+b_*)}-e^{\kappa(t'+a_*)}\right)^2\left(-e^{-\kappa(t-b_*)}+e^{-\kappa(t'-a_*)}\right)^2}{(\kappa\delta)^4 e^{2\kappa(b_*+a_*)}}. \tag{10.12}$$

Since the surface term is independent of t', we can immediately extremize with respect to t'. As in the BPP model (see Sec. 9.1), at late times one finds $t' = t$. Consequently, the semiclassical entropy (10.12) reduces to:

$$S_{semi-cl} = \frac{1}{3}(\rho_I+\rho_b) + \frac{2}{3}\ln\left(e^{\kappa b_*}-e^{\kappa a_*}\right) - \frac{2}{3}\ln(\kappa\delta). \tag{10.13}$$

We now proceed to analyze the surface term in the fine-grained entropy formula (1.6). It is given by:

$$\frac{A[I]}{4G_N} = 2\frac{4\pi(\lambda a)^2}{4G\hbar}\mathrm{x}_I^2, \tag{10.14}$$

where we have used the reduced field x defined in Eq. (5.39). This expression coincides with the Bekenstein–Hawking entropy (1.4). The factor of two appears because the spacetime contains two asymptotically flat regions. Note that, unlike in the BPP model, we do not use the quantum-corrected area term (8.83). Instead, we employ the purely classical area obtained via dimensional reduction, as the model is derived from the four-dimensional Einstein–Hilbert action. Summing Eqs. (10.13) and (10.14) then gives the generalized entropy in the form:

$$S_{gen} = \frac{2\pi(\lambda a)^2}{G\hbar}\mathrm{x}_I^2 + \frac{1}{3}(\rho_a+\rho_b) + \frac{2}{3}\ln\left(e^{\kappa b_*}-e^{\kappa a_*}\right) - \frac{2}{3}\ln(\kappa\delta). \tag{10.15}$$

The last step in evaluating the fine-grained entropy is to extremize the generalized entropy (10.15) with respect to the island location a_*:

$$\partial_{a_*}S_{gen} = \left[\frac{4\pi(\lambda a)^2}{G\hbar}\mathrm{x}_I + \frac{1}{3}\frac{\mathrm{d}\rho}{\mathrm{dx}}\bigg|_I\right]\frac{\mathrm{dx}_I}{\mathrm{d}a_*} - \frac{2}{3}\frac{\kappa}{e^{\kappa(b_*-a_*)}-1} = 0, \tag{10.16}$$

which yields:

$$-\left[\mathrm{x}_I + \frac{\varepsilon}{(\lambda a)^2}\frac{\mathrm{d}\rho}{\mathrm{dx}}\bigg|_I\right]\Lambda(a)\mathcal{D}(a) = \frac{\varepsilon}{(\lambda a)^2}\frac{2\kappa a}{e^{\kappa(b_*-a_*)}-1}, \tag{10.17}$$

where we have used the definition of the tortoise coordinate Eq. (3.18). We anticipate that the QES is located close to, but outside, the horizon. Hence, we parametrize its position as $\mathrm{x}_I = 1+z$, where $z \ll 1$, since $\mathrm{x_H} = 1$. Expanding the left-hand side of (10.17) in powers of small x up to first order, we obtain:

$$\mathrm{LHS} \approx -\left[\mathrm{x_H} + \frac{\varepsilon}{(\lambda a)^2}\frac{\mathrm{d}\rho}{\mathrm{dx}}\bigg|_H\right]\cancelto{0}{\Lambda(\mathrm{x_H})}\mathcal{D}(\mathrm{x_H}) - \left[\mathrm{x_H} + \frac{\varepsilon}{(\lambda a)^2}\frac{\mathrm{d}\rho}{\mathrm{dx}}\right]\mathcal{D}\frac{\mathrm{d}\Lambda}{\mathrm{dx}}\bigg|_H z. \tag{10.18}$$

The first term vanishes because $\Lambda(\mathrm{x_H}) = 0$ by the definition of the horizon. For the second term, we use $\mathcal{D}\frac{\mathrm{d}\Lambda}{\mathrm{dx}}\Big|_H = -2\kappa a$, which follows from the definition of the surface gravity in Eq. (5.89). Next, we examine the right-hand side of Eq. (10.17). We expand $e^{2\kappa a_*}$ around the horizon and find:

$$e^{2\kappa a_*} = e^{\mathrm{x}_I}\left(\mathrm{x}_I - 1\right)\left[1 + \frac{\varepsilon}{4(\lambda a)^2}\left(\left(1 - \mathrm{x}_I - \frac{1}{\mathrm{x}_I - 1}\right)\ln \mathrm{x}_I + \frac{5}{2}\mathrm{x}_I - \frac{3}{2}\right)\right] \approx ze, \tag{10.19}$$

where we have explicitly exploited the divergent behavior of the tortoise coordinate in Eq. (5.91). Consequently, the right-hand side of Eq.(10.17) becomes:

$$\mathrm{RHS} \approx \frac{2\kappa a\varepsilon}{(\lambda a)^2} e^{-\kappa b_*} e^{\kappa a_*}\left(1 + e^{-\kappa b_*} e^{\kappa a_*}\right) \approx \frac{2\kappa a\varepsilon}{(\lambda a)^2} e^{-\kappa b_*}\sqrt{ze}\left(1 + e^{-\kappa b_*}\sqrt{ze}\right). \tag{10.20}$$

Combining Eqs. (10.18) and (10.20), we arrive at the following solution for z:

$$z = \frac{\varepsilon^2}{(\lambda a)^4}\frac{e^{1-2\kappa b_*}}{\left[1 + \varepsilon\left(\frac{\mathrm{d}\rho}{\mathrm{dx}}\Big|_{\mathrm{H}} - e^{1-2\kappa b_*}\right)\right]^2} \tag{10.21}$$

Very careful computation of the derivative of the metric in the Kruskal coordinates yields $\frac{\mathrm{d}\rho}{\mathrm{dx}}\Big|_{\mathrm{H}} = 1$. Finally, using Eqs. (4.110) and (5.91) and reinstating $\varepsilon = \frac{\hbar G}{12\pi}$, we arrive at:

$$\mathrm{x}_I = 1 + \left(\frac{\hbar G}{12\pi(\lambda a)^2}\right)^2 e^{1-2\kappa b_*}\left[1 - \frac{\hbar G}{6\pi(\lambda a)^2}\left(1 - e^{1-2\kappa b_*}\right)\right]. \tag{10.22}$$

Note that the expression (10.22) for the island position matches precisely the leading-order result of [59] in the ε expansion. The key difference in our analysis is that we also incorporate the back-reaction of the radiation, so that the inclusion of quantum effects still preserves the appearance of an island in the vicinity of the quantum-corrected horizon. In addition, the island location does not coincide with the result in [42], because here we employed a different tortoise coordinate.

Next, we substitute the island position (10.22) into Eq. (10.15) to compute the late-time fine-grained entropy. Since the island forms very close to the quantum-corrected horizon, we first expand around the horizon position:

$$S_{FG} = S_{gen}(a) - \frac{\hbar G}{36\pi(\lambda a)^2} e^{1-2\kappa b_*} + \mathcal{O}(\hbar^2)\,. \tag{10.23}$$

The second term can be neglected, as it is of order $\mathcal{O}(\hbar)$, while the fine-grained entropy scales as $S_{FG} = (\mathcal{O}(1) + \hbar\mathcal{O}(1))/\hbar$. Consequently, we obtain:

$$S_{FG} = \frac{2\pi(\lambda a)^2}{G\hbar} + \frac{1}{3}\left(\rho_{\mathrm{H}} + \rho_b\right) + \frac{2}{3}\ln\frac{e^{\kappa b_*}}{\kappa\delta} = 2\left[\frac{\pi(\lambda a)^2}{G\hbar} + \frac{1}{12}\ln\frac{e^{4\kappa b_*}}{(\kappa\delta)^4 e^{-2\rho_{\mathrm{H}}} e^{-2\rho_b}}\right]. \tag{10.24}$$

To leading order, the expression (10.24) matches precisely the classical Bekenstein-Hawking entropy (1.4), implying $S_{gen} = 2S_{BH}$, as anticipated. We return to the role of the quantum correction term in the next subsection. The fine-grained entropy of the Hawking radiation is therefore given by:

$$S_{FG} = \min\left\{\frac{1}{3}\kappa t, 2S_{BH}\right\}. \tag{10.25}$$

To evaluate the Page time, we employ the classical value of the entropy, because the quantum correction becomes negligible in the large-mass regime. The Page time t_P is therefore determined by:

$$\frac{1}{3}\kappa c t_P = \frac{2\pi c^3(\lambda a)^2}{G\hbar} \quad \Longrightarrow \quad t_P = \frac{96\pi M^3 G^2}{\hbar\lambda^4 c^4}. \tag{10.26}$$

10.1.3 Relation to the Wald entropy

To analyze the second term in Eq. (10.24), we employ the quantum-corrected thermodynamic entropy, given by the Wald entropy formula. In this approach, the black hole entropy is interpreted as a conserved charge associated with the horizon and is expressed as

$$S_{Wald} = -2\pi \int_{\mathrm{H}} dA \frac{\partial \mathcal{L}}{\partial \mathcal{R}_{\mu\nu\rho\sigma}} \varepsilon_{\mu\nu}\varepsilon_{\rho\sigma}, \tag{10.27}$$

where $\varepsilon_{\mu\nu}$ is the binormal satisfying $\varepsilon_{\mu\nu}\varepsilon^{\mu\nu} = -2$, dA is the infinitesimal area element on the event horizon, and $\mathcal{L}$ is the Lagrangian density specifying the theory. A straightforward evaluation for the DREH theory (2.19) coupled to the Polyakov–Liouville quantum correction term (3.72) gives

$$S_{Wald} = \frac{\pi(\lambda a)^2}{G\hbar} - \frac{1}{12}\psi(a). \tag{10.28}$$

We therefore need the exact solution for the auxiliary field. Substituting the solution for ψ (3.76) together with the Hartle–Hawking state condition (3.97), $t_\pm(x^\pm) = 0$, and the explicit expressions for the $t_\pm$ functions (3.78), we obtain the following differential equation for $f_\pm$:

$$\frac{1}{2}\partial_\pm^2 f_\pm - \frac{1}{4}(\partial_\pm f_\pm)^2 = 0. \tag{10.29}$$

Solving this equation yields:

$$f_\pm(x^\pm) = -2\ln\frac{x^\pm + c_\pm}{\delta} + d_\pm, \tag{10.30}$$

where $c_\pm$ and $d_\pm$ are integration constants. We interpret the constants $c_\pm$ as marking positions in spacetime. To ensure that ψ is invariant under local Lorentz transformations, we impose $d_+ + d_- = -2\rho_c$. Implementing this condition leads to

$$\psi(r) = -\ln\frac{(x^+ + c_+)^2(x^- + c_-)^2}{\delta^4 e^{-2\rho}e^{-2\rho_c}}, \tag{10.31}$$

where $c_\pm$ must be chosen on the cut-off hypersurface which defines a region belonging to the black hole (see Figs. 10.3 and 10.4). This implies $\kappa^2 c_+ c_- = -e^{2\kappa b_*}$. To evaluate Wald's entropy, we insert Eq. (10.31) at the horizon, where $x_H^+ = x_H^- = 0$. Wald's entropy then takes the form of a quantum-corrected Bekenstein–Hawking formula:

$$S_{Wald} = \frac{\pi(\lambda a)^2}{G\hbar} + \frac{1}{12}\ln\frac{(e^{2\kappa b_*})^2}{(\kappa\delta)^4 e^{-2\rho_{\mathrm{H}}}e^{-2\rho_b}}. \tag{10.32}$$

Comparing this with Eq. (10.24), we see that, to first order in perturbation theory, it coincides with precisely twice the Wald entropy (10.32). Hence, the Page curve is correctly reproduced in the eternal black hole solution of the DREH model. The fine-grained entropy of the radiation increases monotonically until it saturates at the coarse-grained Bekenstein–Hawking value, after which it stays fixed at $2S_{BH}$. Furthermore, Hawking's result for the generalized entropy in the no-island scenario can likewise be recovered from the Wald formula (10.28).

10.2 Page curve in the classical collapse scenario

In this section, we examine the Page curve for the classical gravitational collapse setup within the DREH model, as introduced in Sec. 5.1.3. Although we cannot determine the final stage of evaporation—since it lies at future time infinity in the classical limit—we can nonetheless extract some information about the qualitative behavior of the Page curve at zeroth order in ε. At this order, however, one does not expect a decreasing contribution to the entropy, as such behavior arises only once quantum corrections are taken into account. The time evolution of the fine-grained entropy of Hawking radiation is governed by the QES formula (1.6). As usual, we analyze two distinct configurations: the no-island configuration and the island configuration.

Fig. 10.3 shows the spacetime of an evaporating black hole in the DREH model (5.150-5.153). This figure corresponds to Fig. 3.3, where the general collapse scenario is illustrated. The event horizon is indicated by a dashed purple line, and the apparent horizon by a solid purple line. The shockwaves are drawn in blue, while the singularity and the spacetime boundary are both shown in black. Future and past null infinities are represented by green lines and denoted by $\mathscr{J}^+$ and $\mathscr{J}^-$, respectively. Likewise, future and past timelike infinities and spatial infinity are marked by $i^\pm$ and $i^)$, respectively. The δ and $\hat{x}$ axes are explicitly displayed, corresponding to the coordinates defined in Eq. (3.107). The coordinates of the end-point of the evaporation $(\delta_E, \hat{x}_E)$, are shown along the respective axes.

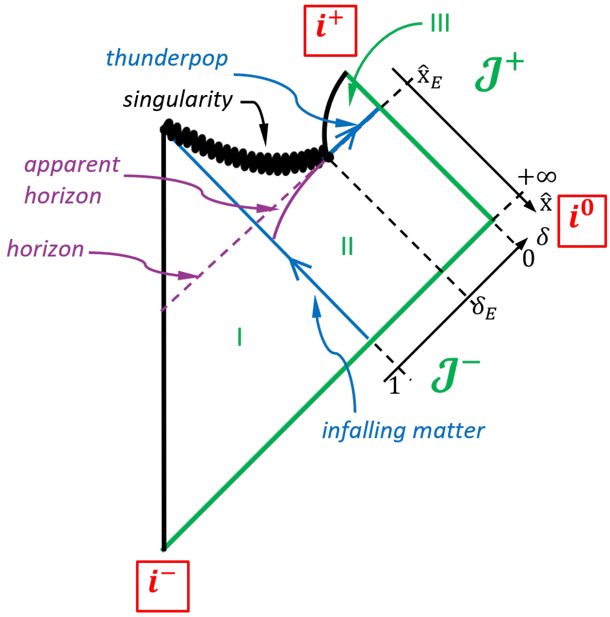

Figure 10.3: Penrose diagram of the quantum-corrected gravitational collapse scenario.

The spacetime is divided into three regions, separated by two shockwaves. Region I corresponds to the initial Minkowski spacetime. Upon crossing the $\delta = 1$ hypersurface, one enters region II, which contains the evaporating black hole. Finally, region III describes the end-state geometry, namely the quantum-corrected Minkowski spacetime given by Eq. (5.84). The purely classical collapse is recovered by pushing the $\delta = \delta_E$ hypersurface all the way to future null infinity $\mathscr{J}^+$, thereby eliminating the third region. The discussion here is largely based on [43].

10.2.1 No-island configuration

We begin by considering the setup without an island. In this case, the fine-grained entropy (1.6) simplifies to just the semiclassical entropy contribution. Because the vacuum is specified in the asymptotically flat coordinates of region I of the spacetime (see Fig. 10.3), the entanglement entropy must likewise be written in these coordinates. The evaporating black hole possesses a spacetime boundary on which reflective boundary conditions are imposed. Consequently, the appropriate expression for the entropy of the quantum matter fields is given by Eq. (8.55), namely:

$$S_{semi-cl} = \frac{1}{12} \ln \frac{(\sigma_S^+ - \sigma_{\bar{S}}^+)^2}{4\epsilon^2 e^{-2\rho_S(\sigma)}}. \tag{10.33}$$

The label S denotes the boundary of the black hole region, while the label $\bar{S}$ refers to the mirror image of this point across the spacetime boundary, as illustrated in Fig. 10.4. We employ the (t, r_*) coordinate system. On the cut-off surface, the coordinates are given by (t, b_*), or equivalently (t, b), where

$$\frac{b}{a} + \ln\left(\frac{b}{a} - 1\right) = \frac{b_*}{a}. \tag{10.34}$$

Note that the time coordinate t is defined with respect to the asymptotically flat coordinates of region II, given in Eqs. (5.38) and (5.37), namely $t = \frac{\hat{\sigma}^+ - \hat{\sigma}^-}{2}$. The cut-off hypersurface is taken to lie close to asymptotic infinity, which requires b_* to be very large. Therefore, throughout the rest of this work we use the following approximation:

$$\frac{b_*}{a} \gg \frac{(\lambda a)^2}{\varepsilon}. \tag{10.35}$$

Note that we have relabeled the UV cut-off from the standard notation δ of Chap. 8, since δ is a coordinate within this setting.

The classical collapse configuration is depicted in Fig. 10.4. The location of region A, which contains the degrees of freedom inaccessible to an asymptotic observer in the no-island classical scenario, is marked in red. The cut-off hypersurface is drawn in purple, and a time coordinate along this hypersurface, denoted by τ and introduced in Eq. (10.37), parameterizes it. The radiation degrees of freedom occupy a causal diamond based on a constant-time slice, indicated in blue. The coordinates of all relevant points—$(\delta_S, \hat{x}_S)$ and their images under reflection from the the spacetime boundary, $(\delta_{\bar{S}})$—are shown on both the δ- and $\hat{x}$-axes.

The reflective boundary condition at $x = 0$ enforces $\sigma^+_{\bar{S}} = \sigma^-_S$. The onset of evaporation is determined by the intersection of the hypersurfaces $\sigma^+ = \sigma^+_0$ and $r_* = b_*$, yielding $t_0 = \sigma^+_0 - b_*$. The evaporation time is then defined as $\tau = t - t_0$. Employing Eq. (5.40), the cut-off hypersurface in region II of the the spacetime takes the form:

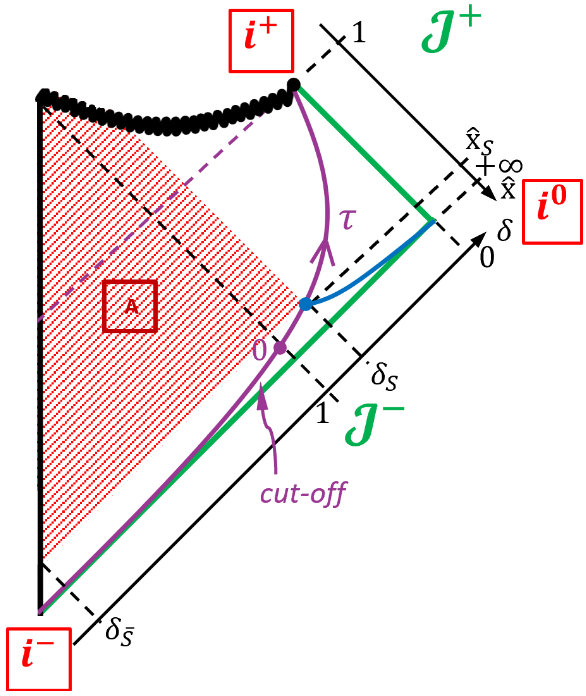

Figure 10.4: Penrose diagram illustrating the no-island case within the classical collapse scenario.

$$\frac{b_*}{a} = -\ln \delta_S + \hat{x}_S + \ln(\hat{x}_S - 1). \tag{10.36}$$

Note that the cut-off surface lies in the region exterior to the black hole event horizon, defined by Eq. (5.41), which entails $\hat{x}_S > 1$. Using Eqs. (5.37) and (5.38), one readily finds that the evaporation time τ is related to $\hat{x}_S$ by the following transcendental relation:

$$\hat{x}_S + \ln(\hat{x}_S - 1) = \frac{b_*}{a} - \frac{\tau}{2a}. \tag{10.37}$$

Imposing the condition $S_{FG}(0) = 0$ removes the UV divergences in the expression for the entanglement entropy (10.33). Expressed in terms of $\hat{x}_S$, the fine-grained entropy evaluated on Hawking's saddle is

$$S_H(\hat{x}_S) = \frac{1}{12} \ln \frac{a^2(b-a)\hat{x}_S \left(\frac{b_*}{a} - \ln(\hat{x}_S - 1)\right)^2}{b^3(\hat{x}_S - 1)}. \tag{10.38}$$

An explicit analytic form of the fine-grained entropy (10.38) as a function of the evaporation time τ cannot be obtained because one would have to solve the transcendental Eq. (10.37), which links τ to the coordinate $\hat{x}_S$. Nevertheless, one can extract the behavior of the fine-grained entropy both at the beginning of evaporation and at late times. At the beginning of the evaporation ($\tau \to 0$), Eq. (10.37) can be solved perturbatively:

$$\hat{x}_S^{(0)} = \frac{b}{a} - \frac{b-a}{2ab}\tau. \tag{10.39}$$

Inserting the result (10.39) into Eq. (10.38) and expanding in powers of τ, one obtains the following early-time expression for the fine-grained entropy:

$$S_H^{(0)}(\tau) = \frac{a\tau}{8b^2}. \tag{10.40}$$

This behavior differs from the eternal black hole case, where the dependence is quadratic (10.5). At late times, the factor $\exp\left\{\left(\frac{b_*}{a} - \frac{\tau}{2a}\right)\right\}$ becomes very small, allowing us to expand $\hat{x}_S$ in powers of this quantity:

$$\hat{x}_S^{(\infty)} = 1 + e^{\frac{b_*}{a} - 1} e^{-\frac{\tau}{2a}}. \tag{10.41}$$

Substituting Eq. (10.41) into Eq. (10.38) yields the anticipated Hawking result of a linearly increasing fine-grained entropy at late times [16]:

$$S_H^{(\infty)}(\tau) = \frac{\tau}{24a} + \frac{1}{12} \ln \frac{(b-a)\tau^2}{4b^3} - \frac{1}{12}\left(\frac{b_*}{a} - 1\right). \tag{10.42}$$

Observe that, in the late-time regime, the leading contribution in Eq. (10.42) is of the form $\frac{\kappa\tau}{12}$, where $\kappa = \frac{1}{2a}$ (see App. D.5) is the usual surface gravity of a Schwarzschild black hole. This is consistent with the fine-grained entropy obtained in various 2D dilaton gravity models [40, 41]. We explicitly confirm this within the BPP model in Sec. 9.2.

10.2.2 Island case

Analogously to the BPP model, the projection splits the inaccessible region A into two non-overlapping segments along past null infinity $\mathcal{J}^-$. Consequently, the appropriate expression for the semi-classical entropy in the presence of an island is given by Eq. (8.61), namely:

$$S_{semi-cl} = \frac{1}{12} \ln \frac{(\sigma_S^+ - \sigma_I^+)^2(\sigma_{\bar{S}}^+ - \sigma_{\bar{I}}^+)^2(\sigma_{\bar{S}}^+ - \sigma_S^+)^2(\sigma_{\bar{I}}^+ - \sigma_I^+)^2}{\epsilon^4(\sigma_{\bar{I}}^+ - \sigma_S^+)^2(\sigma_{\bar{S}}^+ - \sigma_I^+)^2 e^{-2\rho(\sigma_S)}e^{-2\rho(\sigma_I)}}. \tag{10.43}$$

Here the reflected points obey $\sigma_{\bar{I}}^+ = \sigma_I^-$ and $\sigma_{\bar{S}}^+ = \sigma_S^-$. To verify that Eq. (10.43) remains valid when the island vanishes, we consider the limit $\sigma_I^\pm \to \sigma_M^\pm$, where M denotes the point at which the island region meets the spacetime boundary. Since a UV cut-off is present, distances should not shrink to zero; instead, they should approach this UV cut-off. Implementing the limit $\sigma_I^\pm \to \sigma_M^\pm$, we obtain:

$$\epsilon^2 = \lim_{I\to M} g_{\mu\nu}(\sigma_I^\mu - \sigma_M^\mu)(\sigma_I^\nu - \sigma_M^\nu). \tag{10.44}$$

The island hypersurface is specified by the condition $\sigma^+ + \sigma^- = \text{const}$. Using the relation $\sigma_M^+ = \sigma_M^- = \frac{1}{2}(\sigma_I^+ + \sigma_I^-)$, one can straightforwardly verify that Eq. (10.43) reduces to Eq. (10.33) in the limit $I \to M$. The same regularization as in Eq. (10.38) must be applied. The expression (10.43) depends both on τ and on the location of the island. The τ-dependence enters through $\sigma_S^+ = \sigma_0^+ + \tau$ and $\sigma_S^- = \sigma_0^+ - 2a\hat{\mathrm{x}}_S(\tau)$.

Fig. 10.5 illustrates this whole scenario. The location of the region A, which contains the inaccessible degrees of freedom when an island region I is present in the classical case, is indicated in red. The cut-off hypersurface, shown in purple, is parametrized by the time coordinate τ along it and originates at the incoming shockwave. The island-boundary hypersurface, also drawn in purple, passes through region A. The $\Delta\tau$-axis is aligned with this hypersurface, with its zero point defined at the ingoing shockwave. The radiation degrees of freedom occupy both a causal diamond built over a constant-time slice and the island region; these are depicted in blue. The coordinates of all relevant points (δ_S, δ_I, $\hat{\mathrm{x}}_S$, $\hat{\mathrm{x}}_I$), along with those obtained via reflection from the spacetime boundary ($\delta_{\bar{S}}$, $\delta_{\bar{I}}$), are displayed on both the δ-axis and the $\hat{\mathrm{x}}$-axis.

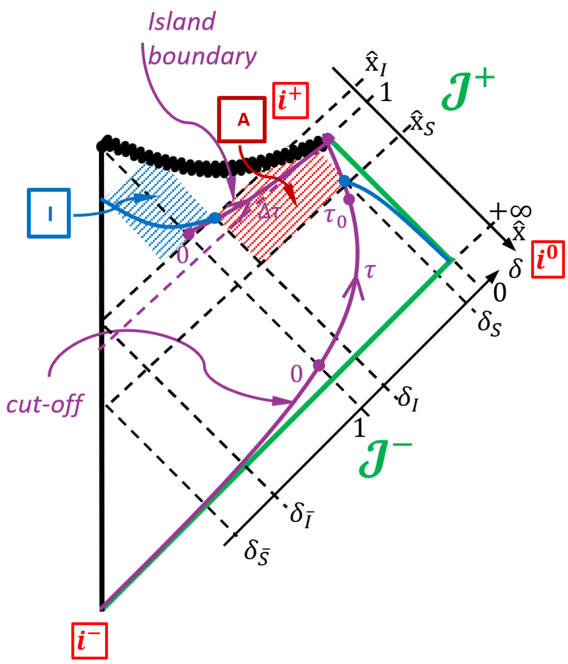

Figure 10.5: Penrose diagram illustrating the island case within the classical collapse scenario.

Next, we include the island's area contribution. Because the DREH model is obtained via dimensional reduction from the 4D Einstein–Hilbert action, this area term takes the usual Bekenstein–Hawking form (1.4), namely

$$\frac{A[I]}{4G_{\mathrm{N}}^{(4)}} = \frac{4\pi\lambda^2 a^2}{4G\hbar}\mathrm{x}_I^2 = \frac{(\lambda a)^2}{12\varepsilon}\mathrm{x}_I^2. \tag{10.45}$$

The generalized entropy is then given by

$$\begin{aligned} S_{gen}(\tau, \sigma_I^+, \sigma_I^-) =& \frac{(\lambda a)^2}{12\varepsilon}\mathrm{x}_I^2 \\ &+ \frac{1}{12}\ln\left[\frac{4a^2(b-a)\hat{\mathrm{x}}_S\left(\frac{b_*}{a} - \ln(\hat{\mathrm{x}}_S - 1)\right)^2}{b^3(\hat{\mathrm{x}}_S - 1)} \frac{(\sigma_S^+ - \sigma_I^+)^2(\sigma_S^- - \sigma_I^-)^2(\sigma_I^+ - \sigma_I^-)^2}{\epsilon^2(\sigma_S^+ - \sigma_I^-)^2(\sigma_I^+ - \sigma_S^-)^2 e^{-2\rho(\sigma_I)}}\right]. \end{aligned} \tag{10.46}$$

The dependence $\mathrm{x}_I(\sigma_I^+, \sigma_I^-)$ is fixed by Eq. (5.152), while $\rho(\sigma_I^+, \sigma_I^-)$ is determined by Eq. (5.150). The parameter τ enters only through $\hat{\mathrm{x}}_S = \hat{\mathrm{x}}_S(\tau)$ via Eq. (10.36). According to the fine-grained entropy prescription (1.6), the expression (10.46) must be extremized with respect to the island location (σ_I^+, σ_I^-). Implementing this extremization with the help of Eqs. (5.152) and (5.150) leads to

$$1 - \mathrm{x}_I = \tilde{\varepsilon}\left[\frac{1}{2\mathrm{x}_I^2} + \frac{\hat{\mathrm{x}}_S - \ln\delta_S}{(\ln\delta_I - \ln\delta_S)(\ln\delta_I - \hat{\mathrm{x}}_S)} + \frac{1}{\hat{\mathrm{x}}_I - \ln\delta_I}\right], \tag{10.47}$$

$$1 - \mathrm{x}_I = \tilde{\varepsilon}\left[\frac{1}{2\mathrm{x}_I^2} - \frac{1}{2\hat{\mathrm{x}}_I^2} + \frac{\hat{\mathrm{x}}_I - 1}{\hat{\mathrm{x}}_I}\left(\frac{\hat{\mathrm{x}}_S - \ln\delta_S}{(\ln\delta_I - \ln\delta_S)(\ln\delta_I - \hat{\mathrm{x}}_S)} + \frac{1}{\hat{\mathrm{x}}_I - \ln\delta_I}\right)\right], \tag{10.48}$$

where we have introduced $\tilde{\varepsilon} = \frac{\varepsilon}{(\lambda a)^2}$. We first determine the island position along the initial shockwave, that is, on the hypersurface $\delta_I = 1$. Setting $\delta_I = 1$ and $\hat{\mathrm{x}}_I = \mathrm{x}_I$, Eqs. (10.48–10.47) simplify to

$$1 - \mathrm{x}_I = \tilde{\varepsilon}\left[\frac{1}{2\mathrm{x}_I^2} + \frac{1}{\mathrm{x}_I} - \frac{\ln\delta_S - \hat{\mathrm{x}}_S}{\hat{\mathrm{x}}_S\ln\delta_S}\right], \tag{10.49}$$

$$\mathrm{x}_I^2 = \tilde{\varepsilon}\left[-1 + \frac{\ln\delta_S}{\mathrm{x}_I - \ln\delta_S} - \frac{\hat{\mathrm{x}}_S}{\mathrm{x}_I - \hat{\mathrm{x}}_S}\right]. \tag{10.50}$$

Eq. (10.49) is a cubic in x_I and could be solved exactly, but it is sufficient to find a perturbative solution up to second order in $\tilde{\varepsilon}$. This yields

$$\mathrm{x}_I = 1 - \tilde{\varepsilon}\left(\frac{3}{2} - \zeta\right)(1 + 2\tilde{\varepsilon}), \tag{10.51}$$

where we have defined $\zeta = \frac{\ln\delta_S - \hat{\mathrm{x}}_S}{\hat{\mathrm{x}}_S\ln\delta_S}$. By writing $\delta_S = \delta_S(\hat{\mathrm{x}}_S, \zeta)$ and inserting the solution (10.51) into the second Eq. (10.50), we obtain an equation for $\hat{\mathrm{x}}_S$. Solving it gives

$$\hat{\mathrm{x}}_S = 1 + \tilde{\varepsilon}\left(\zeta - \frac{1}{2}\right) + \tilde{\varepsilon}^2\left(\zeta - \frac{3}{2} - \frac{1}{\zeta}\right). \tag{10.52}$$

Next, Eq. (10.36) becomes an equation for ζ:

$$\zeta = \frac{1}{\hat{\mathrm{x}}_S} + \frac{1}{\frac{b_*}{a} - \hat{\mathrm{x}}_S - \ln(\hat{\mathrm{x}}_S - 1)}. \tag{10.53}$$

Employing the approximation (10.35), the second term in Eq. (10.53) can be neglected, leaving

$$\zeta = 1 - \frac{\tilde{\varepsilon}}{2}. \tag{10.54}$$

Substituting Eq. (10.54) into Eqs. (10.51) and (10.52), and using $\frac{\tau_0}{2a} = -\ln\delta_S$, we obtain the final expression for the island position along the $\delta_I = 1$ hypersurface, i.e. at the onset of evaporation.

$$\delta_I = 1, \tag{10.55}$$

$$\mathrm{x}_I = 1 - \frac{\tilde{\varepsilon}}{2}(1 + 3\tilde{\varepsilon}) = \hat{\mathrm{x}}_I, \tag{10.56}$$

$$\hat{\mathrm{x}}_S = 1 + \frac{\tilde{\varepsilon}}{2}(1 - 4\tilde{\varepsilon}), \tag{10.57}$$

$$\frac{\tau_0}{2a} = \frac{b_* - a}{a} - \ln\frac{\tilde{\varepsilon}}{2} + \frac{7}{2}\tilde{\varepsilon} = -\ln\delta_S^{(0)}. \tag{10.58}$$

We now turn to determining how the island hypersurface penetrates into region II of the spacetime (see Fig. 10.5). From Eq. (10.58), we see that the island first appears (along the $\delta_I = 1$ hypersurface) only at late times, since $\tau_0/a \gg 1/\tilde{\varepsilon}$. Consequently, we are justified in taking the limit $|\ln \delta_S| \to \infty$ in Eqs. (10.47) and (10.48). In this late-time regime, these equations reduce to:

$$1 - \mathrm{x}_I = \tilde{\varepsilon}\left[\frac{1}{2\mathrm{x}_I^2} - \frac{1}{\hat{\mathrm{x}}_S - \ln\delta_I} + \frac{1}{\hat{\mathrm{x}}_I - \ln\delta_I}\right], \tag{10.59}$$

$$1 - \mathrm{x}_I = \tilde{\varepsilon}\left[\frac{1}{2\mathrm{x}_I^2} - \frac{1}{2\hat{\mathrm{x}}_I^2} + \frac{\hat{\mathrm{x}}_I - 1}{\hat{\mathrm{x}}_I}\left(\frac{1}{\hat{\mathrm{x}}_I - \hat{\mathrm{x}}_S} + \frac{1}{\hat{\mathrm{x}}_I - \ln\delta_I}\right)\right]. \tag{10.60}$$

Motivated by the expressions for the island position along the $\delta_I = 1$ hypersurface in Eqs. (10.55-10.58), we introduce the ansatz

$$\mathrm{x}_I = 1 - \xi, \quad \hat{\mathrm{x}}_I = 1 - \hat{\xi}, \quad \hat{\mathrm{x}}_S = 1 + \mu, \tag{10.61}$$

for the location of the island at arbitrary time $\tau \geqslant \tau_0$. Here, ξ, $\hat{\xi}$, and μ are small functions of δ_I, each expanded to second order in $\tilde{\varepsilon}$. With this substitution, Eqs. (10.59-10.60) take the form

$$\xi = \tilde{\varepsilon}\left[\frac{1}{2} + \xi + \frac{\mu + \hat{\xi}}{(1 - \ln\delta_I)^2}\right], \tag{10.62}$$

$$\xi = \tilde{\varepsilon}\left[\xi - \hat{\xi} + \frac{\hat{\xi}}{\hat{\xi} + \mu}(1 + \hat{\xi}) - \frac{\hat{\xi}}{1 - \ln\delta_I}\right]. \tag{10.63}$$

Equating Eqs. (10.62) and (10.63) yields

$$\frac{1}{2} + \hat{\xi} + \frac{\mu + \hat{\xi}}{(1 - \ln\delta_I)^2} = \frac{\hat{\xi}}{\hat{\xi} + \mu}(1 + \hat{\xi}) - \frac{\hat{\xi}}{1 - \ln\delta_I}. \tag{10.64}$$

On the right-hand side of Eq. (10.64), the only contribution of order $\mathcal{O}(1)$ is $\hat{\xi}/(\hat{\xi} + \mu)$. We therefore infer that this term must be of the form:

$$\frac{\hat{\xi}}{\hat{\xi} + \mu} = \frac{1}{2} + \eta, \tag{10.65}$$

where η is a new quantity of order $\tilde{\varepsilon}$. Substituting Eq. (10.65) into Eq. (10.64) then gives

$$\eta = \frac{1}{2}\hat{\xi} + \frac{\hat{\xi}}{1 - \ln\delta_I} + \frac{\mu + \hat{\xi}}{(1 - \ln\delta_I)^2}. \tag{10.66}$$

Using Eqs. (10.65) and (10.66), we can straightforwardly solve for ξ and $\hat{\xi}$ in terms of μ and δ_I:

$$\xi = \frac{\tilde{\varepsilon}}{2}(1 + \tilde{\varepsilon})\left[1 + \frac{4\mu}{(1 - \ln\delta_I)^2}\right], \tag{10.67}$$

$$\hat{\xi} = \mu\left[1 + 4\mu\left(\frac{1}{2} + \frac{1}{1 - \ln\delta_I} + \frac{2}{(1 - \ln\delta_I)^2}\right)\right]. \tag{10.68}$$

The next step is to determine $\delta_I = \delta_I(\mu)$ using Eq. (5.152). Because this equation contains logarithmic terms, δ_I can only be fixed to first order in $\tilde{\varepsilon}$, even though the other quantities are known to second order. Carrying this out, we obtain

$$\delta_I = \frac{\hat{\xi}}{\xi}(1 + \xi - \hat{\xi}). \tag{10.69}$$

Inserting Eqs. (10.67) and (10.68) into Eq. (10.69) then leads to the expression

$$\delta_I = \frac{\mu}{\tilde{\varepsilon}} (2 - \tilde{\varepsilon}) \left[1 + 4\mu \left(\frac{1}{4} + \frac{1}{1 - \ln \delta_I} + \frac{1}{(1 - \ln \delta_I)^2} \right) \right] . \tag{10.70}$$

Finally, we determine μ as a function of the evaporation time τ from Eq. (10.36), which yields

$$\mu = \frac{\tilde{\varepsilon}}{2} \frac{\delta_S(\tau)}{\delta_S(\tau_0)} \left(1 - \frac{7}{2}\tilde{\varepsilon} \right) \left(1 - \frac{\tilde{\varepsilon}}{2} \frac{\delta_S(\tau)}{\delta_S(\tau_0)} \right) . \tag{10.71}$$

Combining Eqs. (10.67-10.71), we obtain the position of the island as a function of the time elapsed since its formation, $\Delta\tau = \tau - \tau_0$. This provides an effective parametrization of the island hypersurface depicted in Fig. 10.5.

$$\delta_I = e^{-\frac{\Delta\tau}{2a}} (1 - 4\tilde{\varepsilon}) \left[1 + 2\tilde{\varepsilon} \frac{2 + \frac{\Delta\tau}{2a}}{\left(1 + \frac{\Delta\tau}{2a}\right)^2} e^{-\frac{\Delta\tau}{2a}} \right] , \tag{10.72}$$

$$\hat{\mathrm{x}}_I = 1 - \frac{\tilde{\varepsilon}}{2} e^{-\frac{\Delta\tau}{2a}} \left(1 - \frac{7}{2}\tilde{\varepsilon} \right) \left[1 + \frac{\tilde{\varepsilon}}{2} \left(1 + 4 \frac{3 + \frac{\Delta\tau}{2a}}{\left(1 + \frac{\Delta\tau}{2a}\right)^2} \right) e^{-\frac{\Delta\tau}{2a}} \right] , \tag{10.73}$$

$$\mathrm{x}_I = 1 - \frac{\tilde{\varepsilon}}{2} (1 + \tilde{\varepsilon}) \left[1 + \frac{2\tilde{\varepsilon}}{\left(1 + \frac{\Delta\tau}{2a}\right)^2} e^{-\frac{\Delta\tau}{2a}} \right] , \tag{10.74}$$

$$\hat{\mathrm{x}}_S = 1 + \frac{\tilde{\varepsilon}}{2} e^{-\frac{\Delta\tau}{2a}} \left(1 - \frac{7}{2}\tilde{\varepsilon} \right) \left[1 - \frac{\tilde{\varepsilon}}{2} e^{-\frac{\Delta\tau}{2a}} \right] . \tag{10.75}$$

We infer that the island forms behind the horizon, as anticipated. The first consistency test is to check whether Eqs. (10.72-10.75) reduce to the initial solution (10.55-10.57) in the limit $\Delta\tau \to 0$. A straightforward evaluation of this limit confirms that they do. Furthermore, in the opposite limit $\Delta\tau \to \infty$ we obtain $\delta_I \to 0$ and $\hat{\mathrm{x}}_I \to 1$, implying that the island extends to future time infinity. This is consistent with the absence of quantum corrections. In this limit we also find $\hat{\mathrm{x}} \to 1$. It is noteworthy that both the island and the cutoff surface almost reflect the position of the horizon at $\hat{\mathrm{x}}_H = 1$.

We now proceed to compute the fine-grained entropy of the radiation, given by Eq. (10.46), evaluated on the island hypersurface. A direct computation leads to:

$$S_{RW} = \frac{(\lambda a)^2}{12\varepsilon} - \frac{1}{12} - \frac{\varepsilon}{24(\lambda a)^2} + \frac{1}{12} \ln \left(\frac{\varepsilon}{2(\lambda a)^2} \frac{b - a}{b} \right) + \frac{1}{6} \ln \frac{-8a^2 \ln \delta_S^{(0)}}{\epsilon^2} - \frac{\varepsilon}{6(\lambda a)^2} \frac{1 - \frac{\Delta\tau}{2a}}{\left(1 + \frac{\Delta\tau}{2a}\right)^2} e^{-\frac{\Delta\tau}{2a}} . \tag{10.76}$$

Expression (10.76) consists of a constant contribution and an exponentially decaying contribution. The constant piece must be regularized because it depends on the UV cutoff ϵ. Discarding the UV-sensitive part of this constant term, the leading contribution is precisely the Bekenstein–Hawking entropy (1.4), namely $S_{BH}^{(0)} = \frac{(\lambda a)^2}{12\varepsilon}$. Hence we can interpret the full constant part as the quantum-corrected Bekenstein–Hawking entropy S_{BH}^{corr}. Then, fine-grained entropy at late times is given by the following formula:

$$S_{FG} = \min \left\{ \frac{\Delta\tau}{24a} + \frac{1}{6} \ln \frac{\tau}{2b} - \frac{1}{12} \ln \frac{\varepsilon}{2(\lambda a)^2} , S_{BH}^{\mathrm{corr}} - \frac{\varepsilon}{6(\lambda a)^2} \frac{1 - \frac{\Delta\tau}{2a}}{\left(1 + \frac{\Delta\tau}{2a}\right)^2} e^{-\frac{\Delta\tau}{2a}} \right\} , \tag{10.77}$$

From Eq. (10.77) it follows that, at late times, the fine-grained entropy approaches a constant value close to the black hole's Bekenstein–Hawking entropy. Consequently, without including the back-reaction of quantum fields on the spacetime geometry, we do not obtain the correct Page curve and instead recover the same behavior as for an eternal black hole [42]. This outcome is natural, since the classical solution in region II is intrinsically static. Only by analyzing both regions simultaneously does one see that the entire spacetime is actually non-static, due to the discontinuity across the infalling shockwave hypersurface. Nevertheless, the extremization procedure at least guarantees that the coarse-grained entropy bound is not exceeded.

In Fig. 10.6, the Page curve for the classical collapse setup, defined in Eq. (10.77), is shown. The blue curve denotes the fine-grained entropy evaluated on Hawking's saddle point, while the red curve indicates the entropy obtained from the replica-wormhole saddle point at late times. The purple curve illustrates the late-time asymptotic behavior of the fine-grained entropy on Hawking's saddle point. This figure clearly demonstrates how incorporating an island contrasts with the standard Hawking prediction.

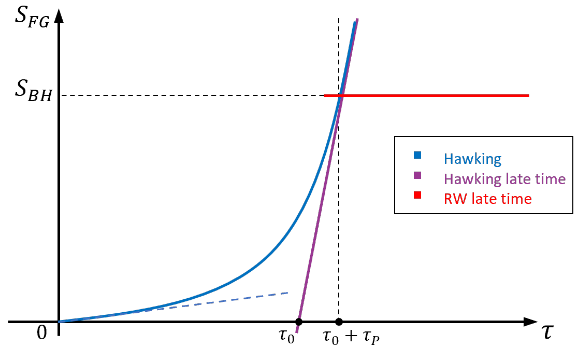

Figure 10.6: Page curve for the classical collapse scenario in the DREH model.

To determine the time at which the phase transition takes place, namely the Page time, we match the leading contributions in Eq. (10.77). This yields the Page time:

$$\tau_P = 24aS^{\text{corr}}_{BH}. \tag{10.78}$$

Expression (10.78) agrees with the result found for the eternal black hole (10.26). The relation between the time variable used in the eternal black hole case and Eq. (10.78) is $t_P = \frac{1}{2}\tau_P$. This factor-of-two difference arises because the eternal black hole possesses two asymptotically flat regions, which makes the coarse-grained entropy twice as large.

10.3 Page curve for the quantum-corrected collapse scenario

We now turn to the analysis of the Page curve for the quantum-corrected collapse setup introduced in Sec. 5.3. In the previous section, we saw that, for a purely classical evaporating black hole, the replica-wormhole saddle point fails to produce the decreasing part of the fine-grained entropy required to obtain the Page curve. By employing the fine-grained entropy formula (1.6), we demonstrate that this problem is resolved once quantum corrections are incorporated. In this way, we recover the expected decreasing contribution from the replica-wormhole saddle point. The structure of this section parallels that of the earlier ones: we begin by examining the no-island configuration and then move on to the island configuration. The derivation is based on [43].

10.3.1 No-island configuration

Here we examine how incorporating the back-reaction of quantum fields into the fine-grained entropy affects its evaluation along Hawking's saddle point. No significant deviations from the results of Sec. 10.2.1 are anticipated. We demonstrate that this procedure once more leads to Hawking's information loss paradox [16]. The fine-grained entropy (1.6) effectively reduces to its semi-classical contribution, given by the same expression (8.55) as in the purely classical analysis:

$$S_{semi-cl} = \frac{1}{12} \ln \frac{(\sigma_S^+ - \sigma_{\bar{S}}^+)^2}{4\epsilon^2 e^{-2\rho_S(\sigma)}}. \tag{10.79}$$

As in Sec. 10.2.1, the cut-off surface (10.36) is specified by the condition $r_* = b_*$. Substituting the expression (5.176) for the tortoise coordinate, we obtain the following relation defining the cut-off hypersurface:

$$\frac{b_*}{a} - \frac{\tau}{2a} = \mathcal{J}(\hat{\mathrm{x}}_S) - \frac{9}{2} - \frac{\tilde{\varepsilon}}{8}\left[(2\hat{\mathrm{x}}_S + 3)\ln \hat{\mathrm{x}}_S + 5\hat{\mathrm{x}}_S - 2\mathrm{L}_S\right], \tag{10.80}$$

where, as before, the evaporation time is introduced via $-\ln \delta_S = \frac{\tau}{2a}$ in complete analogy with Eq. (10.37).

The appropriate Penrose diagram for the no-island configuration in the quantum-corrected collapse scenario is presented in Fig. 10.7. It contains the same key hypersurfaces, points (δ_S, $\hat{\mathrm{x}}_S$, $\delta_{\bar{S}}$), and associated coordinate axes δ and $\hat{\mathrm{x}}$ as in the classical collapse case shown in Fig. 10.4. The essential distinction is the emergence of region III, which represents the remnant spacetime after the black hole has completely evaporated. The evaporation end-point $(\delta_E, \hat{\mathrm{x}}_E)$ is explicitly indicated. The newly formed region lies beyond this point and is characterized by $\delta < \delta_E$ and $\hat{\mathrm{x}} < \hat{\mathrm{x}}_E$. As before, the region A containing the inaccessible degrees of freedom is highlighted in red, while the cut-off hypersurface and the apparent horizon are drawn in purple. The constant-time slice associated with the radiation's degrees of freedom appears in blue. We continue to assume the validity of approximation (10.35), namely

$$b_*\tilde{\varepsilon} \gg a.$$

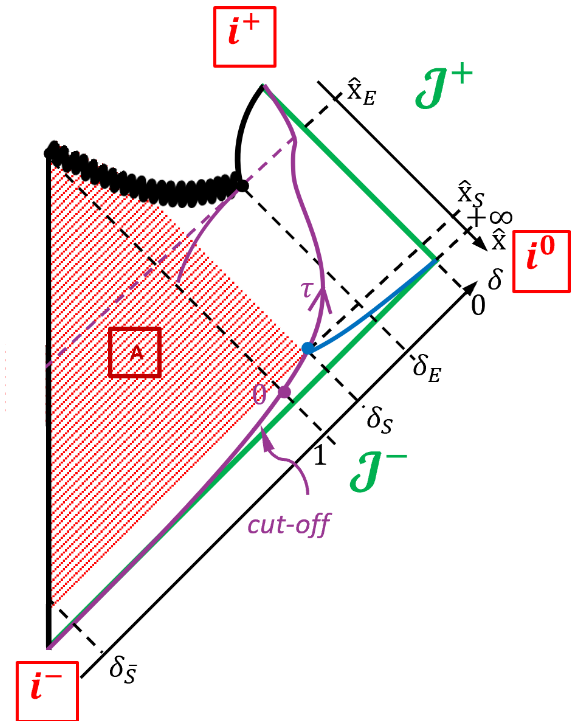

Figure 10.7: Penrose diagram illustrating the no-island case within the quantum-corrected collapse scenario.

We now evaluate the fine-grained entropy along Hawking's saddle point (10.79). Imposing the regularization condition $S_H(0) = 0$ gives

$$S_H(\tau) = \frac{1}{12} \ln \left(\frac{a^2}{b^2} \left(\frac{\tau}{2a} + \hat{\mathrm{x}}_S \right)^2 \frac{\mathrm{F}_S^+ \mathrm{F}_S^- e^{2\rho_S}}{\mathrm{F}_S^- \mathrm{F}_S^+} \right). \tag{10.81}$$

Let us study the behavior of Eq. (10.81) at the beginning of the evaporation, i.e. for $\tau \to 0$, in direct analogy with the classical analysis of Sec. 10.2.1. The first step is to solve the transcendental Eq. (10.80) for $\hat{\mathrm{x}}_S$ as a function of τ. At $\tau = 0$ we obtain $\hat{\mathrm{x}}_S = \mathrm{x}_S = \frac{b}{a}$, implying that for small τ we can write $\hat{\mathrm{x}}_S = \frac{b}{a} + \eta$, with η a small parameter. Expanding Eq. (10.36) in this regime, we find

$$\hat{\mathrm{x}}_S^{(0)} = \frac{b}{a} - \frac{b-a}{2ab}\tau \left\{ 1 - \frac{\tilde{\varepsilon}}{8} \left[2\ln\left(1 - \frac{a}{b}\right) + \frac{2a}{b-a} - \frac{a^2}{b^2} \right] \right\}. \tag{10.82}$$

Keeping only the leading term in the $\frac{a}{b} \to 0$ expansion, this simplifies to

$$\hat{\mathrm{x}}_S^{(0)} = \frac{b}{a} - \frac{b-a}{2ab}\tau \left(1 - \frac{\tilde{\varepsilon}}{6}\frac{a^3}{b^3} \right). \tag{10.83}$$

In comparison with Eq. (10.39), we observe a small shift induced by quantum corrections. A straightforward evaluation of the fine-grained entropy (10.81) then gives

$$S_H^{(0)}(\tau) = \frac{a\tau}{8b^2} \left(1 + \frac{\tilde{\varepsilon}}{4}\frac{b^2}{a^2} \right), \tag{10.84}$$

where, again, we have retained only the dominant contribution in the $\frac{a}{b} \to 0$ expansion. Comparing this with Eq. (10.40), we once more see that the effect of quantum corrections is a small modification.

Next, we turn to the late-time analysis of formula (10.81). Since at late times one has $\hat{\mathrm{x}}_S = 1 + \tilde{\varepsilon}\mu$, we expand Eq. (10.80) around the point $\hat{\mathrm{x}}_S = 1$:

$$\frac{b_* - a}{b_*} - \frac{\tau}{2a} = \left(1 + \frac{11}{8}\tilde{\varepsilon} \right) \frac{4}{\tilde{\varepsilon}} \left(e^{\frac{\tilde{\varepsilon}}{4}\ln\left(\tilde{\varepsilon}\left(\mu - \frac{1}{4}\right)\right)} - 1 \right) + \tilde{\varepsilon}\mu. \tag{10.85}$$

The solution of Eq. (10.85) can be written as

$$\hat{\mathrm{x}}_S^{(\infty)} = 1 + \frac{\tilde{\varepsilon}}{4} \left(1 + 3e^{-\frac{\tau - \tau_0}{2\bar{a}}} \right), \tag{10.86}$$

where τ_0 will be introduced below via Eq. (10.103). For convenience, we define $\Delta\tau = \tau - \tau_0$. Since the metric becomes asymptotically flat at late times, we may approximate $\mathrm{F}_S^+ \mathrm{F}_S^- e^{2\rho_S} \approx -1$. In the regime $\hat{\mathrm{x}}_S \approx 1$, the coordinate transformations simplify to

$$\mathrm{F}_S^- \approx \hat{\mathrm{x}}_S^{(\infty)} - 1 - \frac{\tilde{\varepsilon}}{4} = \frac{3}{4}\tilde{\varepsilon} e^{-\frac{\Delta\tau}{2\bar{a}}}. \tag{10.87}$$

Substituting Eqs. (10.86) and (10.87) into Eq. (10.81), we obtain:

$$S_H^{(\infty)}(\tau) = \frac{\tau - \tau_0}{24\bar{a}} + \frac{1}{6}\ln\frac{\tau}{2b} - \frac{1}{12}\ln\left(-\frac{3\tilde{\varepsilon}}{4}\mathrm{F}_\infty^+ \right), \tag{10.88}$$

where F_∞^+ denotes the late-time value of the coordinate transformation, $\sigma^+ \to \infty$. Thus, for the Hawking saddle point, the fine-grained entropy exhibits linear growth both at early and at late times; only the slope of the linear dependence changes. Comparing with Eq. (10.42), we find that the entropy shows the same qualitative behavior as in the classical case, but with the surface gravity replaced by its quantum-corrected value, given later in Eq. (10.117).

10.3.2 Island configuration

We now analyze the replica-wormhole saddle point in the quantum-corrected setup. We demonstrate that, unlike in the classical island configuration discussed in Sec. 10.2.2, the contribution to the entropy here decreases, thereby yielding the Page curve. In the quantum-corrected geometry, the same expressions (10.45) and (10.43) still apply to the corresponding terms in the fine-grained entropy (1.6). Consequently, we can proceed directly with the extremization, which leads to the following equations determining the island position:

$$\mathrm{x}_I\partial_+\mathrm{x}_I + \tilde{\varepsilon}\partial_+\rho_I = -\frac{\tilde{\varepsilon}}{2a}\left[\frac{\hat{\mathrm{x}}_S - \ln\delta_S}{(\ln\delta_I - \ln\delta_S)(\ln\delta_I - \hat{\mathrm{x}}_S)} + \frac{1}{\hat{\mathrm{x}}_I - \ln\delta_I}\right], \tag{10.89}$$

$$\mathrm{x}_I\partial_-\mathrm{x}_I + \tilde{\varepsilon}\partial_-\rho_I = \frac{\tilde{\varepsilon}}{2a}\left[\frac{\hat{\mathrm{x}}_S - \ln\delta_S}{(\hat{\mathrm{x}}_I - \ln\delta_S)(\hat{\mathrm{x}}_I - \hat{\mathrm{x}}_S)} + \frac{1}{\hat{\mathrm{x}}_I - \ln\delta_I}\right]. \tag{10.90}$$

As in the classical analysis, we first determine the location of the island along the infalling shockwave and subsequently extend it into region II of the spacetime, where the evaporating black hole resides.

The Penrose diagram for the quantum-corrected island configuration is displayed in Fig. 10.8. The region A, which contains the inaccessible degrees of freedom, is shown in red, while the island region I is indicated in blue. The cut-off hypersurface, together with the τ-axis that parametrizes it, is drawn in purple. Likewise, the island-boundary hypersurface and its parametrizing $\Delta\tau$-axis are also depicted in purple. The radiation degrees of freedom occupy a causal diamond built over a constant-time slice, indicated in blue as well. The coordinates of all relevant points (δ_S, δ_I, $\hat{\mathrm{x}}_S$, $\hat{\mathrm{x}}_I$, $\hat{\mathrm{x}}_E$, δ_E), along with those obtained by reflecting them across the spacetime boundary ($\delta_{\bar{S}}$, $\delta_{\bar{I}}$), are marked on both the δ-axis and the $\hat{\mathrm{x}}$-axis. The corresponding classical configuration is shown in Fig. 10.5. The key difference between the two diagrams is that only the quantum-corrected one contains remnant spacetime in region III.

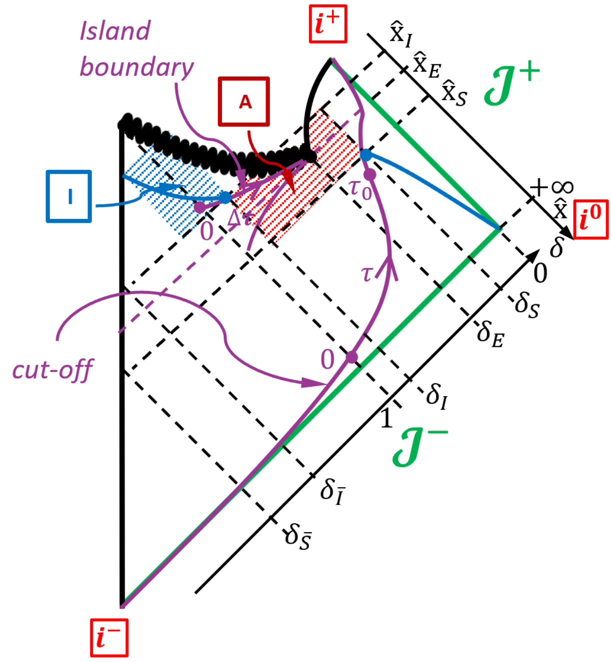

Figure 10.8: Penrose diagram illustrating the island case within the quantum-corrected collapse scenario.

We now analyze how the island appears along the $\delta_I = 1$ hypersurface, following the same procedure as in Sec. 10.2.2. Along this hypersurface, we impose a continuity condition (see [111]), which leads to

$$\mathrm{x}_I\partial_+\mathrm{x}_I + \tilde{\varepsilon}\partial_+\rho_I = \frac{\mathrm{x}_I - 1}{2a}, \tag{10.91}$$

$$\mathrm{x}_I\partial_-\mathrm{x}_I + \tilde{\varepsilon}\partial_-\rho_I = -\frac{\mathrm{x}_I}{2a}. \tag{10.92}$$

Using these continuity relations, Eqs. (10.89) and (10.90) take the form

$$1 - \mathrm{x}_I = \tilde{\varepsilon}\left[\frac{1}{\mathrm{x}_I} - \frac{\ln\delta_S - \hat{\mathrm{x}}_S}{\hat{\mathrm{x}}_S\ln\delta_S}\right], \tag{10.93}$$

$$\mathrm{x}_I^2 = \tilde{\varepsilon}\left[-1 + \frac{\ln\delta_S}{\mathrm{x}_I - \ln\delta_S} - \frac{\hat{\mathrm{x}}_S}{\mathrm{x}_I - \hat{\mathrm{x}}_S}\right]. \tag{10.94}$$

Observe that the second Eq. (10.94) coincides exactly with the classical Eq. (10.50), whereas the first one (10.93) is simpler than its classical analogue (10.49), reducing to a straightforward quadratic equation. As before, we introduce

$$\zeta = \frac{\ln\delta_S - \hat{\mathrm{x}}_S}{\hat{\mathrm{x}}_S\ln\delta_S}. \tag{10.95}$$

Both equations can then be solved exactly in terms of ζ, yielding

$$\mathrm{x}_I = \frac{1+\tilde{\varepsilon}\zeta}{2}\left[1 + \sqrt{1 - \frac{4\tilde{\varepsilon}}{(1+\tilde{\varepsilon}\zeta)^2}}\right], \tag{10.96}$$

$$\hat{\mathrm{x}}_S = \mathrm{x}_I\frac{1 + \frac{1}{2}\zeta\mathrm{x}_I\left(1 + \sqrt{1 + \frac{4\tilde{\varepsilon}}{\zeta\mathrm{x}_I^2(1+\tilde{\varepsilon}\zeta)}}\right)}{1 + \frac{\zeta\mathrm{x}_I^2}{1+\tilde{\varepsilon}\zeta}}. \tag{10.97}$$

Note that this solution is fully non-perturbative. To extract quantitative estimates, we expand Eqs. (10.96) and (10.97) in powers of $\tilde{\varepsilon}$ up to second order:

$$\mathrm{x}_I = 1 + \tilde{\varepsilon}(1+\tilde{\varepsilon})(\zeta - 1), \tag{10.98}$$

$$\hat{\mathrm{x}}_S = 1 + \tilde{\varepsilon}\left(\zeta - \frac{\tilde{\varepsilon}}{\zeta}\right). \tag{10.99}$$

Next, we evaluate $\zeta = \frac{1}{\hat{\mathrm{x}}_S} - \frac{1}{\ln\delta_S}$. As in the classical analysis, we assume $\ln\delta_S \gg 1$, so the second term can be neglected. This gives $\zeta = 1 - \tilde{\varepsilon}(1+\tilde{\varepsilon})$. Finally, we determine τ_0 from Eq. (10.80). Plugging this expression for ζ into Eqs. (10.98) and (10.99), the island's position along the $\delta_I = 1$ hypersurface becomes

$$\delta_I = 1, \tag{10.100}$$

$$\mathrm{x}_I = 1 - \tilde{\varepsilon}^2 = \hat{\mathrm{x}}_I, \tag{10.101}$$

$$\hat{\mathrm{x}}_S = 1 + \tilde{\varepsilon}(1 - 2\tilde{\varepsilon}), \tag{10.102}$$

$$\frac{\tau_0}{2a} = \frac{b_* - a}{a} - \left(1 + \frac{11}{8}\tilde{\varepsilon}\right)\frac{4}{\tilde{\varepsilon}}\left(e^{\frac{\tilde{\varepsilon}}{4}\ln\frac{3\tilde{\varepsilon}}{4}} - 1\right) - \tilde{\varepsilon}. \tag{10.103}$$

Comparing Eqs. (10.100–10.103) with the classical expressions (10.55–10.58), we find that the leading correction to the island position x_I along the $\delta_I = 1$ hypersurface now appears at order $\mathcal{O}(\tilde{\varepsilon}^2)$, in contrast to the classical case, where it is of order $\mathcal{O}(\tilde{\varepsilon})$. Furthermore, the formation time of the island τ_0 agrees with the classical result up to terms of order $\mathcal{O}(1)$. Deviations at higher orders are expected, as they arise from incorporating quantum corrections to the metric.

We now generalize the solution for the island position to arbitrary times $\tau > \tau_0$. Since $b_*\tilde{\varepsilon} \gg a$, we can safely disregard terms of order $1/\ln\delta_S$, as in the purely classical analysis. With this approximation, Eqs. (10.89) and (10.90) take the form

$$\mathrm{x}_I\partial_+\mathrm{x}_I + \tilde{\varepsilon}\partial_+\rho_I = \frac{\tilde{\varepsilon}}{2a}\left[\frac{1}{\hat{\mathrm{x}}_S - \ln\delta_I} - \frac{1}{\hat{\mathrm{x}}_I - \ln\delta_I}\right], \tag{10.104}$$

$$\mathrm{x}_I\partial_-\mathrm{x}_I + \tilde{\varepsilon}\partial_-\rho_I = \frac{\tilde{\varepsilon}}{2a}\left[\frac{1}{\hat{\mathrm{x}}_I - \hat{\mathrm{x}}_S} + \frac{1}{\hat{\mathrm{x}}_I - \ln\delta_I}\right]. \tag{10.105}$$

We adopt the following ansatz:

$$\mathrm{y}_I = 1 + \xi, \quad \hat{\mathrm{x}}_I = 1 + \hat{\xi}, \quad \hat{\mathrm{x}}_S = 1 + \mu, \tag{10.106}$$

where ξ, $\hat{\xi}$ and μ are quantities of order $\mathcal{O}(\tilde{\varepsilon})$. Inserting this ansatz into the expressions (5.157–5.158) for the derivatives of the dilaton field, together with Eqs. (5.182–5.183) for the derivatives of the metric, we find

$$\partial_+ \mathrm{x}_I = \frac{1}{2a}\left(1 - \frac{1}{\sqrt{\mathrm{y}_I^2 - \tilde{\varepsilon}}}\right), \tag{10.107}$$

$$\partial_- \mathrm{x}_I = -\frac{1}{2a\mathrm{F}_I^-}\left(1 - \frac{1 - \frac{\tilde{\varepsilon}}{4}}{\sqrt{\mathrm{y}_I^2 - \tilde{\varepsilon}}}\right), \tag{10.108}$$

$$\partial_+ \rho = \frac{1}{4a\tilde{a}_I}\frac{\mathrm{y}_I}{(\mathrm{y}_I^2 - \tilde{\varepsilon})^{\frac{3}{2}}}, \tag{10.109}$$

$$\partial_- \rho = -\frac{1}{4a\mathrm{F}_I^-}\left(\frac{\hat{\mathrm{x}}_I^2 - 1}{\hat{\mathrm{x}}_I^2} - \frac{1}{\tilde{a}_I}\frac{\mathrm{y}_I^2 - 1}{\mathrm{y}_I^2}\right), \tag{10.110}$$

where y and $\tilde{a}$ are defined via Eq. (5.156). Using Eqs. (10.107) and (5.182), Eq. (10.104) simplifies to $\mathrm{y}_I = 1$, i.e. $\xi = 0$. Note that we can determine the island position only up to $\mathcal{O}(\tilde{\varepsilon})$, since the solution itself is of that order. Consequently, the left-hand side of Eq. (10.104) vanishes. The quantity $\hat{\xi}$ then follows straightforwardly from Eq. (5.181), giving

$$\hat{\xi} = \frac{1}{4}(1 - \delta_I). \tag{10.111}$$

From Eq. (5.184) we infer that

$$\mathrm{F}^-(\hat{\mathrm{x}}_I) = \hat{\xi} - \frac{\tilde{\varepsilon}}{4}. \tag{10.112}$$

Substituting Eq. (10.112) into Eq. (10.105) yields

$$\frac{\tilde{\varepsilon}}{4} = \tilde{\varepsilon}\frac{\hat{\xi} - \frac{\tilde{\varepsilon}}{4}}{\hat{\xi} - \mu}. \tag{10.113}$$

Solving Eq. (10.113) and using Eq. (10.111), we obtain:

$$\mu = \frac{1}{4}\left(1 + 3\delta_I\right). \tag{10.114}$$

By inserting $\Delta\tau = \tau - \tau_0$ into Eq. (10.85), we derive the following relation for μ:

$$-\frac{\Delta\tau}{2a}\left(1 - \frac{11}{8}\tilde{\varepsilon}\right)e^{-\frac{\tilde{\varepsilon}}{4}\ln\frac{3\tilde{\varepsilon}}{4}} = \frac{4}{\tilde{\varepsilon}}\left(e^{\frac{\tilde{\varepsilon}}{4}\ln\frac{4\mu-1}{3}} - 1\right) + \tilde{\varepsilon}(\mu - 1). \tag{10.115}$$

Because the right-hand side of Eq. (10.115) contains logarithms, the equation is correct up to $\mathcal{O}(1)$. Taking the limit $\tilde{\varepsilon} \to 0$ and solving for μ gives

$$\mu = \frac{1}{4}\left(1 + 3e^{-\frac{\Delta\tau}{2\bar{a}}}\right), \tag{10.116}$$

where we have introduced a new constant $\bar{a}$, which can be interpreted as quantum-corrected surface gravity:

$$\kappa = \frac{1}{2\bar{a}} = \frac{1}{2a}\left(1 - \frac{11}{8}\tilde{\varepsilon}\right)e^{-\frac{\tilde{\varepsilon}}{4}\ln\frac{3\tilde{\varepsilon}}{4}}. \tag{10.117}$$

Combining Eqs. (10.111), (10.114) and (10.116), we find the following expressions for the island position:

$$\delta_I = e^{-\frac{\Delta\tau}{2\bar{a}}}, \tag{10.118}$$

$$\hat{\mathrm{x}}_I = 1 + \frac{\tilde{\varepsilon}}{4}\left(1 - e^{-\frac{\Delta\tau}{2\bar{a}}}\right), \tag{10.119}$$

$$\mathrm{x}_I = 1 - \frac{\tilde{\varepsilon}}{4}\frac{\Delta\tau}{2\bar{a}}, \tag{10.120}$$

$$\hat{\mathrm{x}}_S = 1 + \frac{\tilde{\varepsilon}}{4}\left(1 + 3e^{-\frac{\Delta\tau}{2\bar{a}}}\right). \tag{10.121}$$

The island thus emerges behind the event horizon, as expected for an evaporating black hole. Comparing Eqs. (5.189) and (10.119), we see that the island and the apparent horizon are symmetric with respect to the event horizon (5.208). Moreover, the island intersects the singularity slightly before the end-point of the evaporation, just as in the BPP model (see Sec. 9.2.3). In the limit $\Delta\tau \to 0$, the relations (10.118–10.121) reduce to Eqs. (10.101–10.103). Unlike in the classical case, where x_I tends to a constant value at late times (10.74), here x_I decreases with time, which is precisely what is required to reproduce the Page curve, since the island must reach the singularity in a finite time.

We now evaluate the contribution of the replica–wormhole saddle to the fine-grained entropy. We begin with the semi-classical entropy term in Eq. (1.6). Substituting the island location (10.118–10.121) into Eq. (10.43), we obtain

$$S_{semi-cl-\mathrm{RW}} = \frac{1}{12}\ln\left(\frac{4\tilde{\varepsilon}\left(-\ln\delta_S^{(0)}\right)^2}{-3\mathrm{F}_\infty^+(\kappa\epsilon)^4}\right) - \frac{\tilde{\varepsilon}}{6}\frac{1}{1+\frac{\Delta\tau}{2\bar{a}}}e^{-\frac{\Delta\tau}{2\bar{a}}}, \tag{10.122}$$

where we used

$$\begin{aligned}
&\tilde{\mathrm{F}}^+\mathrm{F}^-e^{2\rho}\Big|_I = \frac{\tilde{\varepsilon}}{4} \;\wedge\; \mathrm{F}_I^- = -\frac{\tilde{\varepsilon}}{4}\delta_I \;\wedge\; \tilde{\mathrm{F}}_I^+ = -1,\\
&\mathrm{F}^+\mathrm{F}^-e^{2\rho}\Big|_S = -1 \;\wedge\; \mathrm{F}_S^- = \frac{3}{4}\tilde{\varepsilon}\delta_I \;\wedge\; \mathrm{F}_S^+ = \mathrm{F}_\infty^+,\\
&\text{Coord-part} = \left(-\ln\delta_S^{(0)}\tilde{\varepsilon}\delta_I\right)^2\left(1 - \frac{2\tilde{\varepsilon}\delta_I}{1-\ln\delta_I}\right).
\end{aligned} \tag{10.123}$$

In Eq. (10.123), $\tilde{\mathrm{F}}_I^+$ denotes a coordinate redefinition relative to the σ^+ coordinate, while F_S^+ is a coordinate transformation with respect to $\hat{\sigma}^+$. Moreover, "Coord-part" refers to the portion of Eq. (10.43) inside the logarithm that depends explicitly on the σ coordinates. Since the expression in Eq. (10.122) still involves the UV cut-off ϵ, we must perform a regularization. Next, we consider the area term appearing in Eq. (10.45). Plugging in Eq. (10.120) gives

$$\frac{A[\partial I]}{4G_\mathrm{N}^{(4)}} = \frac{1}{12\tilde{\varepsilon}}\left(1 - \frac{\tilde{\varepsilon}}{4}\frac{\Delta\tau}{2\bar{a}}\right)^2. \tag{10.124}$$

To fix the regularization, we impose that the island hits the singularity near the end of evaporation, ensuring that the fine-grained entropy vanishes at the evaporation end-point. Taking this requirement together with the minimization prescription (1.6), we arrive at the final expression for the late-time limit of the fine-grained entropy of Hawking radiation:

$$\begin{aligned} S_{FG} = \min \Bigg\{ & \frac{\Delta\tau}{24\bar{a}} + \frac{1}{6}\ln\frac{\tau}{2b} - \frac{1}{12}\ln\left(\frac{-3\varepsilon \mathrm{F}^{+}_{\infty}}{4(\lambda a)^2}\right), \\ & \frac{(\lambda a)^2}{12\varepsilon}\left(1 - \frac{\varepsilon}{4(\lambda a)^2}\frac{\Delta\tau}{2\bar{a}}\right)^2 - \frac{1}{12} - \frac{\varepsilon}{6(\lambda a)^2}\frac{1}{1+\frac{\Delta\tau}{2\bar{a}}}e^{-\frac{\Delta\tau}{2\bar{a}}} \Bigg\}. \end{aligned} \tag{10.125}$$

The Page time is then determined by equating the two branches inside Eq. (10.125). This yields

$$\kappa\tau_P = \frac{4(\lambda a)^2}{\varepsilon}\left(3 - 2\sqrt{2}\right). \tag{10.126}$$

At $\tau = \tau_P$, the fine-grained entropy reaches its peak value,

$$S^{\max}_{FG} = \frac{4}{3+2\sqrt{2}} S^{(\mathrm{class})}_{BH}. \tag{10.127}$$

Eq. (10.127) shows that at all times the fine-grained entropy of the Hawking radiation remains below the coarse-grained (thermodynamic) bound set by the classical Bekenstein–Hawking entropy (1.4), as expected.

The resulting Page curve for the quantum-corrected collapse scenario is shown in Fig. 10.10. The blue line denotes the fine-grained entropy evaluated on Hawking's saddle point, whereas the red line depicts the entropy along the replica-wormhole saddle point at late times. The purple line illustrates the late-time asymptotic behavior of the fine-grained entropy on Hawking's saddle point.

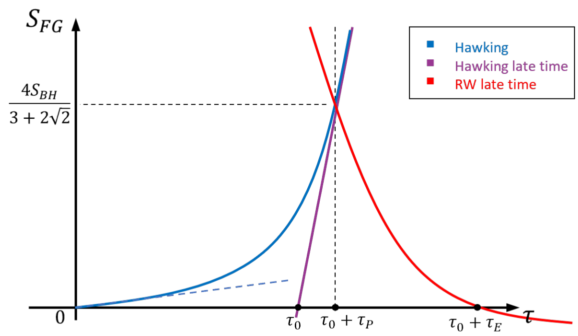

Figure 10.10: Page curve for the quantum-corrected collapse scenario in the DREH model.

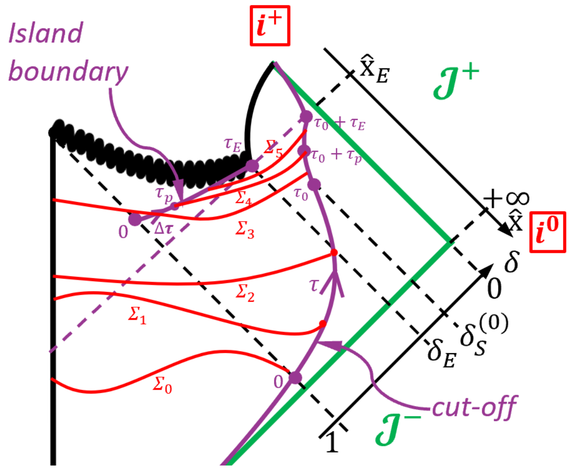

Figure 10.9: The complete process of black hole evaporation.

The evaporation process is depicted in Fig. 10.9. The purple curve outside the horizon denotes the cut-off hypersurface, parameterized by the evaporation time τ. The second purple curve indicates the time-dependent location of the island, parameterized by $\Delta\tau$. Both τ and $\Delta\tau$ are initialized at zero along the $\delta = 1$ hypersurface. The red curves represent the region A, which contains the degrees of freedom that are inaccessible to the asymptotic observer.

Let us now summarize the overall mechanism of black hole evaporation. As τ increases, the black hole begins to evaporate. Initially, the minimum of the fine-grained entropy (10.125) is determined by Hawking's saddle point, so the red curves terminate at the spacetime boundary $\mathrm{x} = 0$. When τ reaches $\tau = \tau_0$, an island first appears inside region II of the spacetime.

This moment is characterized by $\Delta\tau = 0$ along the island-boundary curve. At this stage, the fine-grained entropy is still dominated by the Hawking contribution, and thus the red curves continue to end at the spacetime boundary. At $\tau = \tau_0 + \tau_P$, or equivalently $\Delta\tau = \tau_P$, a phase transition takes place. From that time on, the red curves terminate on the island boundary instead. The evaporation proceeds until $\tau_f = \tau_0 + \tau_E$, that is, until the island meets the singularity, meaning $\Delta\tau \approx \tau_E$. The instant $\tau = \tau_f$ coincides with the point at which the cut-off surface enters region III of the spacetime, thereby leaving the domain in which black hole radiation is present.

Note that we cannot precisely determine what occurs at the very end of the evaporation process, because at this stage the remaining distance to the end-point becomes so small that it is comparable to the Planck length. Consequently, quantum gravity effects become relevant, and the semi-classical approximation is no longer valid. Moreover, in this regime the perturbative treatment also breaks down (see Sec. 5.3). Nevertheless, we can still trust the reproduction of the Page curve up to its last few points.

Chapter 11

Page curve in the DR5DCS model

In this chapter we explore a range of thermodynamic properties arising in the dimensionally reduced 5DCS model of two-dimensional dilaton gravity. The theory naturally separates into two distinct sectors. The equations of motion for the Riemannian sector are solved in Chap. 6, where both eternal and evaporating black hole scenarios are constructed. In what follows we focus exclusively on the eternal black hole configuration and demonstrate that it correctly reproduces the Page curve. The analysis parallels that carried out for the BPP and DREH models.

For the theory with non-vanishing torsion, no island rule prescription is currently available in the literature. Our objective, therefore, is to test whether the standard fine-grained entropy formula for gravitational systems (1.6) can still yield the Page curve. By examining the quantum-corrected black hole solution of Sec. 7.4, we find that it does so successfully. Nevertheless, the presence of torsion imposes a particular constraint on where the cut-off hypersurface may be placed, in contrast to the Riemannian case, where the cut-off can be chosen arbitrarily within the thermal bath regions.

This chapter is organized into four sections. Since we now consider spacetimes that are asymptotically AdS, we must first relax the reflective boundary conditions typically imposed at the AdS boundary. Implementing the new transparent conditions effectively introduces two asymptotically flat regions, each attached to the black hole exterior at the asymptotic boundary. How these thermal bath regions are incorporated in both the eternal and evaporating black hole setups is the main subject of Sec. 11.1.

In Sec. 11.2 we then analyze the coarse-grained entropy of both the Riemannian black hole and the black hole with torsion. Employing the Wald entropy formula, we derive the thermodynamic entropy and thereby obtain the area term appearing in the island formula. Furthermore, we explicitly verify that the first law of thermodynamics is satisfied for the general vacuum solutions in both the torsionless and torsionful cases.

Next, in Sec. 11.3, we determine the Page curve for the eternal black hole in the Riemannian sector constructed in Sec. 6.2.3. We use the standard approach: we first examine the no-island configuration, which leads to the Hawking information-loss paradox, and then introduce an island. The latter produces a well-defined Page curve and thus resolves the paradox.

Finally, Sec. 11.4 is devoted to applying the island rule to spacetimes with non-vanishing torsion. We begin by studying the role of the θ field through the computation of the Page curve for the general vacuum solution of Sec. 7.1.1. We then proceed to the solution of the gravitational field equations coupled to the Polyakov–Liouville quantum corrections to the scalar field action introduced in Sec. 7.4.

11.1 Coupling the black hole to the thermal bath

When the spacetime has AdS-like asymptotic behavior, the usual Page-curve calculation ceases to be applicable. There are two main reasons for this. First, as already pointed out at the end of Sec. 6.1.3, null rays can reach the asymptotic boundary in a finite value of the affine parameter. Consequently, one imposes reflective boundary conditions at this boundary, effectively turning the spacetime into a confining cavity for the fields living on it. In such a configuration, outgoing light rays bounce off the asymptotic boundary and eventually fall back into the black hole. From the standpoint of Hawking radiation, this implies that the radiation is inevitably reabsorbed by the black hole.

To meaningfully discuss Hawking radiation, one must introduce a well-defined radiation region R in which the radiation quanta are collected. In an asymptotically flat spacetime, this region is located near the future null infinity $\mathcal{J}^+$, because outgoing quanta cannot actually arrive at $\mathcal{J}^+$ in finite time. As a result, the quanta accumulate within this intermediate region, where one can perform well-defined measurements on them—such as computing the entanglement entropy of Hawking radiation.

In contrast, if the spacetime is asymptotically AdS, there is no infinitely large subregion R from which Hawking quanta can be extracted. To resolve this, one must replace the usual reflective boundary conditions with transparent ones. Then the Hawking quanta simply pass through the AdS boundary and emerge into a different spacetime region, which is smoothly connected along the AdS asymptotic boundary to the exterior of the black hole. This region is referred to as the *thermal bath region*. It is there that the Hawking quanta are accumulated. It is now clear that this region must have asymptotically flat, Minkowski-like behavior, so that a portion of it, or possibly the entire region, can effectively serve as the infinite radiation subregion R.

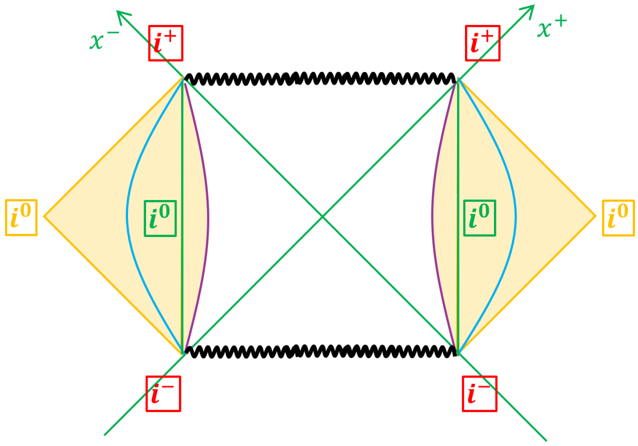

Figure 11.1: Penrose diagram depicting coupling of the AdS asymptotic region to the thermal bath for an eternal BTZ black hole.

In Fig. 11.1, the Penrose diagram of the eternal BTZ black hole (shown previously in Fig. 6.1) is extended by attaching a bath region that is smoothly joined to the AdS boundary. This region is highlighted in yellow. The resulting diagram is very similar to the Penrose diagram of the eternal Schwarzschild black hole in Fig. C.6.

Once the bath is included, there exists a clearly defined region of spacetime into which the Hawking quanta can escape. This region is infinite, so after the quanta enter it, they cannot reflect back and re-emerge into the asymptotic AdS region. Yet a further question remains: where exactly is the cut-off hypersurface located? According to the central dogma (see Sec. 8.4.1), the cut-off surface must lie in a portion of spacetime where gravity is weak. For an asymptotically flat spacetime, this corresponds to a neighborhood of $\mathcal{J}^+$, because there the effective gravitational coupling goes to zero and the metric approaches the flat Minkowski form. In that region gravity is effectively switched off, and the outgoing Hawking modes can be treated using standard quantum field theory on a fixed background.

We now clarify in more detail why the radiation subregion R must lie in a weakly gravitating domain. Suppose that we know the exact quantum state of the full system, consisting of both the black hole and its radiation. The density matrix of the radiation is obtained by tracing out the black hole degrees of freedom that reside below the cut-off hypersurface. To perform this trace, the total Hilbert space must admit a well-defined factorization $\mathcal{H} = \mathcal{H}_{\text{grav}} \otimes \mathcal{H}_{\text{rad}}$; once this factorization is available and the full quantum state is known, the partial trace can be computed simply. However, if the region of spacetime over which we trace is still gravitating, this factorization is no longer well defined, and the partial trace cannot be computed.

The underlying reason is intimately connected to the diffeomorphism and local Lorentz constraints, which are an inherent feature of any gravitational theory. A proper Dirac quantization of gravity has to incorporate the entire symmetry structure of the gravitational theory [81]. In this framework, gravity is formulated via the localization of the group $SO(1,3,\mathbb{R})$. Within the Hamiltonian approach, gauging this symmetry gives rise to ten first-class constraints. Upon quantization, these constraints become operators that must annihilate all physical states:

$$\hat{\mathcal{H}}\,|\Psi\rangle = 0, \qquad \hat{\mathcal{H}}_i\,|\Psi\rangle = 0, \qquad \hat{\mathcal{J}}_{ab}\,|\Psi\rangle = 0. \tag{11.1}$$

Any physical, gauge-invariant operator is required to commute with all these first-class constraints. A sharply localized bulk operator $\hat{\mathcal{O}}(x)$ in a given subregion cannot satisfy this condition, because the constraints act locally at every point in space. To render $\hat{\mathcal{O}}(x)$ genuinely physical, one must gravitationally dress it, meaning that the gravitational field has to be line-integrated from the point x to a boundary where the gauge parameters vanish. In practice, this attaches a gravitational Wilson line extending from the operator's position all the way to an asymptotic boundary. Consequently, physical operators are intrinsically nonlocal, being distributed across the whole spacetime, and this nonlocality prevents any factorization of the physical Hilbert space into a component associated only with a subregion in which gravity remains dynamical.

When gravity is switched off, or is sufficiently weak, these constraints effectively disappear and the Hilbert space can be factorized into a part corresponding to the chosen subregion. In asymptotically flat spacetimes, this situation arises near the $\mathcal{J}^+$ hypersurface. By contrast, in AdS-asymptotic spacetimes, this factorization never takes place, since gravity remains strong all the way to the boundary and the metric diverges there. Introducing a thermal bath region resolves this issue as well: because this region is modeled as flat Minkowski space, gravity is entirely turned off there. Hence, the cut-off hypersurface must lie within the thermal bath region. It is illustrated by the light blue line in Fig. 11.1.

From the perspective of the island formula (1.6), once an island is included, it appears as though we are also performing a partial trace over the island region. Since this region lies close to the horizon, it is clear from the above discussion that such a trace is not strictly well-defined. Nevertheless, the emergence of the QES is merely a byproduct of the replica trick and encodes the semi-classical computation of the trace of the full quantum state restricted to the radiation subregion R. In the semi-classical picture the spacetime geometry is held fixed and does not fluctuate, so the tracing operation acts only on the Hilbert space of the quantum fields, which does admit a decomposition into distinct spacetime regions, as is standard in quantum field theory on curved backgrounds. We are thus led to conclude that the island formula is reliable, as it is applied within the domain of validity of the semiclassical approximation.

Up to this point, our analysis has focused solely on the eternal black hole scenario. However, extension to the case of a classical gravitational collapse and an evaporating black hole scenario is straightforward. In both setups, null rays still reach the asymptotic boundary in finite time.

Consequently, the thermal bath region must again be included. In the collapse scenario, it stretches from the point on the spatial infinity hypersurface i^0 from which the infalling matter shockwave originates, up to future time infinity i^+. In principle, one should analytically continue this region to times before the collapse, but this extension does not affect the computation of the Page curve, and we do not pursue it further.

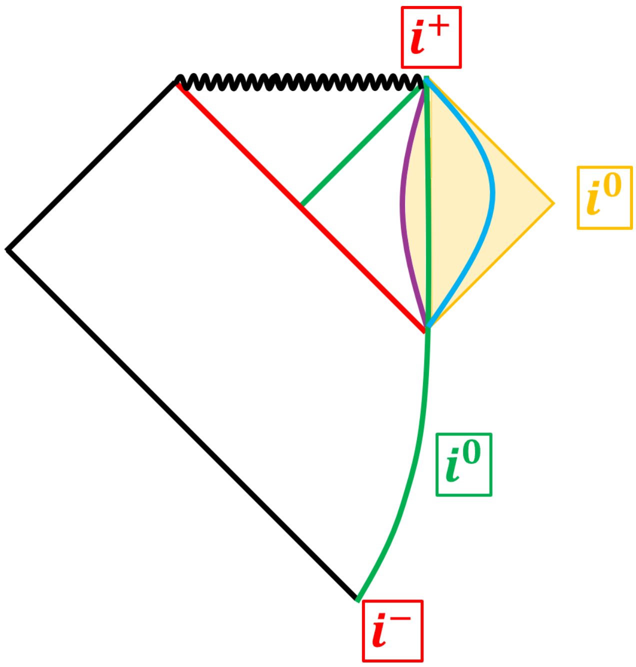

Figure 11.2: Penrose diagram depicting coupling of the AdS asymptotic region to the thermal bath for the classical gravitational collapse scenario.

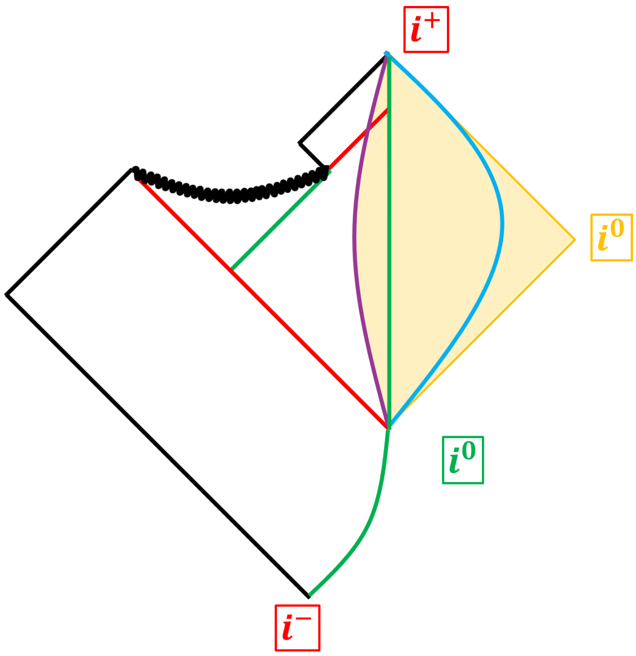

Figure 11.3: Penrose diagram depicting coupling of the AdS asymptotic region to the thermal bath for the evaporating black hole scenario.

Let us begin by examining the classical gravitational collapse scenario. The coupling to the thermal bath is shown in Fig. 11.2. As before, the bath region is highlighted in yellow and the cut-off hypersurface is represented by a light blue line within this region. The diagram is an extension of the diagram in Fig. 6.3, but now the confining coordinates $\mathrm{x}^{\pm}$ defined in Eq. (6.31) are constructed with respect to the coordinates $\hat{\sigma}^{\pm}$. As a result, after the collapse the spacetime boundaries are rendered as straight lines, in contrast to Fig. 6.3, where the confining coordinates are defined relative to the $\sigma^{\pm}$ coordinates of the pre-collapse region. Because there is no evaporation, region II of the spacetime is static, implying that future time infinity lies at the intersection of the event horizon and the singularity. In the bath region, the cut-off hypersurface ends precisely at this same point.

The evaporating black hole case is depicted in Fig. 11.3. Once more, we employ confining coordinates built upon the $\hat{\sigma}^{\pm}$ coordinates so that the boundaries of regions II and III appear as straight lines, in contrast to Fig. 6.4. The key distinction from the previous setup is the appearance of a black hole remnant in region III of the spacetime after the thunderpop. The thermal bath region—again shown in yellow—now borders both the black hole region II and the remnant region III. The cut-off hypersurface, drawn in light blue, now terminates at the future time infinity of the remnant black hole region.

11.1.1 Junction condition at the asymptotic boundary

Thus far, we have explained why including the thermal bath region is essential for studying Hawking radiation in an asymptotically AdS spacetime. We have not yet, however, specified how this region is to be attached at the AdS boundary. The procedure can be straightforwardly generalized to any AdS-like geometry in which spatial infinity is a time-like hypersurface and outgoing Hawking quanta reach this boundary in a finite time. This feature is tied to the fact that the metric diverges at infinity. Near spatial infinity in an AdS-asymptotic spacetime, the metric takes the form

$$\mathrm{d}s^2 = -\frac{1}{\epsilon^2}\mathrm{d}\sigma^+\mathrm{d}\sigma^-, \quad \epsilon \to 0. \tag{11.2}$$

Because the metric in Eq. (11.2) diverges at the AdS boundary, it cannot be smoothly matched to the Minkowski metric directly on that hypersurface. Instead, we terminate the AdS region at a small but finite distance $\mathrm{z} = \epsilon$ from the boundary, and impose the junction conditions with flat Minkowski spacetime on this hypersurface. In Figs. 11.1, 11.2 and 11.3, this matching surface is depicted by a purple line. To implement this construction, we must first analytically continue the σ coordinates into the thermal bath region as well. We begin by addressing this step in the context of a classical BTZ black hole. The tortoise coordinate is defined in Eq. (6.29), which we reproduce here for convenience:

$$\frac{\sigma}{l} = \frac{1}{2\sqrt{\mu}}\ln\left|\frac{\mathrm{x}-\sqrt{\mu}}{\mathrm{x}+\sqrt{\mu}}\right|. \tag{11.3}$$

As already explained in Sec. 6.1.3, the horizon is located at $\sigma_{\mathrm{H}} \to -\infty$, whereas spatial infinity is at $\sigma_{i^0} = 0$, which follows straightforwardly from taking the limit $\mathrm{x} \to \infty$ in Eq. (11.3). To extend the geometry into the bath region, we simply allow the σ coordinate to take positive values. In this parametrization, the limit $\sigma \to \infty$ corresponds to $\mathrm{x} \to -1/\sqrt{\mu}$. Since the quantum state is defined with respect to Kruskal coordinates, which in region I are given by

$$\kappa x^+ = e^{\kappa\sigma^+} \quad \wedge \quad \kappa x^- = -e^{-\kappa\sigma^-}, \tag{11.4}$$

extending σ to positive values also analytically continues these functions, implying

$$\sigma \to +\infty \quad \Longrightarrow \quad x^+ \to \infty \;\; \wedge \;\; x^- \to \infty \quad \Longrightarrow \quad \mathrm{x}^+ = \frac{\pi}{2} \;\; \wedge \;\; \mathrm{x}^- = -\frac{\pi}{2}. \tag{11.5}$$

Hence, we indeed recover the right Rindler wedge of Minkowski spacetime, as intended. Having now specified the full coordinate patch, we can straightforwardly analytically continue both the metric and the dilaton field across the hypersurface $\mathrm{x} = 1/\epsilon$. In particular, the metric function Λ in quadrant I takes the form

$$\Lambda = \begin{cases} -\left(\mathrm{x}^2 - \mu\right), & \sigma \leqslant -\epsilon, \\ -\dfrac{1}{\epsilon^2}, & \sigma > -\epsilon \end{cases} \tag{11.6}$$

To obtain the exact Minkowski metric, we simply rescale the coordinates so that the factor $1/\epsilon$ is absorbed. However, when computing the von Neumann entropy of any region lying inside the thermal bath, the metric must be written in coordinates suitable for defining the quantum state—Kruskal coordinates in the case of the eternal black hole. Rewriting the metric in this way reintroduces the divergent $1/\epsilon$ contribution, but this small parameter can be absorbed into the UV cut-off. Consequently, the entropy remains finite and well defined in the limit $\epsilon \to 0$.

Once quantum corrections are taken into account, they can shift the asymptotic boundary to a slightly negative value of the σ coordinate, denoted by $\sigma = \sigma_{i^0}$. At this point the metric becomes divergent, so we impose the junction conditions at $\sigma = \sigma_{i^0} - \epsilon$ instead. If additional fields are present, as in the full DR5DCS theory, one must inspect their equations of motion to determine how to analytically continue them into the bath region. However, since these fields do not contribute to the von Neumann entropy, the precise details of their analytic continuation are not especially important for investigating the fine-grained entropy.

For the evaporating black hole, the $\hat{\sigma}^{\pm}$ coordinates are analytically continued in the same way as the $\sigma^{\pm}$ coordinates in the eternal black hole case. From the definition of the asymptotic boundary of the evaporating black hole, it is again located at a finite value of the $\hat{\sigma}$ coordinate, and the metric still displays the same $1/\epsilon^2$-type divergence. Consequently, the same procedure can be used in this scenario as well.

11.2 Coarse-grained entropy via Wald formula

As a prerequisite to computing the Page curve, we must first obtain the effective area term. In the model under consideration, this term is given by the analogue of the Bekenstein–Hawking entropy evaluated on the island hypersurface. Consequently, our initial step is to compute the coarse-grained entropy in the DR5DCS model. For this purpose, we use the Wald formula (10.28), which in two-dimensional spacetime simplifies to:

$$S_{\text{Wald}} = -\frac{2\pi}{\hbar}\int_{\text{H}} \mathrm{d}A \frac{\partial \mathcal{L}}{\partial R_{\mu\nu\rho\sigma}} \varepsilon_{\mu\nu}\varepsilon_{\rho\sigma} \quad \Longrightarrow \quad S_{\text{Wald}} = \frac{4\pi}{\hbar}\frac{\partial \mathcal{L}}{\partial R}\bigg|_{\text{H}}. \tag{11.7}$$

This form is applicable provided that the Lagrangian has no explicit dependence on the spin connection and that it enters only through covariant derivatives of the fields [139]. We now evaluate the Wald entropy corresponding to the Riemannian action (6.1). A straightforward calculation gives:

$$S_{\text{R}} = \frac{4k\pi^3}{\hbar}\mathrm{x}\left(\mathrm{x}^2+3\right)\bigg|_{\text{H}}. \tag{11.8}$$

Recalling that the Hawking temperature is expressed in terms of the surface gravity appearing in Eq. (6.21) as:

$$T = \frac{\hbar\kappa}{2\pi} \quad \Longrightarrow \quad T = \frac{\hbar\sqrt{\mu}}{2\pi l}. \tag{11.9}$$

and using that the horizon is located at $\mathrm{x}_{\text{H}} = \sqrt{\mu}$ yields the following thermodynamic relation:

$$T\mathrm{d}S_{\text{R}} = \frac{3k\pi^2}{l}(\mu+1)\mathrm{d}\mu \quad \Longrightarrow \quad T\mathrm{d}S_{\text{R}} = \mathrm{d}M, \tag{11.10}$$

where the mass M is defined in Eq. (6.52). This verifies that the first law of thermodynamics is satisfied.

We now turn to the full DR5DCS theory. Since all the conditions required to apply the Wald entropy formula (11.11) are fulfilled for the general action in Eq. (7.1), we can evaluate it and get:

$$S = \frac{4k\pi^3}{\hbar}\mathrm{x}\left[\mathrm{x}^2+3\left(1-\Phi^2-\theta^2\right)\right]_{\text{H}}. \tag{11.11}$$

We first compute the Wald entropy corresponding to the general vacuum configuration (7.35) of the full DR5DCS theory. Using $\Lambda = -\bar{\mathrm{x}}^2 + \mu$, the horizon is located at $\bar{\mathrm{x}} = \sqrt{\mu}$, which implies $\mathrm{x} = -\phi^{\perp}\sqrt{\mu}$. Plugging the explicit solution for θ into Eq. (11.11) yields:

$$S = \frac{12k\pi^3}{\hbar}\eta\sqrt{\mu}, \tag{11.12}$$

which is valid for an arbitrary function $\phi^{\perp}(\bar{\mathrm{x}})$. This immediately clarifies the role of the constant η. However, as explained in Sec. 7.1.2, the physically relevant solutions arising from gravitational collapse fix the gauge freedom in $\phi^{\perp}$ by imposing $\phi^{\perp} = -1$, which in turn enforces $\theta^2 = \text{const}$. Since θ must be continuous, it is naturally interpreted as a fundamental constant of the theory. In this case, we have:

$$\eta = \frac{1}{3}(\mu + 3) - \theta^2 \quad \Longrightarrow \quad S = \frac{4k\pi^3}{\hbar}\sqrt{\mu}\Big[\mu + 3\left(1 - \theta^2\right)\Big]. \tag{11.13}$$

To verify that the first law is satisfied by the vacuum solutions of the full theory, we differentiate Eq. (11.13) with respect to μ and find:

$$T\mathrm{d}S = \frac{3k\pi^2}{l}\left(\mu + 1 - \theta^2\right)\mathrm{d}\mu \quad \Longrightarrow \quad T\mathrm{d}S = \mathrm{d}M, \tag{11.14}$$

where we have used the mass relation in Eq. (7.54). The black-hole temperature is given by Eq. (11.9). We emphasize that the same conclusion—that θ must be regarded as a fundamental constant—is also reached in [89].

Finally, let us evaluate the entropy for a solution with a non-vanishing EMT. Eq. (11.11) simplifies to:

$$S = -\frac{12k\pi^3}{\hbar}\begin{cases} \cos^2\mathrm{z}\left[-\dfrac{D\sin^2\mathrm{z}}{\sqrt{-\Lambda} - \frac{P}{2}\sin\mathrm{z}} + \eta\cos\mathrm{z}\right]_{\mathrm{H}}, & \Lambda > 0, \\ \cosh^2\mathrm{z}\left[\dfrac{D\sinh^2\mathrm{z}}{\sqrt{-\Lambda} - \frac{P}{2}\sinh\mathrm{z}} + \eta\cosh\mathrm{z}\right]_{\mathrm{H}}, & \Lambda < 0, \;\; \mathrm{x}^2 + \Lambda\phi^{\perp 2} > 0, \\ \sinh^2\mathrm{z}\left[\dfrac{D\cosh^2\mathrm{z}}{\sqrt{-\Lambda} + \frac{P}{2}\cosh\mathrm{z}} - \eta\sinh\mathrm{z}\right]_{\mathrm{H}}, & \Lambda < 0, \;\; \mathrm{x}^2 + \Lambda\phi^{\perp 2} > 0, \\ \dfrac{\eta}{P}\left[\pm\sqrt{-\Lambda}e^{\pm 2\mathrm{z}} + \dfrac{P}{2}e^{\pm\mathrm{z}} + De^{\pm 3\mathrm{z}}\right]_{\mathrm{H}}, & \Lambda < 0, \;\; \mathrm{x}^2 + \Lambda\phi^{\perp 2} = 0, \end{cases} \tag{11.15}$$

where we have retained the general form of the expressions without imposing the horizon condition, since in the island setup they are instead evaluated at the island boundary. For the coarse-grained entropy we evaluate at the horizon, where $\Lambda = 0$. In this case the previous expressions reduce to:

$$S = -\frac{12k\pi^3}{\hbar}\begin{cases} \cos^2\mathrm{z}\left(\dfrac{2D}{P}\sin\mathrm{z} + \eta\cos\mathrm{z}\right)_{\mathrm{H}}, & \Lambda > 0, \\ \cosh^2\mathrm{z}\left(-\dfrac{2D}{P}\sinh\mathrm{z} + \eta\cosh\mathrm{z}\right)_{\mathrm{H}}, & \Lambda < 0, \;\; \mathrm{x}^2 + \Lambda\phi^{\perp 2} > 0, \\ \sinh^2\mathrm{z}\left(\dfrac{2D}{P}\cosh\mathrm{z} - \eta\sinh\mathrm{z}\right)_{\mathrm{H}}, & \Lambda < 0, \;\; \mathrm{x}^2 + \Lambda\phi^{\perp 2} < 0, \\ \dfrac{\eta}{2}\left[e^{\pm\mathrm{z}} + \dfrac{2D}{P}e^{\pm 3\mathrm{z}}\right]_{\mathrm{H}}, & \Lambda < 0, \;\; \mathrm{x}^2 + \Lambda\phi^{\perp 2} = 0. \end{cases} \tag{11.16}$$

As a final illustration, let us evaluate these formulas for the case of the BTZ metric, characterized by $\Lambda = -\bar{\mathrm{x}} + \mu$. We first determine the horizon position in terms of the z coordinate:

$$\frac{\mathrm{dz}}{\mathrm{d}\bar{\mathrm{x}}} = -\frac{1}{\sqrt{-\Lambda}} \quad \Longrightarrow \quad \bar{\mathrm{x}} = \sqrt{\mu}\cosh \mathrm{z}, \;\; \mathrm{z} < 0 \quad \Longrightarrow \quad \mathrm{z_H} = 0. \tag{11.17}$$

Substituting this result into Eq. (11.16) we obtain:

$$S = -\frac{12k\pi^3}{\hbar}\begin{cases} \eta, & \Lambda > 0, \\ \eta, & \Lambda < 0, \;\; \mathrm{x}^2 + \Lambda\phi^{\perp 2} > 0, \\ 0, & \Lambda < 0, \;\; \mathrm{x}^2 + \Lambda\phi^{\perp 2} < 0, \\ \frac{\eta}{2}\left(1 + \frac{2D}{P}\right), & \Lambda < 0, \;\; \mathrm{x}^2 + \Lambda\phi^{\perp 2} = 0. \end{cases} \tag{11.18}$$

Lastly, for the quantum-corrected geometry with a non-vanishing θ field, derived in Sec. 7.4, the entropy is evaluated at the outer horizon, located at $\mathrm{z} = \mathrm{z}_+$..

11.3 Eternal black hole scenario in the Riemannian sector

In this section, we derive the Page curve for an eternal black hole in the Riemannian sector of dimensionally reduced five-dimensional Chern–Simons gravity. The setup for the eternal black hole is introduced in Sec. 6.2.3. Our analysis closely parallels the calculations performed in Secs. 9.1 and 10.1 for the BPP and DREH models. Since the general procedure is already well established there, we refrain from repeating the same level of detail. To obtain the Page curve, we employ the island formula (1.6). As usual, we first evaluate the entropy in the absence of an island, which leads to the information-loss paradox, and then resolve this paradox by incorporating the island.

11.3.1 No-Island configuration

The eternal black hole scenario corresponds to the Hartle–Hawking quantum state (3.97), so the EMT is normal-ordered with respect to Kruskal coordinates, and the appropriate expression for the semiclassical entropy in the absence of an island is given in Eq. (8.51). For convenience, we reproduce it here:

$$S_{semi-cl} = \frac{1}{12}\ln\frac{(x_R^+ - x_L^+)^2(x_R^- - x_L^-)^2}{\delta^4 e^{-2\rho_R} e^{-2\rho_L}}. \tag{11.19}$$

As usual, the subscripts R/L denote the two thermal bath regions on the right and left sides of the spacetime, illustrated in Fig. 11.4. To correctly capture the time dependence of the fine-grained entropy, we move to the (t, σ) coordinate system, since time is defined in terms of the σ coordinate. The quantity δ represents the UV cut-off. Compared with Fig. 11.2, we observe that both spatial infinity i^0 and the singularity are now curved.

From Eq. (6.97), we see that the σ coordinate does not go to zero as x $\to 0$ or x $\to \infty$. Instead, we obtain

$$\sigma_{i^0} = -\frac{\varepsilon}{4\kappa(\mu+1)}, \quad \sigma_{\rm S} = \frac{\varepsilon}{4\kappa(\mu+1)}. \tag{11.20}$$

Consequently, the spatial infinity hypersurface i^0 in region I is slightly bent inward, and an analogous statement holds for the singularity hypersurface in region II. The cut-off hypersurface is depicted in light blue within the thermal bath regions, which are shaded in yellow. The constant-time slices supporting the radiation degrees of freedom are drawn in red in both wedges.

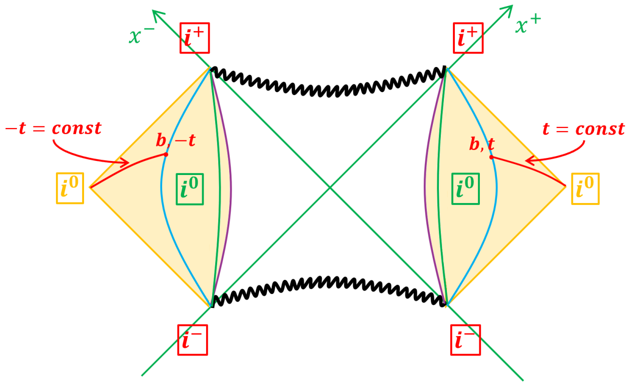

Figure 11.4: Penrose diagram depicting the no-island configuration for the eternal black hole in the DR5DCS model.

The $t =$ const. slice on the right-hand side corresponds to the $-t =$ const. slice on the left, since time runs in the opposite direction in the left wedge. Employing the Kruskal coordinates defined via the quantum-corrected surface gravity in Eq. (6.95), and rewriting them in terms of the time coordinate, one recovers the standard expression for the entanglement entropy (11.19) in the no-island configuration:

$$S_{FG} = \frac{1}{3}\ln\Big[\cosh(\kappa t)\Big], \qquad \kappa = \frac{\sqrt{\mu}}{l}\left[1 - \frac{\varepsilon}{2(\mu+1)\sqrt{\mu}}\right]. \tag{11.21}$$

Here, the UV divergence has been regularized such that $S_{FG}(0) = 0$. Evaluating the early- and late-time limits of Eq. (11.21) gives:

$$S_{FG} = \frac{1}{6}(\kappa t)^2, \;\; \kappa t \ll 1 \quad \wedge \quad S_{FG} \approx \frac{1}{3}\kappa t - \frac{1}{3}\ln 2, \;\; \kappa t \gg 1. \tag{11.22}$$

Thus, the fine-grained entropy of the radiation grows monotonically, in agreement with Hawking's original result [16]. As anticipated, the fine-grained entropy evaluated along Hawking's saddle point exhibits the same behavior as in the BPP and DREH models.

11.3.2 Island configuration

In the presence of an island, the expression for the entanglement entropy of quantum fields becomes more involved, since the region inaccessible to the asymptotic observer is now split into two disconnected components. The appropriate formula is written in Eq. (8.60); for clarity we reproduce it here:

$$S_{semi-cl} = \frac{1}{6}\ln\frac{d_{12}^2 d_{23}^2 d_{14}^2 d_{34}^2}{\delta^4 d_{24}^2 d_{13}^2 e^{-\rho_1} e^{-\rho_2} e^{-\rho_3} e^{-\rho_4}}, \tag{11.23}$$

where d_{ij} represent the usual Minkowski separation between the spacetime points defined in Eq. (10.8). The indices i and j are assigned such that $(1,2,3,4) \longleftrightarrow (Ra, Rb, La, Lb)$. Here, R refers to the right thermal bath region, and L refers to the left thermal bath region.

The eternal black hole scenario with an island region is shown in Fig. 11.5. The cutoff hypersurface, depicted in light blue, is parametrized by (t, b_*). It is located within the thermal bath regions, which are shaded in yellow. The constant-time slices, t = const., in both thermal bath regions are drawn in red. The island region I lies close to the horizon, as is typical for an eternal black hole. It is colored blue, and its boundary is specified by (t', a_*). The way in which the island region splits the previously inaccessible region is now manifest. The singularity and the AdS boundary remain slightly curved, since they are still determined by Eq. (11.20).

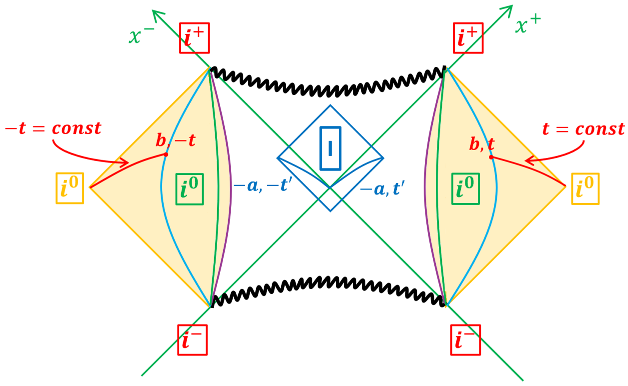

Figure 11.5: Penrose diagram depicting the island configuration for the eternal black hole in the DR5DCS model.

Since we anticipate that including the island resolves the information-loss paradox by contributing a constant term to the fine-grained entropy only at late times, we immediately take the late-time limit. The subsequent calculation of the entanglement entropy of quantum fields in Eq. (11.23) is identical to the analysis in Sec. 10.1. In this limit, one first shows that the factor $d_{23}^2 d_{14}^2/(d_{24}^2 d_{13}^2) \approx 1$, so it can be dropped from Eq. (11.23). We then extremize this entanglement entropy with respect to the island time coordinate t', since in a static spacetime the area term is time-independent. After carrying out these steps, the semi-classical entropy (11.23) simplifies to Eq. (10.13), which we reproduce here:

$$S_{semi-cl} = \frac{1}{3}(\rho_a + \rho_b) + \frac{2}{3}\ln\left(e^{\kappa b_*} - e^{\kappa a_*}\right) - \frac{2}{3}\ln(\kappa\delta). \tag{11.24}$$

We now turn to the area term in the island formula (1.6). This is the model-dependent part of the construction, since the semi-classical entropy consistently takes the universal form discussed above. The area term is given by the Bekenstein–Hawking entropy appropriate to the specific model. In the previous section we obtained this entropy using the Wald entropy formula. Consequently, the area term is provided by Eq. (11.8), multiplied by a factor of two to account for the two thermal bath regions, and evaluated on the island boundary hypersurface. The generalized entropy is then obtained by adding this area term to the semi-classical entropy (11.24), and takes the form:

$$S_{gen} = \frac{8k\pi^3}{\hbar} a\left(a^2 + 3\right) + \frac{1}{3}(\rho_a + \rho_b) + \frac{2}{3}\ln\left(e^{\kappa b_*} - e^{\kappa a_*}\right) - \frac{2}{3}\ln(\kappa\delta). \tag{11.25}$$

Extremizing the generalized entropy (11.25) with respect to the island location leads to:

$$\left(a^2 + 1 + \varepsilon \frac{\mathrm{d}\rho_K}{\mathrm{dx}}\bigg|_a\right)\frac{\mathrm{da}}{\mathrm{da}_*} = \frac{2\varepsilon\kappa}{e^{\kappa(b_*-a_*)} - 1}, \tag{11.26}$$

with $\varepsilon = \frac{\hbar}{72k\pi^3}$. Here, the subscript K in ρ_K emphasizes that the metric is evaluated in Kruskal coordinates. As in the DREH model, when solving Eq. (11.26) one must proceed carefully, since the island is expected to lie very close to the event horizon. Thus, we adopt a perturbative ansatz of the form $a = \sqrt{\mu} + z$ with $z \ll \sqrt{\mu}$. We begin with the left-hand side (LHS):

$$\frac{\mathrm{da}}{\mathrm{da}_*} = -\frac{\Lambda}{l} \implies \text{LHS} = -\frac{\Lambda}{l}\left(a^2 + 1 + \varepsilon\frac{\mathrm{d}\rho_K}{\mathrm{dx}}\bigg|_a\right) \approx -\frac{z}{l}\left(a^2 + 1 + \varepsilon\frac{\mathrm{d}\rho_K}{\mathrm{dx}}\right)\frac{\mathrm{d}\Lambda}{\mathrm{dx}}\bigg|_a. \tag{11.27}$$

The computation of the right-hand side relies on the well-defined pole of the tortoise coordinate in Eq. (6.97). One finds:

$$e^{2\kappa a_*} = e^{2\kappa\sigma_{\rm H}} + 2\kappa z \lim_{{\rm x}\to{\rm x_H}} e^{2\kappa\sigma}\frac{{\rm d}\sigma}{{\rm dx}} = -2\kappa l z \lim_{{\rm x}\to{\rm x_H}} \frac{{\rm x}-{\rm x_H}}{{\rm x}+{\rm x_H}}\left[1-\frac{\varepsilon}{\mu+1}\frac{{\rm x}-{\rm x_H}}{{\rm x}+{\rm x_H}}\right]\frac{1}{\Lambda} = \frac{z}{2\sqrt{\mu}}. \quad (11.28)$$

The first term vanishes because $\sigma_{\rm H} \to -\infty$. With this, the right-hand side of Eq. (11.26) is straightforward to evaluate and becomes:

$$\text{RHS} = 2\varepsilon\kappa e^{-\kappa b_*}\sqrt{\frac{z}{2\sqrt{\mu}}}\left(1+e^{-\kappa b_*}\sqrt{\frac{z}{2\sqrt{\mu}}}\right). \quad (11.29)$$

Equating the LHS from Eq. (11.27) with the RHS from Eq. 11.29 and solving for z yields:

$$z = \frac{1}{2\sqrt{\mu}}\frac{\varepsilon^2 e^{-2\kappa b_*}}{\left[\mu+1+\varepsilon\left(\frac{{\rm d}\rho_K}{{\rm dx}}-\frac{1}{2\sqrt{\mu}}e^{-2\kappa b_*}\right)\right]^2}. \quad (11.30)$$

An explicit evaluation of the derivative of the metric in Kruskal coordinates gives $\rho_K' = 1/(2\kappa l)$. Consequently, the island position is

$$a = \sqrt{\mu} + \frac{\varepsilon^2}{2(\mu+1)^2\sqrt{\mu}}e^{-2\kappa b_*}\left[1-\frac{\varepsilon}{2(\mu+1)\sqrt{\mu}}\left(1-e^{-2\kappa b_*}\right)\right]. \quad (11.31)$$

Comparing this with the island position for the eternal black hole case given in Eq. (10.22), we observe that Eq. (11.31) has precisely the same functional structure.

Next, we proceed to compute the fine-grained entropy along the replica-wormholes saddle. Plugging the island position (11.31) into the generalized entropy formula (11.25) yields a contribution to the generalized entropy evaluated at the horizon plus a term of order ε, exactly as in the DREH model (see Sec. 10.1). Since the generalized entropy contains a leading term of order $1/\varepsilon$, the $\mathcal{O}(\varepsilon)$ contribution can be safely neglected. Consequently, the generalized entropy simplifies to

$$S_{FG} = 2\left[\frac{4k\pi^3}{\hbar}\sqrt{\mu}\,(\mu+3) + \frac{1}{12}\ln\frac{e^{4\kappa b_*}}{(\kappa\delta)^4 e^{-2\rho_H}e^{-2\rho_b}}\right]. \quad (11.32)$$

To leading order, the result in Eq. (11.32) exactly reproduces the classical Bekenstein–Hawking entropy (11.8) for the DR5DCS setup, so that $S_{gen} = 2S_{BH}$, as anticipated. The Wald entropy for the full gravity-plus–Hawking-radiation system gives the coarse-grained entropy via the Wald formula. Once quantum corrections are incorporated, an extra curvature term appears in the action of the form $\propto \int {\rm d}^2x\sqrt{-g}\psi R$. As shown in Sec. 10.1.3, the corresponding contribution to the Wald entropy coincides exactly with the quantum correction in Eq. (11.32). Hence, Eq. (11.32) can be interpreted as a quantum-corrected Bekenstein–Hawking entropy, in direct analogy with the DREH model. The fine-grained entropy of Hawking radiation is thus

$$S_{FG} = \min\left\{\frac{1}{3}\kappa t, 2S_{BH}\right\}. \quad (11.33)$$

Finally we evaluate the Page time. We use the classical entropy, since the quantum correction is suppressed in the large-mass regime. The Page time t_P is then defined by

$$\frac{1}{3}\kappa c t_P = \frac{4k\pi^3 c^3}{\hbar}\sqrt{\mu}\,(\mu+3) \quad\Longrightarrow\quad t_P = \frac{12k\pi^3 l c^2}{\hbar}(\mu+3), \quad (11.34)$$

where we have reinstated all physical constants. In the large-mass limit, one has $\mu+3 \propto \sqrt{M}$, implying that the Page time scales as $T_P \propto \sqrt{M}$ in the DR5DCS model.

11.4 Page curve when non-vanishing torsion is present

In this section, we aim to gain insight into the behavior of the Page curve once torsion is taken into account. Although the appropriate generalization of the island formula for theories with non-vanishing torsion is not known, we will assume that the semi-classical contribution is unchanged, and that the area term is still determined by the Wald entropy formula derived in Sec. 11.2, evaluated on the island hypersurface. To this end, we first compute the Page curve for the general vacuum solution without including the back-reaction of quantum fields on the geometry, as obtained in Sec. 7.1.1. We then incorporate back-reaction and thus use the solution with singular horizons discussed in Sec. 7.4. Since we restrict our analysis to eternal black hole setups, the EMT is normal-ordered in Kruskal coordinates, and the semi-classical entropy of quantum fields on the fixed background is given by the same formulas as in the previous section—namely, Eq. (11.21) for the no-island configuration and Eq. (11.23) for the island configuration. For convenience, we reproduce these expressions here:

$$S_{semi-cl} = \begin{cases} \dfrac{1}{3}\ln\left[\cosh\left(\kappa t\right)\right], & \text{Hawking saddle,} \\ \dfrac{1}{3}(\rho_a+\rho_b) + \dfrac{2}{3}\ln\left(e^{\kappa b_*} - e^{\kappa a_*}\right) - \dfrac{2}{3}\ln\left(\kappa\delta\right), & \text{late-time RW saddle,} \end{cases} \tag{11.35}$$

where the only model-dependent parameter is the surface gravity κ. This is because the Kruskal coordinates are always related to the Killing time and the tortoise coordinate in the same manner, as detailed in App. D.5.

11.4.1 The general static vacuum solution case

The general vacuum solution with a nonzero θ field is given in Eq. (6.20). It contains an arbitrary function $\phi^\perp$ associated with residual gauge freedom. In Sec. 7.1.2 we demonstrate that, once gravitational collapse is taken into account, this function is fixed to $\phi^\perp = -1$, which is therefore the physical value adopted here. As shown in Sec. 7.4, this solution is not continuously connected to the Polyakov–Liouville quantum-corrected solution including back-reaction. The aim of this section is to determine how the inclusion of the $\theta \neq 0$ term in the area contribution modifies the Page-curve computation. The coarse-grained entropy for this solution is given in Eq. (11.13). Replacing the event horizon with a generic island location leads to

$$\frac{A[I]}{4G} = \frac{8k\pi^3}{\hbar}a\left[a^2 + 3\left(1-\theta^2\right)\right], \tag{11.36}$$

where the factor of 2 arises from the two thermal bath regions. The generalized entropy then becomes

$$S_{gen} = \frac{8k\pi^3}{\hbar}a\left[a^2 + 3\left(1-\theta^2\right)\right] + \frac{1}{3}(\rho_a+\rho_b) + \frac{2}{3}\ln\left(e^{\kappa b_*} - e^{\kappa a_*}\right) - \frac{2}{3}\ln\left(\kappa\delta\right). \tag{11.37}$$

The only modification with respect to Eq. (11.25) is the appearance of the constant θ term. Consequently, the computation proceeds exactly as in the previous section, except that the factor $\mu+1$ is replaced by $\mu+1-\theta^2$. Hence, the fine-grained entropy still saturates at late times at twice the coarse-grained entropy of the complete gravitational theory coupled to the matter fields. The island position is determined by

$$a = \sqrt{\mu} + \frac{\varepsilon^2}{2\left(\mu+1-\theta^2\right)^2\sqrt{\mu}}e^{-2\kappa b_*}\left[1 - \frac{\varepsilon}{2\left(\mu+1-\theta^2\right)\sqrt{\mu}}\left(1-e^{-2\kappa b_*}\right)\right], \tag{11.38}$$

and the Page time reads:

$$t_P = \frac{12k\pi^3 lc^2}{\hbar}\left(\mu + 3\left(1-\theta^2\right)\right). \tag{11.39}$$

We immediately observe a potential problem, since this Page time can become negative. However, this issue is directly tied to the possibility of negative entropy:

$$S > 0 \quad \implies \quad \theta^2 < 1 + \frac{1}{3}\mu \quad \implies \quad \eta > 0, \tag{11.40}$$

where in the last step we have inserted the explicit solution for θ. We thus conclude that this Page-curve analysis is consistent only when $\eta > 0$, and this same condition is intimately related to the non-negativity of the coarse-grained entropy. Therefore, it should be imposed independently of any Page-curve considerations. Although we cannot definitively assert that the island formula remains valid in a theory with nonzero torsion, if it does, then we have succeeded in reproducing the Page curve for this vacuum solution in the absence of matter back-reaction.

11.4.2 Eternal black hole scenario with non-zero torsion

In this section, we evaluate the fine-grained entropy of the eternal black hole solution including the matter back-reaction introduced in Sec. 7.4. The EMT must be normal-ordered in Kruskal coordinates, so we focus on the non-extremal configuration, since the extremal one is associated with the Boulware vacuum, where the EMT is normal-ordered in the $\sigma^\pm$ coordinates tied to the Killing time.

The Penrose diagram corresponding to the no-island setup is shown in Fig. 11.6. The key distinction from previous Page-curve computations is the presence of two horizons. This situation is analogous to the Reissner–Nordström or rotating BTZ black hole. These horizons are drawn in green, along with the spatial infinities of the AdS-asymptotic regions. The thermal bath regions are attached to the AdS-asymptotic regions along the purple hypersurfaces and are shaded in yellow. The constant-time slices supporting the radiation degrees of freedom are indicated in red; they start at the spatial infinity of the bath regions and terminate at the cut-off hypersurfaces, which are shown in light blue.

This entire pattern repeats infinitely many times, just as in the original Penrose diagram of Fig. 7.3. Nonetheless, for the purpose of computing the Page curve it suffices to focus on the portion of the diagram associated with a single bifurcation point, since Hawking radiation cannot propagate between different bifurcation points.

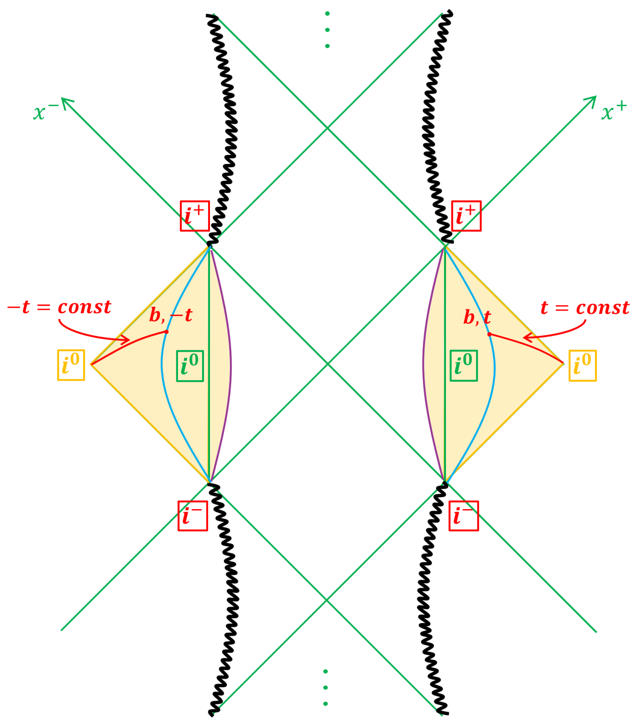

Figure 11.6: Penrose diagram depicting the no-island case for the eternal black hole in the Full DR5DCS model with matter back-reaction.

Even in this regime, Eq. (11.35) remains valid and therefore yields the correct expression for the Hawking saddle contribution to the fine-grained entropy:

$$S_{FG} = \frac{1}{3}\ln\left[\cosh\left(\kappa t\right)\right]. \tag{11.41}$$

We can therefore proceed directly to analyzing the location of the island.

The Penrose diagram corresponding to the island configuration is displayed in Fig. 11.7. All the relevant hypersurfaces previously depicted in Fig. 11.6 are also represented here. In addition, the island region is highlighted in blue. The island boundary in the right AdS-asymptotic region is labeled by (t', a_*), whereas in the left AdS-asymptotic region it is labeled by $(-t', a_*)$, reflecting the fact that the time-like Killing vector reverses direction in the left wedge of the spacetime.

We anticipate that the island lies close to, but outside, the outer event horizon, as illustrated in Fig. 11.7. By evaluating the coarse-grained entropy in Eq. (11.15) at the island, we obtain the area contribution in Eq. (1.6). We must examine the behavior in all four possible cases for the field content of the theory. In each case, we denote the area term as:

$$\frac{A[I]}{4G} = -\frac{24k\pi^3}{\hbar}F(a), \tag{11.42}$$

where a specifies the island location. The generalized entropy formula then takes the form:

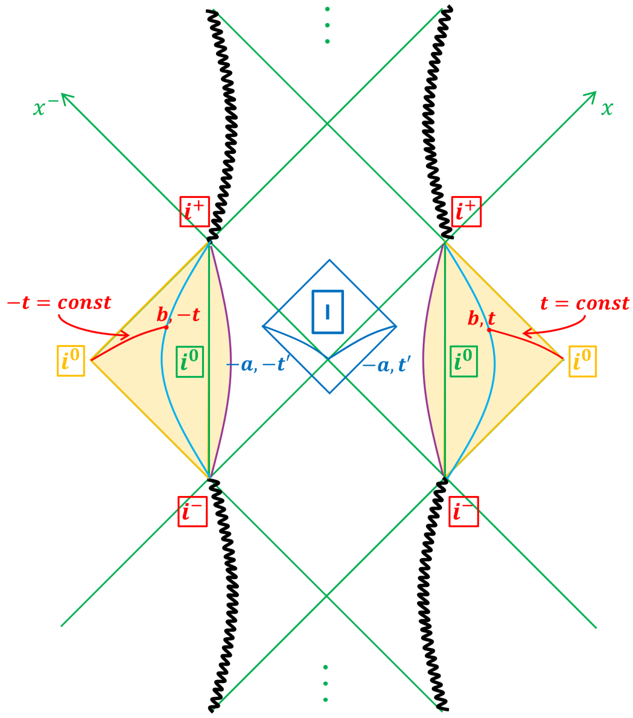

Figure 11.7: Penrose diagram depicting the island case for the eternal black hole in the Full DR5DCS model with matter back-reaction.

$$S_{gen} = -\frac{24k\pi^3}{\hbar}F(a) + \frac{1}{3}(\rho_a + \rho_b) + \frac{2}{3}\ln\left(e^{\kappa b_*} - e^{\kappa a_*}\right) - \frac{2}{3}\ln\left(\kappa\delta\right). \tag{11.43}$$

Extremizing Eq. (11.43) with respect to the island position a_* leads to:

$$\left[-F'(a) + \varepsilon\frac{\mathrm{d}\rho_{\mathrm{K}}}{\mathrm{dz}}\bigg|_a\right]\frac{\mathrm{da}}{\mathrm{d}a_*} = \frac{2\varepsilon\kappa}{e^{\kappa(b_* - a_*)} - 1}. \tag{11.44}$$

Since the island is expected to lie close to the outer horizon, we adopt the ansatz $a = \mathrm{z}_+ + x$ and expand the left-hand side of Eq. (11.44). Using the relations:

$$l\frac{\mathrm{da}}{\mathrm{d}a_*} = \sqrt{-\Lambda}, \qquad e^{\kappa a_*} = \frac{a - \mathrm{z}_+}{a - \mathrm{z}_-}, \qquad \frac{\mathrm{d}\rho_{\mathrm{K}}}{\mathrm{dz}}\bigg|_{\mathrm{z}_+} = \frac{2}{\kappa l}, \tag{11.45}$$

the solution of Eq. (11.44) for x becomes:

$$x = -\frac{2\varepsilon}{e^{\kappa b_*} - 1}\left[\frac{\kappa l}{D}e^{\kappa b_*} + \frac{1}{F'(\mathrm{z}_+) + \frac{2\varepsilon}{\kappa l}}\right], \tag{11.46}$$

where we have taken $F'(a)$ to be regular in a neighborhood of the outer horizon. In the limit of very large b_*, this expression no longer depends on the function F, and the QES sits at the inner horizon, since:

$$x = -\frac{2\varepsilon\kappa l}{D} \quad \Longrightarrow \quad a = \mathrm{z}_+ - \frac{2\varepsilon\kappa l}{D} = \mathrm{z}_-. \tag{11.47}$$

Note that, in addition to this QES, both horizons also satisfy Eq. (11.44). For the outer horizon, this is immediate, since both sides of the equation vanish there. For the inner horizon, on the other hand, the function F' remains well defined everywhere. At the same time, the derivative of the metric in Kruskal coordinates associated with the first bifurcation point diverges at the inner horizon, implying

$$\left.\frac{\mathrm{d}\rho_{\mathrm{K}}}{\mathrm{dz}}\sqrt{-\Lambda}\right|_{\mathrm{z}_-} = -2\varepsilon\kappa. \tag{11.48}$$

Since the left-hand side of Eq. (11.44) is equal to this same quantity, we deduce that the inner horizon is also a solution of the equation.

Each of these quantum extremal surfaces yields the expected behavior of the fine-grained entropy, since they are all situated near the horizons, which are separated by a distance of order $\mathcal{O}(\varepsilon)$. Consequently, the Page curve is correctly reproduced. Nonetheless, one must pay attention to the precise position of these QESs. The surface at the outer horizon is the most physically reasonable, as it is the outermost of the three. Still, we generally do not expect the QES to lie exactly on the outer horizon, but rather slightly outside of it. The only candidate that can realize this feature is the one shifted away from the outer horizon by the amount specified in Eq. (11.46). Its exact location is given by

$$a = \mathrm{z}_+ - \frac{2\varepsilon}{e^{\kappa b_*} - 1}\left[\frac{\kappa l}{D}e^{\kappa b_*} + \frac{1}{F'(\mathrm{z}_+) + \frac{2\varepsilon}{\kappa l}}\right]. \tag{11.49}$$

In most physically relevant regimes, the parameter $F'(\mathrm{z}_+)$ is positive. This would place the island below the inner horizon, which is typically not acceptable physically. However, because gravity is turned off in the thermal bath regions, we are free to move the cut-off surface all the way to the boundary of the thermal bath. As this boundary is shifted inward from the AdS boundary, it corresponds to a negative value of the σ coordinate. As a result, b_* becomes a small negative number, so that the island is pushed outward into the black hole exterior region, as illustrated in Fig. 11.7.

Finally, we stress that this behavior may simply reflect the use of an incorrect island-rule formula in the presence of torsion, since the general prescription for theories with non-vanishing torsion is not yet established. Despite this caveat, the goal of this section was to test whether one can still obtain the Page curve in a theory with non-zero torsion by applying the standard island rule, taking the area term from the Wald entropy formula. Our conclusion is affirmative. However, we also find that turning on torsion imposes a restrictive condition: the cut-off hypersurfaces must lie close to the interface between the bath region and the asymptotically AdS black hole exterior. This is in contrast to the Riemannian case analyzed in Sec. 11.3, where the cut-off hypersurface can be placed at an arbitrary position within the bath.

Chapter 12

Conclusion

In this dissertation, we employ two-dimensional dilaton gravity as our main framework for probing quantum gravity effects within a semiclassical approximation. In this approach, the matter fields are quantized while the spacetime background is treated classically. The central question we aim to address is: Can a black hole be regarded as an ordinary quantum system? If so, its time evolution must be unitary. One strategy to investigate this is to compute the entanglement entropy of the Hawking radiation and examine whether it reproduces the Page curve. Although this can be attempted in the context of an eternal black hole, a more significant result is to obtain the Page curve for a genuinely evaporating black hole. To describe such an evaporating black hole, it is not sufficient to quantize only the matter fields; one must also incorporate the back-reaction of the quantum fields on the classical geometry. Consequently, our first task is to formulate a consistent evaporating black hole scenario.

In Chap. 3, we developed a general formalism that accommodates both eternal and evaporating black hole configurations within two-dimensional dilaton gravity. The central element of this construction is a symmetric ansatz for arbitrary scalar, vector, tensor, or spinor fields in a 2D spacetime that admits a Killing vector. When the Killing vector is time-like we analyze black-hole-type solutions; when it is a space-like we instead study cosmological solutions. This ansatz exploits a distinctive feature of two-dimensional spacetimes: the Hodge dual of 1-form is still an 1-form, a property that holds only in two dimensions. Hence, given a Killing vector field, that vector and its Hodge dual together span the full space of 1-forms. This observation enables us to express any physical observable in terms of a single coordinate orthogonal to the Killing direction, rendering it independent of the coordinate associated with the Killing vector.

In this framework, the equations of motion simplify to a one-dimensional system, which is easier to solve. Yet this is not the only advantage of this construction. We demonstrated that the most general solution in any 2D theory—specified by the metric function Λ, the derivative of the dilaton field $\mathcal{D}$, and the tortoise coordinate $\frac{\sigma}{l}$—and even when coupled to matter, can be fully characterized by $(\mathrm{F}^{+}, \mathrm{F}^{-}, C, f)$. The functions $\mathrm{F}^{\pm}$ encode the coordinate transformations that map arbitrary coordinates to Eddington–Finkelstein-like coordinates adapted to the Killing vector; equivalently, they may be seen as the components of the Killing vector in the original coordinate system. The remaining two structures, C and f, represent respectively a set of constants corresponding to the conserved charges of the theory, and a set of arbitrary functions corresponding to residual gauge freedoms, typically originating from the dimensional reduction procedure by which the given 2D dilaton gravity theory is obtained.

We then showed that by employing static vacuum solutions written in this form, one can construct non-stationary spacetimes describing classical gravitational collapse. Concretely, the

Killing vector becomes discontinuous across the ingoing matter shockwave, so that each region of spacetime on either side of the shockwave is individually stationary, while the full spacetime lacks a single global Killing vector. This patchwise construction yields a genuine collapse geometry, and we demonstrated that, within this setup, one recovers the correct expression for the mass of the spacetime by starting from a massless background solution before introducing the ingoing shockwave.

It is then clear that if one includes quantum corrections and selects a quantum state such that the resulting geometry is stationary—for instance, the Hartle–Hawking or Boulware state—the same formalism still applies. In that case, the quantum expectation value of the EMT must satisfy the static ansatz, and the problem again reduces to one dimension. By contrast, for an evaporating black hole, one has to take into account the quantum back-reaction of the matter fields on the geometry. The corresponding solution is genuinely non-stationary, and at first sight this appears to invalidate our static ansatz. However, this is not the case if, from that point onward, one treats the problem perturbatively in the natural expansion parameter $\hbar$.

Because the quantum-corrected energy–momentum tensor is proportional to $\hbar$ at first order in perturbation theory, one evaluates it on the zeroth-order background solution. That zeroth-order solution coincides with the classical gravitational collapse obtained from the static ansatz. After obtaining the first-order correction, one could, at least in principle, continue to compute higher-order terms iteratively. Nevertheless, we demonstrate in explicit models that the first-order correction already suffices to construct a consistent quantum-corrected evaporating black hole geometry and, in turn, to determine its Page curve.

It is crucial to identify a well-defined pole in the tortoise coordinate in both eternal and evaporating black hole setups. All hypersurfaces of interest are located near the classical horizon, which corresponds to a clear pole of the classical tortoise coordinate. One therefore naturally adopts the dilaton as a radial coordinate, so that the tortoise coordinate relation becomes the only way to switch between the radial coordinate and Eddington–Finkelstein–type coordinates. In generic dilaton gravity theories there is a single pole in the tortoise coordinate, shifted slightly away from the pole in the classical solution. This is straightforward in the eternal black hole case, but for an evaporating black hole one must first introduce coordinates adapted to the evaporation process and then re-express the position of the pole in terms of these new coordinates.

In the following three chapters, we apply this framework in three models of 2D dilaton gravity. First, as a comparison sector, we reproduce a well known result for both the eternal and the evaporating black holes within the BPP model, and show that the symmetric ansatz together with the first-order perturbative expansion is enough to reproduce the correct evolution of the spacetime, from the initial spacetime, through the evaporating black hole region and finally to the black hole remanent spacetime which is what is left after the black hole fully evaporates. The most problematic step in this process is to find the end-point of evaporation, as it is well known that it is not analytical in $\hbar$, since it is proportional to $\sim \exp\left(-\frac{\alpha}{\hbar}\right)$. However, we showed that a good choice of coordinates mends this issue. We call these $(\delta, \hat{\mathrm{x}})$ coordinates the evaporation-adapted coordinates. Now that the end-point is found, continuously matching the solution across the $\hat{\mathrm{x}} = \hat{\mathrm{x}}_{\mathrm{E}}$ hypersurface is a straightforward process. Thus, we can also conclude the final state of black hole evolution as well as the end-state geometry.

We then applied the same framework to the DREH model and to the Riemannian sector of the DR5DCS model, successfully formulating both the eternal and evaporating black hole scenarios. Next, in Chaps. 10 and 11, we take this analysis further and demonstrate that the framework accurately reproduces the Page curve in both the DREH model and the Riemannian sector of the DR5DCS model. For the eternal black hole, the computation turns out to be straightforward once the appropriate pole of the tortoise coordinate is identified. In contrast, for the evaporating black hole solution, one must first determine the location of the island boundary across the ingoing shockwave and then extend that solution into the region where the evaporating black hole resides. Because the island also forms near the classical horizon, having a well-defined pole for the tortoise coordinate is crucial. We showed that the same qualitative behavior arises in the DREH model: the island hypersurface perfectly mirrors the apparent horizon across the quantum-corrected horizon, which is specified by the endpoint of evaporation, $\hat{\mathrm{x}} = \hat{\mathrm{x}}_{\mathrm{E}}$.

The second line of research in this dissertation focuses on how torsion affects the thermodynamic properties of gravitational systems. From the standpoint of coarse-grained entropy, numerous questions remain unresolved about the role of torsion in black hole thermodynamics. In certain models, torsion leads to a well-defined conserved quantity, often called torsion hair, whereas in others it effectively becomes a fundamental constant of spacetime. In the latter case, the first law of thermodynamics does not treat torsion as a thermodynamic variable, but rather as a fixed parameter. This already makes the study of torsion in classical gravity an important and active field of research.

Nonetheless, this is not the direction pursued in the present work. Here, torsion is of interest because its impact on the island formula (1.6), and hence on the Page curve, is presently unknown. The objective of this thesis is therefore to obtain well-defined solutions with torsion, so that in future studies one can analyze the fine-grained entropy in a gravitational system that includes torsion. A suitable framework featuring a well-known BTZ-like black hole solution with non-zero torsion is a five-dimensional Chern-Simons theory. However, for studying fine-grained entropy, it is crucial to have a well-defined solution with non-zero torsion in two-dimensional spacetime. To this end, we preformed a dimensional reduction of the 5DCS theory over a three-sphere, yielding an effective 2D theory. The resulting model is a two-dimensional dilaton gravity theory that not only contains extra fields originating from the five-dimensional torsion, but also admits solutions with non-vanishing torsion in 2D.

To obtain these solutions, we examined various ways of coupling matter to gravity within the DR5DCS framework, choosing to treat matter as minimally coupled to the gravitational field. In this setup, we demonstrated that a real scalar field theory with a standard mass term yields a cosmological solution describing a spacetime that oscillates between big bang and big crunch events, with additional sudden curvature singularities appearing in between. Furthermore, we showed that when a local $U(1)$ symmetry is introduced—thereby generating an interaction between a massless complex scalar field and the electromagnetic field—the resulting geometry is again cosmological. Although the broader objective is to study the fine-grained entropy of cosmological spacetimes, this is not our present focus.

We found that pure electrodynamics alone does not support solutions with non-zero torsion. However, once the theory is restricted to its Riemannian sector, a charged black hole solution with a single horizon appears. This configuration is relevant for computing the Page curve and for analyzing how electric charge influences the fine-grained entropy in this model. Nevertheless, within this line of work our main interest lies in solutions featuring non-vanishing torsion. We also analyzed ideal fluid hydrodynamics and showed that, in this case, the metric function Λ remains undetermined, indicating a residual gauge symmetry. Yet, when an additional field—such as the electromagnetic field or a massless scalar field—is included, the metric is forced to be flat. Consequently, we arrive at a Minkowski vacuum solution endowed with non-zero torsion.

Finally, the most intriguing configurations appear when gravity is coupled to Dirac spinors. In this framework, a fermionic soliton-star solution arises. It exhibits a clearly defined phase transition. In the upper phase, the fermion density profile is distributed across the whole spacetime, the curvature remains finite, and no horizons are present. Thus, this describes a completely regular fermionic star. Moreover, one can impose appropriate junction conditions so that the star becomes a compact object smoothly matched to a generic BTZ-like vacuum solution, thereby behaving as a genuine star. Once the critical threshold is exceeded, however, the fermionic matter collapses and localizes at a specific point in spacetime. At that location, the fermion density diverges and in turn generates a curvature singularity, while at the same time a Killing horizon forms precisely there. This singular horizon is non-extremal, as it possesses a non-zero surface gravity, and is therefore unstable. Nonetheless, we anticipate that including quantum corrections will remove or dress this singularity, while the fermions remain condensed in the lower phase at this same location.

Future work

In the first research program, a concrete method was developed for computing both eternal and evaporating black hole solutions, and this method was implemented in a physically relevant, dimensionally reduced model of Einstein–Hilbert gravity. Using this framework, the Page curve was obtained for both eternal and evaporating Schwarzschild black holes, which might suggest that this line of investigation is essentially complete. Nevertheless, there remain many important models for which the Page curve has not yet been derived, particularly in the context of evaporating black holes. Such models include, but are not limited to, Reissner–Nordström, Kerr–Newman, BTZ, and others.

A further direction is to use the new method to compute the Page curve via non-physical, ghost-like fields in a hybrid state—for example, a Hartle–Hawking state for physical fields combined with a Boulware state for non-physical ones. In this setup, the entanglement entropy shows Page-curve behavior without an island. These extra fields can render the effective central charge negative and remove the space-time singularity, which appears to drive the Page-curve-like evolution. It would be interesting to connect this approach to the standard Lewkowycz–Maldacena derivation of the island formula: Can these non-physical fields be interpreted within the gravitational path integral, and how do the resulting Page curves quantitatively compare? One may also further generalize the hybrid quantum state to entangled quantum states.

The second research program has a natural extension. Up to now, only the minimally-coupled matter theories have been analyzed, even though the general equations for non-minimally coupled fields are already available. Therefore, it is important to investigate the behavior of torsion in this broader framework as well. Existing results already suggest the presence of highly nontrivial phase transitions in the minimally coupled case, so one anticipates even richer dynamics when matter is coupled non-minimally.

Another possible line of inquiry is to incorporate quantum corrections and examine whether they can resolve the singular horizons that arise in fermionic star solutions. Finally, to construct more physically relevant models of 2D dilaton gravity with torsion, one should perform a dimensional reduction of the 4D Einstein–Cartan theory, employing the most general spherically symmetric ansatz for both the vielbein and the spin connection. Ultimately, the main goal of this research program is to determine how the island formula is modified in the presence of non-vanishing torsion.

The ultimate aim of including torsion is to explore how it affects fine-grained quantities of the gravitational theories. This issue has already been partially addressed in Sec. 11.4. There, we demonstrated that torsion imposes strong constraints on the boundary of the black hole region, using the standard island prescription with the area term provided by the Wald entropy formula. This represents only an initial step toward identifying the appropriate modification of the island rule in the presence of torsion, and it should be investigated more thoroughly in future studies.

References

[1] Ahmed Almheiri, Thomas Hartman, Juan Maldacena, Edgar Shaghoulian, and Amirhossein Tajdini. The entropy of hawking radiation. *Reviews of Modern Physics*, 93 (3), Jul 2021. ISSN 1539-0756. doi: 10.1103/revmodphys.93.035002. URL http://dx.doi.org/10.1103/RevModPhys.93.035002.

[2] A. Einstein. Die grundlage der allgemeinen relativitätstheorie. *Annalen der Physik*, 354(7):769–822, 1916. doi: https://doi.org/10.1002/andp.19163540702. URL https://onlinelibrary.wiley.com/doi/abs/10.1002/andp.19163540702.

[3] Karl Schwarzschild. On the gravitational field of a mass point according to Einstein's theory. *Sitzungsber. Preuss. Akad. Wiss. Berlin (Math. Phys.)*, 1916:189–196, 1916.

[4] Roy P. Kerr. Gravitational field of a spinning mass as an example of algebraically special metrics. *Phys. Rev. Lett.*, 11:237–238, Sep 1963. doi: 10.1103/PhysRevLett.11.237. URL https://link.aps.org/doi/10.1103/PhysRevLett.11.237.

[5] E T. Newman, R. Couch, K. Chinnapared, A. Exton, A. Prakash, and R. Torrence. Metric of a Rotating, Charged Mass. *J. Math. Phys.*, 6:918–919, 1965. doi: 10.1063/1.1704351.

[6] Larry Smarr. Mass formula for kerr black holes. *Phys. Rev. Lett.*, 30:71–73, Jan 1973. doi: 10.1103/PhysRevLett.30.71. URL https://link.aps.org/doi/10.1103/PhysRevLett.30.71.

[7] B. Carter. Black holes equilibrium states. In *Les Houches Summer School of Theoretical Physics: Black Holes*, pages 57–214, 1973.

[8] Herbert B Callen. *Thermodynamics and an introduction to thermostatistics; 2nd ed.* Wiley, New York, NY, 1985. URL https://cds.cern.ch/record/450289.

[9] S. W. Hawking. Black holes in general relativity. *Commun. Math. Phys.*, 25:152–166, 1972. doi: 10.1007/BF01877517.

[10] James M. Bardeen, B. Carter, and S. W. Hawking. The Four laws of black hole mechanics. *Commun. Math. Phys.*, 31:161–170, 1973. doi: 10.1007/BF01645742.

[11] S. W. Hawking. Black hole explosions. *Nature*, 248:30–31, 1974. doi: 10.1038/248030a0.

[12] S. W. Hawking. Particle Creation by Black Holes. *Commun. Math. Phys.*, 43:199–220, 1975. doi: 10.1007/BF02345020. [Erratum: Commun.Math.Phys. 46, 206 (1976)].

[13] S. W. Hawking. Black holes and thermodynamics. *Phys. Rev. D*, 13:191–197, Jan 1976. doi: 10.1103/PhysRevD.13.191. URL https://link.aps.org/doi/10.1103/PhysRevD.13.191.

[14] Jacob Bekenstein. Black holes and the second law. *Lettere al Nuovo Cimento (1971-1985)*, 4:737–740, 1972.

[15] Jacob D. Bekenstein. Black holes and entropy. *Phys. Rev. D*, 7:2333–2346, Apr 1973. doi: 10.1103/PhysRevD.7.2333. URL https://link.aps.org/doi/10.1103/PhysRevD.7.2333.

[16] S. W. Hawking. Breakdown of predictability in gravitational collapse. *Phys. Rev. D*, 14:2460–2473, Nov 1976. doi: 10.1103/PhysRevD.14.2460. URL https://link.aps.org/doi/10.1103/PhysRevD.14.2460.

[17] Don N. Page. Information in black hole radiation. *Physical Review Letters*, 71(23):3743–3746, Dec 1993. ISSN 0031-9007. doi: 10.1103/physrevlett.71.3743. URL http://dx.doi.org/10.1103/PhysRevLett.71.3743.

[18] Don N Page. Time dependence of hawking radiation entropy. *Journal of Cosmology and Astroparticle Physics*, 2013(09):028–028, Sep 2013. ISSN 1475-7516. doi: 10.1088/1475-7516/2013/09/028. URL http://dx.doi.org/10.1088/1475-7516/2013/09/028.

[19] Curtis G. Callan, Steven B. Giddings, Jeffrey A. Harvey, and Andrew Strominger. Evanescent black holes. *Physical Review D*, 45(4):R1005–R1009, Feb 1992. ISSN 0556-2821. doi: 10.1103/physrevd.45.r1005. URL http://dx.doi.org/10.1103/PhysRevD.45.R1005.

[20] R. Jackiw. Lower Dimensional Gravity. *Nucl. Phys. B*, 252:343–356, 1985. doi: 10.1016/0550-3213(85)90448-1.

[21] C. Teitelboim. Gravitation and Hamiltonian Structure in Two Space-Time Dimensions. *Phys. Lett. B*, 126:41–45, 1983. doi: 10.1016/0370-2693(83)90012-6.

[22] Alexander M. Polyakov. Quantum geometry of bosonic strings. *Physics Letters B*, 103:207–210, 1981.

[23] Jorge G. Russo, Leonard Susskind, and Lárus Thorlacius. End point of hawking radiation. *Phys. Rev. D*, 46:3444–3449, Oct 1992. doi: 10.1103/PhysRevD.46.3444. URL https://link.aps.org/doi/10.1103/PhysRevD.46.3444.

[24] Jorge G. Russo, Leonard Susskind, and Larus Thorlacius. Cosmic censorship in two-dimensional gravity. *Phys. Rev. D*, 47:533–539, Jan 1993. doi: 10.1103/PhysRevD.47.533. URL https://link.aps.org/doi/10.1103/PhysRevD.47.533.

[25] Sukanta Bose, Leonard Parker, and Yoav Peleg. Semi-infinite throat as the end-state geometry of two-dimensional black hole evaporation. *Physical Review D*, 52(6):3512–3517, Sep 1995. ISSN 0556-2821. doi: 10.1103/physrevd.52.3512. URL http://dx.doi.org/10.1103/PhysRevD.52.3512.

[26] Thomas M. Fiola, John Preskill, Andrew Strominger, and Sandip P. Trivedi. Black hole thermodynamics and information loss in two dimensions. *Physical Review D*, 50(6):3987–4014, Sep 1994. ISSN 0556-2821. doi: 10.1103/physrevd.50.3987. URL http://dx.doi.org/10.1103/PhysRevD.50.3987.

[27] Gerard 't Hooft. Dimensional reduction in quantum gravity. *Conf. Proc. C*, 930308:284–296, 1993.

[28] Leonard Susskind. The world as a hologram. *Journal of Mathematical Physics*, 36(11): 6377–6396, Nov 1995. ISSN 1089-7658. doi: 10.1063/1.531249. URL http://dx.doi.org/10.1063/1.531249.

[29] Juan Martin Maldacena. The Large N limit of superconformal field theories and supergravity. *Adv. Theor. Math. Phys.*, 2:231–252, 1998. doi: 10.1023/A:1026654312961.

[30] Shinsei Ryu and Tadashi Takayanagi. Holographic derivation of entanglement entropy from the anti–de sitter space/conformal field theory correspondence. *Phys. Rev. Lett.*, 96:181602, May 2006. doi: 10.1103/PhysRevLett.96.181602. URL https://link.aps.org/doi/10.1103/PhysRevLett.96.181602.

[31] Veronika E. Hubeny, Mukund Rangamani, and Tadashi Takayanagi. A covariant holographic entanglement entropy proposal. *Journal of High Energy Physics*, 2007:062–062, 2007.

[32] G. W. Gibbons and S. W. Hawking. Cosmological event horizons, thermodynamics, and particle creation. *Phys. Rev. D*, 15:2738–2751, May 1977. doi: 10.1103/PhysRevD.15.2738. URL https://link.aps.org/doi/10.1103/PhysRevD.15.2738.

[33] Aitor Lewkowycz and Juan Martin Maldacena. Generalized gravitational entropy. *Journal of High Energy Physics*, 2013:1–29, 2013.

[34] Thomas Faulkner, Aitor Lewkowycz, and Juan Maldacena. Quantum corrections to holographic entanglement entropy. *Journal of High Energy Physics*, 2013(11), Nov 2013. ISSN 1029-8479. doi: 10.1007/jhep11(2013)074. URL http://dx.doi.org/10.1007/JHEP11(2013)074.

[35] Ahmed Almheiri, Raghu Mahajan, Juan Maldacena, and Ying Zhao. The page curve of hawking radiation from semiclassical geometry. *Journal of High Energy Physics*, 2020(3), Mar 2020. ISSN 1029-8479. doi: 10.1007/jhep03(2020)149. URL http://dx.doi.org/10.1007/JHEP03(2020)149.

[36] Ahmed Almheiri, Netta Engelhardt, Donald Marolf, and Henry Maxfield. The entropy of bulk quantum fields and the entanglement wedge of an evaporating black hole. *Journal of High Energy Physics*, 2019(12), Dec 2019. ISSN 1029-8479. doi: 10.1007/jhep12(2019)063. URL http://dx.doi.org/10.1007/JHEP12(2019)063.

[37] Geoffrey Penington. Entanglement wedge reconstruction and the information paradox, 2020.

[38] Ahmed Almheiri, Thomas Hartman, Juan Maldacena, Edgar Shaghoulian, and Amirhossein Tajdini. Replica wormholes and the entropy of hawking radiation. *Journal of High Energy Physics*, 2020(5), May 2020. ISSN 1029-8479. doi: 10.1007/jhep05(2020)013. URL http://dx.doi.org/10.1007/JHEP05(2020)013.

[39] Ahmed Almheiri, Raghu Mahajan, and Juan Maldacena. Islands outside the horizon, 2019.

[40] Thomas Hartman, Edgar Shaghoulian, and Andrew Strominger. Islands in asymptotically flat 2d gravity. *Journal of High Energy Physics*, 2020(7), Jul 2020. ISSN 1029-8479. doi: 10.1007/jhep07(2020)022. URL http://dx.doi.org/10.1007/JHEP07(2020)022.

[41] Xuanhua Wang, Ran Li, and Jin Wang. Page curves for a family of exactly solvable evaporating black holes. *Physical Review D*, 103(12), Jun 2021. ISSN 2470-0029. doi: 10.1103/physrevd.103.126026. URL http://dx.doi.org/10.1103/PhysRevD.103.126026.

[42] Stefan Đorđević, Aleksandra Gočanin, Dragoljub Gočanin, and Voja Radovanović. Page curve for an eternal schwarzschild black hole in a dimensionally reduced model of dilaton gravity. *Phys. Rev. D*, 106:105015, Nov 2022. doi: 10.1103/PhysRevD.106.105015. URL https://link.aps.org/doi/10.1103/PhysRevD.106.105015.

[43] Stefan Đorđević and Voja Radovanović. Page curve for an evaporating schwarzschild black hole in dimensionally reduced model of dilaton gravity. *Phys. Rev. D*, 113:105020, May 2026. doi: 10.1103/nc2z-hx6s. URL https://link.aps.org/doi/10.1103/nc2z-hx6s.

[44] Geoff Penington, Stephen H. Shenker, Douglas Stanford, and Zhenbin Yang. Replica wormholes and the black hole interior, 2020. URL https://arxiv.org/abs/1911.11977.

[45] Friðrik Freyr Gautason, Lukas Schneiderbauer, Watse Sybesma, and Lárus Thorlacius. Page Curve for an Evaporating Black Hole. *JHEP*, 05:091, 2020. doi: 10.1007/JHEP05(2020)091.

[46] Ahmed Almheiri, Raghu Mahajan, and Juan Maldacena. Islands outside the horizon, 2023. URL https://arxiv.org/abs/1910.11077.

[47] Ahmed Almheiri, Netta Engelhardt, Donald Marolf, and Henry Maxfield. The entropy of bulk quantum fields and the entanglement wedge of an evaporating black hole. *Journal of High Energy Physics*, 2019(12), December 2019. ISSN 1029-8479. doi: 10.1007/jhep12(2019)063. URL http://dx.doi.org/10.1007/JHEP12(2019)063.

[48] Hong Zhe Chen, Zachary Fisher, Juan Hernandez, Robert C. Myers, and Shan-Ming Ruan. Information flow in black hole evaporation. *Journal of High Energy Physics*, 2020(3), March 2020. ISSN 1029-8479. doi: 10.1007/jhep03(2020)152. URL http://dx.doi.org/10.1007/JHEP03(2020)152.

[49] Yiming Chen. Pulling Out the Island with Modular Flow. *JHEP*, 03:033, 2020. doi: 10.1007/JHEP03(2020)033.

[50] Chris Akers, Netta Engelhardt, Geoff Penington, and Mykhaylo Usatyuk. Quantum maximin surfaces, 2020. URL https://arxiv.org/abs/1912.02799.

[51] Hong Liu and Shreya Vardhan. A dynamical mechanism for the Page curve from quantum chaos. *JHEP*, 03:088, 2021. doi: 10.1007/JHEP03(2021)088.

[52] Donald Marolf and Henry Maxfield. Transcending the ensemble: baby universes, spacetime wormholes, and the order and disorder of black hole information. *Journal of High Energy Physics*, 2020(8), August 2020. ISSN 1029-8479. doi: 10.1007/jhep08(2020)044. URL http://dx.doi.org/10.1007/JHEP08(2020)044.

[53] Vijay Balasubramanian, Arjun Kar, Onkar Parrikar, Gábor Sárosi, and Tomonori Ugajin. Geometric secret sharing in a model of Hawking radiation. *JHEP*, 01:177, 2021. doi: 10.1007/JHEP01(2021)177.

[54] Aranya Bhattacharya. Multipartite purification, multiboundary wormholes, and islands in AdS_3/CFT_2. *Phys. Rev. D*, 102(4):046013, 2020. doi: 10.1103/PhysRevD.102.046013.

[55] Kanato Goto, Thomas Hartman, and Amirhossein Tajdini. Replica wormholes for an evaporating 2d black hole. *Journal of High Energy Physics*, 2021(4), April 2021. ISSN 1029-8479. doi: 10.1007/jhep04(2021)289. URL http://dx.doi.org/10.1007/JHEP04(2021)289.

[56] Herman Verlinde. Er = epr revisited: On the entropy of an einstein-rosen bridge, 2020. URL https://arxiv.org/abs/2003.13117.

[57] Takanori Anegawa and Norihiro Iizuka. Notes on islands in asymptotically flat 2d dilaton black holes. *Journal of High Energy Physics*, 2020(7), Jul 2020. ISSN 1029-8479. doi: 10.1007/jhep07(2020)036. URL http://dx.doi.org/10.1007/JHEP07(2020)036.

[58] Friðrik Freyr Gautason, Lukas Schneiderbauer, Watse Sybesma, and Lárus Thorlacius. Page curve for an evaporating black hole. *Journal of High Energy Physics*, 2020(5), May 2020. ISSN 1029-8479. doi: 10.1007/jhep05(2020)091. URL http://dx.doi.org/10.1007/JHEP05(2020)091.

[59] Koji Hashimoto, Norihiro Iizuka, and Yoshinori Matsuo. Islands in schwarzschild black holes. *Journal of High Energy Physics*, 2020(6), Jun 2020. ISSN 1029-8479. doi: 10.1007/jhep06(2020)085. URL http://dx.doi.org/10.1007/JHEP06(2020)085.

[60] Ming-Hui Yu and Xian-Hui Ge. Islands and Page curves in charged dilaton black holes. *Eur. Phys. J. C*, 82(1):14, 2022. doi: 10.1140/epjc/s10052-021-09932-w.

[61] Xuanhua Wang, Ran Li, and Jin Wang. Islands and Page curves of Reissner-Nordström black holes. *JHEP*, 04:103, 2021. doi: 10.1007/JHEP04(2021)103.

[62] Ahmed Almheiri, Raghu Mahajan, and Jorge E. Santos. Entanglement islands in higher dimensions. *SciPost Phys.*, 9(1):001, 2020. doi: 10.21468/SciPostPhys.9.1.001.

[63] Chen-Wei Tong, Dong-Hui Du, and Jia-Rui Sun. Island of Reissner-Nordström anti–de Sitter black holes in the large D limit. *Phys. Rev. D*, 109(10):104053, 2024. doi: 10.1103/PhysRevD.109.104053.

[64] Liqiang Wang and Ran Li. Entanglement islands and the Page curve of Hawking radiation for rotating Kerr black holes. *Phys. Rev. D*, 110(6):066012, 2024. doi: 10.1103/PhysRevD.110.066012.

[65] D. S. Ageev, I. Ya. Aref'eva, A. I. Belokon, A. V. Ermakov, V. V. Pushkarev, and T. A. Rusalev. Infrared regularization and finite size dynamics of entanglement entropy in Schwarzschild black hole. *Phys. Rev. D*, 108(4):046005, 2023. doi: 10.1103/PhysRevD.108.046005.

[66] Chih-Hung Wu and Jiuci Xu. Islands in non-minimal dilaton gravity: exploring effective theories for black hole evaporation. *JHEP*, 10:094, 2023. doi: 10.1007/JHEP10(2023)094.

[67] D. S. Ageev, I. Ya. Aref'eva, A. I. Belokon, V. V. Pushkarev, and T. A. Rusalev. Entanglement entropy in de Sitter: no pure states for conformal matter. *JHEP*, 05:308, 2024. doi: 10.1007/JHEP05(2024)308.

[68] Aleksandr I. Belokon. Finite entangling regions and information paradox in charged black holes. *Theor. Math. Phys.*, 222(1):154–169, 2025. doi: 10.1134/S004057792501012X.

[69] Gopal Yadav and Nitin Joshi. Cosmological and black hole islands in multi-event horizon spacetimes. *Phys. Rev. D*, 107(2):026009, 2023. doi: 10.1103/PhysRevD.107.026009.

[70] Aron C Wall. Maximin surfaces, and the strong subadditivity of the covariant holographic entanglement entropy. *Classical and Quantum Gravity*, 31(22):225007, Nov 2014. ISSN 1361-6382. doi: 10.1088/0264-9381/31/22/225007. URL http://dx.doi.org/10.1088/0264-9381/31/22/225007.

[71] Bartłomiej Czech, Joanna L Karczmarek, Fernando Nogueira, and Mark Van Raamsdonk. The gravity dual of a density matrix. *Classical and Quantum Gravity*, 29(15):155009, Jul 2012. ISSN 1361-6382. doi: 10.1088/0264-9381/29/15/155009. URL http://dx.doi.org/10.1088/0264-9381/29/15/155009.

[72] Matthew Headrick, Veronika E. Hubeny, Albion Lawrence, and Mukund Rangamani. Causality and holographic entanglement entropy. *Journal of High Energy Physics*, 2014 (12), Dec 2014. ISSN 1029-8479. doi: 10.1007/jhep12(2014)162. URL http://dx.doi.org/10.1007/JHEP12(2014)162.

[73] Shiin-Shen Chern and James Simons. Characteristic forms and geometric invariants. *Annals Math.*, 99:48–69, 1974. doi: 10.2307/1971013.

[74] S. Deser, R. Jackiw, and S. Templeton. Topologically massive gauge theories. *Annals of Physics*, 281:409–449, 04 2000. doi: 10.1006/aphy.2000.6013.

[75] Edward Witten. Quantum Field Theory and the Jones Polynomial. *Commun. Math. Phys.*, 121:351–399, 1989. doi: 10.1007/BF01217730.

[76] A. Achucarro and P. K. Townsend. A Chern-Simons Action for Three-Dimensional anti-De Sitter Supergravity Theories. *Phys. Lett. B*, 180:89, 1986. doi: 10.1016/0370-2693(86)90140-1.

[77] Edward Witten. (2+1)-Dimensional Gravity as an Exactly Soluble System. *Nucl. Phys. B*, 311:46, 1988. doi: 10.1016/0550-3213(88)90143-5.

[78] Máximo Bañados, Claudio Teitelboim, and Jorge Zanelli. Black hole in three-dimensional spacetime. *Physical Review Letters*, 69(13):1849–1851, September 1992. ISSN 0031-9007. doi: 10.1103/physrevlett.69.1849. URL http://dx.doi.org/10.1103/PhysRevLett.69.1849.

[79] Ali H. Chamseddine. Topological Gauge Theory of Gravity in Five-dimensions and All Odd Dimensions. *Phys. Lett. B*, 233:291–294, 1989. doi: 10.1016/0370-2693(89)91312-9.

[80] Andrew Strominger and Cumrun Vafa. Microscopic origin of the Bekenstein-Hawking entropy. *Phys. Lett. B*, 379:99–104, 1996. doi: 10.1016/0370-2693(96)00345-0.

[81] Milutin Blagojević. *Gravitation and Gauge Symmetries*. CRC Press, Boca Raton, 2002. ISBN 978-0-429-18716-2. doi: 10.1201/9781420034264.

[82] D. Lovelock. The Einstein tensor and its generalizations. *J. Math. Phys.*, 12:498–501, 1971. doi: 10.1063/1.1665613.

[83] Jorge Zanelli. Chern–simons forms in gravitation theories. *Classical and Quantum Gravity*, 29(13):133001, 2012. doi: 10.1088/0264-9381/29/13/133001.

[84] J. David Brown and Marc Henneaux. Central charges in the canonical realization of asymptotic symmetries: An example from three-dimensional gravity. *Communications in Mathematical Physics*, 104(2):207–226, 1986. doi: 10.1007/BF01211153.

[85] Olivera Mišković and Rodrigo Olea. On boundary conditions in three-dimensional AdS gravity. *Physics Letters B*, 640(2):101–107, 2006. doi: 10.1016/j.physletb.2006.07.045.

[86] Rodrigo Aros. Charges and the boundary in chern-simons gravity. *Physical Review D*, 73 (4), 2006. doi: 10.1103/physrevd.73.044023.

[87] Karim Ait Moussa, Gérard Clément, Hakim Guennoune, and Cédric Leygnac. Three-dimensional chern-simons black holes. *Physical Review D*, 78(6), 2008. doi: 10.1103/physrevd.78.064065.

[88] Luis Avilés, Patrick Concha, Javier Matulich, Evelyn Rodríguez, and David Tempo. Maxwell chern-simons gravity in 3d: Thermodynamics of cosmological solutions and black holes with torsion. *arXiv preprint*, 2025. doi: 10.48550/arxiv.2510.25559.

[89] Laura Andrianopoli, Dušan Đorđević, and Olivera Miskovic. Thermodynamics of Chern-Simons AdS_5 black holes coupled to SU(2) solitons. 4 2026.

[90] Kazunori Akiyama et al. First M87 Event Horizon Telescope Results. I. The Shadow of the Supermassive Black Hole. *Astrophys. J. Lett.*, 875(1):L1, 2019. doi: 10.3847/2041-8213/ab0ec7.

[91] B. P. Abbott et al. Observation of gravitational waves from a binary black hole merger. *Phys. Rev. Lett.*, 116:061102, Feb 2016. doi: 10.1103/PhysRevLett.116.061102. URL https://link.aps.org/doi/10.1103/PhysRevLett.116.061102.

[92] John D. Barrow. Sudden future singularities. *Classical and Quantum Gravity*, 21(3): L79–L82, 2004. doi: 10.1088/0264-9381/21/3/L01.

[93] Jaume de Haro, Shin'ichi Nojiri, S. D. Odintsov, V. K. Oikonomou, and Supriya Pan. Finite-time cosmological singularities and the possible fate of the universe. *Physics Reports*, 1034:1–114, 2023. doi: 10.1016/j.physrep.2023.09.003.

[94] TH. KALUZA. On the unification problem in physics. *International Journal of Modern Physics D*, 27(14):1870001, October 2018. ISSN 1793-6594. doi: 10.1142/s0218271818700017. URL http://dx.doi.org/10.1142/S0218271818700017.

[95] Oskar Klein. Quantentheorie und fünfdimensionale relativitätstheorie. *Zeitschrift für Physik*, 37(12):895–906, 1926. doi: 10.1007/bf01397481. URL https://doi.org.

[96] David G. Boulware and S. Deser. String-generated gravity models. *Phys. Rev. Lett.*, 55: 2656–2660, Dec 1985. doi: 10.1103/PhysRevLett.55.2656. URL https://link.aps.org/doi/10.1103/PhysRevLett.55.2656.

[97] D. Lovelock. The Einstein tensor and its generalizations. *J. Math. Phys.*, 12:498–501, 1971. doi: 10.1063/1.1665613.

[98] Maja Buric, Voja Radovanovic, and Aleksandar R. Mikovic. One loop correction for Schwarzschild black hole via 2-D dilaton gravity. *Phys. Rev. D*, 59:084002, 1999. doi: 10.1103/PhysRevD.59.084002.

[99] Dušan Đorđević and Dragoljub Gočanin. Noncommutative $d = 5$ chern–simons gravity: Kaluza–klein reduction and chiral gravitational anomaly. *The European Physical Journal C*, 82(8), August 2022. ISSN 1434-6052. doi: 10.1140/epjc/s10052-022-10657-7. URL http://dx.doi.org/10.1140/epjc/s10052-022-10657-7.

[100] Maximo Banados, Claudio Teitelboim, and Jorge Zanelli. Dimensionally continued black holes. *Phys. Rev. D*, 49:975–986, 1994. doi: 10.1103/PhysRevD.49.975.

[101] Fabrizio Canfora, Alex Giacomini, and Ricardo Troncoso. Black holes, parallelizable horizons and half-BPS states for the Einstein-Gauss-Bonnet theory in five dimensions. *Phys. Rev. D*, 77:024002, 2008. doi: 10.1103/PhysRevD.77.024002.

[102] Branislav Cvetković and Dejan Simić. A black hole with torsion in 5D Lovelock gravity. *Class. Quant. Grav.*, 35(5):055005, 2018. doi: 10.1088/1361-6382/aaa3a7.

[103] Yvonne Kosmann. Dérivées de lie des spineurs. *Annali di Matematica Pura ed Applicata*, 91:317–395, 1972.

[104] Tomas Ortin. A Note on Lie-Lorentz derivatives. *Class. Quant. Grav.*, 19:L143–L150, 2002. doi: 10.1088/0264-9381/19/15/101.

[105] A. A. Belavin, A. M. Polyakov, and A. B. Zamolodchikov. Infinite conformal symmetry in two-dimensional quantum field theory. *Nuclear Physics B*, 241(2):333–380, 1984. doi: 10.1016/0550-3213(84)90052-X.

[106] Sean M. Carroll. *Spacetime and Geometry*. Cambridge University Press, 7 2019. ISBN 978-0-8053-8732-2, 978-1-108-48839-6, 978-1-108-77555-7.

[107] J. B. Hartle and S. W. Hawking. Path Integral Derivation of Black Hole Radiance. *Phys. Rev. D*, 13:2188–2203, 1976. doi: 10.1103/PhysRevD.13.2188.

[108] Yohan Potaux, Sergey N. Solodukhin, and Debajyoti Sarkar. Spacetime structure, asymptotic radiation, and information recovery for a quantum hybrid state. *Physical Review Letters*, 130(26), June 2023. ISSN 1079-7114. doi: 10.1103/physrevlett.130.261501. URL http://dx.doi.org/10.1103/PhysRevLett.130.261501.

[109] Yohan Potaux, Debajyoti Sarkar, and Sergey N. Solodukhin. Hybrid quantum states in 2d dilaton gravity. *Physical Review D*, 108(12), December 2023. ISSN 2470-0029. doi: 10.1103/physrevd.108.125012. URL http://dx.doi.org/10.1103/PhysRevD.108.125012.

[110] Yohan Potaux, Debajyoti Sarkar, and Sergey N. Solodukhin. Islands for black holes in a hybrid quantum state, 2024. URL https://arxiv.org/abs/2411.09574.

[111] Stefan Đorđević and Voja Radovanović. Collapse scenario and final state of evaporation for schwarzschild black hole in dimensionally reduced model of dilaton gravity. *Phys. Rev. D*, 113:105010, May 2026. doi: 10.1103/q2n7-qnc1. URL https://link.aps.org/doi/10.1103/q2n7-qnc1.

[112] A. Fabbri, S. Farese, J. Navarro-Salas, G. J. Olmo, and H. Sanchis-Alepuz. Semiclassical zero-temperature corrections to schwarzschild spacetime and holography. *Physical Review D*, 73(10), May 2006. ISSN 1550-2368. doi: 10.1103/physrevd.73.104023. URL http://dx.doi.org/10.1103/PhysRevD.73.104023.

[113] Pei-Ming Ho, Yoshinori Matsuo, and Yuki Yokokura. Analytic description of semiclassical black-hole geometry. *Physical Review D*, 102(2), July 2020. ISSN 2470-0029. doi: 10.1103/physrevd.102.024090. URL http://dx.doi.org/10.1103/PhysRevD.102.024090.

[114] Adrián del Río, F. Javier Marañón-González, and José Navarro-Salas. Singularity resolution in spherically reduced 2D semiclassical gravity with negative central charge. *Phys. Rev. D*, 111(4):045025, 2025. doi: 10.1103/PhysRevD.111.045025.

[115] Maja Burić and Voja Radovanović. Quantum corrections for an (anti)evaporating black hole. *Physical Review D*, 63(4), Jan 2001. ISSN 1089-4918. doi: 10.1103/physrevd.63.044020. URL http://dx.doi.org/10.1103/PhysRevD.63.044020.

[116] Jose P. S. Lemos. Thermodynamics of the two-dimensional black hole in the Teitelboim-Jackiw theory. *Phys. Rev. D*, 54:6206–6212, 1996. doi: 10.1103/PhysRevD.54.6206.

[117] Laura Andrianopoli, Gaston Giribet, Darío López Díaz, and Olivera Miskovic. Black holes with topological charges in Chern-Simons AdS_5 supergravity. *JHEP*, 11:123, 2021. doi: 10.1007/JHEP11(2021)123.

[118] Juan Crisostomo, Ricardo Troncoso, and Jorge Zanelli. Black hole scan. *Phys. Rev. D*, 62:084013, 2000. doi: 10.1103/PhysRevD.62.084013.

[119] Máximo Bañados, Marc Henneaux, Claudio Teitelboim, and Jorge Zanelli. Geometry of the 2+1 black hole. *Phys. Rev. D*, 48:1506–1525, Aug 1993. doi: 10.1103/PhysRevD.48.1506. URL https://link.aps.org/doi/10.1103/PhysRevD.48.1506.

[120] M. Banados, A. Schwimmer, and S. Theisen. Chern-Simons gravity and holographic anomalies. *JHEP*, 05:039, 2004. doi: 10.1088/1126-6708/2004/05/039.

[121] Farshid Soltani. Global kruskal-szekeres coordinates for reissner-nordström spacetime. *Physical Review D*, 108(12), December 2023. ISSN 2470-0029. doi: 10.1103/physrevd.108.124002. URL http://dx.doi.org/10.1103/PhysRevD.108.124002.

[122] Stephen A. Fulling. Nonuniqueness of canonical field quantization in riemannian space-time. *Physical Review D*, 7:2850–2862, 1973.

[123] P Davies. Scalar production in schwarzschild and rindler metrics. *Journal of Physics A: Mathematical and General*, 8:609, 01 2001. doi: 10.1088/0305-4470/8/4/022.

[124] W. G. Unruh. Notes on black-hole evaporation. *Physical Review D*, 14:870–892, 1976.

[125] C. Holzhey. Ph.d. thesis. *unpublished*, 1993.

[126] Xi Dong, Aitor Lewkowycz, and Mukund Rangamani. Deriving covariant holographic entanglement. *Journal of High Energy Physics*, 2016(11), Nov 2016. ISSN 1029-8479. doi: 10.1007/jhep11(2016)028. URL http://dx.doi.org/10.1007/JHEP11(2016)028.

[127] Geoff Penington, Stephen H. Shenker, Douglas Stanford, and Zhenbin Yang. Replica wormholes and the black hole interior, 2020.

[128] Xi Dong and Aitor Lewkowycz. Entropy, extremality, euclidean variations, and the equations of motion. *Journal of High Energy Physics*, 2018(1), Jan 2018. ISSN 1029-8479. doi: 10.1007/jhep01(2018)081. URL http://dx.doi.org/10.1007/JHEP01(2018)081.

[129] J. Maldacena and L. Susskind. Cool horizons for entangled black holes. *Fortschritte der Physik*, 61(9):781–811, Aug 2013. ISSN 0015-8208. doi: 10.1002/prop.201300020. URL http://dx.doi.org/10.1002/prop.201300020.

[130] Ping Gao, Daniel Louis Jafferis, and Aron C. Wall. Traversable wormholes via a double trace deformation. *Journal of High Energy Physics*, 2017(12), Dec 2017. ISSN 1029-8479. doi: 10.1007/jhep12(2017)151. URL http://dx.doi.org/10.1007/JHEP12(2017)151.

[131] Daniel L. Jafferis, Aitor Lewkowycz, Juan Maldacena, and S. Josephine Suh. Relative entropy equals bulk relative entropy. *Journal of High Energy Physics*, 2016(6), Jun 2016. ISSN 1029-8479. doi: 10.1007/jhep06(2016)004. URL http://dx.doi.org/10.1007/JHEP06(2016)004.

[132] Xi Dong, Daniel Harlow, and Aron C. Wall. Reconstruction of bulk operators within the entanglement wedge in gauge-gravity duality. *Physical Review Letters*, 117(2), Jul 2016. ISSN 1079-7114. doi: 10.1103/physrevlett.117.021601. URL http://dx.doi.org/10.1103/PhysRevLett.117.021601.

[133] Ahmed Almheiri, Xi Dong, and Daniel Harlow. Bulk locality and quantum error correction in ads/cft. *Journal of High Energy Physics*, 2015(4), Apr 2015. ISSN 1029-8479. doi: 10.1007/jhep04(2015)163. URL http://dx.doi.org/10.1007/JHEP04(2015)163.

[134] Masanori Ohya and Dénes Petz. *Quantum Entropy and Its Use*. Springer-Verlag, Berlin, Heidelberg, 2nd edition, 2004. ISBN 978-3-540-20806-8. doi: 10.1007/1-4020-4876-9_6.

[135] Jordan Cotler, Patrick Hayden, Geoffrey Penington, Grant Salton, Brian Swingle, and Michael Walter. Entanglement wedge reconstruction via universal recovery channels. *Physical Review X*, 9(3), Jul 2019. ISSN 2160-3308. doi: 10.1103/physrevx.9.031011. URL http://dx.doi.org/10.1103/PhysRevX.9.031011.

[136] Adam R. Brown, Hrant Gharibyan, Geoff Penington, and Leonard Susskind. The python's lunch: geometric obstructions to decoding hawking radiation, 2019.

[137] Isaac Kim, Eugene Tang, and John Preskill. The ghost in the radiation: robust encodings of the black hole interior. *Journal of High Energy Physics*, 2020(6), Jun 2020. ISSN 1029-8479. doi: 10.1007/jhep06(2020)031. URL http://dx.doi.org/10.1007/JHEP06(2020)031.

[138] C. J. Wheeler, edited by DeWitt and B. DeWitt, editors. *Relativité, Groupes et Topologie: Proceedings, Ecole d'été de Physique Théorique, Session XIII, Les Houches, France, Jul 1 - Aug 24, 1963*, New York, 1964. Gordon and Breach.

[139] Vivek Iyer and Robert M. Wald. Some properties of the noether charge and a proposal for dynamical black hole entropy. *Phys. Rev. D*, 50:846–864, Jul 1994. doi: 10.1103/PhysRevD.50.846. URL https://link.aps.org/doi/10.1103/PhysRevD.50.846.

APPENDICES

Appendix A

Riemann-Cartan geometry and spinors

The key distinction between Riemannian and Riemann-Cartan geometries lies in the presence of a non-vanishing torsion in the latter case. Then, the geometry is determined by two fundamental fields: vielbeins e^a and spin-connection ω^{ab}. Vielbeins $e^a = e^a{}_\mu \mathrm{d}x^\mu$ represent a specific basis in a 1-form space. They also satisfy the condition of orthogonality, so that the metric has a following form:

$$g = \eta_{ab} e^a \otimes e^b. \tag{A.1}$$

In this basis, the components of the metric are η_{ab}, that is, a flat Minkowski metric. For this reason, the frame defined by e^a is called local Lorentz frame, and the Latin indices $a, b, c, ...$ $(\hat{0}, \hat{1}, \hat{2}, ...)$ are called the local Lorentz indices. On the other hand, global space-time indices are denoted by Greek letters $\mu, \nu, \rho, ...$ $(0, 1, 2, ...)$. We adopt the $(-, +)$ signature, and adhere to the convention $\varepsilon^{\hat{0}\hat{1}} = +1$ for the Levi-Civita tensor. The vector field space is spanned by inverse vielbein $e_a = e_a{}^\mu \partial_\mu$, so that the relations of biorthogonality are satisfied:

$$e^a{}_\mu e_b{}^\mu = \delta^a{}_b, \qquad e^a{}_\mu e_a{}^\nu = \delta_\mu{}^\nu. \tag{A.2}$$

The construction of a Riemannian space equipped with the Levi-Civita connection does not allow for the non-vanishing torsion. Riemann-Cartan spaces are equipped with spin-connection which allows for non-zero torsion. For the purpose of defining parallel transport of different objects on a manifold, a Riemann-Cartan covariant derivative is defined by:

$$\mathrm{D} = \mathrm{d} + \frac{1}{2}\omega^{ab}\Sigma_{ab} \equiv \tilde{\nabla}_\mu \mathrm{d}x^\mu, \tag{A.3}$$

where d represents the exterior derivative, and Σ_{ab} denotes the local Lorentz generators within a specific representation of the Lorentz group, under which the corresponding object transforms. For example, in a case of a vector field, generators are given by:

$$(\Sigma_{ab})^c{}_d = \delta_a{}^c \eta_{bd} - \delta_b{}^c \eta_{ad}. \tag{A.4}$$

Using Eq. (A.4) the action of the Riemann-Cartan covariant derivative on a vector field $A = A^a e_a$is given by:

$$\mathrm{D}A^a \equiv \tilde{\nabla}_\mu A^a \mathrm{d}x^\mu = \left(\partial_\mu A^a + \omega^a{}_{b\mu} A^b\right) \mathrm{d}x^\mu. \tag{A.5}$$

On the other hand, the Riemann-Cartan connection coefficients $\tilde{\Gamma}^\rho_{\nu\mu}$ are defined as usual:

$$\tilde{\nabla}_\mu A^\nu = \partial_\mu A^\nu + \tilde{\Gamma}^\nu_{\rho\mu} A^\rho. \tag{A.6}$$

Demanding that these two Eqs. (A.5) and (A.6) are consistent yields the metricity condition:

$$\tilde{\nabla}_\mu e^a{}_\nu \equiv \partial_\mu e^a{}_\nu + \omega^{ab}{}_\mu e_{b\nu} - \tilde{\Gamma}^\rho_{\nu\mu} e^a{}_\rho = 0. \tag{A.7}$$

After preforming antisymmetrization with respect to μ and ν indices and solving for $\omega^{ab}{}_\mu$ results into:

$$\omega^{ab}{}_\mu = \Delta^{ab}{}_\mu + \mathrm{K}^{ab}{}_\mu, \tag{A.8}$$

where $\mathrm{K}^{ab}{}_\mu$ is contorsion, while $\Delta^{ab}{}_\mu$ is called Ricci coefficient of rotation. They are given by:

$$\mathrm{K}_{\mu\rho\nu} = -\frac{1}{2}\left(T_{\mu\rho\nu} - T_{\nu\mu\rho} + T_{\rho\nu\mu}\right), \tag{A.9}$$

$$\Delta_{abc} = \frac{1}{2}\left(c_{abc} - c_{cab} + c_{bca}\right), \tag{A.10}$$

where $T^\mu{}_{\nu\rho} = \tilde{\Gamma}^\mu_{\rho\nu} - \tilde{\Gamma}^\mu_{\nu\rho}$ and $c^a{}_{\mu\nu} = \partial_\mu e^a{}_\nu - \partial_\nu e^a{}_\mu$. Since $T^\mu{}_{\nu\rho}$ is the antisymmetric part of the connection coefficients, $\tilde{\Gamma}^\rho_{\mu\nu}$ are expressed as:

$$\tilde{\Gamma}^\rho_{\mu\nu} = \Gamma^\rho_{\mu\nu} + \mathrm{K}^\rho{}_{\mu\nu}, \tag{A.11}$$

where $\Gamma^\rho_{\mu\nu}$ are the Christoffel symbols. Then the decomposition of the Riemann-Cartan covariant derivative into the Riemannian part and the remainder is as follows:

$$\tilde{\nabla}_\nu A_\mu = \nabla_\nu A_\mu - \mathrm{K}^\rho{}_{\mu\nu} A_\rho, \tag{A.12}$$

where ∇_μ is the covariant derivative with respect to the Christoffel symbols. The torsion and the curvature are defined as covariant derivatives of the spin-connection and the vielbein in the following manner:

$$\tilde{R}^{ab} = \mathrm{d}\omega^{ab} + \omega^a{}_c \wedge \omega^{cb}, \tag{A.13}$$

$$T^a = \mathrm{d}e^a + \omega^a{}_b \wedge e^b. \tag{A.14}$$

Then it is easy to show that the components of torsion $T^\mu{}_{\nu\rho}$ are indeed the antisymmetric part of the connection coefficients $\tilde{\Gamma}^\mu_{\nu\rho}$. The two-dimensional space-time has higher symmetry, which results in the simplified expressions for the spin-connection, contorsion, and curvature:

$$\begin{aligned}
&\omega^{ab}{}_\mu = \varepsilon^{ab}\omega_\mu, \quad \mathrm{K}^{ab}{}_\mu = \varepsilon^{ab}\mathrm{K}_\mu, \quad \Delta^{ab}{}_\mu = \varepsilon^{ab}\Delta_\mu, \\
&\tilde{R}^{ab}{}_{\mu\nu} = -\frac{1}{2}\varepsilon^{ab}\varepsilon_{\mu\nu}\tilde{R}, \quad \tilde{R} = 2\varepsilon^{\mu\nu}\partial_\mu\omega_\nu, \quad R = 2\varepsilon^{\mu\nu}\partial_\mu\Delta_\nu, \\
&T^a{}_{\mu\nu} = e^a{}_\alpha \mathrm{K}^\alpha \varepsilon_{\mu\nu},
\end{aligned} \tag{A.15}$$

where R is the Riemannian part of the scalar curvature. The following two identities involving the Levi-Civita tensor always hold in a two-dimensional spacetime:

$$\varepsilon_{\alpha\beta}\varepsilon_{\gamma\delta} = -g_{\alpha\gamma}g_{\beta\delta} + g_{\alpha\delta}g_{\beta\gamma}, \tag{A.16}$$

$$g_{\alpha\beta}\varepsilon_{\gamma\delta} + g_{\beta\gamma}\varepsilon_{\delta\alpha} + g_{\delta\beta}\varepsilon_{\alpha\gamma} = 0. \tag{A.17}$$

With this newly defined notation, we can now move on to rewriting the Dirac equation for a massive spinor field in curved space-time. The minimal coupling to the geometry gives the following:

$$\left(\gamma^\mu\tilde{\nabla}_\mu - m\right)\psi = 0, \tag{A.18}$$

where $\tilde{\nabla}_\mu$ represents the covariant derivative within the spinor representation and $\gamma^\mu = e_a{}^\mu \gamma^a$ are the coordinate-dependent γ-matrices due to their requirement to satisfy the Clifford algebra associated with the metric $g_{\mu\nu}$. Notice that the covariant derivative in Eq. (A.18) lacks an imaginary unit prefix. This is because the signature is $(-,+)$ instead of the usual $(+,-)$ typically used in the context of the Dirac equation. Additionally, we define local γ-matrices γ^a that adhere to the Clifford algebra corresponding to the metric η_{ab}, specifically:

$$\{\gamma^a, \gamma^b\} = 2\eta^{ab}. \tag{A.19}$$

Next, we make the following choice:

$$\gamma^{\hat{0}} = i\sigma_1 \quad \wedge \quad \gamma^{\hat{1}} = \sigma_2, \tag{A.20}$$

where $\sigma_{1,2}$ are Pauli matrices. Now the generators of the Lorentz group in two dimensions can be expressed as:

$$\Sigma_{ab} \equiv \frac{1}{4}\left[\gamma_a, \gamma_b\right] = -\frac{\sigma_3}{2}\varepsilon_{ab} \tag{A.21}$$

The Lorentz conjugate is given by the following:

$$\bar{\psi} = i\psi^\dagger \gamma^{\hat{0}}. \tag{A.22}$$

Lorentz covariant derivatives for the spinor field and its conjugate are:

$$\tilde{\nabla}_\mu \psi = \left(\partial_\mu + \omega_\mu \frac{\sigma_3}{2}\right)\psi, \quad \tilde{\nabla}_\mu \bar{\psi} = \partial_\mu \bar{\psi} - \bar{\psi}\frac{\sigma_3}{2}\omega_\mu. \tag{A.23}$$

Finally, the symmetrized action for the massive Dirac fermion is expressed as:

$$S_D = -\int \mathrm{d}^2x\sqrt{-g}\left[\frac{1}{2}\bar{\psi}\gamma^\mu\tilde{\nabla}_\mu\psi - \frac{1}{2}\tilde{\nabla}_\mu\bar{\psi}\gamma^\mu\psi - m\bar{\psi}\psi\right]. \tag{A.24}$$

For the metric written in a conformal gauge $\mathrm{d}s^2 = -e^{2\rho}\mathrm{d}x^+\mathrm{d}x^-$, the appropriate choice of vielbeins is given by:

$$e^{\hat{+}}{}_- = e^{\hat{-}}{}_+ = 0, \tag{A.25}$$
$$e^{\hat{+}}{}_+ = e^{\hat{-}}{}_- = e^\rho, \tag{A.26}$$

and the inverse vielbeins are:

$$e_{\hat{+}}{}^- = e_{\hat{-}}{}^+ = 0, \tag{A.27}$$
$$e_{\hat{+}}{}^+ = e_{\hat{-}}{}^- = e^{-\rho}, \tag{A.28}$$

The Ricci rotation coefficients can be represented using the metric as follows:

$$\Delta_\mu = \frac{1}{2}\varepsilon^{\alpha\beta}\left(\partial_\alpha g_{\mu\beta} - e^a{}_\beta \partial_\mu e_{a\alpha}\right) \tag{A.29}$$

Substituting metric in a conformal gauge results in:

$$\Delta_+ = \partial_+\rho \quad \wedge \quad \Delta_- = -\partial_-\rho. \tag{A.30}$$

Appendix B

Transcendental equation solution

Here we solve the transcendental Eq. (5.102), that is:

$$e^{\hat{\mathrm{x}}}(\hat{\mathrm{x}}-1)=\delta e^{\mathrm{x}}(\mathrm{x}-1), \tag{B.1}$$

when $\delta \leqslant 1$, $\hat{\mathrm{x}} \geqslant 0$ and $\mathrm{x} \geqslant 0$. Notice that when $\delta = 1$, we have a simple solution $\hat{\mathrm{x}} = \mathrm{x}$. This is the only solution, since both functions are monotonically increasing, which implies that they intersect at most once. This is true simply because when $\sigma^+ = \sigma_0^+$, the metric becomes that of the Minkowski space-time (see Sec. 5.1.3). This fact will be extensively used as well as the fact that $\delta < 1$ when $\sigma^+ > \sigma_0^+$. Two cases will be studied, since the function on the right-hand side of Eq. (B.1) behaves differently depending on whether $\mathrm{x} \geqslant 1$ or $\mathrm{x} \leqslant 1$.

It is important to further discuss the condition $\hat{\mathrm{x}} \geqslant 0$. Fig. 3.2 shows space-time. In part I of space-time the boundary is defined by $\mathrm{x} = 0$. The formation of the singularity happens when the collapsing matter's world-line $\sigma^+ = \sigma_0^+$ hits the boundary of space-time. This corresponds to $\hat{\mathrm{x}} = 0$, which implies that $\hat{\mathrm{x}} \geqslant 0$.

Theorem 1. *The solution to Eq. (B.1)* $\hat{\mathrm{x}} = \hat{\mathrm{x}}(\mathrm{x}, \delta)$, *when* $\delta \leqslant 1$, $\hat{\mathrm{x}} \geqslant 0$ *and* $\mathrm{x} \geqslant 1$ *is given by the following functional series:*

$$\hat{\mathrm{x}}(\mathrm{x},\delta)=\mathrm{x}-\sum_{n=1}^{\infty}\frac{(1-\delta)^n}{n!}\left(1-\frac{1}{\mathrm{x}}\right)^n \mathrm{P}_{n-1}\left(\frac{1}{\mathrm{x}}\right), \tag{B.2}$$

where $\mathrm{P}_n(x)$ *are polynomials of the* n*-th degree, defined by the following recurrence relation,*

$$\mathrm{P}_n(x)=\left[n(x+1)+x^2\frac{\mathrm{d}}{\mathrm{d}x}\right]\mathrm{P}_{n-1}(x), \tag{B.3}$$

and the initial condition $\mathrm{P}_0(x) = 1$.

Proof. We expand the function $\hat{\mathrm{x}} = \hat{\mathrm{x}}(\mathrm{x}, \delta)$ in a Taylor series around $\delta = 1$:

$$\hat{\mathrm{x}}=\mathrm{x}+\sum_{n=1}^{\infty}\frac{1}{n!}\frac{\partial^n\hat{\mathrm{x}}}{\partial\delta^n}\bigg|_{\delta=1}(\delta-1)^n\,, \tag{B.4}$$

where we have used the fact that $\hat{\mathrm{x}}(\mathrm{x}, 1) = \mathrm{x}$. The differential of the function $\hat{\mathrm{x}} = \hat{\mathrm{x}}(x, \delta)$ is given by:

$$\mathrm{d}\hat{\mathrm{x}}=\frac{e^{\mathrm{x}}(\mathrm{x}-1)}{\hat{\mathrm{x}}e^{\hat{\mathrm{x}}}}\mathrm{d}\delta+\delta\frac{\mathrm{x}e^{\mathrm{x}}}{\hat{\mathrm{x}}e^{\hat{\mathrm{x}}}}\mathrm{d}\mathrm{x}. \tag{B.5}$$

The n-th derivative can be written in the following form:

$$\frac{\partial^n \hat{\mathrm{x}}}{\partial \delta^n} = e^{n\mathrm{x}}(\mathrm{x}-1)^n \left(\frac{e^{-\hat{\mathrm{x}}}}{\hat{\mathrm{x}}}\frac{\mathrm{d}}{\mathrm{d}\hat{\mathrm{x}}}\right)^{n-1} \frac{e^{-\hat{\mathrm{x}}}}{\hat{\mathrm{x}}}. \tag{B.6}$$

Demanding that $\delta = 1$ is equivalent to replacing $\hat{\mathrm{x}} = \mathrm{x}$ on the right hand side of Eq. (B.6). We define the array of polynomials $\mathrm{P}_n\left(\frac{1}{\mathrm{x}}\right)$ by:

$$\mathrm{P}_{n-1}\left(\frac{1}{\mathrm{x}}\right) = (-1)^{n-1}\mathrm{x}^n e^{n\mathrm{x}} \left(\frac{e^{-\mathrm{x}}}{\mathrm{x}}\frac{\mathrm{d}}{\mathrm{dx}}\right)^{n-1} \frac{e^{-\mathrm{x}}}{\mathrm{x}}. \tag{B.7}$$

Using mathematical induction, it is easy to show that the Rodrigues formula (Eq. (B.7)) really defines polynomials of degree $n-1$. With the help of Eq. (B.7) it is straight forward to derive a recurrence relation for the $\mathrm{P}_n(1/\mathrm{x})$ polynomials, which is given by:

$$\mathrm{P}_n\left(\frac{1}{\mathrm{x}}\right) = \left[n\left(1+\frac{1}{\mathrm{x}}\right) - \frac{\mathrm{d}}{\mathrm{dx}}\right] \mathrm{P}_{n-1}\left(\frac{1}{\mathrm{x}}\right). \tag{B.8}$$

From this relation, the recurrence relation (B.3) is directly derived by the substitution $x = 1/\mathrm{x}$. Replacing $n = 1$ in Eq. (B.7), the initial condition reads $\mathrm{P}_0(x) = 1$. □

To properly use Eq. (B.2), it is important to show that this series is uniformly convergent. If so, then the solution of Eq. (B.1) when $\mathrm{x} \geqslant 1$ is given by Eq. (B.2).

Theorem 2. *The series $\sum_{n=1}^{\infty} \frac{(1-\delta)^n}{n!} f_n(\mathrm{x})$ is uniformly convergent when $\mathrm{x} \geqslant 1$. The functional array $f_n(x)$ is defined by the following equation:*

$$f_n(x) = \left(1-\frac{1}{x}\right)^n \mathrm{P}_{n-1}\left(\frac{1}{x}\right). \tag{B.9}$$

Proof. To prove this theorem, we need to prove the following lemma first.

Lemma 1. *The functions $f_n(x)$ are monotonically increasing functions of x when $x \geqslant 1$.*

Proof. We will calculate the derivative of the function $f_n(x)$, and show that it is positive when $x > 1$. Using Eq. (B.8) the derivative of the polynomial $\mathrm{P}_{n-1}(x)$ can be eliminated, resulting in:

$$\frac{\mathrm{d}f_n(x)}{\mathrm{d}x} = \left(1-\frac{1}{x}\right)^{n-1} \left[n\mathrm{P}_{n-1}\left(\frac{1}{x}\right) - \left(1-\frac{1}{x}\right)\mathrm{P}_n\left(\frac{1}{x}\right)\right]. \tag{B.10}$$

Since $x > 1$, $f_n'(x) > 0$ is equivalent to proving that

$$n\mathrm{P}_{n-1}\left(\frac{1}{x}\right) > \left(1-\frac{1}{x}\right)\mathrm{P}_n\left(\frac{1}{x}\right), \ \forall n \geqslant 1. \tag{B.11}$$

We write the polynomials in terms of their coefficients as $\mathrm{P}_n(x) = \sum_{k=0}^{n} a_n^{(k)} x^k$. Eq. (B.11) now takes the following form:

$$n a_{n-1}^{(0)} - a_n^{(0)} + \sum_{k=1}^{n-1}\left[n a_{n-1}^{(k)} + a_n^{(k-1)} - a_n^{(k)}\right]\frac{1}{x^k} + \left[a_n^{(n-1)} - a_n^{(n)}\right]\frac{1}{x^n} + a_n^{(n)}\frac{1}{x^{n+1}} > 0. \tag{B.12}$$

We will show that coefficient of every order in Eq. (B.12) is greater than 0. To do this we need the recurrence relation between the coefficients $a_n^{(k)}$, which is easily derived using recurrence relation (B.3). The result is given by:

$$k = 0: \; a_n^{(0)} = n a_{n-1}^{(0)}, \tag{B.13}$$

$$k = 1: \; a_n^{(1)} = n a_{n-1}^{(1)} + n a_{n-1}^{(0)}, \tag{B.14}$$

$$1 < k < n: \; a_n^{(k)} = n a_{n-1}^{(k)} + (n + k - 1) a_{n-1}^{(k-1)}, \tag{B.15}$$

$$k = n: \; a_n^{(n)} = (2n - 1) a_{n-1}^{(n-1)}. \tag{B.16}$$

Together with the initial condition $a_0^{(0)} = 1$, Eqs. (B.13) through (B.16) give $a_n^{(0)} = n!$, $a_n^{(1)} = nn!$ and $a_n^{(n)} = (2n-1)!!$ respectively. Now, we return to proving the inequality (B.12). From Eq. (B.13) it follows that the $k = 0$ term in the (B.12) vanishes. The first-order term vanishes because $a_n^{(1)} = nn!$. Now, the inequality (B.12) nay be recast as:

$$(\forall k \in \{2, 3, ..., n-1\}) \; n a_{n-1}^{(k)} + a_n^{(k-1)} - a_n^{(k)} > 0. \tag{B.17}$$

With the help of the relation (B.15), the inequality (B.17) can be rewritten in the following form:

$$(n + k - 2) a_{n-1}^{(k-2)} > (k - 1) a_{n-1}^{(k-1)}. \tag{B.18}$$

Shifting $k - 1$ to k, and $n - 1$ to n, we arrive at the following expression:

$$(\forall k \in \{1, 2, ..., n-1\}) \; (n + k) a_n^{(k-1)} > k a_n^{(k)}. \tag{B.19}$$

Now, we apply mathematical induction to prove this inequality. First, we prove the relation for $n = 3$ (the base case of the induction). The coefficients of the polynomial $\mathrm{P}_3(x) = 15x^3 + 25x^2 + 18x + 6$ clearly satisfy relations (B.19). We need to prove that the relation holds for $n + 1$ if relation (B.19) is satisfied for n (induction hypothesis):

$$(\forall k \in \{1, 2, ..., n\}) \; (n + k + 1) a_{n+1}^{(k-1)} > k a_{n+1}^{(k)}. \tag{B.20}$$

Using relation (B.15), the inequality (B.20) can be rewritten as:

$$\begin{aligned}(\forall k \in \{2, ..., n\}) \; &(n+1) \left[(n+k) a_n^{(k-1)} - k a_n^{(k)}\right] \\ &+ (n + k + 1) \left[(n + k - 1) a_n^{(k-2)} - (k-1) a_n^{(k-1)}\right] > 0.\end{aligned} \tag{B.21}$$

Following from the hypothesis, both terms are greater then 0. Only two cases remain to be proven: $k = 1$ and $k = n$. In the case of $k = 1$, the relation is given by $(n+2) a_{n+1}^{(0)} > a_{n+1}^{(1)}$. Using the closed forms for these two coefficients, $(n + 2)(n + 1)! > (n + 1)(n + 1)!$, which is clearly satisfied. In the case of $k = n$, we are allowed to use formula (B.21), which takes the following form:

$$(n+1)n \left[2a_n^{(n-1)} - a_n^{(n)}\right] + (2n+1) \left[(2n-1) a_n^{(n-2)} - (n-1) a_n^{(n-1)}\right] > 0. \tag{B.22}$$

The second term is greater then zero (from the hypothesis). Using relation (B.15) we get

$$2a_n^{(n-1)} > 2n a_{n-1}^{(n-1)} = 2n(2n-3)!! > (2n-1)!! = a_n^{(n)}. \tag{B.23}$$

With this, the mathematical induction is finished and we have proven inequality (B.19), and subsequently the inequality (B.17).

The last remaining part of inequality (B.12) that needs to be proven is the relation $(\forall n \geqslant 1) a_n^{(n-1)} > a_n^{(n)}$. Using the relation (B.15) (and the result $a_n^{(n)} = (2n-1)!!$) repeatedly, it is easy to arrive at the following expression for the closed form of $a_n^{(n-1)}$:

$$a_n^{(n-1)} = \sum_{k=0}^{n-1} \frac{2^k (n-k)(n-1)!(2(n-k)-3)!!}{(n-k-1)!}. \tag{B.24}$$

The zeroth term in this sum is equal to $n(2n-3)!!$, and every other term is greater then $(2n-3)!!$, which means that: $a_n^{(n-1)} > (2n-1)(2n-3)!! = a_n^{(n)}$. This is what we needed to prove.

With this, we have proven inequality (B.12) and subsequently inequality (B.11), thus proving the lemma. □

To prove theorem 2, the Weierstrass criterion will be used. Lemma 1 implies that

$$(\forall x \geqslant 1) f_n(x) < \lim_{x\to\infty} f_n(x) = a_{n-1}^{(0)} = (n-1)!, \tag{B.25}$$

$\forall n \geqslant 1$. The inequality (B.25) implies the following inequality for the coefficients of the series $\sum_{n=1}^{\infty} \frac{(1-\delta)^n}{n!} f_n(x)$:

$$(\forall n \geqslant 1)(\forall x \geqslant 1) \left| \frac{(1-\delta)^n}{n!} f_n(x) \right| < \frac{(1-\delta)^n}{n}. \tag{B.26}$$

The next step is to prove that the series $\sum_{n=1}^{\infty} \frac{(1-\delta)^n}{n}$ converges. By the comparison test, this is true for $|1-\delta| < 1$, which is satisfied. Then, according to the Weierstrass criterion, the series $\sum_{n=1}^{\infty} \frac{(1-\delta)^n}{n!} f_n(x)$ converges uniformly. □

This result is important because the infinite sum may exchange places with integrals and limits with respect to x, which will be used in the main text. Now we move on to the case when $x < 1$.

Theorem 3. *The solution to Eq. (B.1)* $\hat{\mathrm{x}} = \hat{\mathrm{x}}(\mathrm{x}, \delta)$*, when* $\delta \leqslant 1$*,* $\hat{\mathrm{x}} \geqslant 0$ *and* $0 \leqslant \mathrm{x} \leqslant 1$ *is given by the following functional series:*

$$\hat{\mathrm{x}}(\mathrm{x}, \delta) = 1 - \sum_{n=1}^{\infty} \frac{\delta^n}{n!} \mathrm{P}_{n-1}(1) e^{n(\mathrm{x}-1)} (1-\mathrm{x})^n, \tag{B.27}$$

where $\mathrm{P}_n(x)$ *are the polynomials defined in theorem 1.*

Proof. If $0 \leqslant \mathrm{x} \leqslant 1$, then $0 \leqslant e^{\mathrm{x}}(1-\mathrm{x}) \leqslant 1$, which means that we can choose $\tilde{\delta} = \delta e^{\mathrm{x}}(1-\mathrm{x})$ as a small parameter, and expand the solution as a Taylor series with respect to $\tilde{\delta}$ around $\tilde{\delta} = 0$,

$$\hat{\mathrm{x}}(\tilde{\delta}) = \hat{\mathrm{x}}(0) + \sum_{n=1}^{\infty} \frac{\tilde{\delta}^n}{n!} \frac{\mathrm{d}^n \hat{\mathrm{x}}}{\mathrm{d}\tilde{\delta}^n}\bigg|_{\tilde{\delta}=0}. \tag{B.28}$$

The equation we are solving, in terms of $\hat{\mathrm{x}} = \hat{\mathrm{x}}(\tilde{\delta})$, is given by:

$$e^{\hat{\mathrm{x}}(\tilde{\delta})}(1 - \hat{\mathrm{x}}(\tilde{\delta})) = \tilde{\delta}. \tag{B.29}$$

With the help of the Eq. (B.29) the n-th derivative of the function $\hat{\mathrm{x}}(\tilde{\delta})$ is given by

$$\frac{\mathrm{d}^n\hat{\mathrm{x}}}{\mathrm{d}\tilde{\delta}^n} = (-1)^n \left(\frac{e^{-\hat{\mathrm{x}}}}{\hat{\mathrm{x}}}\frac{\mathrm{d}}{\mathrm{d}\hat{\mathrm{x}}}\right)^{n-1}\frac{e^{-\hat{\mathrm{x}}}}{\hat{\mathrm{x}}} = -\frac{e^{-n\hat{\mathrm{x}}}}{\hat{\mathrm{x}}^n}\mathrm{P}_{n-1}\left(\frac{1}{\hat{\mathrm{x}}}\right), \tag{B.30}$$

where Eq. (B.7) has been used. Using the fact that $\hat{\mathrm{x}} = 1$ when $\tilde{\delta} = 0$ we arrive at the following expression:

$$\frac{\mathrm{d}^n\hat{\mathrm{x}}}{\mathrm{d}\tilde{\delta}^n} = -e^{-n}\mathrm{P}_{n-1}(1). \tag{B.31}$$

Changing this result in formula (B.28) we find $\tilde{\delta} = \delta e^{\mathrm{x}}(1-\mathrm{x})$ and we have derived formula (B.27). $\square$

To be able to use this result (B.27), once again we need to prove that the series appearing in Eq. (B.27) is uniformly convergent.

Theorem 4. *The series* $\sum_{n=1}^{\infty}\frac{\delta^n}{n!}\mathrm{P}_{n-1}(1)e^{n(x-1)}(1-x)^n$ *is uniformly convergent when* $0 \leqslant x \leqslant 1$.

Proof. Since $0 \leqslant x \leqslant 1$, we have $e^{nx}(1-x)^n < 1$, which means

$$\left|\frac{\delta^n}{n!}\mathrm{P}_{n-1}(1)e^{n(x-1)}(1-x)^n\right| < \frac{\delta^n}{n!}\mathrm{P}_{n-1}(1)e^{-n}, \tag{B.32}$$

$\forall 0 \leqslant x \leqslant 1$ and $\forall n \geqslant 1$. The next step is to prove that the series $\sum_{n=1}^{\infty}\frac{\delta^n}{n!}\mathrm{P}_{n-1}(1)e^{-n}$ is convergent. To be able to do this, we need a closed form for $\mathrm{P}_{n-1}(1)$, which will be derived in the following lemma, without proof.

Lemma 2. *The polynomials defined in theorem 1 have the following property:* $\mathrm{P}_n(1) = (n+1)^n$, $\forall n \geqslant 0$.

Now we can use the comparison test to check if the series $\sum_{n=1}^{\infty}\frac{\delta^n}{n!}\mathrm{P}_{n-1}(1)e^{-n}$ is convergent. Using lemma 2 we get

$$\frac{\frac{\delta^{n+1}}{(n+1)!}(n+1)^n e^{-(n+1)}}{\frac{\delta^n}{n!}n^{n-1}e^{-n}} = \frac{\delta}{e}\left(1+\frac{1}{n}\right)^{n-1} \underset{n\to\infty}{\longrightarrow} \delta, \tag{B.33}$$

which means that the series is convergent when $\delta < 1$. This requirement is satisfied by the theorem statement. Then, according to the Weierstrass criterion, the series $\sum_{n=1}^{\infty}\frac{\delta^n}{n!}\mathrm{P}_{n-1}(1)e^{n(x-1)}(1-x)^n$ converges uniformly. $\square$

Sometimes functions of $\hat{\mathrm{x}}$ will appear in our calculations (for example, $\ln\hat{\mathrm{x}}$). Similar expressions to those of theorems 1 and 3 are needed for these functions.

Theorem 5. *The differentiable function* $\mathrm{F}(\hat{\mathrm{x}}(\mathrm{x},\delta))$, *where* $\hat{\mathrm{x}}$ *is a solution of the Eq. (B.1), when* $\delta \leqslant 1$, $\hat{\mathrm{x}} \geqslant 0$ *and* $\mathrm{x} \geqslant 1$, *is given by the following functional series:*

$$\mathrm{F}(\hat{\mathrm{x}}) = \mathrm{F}(\mathrm{x}) - \sum_{n=1}^{\infty}\frac{(1-\delta)^n}{n!}\left(1-\frac{1}{\mathrm{x}}\right)^n \mathrm{F}_{n-1}\left(\frac{1}{\mathrm{x}}\right), \tag{B.34}$$

where $\mathrm{F}_n(x)$ *is an array of functions, defined by the following recurrence relation,*

$$\mathrm{F}_n(x) = \left[n(x+1) + x^2\frac{\mathrm{d}}{\mathrm{dx}}\right]\mathrm{F}_{n-1}(x), \tag{B.35}$$

and the initial condition $\mathrm{F}_0(x) = -x^2\frac{\mathrm{dF}(1/x)}{\mathrm{d}x}$.

Proof. The proof is analogous to that of theorem 1. We start by writing the Taylor series of the function $\mathrm{F}(\mathrm{x}, \delta)$ around the point $\delta = 1$:

$$\mathrm{F}(\hat{\mathrm{x}}) = \mathrm{F}(\mathrm{x}) + \sum_{n=1}^{\infty} \frac{1}{n!} \frac{\partial^n \mathrm{F}(\hat{\mathrm{x}})}{\partial \delta^n}\bigg|_{\delta=1} (\delta - 1)^n. \tag{B.36}$$

The n-th derivative is now given by the following expression:

$$\frac{\partial^n \mathrm{F}(\hat{\mathrm{x}})}{\partial \delta^n} = e^{n\mathrm{x}}(\mathrm{x}-1)^n \left(\frac{e^{-\hat{\mathrm{x}}}}{\hat{\mathrm{x}}}\frac{\mathrm{d}}{\mathrm{d}\hat{\mathrm{x}}}\right)^{n-1} \frac{e^{-\hat{\mathrm{x}}}}{\hat{\mathrm{x}}}\frac{\mathrm{dF}(\hat{\mathrm{x}})}{\mathrm{d}\hat{\mathrm{x}}}. \tag{B.37}$$

The same way as in the theorem 1 we define an array of functions:

$$\mathrm{F}_{n-1}\left(\frac{1}{\mathrm{x}}\right) = (-1)^{n-1}\mathrm{x}^n e^{n\mathrm{x}} \left(\frac{e^{-\mathrm{x}}}{\mathrm{x}}\frac{\mathrm{d}}{\mathrm{dx}}\right)^{n-1} \frac{e^{-\mathrm{x}}}{\mathrm{x}}\frac{\mathrm{dF}(\mathrm{x})}{\mathrm{dx}}. \tag{B.38}$$

It is now obvious that the recurrence relation for the functions F_n would be the same as for the polynomials defined in the theorem 1. The only difference would be the initial condition, which is now given by $\mathrm{F}_0(1/\mathrm{x}) = \frac{\mathrm{dF(x)}}{\mathrm{dx}}$. Applying the substitution $\mathrm{x} \mapsto 1/\mathrm{x}$, we arrive at the expression given in the statement of the theorem. □

Once again, the question of uniform convergence must be asked. This time, it depends on the form of the function $\mathrm{F}(\hat{\mathrm{x}})$. The first requirement is that F does not diverge when $\hat{\mathrm{x}} \to \infty$, since the radius of convergence would depend on x, and the discussion of uniform convergence would become meaningless. From the proof of theorem 2 we can see that the necessary condition is:

$$(\forall \mathrm{x} \geqslant 1)(\exists n_0)(\forall n \geqslant n_0)\left|\left(1 - \frac{1}{\mathrm{x}}\right)^n \mathrm{F}_{n-1}\left(\frac{1}{\mathrm{x}}\right)\right| < n!. \tag{B.39}$$

The function $\ln \hat{\mathrm{x}}$ is the only one directly involved in the calculation. Since this is the case, we will take extra care of this function.

Corollary 1. *The function* $\ln \hat{\mathrm{x}}(\mathrm{x}, \delta)$ *when* $\delta \leqslant 1$, $\hat{\mathrm{x}} \geqslant 0$ *and* $\mathrm{x} \geqslant 1$, *is given by the following functional series:*

$$\ln \hat{\mathrm{x}} = \ln \mathrm{x} - \sum_{n=1}^{\infty} \frac{(1-\delta)^n}{n!} \left(1 - \frac{1}{\mathrm{x}}\right)^n \mathrm{Q}_{n-1}\left(\frac{1}{\mathrm{x}}\right), \tag{B.40}$$

where $\mathrm{Q}_n(x)$ *are polynomials of degree* $n+1$, *defined by the following recurrence relation:*

$$\mathrm{Q}_n(x) = \left[n(x+1) + x^2\frac{\mathrm{d}}{\mathrm{d}x}\right] \mathrm{Q}_{n-1}(x), \tag{B.41}$$

and the initial condition $\mathrm{Q}_0(x) = x$.

Proof. This corollary is a direct consequence of theorem 5. The initial condition is obvious since $-x^2(\ln(1/x))' = x$. We only need to prove that Q_n are polynomials of degree $n+1$, which follows directly from the recurrence relation (B.41) since it increases the degree of the polynomial by one, and the degree of the zeroth polynomial is 1. This concludes the proof. □

Theorem 6. *The series* $\sum_{n=1}^{\infty} \frac{(1-\delta)^n}{n!} f_n(x)$ *is uniformly convergent when* $\mathrm{x} \geqslant 1$. *The functional array* $f_n(x)$ *is defined by the following equation:*

$$f_n(x) = x\left(1 - \frac{1}{x}\right)^{n+1} \mathrm{Q}_{n-1}\left(\frac{1}{x}\right). \tag{B.42}$$

Proof. This proof will not be as detailed as the previous proofs since it is based on the same ideas. By mathematical induction, it is easy to prove that the functions $f_n(x)$ are monotonically increasing, the same way as in lemma 1. This fact implies that the functions $f_n(x)$ take their maximum value when $x \to \infty$. Then, the recurrence relations (B.41) tell us that the maximal value is $(n-1)!$. The rest of the proof is exactly the same as in theorem 2. □

Now we examine the $x < 1$ case.

Theorem 7. *The function* $\ln \hat{\mathrm{x}}(\mathrm{x}, \delta)$*, when* $\delta \leqslant 1$*,* $\hat{\mathrm{x}} \geqslant 0$ *and* $0 \leqslant \mathrm{x} \leqslant 1$ *is given by the following functional series:*

$$\ln \hat{\mathrm{x}} = -\sum_{n=1}^{\infty} \frac{\delta^n}{n!} \mathrm{Q}_{n-1}(1) e^{n(\mathrm{x}-1)} (1-\mathrm{x})^n, \tag{B.43}$$

where $\mathrm{Q}_n(x)$ *are the polynomials defined in corollary 1.*

Proof. The proof of this theorem is essentially the same as the proof of theorem 3. The only difference is the appearance of the polynomials Q_n instead of the polynomials P_n. □

Finally, we need to prove the uniform convergence of the series appearing in Eq. (B.43).

Theorem 8. *When* $0 \leqslant x \leqslant 1$*, the functional series* $\sum_{n=1}^{\infty} \frac{\delta^n}{n!} \mathrm{Q}_{n-1}(1) e^{n(x-1)} (1-x)^n$ *is uniformly convergent.*

Proof. As in theorem 4, we can write:

$$\left| \frac{\delta^n}{n!} \mathrm{Q}_{n-1}(1) e^{n(x-1)} (1-x)^n \right| < \frac{\delta^n}{n!} \mathrm{Q}_{n-1}(1) e^{-n}. \tag{B.44}$$

Now we need the closed form of $\mathrm{Q}_{n-1}(1)$, which will be given by the following lemma without proof.

Lemma 3. *The polynomials defined in corollary 1 have the following property:* $(\forall n \geqslant 1)\ \mathrm{Q}_{n-1}(1) = (n-1)! \sum_{k=0}^{n-1} \frac{n^k}{k!}$.

Using lemma 3, the following inequality holds:

$$\mathrm{Q}_{n-1}(1) = (n-1)! \sum_{k=1}^{n-1} \frac{n^k}{k!} < (n-1)! e^n. \tag{B.45}$$

Using Eq. (B.45), the inequality (B.44) becomes:

$$\left| \frac{\delta^n}{n!} \mathrm{Q}_{n-1}(1) e^{n(x-1)} (1-x)^n \right| < \frac{\delta^n}{n}. \tag{B.46}$$

The next step would be to prove the convergence of the series $\sum_{n=1}^{\infty} \frac{\delta^n}{n}$. This series is convergent by the comparison test when $\delta < 1$, which is satisfied. □

Appendix C

Review of the Schwarzschild solution

In this Appendix, we revisit the standard four-dimensional Schwarzschild solution. This solution is the most general spherically symmetric and static solution to the vacuum Einstein field equations. In the vacuum case, Einstein's equations simplify to the requirement that the Ricci curvature tensor vanishes:

$$\mathcal{R}_{\mu\nu} = 0, \tag{C.1}$$

The fact that the Schwarzschild metric is the unique static, spherically symmetric vacuum solution is a key consequence of Birkhoff's theorem. A precise formulation of the theorem states: any spherically symmetric solution of Einstein's field equations must be static and asymptotically flat. The converse statement, known as Israel's theorem, is also valid. Because the Schwarzschild solution is the only static and asymptotically flat solution of this kind, the spacetime outside any spherically symmetric object, such as a star or a black hole, is necessarily described by a region of the maximally extended Schwarzschild geometry.

A straightforward extension of this result exists for the Einstein–Maxwell theory: one simply replaces the Schwarzschild solution with the Reissner–Nordström solution. In contrast, no such generalization is known for stationary but non-static spacetimes, such as the most general Kerr–Newman black hole solution, which describes a rotating charged black hole. The presence of rotation violates the static condition of the spacetime, even though a time-like Killing vector (corresponding to time-translation invariance) is still present. A spacetime is called static if, in addition to admitting a timelike Killing vector, it is also invariant under time reversal. Rotating black holes do not possess this time-reversal symmetry.

The chapter is organized in four sections. In Sec. C.1, we obtain the most general static, spherically symmetric solution of Einstein's field equations. The subsequent Sec. C.2 shows that the Schwarzschild solution exhibits a singularity by explicitly evaluating the Kretschmann scalar. Sec. C.3 then examines the analytic continuation to the maximally extended Schwarzschild solution. Finally, Sec. C.4 introduces a concept of the conformal Penrose diagram and derives it explicitly for the Schwarzschild solution. The chapter closely follows the treatment given in Chapter 4 of Carroll's book [106].

C.1 The Schwarzschild spacetime metric

In this section, we solve the vacuum Einstein field equations. The most general spherically symmetric metric can be written in the form

$$\mathrm{d}s^2 = g_{aa}\mathrm{d}a^2 + 2g_{ar}\mathrm{d}a\mathrm{d}r + g_{rr}\mathrm{d}r^2 + r^2\left(\mathrm{d}\theta^2 + \sin^2\theta\mathrm{d}\phi^2\right). \tag{C.2}$$

Because of spherical symmetry, the metric components g_{ar}, g_{rr}, and g_{aa} depend only on the radial and temporal coordinates. One can demonstrate that this metric can be brought into diagonal form by introducing a new time coordinate whose differential is given by

$$\mathrm{d}t = I(a, r)\left(g_{aa}\mathrm{d}a + g_{ar}\mathrm{d}r\right), \tag{C.3}$$

where I is chosen so that this expression is an exact differential. In terms of this new coordinate, the metric takes the form:

$$\mathrm{d}s^2 = \frac{\mathrm{d}t^2}{I^2 g_{aa}} + \left(g_{rr} - \frac{g_{ar}^2}{g_{aa}}\right)\mathrm{d}r^2 + r^2\left(\mathrm{d}\theta^2 + \sin^2\theta\mathrm{d}\phi^2\right). \tag{C.4}$$

Since we started from the most general spherically symmetric line element, we can infer that imposing a diagonal form for the metric does not restrict the generality of the resulting solution. Therefore, we choose the ansatz:

$$\mathrm{d}s^2 = -e^{2\alpha(t,r)}\mathrm{d}t^2 + e^{2\beta(t,r)}\mathrm{d}r^2 + r^2\left(\mathrm{d}\theta^2 + \sin^2\theta\mathrm{d}\phi^2\right). \tag{C.5}$$

We now proceed to calculate the Christoffel symbols, which are defined as

$$\Gamma^\rho_{\mu\nu} = \frac{1}{2}e^{\rho\lambda}\Big[\partial_\mu g_{\nu\lambda} + \partial_\nu g_{\mu\lambda} - \partial_\lambda g_{\mu\nu}\Big]. \tag{C.6}$$

Substituting the ansatz (C.5) into this expression and exploiting the fact that the metric is diagonal, we find the following non-vanishing Christoffel symbols:

$$\begin{aligned}
&\Gamma^r_{tt} = e^{2(\alpha-\beta)}\partial_r\alpha, \quad \Gamma^t_{rr} = e^{-2(\alpha-\beta)}\partial_t\beta, \quad \Gamma^t_{rt} = \partial_r\alpha, \quad \Gamma^r_{tr} = \partial_t\beta,\\
&\Gamma^r_{\theta\theta} = -re^{-2\beta}, \quad \Gamma^r_{\phi\phi} = -r\sin^2\theta e^{-2\beta}, \quad \Gamma^\theta_{r\theta} = \frac{1}{r}, \quad \Gamma^\phi_{r\phi} = \frac{1}{r},\\
&\Gamma^\theta_{\phi\phi} = -\sin\theta\cos\theta, \quad \Gamma^\phi_{\theta\phi} = \cot\theta, \quad \Gamma^t_{tt} = \partial_t\alpha, \quad \Gamma^r_{rr} = \partial_r\beta.
\end{aligned} \tag{C.7}$$

To obtain the solutions of the equations of motion, we must next compute the components of the Ricci tensor. In particular, we use:

$$\mathcal{R}_{\mu\nu} = \mathcal{R}^\rho{}_{\mu\rho\nu} = \partial_\rho\Gamma^\rho_{\mu\nu} - \partial_\nu\Gamma^\rho_{\mu\rho} + \Gamma^\rho_{\alpha\rho}\Gamma^\alpha_{\mu\nu} - \Gamma^\rho_{\nu\alpha}\Gamma^\alpha_{\mu\rho}. \tag{C.8}$$

Inserting the Christoffel symbols (C.7) together with the ansatz (C.5) into Eq. (C.8), we obtain:

$$\mathcal{R}_{tt} = -\Big[\partial_t^2\beta + (\partial_t\beta)^2 - \partial_t\alpha\partial_t\beta\Big] + \Big[\partial_r^2\alpha + (\partial_r\alpha)^2 - \partial_r\alpha\partial_r\beta + \frac{2}{r}\partial_r\alpha\Big]e^{2(\alpha-\beta)}, \tag{C.9}$$

$$\mathcal{R}_{rr} = -\Big[\partial_r^2\alpha + (\partial_r\alpha)^2 - \partial_r\alpha\partial_r\beta - \frac{2}{r}\partial_r\beta\Big] + \Big[\partial_t^2\beta + (\partial_t\beta)^2 - \partial_t\alpha\partial_t\beta\Big]e^{2(\beta-\alpha)}, \tag{C.10}$$

$$\mathcal{R}_{\theta\theta} = 1 + \Big[r\partial_r(\beta-\alpha) - 1\Big]e^{-2\beta}, \tag{C.11}$$

$$\mathcal{R}_{\phi\phi} = \Big\{1 + \Big[r\partial_r(\beta-\alpha) - 1\Big]e^{-2\beta}\Big\}\sin^2\theta, \tag{C.12}$$

$$\mathcal{R}_{rt} = \frac{2}{r}\partial_t\beta. \tag{C.13}$$

These are precisely the non-zero components of the Ricci tensor. The equations of motion require the Ricci tensor to vanish. From Eq. (C.13), we immediately deduce that $\beta = \beta(r)$ only. Consequently, Eqs. (C.9) and (C.10) simplify to:

$$\left.\begin{aligned}
\partial_r^2\alpha + (\partial_r\alpha)^2 - \partial_r\alpha\partial_r\beta + \tfrac{2}{r}\partial_r\alpha = 0\\
\partial_r^2\alpha + (\partial_r\alpha)^2 - \partial_r\alpha\partial_r\beta - \tfrac{2}{r}\partial_r\beta = 0
\end{aligned}\right\} \implies \quad \partial_r\alpha = -\partial_r\beta. \tag{C.14}$$

Inserting this relation into Eq. (C.11) yields the solution for the function β:

$$2r\frac{\mathrm{d}\beta}{\mathrm{d}r} - 1 = -e^{2\beta} \quad \Longrightarrow \quad e^{2\beta} = \frac{1}{1-\frac{C}{r}}, \tag{C.15}$$

where C is an integration constant. A direct substitution into Eq. (C.10) confirms that this equation is satisfied for any constant C. The remaining task is to determine $\alpha(r,t)$. Using $\partial_r\alpha = -\partial_r\beta$, we conclude:

$$\alpha(t,r) = -\beta(r) + f(t) \quad \Longrightarrow \quad e^{2\alpha(t,r)}\mathrm{d}t^2 = e^{-2\beta(r)}\mathrm{d}t'^2, \quad \text{where}: \ \frac{\mathrm{d}t'}{\mathrm{d}t} = e^{f(t)}. \tag{C.16}$$

By carrying out this coordinate transformation, we have fully removed the time dependence from the metric. Consequently, we have indeed arrived at a stationary solution, as anticipated. It is evident that the constant C must be connected to the mass of the spacetime, or equivalently to the compact, spherically symmetric object for which this is the exterior solution. To find the explicit form of this relation, one has to evaluate the non-relativistic limit of Einstein's field equations, a calculation we will not perform here. In that limit, the non-relativistic gravitational potential can be associated with the quantity $\phi(r) = -\frac{1}{2}h_{00}$, where the metric is written as $g_{\mu\nu} = \eta_{\mu\nu} + h_{\mu\nu}$, corresponding to a perturbative expansion around flat Minkowski spacetime $\eta_{\mu\nu}$. Since, in the non-relativistic regime, the potential is known to satisfy

$$\phi(r) = -G\frac{M}{r} \quad \Longrightarrow \quad -\frac{1}{2}h_{00}(r) = -\frac{C}{2r} = \frac{GM}{r} \quad \Longrightarrow \quad C = 2GM. \tag{C.17}$$

Thus, the spacetime geometry surrounding a static, spherically symmetric mass distribution is described by the following metric:

$$\mathrm{d}s^2 = -\left(1-\frac{2GM}{r}\right)\mathrm{d}t^2 + \frac{\mathrm{d}r^2}{1-\frac{2GM}{r}} + r^2\left(\mathrm{d}\theta^2 + \sin^2\theta\,\mathrm{d}\phi^2\right), \tag{C.18}$$

which is precisely the Schwarzschild spacetime.

C.2 The singularity

One of the key notions in black hole physics is that of a singularity. Inspecting the metric (C.18), we immediately observe that it becomes divergent at $r = 0$ and $r = 2GM$. Our aim is to determine whether these divergences correspond to genuine singularities or are simply artifacts of the chosen coordinate system, i.e. coordinate singularities. To address this, we must examine quantities that remain invariant under diffeomorphisms (coordinate transformations). Two such invariants are already known:

$$\mathcal{R} = g^{\mu\nu}\mathcal{R}_{\mu\nu} = 0 \quad \wedge \quad \mathcal{R}^{\mu\nu}\mathcal{R}_{\mu\nu} = 0. \tag{C.19}$$

Neither of these invariants diverges at $r = 0$ nor at $r = 2GM$. There is, however, another invariant we must still evaluate: the Kretschmann scalar $\mathcal{R}^{\mu\nu\rho\sigma}\mathcal{R}_{\mu\nu\rho\sigma}$. To compute this quantity, we first need the components of the Riemann curvature tensor, which in turn require knowledge of the Christoffel symbols. Using the formulas in Eq. (C.7), we find for the Christoffel symbols:

$$\begin{aligned}
&\Gamma^r_{tt} = \left(1-\frac{2GM}{r}\right)\frac{GM}{r^2}, \quad \Gamma^r_{\theta\theta} = 2GM - r, \quad \Gamma^r_{\phi\phi} = (2GM - r)\sin^2\theta, \\
&\Gamma^r_{rr} = -\frac{1}{1-\frac{2GM}{r}}\frac{GM}{r^2}, \quad \Gamma^t_{rt} = \frac{1}{1-\frac{2GM}{r}}\frac{GM}{r^2}, \\
&\Gamma^\theta_{r\theta} = \frac{1}{r}, \quad \Gamma^\phi_{r\phi} = \frac{1}{r}, \quad \Gamma^\theta_{\phi\phi} = -\sin\theta\cos\theta, \quad \Gamma^\phi_{\theta\phi} = \cot\theta.
\end{aligned} \tag{C.20}$$

All other Christoffel symbols vanish. The next step is to calculate the components of the Riemann curvature tensor. Starting from the definition

$$\mathcal{R}^{\rho}{}_{\mu\sigma\nu} = \partial_\sigma \Gamma^{\rho}_{\mu\nu} - \partial_\nu \Gamma^{\rho}_{\mu\sigma} + \Gamma^{\rho}_{\alpha\sigma}\Gamma^{\alpha}_{\mu\nu} - \Gamma^{\rho}_{\nu\alpha}\Gamma^{\alpha}_{\mu\sigma}, \tag{C.21}$$

we find the non-vanishing components:

$$\begin{aligned}
\mathcal{R}^{\theta}{}_{t\theta t} &= \mathcal{R}^{\phi}{}_{t\phi t} = \left(1 - \frac{2GM}{r}\right)\frac{GM}{r^3}, & \mathcal{R}^{r}{}_{trt} &= -\left(1 - \frac{2GM}{r}\right)\frac{2GM}{r^3},\\
\mathcal{R}^{\theta}{}_{r\theta r} &= \mathcal{R}^{\phi}{}_{r\phi r} = -\frac{1}{1-\frac{2GM}{r}}\frac{GM}{r^3}, & \mathcal{R}^{t}{}_{rtr} &= \frac{1}{1-\frac{2GM}{r}}\frac{2GM}{r^3},\\
\mathcal{R}^{t}{}_{\theta t\theta} &= \mathcal{R}^{r}{}_{\theta r\theta} = -\frac{GM}{r}, & \mathcal{R}^{\phi}{}_{\theta\phi\theta} &= \frac{2GM}{r},\\
\mathcal{R}^{t}{}_{\phi t\phi} &= \mathcal{R}^{r}{}_{\phi r\phi} = -\frac{GM}{r}\sin^2\theta, & \mathcal{R}^{\theta}{}_{\phi\theta\phi} &= \frac{2GM}{r}\sin^2\theta.
\end{aligned} \tag{C.22}$$

To ensure the internal consistency of our results, we must verify that the Ricci tensor indeed vanishes. A straightforward calculation shows that $\mathcal{R}_{\mu\nu} = 0$. We can therefore proceed to compute the Kretschmann scalar:

$$\mathcal{R}^{\mu\nu\rho\sigma}\mathcal{R}_{\mu\nu\rho\sigma} = \frac{48(GM)^2}{r^6}. \tag{C.23}$$

We see that this quantity becomes infinite at $r = 0$. Because it is invariant under coordinate transformations, it will diverge in every coordinate system, and we therefore identify $r = 0$ as a genuine (physical) singularity. In the following sections, we will explicitly demonstrate how the apparent singularity at $r = 2GM$ can be removed by performing an appropriate change of coordinates. Furthermore, in the limit $r \to \infty$, the metric reduces to the Minkowski metric, indicating that the spacetime is asymptotically flat.

Given the Christoffel symbols and the Riemann curvature tensor components, one could in principle determine the geodesics and study geodesic deviation. We will not carry out this analysis here, as it is not essential for discussing black hole thermodynamics. We therefore summarize: The Schwarzschild metric represents an asymptotically flat spacetime containing a singularity at $r = 0$. The parameter $r_s = 2GM$ is referred to as the Schwarzschild radius.

C.3 The maximally extended Schwarzschild solution

In this section, we outline a systematic method for constructing the maximally extended spacetime, using the Schwarzschild solution as a representative case. In this setting, the full causal structure of the spacetime is made explicitly transparent. This requirement means that we must find a coordinate system in which massless particles always move at an angle of 45° at every point in spacetime. Equivalently, the light cones must look the same as in Minkowski space. The situation becomes much more involved, however, once we additionally demand that the metric remain regular over the entire spacetime, with the sole exception of the singularity at $r = 0$.

We begin by examining the causal structure. Light rays travel along null hypersurfaces. To focus on radial light rays, we fix the angular coordinates θ and ϕ to arbitrary constant values. Under this restriction, we find:

$$\mathrm{d}s^2 = 0 \quad \Longrightarrow \quad \frac{\mathrm{d}t}{\mathrm{d}r} = \pm\frac{1}{1-\frac{2GM}{r}}. \tag{C.24}$$

The signs $\pm$ distinguish ingoing from outgoing light rays. Integrating this equation yields their paths:

$$t = \pm\left[r + 2GM \ln\left(\frac{r}{2GM} - 1\right)\right] + const. \tag{C.25}$$

In Fig. C.1, the plots of the functions introduced in Eq. (C.25) are shown. The figure makes it evident that, as one approaches the hypersurface $r = 2GM$, the corresponding light cones become increasingly narrow and, in the limit $r \to 2GM$, they degenerate and effectively close at $r = 2GM$. The cones depict the causal relation between future and past. As we get closer to $r = 2GM$, the amount of information we can extract steadily decreases, and precisely at $r = 2GM$ it becomes impossible to distinguish between future and past.

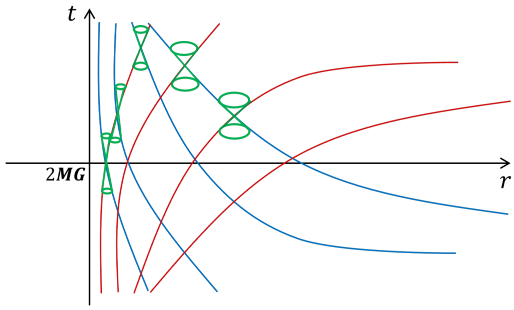

Figure C.1: Closing of light cones in (t, r) coordinates.

Because the spacetime we are studying is static, it necessarily possesses a time-like Killing vector field $\xi = \partial_t$. In order to examine the causal structure, the temporal coordinate must remain unchanged. This implies that the spatial coordinate must be redefined so that the light cones appear tilted at an angle of 45° everywhere in spacetime. To implement this, we first rewrite metric (C.18) by introducing the tortoise coordinate as follows:

$$\mathrm{d}s^2 = \left(1 - \frac{2GM}{r}\right)\left(-\mathrm{d}t^2 + \mathrm{d}r_*^2\right) + r^2\mathrm{d}\Omega^2, \tag{C.26}$$

By comparing this metric with the Schwarzschild form Eq. (C.18), we identify the tortoise coordinate r_*:

$$\frac{\mathrm{d}r_*}{\mathrm{d}r} = \frac{\mathrm{d}r}{1 - \frac{2GM}{r}} \quad\Longrightarrow\quad r_* = r + 2GM \ln\left|\frac{r}{2GM} - 1\right|. \tag{C.27}$$

Note that this coordinate (including the absolute value) is well defined both in the region $r > 2GM$ and in the region $r < 2GM$. Thus, the manifold splits into two coordinate patches: one covering $r > 2GM$ and the other covering $r < 2GM$. From this we obtain, for null curves,

$$\mathrm{d}s^2 = 0 \quad\Longrightarrow\quad \frac{\mathrm{d}t}{\mathrm{d}r_*} = 0 \quad\Longrightarrow\quad t = r_* + const, \tag{C.28}$$

which shows that the light cones have exactly the same structure as in Minkowski spacetime. However, the condition that the metric be regular everywhere except at $r = 0$ is still not satisfied. The problematic hypersurface at $r = 2GM$ remains; under the tortoise coordinate transformation it is merely pushed to $r_* \to -\infty$. To go further, we introduce the Eddington–Finkelstein coordinates, which are adapted to the outgoing and ingoing null geodesics in the (t, r_*) system. These are defined by:

$$\sigma^{\pm} = t \pm r_* \quad\Longrightarrow\quad \mathrm{d}s^2 = -\left(1 - \frac{2GM}{r}\right)\mathrm{d}\sigma^+\mathrm{d}\sigma^- + r^2\left(\mathrm{d}\theta^2 + \sin^2\theta\mathrm{d}\phi^2\right). \tag{C.29}$$

We first transform to the (σ^+, r) coordinate system, in which the metric takes the form

$$\mathrm{d}s^2 = -\left(1 - \frac{2GM}{r}\right)\mathrm{d}\sigma^{+2} + 2\mathrm{d}\sigma^+\mathrm{d}r + r^2(\mathrm{d}\theta^2 + \sin^2\theta\mathrm{d}\phi^2). \tag{C.30}$$

In these coordinates, the light cones are determined by the following relations:

$$\mathrm{d}s^2 = 0 \quad \Longrightarrow \quad \frac{\mathrm{d}\sigma^+}{\mathrm{d}r} = 0 \quad \wedge \quad \frac{\mathrm{d}\sigma^+}{\mathrm{d}r} = \frac{2}{1 - \frac{2GM}{r}}. \tag{C.31}$$

The first equation describes incoming light rays (shown in blue in Fig. C.2), whereas the second equation describes outgoing light rays (shown in red). Observe that by introducing these coordinates, we have eliminated the issue of requiring two separate charts that appeared when we used the coordinate r_*. From the figure, one can see that a freely falling observer can still send information about their position as long as they have not crossed $r = 2GM$. Once $r < 2GM$, however, every timelike (and even null) trajectory is inevitably directed toward the singularity at $r = 0$.

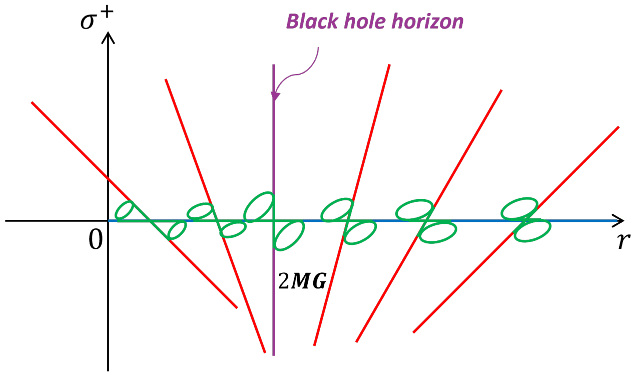

Figure C.2: Light cones in (σ^+, r) coordinates.

We therefore find that once particles cross into the region $r < 2GM$, they can no longer alter their trajectory and come back. Their subsequent evolution is completely fixed. The spatial coordinate r effectively takes on the role of a time-like direction. All particles are unavoidably driven toward the singularity. Note also that for $r < 2GM$ it is not even possible to remain at a constant value of r. Because of this, the surface $r = 2GM$ is referred to as the *future event horizon*. Since not even light can escape from the region enclosed by this horizon, we have no access to what happens inside. Black holes owe their very name to this feature. The singularity at $r = 0$ is known as the *black hole singularity*. We now switch to the (σ^-, r) coordinate system, in terms of which the metric takes the form:

$$\mathrm{d}s^2 = -\left(1 - \frac{2GM}{r}\right)\mathrm{d}\sigma^{-2} - 2\mathrm{d}\sigma^-\mathrm{d}r + r^2(\mathrm{d}\theta^2 + \sin^2\theta\mathrm{d}\phi^2), \tag{C.32}$$

while the light cones satisfy:

$$\mathrm{d}s^2 = 0 \quad \Longrightarrow \quad \frac{\mathrm{d}\sigma^-}{\mathrm{d}r} = 0 \quad \wedge \quad \frac{\mathrm{d}\sigma^-}{\mathrm{d}r} = -\frac{2}{1 - \frac{2GM}{r}}. \tag{C.33}$$

In the (σ^-, r) coordinates, the first equation describes outgoing light rays, while the second one describes incoming rays. We observe that, in this setup, a freely falling observer can still transmit information about their position even when they are in the region $r < 2GM$. However, they are unable to send information toward the singularity. Thus, the singularity constitutes the past endpoint of all particles that have been in the region $r < 2GM$. For $r > 2GM$, the observer is free to move in both directions along the r-axis, just as in the earlier coordinate choice.

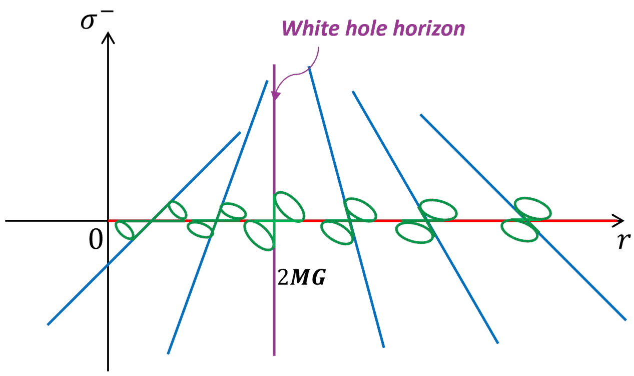

Figure C.3: Light cones in (σ^-, r) coordinates.

For the reasons given above, the surface $r = 2GM$ is called the *past event horizon* in this context, while the singularity at $r = 0$ is referred to as the *white hole singularity*. This configuration does not correspond to any physical phenomenon occurring in nature; it simply reflects a different possible choice of coordinates.

Up to this point, we have attached both a white-hole region and a black-hole region to the asymptotically flat exterior specified by $r > 2GM$. Nevertheless, this spacetime is still not the maximally extended Schwarzschild solution. A solution is maximally extended when every geodesic can be prolonged until it reaches the largest allowed value of its affine parameter, or else ends at the singularity. In the (t, r) coordinate patch, this condition is not met. The time coordinate t ranges over the entire real line, $-\infty < t < \infty$, while the radial coordinate r is confined to $2GM < r < \infty$. One finds that there is, in fact, an additional asymptotically flat region.

In the (σ^+, σ^-) coordinates we still face an issue. This arises because the tortoise coordinate r_* behaves differently in the regions $r > 2GM$ and $r < 2GM$, causing σ^+ and σ^- to cover the full range of values in both regions. What we want instead are coordinates $x^\pm = x^\pm(\sigma^\pm)$ for which the metric is smooth everywhere except at the singularity $r = 0$, and which each run from $-\infty$ to ∞ throughout the entire spacetime. To this end, let us introduce a transformation of the form:

$$\mathrm{d}x^+\mathrm{d}x^- = \begin{cases} e^{\frac{r_*}{2GM}}\mathrm{d}\sigma^+\mathrm{d}\sigma^-, & r > 2GM, \\ -e^{\frac{r_*}{2GM}}\mathrm{d}\sigma^+\mathrm{d}\sigma^-, & r < 2GM. \end{cases} \tag{C.34}$$

In App. D.5 we justify this particular choice of coordinate transformation. After carrying out the computation, we find that in both regions the metric takes the same form:

$$\mathrm{d}s^2 = -\frac{2GM}{r}e^{-\frac{r}{2GM}}\mathrm{d}x^+\mathrm{d}x^- + r^2\left(\mathrm{d}\theta^2 + \sin^2\theta\mathrm{d}\phi^2\right). \tag{C.35}$$

We see that this metric is indeed regular everywhere except at $r = 0$. It has the same expression for $r < 2GM$ and $r > 2GM$, and the light cones coincide with those in Minkowski space. What remains is to check that the coordinates $x^\pm$ actually range over the entire interval $(-\infty, \infty)$. If this condition is satisfied, we will have obtained the maximally extended Schwarzschild solution.

- First, consider the case $r > 2GM$. We have two possible choices:

$$\mathrm{d}x^+\mathrm{d}x^- = \left(e^{-\frac{\sigma^-}{4GM}}\mathrm{d}\sigma^-\right)\left(e^{\frac{\sigma^+}{4GM}}\mathrm{d}\sigma^+\right) \implies \frac{x^+}{4GM} = e^{\frac{\sigma^+}{4GM}} \quad \wedge \quad \frac{x^-}{4GM} = -e^{-\frac{\sigma^-}{4GM}}, \tag{C.36}$$

$$\mathrm{d}x^+\mathrm{d}x^- = \left(-e^{-\frac{\sigma^-}{4GM}}\mathrm{d}\sigma^-\right)\left(-e^{\frac{\sigma^+}{4GM}}\mathrm{d}\sigma^+\right) \implies \frac{x^+}{4GM} = -e^{\frac{\sigma^+}{4GM}} \quad \wedge \quad \frac{x^-}{4GM} = e^{-\frac{\sigma^-}{4GM}}. \tag{C.37}$$

  The first option corresponds to $x^+ \in (0, \infty)$ and $x^- \in (-\infty, 0)$ (quadrant I), while the second option corresponds to $x^+ \in (-\infty, 0)$ and $x^- \in (0, \infty)$ (quadrant II).

- Next, we turn to the case $r < 2GM$. Once more, there are two possible choices:

$$\mathrm{d}x^+\mathrm{d}x^- = \left(-e^{-\frac{\sigma^-}{4GM}}\mathrm{d}\sigma^-\right)\left(e^{\frac{\sigma^+}{4GM}}\mathrm{d}\sigma^+\right) \implies \frac{x^+}{4GM} = e^{\frac{\sigma^+}{4GM}} \quad \wedge \quad \frac{x^-}{4GM} = e^{-\frac{\sigma^-}{4GM}}, \tag{C.38}$$

$$\mathrm{d}x^+\mathrm{d}x^- = \left(e^{-\frac{\sigma^-}{4GM}}\mathrm{d}\sigma^-\right)\left(-e^{\frac{\sigma^+}{4GM}}\mathrm{d}\sigma^+\right) \implies \frac{x^+}{4GM} = -e^{\frac{\sigma^+}{4GM}} \quad \wedge \quad \frac{x^-}{4GM} = -e^{-\frac{\sigma^-}{4GM}}. \tag{C.39}$$

  The first option corresponds to $x^+ \in (0, \infty)$ and $x^- \in (0, \infty)$ (quadrant III), whereas the second one corresponds to $x^+ \in (-\infty, 0)$ and $x^- \in (-\infty, 0)$ (quadrant IV).

We observe that, through this transformation, the coordinates $x^{\pm}$ now span the entire two-dimensional plane. The coordinates introduced in this section are known as Kruskal coordinates. They are the coordinate system that describes the maximally extended Schwarzschild solution. Fig. C.4 illustrates how the coordinates $x^{\pm}$ partition the two-dimensional plane into four distinct quadrants.

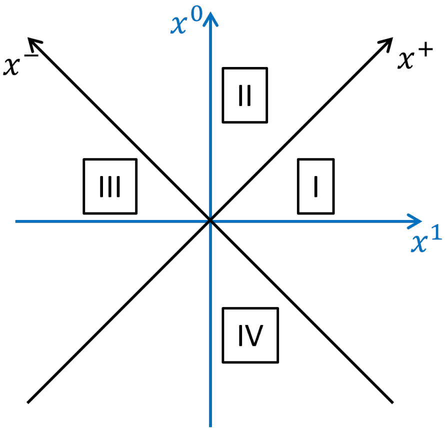

Figure C.4: Regions of spacetime diagrams.

To make the structure of spacetime more transparent, we plot the curves of constant t and constant r on the Kruskal diagram shown in Fig. C.5. These curves satisfy

$$\frac{x^0}{x^1} = \tanh\left(\frac{t}{4GM}\right) = \text{const.}$$

and

$$(x^1)^2 - (x^0)^2 = f(r) = \text{const.},$$

in regions I and III. In contrast, in regions II and IV they obey

$$(x^0)^2 - (x^1)^2 = f'(r) = \text{const.}$$

Thus, curves of fixed r appear as hyperbolas, whereas curves of fixed t are straight lines that intersect at the origin of the coordinate system.

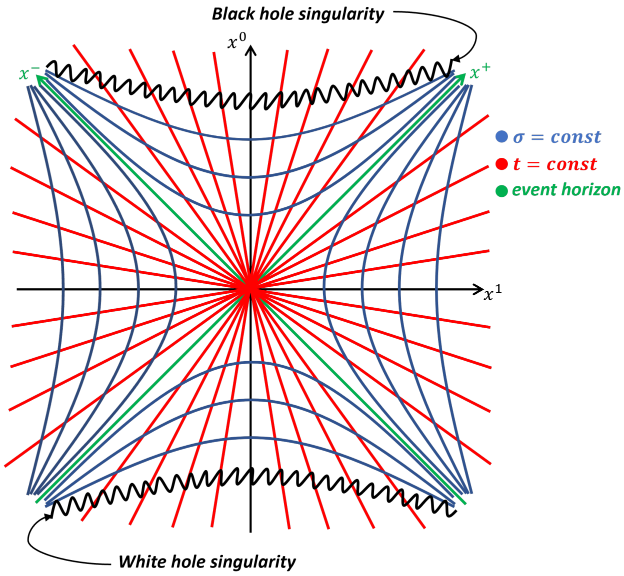

Figure C.5: Kruskal diagram.

In summary, this spacetime is composed of two asymptotically flat regions, I and III, and two regions containing singularities: region II, associated with the black hole singularity, and region IV, associated with the white hole singularity. The singularity lines at $r = 0$ correspond to the outermost hyperbolae in regions I and III, and are described by

$$(x^0)^2 - (x^1)^2 = (4GM)^2 \quad \Longleftrightarrow \quad x^+x^- = (4GM)^2, \tag{C.40}$$

whereas the event horizons are given by the hypersurfaces $x^+ = 0$ and $x^- = 0$. Recall that the original (t, r) coordinates only covered quadrants I and II of the spacetime shown in Fig. C.4.

C.4 Conformal diagram

Conformal or Penrose diagrams represent spacetime diagrams constructed by means of a coordinate transformation that satisfies the following two conditions:

1. The causal structure of spacetime is visible in the diagram. This means that the light cones are oriented at an angle of 45°.
2. Spacetime is compactified, so that infinity becomes a finite boundary on the diagram. The complete structure of spacetime is thus represented.

To fulfill the second requirement, one typically introduces coordinate transformations that involve inverse trigonometric functions. We now proceed to construct the conformal diagram of the static Schwarzschild black hole. We start from the metric of the maximally extended Schwarzschild spacetime, written in terms of the Kruskal coordinates $x^{\pm}$ obtained in the previous section. We then compactify these coordinates as follows:

$$\frac{X^+}{4GM} = \arctan\left(\frac{x^+}{4GM}\right) \quad \wedge \quad \frac{X^-}{4GM} = \arctan\left(\frac{x^-}{4GM}\right). \tag{C.41}$$

Since the original coordinates $x^{\pm}$ range over $(-\infty, \infty)$, the transformed coordinates $X^{\pm}$ take values in $(-2\pi GM, 2\pi GM)$. Thus, the second condition is indeed met. Rewriting the metric in terms of $X^{\pm}$, we find:

$$\mathrm{d}s^2 = -\frac{2GM}{r} e^{-\frac{r}{2GM}} \frac{\mathrm{d}X^+ \mathrm{d}X^-}{\cos^2\left(\frac{X^+}{4GM}\right)\cos^2\left(\frac{X^-}{4GM}\right)} + r^2\left(\mathrm{d}\theta^2 + \sin^2\theta\, \mathrm{d}\phi^2\right). \tag{C.42}$$

From this expression it is evident that the causal structure is preserved, so both required conditions are satisfied. We now locate the singularity line on the diagram. The singularity condition reads

$$x^+x^- = (4GM)^2 \quad \Longleftrightarrow \quad \tan\left(\frac{X^+}{4GM}\right)\tan\left(\frac{X^-}{4GM}\right) = 1. \tag{C.43}$$

Applying the addition formula for the tangent function yields

$$\tan\left(\frac{X^+ + X^-}{4GM}\right) = \frac{\tan\left(\frac{X^+}{4GM}\right) + \tan\left(\frac{X^-}{4GM}\right)}{1 - \tan\left(\frac{X^+}{4GM}\right)\tan\left(\frac{X^-}{4GM}\right)} \to \infty. \tag{C.44}$$

Because this expression diverges, and $\tan y$ diverges when $y = \pm\frac{\pi}{2}$, we infer that the singularities of the black hole and white hole are located at

$$X^+ + X^- = \pm 2\pi GM. \tag{C.45}$$

For the hypersurfaces $r = $ const. and $t = $ const., we obtain the following relations:

$$\begin{aligned} r = const. \quad &\Longleftrightarrow \quad x^+x^- = const. \quad &&\Longrightarrow \quad \tan\left(\frac{X^+}{4GM}\right)\tan\left(\frac{X^-}{4GM}\right) = const., \\ t = const. \quad &\Longleftrightarrow \quad \frac{x^+ - x^-}{x^+ + x^-} = const. \quad &&\Longrightarrow \quad \frac{\tan\left(\frac{X^+}{4GM}\right) - \tan\left(\frac{X^-}{4GM}\right)}{\tan\left(\frac{X^+}{4GM}\right) + \tan\left(\frac{X^-}{4GM}\right)} = const. \end{aligned} \tag{C.46}$$

It is clear that future null infinity in the right asymptotically flat region, $\mathscr{J}^+$, is reached in the limit $x^+ \to \infty$, which corresponds to $X^+ = 2\pi GM$. Similarly, past null infinity $\mathscr{J}^-$ arises when $x^- \to -\infty$, i.e. when $X^- = -2\pi GM$. The point where these two null hypersurfaces intersect is denoted by i^0 and represents spatial infinity; in the (X^+, X^-) plane this is the point $(2\pi GM, -2\pi GM)$.

Future timelike infinity i^+ is found at the intersection of the black hole singularity line with $\mathcal{J}^+$, namely at $(2\pi GM, 0)$. Conversely, past timelike infinity i^- is located where the white hole singularity line meets $\mathcal{J}^-$, that is, at $(0, -2\pi GM)$. All these identifications follow directly from the expressions for constant r and constant t hypersurfaces (C.46).

Up to this point, we have focused exclusively on the right asymptotically flat region. In the left asymptotically flat region, the entire configuration is obtained by reflecting this structure across the line $X^+ + X^- = 0$. The past and future event horizons are given by $x^+ = 0$ and $x^- = 0$, which, in the conformal diagram, correspond to the null hypersurfaces $X^+ = 0$ and $X^- = 0$. The resulting conformal diagram is depicted in Fig. C.6.

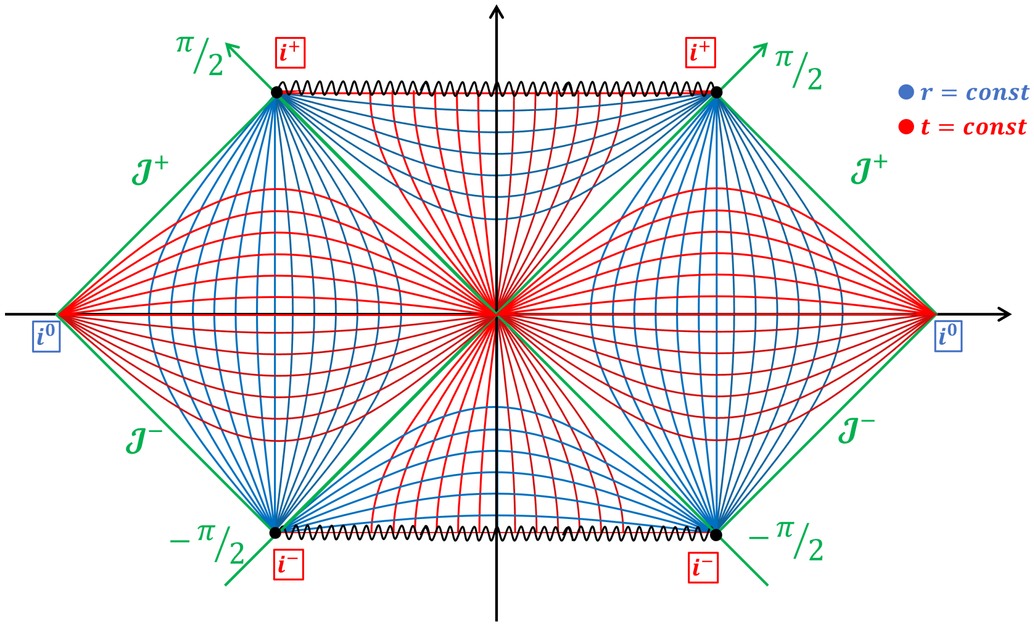

Figure C.6: Conformal diagram of the maximally extended Schwarzschild solution.

On this conformal diagram, just as on the Kruskal diagram, one can clearly see that once the future event horizon is crossed, reaching the singularity becomes unavoidable. By maximally extending the Schwarzschild solution, we obtain a region representing the black hole, another representing the white hole, our own asymptotically flat universe, and a second asymptotically flat universe linked to ours by a wormhole that passes through the point $(0, 0)$ on the conformal diagram. We also know, however, that such a configuration does not occur in nature. This naturally raises the question: What is the conformal diagram of a realistic gravitational collapse?

If objects in the universe do not evolve, then nothing interesting happens, and spacetime appears as Minkowski space. However, this is not the case. Consider a star. Throughout its lifetime, it burns nuclear fuel and in this way generates nuclear pressure. This pressure is in equilibrium with the gravitational pressure for most of the star's life. However, toward the end of its lifetime, the star exhausts its nuclear fuel, and the gravitational pressure becomes increasingly stronger. As gravitational attraction intensifies, gravitational collapse occurs. This event involves a reduction of the star's radius due to its own gravity. It is accompanied by an explosion in which the outer layers of the star's mass are expelled. If the mass exceeds a certain limit, gravitational contraction proceeds below the Schwarzschild radius. As a result, a singularity forms and the star becomes a black hole.

All that we have described can be represented on the portion of the conformal diagram of the maximally extended Schwarzschild solution corresponding to the right asymptotically flat region and the region where the black hole singularity exists. In Fig. C.7, the diagram describing gravitational collapse is shown. The region shaded in green represents the domain in which matter undergoes collapse. The Schwarzschild solution is valid in the region outside the domain where matter exists. This diagram contains an additional part that we do not expect based on the Schwarzschild conformal diagram. It is the region that appears after the singularity disappears, and is due to the phenomenon of Hawking radiation.

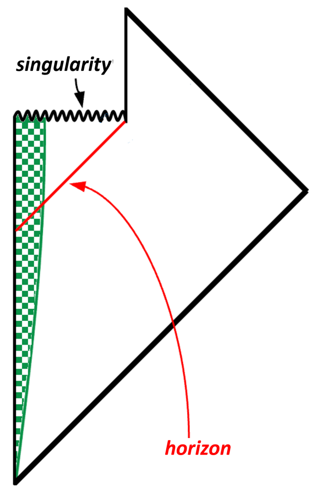

Figure C.7: Conformal diagram depicting a Schwarzschild black hole formed via the gravitational collapse of a star.

Thus, Fig. C.7 represents the Penrose diagram of the gravitational collapse of a star into a black hole, followed by the evaporation of the black hole. It turns out that, due to quantum corrections, black holes radiate, so that after a very long period of time the black hole emits all of its mass. The singularity disappears, leaving behind a black hole remanent spacetime, which in most cases corresponds to the quantum-corrected flat Minkowski space.

Appendix D

Quantum fields in curved spacetime

Hawking radiation is a phenomenon that states that black holes act as thermal objects at specific Hawking temperatures and consequently emit radiation. This radiation is defined with respect to an asymptotic observer. Since a black hole cannot classically emit matter, Hawking radiation necessarily arises from quantum effects. Nonetheless, its derivation does not require a complete theory of quantum gravity. It suffices to quantize the matter fields on a fixed classical spacetime background. If one aims to study an evaporating black hole, however, the quantum back-reaction of these matter fields on the classical geometry must be included, typically via the one-loop effective action.

For this reason, a basic understanding of quantum field theory (QFT) in curved spacetime is essential. As our discussion mainly involves scalar matter fields, we formulate QFT in curved spacetime in terms of scalar fields. In this appendix, with the exception of Sec. D.5, we largely follow Chapter 9 of Carroll's text [106].

The appendix is organized as follows. Sec. D.1 outlines how standard canonical quantization is modified when the background spacetime is curved. Sec. D.2 then shows how conventional quantum-mechanical Bogoliubov transformations relate vacuum states defined in different coordinate systems, with the Unruh effect serving as the main example in Sec. D.3. The remaining sections are more technical. Sec. D.4 introduces the concepts of event horizons and Killing horizons, which are further developed in Sec. D.5, where we analyze the regularity of the metric at the horizon and define the surface gravity. The final Sec. D.6 is devoted to a qualitative explanation of the phenomenon of Hawking radiation.

D.1 Canonical quantization in curved spacetime

To proceed with quantization, one must define the field momentum in curved spacetime and, correspondingly, formulate the Hamiltonian formalism in curved spacetime. The scalar field Lagrangian, derived via minimal coupling, is expressed as:

$$\mathcal{L} = \sqrt{-g}\left[-\frac{1}{2}g^{\mu\nu}\nabla_\mu\phi\nabla_\nu\phi - \frac{m^2}{2}\phi^2 - \frac{1}{2}\xi\mathcal{R}\phi^2\right], \tag{D.1}$$

where we have additionally introduced a term that couples the curvature to the scalar field. The interaction constant ξ may assume several distinct values. Minimal coupling corresponds to the choice $\xi = 0$. For conformal coupling, one instead has $\xi = \frac{n-2}{4(n-1)}$. This particular value describes the situation in which both the metric and a massless scalar field remain invariant under conformal transformations. In physical reality, however, there is no requirement that either of these two special cases must hold. Here, n denotes the total number of spacetime dimensions under consideration. Note that in two dimensions the usual action is conformally invariant. We now proceed to generalize the Hamiltonian formalism to curved spacetime. The field momentum and the Euler–Lagrange equations take the following generalized form:

$$\pi = \frac{\partial \mathcal{L}}{\partial(\nabla_0 \phi)}, \quad \nabla_\mu \frac{\partial \mathcal{L}}{\partial(\nabla_\mu \phi)} - \frac{\partial \mathcal{L}}{\partial \phi} = 0. \tag{D.2}$$

A straightforward computation based on Eqs. (D.1) and (D.2) leads to the following equations of motion:

$$\left(\Box - m^2 - \xi \mathcal{R}\right) \phi = 0. \tag{D.3}$$

The same result could also have been obtained using the standard quantum field theory approach, namely by deriving and solving the Euler–Lagrange equations directly, without invoking the minimal substitution principle. To proceed, we must first introduce an inner product on the space of functionals defined over the curved manifold. We select an arbitrary spacelike hypersurface Σ with induced metric γ_{ij} and unit normal vector n^μ. We then generalize the flat-spacetime scalar product as follows:

$$(\phi_1, \phi_2) = -i \int_\Sigma d^{n-1}x \sqrt{\gamma}\, n^\mu \Big(\phi_1 \nabla_\mu \phi_2^* - \phi_2^* \nabla_\mu \phi_1 \Big). \tag{D.4}$$

This scalar product is independent of the particular choice of spacelike hypersurface Σ, which is essential for it to be well defined. The subsequent step is to solve the equations of motion. As in ordinary quantum mechanics, this means identifying a complete set of functions that constitute a basis for the Hilbert space on the curved manifold. By analogy with flat spacetime, we would like to decompose the field into positive- and negative-frequency modes. However, this may not be feasible in general because it is not always possible to separate time and space variables. If a timelike Killing vector exists, the spacetime is stationary and there is a conserved energy, which allows us to assign definite energies to the modes. Yet such a Killing vector need not exist in every case. What we can always construct, however, is a complete orthogonal set of solutions satisfying:

$$(\forall i, j \in \mathbb{N}) \;\; (f_i, f_j) = \delta_{ij} \;\; \wedge \;\; (f_i^*, f_j^*) = -\delta_{ij}. \tag{D.5}$$

For the moment, the index i is taken to be discrete; the extension to a continuous index is straightforward. With this basis, the field can be expanded as follows:

$$\phi = \sum_i \Big(a_i f_i + a_i^\dagger f_i^* \Big). \tag{D.6}$$

At this stage, a_i and $a_i^\dagger$ are simply complex coefficients. We now proceed to canonically quantize the scalar field. The method parallels the flat-spacetime case, with one modification in the commutator between the field and its conjugate momentum. We impose equal-time commutation relations of the form:

$$\Big[\phi(t,\vec{x}), \phi(t,\vec{x}^{\,\prime})\Big] = 0, \;\; \Big[\pi(t,\vec{x}), \pi(t,\vec{x}^{\,\prime})\Big] = 0, \;\; \Big[\phi(t,\vec{x}), \pi(t,\vec{x}^{\,\prime})\Big] = \frac{i\hbar}{\sqrt{-g}} \delta^{(n-1)} \Big(\vec{x} - \vec{x}^{\,\prime}\Big). \tag{D.7}$$

Upon quantization, the coefficients a_i and $a_i^\dagger$ are promoted to annihilation and creation operators, respectively. Enforcing the canonical commutation relations and using the orthogonality of the mode functions yields the familiar algebra for these operators:

$$(\forall i, j \in \mathbb{N}) \;\; [a_i, a_j] = 0 \;\; \wedge \;\; \left[a_i^\dagger, a_j^\dagger\right] = 0 \;\; \wedge \;\; \left[a_i, a_j^\dagger\right] = 1. \tag{D.8}$$

Finally, we define the vacuum state corresponding to this particular set of modes in direct analogy with the flat-spacetime case, and from it construct the associated Fock space basis:

$$(\forall i \in \mathbb{N}) \;\; a_i \left|0_f\right\rangle = 0 \quad \Longrightarrow \quad \left|n_1, n_2, ...\right\rangle = \frac{\left(a_1^\dagger\right)^{n_1} \left(a_2^\dagger\right)^{n_2} ...}{\sqrt{n_1! n_2! ...}} \left|0_f\right\rangle. \tag{D.9}$$

Gravity is described by a theory that is invariant under diffeomorphisms, meaning it does not depend on the particular choice of coordinates. To define the basis $\{f_i \mid i \in \mathbb{N}\}$, we must first fix a coordinate system; only then can we solve the equations of motion in that system. Any complete set of mode functions constructed within a given coordinate system leads to a set of annihilation operators that define the same vacuum state. If, however, we switch to a different coordinate system, solve the equations of motion there, and define a new basis $\{g_i \mid i \in \mathbb{N}\}$, we obtain a different family of annihilation operators, which now annihilate a new vacuum $\left|0_g\right\rangle$:

$$\phi = \sum_i \left[b_i g_i + b_i^\dagger g_i^*\right] \;\; \wedge \;\; (\forall i, j \in \mathbb{N}) \;\; [a_i, a_j] = 0 \;\; \wedge \;\; \left[a_i^\dagger, a_j^\dagger\right] = 0 \;\; \wedge \;\; \left[a_i, a_j^\dagger\right] = 1$$
$$\Longrightarrow \;\; (\forall i \in \mathbb{N}) \;\; b_i \left|0_g\right\rangle = 0. \tag{D.10}$$

These two vacuum states are fundamentally different. In a gravitational context, selecting a particular coordinate system corresponds to choosing a particular observer associated with that system; choosing another coordinate system corresponds to a different observer. In flat spacetime, only Lorentz transformations are allowed (instead of general diffeomorphisms), and these transformations leave the vacuum invariant. Consequently, all inertial observers agree on the nature of the vacuum. In curved spacetime this agreement breaks down: different observers correspond to different vacuum states. This is the hallmark of quantum field theory in curved spacetime and leads to the conclusion that what one observer perceives as vacuum can appear as a nontrivial particle spectrum to another. This is exactly the kind of situation realized in the Unruh and Hawking effects.

D.2 Bogoliubov transformations

In Sec. D.1 we showed that each choice of coordinates leads to a different basis. Because these are all bases of the same Hilbert space (as we are working on a single manifold), there must be transformations that map one basis into another. These are known as Bogoliubov transformations. They frequently appear in condensed matter physics in the study of many-body systems, where the experimentally observed excitations are collective in nature. A standard example is provided by the BCS theory of superconductivity. The particular Bogoliubov transformation connecting the g_i modes and the f_i modes, introduced in Eqs. (D.10) and (D.6), respectively, is as follows:

$$g_i = \sum_j \left[\alpha_{ij} f_j + \beta_{ij} f_j^*\right], \quad f_i = \sum_j \left[\alpha_{ji}^* g_j - \beta_{ji} g_j^*\right], \tag{D.11}$$

where α_{ij} and β_{ij} are the Bogoliubov coefficients. It is straightforward to extract these coefficients using the scalar product (D.4):

$$\alpha_{ij} = (g_i, f_j), \quad \beta_{ij} = -\left(g_i, f_j^*\right). \tag{D.12}$$

Since the same field is being expanded in two different bases, the Bogoliubov relations between the mode functions induce corresponding Bogoliubov relations among the annihilation and creation operators:

$$b_i = \sum_j \left[\alpha_{ij}^* a_j - \beta_{ij}^* a_j^\dagger\right], \quad b_i^\dagger = \sum_j \left[-\beta_{ij} a_j + \alpha_{ij} a_j^\dagger\right], \tag{D.13}$$

$$a_i = \sum_j \left[\alpha_{ji} b_j + \beta_{ji}^* b_j^\dagger\right], \quad a_i^\dagger = \sum_j \left[\beta_{ji} b_j + \alpha_{ji}^* b_j^\dagger\right]. \tag{D.14}$$

The mutual orthogonality of the f- and g-bases then yields a set of constraints on the Bogoliubov coefficients. Conversely, these same constraints guarantee that the commutation relations between creation and annihilation operators remain invariant under a change of coordinates.

We now demonstrate how this formalism implies that distinct observers associate different vacuum states with the same physical situation. Let observer A employ the coordinates tied to the f-basis, and observer B use those corresponding to the g-basis. Assume the quantum state is such that observer A detects no particles, i.e. $|\psi\rangle = |0_f\rangle$. Our objective is to determine what observer B perceives in this same state. To do so, we evaluate the expectation value of the occupation numbers defined with respect to observer B's particle notion:

$$\begin{aligned} \langle 0_f|\, n_{ig}\, |0_f\rangle = \langle 0_f|\, b_i^\dagger b_i\, |0_f\rangle &= \langle 0_f| \sum_{j,k} \left(-\beta_{ij} a_j + \cancelto{0}{\alpha_{ij} a_j^\dagger}\right)\left(\cancelto{0}{\alpha_{ik}^* a_k} - \beta_{ik}^* a_k^\dagger\right) |0_f\rangle \\ &= \sum_{j,k} \beta_{ij}\beta_{ik}^* \langle 0_f|\, a_j a_k^\dagger\, |0_f\rangle = \sum_{j,k} \beta_{ij}\beta_{ik}^* \delta_{jk} = \sum_j |\beta_{ij}|^2. \end{aligned} \tag{D.15}$$

This leads directly to the following conclusion:

$$(\forall i \in \mathbb{N}) \ \ \langle 0_f|\, n_{if}\, |0_f\rangle = 0 \ \wedge \ \langle 0_f|\, n_{ig}\, |0_f\rangle = \sum_j |\beta_{ij}|^2. \tag{D.16}$$

This relation implies that although observer A detects no particle spectrum, observer B does register a particle spectrum as long as at least one Bogoliubov coefficient is nonzero. The key question then becomes how these particles are actually measured. Given a specific detector in curved spacetime, we must determine how to define the positive- and negative-frequency modes associated with it. The most natural proposal is to impose

$$\frac{D}{\mathrm{d}\tau} f_i = -i\omega_i f_i. \tag{D.17}$$

If we can find modes that satisfy this condition, the issue is essentially settled. However, this construction cannot always be carried out. It is guaranteed to work when the metric is static, in which case we can choose coordinates such that

$$\partial_0 g_{\mu\nu} = 0 \quad \wedge \quad g_{0i} = 0. \tag{D.18}$$

We now make explicit the form of the $\Box$ operator:

$$\Box = g^{00}\partial_0^2 + g^{ij}\partial_i\partial_j - g^{00}\Gamma^i_{00}\partial_i - g^{ij}\Gamma^k_{ij}\partial_k. \tag{D.19}$$

Under these conditions, the Klein–Gordon equation allows a separation of variables into temporal and spatial components:

$$\partial_0^2\phi = \frac{1}{g^{00}}\left[-g^{ij}\partial_i\partial_j + g^{00}\Gamma^i_{00}\partial_i + g^{ij}\Gamma^k_{ij}\partial_k + m^2 + \xi\mathcal{R}\right]\phi. \tag{D.20}$$

We can now straightforwardly introduce the ansatz of the form $f_\omega(t,\vec{x}) = e^{-i\omega t}F_\omega(\vec{x})$. In this way we define the positive-frequency modes. Taking the complex conjugate of this relation then yields the negative-frequency modes. Clearly, these modes obey

$$\partial_0 f_\omega = -i\omega f_\omega \quad \Longrightarrow \quad \mathcal{L}_\xi f_\omega = -i\omega f_\omega, \tag{D.21}$$

where the second equality is the coordinate-independent form, written in terms of the Killing vector ξ. In the chosen coordinate system, this Killing vector simply corresponds to $\xi = \partial_0$.

D.3 Unruh effect

The Unruh effect describes how a uniformly accelerated observer in the Minkowski vacuum experiences a particle spectrum corresponding to a thermal bath, with a temperature proportional to that observer's proper acceleration. An observer undergoing such a motion is referred to as a Rindler observer. Our first step is to identify the coordinate system that is natural to this Rindler observer. Since acceleration is only meaningfully defined in the observer's own reference frame, let us denote this proper acceleration by a. Working in Minkowski spacetime, we must then ask: How does this acceleration behave under Lorentz transformations?

To address this, consider an inertial frame $S^{'}$ moving with constant velocity u along the positive x-axis with respect to the laboratory frame S. Suppose further that a body moves with velocity $v^{'}$ in $S^{'}$. The corresponding velocity v as measured in S follows the relativistic velocity addition formula:

$$v = \frac{\mathrm{d}x}{\mathrm{d}t} = \frac{\mathrm{d}x^{'} + u\mathrm{d}t^{'}}{\mathrm{d}t^{'} + \frac{u}{c^2}\mathrm{d}x^{'}} = \frac{v^{'} + u}{1 + \frac{uv^{'}}{c^2}}. \tag{D.22}$$

Our next goal is to derive the corresponding transformation law for acceleration (where a_l denotes acceleration in the laboratory system S):

$$a_l = \frac{\mathrm{d}v}{\mathrm{d}t} = \frac{\mathrm{d}v}{\mathrm{d}v^{'}}\frac{\mathrm{d}v^{'}}{\mathrm{d}t^{'}}\frac{\mathrm{d}t^{'}}{\mathrm{d}t} = a\left(\frac{\sqrt{1-\frac{u^2}{c^2}}}{1+\frac{uv^{'}}{c^2}}\right)^3. \tag{D.23}$$

This is the general transformation rule for acceleration under Lorentz transformations. Our discussion is restricted to the special case in which the body is at rest in the S' frame, which is the proper frame attached to the body. In other words, from this point on we take S' to be the frame comoving with the observer. Consequently, we have $u = v$ and $v' = 0$. Hence,

$$a_l = \frac{a}{\gamma^3} \quad \Longrightarrow \quad \frac{dv}{dt} = a\left(1 - \frac{v^2}{c^2}\right)^{\frac{3}{2}} \quad \Longrightarrow \quad v(t) = \frac{at}{\sqrt{1+\left(\frac{at}{c}\right)^2}}. \tag{D.24}$$

This expression is valid for the initial condition $v(0) = 0$. We now compute how the observer's position evolves in time:

$$\frac{\mathrm{d}x}{\mathrm{d}t} = v \quad \Longrightarrow \quad x(t) = \frac{c^2}{a}\left(\sqrt{1+\left(\frac{at}{c}\right)^2} - 1\right) + x_0. \tag{D.25}$$

Next, we determine $t(\tau)$, since we wish to rewrite all quantities in terms of the proper time:

$$\frac{\mathrm{d}t}{\mathrm{d}\tau} = \gamma = \frac{1}{\sqrt{1-\frac{v^2}{c^2}}} \quad \Longrightarrow \quad t(\tau) = \frac{c}{a}\sinh\left(\frac{a\tau}{c}\right). \tag{D.26}$$

The integration constant is chosen so that $t(0) = 0$. With this, we can also express x as a function of the proper time:

$$x(\tau) = \frac{c^2}{a}\sqrt{1+\sinh^2\left(\frac{a\tau}{c}\right)} + x_0 - \frac{c^2}{a} \quad \Longrightarrow \quad x(\tau) = \frac{c^2}{a}\cosh\left(\frac{at}{c}\right) + x_0 - \frac{c^2}{a}. \tag{D.27}$$

We may set the initial position (or coordinate origin) such that $x_0 = \frac{c^2}{a}$. With this convention, and choosing units where $c = 1$, the coordinate transformations become

$$t(\tau) = \frac{1}{a}\sinh(a\tau) \quad \wedge \quad x(\tau) = \frac{1}{a}\cosh(a\tau). \tag{D.28}$$

Thus, the worldline is a hyperbola in Minkowski space, with the proper time serving as the parameter.

$$(ax)^2 - (at)^2 = 1. \tag{D.29}$$

An observer following a geodesic inevitably reaches future timelike infinity. In contrast, a uniformly accelerated observer does not approach timelike infinity; instead, their worldline becomes asymptotically tangent to the light cone. Our aim is to introduce coordinates adapted to this uniformly accelerated observer. The new time coordinate should coincide with the observer's proper time, and the observer should remain fixed at the origin of the new spatial coordinate, reflecting the fact that they are at rest in this coordinate system. Consider the coordinate transformation

$$t = \frac{1}{a}e^{a\xi}\sinh(a\eta) \quad \wedge \quad x = \frac{1}{a}e^{a\xi}\cosh(a\eta)\,. \tag{D.30}$$

The coordinates (η, ξ) defined in this way are known as Rindler coordinates. The uniformly accelerated observer follows the worldline $\xi = 0$, precisely as required. Furthermore, the time coordinate satisfies $\eta = \tau$, where τ is the proper time of the uniformly accelerated observer.

The domain of these coordinates is $\mathbb{R}$, indicating that they are maximally extended. It is clear that this observer can access only the first quadrant. The light cone sets the boundaries of this accessible region. This observer possesses two Rindler horizons: the hypersurface $x^+ = 0$ is referred to as the future Rindler horizon, and the hypersurface $x^- = 0$ is known as the past Rindler horizon. In these coordinates, the structure of spacetime closely mimics the Schwarzschild geometry in region I. The Rindler wedge together with constant-coordinate hypersurfaces is presented in Fig. D.1.

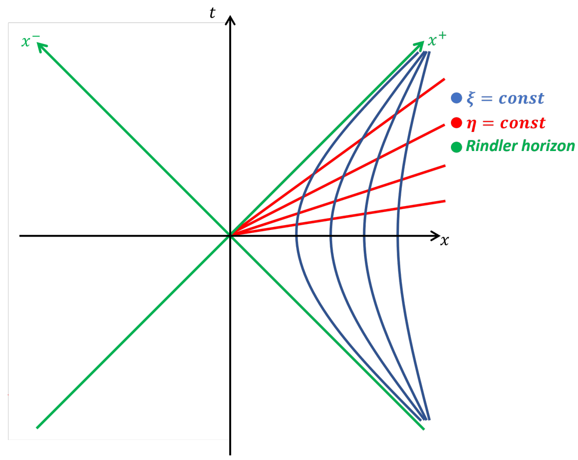

Figure D.1: Constant coordinate hypersurfaces in Rindler coordinates.

From now on, we restrict our attention to the two-dimensional case. In Rindler coordinates the metric can be written as

$$ds^2 = e^{2a\xi}\left(-d\eta^2 + d\xi^2\right). \tag{D.31}$$

Notice that the metric is independent of η. Consequently, in these coordinates there is a Killing vector $K = \partial_\eta$. To understand what this vector represents physically, let us express it in the (x, t) coordinates. After performing the transformation we find

$$K = a\left(x\partial_t + t\partial_x\right), \qquad K^\mu K_\mu = -e^{2a\xi} = a(t-x). \tag{D.32}$$

Thus, in region I this Killing vector is timelike, as expected, since η plays the role of time there. However, it becomes spacelike upon crossing the Rindler horizons, which shows that it represents a Killing horizon. Next, we introduce light-cone coordinates $\sigma^\pm = \eta \pm \xi$:

$$x^+ = t + x = \frac{1}{a}e^{a\xi}\left[\sinh(a\eta) + \cosh(a\eta)\right] = \frac{1}{a}e^{a(\xi+\eta)} \qquad \Longrightarrow \qquad ax^+ = e^{a\sigma^+}, \tag{D.33}$$

$$x^- = t - x = \frac{1}{a}e^{a\xi}\left[\sinh(a\eta) - \cosh(a\eta)\right] = -\frac{1}{a}e^{a(\xi-\eta)} \qquad \Longrightarrow \qquad ax^- = -e^{-a\sigma^-}. \tag{D.34}$$

In Sec. 8.2.1 we focused on the Rindler observer. There we also derived the Bogoliubov coefficients for the case in which the quantum state is the Minkowski vacuum, and we showed that a Rindler observer detects a particle spectrum in this state. Furthermore, this spectrum turns out to be exactly thermal, with temperature

$$T = \frac{\hbar a}{2\pi k_B c}. \tag{D.35}$$

Here we have reinstated the fundamental constants. The temperature is directly proportional to the observer's proper acceleration. This value corresponds to the observer located at $x = 0$. We can now ask: what temperature is measured by an observer situated at an arbitrary ξ? The computation proceeds in precisely the same way as for the observer at $\xi = 0$; the only change is the observer's proper acceleration α. His trajectory must satisfy

$$t = \frac{1}{\alpha}\sinh\left(\alpha\tau'\right) = \frac{1}{a}e^{a\xi}\sinh(a\eta) \quad \wedge \quad x = \frac{1}{\alpha}\cosh\left(\alpha\tau'\right) = \frac{1}{a}e^{a\xi}\cosh(a\eta), \tag{D.36}$$

where τ' denotes this observer's proper time. From these relations we infer his trajectory in (η, ξ) coordinates:

$$\eta = \frac{\alpha}{a}\tau' \quad \wedge \quad \xi = \frac{1}{a}\ln\frac{a}{\alpha}. \tag{D.37}$$

We therefore deduce that the temperature measured by this observer is:

$$T' = \frac{\hbar\alpha}{2\pi k_B c} = \frac{\hbar a}{2\pi k_B c}e^{-a\xi} \quad \Longrightarrow \quad T' = Te^{-a\xi}. \tag{D.38}$$

We observe that the temperature vanishes in the limit $\xi \to \infty$. This is indeed what one should expect, because as we move toward infinity the Rindler hyperbolae become increasingly flat, and Minkowski space is effectively recovered. It is important to explain how this can be consistent. An inertial (Minkowski) observer does not measure any particles, whereas a Rindler observer perceives a thermal spectrum of particles. For the Rindler observer to register these particles, they must carry a detector. To keep this detector accelerating, work must be done on it continuously. From the viewpoint of the inertial observer, the detector is both absorbing and emitting particles at the same time, while from the Rindler observer's frame it is simply detecting particles and maintaining its accelerated motion.

D.4 Event horizon and Kiling horizons

We now address the question of how to identify the event horizon of a black hole. In App. C, we approached this by examining the behavior of the metric at $r = 2GM$. But what is the appropriate procedure when we are instead given a general metric? In particular, we ask: does an event horizon exist, and if so, how can we locate it?

For a static, asymptotically flat spacetime with spherical topology, one can always find a coordinate system in which the position of the event horizon is straightforward to determine. In such a spacetime there exists a timelike Killing vector field ∂_t. We may then choose coordinates so that $\partial_t g_{\mu\nu} = 0$. On each hypersurface $t = \text{const.}$, we select spatial coordinates (r, θ, ϕ) such that the metric approaches the flat metric at spatial infinity.

With a suitable choice of coordinates, we can conceptually begin at spatial infinity, where the metric is approximately flat, and move inward toward the singularity using r as a radial coordinate. We examine the family of hypersurfaces defined by $r = \text{const.}$. For large r, these hypersurfaces are spacelike, but as we move inward there will be some critical radius $r = r_H$ at which their character changes: for $r < r_H$ they become timelike hypersurfaces. Consequently, the hypersurface at $r = r_H$ itself must be null. If our coordinate choice is poor, this null property may hold only in certain regions, complicating the interpretation. In any case, beyond this null hypersurface, light rays cannot propagate out to infinity, so this surface is in fact the event horizon. Thus, event horizons are null hypersurfaces.

This observation indicates how to locate the event horizon from the metric. Consider the one-form $\partial_\mu r$, which is normal to the hypersurfaces $r = \text{const.}$. At the radius where these hypersurfaces become null, this normal vector must itself be null, i.e.:

$$0 = g^{\mu\nu}\partial_\mu r \partial_\nu r = g^{rr} \quad \Longrightarrow \quad g^{rr}(r_H) = 0. \tag{D.39}$$

In Sec. D.3 we encountered the concept of a Killing horizon. This is a hypersurface on which a certain Killing vector becomes null. One can show that any event horizon in a stationary, asymptotically flat spacetime is in fact a Killing horizon associated with some Killing field ξ. If the spacetime is also static (which is automatically true in two dimensions), then this Killing field is simply $\xi = \partial_t$. The reverse statement, however, is not generally valid: a Killing horizon need not be an event horizon. As discussed in the previous section, the Rindler horizons provide an example: they are Killing horizons but not event horizons. By definition, a Killing horizon is characterized by the condition $\xi^\mu \xi_\mu = 0$ on the horizon. Consequently, $\nabla_\nu(\xi^\mu \xi_\mu)$ defines a one-form normal to the Killing horizon. At the same time, we also know that ξ^μ itself is normal to this horizon. From this it follows that

$$\nabla_\nu \left(\xi^\mu \xi_\mu\right) = 2\kappa \xi_\nu \quad \implies \quad \xi^\mu \nabla_\mu \xi^\nu = -\kappa \xi^\nu, \tag{D.40}$$

where κ is a constant over the Killing horizon, known as the surface gravity. Making use of Frobenius' theorem, $\xi \wedge d\xi = 0$, one can readily compute κ and finds

$$\kappa^2 = -\frac{1}{2} \nabla^\mu \xi^\nu \nabla_\mu \xi_\nu. \tag{D.41}$$

We will always understand this expression to be evaluated on the horizon. At first glance κ appears to be arbitrary, since multiplying a Killing vector by any constant yields another Killing vector. However, in a static, asymptotically flat spacetime the timelike Killing vector can be uniquely fixed by imposing the following convention:

$$\xi^\mu \xi_\mu \to -1, \quad \text{when } r \to \infty. \tag{D.42}$$

A static observer has a four-velocity that is proportional to the timelike Killing vector. The proportionality factor between the Killing vector and the four-velocity of a stationary observer is defined as the redshift factor:

$$\xi^\mu = V(x) U^\mu \ \wedge \ U^\mu U_\mu = -1 \quad \implies \quad V(x) = \sqrt{-\xi^\mu \xi_\mu}. \tag{D.43}$$

This quantity is called the redshift factor because it determines how photon frequencies measured by static observers at different spatial locations are related via gravitational redshift. Consider a photon with four-momentum p^μ. Its conserved energy, defined using the timelike Killing vector, is $E = -\xi^\mu p_\mu$. For a stationary observer with four-velocity U^μ, the photon energy measured in that observer's frame is $\omega = -U^\mu p_\mu$. We now derive the relation between the photon frequencies recorded by two stationary observers located at different points in space:

$$\frac{\omega_1}{\omega_2} = \frac{-U_1^\mu p_\mu}{-U_2^\nu p_\nu} = \frac{V(x_2)\xi^\mu p_\mu}{V(x_1)\xi^\nu p_\nu} = \frac{V(x_2)E}{V(x_1)E} = \frac{V(x_2)}{V(x_1)}. \tag{D.44}$$

Next, we compute the four-acceleration of a stationary observer:

$$\begin{aligned} a^\mu &= \frac{DU^\mu}{d\tau} = \frac{dx^\nu}{d\tau}\nabla_\nu U^\mu = U^\nu \nabla_\nu U^\mu = \frac{\xi^\nu}{V}\nabla_\nu\left(\frac{\xi^\mu}{V}\right) = \xi^\mu \xi^\nu \nabla_\nu \left(\frac{1}{V}\right) + \frac{1}{V^2}\xi^\nu \nabla_\nu \xi^\mu \\ &= \xi^\mu \cancelto{0}{\partial_t \left(\frac{1}{V}\right)} - \frac{1}{V^2}\xi^\nu \nabla^\mu \xi_\nu = -\frac{1}{2V^2}\nabla^\mu\left(\xi^\nu \xi_\nu\right) = \frac{1}{2V^2}\nabla^\mu\left(V^2\right) = \nabla^\mu \ln V. \end{aligned} \tag{D.45}$$

The first equality in the second line is justified for two reasons. First, $V(x)$ is time-independent, so the time derivative vanishes. Second, we used the Killing equation $\nabla_\nu \xi^\mu = -\nabla^\mu \xi_\nu$. In the next step, we insert the defining relation for the surface gravity (D.40):

$$a^\mu = -\frac{1}{2V^2}\nabla^\mu \left(\xi^\nu \xi_\nu\right) = -\frac{\kappa}{V^2}\xi^\mu \quad \Longrightarrow \quad a^2 = -a^\mu a_\mu = \frac{\kappa^2}{V^4}\xi^\mu \xi_\mu = \frac{\kappa^2}{V^2}. \tag{D.46}$$

This relation yields another, conceptually more straightforward, method for determining the surface gravity:

$$\kappa = aV \quad \wedge \quad \kappa = \sqrt{\nabla^\mu V \nabla_\mu V}. \tag{D.47}$$

Again, this expression is to be evaluated on the horizon. Let us now interpret the result. Consider what the following relation encodes:

$$a^{'} = \frac{V_1}{V_2}a. \tag{D.48}$$

This quantity represents the acceleration assigned by the observer at position 2 to an observer at position 1 who measures a proper acceleration a. In our setup we take $V_1 = V$, the value of the redshift factor on the horizon, and $V_2 = 1$, which by Eq. (D.42) corresponds to spatial infinity. We can thus infer the physical meaning of the surface gravity: In a static, asymptotically flat spacetime, the surface gravity is the acceleration of a static observer arbitrarily close to the event horizon, as redshifted to (i.e. as measured by) an observer at infinity.

For this statement to hold, the spacetime must be static; otherwise, the surface gravity defined on the horizon cannot be given this interpretation. In a stationary spacetime, there is still a timelike Killing vector, but the problem is that it does not become null on the event horizon. Instead, it is null on a different hypersurface located outside the horizon, known as the ergosurface. The event horizon is still a Killing horizon, but now with respect to a linear combination of the two Killing vectors that exist in this situation, namely $\partial_t + \Omega_H \partial_\phi$. The parameter Ω_H is called the angular velocity of the horizon. We will not analyze stationary but non-static solutions any further, because in two dimensions every stationary solution is also static.

D.5 Regularity of the metric at the horizon

Since the singularity at $r = 2GM$ in the Schwarzschild solution is merely a coordinate singularity, there must exist a coordinate system that remains regular on this hypersurface (see App. C.3). We now show that, at the instant an observer in radial free fall crosses the event horizon, they notice nothing peculiar. Our analysis applies to a static spacetime with spherically symmetric topology. We take the metric in the following form:

$$ds^2 = g_{tt}dt^2 + g_{rr}dr^2 + r^2\left(d\theta^2 + \sin^2\theta\, d\phi^2\right), \tag{D.49}$$

and assume that $g_{tt} = g_{tt}(r)$ and $g_{rr} = g_{rr}(r)$. We now demonstrate that any such metric can be re-expressed so that the relation $g_{tt} = -g^{rr}$ holds:

$$ds^2 = g_{tt}\left(dt^2 + \frac{g_{rr}}{g_{tt}}dr^2\right) + r^2 d\Omega^2 = g_{tt}\left(dt^2 + \frac{dr'^2}{g_{tt}^2}\right) + r^2 d\Omega^2. \tag{D.50}$$

In doing so, we have introduced a new radial coordinate $r' = r'(r)$, defined via

$$\frac{g_{rr}}{g_{tt}}dr^2 = \frac{dr'^2}{g_{tt}^2} \quad \Longrightarrow \quad \frac{dr'}{dr} = \sqrt{g_{rr}g_{tt}}. \tag{D.51}$$

Having reduced the problem to evaluating this integral, we are free to assume that the metric is written in a form such that $g_{tt} = -g^{rr}$. From the previous section we know that the horizon is located by the condition $g^{rr}(r_H) = 0$. Let us expand the metric about this radial value, i.e. set $r = r_H + \varepsilon$:

$$\begin{aligned} \mathrm{d}s^2 &= \left(\cancelto{0}{g_{tt}(r_H)} + \partial_r g_{tt}(r_H)\,\varepsilon\right)\mathrm{d}t^2 + \frac{\mathrm{d}\varepsilon^2}{\cancelto{0}{g^{rr}(r_H)} + \partial_r g^{rr}(r_H)\,\varepsilon} + f(\varepsilon)\mathrm{d}\Omega^2 \\ &= \partial_r g_{tt}(r_H)\,\varepsilon\,\mathrm{d}t^2 + \frac{\mathrm{d}\varepsilon^2}{\partial_r g^{rr}(r_H)\,\varepsilon} + f(\varepsilon)\mathrm{d}\Omega^2. \end{aligned} \tag{D.52}$$

We now define a new coordinate ρ by requiring

$$\mathrm{d}\rho^2 = \frac{\mathrm{d}\varepsilon^2}{\partial_r g^{rr}(r_H)}\varepsilon \quad \Longrightarrow \quad \frac{\mathrm{d}\rho}{\mathrm{d}\varepsilon} = \frac{1}{\sqrt{\partial_r g^{rr}(r_H)\varepsilon}} \quad \Longrightarrow \quad \varepsilon = \frac{1}{4}\rho^2\partial_r g^{rr}(r_H). \tag{D.53}$$

In terms of ρ, the metric becomes

$$\mathrm{d}s^2 = -\left(\frac{1}{2}\partial_r g^{rr}(r_H)\right)^2 \mathrm{d}t^2 + \mathrm{d}\rho^2 + f(\rho)\mathrm{d}\Omega^2. \tag{D.54}$$

We now compute the surface gravity for this metric:

$$V = \sqrt{-\xi^\mu\xi_\mu} = \sqrt{-g_{\mu\nu}\xi^\mu\xi^\nu} = \sqrt{-g_{tt}} \implies \kappa = \sqrt{\nabla^\mu V \nabla_\mu V} = \sqrt{g^{rr}\left(\partial_r V\right)^2}. \tag{D.55}$$

$$\Longrightarrow \kappa = -\frac{1}{2}\sqrt{\frac{g^{rr}}{-g_{tt}}}\,\partial_r g_{tt} = \frac{1}{2}\partial_r g^{rr}(r_H). \tag{D.56}$$

This is exactly the quantity that appears in front of dt^2 in the metric. We can therefore rewrite the metric as

$$\mathrm{d}s^2 = -\kappa^2\rho^2\mathrm{d}t^2 + \mathrm{d}\rho^2 = -\rho^2\mathrm{d}\theta^2 + \mathrm{d}\rho^2, \tag{D.57}$$

where we have introduced the rescaled time coordinate $\theta = \kappa t$. By now defining new coordinates (T, X) as

$$X = \rho\cosh\theta \quad \wedge \quad T = \rho\sinh\theta \quad \Longrightarrow \quad \mathrm{d}s^2 = -\mathrm{d}T^2 + \mathrm{d}X^2, \tag{D.58}$$

we see that the metric reduces locally to that of Minkowski spacetime. We thus confirm that a freely falling observer indeed experiences nothing unusual when crossing the horizon. We are now ready to examine how the tortoise coordinate (C.27) behaves in the vicinity of the horizon:

$$\mathrm{d}s^2 = g_{tt}\mathrm{d}t^2 + g_{rr}\mathrm{d}r^2 + f(r)\mathrm{d}\Omega^2 = g_{tt}\left(\mathrm{d}t^2 + \frac{g_{rr}}{g_{tt}}\mathrm{d}r^2\right) + f(r)\mathrm{d}\Omega^2 \implies \frac{\mathrm{d}r_*}{\mathrm{d}r} = g_{rr}. \tag{D.59}$$

We can now expand this relation and arrive at:

$$\frac{\mathrm{d}r_*}{\mathrm{d}\varepsilon} = \frac{1}{\cancelto{0}{g^{rr}(r_H)} + \partial_r g^{rr}(r_H)\varepsilon} \quad \implies \quad 2\kappa r_* = \ln\varepsilon + C', \tag{D.60}$$

where C' is an integration constant that needs to be fixed appropriately. As expected, this expression diverges to minus infinity as we approach the horizon. Next, we determine the relation between r_* and ρ:

$$2\kappa r_* = \ln\left(C^2\rho^2\right) \quad \implies \quad C\rho = e^{\kappa r_*}. \tag{D.61}$$

Substituting this expression into the defining relations of the (X, T) coordinates yields:

$$X = Ce^{\kappa r_*}\cosh(\kappa t) \quad \wedge \quad T = Ce^{\kappa r_*}\sinh(\kappa t). \tag{D.62}$$

We see that this reproduces the Rindler coordinate system. The only remaining free parameter is C. By recalling the standard definition of Rindler coordinates, we immediately identify $C = 1/\kappa$. We can thus express the transformation rule for the light-cone coordinates, $\sigma^\pm = t \pm x \mapsto x^\pm = T \pm X$, as:

$$\kappa x^+ = e^{\kappa\sigma^+} \quad \wedge \quad \kappa x^- = -e^{-\kappa\sigma^-}. \tag{D.63}$$

This relation specifies the coordinates in which the metric remains regular at the event horizon. In this way, we have systematically arrived at the Kruskal coordinates. For the Schwarzschild solution, one has $\kappa = 1/(4GM)$. We now analytically continue this coordinate transformation so that it is valid over the entire spacetime, and not merely in the near-horizon region. In doing so, we directly obtain the maximally extended geometry. This construction is very general: it applies not only to static spacetimes, but also to stationary ones.

D.6 Hawking effect

The Hawking effect refers to the phenomenon in which black holes emit particles with a thermal spectrum characterized by the Hawking temperature. In other words, a stationary observer situated far away from the black hole measures a thermal distribution of particles. From the derivations discussed so far, we infer that there must also be an observer for whom the state appears as vacuum. The previous section demonstrated that an observer in free fall experiences nothing unusual when passing through the event horizon. In this frame, the metric reduces to the Minkowski spacetime metric, implying that such an observer perceives the Minkowski vacuum. This vacuum is one of the admissible quantum states for the system and is known as the Hartle–Hawking state. Because the metric is regular throughout the entire spacetime, this state represents a black hole in thermal equilibrium with its environment.

Our aim is to determine the temperature of the particles that arrive in the asymptotically flat region at $\mathscr{J}^+$. We begin by evaluating the redshift factor in Schwarzschild spacetime:

$$V = \sqrt{-\xi^\mu \xi_\mu} = \sqrt{-g_{\mu\nu}\xi^\mu \xi^\nu} = \sqrt{-g_{tt}} \quad \Longrightarrow \quad V = \sqrt{1 - \frac{2GM}{r}}. \tag{D.64}$$

The next step is to compute the acceleration experienced by an observer freely falling at the horizon:

$$a = \sqrt{\nabla_\mu \ln V \nabla^\mu \ln V} = \frac{\sqrt{g^{rr}}}{V}\partial_r V = \frac{1}{2\sqrt{g^{rr}}}\partial_r g_{rr} \quad \Longrightarrow \quad a = \frac{GM}{r^2\sqrt{1 - \frac{2GM}{r}}}. \tag{D.65}$$

We observe that this proper acceleration becomes infinite exactly at the horizon. A freely falling observer crossing the horizon locally experiences Minkowski spacetime, yet is subject to a very large inward gravitational pull toward the black hole. Consequently, a static observer hovering just outside the horizon effectively behaves like a Rindler observer, counteracting this acceleration in order to remain at a fixed radial position relative to the event horizon. Such an observer therefore measures a thermal particle spectrum (analogous to that seen by a Rindler observer) with temperature $\frac{a}{2\pi}$. However, our focus is on what a distant observer at spatial infinity detects. This asymptotic observer also detects these particles, but with a temperature that has been modified by gravitational gravitational redshift. Therefore, we can write that the temperature detected by this observer is given by:

$$T = \lim_{r_1 \to 2GM} \lim_{r_2 \to \infty} \frac{V(r_1)}{V(r_2)} \frac{a}{2\pi} = \frac{1}{2\pi} \lim_{r \to 2GM} \frac{\sqrt{1 - \frac{2GM}{r}}}{r^2\sqrt{1 - \frac{2GM}{r}}} = \frac{1}{8\pi GM}. \tag{D.66}$$

Upon reinstating all the physical constants, the Hawking temperature takes the form

$$T = \frac{\hbar c^3}{8\pi G k_B M}. \tag{D.67}$$

Thus, the temperature scales inversely with the mass. This behavior is initially surprising, as it indicates that black holes have a negative heat capacity. It is important to stress that this is the temperature of the emitted radiation; nonetheless, because this radiation is in thermal equilibrium with the black hole (the underlying quantum state being everywhere regular, namely the Hartle–Hawking state), it can also be identified as the temperature of the black hole itself.

We can now use standard thermodynamic relations to determine the entropy of the black hole. We start from Einstein's mass–energy relation, $E = Mc^2$, and combine it with the thermodynamic identity $dE = T\,dS$. Integrating with respect to M, we arrive at the expression:

$$S = k_B \frac{4\pi G M^2}{\hbar c}. \tag{D.68}$$

Since the Schwarzschild radius is proportional to M, the quantity M^2 is proportional to the horizon area. Consequently, the entropy is proportional to the area of the event horizon. In this way, we recover the Bekenstein–Hawking entropy formula (1.4). The final relations connecting the mass, temperature, and entropy of a black hole can be summarized as

$$E = Mc^2 \quad \wedge \quad T = \frac{\kappa}{2\pi} \quad \wedge \quad S = \frac{A}{4 l_p^2}. \tag{D.69}$$

Remarkably, these relations are quite general and hold for nearly all black hole solutions, whether static or stationary. Finally, recall that the acceleration of a Rindler observer coincides with surface gravity $\kappa = a$, providing yet another confirmation of the equivalence principle.

Biografija

Stefan Đorđević rođen je 1997. godine u Beogradu. Osnovnu školu „Ćirilo i Metodije" završio je 2012. godine u Beogradu, dok je „Matematičku gimnaziju" u Beogradu završio 2016. godine. Osnovne studije fizike završava 2020. godine na Fizičkom fakultetu Univerziteta u Beogradu, na smeru teorijska i eksperimentalna fizika, sa prosečnom ocenom 10.00. Iste godine završva i osnovne studije elektrotehnike i računarstva na Elektrotehničkom fakultetu, Univerziteta u Beogradu sa prosečnom ocenom 10.00 kao student generacije. Naredne, 2021. godine završava master studije iz teorijske i eksperimentalne fizike na Fizičkom fakultetu Univerziteta u Beogradu, sa prosečnom ocenom 10.00, odbranivši master rad na temu *"Entropija Hokingovog zračenja u 2D dilatonskoj gravitaciji".* Naredne godine osvaja nagradu „Prof dr Ljubomir Ćirković" za najbolji master rad odbranjen na Fizičkom fakultetu tokom školske 2020/2021. Oktobra 2021. godine upisao je doktorske studije na Fizičkom fakultetu Univerziteta u Beogradu. Od maja 2022. godine je zaposlen na ovom fakultetu, a u zvanje istraživač-saradnik izabran je krajem novembra 2024. godine.

Stefan je držao računske vežbe iz predmeta Relativistička kvantna mehanika na Fizičkom fakultetu. Učestvovao je na većem broju međunarodnih konferencija. Do sada je objavio 4 rada u međunarodnim časopisima. Član je, ili je bio član dva projekta koja su finansirana od strane Fonda za nauku Republike Srbije. Oblasti njegovog interesovanja iz fizike visokih energija su: (kvantna) gravitacija, termodinamika crnih rupa, kvantna teorija polja; kao i oblasti fizike čvrstog stanja: topološka kvantna mehanika, topološki izolatori, kvantni holov efekat, ne-hermitski disipativni sistemi.

Ime i prezime autora: Stefan Đorđević

Broj indeksa: 8008/2021

Izjavljujem

da je doktorska disertacija pod naslovom

Page curve in 2D dilaton gravity (Pejdžova kriva u 2D dilatonskoj gravitaciji)

- rezultat sopstvenog istraživačkog rada;
- da disertacija u celini ni u delovima nije bila predložena za sticanje druge diplome prema studijskim programima drugih visokoškolskih ustanova;
- da su rezultati korektno navedeni i
- da nisam kršio autorska prava i koristio intelektualnu svojinu drugih lica.

Potpis autora

U Beogradu, ____________________ ______________________________

Izjava o istovetnosti štampane i elektronske verzije doktorskog rada

Ime i prezime autora: Stefan Đorđević

Broj indeksa: 8008/2021

Studijski program: kvantna polja, čestice i gravitacija

Naslov rada: Page curve in 2D dilaton gravity

Mentor: prof. dr Voja Radovanović

Izjavljujem da je štampana verzija mog doktorskog rada istovetna elektronskoj verziji koju sam predao/la radi pohranjivanja u Digitalnom repozitorijumu Univerziteta u Beogradu.

Dozvoljavam da se objave moji lični podaci vezani za dobijanje akademskog naziva doktora nauka, kao što su ime i prezime, godina i mesto rođenja i datum odbrane rada.

Ovi lični podaci mogu se objaviti na mrežnim stranicama digitalne biblioteke, u elektronskom katalogu i u publikacijama Univerziteta u Beogradu.

Potpis autora

U Beogradu, ____________________ ____________________________________

Izjava o korišćenju

Ovlašćujem Univerzitetsku biblioteku „Svetozar Marković“ da u Digitalni repozitorijum Univerziteta u Beogradu unese moju doktorsku disertaciju pod naslovom:

Page curve in 2D dilaton gravity (Pejdžova kriva u 2D dilatonskoj gravitaciji)

koja je moje autorsko delo.

Disertaciju sa svim prilozima predao/la sam u elektronskom formatu pogodnom za trajno arhiviranje.

Moju doktorsku disertaciju pohranjenu u Digitalnom repozitorijumu Univerziteta u Beogradu i dostupnu u otvorenom pristupu mogu da koriste svi koji poštuju odredbe sadržane u odabranom tipu licence Kreativne zajednice (Creative Commons) za koju sam se odlučio/la.

1. Autorstvo (CC BY)
2. Autorstvo – nekomercijalno (CC BY-NC)
3. Autorstvo – nekomercijalno – bez prerada (CC BY-NC-ND)
4. Autorstvo – nekomercijalno – deliti pod istim uslovima (CC BY-NC-SA)
5. Autorstvo – bez prerada (CC BY-ND)
6. Autorstvo – deliti pod istim uslovima (CC BY-SA)

(Molimo zaokružiti samo jednu od šest ponuđenih licenci. Kratak opis licence je sastavni deo ove izjave.)

Potpis autora

U Beogradu, ____________________ ________________________

1. **Autorstvo (CC BY)** Dozvoljavate umnožavanje, distribuciju i javno saopštavanje dela, i prerade, ako se navede ime autora na način određen od strane autora ili davaoca licence, čak i u komercijalne svrhe. Ovo je najslobodnija od svih licenci.

2. **Autorstvo – nekomercijalno (CC BY-NC)** Dozvoljavate umnožavanje, distribuciju i javno saopštavanje dela, i prerade, ako se navede ime autora na način određen od strane autora ili davaoca licence. Ova licenca ne dozvoljava komercijalnu upotrebu dela.

3. **Autorstvo – nekomercijalno – bez prerada (CC BY-NC-ND)** Dozvoljavate umnožavanje, distribuciju i javno saopštavanje dela, bez promena, preoblikovanja ili upotrebe dela u svom delu, ako se navede ime autora na način određen od strane autora ili davaoca licence. Ova licenca ne dozvoljava komercijalnu upotrebu dela. U odnosu na ostale licence, ovom licencom se ograničava najveći obim prava korišćenja dela.

4. **Autorstvo – nekomercijalno – deliti pod istim uslovima (CC BY-NC-SA)** Dozvoljavate umnožavanje, distribuciju i javno saopštavanje dela, i prerade, ako se navede ime autora na način određen od strane autora ili davaoca licence i ako se prerada distribuira pod istom ili sličnom licencom. Ova licenca ne dozvoljava komercijalnu upotrebu dela i prerada.

5. **Autorstvo – bez prerada (CC BY-ND)** Dozvoljavate umnožavanje, distribuciju i javno saopštavanje dela, bez promena, preoblikovanja ili upotrebe dela u svom delu, ako se navede ime autora na način određen od strane autora ili davaoca licence. Ova licenca dozvoljava komercijalnu upotrebu dela.

6. **Autorstvo – deliti pod istim uslovima (CC BY-SA)** Dozvoljavate umnožavanje, distribuciju i javno saopštavanje dela, i prerade, ako se navede ime autora na način određen od strane autora ili davaoca licence i ako se prerada distribuira pod istom ili sličnom licencom. Ova licenca dozvoljava komercijalnu upotrebu dela i prerada. Slična je softverskim licencama, odnosno licencama otvorenog koda.